JPRS L/10374

8 March 1982

Translation

MICROWAVE ANTENNAS AND EQUIPMENT: DESIGN OF PHASED ANTENNA ARRAYS

Ed. by

D.I. Voskresenskiy

FBIS FOREIGN BROADCAST INFORMATION SERVICE

NOTE

JPRS publications contain information primarily from foreign newspapers, periodicals and books, but also from news agency transmissions and broadcasts. Materials from foreign-language sources are translated; those from English-language sources are transcribed or reprinted, with the original phrasing and other characteristics retained.

Headlines, editorial reports, and material enclosed in brackets [] are supplied by JPRS. Processing indicators such as [Text] or [Excerpt] in the first line of each item, or following the last line of a brief, indicate how the original information was processed. Where no processing indicator is given, the information was summarized or extracted.

Unfamiliar names rendered phonetically or transliterated are enclosed in parentheses. Words or names preceded by a question mark and enclosed in parentheses were not clear in the original but have been supplied as appropriate in context. Other unattributed parenthetical notes within the body of an item originate with the source. Times within items are as given by source.

The contents of this publication in no way represent the policies, views or attitudes of the U.S. Government.

COPYRIGHT LAWS AND REGULATIONS GOVERNING OWNERSHIP OF MATERIALS REPRODUCED HEREIN REQUIRE THAT DISSEMINATION OF THIS PUBLICATION BE RESTRICTED FOR OFFICIAL USE ONLY.

JPRS L/10374

8 March 1982

MICROWAVE ANTENNAS AND EQUIPMENT:
DESIGN OF PHASED ANTENNA ARRAYS

Moscow ANTENNY I USTROYSTVA SVCH: PROYEKTIROVANIYE FAZIROVANNYKH ANTENNYKH RESHETOK in Russian 1981 (signed to press 13 Apr 81) pp 1-431

[Book edited by Professor D.I. Voskresenskiy: "Microwave Antennas and Equipment (Phased Antenna Array Design): Textbook for the Higher Educational Institutes", approved by the USSR Ministry of Higher and Intermediate Special Education as a textbook for students in the Radioengineering Specialties of the Higher Educational Institutes, Izdatel'stvo "Radio i svyaz'", 1981, 431 pages, 15,000 copies]

CONTENTS

Annotation.......... 1

Foreword.......... 1

Section I. Antenna Arrays.......... 4

Chapter 1. Microwave Antenna Design.......... 4

1.1. Introduction.......... 4

1.2. The Main Requirements Placed on Microwave Antenna Systems and the Possibilities of Using Antenna Arrays.......... 6

1.3. Antennas With Electrical Scanning.......... 11

1.4. Specific Features of Phased Antenna Array Design.......... 13

1.5. Specific Features of Active Array Design.......... 15

Chapter 2. Phased Antenna Arrays.......... 19

2.1. The Determination of the Geometric Characteristics of Phased Antenna Arrays.......... 19

2.2. Mutual Coupling Effects Among Radiators.......... 25

2.3. The Relationship Between the Directivity of a Radiator in an Array and the Directional Characteristics of a Fully Excited Array 28

2.4. Radiators of Phased Antenna Arrays 30

2.5. Wide Angle Matching of Phase Antenna Arrays 37

2.6. Structural Configuration of Phased Antenna Arrays 41

2.7. The Passband of a Phased Antenna Array 47

2.8. Switched Scanning 53

2.9. Switched Phase Shifters 54

2.10. Discrete Phase Shifters and the Suppression of Switching Lobes 56

2.11. Beam Jumps in a Switched Array 59

2.12. Design Procedure 60

Chapter 3. Frequency Scanning Antennas 61

3.1. Fundamental Relationships for a Frequency Scanning Linear Radiator Array 61

3.2. Channelizing Systems of Frequency Scanning Antennas 69

3.3. The Frequency Scanning Slotted Waveguide Array 72

3.4. The Design Procedure for a Frequency Scanning Linear Slotted Waveguide Array 76

Chapter 4. Highly Directional Cylindrical and ARC Antenna Arrays 83

4.1. General Information 83

4.2. The Phase Distribution in Highly Directional Cylindrical Arrays 86

4.3. The Directional Patterns of Cylindrical Pencil Beam Arrays 88

4.4. Directional Patterns of Arc and Cylindrical Arrays 89

4.5. The Directional Gain of Cylindrical and Arc Arrays 94

4.6. Bandwidth Properties of Arc Arrays 98

4.7. Some Structural and Circuit Design Variants for Arc and Cylindrical Arrays 100

4.8. The Design Procedure for Cylindrical Arrays........................ 104

Chapter 5. Slotted Waveguide Arrays.. 107

5.1. The Function and Specific Features of Slotted Waveguide Arrays...... 107

5.2. The Major Parameters of a Slot in a Waveguide...................... 107

5.3. The Types of Slotted Waveguide Arrays.............................. 112

5.4. Methods of Designing Slotted Waveguide Arrays...................... 115

5.5. Matching a Slotted Waveguide Array to a Feed Waveguide............. 121

5.6. The Influence of a Change in Frequency on Antenna Characteristics... 121

5.7. The Directional Properties of Slotted Waveguide Arrays............. 122

5.8. Possible Structural Configurations for Slotted Waveguide Arrays and Structural Design Examples.................................... 126

5.9. A Sample Design Calculation Procedure for Slotted Waveguide Arrays.. 129

Chapter 6. Accounting for Mutual Coupling Effects in Slotted Waveguide Arrays.. 131

6.1. Basic Relationships.. 132

6.2. Planar Slotted Waveguide Array..................................... 135

6.3. An Analysis of Mutual Coupling Effects on the Directional Pattern of an Array... 136

6.4. A Procedure for Synthesizing a Linear Slotted Waveguide Array Taking Electrodynamic Mutual Coupling Effects Into Account......... 141

6.5. A Procedure for Synthesizing a Planar Slotted Waveguide Array Taking Mutual Coupling Into Account............................... 149

6.6. Design Calculation Recommendations................................. 150

Chapter 7. Phased Antenna Arrays With a Hemispherical Scan Space........... 151

7.1. General Governing Laws... 151

7.2. A Hybrid Phased Antenna Array With a Hemispherical Scan Space. Operational Principle. Specific Structural Design Features of a Phased Array With a Dome Shaped Lens............................. 154

7.3. Conformal Phased Antenna Arrays.................................... 156

7.4. Polyhedral Phased Antenna Arrays.................................... 163

Chapter 8. Beam Steering Systems for Phased Antenna Arrays.................. 168

8.1. Phased Antenna Array Control Problems.............................. 168

8.2. Control Algorithms for Phase Shifters.............................. 171

8.3. Algorithms for Generating Directional Patterns of Special Shapes... 175

8.4. Switcher Control Algorithms.. 177

8.5. Adaptation Control Algorithms...................................... 179

8.6. The Design of Beam Steering Systems for a Specified Precision of the Directional Pattern Orientation in Space..................... 184

Section II. Radiating Elements of an Antenna Array.......................... 190

Chapter 9. Printed Circuit Antenna.. 190

9.1. The Function and Specific Features of Printed Circuit Antennas....... 190

9.2. The Major Types of Printed Circuit Antennas and Their Operational Principles... 190

9.3. The Major Characteristics and Design of Printed Circuit Resonator Antennas.. 193

9.4. Antenna Arrays With Resonator Elements.............................. 197

9.5. Printed Circuit Dipole Antennas..................................... 200

9.6. Antenna Arrays With Printed Circuit Dipole Elements.................. 204

9.7. Other Printed Circuit Radiating Systems............................. 207

Chapter 10. Yagi Radiators for Planar Phased Antenna Arrays................. 211

10.1. Phased Arrays of Yagi Radiators.................................... 211

10.2. Analysis of the Electromagnetic Field of a Phased Antenna Array of Yagi Radiators... 211

10.3. The Characteristics of a Yagi Radiator in a Planar Phased Antenna Array.. 213

10.4. The Optimization of a Yagi Radiator in an Array.................... 216

10.5. Designing the Input Circuit of a Yagi Radiator..................... 218

10.6. A Design Procedure for a Yagi Radiator for Phased Antenna Arrays.................... 220

Chapter 11. Approximate Design Calculations for Phased Waveguide Antenna Arrays Taking Mutual Coupling Into Account............ 221

11.1. General Considerations.................... 221

11.2. Design Graphs.................... 221

11.3. Design Recommendations.................... 225

Chapter 12. Wide Angle Matching of the Waveguide Radiators of Planar Phased Antenna Arrays.................... 228

12.1. Methods of Matching Waveguide Radiators in Planar Phased Antenna Arrays.................... 228

12.2. Matching With a Fixed Scanning Angle.................... 233

Chapter 13. Slotted Resonator Radiators for Planar Antenna Arrays.......... 237

13.1. Analysis of the Characteristics of a Slotted Resonator Radiator.................... 237

13.2. The Characteristics of a Slotted Resonator Radiator as a Independent Antenna.................... 241

13.3. The Characteristics of a Slotted Resonator Radiator in a Planar Antenna Array.................... 242

13.4. The Optimization of the Characteristics of a Slotted Resonator Radiator in an Antenna Array.................... 244

13.5. Examples of the Realization of Slotted Resonator Radiators......... 246

13.6. The Design Procedure.................... 247

Chapter 14. Radiating Waveguide Modules With Reflective Phase Shifters.................... 249

14.1. The Modular Design of a Phased Antenna Array.................... 249

14.2. Multiposition Phase Shifter for a Module.................... 250

14.3. Microwave Bridge Devices for Feedthrough Phase Shifters........... 254

14.4. The Design of a Radiating Module of an Antenna Array............... 255

14.5. Waveguide Directional Couplers.................... 258

14.6. An Approximate Design Calculation Procedure for a Radiating Module.. 261

Section III. Active Elements of Antenna Array Modules...................... 264

Chapter 15. Modules of Transmitting Phased Antenna Arrays Using Semiconductor Devices.. 264

15.1. The Major Characteristics of the Active Elements of Modules........ 265

15.2. Major Structural Design Requirements.............................. 267

15.3. Active Semiconductor Devices for Active Phased Antenna Array Modules.. 268

15.4. The Radiation Power of Active Semiconductor Phased Antenna Arrays... 269

15.5. Active Phased Antenna Array Efficiency............................ 274

15.6. Recommendations for the Selection of Module Circuits and Parameters... 276

Chapter 16. Externally Excited Oscillators and Amplifiers Using Power Transistors... 279

16.1. General Information.. 279

16.2. The Equivalent Circuit of a Microwave Transistor.................. 279

16.3. A Time and Harmonic Analysis of Transistor Currents and Voltages... 284

16.4. The Properties of Common Emitter and Common Base Generator Configurations.. 289

16.5. The Procedure and Sequence for the Design Calculations of the Operating Mode of an Oscillator/Amplifier.......................... 293

Chapter 17. Externally Excited Microwave Circuits for Transistor Oscillators and Amplifiers................................... 300

17.1. General Information.. 300

17.2. The Design of the Microwave Networks of Amplifiers and Oscillators... 304

17.3. Oscillator/Amplifier Power Supply Circuits........................ 308

17.4. The Design of Microwave Matching Transformer Networks Using Lumped Elements.. 310

17.5. The Design of a Microwave Matching and Transforming Network Using Elements With Distributed Parameters........................ 320

Chapter 18. Frequency Multipliers Using Nonlinear Capacitance Diodes..... 328

18.1. General Information... 328

18.2. The Selection of the Multiplication Factor for the Frequency Multiplier of an Active Phased Antenna Array Module.............. 329

18.3. The Selection of Nonlinear Capacitance Diode and Its Operating Mode.. 332

18.4. The Power Design Calculation Procedure for the Operational Mode of a Diode in a Parallel Type Multiplier.................... 335

18.5. The Design of the Microwave Input and Output Networks of a Multiplier.. 338

Chapter 19. Microwave Amplifiers and Oscillators Using Avalanche Transit Time Diodes.. 343

19.1. Basic Characteristics.. 343

19.2. The Parameters of IMPATT Diodes and Specific Features of Their Applications in the Modules of Active Phased Transmitting Antenna Arrays.. 345

19.3. Microwave Circuits of Oscillators Using IMPATT Diodes............ 353

19.4. Structural Design Principles.................................... 357

19.5. Principles of Design Calculations of IMPATT Diode Microwave Devices... 360

Section IV. Microwave Hardware... 368

Chapter 20. The Structural Design of Microwave Hybrid Integrated Circuit Components.. 368

20.1. General Information... 368

20.2. The Asymmetrical Transmission Stripline......................... 370

20.3. Printed Circuit Inductance Coils................................. 375

20.4. Capacitors.. 379

Chapter 21. Microwave Phasing Devices (Phase Shifters)................... 383

21.1. Semiconductor Phase Shifters.................................... 384

21.2. Semiconductor Phase Shifters With a Continuous Phase Change....... 386

21.3. Discretely Switched Semiconductor Phase Shifters................. 391

Chapter 22. Microwave Filters... 404

22.1. The Classification of Microwave Filters.......................... 404

22.2. The Design of the Low Frequency Filter Prototype................. 405

22.3. The Structural Execution of Microwave Filters.................... 411

22.4. A Design Procedure for Microwave Filters......................... 415

Chapter 23. Directional Couplers and Directional Filters Using Coupled Striplines... 417

23.1. The Classification of Directional Couplers and Filters and Their Operating Characteristics................................. 418

23.2. The Main Design Equations for Single Section T Mode Coupled Line Directional Couplers.. 420

23.3 Extended Bandwidths Directional Couplers Using Coupled Lines....... 426

23.4. The Characteristic Impedances of Coupled Lines in the Case of in-Phase and Out-of-Phase Excitation.......................... 428

23.5. The Relationship Between the Structural and Electrical Characteristics... 432

23.6. The Major Design Relationships for Single Loop Directional Filters Using Striplines....................................... 435

23.7. The Influence of Tolerances on the Parameters of Directional Couplers... 437

23.8. The Structural Design of Directional Couplers and Filters Using Coupled Striplines.. 440

23.9. The Design Procedure.. 443

Chapter 24. Stripline Microwave Power Distribution Systems.............. 447

24.1. The Function and Major Characteristics of Microwave Power Distribution Systems.. 447

24.2. The Comparative Performance of Various Types of Microwave Power Distribution Systems...................................... 448

24.3. Calculating the Electrical Parameters and Characteristics of Two Channel Power Distributors................................. 450

24.4. The Calculation of the Eletrical Parameters and Characteristics of Multi-Channel Power Distribtuion Systems..................... 455

24.5. An Approximate Design Procedure for Power Distribution Systems.. 457

Bibliography.. 459

Annotation

[Text] Methods of calculating the characteristics of phased antenna arrays (PAA) and active phased antenna arrays (APAA) as well as their components are presented. Arrays with various geometries, types of radiators and control techniques are treated as well as antennas with frequency scanning, switching, multislot, planar, and cylindrical antennas, etc.

The book is intended for students in the radio engineering specialties of the higher educational institutions in the performance of the diploma and course required design, as well as for engineers engaged in the design of phased antenna arrays and active phased antenna arrays.

D.I. Voskresenskiy, V.L. Gostyukhin, R.A. Granovskaya, K.I. Grineva, A.Yu. Grinev, I.I. Gurova, N.S. Davydova, G.P., Zemtsov, M.V. Indenbom, G.I. Koptev, Yu.V. Kotov, S.D. Kremenetskiy, S.M. Mikheyev, B.Ya. Myakishev, T.A. Panina, S.B. Petrov, L.I. Ponomarev, V.V. Popov, A.M. Razdolin, P.A. Solovtsov, V.I. Samoylenko, V.S. Filippov, V.V. Chebyshev, V.N. Shkalikov, V.Ye. Yamaykin.

Reviewers: Department of Antenna Equipment and Radio Wave Propagation of Moscow Power Engineering Institute (head of the department, doctor of the engineering sciences, professor Ye.N. Vasil'yev) and the Department of Communications and Radio Control of Ryazan' Radio Engineering Institute (head of the department, doctor of the engineering sciences, winner of the USSR State Prize, professor V.I. Popovkin)

Editorial Staff for Cybernetics and Computer Engineering Literature

Foreword

Material on the planning and design of phased antenna arrays (PAA), active antenna arrays (APAA) and their components is collected and systematized in this book. Engineering methods are given for electrically scanned antenna design to meet specific technical requirements, as well as the requisite information for design work based on the parameters of existing equipment and a description of existing designs. Special attention is devoted to flight systems.

The book "Microwave antennas and equipment. The planning and design of antenna arrays and their radiating elements" which came out in 1972 under the editorship of D.I. Voskresenskiy, to a known extent generalized the most widespread design techniques. This book contains materials which are an extension of the indicated work; the design methods presented in it supplement and refine the methods treated earlier, taking into account the latest achievements in design automation using computers. The range of problems considered has been significantly expanded: questions of the design of new types of arrays are set forth, as well as active and passive elements.

Considerable attention has been devoted to the construction of active stripline modules with semiconductor devices. Bringing the materials on the indicated topics together in one book, based on the general requirements placed on array elements, as well as the utilization of uniform criteria for a comparative evaluation of these and other elements have significantly simplified the problem of the goal directed design of an array, in particular, the selection of an acceptable variant for the overall array configuration, as well as the type of active and control elements.

The book consists of four sections. General questions of phased array design are treated in the first. Here, questions of antenna design with phase, switching and frequency scanning techniques are presented. Procedures are given for the design of planar and cylindrical arrays, phased arrays with a hemispherical scanning space as well as slotted waveguide arrays.

Procedures are given in the second section for the engineering design of phased array radiating elements, taking their interaction into account. Dipole, stripline, slotted, director, waveguide and other phased array radiators are treated.

The third section is devoted to the design of active phased arrays and their modules. Specific features of the construction and calculation of the characteristics of active phased arrays are presented; structural configurations are given for active reflective and transmission type phased array modules as well as methods of signal phasing in the modules. Modules of various types are compared and possibilities of using various active elements are indicated. Procedures are given for designing the modules of transmitting active phased arrays around various semiconductor elements: oscillator stages using microwave transistors and IMPATT diodes, varactor multipliers, and hybrid IC microwave circuits.

Questions of the design of passive elements of phased arrays are treated in the fourth section. Design procedures are given for directional couplers and coupled line filters as well as multichannel stripline dividers, microwave phase shifters and filters.

Widely known material existing in monographs and the periodical press is collected and systematized in the book, and the published literature of the Problems

Laboratory for Microwave Engineering of Moscow Aviation Institute are also used. Topics from general microwave antenna and equipment theory are not treated; it is assumed that the reader is already familiar with the general course given in the radio engineering departments of the higher educational institutes.

It must be underscored that the design procedures incorporated in the book differ substantially in terms of design precision and complexity. Along with simplified calculations, which make no pretense of exhaustive completeness, some of the latest techniques of computer assisted design are included in the book. Simplified design methods are presented initially, which make it possible to design phased antenna arrays or elements which meet the major technical requirements, in the amount necessary for the course required or diploma design work, as well as in the preliminary developmental work on antenna system designs. Further, where it has proved possible, the authors provide more precise computational methods which make it possible to optimize the device being designed with respect to a particular criterion by means of the programs which have been developed.

A bibliography of the major literature is given at the end of the book, as well as bibliographies for the chapters, which are recommended in the planning and design of the given equipment.

The book is intended for students in the radio engineering specialties when doing their diploma or course required design work, but can also be useful to engineers engaged in the design of antenna arrays.

The book was written by a collective of authors: D.I. Voskresenskiy (the Foreword and Chapter 1); V.S. Fillipov (Chapter 2); R.A. Granovskaya (Chapter 3 and 17); L.I. Ponomarev (Chapter 4); V.L. Gostyukhin (Chapters 5 and 21); S.D. Kremenetskiy (Chapter 6); V.Ye. Yamaykin (Chapter 7); V.I. Samoylenko (Chapter 8); V.V. Chebyshev (Chapter 9); M.V. Indenbom (Chapter 10); K.I. Grineva (Chapter 11); A.M. Razdolin (Chapter 12); A.Yu. Grinev and Yu.V. Kotov (Chapter 13); V.V. Popov and S.M. Mikheyev (Chapter 14); G.P. Zemtsov (Chapter 15); G.I. Koptev and T.A. Panina (Chapter 16); V.N. Shkalikov (Chapter 18); N.S. Davydova (Chapter 19); S.B. Petrov (Chapter 20); B.Ya. Myakishev (Chapter 22); A.Yu. Grinev (Chapter 23); I.I. Gurova, B.Ya. Myakishev and P.A. Solovtsov (Chapter 24). The overall editing of the book was done by D.I. Voskresenskiy.

1. Microwave Antenna Design

1.1. Introduction

The antenna and feedline, which provide for the radiation and reception of radio waves, is an integral part of any radio engineering system. A number of technical requirements are placed on the antenna, which follow from the function of the radio system in which it is used. The conditions for the placement and operation of the antenna influence its characteristics. The feasibility of attaining the requisite directional properties, frequency, power and other characteristics of an antenna depend in many respects on the working frequency band. The last two decades have been marked by the wide scale introduction of radio equipment into the economy and the use of microwave gear. Antennas in the microwave band produce pencil beam radiation with a beam width measured in units and fractions of degrees and have a gain reaching tens and hundreds of thousands. This makes it possible to use the antenna not just for radio wave transmission and reception, but also for direction finding (in radar, navigation and radio astronomy), combating interference, providing for concealed operation of a radio system and for other purposes.

Besides radars, microwave hardware is used in such sectors of electronics as television, radio control, radio navigation, radio communications, telemetry, and accelerators. The successful development of radio astronomy and the mastery of space is related in many respect to the achievements of microwave engineering.

Pencil-beam scanning microwave antennas have become widespread at the present time. The scanning makes it possible to scan the surrounding space, track moving objects and determine their angular coordinates. The replacement of poorly directional or omnidirectional antennas (for example, coupled antennas) with pencil-beam scanning antennas makes it possible to obtain not only a power gain in the system because of the increase in the antenna gain, but also, in a number of cases, to attenuate crosstalk between different radio engineering systems operating at the same time, i.e., provide for electromagnetic compatibility of these systems. In this case, the noise immunity, security and other characteristics of the system can also be improved. With mechanical scanning, which is accomplished by means of rotating the entire antenna, the maximum rate of beam travel in space is limited, and with the presently existing aircraft speeds, proves to be insufficient. For this reason, it became necessary to develop new types of antennas.

The application of phased antenna arrays (PAA's) to produce scanning pencil-beam antennas makes it possible to realize a high space scanning rate and promotes an improvement in the data obtained on the electromagnetic reflection or radiation sources in the surrounding space. Modern microwave devices with vacuum tube or semiconductor devices and electrically controllable media have made it possible to not only create a controlled phase distribution in an antenna array (i.e., effect electrical scanning), but to accomplish the initial processing of the incoming information (summing of the fields, frequency conversion, amplification, etc.) directly in the radio frequency channel of the antenna.

A further improvement in the characteristics of radio systems with phased arrays is possible (resolution, speed, carrying capacity, detection range, interference immunity, etc.) by refining the techniques of processing the signal transmitted and received by the antenna (space-time processing in the general case). The antenna in this case is the primary processing unit and to a significant extent governs the major characteristics of the system as a whole. Usually, far from all of the information contained in the wave impinging on a pencil-beam receiving antenna is used, where the fields in the antenna from the individual radiators are added together in a single radio frequency channel. The most complete information can be obtained by processing each received signal in the antenna array separately, i.e., by processing a series of samples from the spatial distribution of the incident wave. Antennas with different processing techniques are employed, depending on the function of the system and the requirements placed on its characteristics. One of the antenna variants with signal processing is the adaptive array, which in a radio signal processing system can be treated as a dynamic self-tuning space-time filter, in which the directional pattern, frequency properties and other parameters are changed automatically. Other signal processing antennas are also known: self-tuning, artificial aperture, with time modulation of the parameters, digital processing, analog space-time processing using coherent optics methods, etc.

Thus, the antennas being used in practice are very complex systems, having up to tens of thousands and more radiators, active elements and phase shifters, which are controlled by a special computer. The design of such antennas is extremely complex and basically determines the size and cost of the entire radio system.

The characteristics of antennas presently predetermine the major parameters of an entire radio system, for example, in radars, the resolution and precision in the determination of angular coordinates, the rate of beam travel in space and the interference immunity.

The rapid development of microelectronics and its achievements have also found their own place in antenna engineering. Integrated circuit stripline assemblies, stripline and microstrip transmission lines and various microwave devices designed around them (phase shifters, switchers, rectifiers, amplifiers, etc.) have come into widespread use in recent years. However, the potential possibilities for reducing the weight and volume of microelectronic radio equipment can be realized with the appropriate design of the antennas, dispensing with traditional types of them and making a transition to antenna arrays. The fact is that the reflector antenna with a fairing, the drive mechanism, waveguide channel and microwave devices of the aircraft radars in operation has considerable size and weight as compared to the other parts of the radar station. A radar in a microelectronic design using semiconductor microwave devices makes it possible to achieve the greatest reduction in size and weight.

The increasing complexity of antennas during their development and their increasing role in radio systems have led to the expansion of the group of radio specialists working directly in the field of antennas and feedlines. Not only the specialists in these fields must be involved with the calculation of the major characteristics of antennas and microwave devices, but also the designers of the entire radio system and its individual components, which are coupled to the antenna. Their combined efforts during the preliminary design stage make it possible to estimate the ultimately attainable characteristics of the entire radio system, taking into account the feasibility of making the individual components.

The appearance of new types of antennas has led to a substantial expansion and deepening of antenna theory as well as the development of new design techniques. Considerable attention has been devoted to these questions in the literature: a number of monographs have been published [01-013] and a considerable number of papers have published in journals. However, the use of these materials by radio engineers as well as students doing their diploma and course design work also encounters considerable difficulties. Engineering methods of designing prospective phased and active phased antenna arrays, as well as their elements, are presented in this textbook. Considerable attention is devoted to the design of aircraft and mobile antenna systems. The engineering design techniques are supplemented with descriptions of designs of existing antennas and the requisite reference material on the parameters of various microwave devices is given for devices which can be used as the components of phased and active phased antenna arrays.

The cited design techniques are sufficiently simple, based on approximate microwave antenna theory and suitable in the majority of cases for engineering practice. These techniques make it possible in the initial design stages to approximately determine the major parameters and characteristics of the antennas, where these parameters and characteristics can subsequently be made more precise where necessary by means of various more rigorous design methods. Also included in the book are design techniques developed on the basis of mathematical models of antenna arrays and their components, close to the actual ones. The characteristics of director, waveguide, slotted resonator and slotted waveguide radiators of a periodic array are studied and optimized by rigorous electrodynamic methods. The calculated curves and the programs developed in the all-purpose algorithmic languages of Algol-60 and Fortran-IV for the BESM-6 and M-4030 computers are presented. By basing the work on the general procedure for phased antenna array design and using the materials of this book, one can design the radiating aperture of a phased array in a rather well reasoned fashion.

The material presented here is intended for a reader already familiar with the general course on antennas and microwave devices, which is studied in the radio engineering departments of the higher educational institutes.

1.2. The Main Requirements Placed on Microwave Antenna Systems and the Possibilities of Using Antenna Arrays

The major requirements placed on an antenna are governed by the volume of information to be processed (or extracted) and are linked to the range, resolution, precision in the determination of coordinates, speed, reliability, interference immunity and other characteristics of the radio engineering system. Establishing the interrelationship between the characteristics of various radio engineering systems and the characteristics of the antenna and feedline is accomplished in the relevant courses on radar, radio control, etc. Without going into the details of the operation of these systems and establishing the interrelationship cited above, one can state that in the final analysis, antennas and feedlines should assure the appropriate: directionality, power, frequency and direction finding characteristics, control characteristics and other general engineering, operational and economic characteristics.

The requirements for antenna directionality predetermine the shape and width of the spatial directional pattern (in the two main planes), the permissible level of sidelobes, the direction gain (KND) and the polarization characteristics of the antenna. Antennas in the microwave band have needle-shaped, cosecant, fan-shaped, funnel-shaped and other directional pattern shapes. The polarization characteristic determines the following: the polarization of the transmitted and received waves, the permissible coefficient of uniformity of the polarization ellipse when using rotationally polarized waves and the permissible level of cross-polarization in the case of linear polarization of the radiated field. When designing an antenna, the shape of the directional pattern, its width, the sidelobe level, the directional gain and the polarization can be specified. It must be noted that a relationship exists [01] between these characteristics which determine the directionality, and during the design work, frequently only some of them are specified. Thus, in the electrical design, the starting data can be the width of the directional pattern (beam width) or the directional gain. It can be stipulated in this case that it is desirable to keep the sidelobe and cross-polarized radiation levels to a minimum with the given relative antenna dimensions.

The power characteristics of transmitting and receiving antennas make it possible to determine: the signal power at the input to the receiver; the maximum permissible transmission power at which the electrical strength and permissible thermal mode are assured; the power needed to control the beam position in space; the microwave power losses in the antenna and feedline channel as well as the noise power in the receiving antenna. These powers are characterized by the following parameters, as is well known [0.1, 0.2, 0.3, 0.6, 0.7]: the antenna gain, the antenna efficiency and efficiency of the microwave devices which are used, the noise temperature, the input impedence (the matching in the feed channel), the antenna Q [02] and the permissible electrical field intensity. In contrast to mechanically scanned antennas, in which the determination of the power used to control the beam position in space is related to the electrical drive design, in electrically scanned antennas, this power is governed by the losses in the controllable microwave devices, and for this reason can have an impact on the thermal mode of the antenna. When designing microwave scanning antennas, only individual values are specified at times which characterize the power indicators of the antenna. Thus, for example, the power (pulsed and average) of a radio transmitter or the sensitivity of a radio receiver are specified.

One of the tasks of design is to optimize the power characteristics of the antenna being developed, taking into account the existing possibilities and specific set requirements. Optimization reduces to bringing the feasibly attainable characteristics close to the ultimately attainable theoretical characteristics, found for the specified optimality criteria. For example, such criteria can be the maximum gain or minimum noise temperature for the specified relative dimensions and losses in the microwave components being used.

The frequency properties of antennas are characterized by the greatest change in the frequency of the transmitted (received) signal for which the major parameters of the antenna do not go beyond the permissible limits. Depending on the requirements placed on the radio system in which the antenna being designed will be used, the frequency properties are determined with respect to the change in the directionality or the power characteristics. When calculating the frequency properties of the antennas treated in this book, it is expedient to draw a distinction between the requirements placed on the working bandwidth of the antenna and the bandwidth of the transmitted signals. The requisite passband is determined by the condition of the simultaneous transmission or reception by the antenna of a signal with a specified frequency spectrum. The range of frequencies is determined by the condition of antenna operation sequentially in time at different frequencies in the working band, i.e., permits a synchronous change in certain antenna parameters with a change in the working frequency of the radio system. For example, in an electrically scanned antenna array, the phase distribution along the array is varied so as to preserve the direction of the beam in space when the working frequency of the transmitter changes.

In antennas and feedlines, a number of requirements are placed on the spatial scanning characteristics (such as the scanning sector and time, etc.) as well as requirements governing the change in the directional properties during the process of operating and switching the antenna from transmit to receive. These requirements also determine the requisite control characteristics for the antenna and feedline. The starting data with the choice of electromechanical or electrical scanning for the performance of the design calculations for the selected type of antenna are the spatial scanning sector of the beam, the scanning period (pace) or time needed to set the beam to a specified point in space, method of spatial scanning, precision of setting the beam to a specified point in space, etc. The antenna switching time from transmit to receive is also to be included among the control characteristics, as well as the requirements which arise in a number of cases concerning the change during the operational process in the polarization of the transmitted field or the shape of the directional pattern. In mechanically scanned antennas, the beam control characteristics are not related to the electrical design of the antenna and are determined during the design of the rotation mechanisms.

The angular coordinates of objects and the precision in the measurement of these coordinates are determined by means of the direction finding characteristics used in radar, radio direction finding, radio astronomy, etc. The requirements placed on direction finding characteristics depend substantially on the direction finding technique employed (monopulse, radio signal, amplitude, phase DF'ing, etc.).

Antenna using a monopulse direction finding method (monopulse antennas) have become widespread in radar of late, the direction finding characteristics of which are the slope and linearity of the characteristic, the depth of the "null" in the difference pattern and the precision of its setting in a specified direction. The requirements placed on these characteristics, with the exception of the latter, reduce to the creation of a special shape and symmetry in the directional patterns, as well as to obtaining the maximum reception antenna gain. The requisite precision in setting the "null" of the difference pattern in a specified direction, within the bounds of a scanning sector, is governed by the scanning technique and the characteristics of the devices which control the antenna beam position. The realization of the requisite direction finding characteristics is a most important and difficult task for many antennas.

Overall engineering, operational and economic requirements are placed on an antenna, just as on any radio engineering unit, such as: minimal size, weight and cost, high reliability, adaptibility to specified conditions, as well as control and repair convenience. Setting these requirements on an antenna being developed is no less important than setting the electrical requirements, and meeting them is achieved not only through the appropriate structural design solutions, fabrication technology and the use of the requisite materials, but also through the selection of the appropriate scanning method, electrical circuit configuration, operational mode for the system as well as the active elements and microwave devices which are employed.

With the development of various radio engineering systems and the increased complexity of the design and engineering problems solved by them, the requirements placed on the antenna characteristics are also increasing, and in a number of cases, they become contradictory and altogether insoluble when attempting to develop new antennas on analogy with those previously existing and presently in operation. For example, the striving to increase the range and precision of the determination of angular coordinates in radar leads to the requirement of increasing the antennas directionality, which causes an increase in their size and weight. The increase in the flight velocity of aircraft leads to the necessity of increasing the rate of beam motion in space. It is not possible to combine the requirements of increasing the directionality and the rate of beam travel in mechanically scanned antennas because of the inertia in their structure. Similar contradictions also arise during attempts to simultaneously provide for high directionality and the requisite frequency, power and direction finding characteristics. These circumstances force one to dispense with the traditional type of antennas for the given class of radio systems and to change over to antenna arrays.

The use of complex antennas in the form of arrays, consisting of systems of poorly directional or directional radiators, significantly expands the possibilities for realizing the requisite characteristics.

A system of radiators with an electrically controlled phase distribution - a phased antenna array - accomplishes the electrical scanning of the beam in space at a rate which can be several orders of magnitude greater than the speed of mechanical scanning antennas. The setting time to a specified point in space for the beam of a phased array is practically determined by the speed of the electrical phase shifter or the frequency tuning or frequency scanning time, and is not related to the weight or the dimensions of the antenna. With this "inertialless" scanning, new, previously not used methods of spatial scanning and multitarget operation are possible (the simultaneous tracking of several targets in space).

Arrays made of narrow beam antennas make it possible to increase the ultimately realizable resolution, gain and maximum transmitted power. Arrays have been designed and are being designed using large reflectors for the antennas of radio telescopes for space communications, having a resolution of down to minutes of an angle in the centimeter band [0.3]. The arrays make it possible to create multiple function antennas, in which the shape and width of the directional pattern are changed by means of electrically controlled microwave devices, depending on the functions being performed by the radio system.

The realization of different kinds of amplitude-phase distributions is significantly simpler in an antenna array than in reflector, horn, lens and other microwave antennas, since directional couplers, phase shifters, switchers and other components can be inserted in the exciting radiators of the device (power dividers of the antenna array), where these components provide for the requisite distribution or control. Various kinds of amplitude-phase distributions make it possible to realize so-called optimal directional patterns in practice (with minimal sidelobe radiation), as well as directional patterns having deep troughs ("nulls") in the direction of interference near a target outside the main lobe of the antenna.

In terms of the structural design, the use of antenna arrays makes it possible to reduce the longitudinal dimensions (in the direction of the normal to the plane of the array) of pencil-beam antennas, and consequently, the volumes occupied by them, and to use the exterior conducting surface of an object for radiating. A highly directional antenna array made of horns or reflectors has a smaller longitudinal dimension than one horn or reflector antenna with the same directivity. An array of slotted radiators on the convex (conical, cylindrical, spherical, etc.) exterior surface of an aircraft [05], without increasing the aerodynamic resistance, makes it possible to substantially reduce the occupied volume as compared to the corresponding aperture antenna placed in a fairing. Radio specialists have recently been devoting considerable attention to so-called active phased antenna arrays, in which a self-excited oscillator, amplifier, converter, mixer, etc. are connected to each radiator or a group of them. This new approach to the design of the entire radio system, where it is impossible to single out such individual devices as a receiver, transmitter, etc., permits a substantial expansion of system capabilities when processing the incoming information, as well as the construction of adaptive (self-tuning) antennas and achieving better interfacing of the radio system to a computer.

From everything that has been presented here, the role of antenna arrays in modern radio engineering systems, their possibilities in providing for the requisite antenna characteristics as well as for the entire radio system becomes understandable. For this reason, the design principles and methods of calculating the major parameters of prospective phased and active phased antenna arrays with various radiators, geometries and control techniques are set forth in this book.

1.3. Antennas with Electrical Scanning

We shall deal with the specific features of the construction and design of antenna arrays with electrical scanning, which must be taken into account during the planning. It should be noted that up to the present time, no final terminology has been worked out in the field of antenna arrays with electrical scanning, and conclusive engineering techniques for their design are also still lacking. We shall employ borrowed terms and definitions, as well as the most widely disseminated terminology, corresponding to the physics of the processes which take place.

Electrically scanned antennas can be treated in the general case as arrays with a controlled phase or amplitude-phase distribution. Various types of radiators and channelizing systems are used in such antenna arrays, as well as diverse ways of exciting the radiators and controlling the amplitude-phase distribution during scanning. Antenna arrays in this case have the most diverse structural design. However, the directional properties of antenna arrays, when they are correctly designed, can be determined just as for highly directional antennas with a continuous radiating aperture, in which the directional properties depend on the relative dimensions of the aperture (with respect to the wavelength) and the field distribution in it. In linear and planar arrays, the equivalent radiating aperture changes during scanning, i.e., the projection of the aperture onto a plane normal to the direction of the beam, and consequently, the directional properties also change. The changes in the beam width of the array during scanning should be taken into account in the electrical design of the antenna. Graphs which illustrate the change in the directional pattern width, $2\theta_{0.5}$, are shown in Figure 1.1 as a function of the relative antenna size L/λ and the direction of the beam in space, θ.

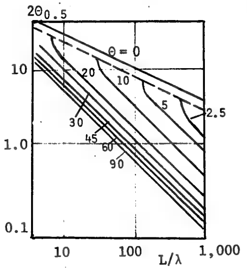

Figure 1.1. Beam width as a function of array length and scanning angle for the case of uniform excitation.

Linear, planar or axially symmetric arrays (annular, conical, cylindrical, spherical), as well as arrays with a more complex shape (surface antenna arrays) find application in practice. Arrays can be both equidistant (with a constant spacing between the radiators) and non-equidistant types. The directional pattern width of each radiator, the number of them and their arrangement in the array are governed by the requirements placed on the directivity of the antenna, the spatial scanning sector and the conditions for the placement and operation of the antenna.

Cylindrical antenna arrays and phased arrays with a hemispherical scan space are also treated in the book. Such arrays can be constructed in the form of convex polyhedra made of planar arrays and arrays which have been given the name "conformal" in foreign literature.

Assuring the specified requirements for an array with electrical scanning during the design work can be achieved with the use of different types of radiators, different spacings between them, array configurations, etc. One of the main tasks of the design work is to find the optimum array variant for the specified requirements, taking into account the existing possibilities for the excitation, placement, fabrication and operating conditions.

The radiators, the number of which in an antenna can reach tens of thousands can be excited by means of waveguides, coaxial lines and striplines as well as other types of channelizing systems using parallel, series, branched and other feed configurations. A spatial excitation technique is also possible which is similar to the method of exciting lenses and reflectors in which one (the primary) irradiator excites all of the radiators of the array simultaneously. The selection of the excitation configuration during the design work is determined by the method of scanning, the permissible losses in the antenna as well as the size and weight.

Beam scanning in a frequency scanning antenna* is achieved by changing the oscillator frequency (in the transmitting antenna) and the receiver (in the receiving antenna). The electrical spacing between the radiators, excited by the channelizing traveling wave systems changes with the change in frequency, and consequently, the phase distribution in the array also changes. The determination of the characteristics of these channelizing systems reduces, primarily, to the design of frequency scanning antennas. Frequency scanning antenna arrays prove to be significantly simpler in their structure than other antenna arrays with electrical scanning, since there are no other elements in them besides the channelizing and radiating devices. The presence of a microwave receiver and generator with a fast response, for example, with electrical frequency tuning is a necessary condition for the design of electrically scanning radio systems. However, the realization of frequency scanning in the case of wide angle and two-dimensional scanning encounters considerable difficulties. Moreover, the use of frequency scanning is not possible in all radio systems.

In the case of a constant working frequency for a radio system, the phase distribution in an antenna with electrical scanning can be controlled by means of phase shifters. This technique has been given the name of phase beam scanning of an antenna array. Ferrite, semiconductor, ferroelectric and other phase shifters have been developed at the present time, in which the phase of the outgoing electromagnetic wave changes either discretely or continuously from 0 to 360° as a function of the control voltage or current. The incorporation of a system of phase shifters in the device exciting the antenna (the power divider) makes it possible to realize electrical scanning, where the phase distribution control is discrete in the majority of cases. This occurs because of the discrete change in the phase shift in a phase shifter or the control current (or voltage), which in turn is due to the specific nature of the operation of the electronic device controlling the beam position. Such an electrical scanning technique, which has been termed switched scanning (or digitally switched scanning in previously published literature), is the most promising at the present time. With the switching technique, as a result of the discrete change in the phase, the directional properties of the phased antenna array also change. These changes should be taken into account when designing switched antennas.

---

*Questions of frequency scanning antenna theory and design were treated most completely for the first time by L.N. Deryugin [010].

The phase distribution of a scanning antenna array can also be controllod by means of mechanical phase shifters, in which the phase change is accomplished by means of mechanically moving or rotating special individual components or parts of the channelizing system of the phase shifter [03]. With such a scanning technique, which is termed electromechanical, the maximum rate of beam travel is governed by the speed of the phase shifter, and because of the low inertia of the devices being moved, can be significantly greater than in mechanically scanned antennas. The calculation of the directional characteristics of antenna arrays with electromechanical scanning is the same as for electrically scanned arrays.

The choice of one scanning technique or the other during antenna design is determined not only by the requisite characteristics, but also by the existing possibilities, the presence of the appropriate electronic devices, the characteristics of the phase shifters and channelizing systems, power considerations, etc.

The transition from mechanical scanning to electrical led to increased complexity in antenna structural design, which was due to the use, for example, of an array of radiators with phase shifters instead of one dish antenna, as well as to a sharp increase in the cost of the antenna unit. The use of phase shifters, channelizing systems and other supplemental devices increases the phase errors and thermal losses in an antenna and reduces the gain. For this reason, it is expedient to change over to electrically scanned antenna arrays only in those cases where the mechanical approach does not assure the requisite beam control characteristics and a certain degradation of the power characteristics and increase in the cost are permissible.

1.4. Specific Features of Phased Antenna Array Design

The further development of microwave antennas led to the working out of new and increased complexity of known methods of computing the main characteristics. The structural and computational design work on the antennas became significantly more complicated because of the increase in the number of parameters governing antenna characteristics, as well as by the striving to optimize the characteristics or compute them more precisely.

The design of scanning antennas with specified characteristics is accomplished with the condition that these characteristics are assured for all antenna beam positions. For this reason, the calculation of the directional, frequency and other properties of arrays must be made for various beam positions in the spatial scanning sector. In this case, the beam width, sidelobe level, directional gain and other characteristics are determined not only by the array parameters, but also by the characteristics of the devices which control the phase distribution (the discrete step for the phase change in a phase shifter, the deviation of the dispersion characteristics of the channelizing systems from the requisite values, etc.).

Complex interaction phenomena occur between the radiators in antenna arrays, which are manifest in a change in the directivity and input impedance of a radiator when it is inserted in the array. As a result, the directional properties and power characteristics of an antenna can change substantially in an array as compared to the characteristics found without taking the interaction into account.

Intense developmental work is under way at the present time on the theory of accounting for interaction in microwave antenna arrays. Engineering methods of calculating the interaction are known only for certain types of radiators and a definite arrangement of them. Taking this interaction into account, which changes when controlling the phase distribution, makes the design of phased microwave arrays considerably more difficult.

The interaction of the radiators in a phased antenna array depends on the type of radiators used, their configuration and affects the antenna characteristics in different ways. Thus, the interaction of resonant poorly directional radiators (resonant dipoles, resonant slot antennas) in an array leads to a substantial change in the input impedance and the resonance properties, so that during scanning, the input impedance of each radiator in the system and the matching of the driving channel depend on the beam direction in space. The change in the distribution of the radiating current (field) and correspondingly, the directional pattern of a radiator, is insignificant in this case.

The interaction of radiators in different types of antenna arrays (for example, of the traveling wave--dielectric rod type, helical antennas, yagi channels or aperture-waveguide antennas, horns) is manifest in a change in the current distribution in the radiator and a corresponding change in the directional pattern of an element. A change in the directional pattern of a radiating element in an array is manifest in a substantial change in its width and in the appearance of deep nulls (indented pattern), something which leads to a significant drop in antenna gain for certain beam positions in space and to the corresponding mismatching of the exciting channel. The mutual influence effect of radiators can be eliminated by means of the appropriate placement of the radiators, a choice of their type and size as well as the use of dielectric coatings and other special measures. For this reason, the design of the radiating elements of arrays is treated in this book along with the general questions of phased array design.

Finding the optimal variant of a scanning antenna for given requirements, taking into account the characteristics of the radiators, phase shifters, channelizing systems and other microwave devices available to the designer, considerably increases the volume of all of the calculations to be performed during the design work.

Individual sections on the theory of microwave antenna arrays and electrical scanning, which have been published in the literature, are intended primarily for specialists in antenna arrays. The study and utilization of this literature in the designs of antennas for various functions require large expenditures of time, which creates difficulties during engineering design work. For this reason, some engineering techniques of designing scanning microwave arrays and their elements are presented in the book, which make it easier for specialists familiar only with the general theory and practice of the application of antenna devices to determine the major characteristics. This has brought about the necessity of introducing a number of approximations and simplifications, something which has influenced the precision in calculating the characteristics and led to a limitation of their range of applicability.

Various methods exist for designing the antennas considered here, which differ in the precision of the results obtained and the degree of complexity of the calculations. The antenna characteristics found by means of the cited engineering procedures can be made more precise by means of more rigorous computational techniques known from the literature (see the bibliographies for the relevant chapters).

Along with the simplified design methods, where it has been possible, more rigorous computational methods are included using computers, which make it possible to optimize the device being developed with respect to one criteria or another by means of the programs which have been worked out.

The design of phased antenna arrays involves the solution of exterior and interior electrodynamic problems from antenna theory. When using approximate analysis methods, the independent solution of the exterior and interior problems can be permitted. The solution of these problems, taking their mutual relationship into account, makes it possible to calculate antenna characteristics and search for the optimum variant of an antenna which best conforms to the set requirements. Such an approach made it possible to create independent methods for the engineering design of electrically scanned antenna arrays, arrays of radiators and their elements.

1.5. Specific Features of Active Array Design

The application of stripline and microstripline hardware makes it possible to a significant extent to reduce the cost, improve the reliability and decrease the size and weight of antenna equipment. Stripline and microstripline devices can be used as channelizing systems, power dividers and directional couplers, filters and circulators, isolators and phase shifters, etc. Such advantages of printed circuit technology as repeatability of the parameters during series production and the capability of integration have made it possible to also use these devices in the structural design of microwave antenna, first in the decimeter and meter bands, and then also in the centimeter band. The yagi (director antenna), microstripline radiators, arrays of dipole radiators, compact resonator slot antennas, etc. can be numbered among them. However, a substantial drawback to stripline devices is the significant losses in the centimeter band and especially in the short wave portion of this band. The insertion of an active element in the microwave channel makes it possible to not only reduce the losses, but to also increase the radiated power, simplify the microwave distribution system and ease the electrical requirements placed on it, as well as to miniaturize the entire antenna system. The insertion of an active element (or device) in a radiator or in its excitation channel transforms the antenna array from a passive reciprocal [sic] device into an active antenna array, and a phased array into an active phased antenna array, in which different active elements are used during reception and transmission. In practice, antenna arrays are broken down into receiving, transmitting and transceiving, depending on the function. The radiator, active elements, phase shifter, lines connecting these microwave elements, etc. are structurally combined into a single device, which has been given the name of an active phased antenna array module.

The most diverse circuit configurations are known at the present time for receiving and transmitting modules. For example, in some circuits, the active element is coupled to each radiator, while in others, it is coupled to a group of radiators. There is a lack of unified terminology to an even greater extent for phased antenna arrays for active arrays.

The designing of the transceiving module of an active phased array with the theoretic and component bases existing at the present time is actually broken down into the solution of two independent problems: the development of the transmitting module and the development of the receiving module. As is well known, modern microelectronics has achieved significant successes; various integrated circuits have been created which are widely used in radio receivers. At the same time, there is a lack of series produced high power microwave integrated circuits for radio transmitting devices. This circumstance has also led to the necessity of a more detailed treatment of the questions of the design of active transmitting modules in this book.

When developing an active phased antenna array module, a solution which provides for minimum antenna cost while assuring all of the requisite characteristics is preferable. As studies show, the cost of the power generated in a circuit, where each radiator is coupled to an individual active element, is higher, however, this is compensated by the less expensive and lower power generators and phase shifters, and the possibility of using more convenient power supplies as well as facilitating the cooling of the elements of an array.

When designing an active transmitting module, one can use either a self-excited oscillator or an externally excited generator (power amplifier), or a string of series connected stages, among which there can be frequency multipliers. Because of frequency multiplication, the distribution system operates at a frequency lower than the output frequency, and as a rule, at a lower power level, which makes it possible to substantially reduce the losses in the system.

The major requirements placed on the active elements of modules are assuring the specified output microwave power, relatively high values of the efficiency (no less than 20 to 40%) and power gain (more than 10 dB), operating mode stability, comparatively wide passband (more than 5%), a small scatter in the parameters of the individual models, operational stability in a wide range of temperature variation, low levels of generator noise, filtering of spurious signals and those outside the passband, as well as a number of structural design (small size and weight) and economic requirements.

Semiconductor microwave devices such as bipolar power microwave transistors, multiplier diodes (varactors and charge storage diodes) as well as microwave diodes (IMPATT diodes and charge transfer diodes) have been finding increasingly wider applications in active modules in recent years.

High power microwave transistors are the most sophisticated semiconductor devices in the microwave band; they have working frequencies which as yet do not exceed 5 to 7 GHz. For this reason, when developing active phased array modules for a working frequency in the 3 centimeter band using these transistors, it is necessary to provide a frequency multiplier, something which leads to the use of an amplifier and multiplier chain in the module. Diodes with a nonlinear p-n junction capacitance are used as the nonlinear element in the multiplier, where these diodes are distinguished by a high input to output signal power conversion gain, small dimensions and weight and which practically require no power from the power supply.

Microwave amplifiers designed around avalanche transit time diodes have a higher output power (by an order of magnitude) and a greater efficiency (up to 5 to 15%) than charge transfer diodes.

Active modules can also be designed around self-excited microwave device oscillators (transistor or diodes) using a system of synchronization from a special frequency source.

The design of the radiating system of an active phased antenna array is closely tied to the development of active modules which assure the requisite characteristics of the antenna array. For this reason, when planning an active phased array, it is necessary to select the circuit configuration of the active modules, compute the operational modes of the generator stages and the microwave networks matching them as well as execute the structural design of the generator circuit components in the form of a hybrid integrated circuit. It should be noted that calculations of semiconductor microwave generators are made at the present time using approximate methods, since the devices themselves are complex nonlinear microwave devices. However, these techniques make it possible to estimate the major power and structural design characteristics of the stages with a precision adequate for practice and to design the radiating system of an active phased antenna array based on them.

The power engineering characteristics (output power, working frequency, efficiency, gain, etc.) of microwave semiconductor devices are treated in the book for the purpose of using them in the active modules of active phased arrays and attention is drawn to the possibility of the appearance of thermal limitations with certain structural design requirements related to the realization of beam scanning in the array. Design procedures are given for the operating conditions of high power microwave transistor oscillators and their matching networks, as well as frequency multipliers using varactors and charge storage diodes, which make it possible to design an active module using an amplifier and multiplier chain.

Special attention is devoted to the design of microwave oscillators and amplifiers around avalanche transit time diodes, which meet many of the major requirements placed on the active elements of active phased array modules in the 3 cm band. Reference materials are also given for the structural design of the components of microwave networks.

2. PHASED ANTENNA ARRAYS

2.1. The Determination of the Geometric Characteristics of Phased Antenna Arrays

Some of the most widespread types of phased antenna arrays are linear and planar arrays. The majority of planar phased arrays consist of identical radiators, positioned at the nodes of a plane coordinate grid with twofold periodicity. The most useful grids are rectangular and triangular (or hexagonal) (Figure 2.1).

It is assumed in an elementary analysis that the directional pattern of a radiator in an array does not differ from the directional pattern of an isolated radiator.

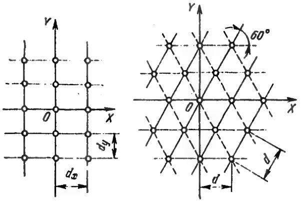

Figure 2.1. Methods of radiator layout.

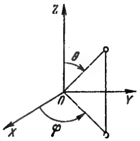

Figure 2.2. Systems of coordinates

The excitation phase for the radiators in an array in the case of narrow beam radiation provides for the in-phase addition of the fields in a specified direction and depends on the position of the radiator in the array:

$$\Phi_{nq}(\theta_{\text{гл}}, \varphi_{\text{гл}}) = -k(X_{nq}\cos\varphi_{\text{гл}} + Y_{nq}\sin\varphi_{\text{гл}})\sin\theta_{\text{гл}}, \tag{2.1}$$

where $k = 2\pi/\gamma$ is the wave number; X_{nq} and Y_{nq} are the coordinates of the radiators in the array; $\theta_{\Gamma Л}$ and $\phi_{\Gamma Л}$ are the angles in a spherical system of coordinates which determine the direction of the main lobe (beam) in space (Figure 2.2).

The directivity function of an array $f(\theta, \phi)$ can be represented in the form of the product of the directivity function of an isolated radiator $F(\theta, \phi)$ times an array factor $F_\Sigma(\theta, \phi)$, which can be treated as the directivity function of an array consisting of isotropic radiators:

$$f(\theta, \varphi) = F(\theta, \varphi)\, F_\Sigma(\theta; \varphi), \tag{2.2}$$

where

$$F_\Sigma(\theta, \varphi) = \sum_{m, n=1}^{M, N} A_{mn}\, e^{i(\Phi_{mn} + \Phi''_{mn})}.$$

In the cited expressions, A_{mn} is the amplitude of the excitation for an array element; $\Phi''_{mn} = k(X_{mn}\cos\varphi + Y_{mn}\sin\varphi)$; ; $\sin\theta$ is the spatial phase shift for the observation direction θ, ϕ.

When the radiators are placed at the nodal points of a coordinate grid with two-fold periodicity, the in-phase addition of the fields of the individual array radiators is possible not only in the direction of the main lobe of the directional pattern, but also in other directions which correspond to the spatial phase shift, which compensates for the phase shift between the radiators due to the excitation. Then, in addition to the main lobe of the array, there also exist diffraction maxima of higher orders. The spatial orientation of the diffraction maxima depends on the spacing between the radiators. With a reduction in the spacing between them, the number of diffraction maxima located in the region of the real nodes, is reduced. It is essential for normal operation of the array that only one main lobe of the array be located in the region of the real nodal points, while there be no diffraction maxima.

When using a rectangular grid, there are no higher order diffraction maxima if the spacing between the radiators in the direction of the coordinate axes satisfies the following conditions:

$$d_x/\lambda \leqslant 1/(\sin\theta_{x\,\max}+1);\ d_y \leqslant 1/(\sin\theta_{y\,\max}+1), \qquad (2.3)$$

where λ is the wavelength; $\theta_{x\,\max}$ and $\theta_{y\,\max}$ are the maximum beam deflection angles in the ZOX and ZOY planes (Figure 2.2).

For a triangular grid, the corresponding condition has the form:

$$\frac{d}{\lambda} \leqslant \frac{2}{\sqrt{3}}\,\frac{1}{1+\sin\theta_{\max}}, \qquad (2.4)$$

where $\theta_{\max}$ is the maximum deflection of the beam from the normal to the array. For example, if $\theta_{\max} = 45°$, then we obtain for rectangular and triangular grids $d_x = d_y = 0.58\ \lambda$ and $d = 0.68\ \lambda$ respectively.

Thus, the use of a triangular grid makes it possible to increase the spacing between the radiators and to reduce the overall number of them. It follows from expressions (2.3) and (3.4) that this reduction amounts to approximately 13% of the number of elements in an array with a rectangular grid.

Conditions (2.3) and (2.4) do not take into account the directional properties of the radiators of an array and determine the ultimate spacings in an array of isotropic radiators. In the case of a limited scanning sector, the use of directional radiators makes it possible to increase the spacing between them as compared to the values determined by (2.3) and (2.4), and to correspondingly reduce the overall number of them.

In fact, if the directional pattern of one radiator of an array is zero or close to it outside the scanning sector (Figure 2.3), then one can allow the existence of higher order diffraction maxima in the region of the real nodal points, increasing the spacing between the radiators as compared to (2.3) and (2.4), and requiring in this case that during all movements of the beam, the diffraction maxima do not fall in the scanning sector. Since the directional pattern of an array is obtained by multiplying the directivity function of a radiator and the array factor, the diffraction maxima are suppressed, since they will be multiplied by small or zero values of the radiator directivity function.

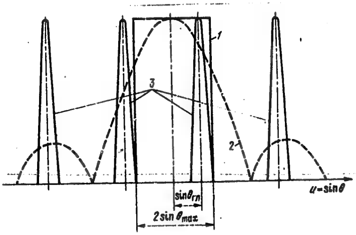

Figure 2.3. Directional patterns of an ideal (1) and a real (2) radiator, and the lobes of the array multiplying factor (3).

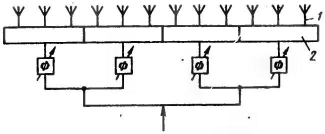

Figure 2.4. A phased antenna array with nonscanning "subarrays".

Key:
1. Subarray radiators;
2. The subarrays.

The advantage gained in the number of radiators as compared to an array of isotropic elements for triangular and rectangular grids is defined by the following expressions:

$$\frac{N_{\text{изотр}}}{N}=\frac{\sqrt{3}}{2\pi}\,\frac{(1+\sin\theta_{max})^2}{\sin^2\theta_{max}};\qquad \frac{N_{\text{изотр}}}{N}=\frac{(1+\sin\theta_{max})^2}{4\sin^2\theta_{max}}. \tag{2.5}$$

[$N_{\text{изотр}} = N_{\text{isotropic}}$]. For example, when $\theta_{max} = 40°$, the number of radiators is reduced by 45% and 39% respectively.

However, the design of a directional radiator, the directivity function of which would fall off rapidly to small values outside the bounds of the scanning sector is a complex problem. The directivity functions of actual radiators differ from the ideal. For this reason, the number of radiators in real scanning arrays is greater than the minimum possible. If the width of the directional pattern of a phased array does not exceed 1°, while the scanning sector in both of the main planes is less than 10°, then the requisite directivity can be obtained by combining conventional poorly directional radiating elements into groups (Figure 2.4). Such groups of radiators will be called subarrays in the following. The radiators of each subarray are excited in phase and produce a directional pattern, the maximum of which is oriented in the direction of the normal to the plane of the array. During scanning, the excitation phases of each of the subarrays, which can be treated as individual antenna radiators, are changed by means of phase shifters. The relative dimensions of the subarrays are chosen in accordance with the specified scanning sector and the permissible level of the higher order diffraction maxima. Since the shape of a subarray directional pattern differs from a rectangular one, when determining the dimensions of subarrays it is necessary to take into account the permissible level of the higher order diffraction maxima, which now fall within the bounds of the main lobe of the directional pattern of the subarrays during scanning (Figure 2.3). Design formulas have the form:

$$L'_{x,y}/\lambda = \alpha/(1+\alpha)\sin\theta_{x,y\,\max}, \tag{2.6}$$

where α is the permissible level of the diffraction maxima relative to the main maximum of the directivity characteristic; $L'_{x,y}$ are the dimensions of the subarray along the X and Y axes respectively (Figure 2.5). The number of lines and columns formed by the subarrays is determined by the expressions:

$$N_{x,y} = \frac{L_{x,y}}{\lambda}\,\frac{1+\alpha}{\alpha}\sin\theta_{xy\,\max}, \tag{2.7}$$

where $L_{x,y}$ are the dimensions of the array aperture along the X and Y axes respectively. The product $N = N_x N_y$ is equal to the number of phase shifters in the array.

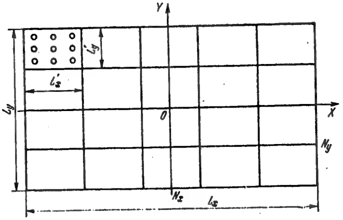

Figure 2.5. The geometry of a plane antenna array with nonscanning subarrays.

If the subarrays are replaced by aperture radiators (for example, horn antennas), then when determining the quantities N_x and N_y, it is necessary to multiply one of them, corresponding to the H-plane of the horn antenna by a factor of 1.5, since the field distribution in this plane falls off towards the edges of the aperture, which leads to a widening of the directional pattern of the horn antenna.

The antenna dimensions are determined by the specified directional gain or width of the directional pattern, the wavelength and the selected amplitude distribution of the field in the antenna aperture. (The choice of the amplitude distribution in the antenna depends on the requisite level of the sidelobes.)

TABLE 2.1.

Таблица 2.1

(1) Закон изменения амплитуды поля (синфазный раскрыв) $A(x)$	(2) Формулы для ДН без учета направленных свойств элементарной площадки $F(u)$		(3) Ширина ДН на уровне половинной мощности $2\theta^{\circ}_{0,5}$	(4) Положение первого нуля θ°_{0}	(5) Уровень первого бокового лепестка, дБ	(6) Коэффициент использования площади раскрыва ν
$A(x)=1$	$\frac{\sin u}{u}$		$50{,}8\frac{\lambda}{L}$	$57{,}3\frac{\lambda}{L}$	—13,2	1,0
$1-(1-\Delta)X^2$	$\frac{\sin u}{u}+$ $+(1-\Delta)\frac{d^2}{du^2}\left(\frac{\sin u}{u}\right)$	$\Delta=0{,}8$	$52{,}7\frac{\lambda}{L}$	$60{,}7\frac{\lambda}{L}$	—15,8	0,994
		$\Delta=0{,}5$	$55{,}6\frac{\lambda}{L}$	$65{,}3\frac{\lambda}{L}$	—17,1	0,970
		$\Delta=0$	$65{,}9\frac{\lambda}{L}$	$81{,}9\frac{\lambda}{L}$	—20,6	0,833
$1-\lvert X\rvert$	$\frac{\sin^2 u/2}{(u/2)^2}$		$73{,}4\frac{\lambda}{L}$	$114{,}6\frac{\lambda}{L}$	—26,4	0,750
$\cos^n\left(\frac{\pi-X}{2}\right)$	n — четное even $\sin u$	$n=1$	$68{,}8\frac{\lambda}{L}$	$85{,}9\frac{\lambda}{L}$	—23	0,810
	$u\prod_{k=1}^{n/2}\left[(2k)^2-\frac{4u^2}{\pi^2}\right]$ n — нечетное odd $\cos u$	$n=2$	$83{,}2\frac{\lambda}{L}$	$114{,}6\frac{\lambda}{L}$	—32	0,667
		$n=3$	$95{,}1\frac{\lambda}{L}$	$143{,}2\frac{\lambda}{L}$	—40	0,575
	$\prod_{k=1}^{\frac{n-1}{2}}\left[(2\kappa-1)^2-\frac{4u^2}{\pi^2}\right]$	$n=4$	$110{,}6\frac{\lambda}{L}$	$171{,}9\frac{\lambda}{L}$	—48	0,515

Key:
1. Law governing the change in the amplitude of the field (in-phase aperture), A(x);
2. Formulas for the directional pattern without taking the directional properties of an elementary area into account, F(u);
3. Directional pattern width at the half power level, $2\theta^{\circ}_{0.5}$;
4. Position of the first null, θ°_{0};
5. Level of the first sidelobe, dB;
6. Aperture area utilization factor, ν.

Some of the radiation characteristics of a rectangular aperture are given in Table 2.1 for various field distributions in the aperture. The data of the table are justified for antennas with a continuous distribution of radiators. However, with a small spacing between the radiators, they are also justified for antenna arrays. As can be seen from the table, the level of the first sidelobe and the nature of the decay in the level of the remaining lobes depend on the specific features of the field amplitude distribution at the edge of the aperture. In the case of a uniform distribution, which has a break at the edge of the aperture, the level of the first sidelobe is -13.2 dB, while the level of the remaining lobes falls off in proportion to 1/u, where u = (kL/2) sinθ.

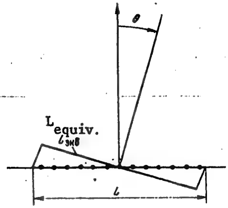

Figure 2.6. The equivalent length of an antenna array.

In the case of triangular and cosine distributions, continuous at the edge of the aperture, but the first derivative of which has a break, the level of the first sidelobe is -26.4 dB and -23 dB respectively, while the level of the remaining lobes falls off proportionally to $1/u^2$. With a cosine-squared distribution, continuous at the edge of the aperture along with the first derivative, the level of the first sidelobe is -32 dB, while the level of the remaining lobes falls off as $1/u^3$.

The data cited in Table 2.1 correspond to the antenna beam orientation in the direction of the normal to the line of position of the radiators in the case of a linear array or to the plane of the aperture in the case of a plane two dimensional array.

To calculate the width of the directional pattern of a linear array with a deviation of the beam from the normal, the concept of equivalent array length is introduced (Figure 2.6):

$$L_{\text{equiv.}} = Nd\cos\theta_{\text{main}} \qquad L_{\text{экв}} = Nd\cos\theta_{\text{гл}}. \qquad (2.8)$$

With an increase in the deviation angle, the equivalent length falls off, while the width of the directional pattern increases in accordance with the formulas of Table 2.1.

In a two-dimensional planar array, with a deviation of the main lobe from the direction of the normal to the aperture in any plane, one can assume that the directional pattern also changes only in this plane; this assertion becomes more precise, the greater the dimensions of the array. For arrays, the length of which is greater than 10 λ, this is well justified.

With a deviation in the main lobe from the normal to the plane of a rectangular array in the main XOZ and YOZ planes, the concept of an equivalent size and equivalent array area can also be introduced to determine the directional pattern width and directional gain:

$$\begin{aligned} L_{x\ \text{equiv}} = L_{x\ \text{экв}} &= N_x\, d_x \cos\theta_{\text{гл}} \ (\text{плоскость } XOZ), \ (\text{XOZ Plane}),\\ L_{y\ \text{экв}} &= N_y d_y \cos\theta_{\text{гл}} \ (\text{плоскость } YOZ);\\ S_{\text{экв}} &= N_x\, N_y\, d_x\, d_y \cos\theta_{\text{гл}}. \end{aligned} \qquad (2.9)$$

where N_x and N_y are the number of rows and columns formed by the radiators of the array, parallel to the X and U axes of the rectangular system of coordinates respectively.

It is not difficult to note that the equivalent values are equal to the projections of the actual geometric characteristics on to a plane perpendicular to the direction of the main lobe. The directional pattern width in the main planes can be found from the formulas of Table 2.1 when the corresponding equivalent dimensions are substituted in them.

To estimate the change in the directional gain of a planar array with a deflection of the directional pattern maxima from the normal to the plane of the array through an angle θ_{main}, one can employ the relationship:

$$D(\theta_{main}) = D_0 \cos\theta_{main} \tag{2.10}$$

where D_0 is the value of the directional gain in the direction of a perpendicular to the plane of the array. Formulas (2.8) - (2.10) are approximate, and their precision is better, the smaller the beam width, i.e., the greater the relative dimensions of the array.

The directional gain of a planar array with the beam oriented in the direction of a normal to its plane can be computed from the following formula:

$$D_0 = 4\pi S\nu/\lambda^2, \tag{2.11}$$

where ν is the aperture area utilization factor and its value is determined by the amplitude distribution; S is the aperture area.

2.2. Mutual Coupling Effects Among Radiators

Numerous theoretical and experimental studies have shown that it is impossible to neglect the mutual influence of array radiators. In accordance with [08], the interaction between radiating elements in an array is manifest as follows:

--The input impedance of the radiating element in an antenna array differs from its impedance in free space and is a function of the scanning angle;

--The directional pattern of the element changes;

--The polarization characteristics are distorted.

In a number of cases, the interaction of the elements in an array leads to a sharp mismatch between the antenna aperture and the feed circuits. Large antenna arrays at such scanning angles become blinded.

One of the most important characteristics of an antenna array is the directional pattern of a single radiator with all of the other radiators loaded into matched loads. In other words, this is the directional pattern of the array when only one radiator in all is excited in it, while all of the others are connected to loads which can be either the output impedances of the generators or the input impedances of the receivers in the case of active arrays, or loads which match the characteristic impedances of the supply feeders. When one radiating element is excited, because of the mutual coupling there is excitation of the adjacent radiators and the directional pattern of this element in the array is produced as a result of the superimposition of the fields of adjacent elements on the field of the excited radiator. In this case, waves are excited in the feeders of adjacent elements loaded into passive loads and a portion of the energy is absorbed in the loads.

For an antenna array of finite dimensions, the radiation resistance and directional pattern of a single radiator depend on its position, since the cross coupling is manifest in different ways for radiating elements located at different points in the array. Consequently, the principle of multiplication of the directivity characteristics can prove to be unacceptable in this case. This applies to arrays with a relatively small number of radiators.

In a large planar antenna array, the characteristics of the radiators of the central region are practically identical and the most important features of their behavior can be described with sufficient precision by the behavior of the radiators of an infinite antenna array. For this reason, an infinite antenna array can successfully serve as a model for the analysis of large planar antenna arrays. In this case, the directivity function of the antenna array can nonetheless be represented in the form of the product of the array factor and the directivity function of a single element, which is determined taking an infinite environment into account.

One of the most important reasons for using an infinite array model consists in the fact that this model can be treated as a periodic structure, for the study of which there are various analytical techniques. In the case of uniform excitation, it is sufficient to calculate the field distribution in one of the cells of this structure. The reflection factor and the radiation characteristics are determined by this field. The specific features of the various analysis techniques for infinite arrays are treated in [08]. Specific features of methods of analyzing other models of phased arrays are also given there.

We shall briefly consider what the effect of phased array blinding consists of. The concepts of hidden resonance, field suppression, nulls of the directional pattern of an element in an array and leaky waves. All of these concepts can be considered valid, but each of them does not exhaust, rather only underscores the different aspects of the phenomenon. Such a diversity in the interpretations of the blinding effect is partially explained by the two different approaches to the study of phased antenna arrays, one of which corresponds to the case of the excitation of all array elements, where the concept of input impedance of the radiator and the reflection factor is used to describe the array properties, while the second involves the excitation of one element with all of the other elements loaded into the impedance of the generators, receivers or into matched passive loads. The concepts of hidden resonance and suppression are explained by the behavior of an array in the case of the first approach to the study of array properties, while directional pattern nulls and leaky waves explain the specific features of array characteristics with the second approach.

The blinding effect can be observed for various radiating element structures. Radiating elements, of which hidden resonance is a characteristic, are shown in Figure 2.7 a-c. Each structure contains regions in which the propagation of surface waves is possible. (Besides the indicated structures, hidden resonance is also possible for director radiators (see Chapter 10)). We shall consider some of the specific features of the occurrence of this phenomenon.

In accordance with the theory of hidden resonance [0.8], the condition for array blinding matches the condition for surface wave propagation in an appropriate radiator structure. For example, a slotted array, ~~excited~~ by waveguides (Figure 2.7b), contains a dielectric layer lying on top of the slots. If a surface waveguide system is mated to this array, where the system is in the form of a dielectric layer on a solid metal shield, then the blinding of the array of narrow slots corresponds to the beam direction in which a phase distribution is established along the array which matches the phase of the surface wave field at the points where the slots are located. In this case, the field in the array over the slots is identical to the surface wave field in the dielectric layer on the metal shield, while the input admittance of the slots is infinitely high. As as result, the waves propagating in the waveguides are completely reflected back to the generators. The array does not radiate anything.

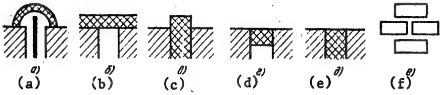

Figure 2.7. Radiating structures in which the effect of blinding is observed.

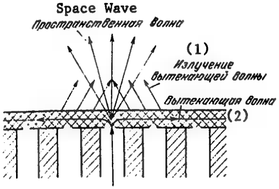

Figure 2.8. A leaky wave in a periodic array with the excitation of a single element.

Key: 1. Leaky wave radiation;
2. Leaky wave.

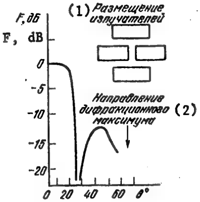

Figure 2.9. Directional pattern of a waveguide array.

Key: 1. Layout of the radiators;
2. Direction of the diffraction maximum.

It is essential to note that the comparison of the indicated guide system and a phased array make sense only for a beam direction in which the blinding of the array takes place.

Examples of radiators for which field suppression is possible are shown in Figure 2.7 d-f. In the region filled with dielectric (Figure 2.7b), the higher modes either propagate or fall in the supercritical mode of the phased array. A slightly supercritical mode is presupposed in the radiators depicted in Figure 2.7 e-f for the initial higher modes, i.e., the dimensions of the waveguides should be rather large. Field suppression occurs as a result of the excitation of higher modes in the waveguides of the array because of the asymmetry of the external field, which occurs during scanning. For a certain scanning angle, the excitation of the higher modes in the waveguide leads to field suppression in the aperture, complete reflection, and consequently to the blinding of the array.

If only one radiating element is excited in an array, while all of the others are loaded into passive loads, the nulls of the directional pattern of the excited radiator correspond to the blinding effect. The appearance of nulls in the directional pattern of the excited element can be related to the excitation of a leaky wave, which entails the removal of energy in a direction opposite to the direction of its propagation (Figure 2.8). Besides the leaky wave, an excited radiator produces a space wave. The interference of the indicated waves in the space above the array leads to the cancellation of their fields in some directions and nulls appear in the directional pattern of the array element, where these nulls are absent in the directional pattern of the same isolated element.

The structure of a waveguide array and the directional pattern of a waveguide radiator corresponding to it [013], calculated taking into account the influence of adjacent radiating elements loaded into passive loads and exhibiting a trough is shown in Figure 2.9.

The phenomenon of blinding is observed when the array beam is oriented within the bounds of the working scanning sector, and for this reason reduces the phased array scanning sector.

2.3. The Relationship Between the Directivity of a Radiator in an Array and the Directional Characteristics of a Fully Excited Array

The convenience and importance of the concept of the directivity characteristic of an element in an array consists in the fact that, first of all, when all of the antenna array radiators are excited, the superimposition of these patterns makes it possible to obtain the true directional pattern of the array, and secondly, an experimentally measured directional pattern of an element in an array can be used, as will be demonstrated in the following, to calculate the reflection factor in the feeders connected to the radiators when all of the array elements are excited. The latter circumstance is especially important when, because of the complexity of the structure of the radiating elements, their theoretic analysis proves to be difficult.

The directivity function of an element in an array corresponds to the gain of the element in the array: the directional pattern of the element in terms of power:

$$g(\theta, \varphi) = F^2(\theta, \varphi). \qquad (2.12)$$

In the case of equal amplitude excitation of the elements of an array, the gain of the array is related to the gain of an element in the array by the simple relationship:

$$G(\theta, \varphi) = Ng(\theta, \varphi). \tag{2.13}$$

This relationship determines one of the major advantages of the utilization of the element directivity characteristic in an array: using this directivity characteristic, one can determine the gain of a fully excited array.

If the generators which drive the radiators are matched to the feedlines running to the radiators and there are no thermal losses, then the difference between the gain of the antenna array and the directional gain is determined by the energy reflected from the radiators back to the generators:

$$G(\theta_0, \varphi) = D(\theta, \varphi)[1 - \Gamma^2(\theta, \varphi)], \tag{2.14}$$

where $\Gamma(\theta, \phi)$ is the reflection factor in the feeders driving the radiators.

Reflections in feedlines are due to mismatching these lines to the input impedances of the radiators of a fully excited array. Since the excitation phase of the array elements changes during scanning, the input impedance of the radiators is a function of θ, ϕ. The coefficient Γ is related to the input impedance of a radiator Z_a by the following relationship known from transmission line theory:

$$\Gamma(\theta, \varphi) = [Z_a(\theta, \varphi) - Z_0]/[Z_a(\theta, \varphi) + Z_0], \tag{2.15}$$

where Z_0 is the characteristic impedance of the feeder to which the radiator is connected.

If there are no higher order diffraction maxima, then the directional gain of the array is determined by the expression:

$$D = (4\pi/\lambda^2) AN \cos\theta, \tag{2.16}$$

where θ is the angle formed by the direction of the main lobe of the directional pattern and the normal to the plane of the array; A is the area allocated for one array element.

By comparing (2.13) -- (2.16), we obtain:

$$g(\theta, \varphi) = (4\pi^2/\lambda^2) A \cos\theta [1 - \Gamma^2(\theta, \varphi)]. \tag{2.17}$$

Expression (2.16) ties together two different operational modes of an antenna array. The gain of an element corresponds to the excitation of just one element in the array, while all the remaining ones are loaded into matched loads. The reflection factor characterizes the reflected power when all of the array elements are excited.

If the value of Z_a is found theoretically, then one can determine $g(\theta, \phi)$ by means of expressions (2.16) and (2.17), and then the gain of the array $G(\theta, \phi)$.

In the case where it is difficult to calculate Z_a and Γ because of the complexity of the analytical description of these quantities, one can experimentally measure $g(\theta, \phi)$ in an array, all of the radiating elements of which with the exception of one are loaded into a matched load. It is enormously simpler to measure $g(\theta, \phi)$ than to experimentally determine $G(\theta, \phi)$ and $Z_a(\theta, \phi)$ in the case where it is necessary to excite all of the array elements. The difficulties in this case are obvious. They are determined by the complexity of the excitation feeder system. Based on the measured $g(\theta, \phi)$, one can determine $|\Gamma|$ and the SWR in the lines leading to the radiators by means of (2.16).

The ideal directional pattern of an element in an array which provides for array matching for any beam direction in space can be derived from expression (2.16). In fact, it follows from (2.16) that $\Gamma = 0$, if:

$$g(0, \varphi) = (4\pi A/\gamma^2)\cos 0. \tag{2.18}$$

Thus, the directivity function of an ideal element in an array has the form:

$$F(\theta, \varphi) = (\sqrt{4\pi A}/\lambda)\sqrt{\cos 0}. \tag{2.19}$$

The efficiency and universal nature of the directivity function of an array radiator is due to the fact that all of the effects related to the interaction of radiating elements are taken into account in it. It must be noted that the introduction of the directivity characteristic of an array radiator is based on the assumption of the identical nature of the directivity functions of all of the radiators, which, generally speaking, is most likely the case in finite arrays. However, in the case of large arrays, the existing differences are insignificant for all of the radiating elements except those which are located at the edges of the array.

2.4. Radiators of Phased Antenna Arrays

Dipoles, open ends of waveguides, dielectric rod, helical and slotted radiators, etc. are used as the radiators of phased antenna arrays. Considerable attention has been devoted in recent years to printed circuit radiators (also see Chapter 9). The choice of a particular type of radiator is governed by the working frequency band, the requirements placed on the shape of the directional pattern of an individual element radiating power, as well as the polarization characteristics and broadband response.

There are three methods used at the present time in the design of radiating elements: 1) the technique of an array with a small number of elements; 2) the technique of waveguide models; 3) the technique of mathematical simulation. The major problem in the design work consists most often in minimizing the reflection factor in a specified scanning sector and frequency range.

In the first case [013], it is necessary to design an array with a relatively small number of radiating elements, to determine the coefficients and subsequently calculate the reflection factor for the center element. Then a matching device is chosen for each element, after which the entire procedure is repeated to confirm the results and improve the matching. The method is extremely laborious and has poor precision for directions close to the angles where the diffraction maxima occur.

Experimental modeling of the operation conditions of a radiating element as a component part of an infinite antenna array is used in the method of waveguide models [0.8] for several values of scanning angles, by means of placing a small number of radiators in a special waveguide unit. One of the drawbacks to the technique is the limited number of directions for which one can experimentally determine the reflection factor. Because of these specific features, the method does not allow for obtaining complete information on the properties of an array radiator in a specified scanning sector and frequency range.

The third method, which is based on the study of a mathematical model of the radiator, is the most promising and has no fundamental limitations on the type of radiators which can be studied. It is applicable to radiating elements which can be "calculated", i.e., for which a solution is known for the corresponding boundary problem as applied to an infinite array. Although the number of types of such radiators is small, there are extremely interesting ones for practical applications among them. These are waveguide radiators and their different variants (waveguide radiators partially and completely filled with a dielectric, or coated with a dielectric layer), dipole and director radiators over a conducting flat surface, as well as dielectric rod and slotted radiators with various excitation methods and certain others. A great advantage of the technique is the fact that mathematical simulation makes it possible to reproduce any changes both in the model which are possible in principle and in an experiment, but which may be difficult to realize. The utilization of the technique substantially curtails the volume of experimental studies related to the development of the radiators, and in a number of cases, even eliminates them.

When using mathematical modeling, the process of developing a radiator can be broken down into four steps:

1) The choice of the type of radiating element and the determination of the parameters of the layout grid for the radiators in the arrays;
2) The calculation and minimization of the reflection factor by means of varying the radiator parameters being changed;
3) Selecting a matching device and matching the radiator;
4) Checking the results obtained with the simplest waveguide model.

The first step was partially described in § 2.2.

If an equivalent circuit is known for the selected matching device and its parameters can be determined, then the matching device can be completely designed and optimized along with the radiator. In this case, the second and third steps are performed simultaneously. It must be kept in mind that in any case, the matching device should be placed closer to the radiator so as not to degrade the frequency properties of the array.

A distinction is drawn between matching phased array radiators for one direction and wide angle matching. Matching for one beam direction is accomplished by conventional methods adopted in microwave engineering (reactive loops, quarter-wave transformers, etc.). Some methods of wide angle matching of radiators are described in § 2.6.

A description of mathematical models and director, slotted and waveguide radiators is given in Chapter 10.

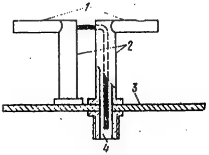

Figure 2.10. Structural design of a dipole radiator.

Key: 1. Dipole arms;
2. Balancing unit;
3. Conducting shield;
4. Feedline input.

Figure 2.11. A dipole phased antenna array.

Dipole radiators in a phased antenna array are usually positioned over a plane conducting surface, which plays the part of a shield and prevents back radiation. Theoretical and experimental studies show that two factors have the greatest impact on the characteristics of a dipole radiator incorporated in an antenna array: the arrangement of the radiators in the array and their postion relative to the conducting shield. A reduction in the step spacing of the array leads not only to the suppression of higher diffraction maxima, but also makes it possible to improve matching in a wide sector of scanning angles. Changing the height of a dipole radiator over the shield leads to an improvement in the matching in the extreme positions of the beam during scanning in the E and H planes.

A parameter which has a considerably lesser impact on matching in the scanning sector is the dipole length, if the initial matching is accomplished in the direction of a normal to the plane of the radiators.

A schematic depiction of the structural design of a dipole radiator positioned above a conducting shield is shown in Figure 2.10. Included in the structure, besides the dipole itself, are a balancing unit and a feedline, which perform the additional functions of mechanical supports holding the arms of the dipole. The presence of the supports can lead to undesirable resonance phenomena under certain conditions.

An example of dipole radiators with good matching is shown in Figure 2.11. Each radiator takes the form of a system of mutually orthogonal, separately excited dipoles, and it can be used to obtain circular polarization, or can be used in arrays with two independent channels with polarization decoupling.

Design practice for such radiators shows that the nonparallel nature of the dipole arms makes it possible to eliminate resonance effects which lead to the blinding of the phased array.

Printed circuit technology can be used to fabricate dipole radiators. Moreover, when printed circuit technology is used, the radiating elements, RF feed networks and phase shifters can be fabricated in a single cycle.

As studies have shown, the use of directors makes it possible to obtain good matching of a phased array in a wide sector of angles through the selection of the length and configuration of the directors.

Waveguide radiators have proved to be one of the most convenient radiators in the centimeter band for phased antenna arrays, for the following reasons:

1) Waveguide radiators are a natural continuation of the waveguide section where a phase shifter is placed;
2) They are characterized by a high transmission power level;
3) The properties of the radiator can be predicted based on analysis and calculations which in this case play the main role in the design work;
4) The computed characteristics of a radiator in a large array can be checked by means of measurements using a simple waveguide model.

The data obtained as a result of analyzing the properties of arrays of waveguide radiators show that with an increase in the dimensions of the waveguides, the influence of the higher harmonics in the aperture of the radiators becomes quite substantial. In contrast to arrays with radiators of relatively small dimensions, for example, half-wave dipoles in which a sharp increase in the reflection factor coincides with the appearance of higher order diffraction maxima in the range of real angles, when waveguide radiators of sufficiently large size are used, a sharp mismatching begins at smaller scanning angles, something which degrades the array properties because of the narrowing of the scanning sector. In this case, the following law is usually observed: the greater the cross-sectional dimensions of the waveguide radiator, the smaller the scanning angles for the onset of sharp mismatching. In important consequence following from this is the conclusion that the spacing between the elements in an array cannot be chosen by working solely from the requirement of a lack of higher order diffraction maxima in the region of real angles. The results of studying waveguide radiators [09] are summarized in Table 2.2, where the limitations on the placement of radiators in rectangular and triangular grids are indicated which prevent the appearance of higher harmonic resonances in the apertures of waveguide radiators.

TABLE 2.2.

Triangular Grid Треугольная сетка			
$\frac{d_y}{\lambda} \geqslant 0,75$	$0,75 \geqslant \frac{d_y}{\lambda} \geqslant 0,6$	$0,6 > \frac{d_y}{\lambda} \geqslant 0,45$	$\frac{dy}{\lambda} < 0,45$
$a/\lambda < 0,7$ $b/\lambda < 0,4$	$a/\lambda < 0,65$ $b/\lambda < 0,4$	$a/\lambda < 0,6$ $b/\lambda < 0,4$	$a/\lambda < 0,75$ $b/\lambda < 0,4$
Rectangular Grid Прямоугольная сетка $a/\lambda < 0,75;\ b/\lambda < 0,5$			

The placement of waveguide radiators in antenna arrays and the designations of the geometric dimensions cited in Table 2.2 are shown in Figure 2.12.

Approximate dimensions of a waveguide radiator can be selected using the data of this table so as to subsequently determine its characteristics and optimize them by experimental processing or modeling on a computer.

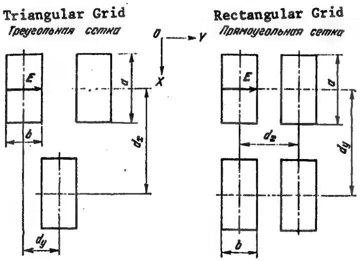

Figure 2.12. Phased antenna array geometry.

Figure 2.13. A phased antenna array of waveguide radiators.

A phased antenna array of waveguide radiators is shown in Figure 2.13. More complex radiating structures, the basis for which are waveguide radiators, are treated in § 2.6.

To obtain circularly polarized radiation or two independent polarizations, both waveguide dimensions should be sufficiently great to assure wave propagation with mutually orthogonal polarizations. On the other hand, the maximum dimensions of the radiators are limited by the step spacing of the array and in the majority of cases, steps must be taken to reduce the cross-section dimensions of the waveguide radiators. Blade inserts (Figure 2.14) are used or a transition is made to coaxial radiators using a H_{11} mode [013] to reduce the dimensions of such waveguides. With the appropriate choice of dimensions of cylindrical conductors for a coaxial radiator (Figure 2.15) which assure the propagation of an H_{11} mode, the cross-sectional dimensions of the radiator can be made less than half a wavelength.

A coaxial line is used for the feed to the radiator. The transition from the feedline to the coaxial radiator is positioned at a spacing of 0.5 λ_0, while the diameter of the inner conductor is chosen so that this spacing is equal to $\lambda_{H\ 11}/4$. This provides for H_{11} mode propagation and the suppression of the T mode. Moreover, a supplemental filter can be inserted between the radiator aperture and the transition adapter for T mode suppression. A standing wave ratio, K_{st}, of less than 3.5 in a passband of 1% was obtained in a scanning sector of ±50% relative to a normal to the plane of the array for the given radiator.

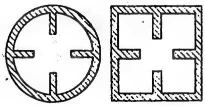

Figure 2.14. The configuration of waveguide radiators with reduced cross-sections.

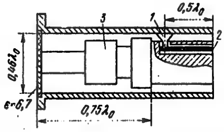

Figure 2.15. A coaxial radiator.

Key:
1. Crossbar transition;
2. Feedline;
3. T mode filter.

Figure 2.16. Radiator with a multimode waveguide section.

Figure 2.17. Waveguide-dipole radiator.

Another type [09] of radiating element with circular or double mutual orthogonal polarization of the field is a radiator (Figure 2.16), the cross-sectional dimensions of which are reduced through the use of an overmoded circular waveguide, excited by two crossed dipoles. The length of the overmoded waveguide section is made small. After matching, the value of K_{st} is ≤ 2.0 within a scanning sector of ± 50% relative to a normal to the plane of the array in a 13% passband.

An example of a radiator with small cross-sectional dimensions having double or circular field polarization is a waveguide-dipole radiator (Figure 2.17). The radiation fields of the printed circuit dipole and the open end of the waveguide are polarized in mutually perpendicular planes. The feed is delivered to the dipole radiator by means of a stripline, placed in the waveguide. Since the dipole radiator is parallel to the wide wall of the waveguide, then in the transverse direction, the size of the waveguide-dipole radiator is determined by the size of the narrow wall of the waveguide.

Printed Circuit Radiators. In those cases where stringent requirements concerning size and weight are placed on a phased antenna array, printed circuit components can be used as the array radiators [013]. These radiators are arranged a short height above a plane conducting shield (about $\lambda/20$); a special feature of them is the possibility of utilizing printed circuit technology in the fabrication of multielement subarrays with microwave feed circuits and radiators, arranged on both sides of the substrate.

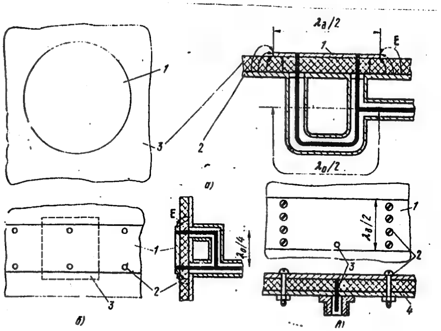

Figure 2.18. Printed circuit radiators.

Key: a. Disk;
b. Two stub strip radiator;
c. Single stub strip radiator.

Different variants of printed circuit radiators exist. In the latest variant ((Figure 2.18a), the printed circuit radiator takes the form of a disk (1), positioned above a metal shield (2) on a dielectric substrate of small thickness (3). The disk is excited by means of two stubs, to which the energy can be delivered either by a coaxial feeder or by means of a stripline, placed on the opposite side of the shield. The stubs are excited out of phase which provides for maximum radiation in the direction of a normal to the plane of the shield. The utilization of two pairs of exciting stubs, positioned in perpendicular planes and excited with a phase shift of 90°, makes it possible to obtain circular polarization of the radiation field.

Another variant of a printed circuit radiator is shown in Figure 2.18b. The array takes the form of a system of metal strips (1) each of which is excited by a definite number of paired stubs (2). The dashed line singles out the individual radiator (3) in this system. The pair of radiator stubs is excited out of phase.

A single stub printed circuit radiator is shown in Figure 2.18c. To simplify the excitation device, one of the stubs is removed in each radiator (3), however, this necessitates the placement of shunting stubs (2) between the individual radiators which electrically couple the strip conductor (1) to the metallic plane (4). Such a structural design in extremely close in terms of its properties to a section of rectangular waveguide with a length of $\lambda_w/2$ filled with a dielectric, excited by a stub positioned near one of its open ends. The fields radiated by the open ends of a waveguide $\lambda_w/2$ long in the direction of a normal to the plane of an array are in phase.

Changing the input impedance of a printed circuit radiator to match it to the feeders can be accomplished by virtue of changing the spacing between the stubs in two stub designs or shifting the stub in single stub structures.

Since the thickness of the dielectric substrate is small, resonance effects which lead to dips in the directional pattern of the printed circuit radiator are absent.

Research has shown that the best matching can be obtained for a disk diameter of 0.6 λ_d (λ_d is the wavelength in the dielectric) and with a strip width of 0.5 λ_d, where the excitation is realized by means of two stubs. In the case of printed circuit radiator excitation by one stub, acceptable matching is achieved when it is placed at the edge of the strip.

Studies show that radiators can be quite well matched. Thus, for an array of single stub radiators, a value of $K_{st} < 1.2$ was obtained in a 12% passband.

2.5. Wide Angle Matching of Phase Antenna Arrays

Mismatching of an array to a feeder system, which is due to the interaction of radiators during scanning, reduces the attainable gain, leads to direction pattern distortions and has a harmful impact on the amplifiers which may be inserted in the array following the radiators. In contrast to conventional matching for one beam direction, the utilization of wide angle matching techniques makes it possible to improve the characteristics of the array throughout the entire scanning sector. For example, in a conventional antenna array intended for scanning in a range of one-third of a hemisphere, at a single frequency with conventional matching, $\Gamma \leq 0.55$ ($K_{st} \leq 3.5$) [0.13]. The maximum gain losses with mismatching in this case amount to 1.6 dB. The application of wide angle matching techniques makes it possible to reduce the losses down to 0.8 dB, which is equivalent to increasing the antenna area by 20%.

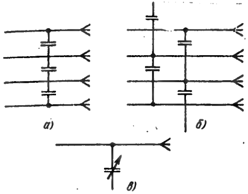

Figure 2.19. The connection of radiators in linear antenna arrays.

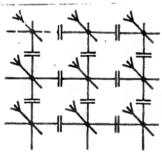

Figure 2.20. An example of radiator connection in a planar antenna array.

Methods of wide angle matching of phased antenna arrays can be broken down into two groups: 1) methods related to modifying the structure of the device exciting the array; 2) methods, the use of which leads to the placement of additional elements in front of the radiating aperture, the reflection from which reduces the change in the input impedance of the radiators during scanning.

The following methods of wide angle matching for phased arrays belonging to group 1 have been described in the literature:

1. The utilization of coupling networks between the elements. Sections of transmission lines or reactive elements, which couple the array radiators, are used as the coupling networks. The methods of coupling the elements can vary. Shown as an example in Figure 2.19 are connections of radiators in a linear array. Such connections are equivalent to the insertion of a reactance in parallel with the radiator, where the reactance depends on the scanning angle. Selection of the coupling network parameters makes it possible to reduce the change in the input impedance during scanning. One of the variants for the insertion of coupling networks in a two-dimensional array is shown in Figure 2.20. In accordance with [013], the use of this configuration in an array of dipole radiators intended for scanning in a conical region of $\theta \leqq 60°$, makes it possible to reduce the range of variation in the reflection coefficient down to $|\Gamma| \leqq 0.26$ ($K_{st} \leqq 1.7$) as compared to $|\Gamma| \leqq 0.67$ ($K_{st} \leqq 5.1$) in the case of conventional matching.

2. Filling the waveguide radiators with a dielectric. In the case considered here, the dimensions of the waveguide radiators and the parameters of the filling medium are chosen so that only one mode propagates.

Such a technique was treated in the study of antenna arrays of plane-parallel waveguides [0.13], which scan in one plane, as well as circular waveguide arrays with a rectangular grid for the radiating elements, which scan in the H-plane [0.13]. An improvement in the matching is achieved when this method is used by virtue of filling the waveguides and through a reduction in the dimensions of the radiating elements, which assures single mode operation of the waveguides. In the case of very small radiating elements, the difference in the power directional patterns of an isolated radiator and an ideal radiator ($\cos\theta$) can serve as a measure of the mismatching during scanning. In the H-plane, the directional pattern of a waveguide radiator expands with a decrease in the dimensions of the waveguide, approaching $\cos^2\theta$. Consequently, a reduction in waveguide dimensions improves the directional pattern of a waveguide radiator in the H-plane. Contrariwise, the directional pattern in the E-plane widens as compared to $\cos\theta$. It follows from this that the filling of waveguides with a dielectric and the reduction in radiator dimensions related to this reduce the mismatching during H-plane scanning and increase it in the case of scanning in the E-plane.

3. The use of waveguide radiators with several propagating modes [09]. In the case of linear arrays, an improvement is achieved in the matching through the choice of the relationship between the amplitudes of the two modes, which are the H_{10} and H_{20} modes in the case of scanning in the E-plane. This method makes it possible to reduce the range of variation in the reflection coefficient in an angular sector of $\theta = \pm 54°$ down to $|\Gamma| \leqq 0.09$ ($K_{st} \leqq 1.2$) as compared to $|\Gamma| \leqq 0.23$ ($K_{st} \leqq 1.6$) when using a single mode: H_{10}. It must be kept in mind that in this case, the directional pattern becomes asymmetrical in the H-plane and a null

appears in one of the directions, which is absent when using only the H_{10} mode.. The indicated defects in the directional pattern are due to the intense excitation of a H_{20} mode and field distribution asymmetry in the waveguide aperture.

4. The use of electronically tuned matching devices. Although this technique can provide for wide angle matching, it requires the insertion of additional control devices in the array, something which greatly increases the cost and reduces the reliability of phased antenna arrays.

5. The use of matching devices which absorb reflected waves in the radiator channels. Circulators and isolators, inserted between each element and the generator can be used as matching devices. This method makes it possible to improve the operational conditions for the generators, but does not reduce the gain losses due to mismatching of the radiators.

The following techniques belong to group II.

1. Inserting conducting partitions in the H-plane of a dipole array (Figure 2.21). These partitions reduce the change in the reflection coefficient during E-plane scanning, without influencing the conditions for matching in the case of H-plane scanning. When this method of matching is employed, a figure of $|\Gamma| \leq 0.23$ ($K_{st} \leq 1.58$) can be obtained in a conical scanning sector of $\theta \leq 60°$, while in the case without partitions, $|\Gamma| \leq 0.45$ ($K_{st} \leq 2.63$) in the same sector. These results are justified for radiators positioned at a spacing of less than half a wavelength. The improvement in the matching in this case is due to the change in the dipole directional pattern in the E-plane, which makes it more similar to the directional pattern of a waveguide radiator. The directional pattern of an isolated dipole is substantially narrower than an ideal radiator pattern, while the directional pattern of a waveguide radiator in the E-plane can be made extremely close to the corresponding directional pattern of a ideal radiator. The utilization of this method for a waveguide array does not lead to a marked improvement in the matching with the conventional configuration of the elements [0.13]. An improvement in the matching proves to be possible only with a reduction in the spacing between the radiators as compared to that defined by expression (2.3) [013].

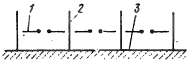

Figure 2.21. A dipole antenna array with matching baffles.

Key: 1. Dipole; 2. Baffle; 3. Conducting shield.

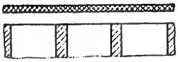

Figure 2.22. A thin dielectric sheet over a waveguide array.

2. The placing of a thick dielectric plate in the aperture of the antenna array. When scanning in the H-plane in an angular sector of $\theta = \pm 72°$, a figure of $K_{st} \leq 1.15$ was obtained for an antenna array of flat waveguides [08] with a dielectric plate, as compared to $K_{st} \leq 2.2$ without the plate. This method is applicable for rectangular and circular waveguides in a rectangular and triangular grid. However, in the case of E-plane scanning, the dielectric plate increases the reflection, which leads to the appearance of resonance dips in the directional pattern of the radiator.

3. The use of a thin dielectric sheet with a high dielectric permittivity, placed a small distance from the waveguide array (Figure 2.22). This sheet acts in a manner similar to a reactance, which changes during scanning. During waveguide simulation, a value of $|\Gamma| \leq 0.38$ ($K_{st} \leq 2.2$) was obtained without the sheet and a value of $|\Gamma| \leq 0.2$ ($K_{st} \leq 1.5$) with the dielectric sheet. A drawback to this technique consists in the fact that there is a tendency towards a reduction in the scanning sector in the E-plane, as well as in other planes which do not coincide with the H-plane, because of resonance phenomena. However, this can be avoided when the thickness of the dielectric is reduced, while the dielectric permittivity is increased.

4. The utilization of a "loaded" conducting plane. One of the examples of the use of this method is an array of flat waveguides, between which short circuited sections of the same waveguides are placed (Figure 2.23a). A waveguide array with a triangular grid for the placement of the radiators, separated by short circuited flat waveguides (Figure 2.23b) can serve as another example. This same method also includes the use of short circuited rectangular waveguides, placed in the gaps between waveguide radiators (Figure 2.23c). In the latter case, total mismatching ($|\Gamma| = 1$) is successfully prevented in planes not coinciding with the H-plane, which is due to the appearance of higher order diffraction maxima or resonance effects, which lead to the blinding of the antenna. The possibility arises in this case for widening the scanning sector to a certain extent as compared to the sector determined by the appearance of higher order diffraction maxima.

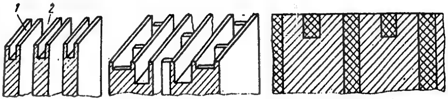

а) (a) б) (b) в) (c)

Figure 2.23. Examples of a "loaded" flat shield.

5. Close spacing of the radiating elements. When the radiating elements are close together, the higher order diffraction maxima move over to the region of imaginary angles and remain in it for any scanning angles. The change in the reactive component of the input admittance of the radiators is reduced in this case and the mismatching is basically due to the change in the resistive component.

The effectiveness differs for the methods of wide angle matching within the passband enumerated above.

The most broadband techniques can be considered the methods of reducing the spacings between the elements, the use of a thin dielectric sheet with a high dielectric permittivity and baffles between the radiators. Reducing the spacing between the radiators is unacceptable in the majority of cases, since it leads to an increase in the number of radiators. The two other methods are applicable both to waveguide and dipole radiators, arranged in triangular and rectangular grids.

A dielectric plate can be employed when scanning in one plane and for matching over a band of frequencies. In the case of a waveguide array, matching is achieved in the H-plane, and in the case of dipoles, is achieved in the E-plane.

2.6. Structural Configuration of Phased Antenna Arrays

Optical type and closed channel power dividers are used to excite phased antenna array radiators.

There are two kinds of antenna array configurations using optical type dividers. In the first case, the energy from the feed irradiator impinges on the collector (Figure 2.24a) array, passes through the RF circuits and phase shifters, and is then reradiated in the requisite direction by another array. In the second case (Figure 2.24b), the collector and reradiating array are combined. The power received from the feed irradiator is reradiated in the requisite direction.

A merit of optical type dividers is simplicity with a large number of radiators. Feed irradiators of the corresponding reflector antennas can be used as the feeds, including monopulse feed irradiators to produce sum and difference directional patterns. An advantage of reflector type arrays is their structural design and operational convenience, which consists in the accessibility of the radiating elements during alignment and replacement from the nonradiating side of the array. An example of the structural realization of a reflective array, intended for installation in an aircraft, is shown in Figure 2.25. In a transmissive array, better characteristics can be obtained by optimizing the collector and reradiating arrays individually.

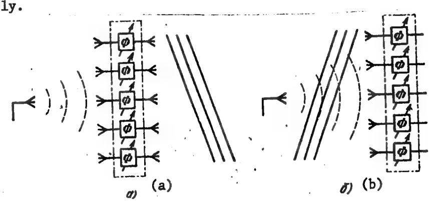

Figure 2.24. Configurations of antenna arrays with optical power dividers.

Energy "spillover" through the edges of an array, similar to what occurs in reflector antennas, must be numbered among the drawbacks to arrays with an optical method of exciting the elements. This leads to a reduction in the surface utilization factor and an increase in the sidelobe radiation background.

Dividers in the form of a closed channel are made using series and parallel power divider circuit configurations (Figure 2.26). In the case of series power division, the phase shifters can be inserted in the lateral branches of the feedline, running to the radiators (Figure 2.26a). In this case, 1/Nth part of the power flows in each of the N phase shifters, while the power losses are governed by the losses introduced by a single phase shifter. The drawback to this circuits is the differing electrical lengths of the path from the antenna input to the radiators, which can lead to phase distortions at the edge of the frequency band. To eliminate phase distortion, it is necessary to inset compensating feeder sections in the lateral branches (see § 2.8).

With a parallel power division circuit (Figure 2.26b), which also permits the use of low power phase shifters, the overall power losses are determined by the losses in a single phase shifter and there is the capability of equalizing the lengths of the individual channels to assure a broadband response. A drawback to the parallel configuration is the complexity of matching when dividing the power among a large number of channels. The double stepped configuration (Figure 2.26c) belongs among parallel division configurations, where in each node of this circuit the power is divided equally or unequally. In the case of equal division, the double stepped configuration can be made to have a broadband response because of the use of feeder sections of equal length from the input to each radiator. In the case of unequal division, the phase and amplitude distortions within the passband in the output lines of the branches will be large, while the passband will be narrower as compared to the case of equal division.

Figure 2.25. A reflector type aircraft phased array.

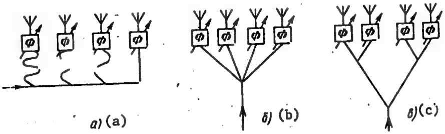

Figure 2.26. Schematics of power dividers in the form of a closed channel.

Various units can be employed as power dividers: waveguide and coaxial Tees, waveguide bridges, directional couplers using coupled striplines, as well as resistive ring power dividers using striplines.

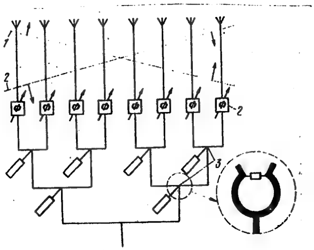

Figure 2.27. A double stepped circuit configuration with hybrid power dividers.

Key:
1. Incident waves;
2. Reflected waves;
3. Hybrid power dividers.

As a result of the mismatching of the radiators during scanning, the antenna system gain is reduced, and something which is no less important, amplitude and phase distortions appear which in turn can substantially change the sidelobe radiation level of the phased array. The latter factor is important for arrays with a requisite low sidelobe level.

In analyzing the impact of radiator mismatching on the shape of the directional pattern and the operational mode of the feeder system, reflections in the radiator feed circuits can be treated as excitation of a plane wave in the radiators and feeder system, where this wave arrives from a direction which is the mirror reflection with respect to the direction of the main lobe (Figure 2.27), as well as subsequent sequential re-reflection of the waves excited in the feeder system from the radiators and the power divider. For arrays consisting of a large number of radiating elements, the reflection coefficients can be considered approximately the same and equal to the reflection coefficient of an infinite array. The reflected waves propagating from the radiators in the feedlines partially pass through to the input of the antenna, and are partially returned to the radiators, again passing through the phase shifters. These waves, in turn, are in part radiated and in part reflected, etc. During the radiation of each repeat wave, additional sidelobes appear in the directional pattern.

Antenna arrays with various types of power dividers have differing sensitivity to mismatching. In the simplest case, when each radiator is excited from a separate generator with a nonreflecting output, the mismatching of the radiators has no effect on the shape of the directional pattern, since the reflected wave is completely absorbed. A similar effect occurs in double stepped circuits, where hybrid connectors are used as the power dividers. For example, resistive ring power dividers using striplines can be employed as the dividers in double stepped circuit configurations (Figure 2.27). In such dividers, a portion of the reflected waves passes through to the antenna input, while the remaining part is absorbed in the resistors. In this case, the reflected waves are not reradiated and the radiators are decoupled. Double stepped power dividers with resistive ring elements can be built using striplines by means of printed circuit technology (Figure 2.28).

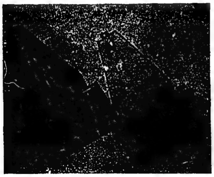

Figure 2.28. A stripline power divider with resistive ring dividers.

Another example of a feeder system which absorbs the reflected wave and provides for decoupling of the radiators is a power divider in which directional couplers are used as the coupling elements (Figure 2.29). The waves reflected from the radiator pass through to the antenna input or are absorbed in the loads of the directional couplers, but are not reradiated by the radiators.

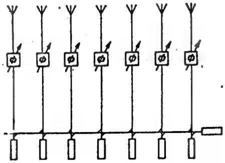

Figure 2.29. A power divider with directional couplers.

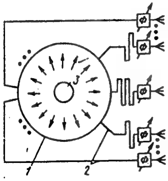

Figure 2.30. A combination power divider circuit using a radial line.

Key:
1. Radial line;
2. Feeders of equal electrical length;
3. Radial line exciter.

A radial line (Figure 2.30) excited in the center by a circular waveguide [013], can be used as a power divider for a linear antenna array. The mode propagating in the radial line excites the radiators of the collector array, which can be the open ends of waveguides or other radiators. The radiating elements of the linear array are coupled to the radiators of the collector array by feeder lines of equal length, for which it is convenient to use flexible coaxial cable sections in the given case.

If a E_{01} mode propagates in a circular waveguide with an azimuthally symmetrical field, then all of the array elements are excited in phase with equal amplitude. However, if a H_{11} mode is excited in the circular waveguide, then the amplitude of the electrical field intensity at the output of the radial line will vary in accordance with a cosinusoidal law. With the simultaneous excitation of H_{11} and E_{01} modes, the resulting field at the output of the radial line is:

$$E_\Sigma = E_{E_{01}} + E_{H_{11}} \cos\varphi = E_{0\Sigma} + E_1 \cos^2(\varphi/2).$$

By choosing the ratio of the modal amplitudes excited in the circular waveguide, one can produce directional patterns with various properties. Beam scanning is accomplished by means of phase shifters inserted in the feedlines. The electrical length of these lines is chosen the same so as not to degrade the frequency response of the divider.

In the case of small scan angle sectors, it is expedient to combine the great capacities of electrical scanning systems and the precision of traditional reflector antennas to reduce the cost of antenna systems [09]. A schematic depiction of such antenna systems is shown in Figure 2.31. The operational principle of the antennas considered here can be described by using as the analog for these devices, reflector systems in which the beam scanning is achieved by shifting the feed radiator from the focal point in a transverse direction. In the case considered here, control of the radiator excitation phase (phasing) of the small feed irradiator arrays is realized so that the field produced by them corresponds in the sense defined here to the field of a shifted radiator. Using the system depicted in Figure 2.31a, scanning can be realized in an angular sector not exceeding 10 times the directional pattern width. A twin reflector, excited by a small phased array (Figure 2.31b) scans in an angular sector of less than 5° with a beam width of less than 1°. An example of the structural design of a transmissive type antenna system (Figure 2.31c) is shown in Figure 2.32. The given antenna is intended for scanning in an angular sector of 14 x 20°. The feed radiator array, with dimensions of 22.5 x 30 cm consists of 824 elements. It is not necessary to use the reflector in the systems described here; a lens antenna can be used in place of it.

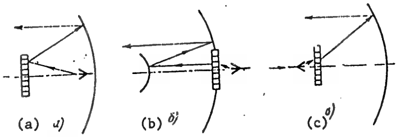

Figure 2.31. Schematics of antenna systems with a limited scan sector.

Figure 2.32. A scanning reflector antenna with an auxiliary phased antenna array.

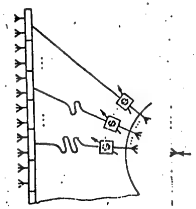

Figure 2.33. A planar spherical transmissive antenna array.

An example of the realization of the optical technique of energy distribution in transmissive arrays is a planar spherical antenna with dual polarization and separate inputs for each polarization. In such an array (Figure 2.33), the spherical wave irradiated by the feed radiator excites the elements of a spherical collector array. Coaxial cables of equal length, in which the phase shifters are inserted, connect the elements of the spherical array to the subarrays of the planar radiating system. Each subarray is controlled by a single phase shifter, since its scan sector is small (See § 2.2).

The spherical shape of the collector array makes it possible to reduce energy losses related to reflection, since the wave incidence angle on the collector array is the same at any point on it and the radiators of the collector array can be quite well matched. In this case, a greater bandwidth is achieved, since the spacings from the feed to the elements of the collector array are the same. A general view of an antenna array and one of the subarrays is shown in Figures 2.34 and 2.35. The radiators of the subarray are symmetrical dipoles. The radiators in each subarray are split into two independent groups, having mutually orthogonal polarization. Each group is controlled by a separate phase shifter. There are two mutually perpendicular dipoles in the collector array corresponding to the indicated groups of radiators. The overall electrical length of the microwave circuits from these dipoles of the collector array to the subarray is the same. Such a system, which takes the form of a controlled lens, is capable of reradiating a wave of any polarization. If the feed radiator radiates two waves with orthogonal polarization, then the field radiated by the antenna system can have either linear or circular polarization, depending on the phase and amplitude relationships between the orthogonal components.

Figure 2.34. General view of a planar spherical antenna array from the radiating array side.

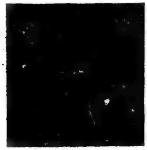

Figure 2.35. General view of a dipole subarray.

The considerable spacing between identically oriented dipoles in the subarrays leads to the appearance of high level diffraction maxima in their directional patterns. However, the sidelobe level of the directional pattern of the entire antenna is substantially less, because of the annular arrangement of the subarrays (Figure 2.34).

2.7. The Passband of a Phased Antenna Array

The major factors which influence the frequency properties of phased arrays are the frequency properties of the radiating aperture, the phase control technique employed (using phase shifters or delay lines), the type of power divider as well as the nature of the received or transmitted signal. Formulas are given in this section for the estimation of the frequency characteristics of a phased antenna array for signals in the form of short and long pulses with a frequency which changes within the bounds of a pulse.

It is assumed in the following in the estimation of the frequency properties of phased arrays that the working bandwidth of some of its devices, such as phase shifters, radiators and directional couplers, for example, is no narrower than the bandwidth of the array, determined by the major factors which are indicated.

In the majority of cases of practical interest, a slight change is permitted in the phased antenna array characteristics within the working passband. For this reason, the effect of each of the indicated factors can be treated separately, and the overall effect determined as the sum of the corresponding contributions.

Frequency Properties of the Radiating Aperture. If the phase distribution remains constant with a change in the frequency, then the beam produced by the aperture is shifted through an angle of [013]:

$$\Delta\theta \simeq -(\Delta f/f)\ \mathrm{tg}\ \theta_{\text{гл}}. \tag{2.20}$$

It follows from formula (2.20) that the size of the aperture and the beam width do not influence the shift. With the same frequency change, the displacement depends on the direction of the beam and it is greater, the more the beam is deflected from the normal to the aperture. The passband, within which the beam displacement does not exceed half of its width, is defined by the relationship:

$$\Delta f/f \approx \lambda/2L \sin\ \theta_{\text{гл}}, \tag{2.21}$$

where L is the dimension of the aperture in the plane running through the normal to the aperture and the direction of the main lobe of the directional pattern.

Frequency shifting of the beam leads to a gain reduction in the original direction. A graph of the change in the gain of a phased array as a function of the argument:

$$u = 0{,}285\,\Delta f\,(\mathrm{tg}\,\theta_{\text{гл}})/2\theta_{0.5}, \tag{2.22}$$

where Δf is the bandwidth (in percent); $\theta_{0.5} = 57\lambda/L \cdot \cos\theta_{\text{main}}$ is the directional pattern width (in degrees), is shown in Figure 2.36.

By using this graph, one can determine the passband of an aperture for a specified permissible change in the gain and for a known beam width and its maximum deflection from the normal to the plane of the array:

$$\Delta f \simeq 3{,}3 u_{\text{доп}} 2\theta_{0.5}/\mathrm{tg}\,\theta_{\max}, \tag{2.23}$$

where $u_{\text{доп}}$ [$u_{\text{perm.}}$] is the argument of the function considered here, corresponding to the permissible reduction in the gain of the phased antenna array. In particular, if the gain reduction should not exceed 1 dB, then for an array with a scanning sector of $|\theta_0| \leq 60°$:

$$\Delta f \simeq 2\theta_{0,5}. \qquad (2.24)$$

The results cited here are justified for a signal in the form of a long pulse with a frequency which changes within the limits of a pulse.

In the case where the signal takes the form of a short pulse of width τ, which corresponds to a passband of Δf = 1/τ, the reduction in the phased array gain occurs because of the fact that for various spectral components, the shaping beam is shifted through different angles, so that the directional pattern of the phased array for a pulsed signal is wider than the directional pattern for the center frequency.

We shall make use of the concept of "aperture filling time", which is defined as the time during which the wave front propagating at the angle θ_{main} passes through the entire aperture:

$$T = L\,(\sin\,\theta_{\text{гл}})/c, \qquad (2.25)$$

where c is the speed of light. Then condition (2.24) is equivalent to the condition:

$$T = \tau \qquad (2.26)$$

The change in antenna gain is plotted in Figure 2.37 as a function of the ratio:

$$u = T/\tau = 0{,}57\;\Delta f\;(\text{tg}\;\;\theta_0)/2\;\;\theta_{0,5}. \qquad (2.27)$$

It follows from this relationship that in the case of short pulses:

$$\Delta f\,[\%] = 1{,}75 u_{\text{доп}}\, 2\theta_{0,5}/\text{tg}\,\theta_{\max}. \qquad (2.28)$$

If a gain reduction of no more that 1 dB is chosen as the criterion for determining the passband, then in a scanning sector of $\theta_{\max} = 60°$, the passband for a pulsed signal is [013]:

$$\Delta f \simeq 4\,\theta_{0,5}. \qquad (2.29)$$

Just as in the preceding case, the aperture bandwidth depends on the beam width, i.e., on the size of the aperture referenced to the wavelength. Increasing the directivity of the aperture leads to a narrowing of the passband.

The Passband and Phase Shifters. Phase shifters used for beam control in phased antenna arrays can be broken down into phase shifters and controlled delay lines. Although this division is arbitrary and a signal delay also occurs in phase shifters, this delay is usually much less than the aperture filling time for any value of the phase at the output. This is due to the fact that the maximum change in the electrical "length" of a phase shifter does not usually exceed 360°. Moreover, the change in the phase at the output of a phase shifter is small within

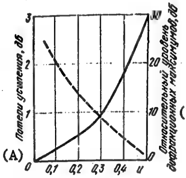

Figure 2.36. The change in aperture gain (——) and level of the diffraction maxima (---) for long pulses.

Key: A. Gain losses, dB;
B. Relative level of the diffraction maxima, dB.

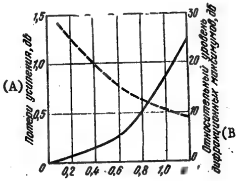

Figure 2.37. The change in the aperture gain (——) and level of the diffraction maxima (---) for signals in the form of short pulses.

Key: A. Gain losses, dB;
B. Relative level of the diffraction maxima, dB

the working passband and it can be disregarded in a first approximation.

Controlled delay lines used for scanning serve to change the signal delay time in the channel of the corresponding radiator, which in the final analysis, as it stands to reason, is equivalent to changing the phase. The maximum signal delay during scanning in angular sector of $|\theta| \leq 90°$ is equal to the aperture filling time. However, despite the seeming equivalence of phase shifters and controlled delay lines, the properties of the phased arrays within the passband differ substantially depending on the type of phase shifters employed.

Let the phase change be accomplished with phase shifters. If the phase relationships at the output of the power divider remain constant, then one can assume that the phase is also constant at the output of the phase shifters. Then the passband of the phased antenna array is governed by the frequency properties of the radiating aperture, something which has already been noted.

If delay lines are used as the phase shifters, then the signal delay time in the channel for each radiator is chosen so that the signals from all of the radiators at the antenna output are added in phase, i.e., so that the spatial delay is cancelled out:

$$T_n = L_n/c \tag{2.30}$$

where L_n is the distance from the n-th radiator to a plane perpendicular to the direction of arrival of the wave passing through the edge radiator (Figure 2.38). The spatial delay does not depend on the frequency. For this reason, if the signal propagation velocity in the delay lines is also independent of the frequency, then the frequency properties of the aperture do not limit the array passband and it is necessary to take other factors into account. Delay lines which possess the indicated properties can be designed around T mode guide systems, the phase velocity of which does not depend on the frequency. Such a delay

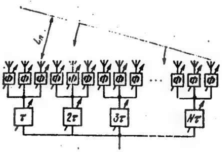

Figure 2.38. Configuration of a phased antenna array with controlled delay lines.

line takes the form of a set of switched coaxial cables of different lengths. However, during wide angle scanning, the use of controlled delay lines in the channel of each radiator does not prove to be possible because of the impermissible increase in antenna cost and structural design in conveniences related to the considerable overall length of the switched cables. For example, when scanning in an angular sector of $\theta_{max} = 60°$, the maximum length of the switched cables differs only slightly from the aperture size. A widening of a phased array bandwidth can nonetheless be attained through delay line control of not individual radiators, but rather groups of radiators (Figure 2.38), while the phase control of individual radiators is accomplished in a group by phase shifters. Even when the aperture is broken down into two subarrays, the passband of a linear array is more than doubled. Doubling the passband of a planar antenna array is accomplished when the array is broken down into four parts. In the general case, to increase the passband by a factor of N times, it is necessary to break a linear antenna array down into N subarrays, and a planar array down into N^2 subarrays, controlled by means of delay lines. By employing the property of array symmetry, the number of delay lines with long cables can be substantially reduced [09].

The directional pattern of an antenna system, the subarrays of which are controlled by means of changing the signal delay time, can be represented in the form:

$$f(\theta, \varphi) = F_n(\theta, \varphi) F_{\Sigma n}(\theta, \varphi); \qquad (2.31)$$

where $F_n(\theta, \phi)$ is the directional pattern of the subarray; $F_{\Sigma n}$ is the multiplying factor for the array, the elements of which are the subarrays.

With a change in the frequency (Figure 2.39), the main lobe of the array factor (1) remains in a constant position, since the phases of the subarray signals are controlled by means of changing the delay time, while the directional pattern of the subarray (2) is moved, just as in the case of a radiating aperture, since the radiators of the subarrays are controlled by phase shifters. For this reason, the frequency properties of the antennas considered here are determined by the frequency properties of the radiating aperture of the subarray. A significant circumstance in the given case is the increase in the level of the sidelobes of the directional pattern for the entire array at frequencies other than the center frequency. This increase is due to the fact that when the main lobe of a subarray directional pattern is shifted relative to the array factor, spurious maxim (3) of the array factor (Figure 2.39) fall in the region of the maxima, where these spurious maxima coincide at the center frequency in terms of direction with the direction of the nulls of the subarray directional pattern. Therefore, the level of sidelobe radiation in the direction of the spurious maxima of the array factor increases. The sidelobe level for various signals is shown as a function

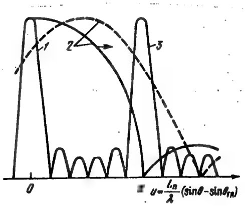

Figure 2.39. The relative shift in the directional pattern of a subarray with phase shifters and the maxima of the array factor with a change in the frequency in an antenna system with delay lines.

of the argument u in Figures 2.37 and 2.38. It follows from the graphs that if the drop in the gain does not exceed 1 dB, this level does not exceed 11 dB. The graphs shown in Figures 2.37 and 2.38 also characterize the change in the gain of an antenna array with subarrays controlled by delay lines, where L in formulas (2.20) - (2.29) is understood to be the corresponding dimension of the subarray.

The Frequency Properties of Power Divider Circuits. The Parallel Circuit Configuration. The various power divider circuits differ substantially in their frequency properties. Parallel and double stepped circuit configurations with equal power division in each branch possess the best frequency properties. This is due to the fact that the electrical length of the paths from the antenna input to each radiator are the same and change identically with a change in frequency. For this reason, the phase distribution remains constant within the passband at the output of power dividers designed in these configurations. Other feed circuits introduce additional phase shifts, which lead to a displacement of the beam of the array.

The Series Circuit Configuration. In the case of series power division (Figure 2.40), where additional transmission line sections are absent (Figure 2.40a), which equalize the signal path length from the antenna input to the radiators, a frequency change which changes the phase relationships at the input to the radiators leads to a deflection of the beam of the antenna array. If a T-mode propagates in the main trunk feeder, then the shift in the beam caused by the linear phase error occurring with the change in the frequency, is determined by the expression [013]:

$$\Delta\vartheta \simeq \frac{\lambda_\Phi}{\lambda}\frac{\Delta f}{f}\frac{1}{\cos\theta_{гл}}, \qquad (2.32)$$

where λ_Φ is the wavelength in the feeder trunk. The beam displacement which is due to the properties of the series feed circuit for the radiators, either adds to the displacement related to the frequency properties of the radiating aperture, or cancels it: if the beam is deflected in the direction of the array input, then the beam displacements add; if the beam is deflected in the direction of the load, then they subtract. The passband, within which the array gain falls off no more than 1 dB with a maximum beam deflection of 60°, is defined by the relationships [013]:

$$\Delta f \simeq \frac{2\theta_{0.5}}{1 + \lambda_\Phi/\lambda} \qquad (2.33)$$

in the case of a long pulse with a changing frequency, and:

$$\Delta f \simeq \frac{4\theta_{0.5}}{1+\lambda_\Phi/\lambda} \qquad (2.34)$$

in the case of a short pulse.

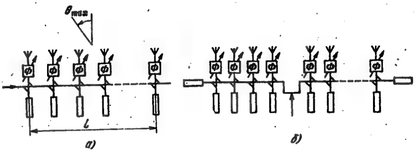

Figure 2.40. A series power division circuit configuration.

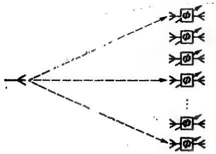

Figure 2.41. An optical power division circuit configuration.

When the main trunk feeder is fed in the center (Figure 2.40b), the system can be treated as two antennas with series power division. If the beam is oriented with respect to the normal to the line of position of the radiators at the center frequency, then when the frequency changes, the beams of each of the halves of the array will move in opposite directions and the overall directional pattern will expand, without changing the direction. As a result, the directivity of the antenna array will be reduced. When the array beam is deflected from the normal, the angular motion of the beam due to the specific features of series power division, adds to the motion of the beam due to the frequency properties of the radiating aperture. For the different halves of the array, these motions are in opposition: for one half, the aperture motion is cancelled by the displacement due to the properties of the power divider, and for the other, the motions add together with the same sign.

In the case of radiation along a normal, the series dividers are worse than parallel dividers, but with a deflection from the normal through an angle of ± 60°, the degradation of the characteristics is approximately the same and does not exceed 0.25 dB for the series circuit.

If the trunk feeder is a dispersion system, then:

$$\Delta f \approx 2\theta_{0.5}\,\lambda/\lambda_\Phi \qquad (2.35)$$

in the case of a long pulse with a changing frequency; and:

$$\Delta f \approx 4\theta_{0.5}\,\lambda/\lambda_\Phi \qquad (2.36)$$

in the case of a short pulse, i.e., the characteristics of the array are degraded.

Optical Circuit Configurations. When using an optical power division configuration, the frequency properties of an antenna array depend on the relative focal distance. If the focal distance is large (Figure 2.41), then the properties of an optical power divider approach the properties of a parallel circuit with feeders of equal length, though if the focal distance is small, the properties of the optical power divider approach those of a series configuration with center excitation. Since with a beam deflection through a maximum angle of ± 60° from a normal to the array aperture, the parallel circuit properties differ insignificantly from the properties of a series, center fed configuration, the frequency properties of optical power dividers in the case of wide angle scanning are practically the same as the properties of a parallel feed circuit with feeders of equal length.

TABLE 2.3.

Type of Power Divider Тип делителя мощности	Bandwidth Полоса частот, %	
	Длинные импульсы Long Pulses	Короткие импульсы Short Pulses
Параллельный двоично-этажный (1)	$2\theta_{0,5}$	$4\theta_{0,5}$
Последовательный: питание с конца (2)	$\frac{2\theta_{0,5}}{1+\lambda/\lambda_\Phi}$	$\frac{4\theta_{0,5}}{1+\lambda/\lambda_\Phi}$
питание с середины	$2\theta_{0,5}\lambda/\lambda_\Phi$	$4\theta_{0,5}\lambda/\lambda_\Phi$
Оптический OPTICAL	$2\theta_{0,5}$	$4\theta_{0,5}$

Key: 1. Parallel double stepped divider;
2. Series: end fed;
center fed.

The indicated results are summarized in Table 2.3. They correspond to a scan sector of ± 60° with a permissible drop in the directivity of no more than 1 dB.

2.8. Switched Scanning

The beam position of a pencil beam antenna array is controlled by changing the phase relationships between the currents in the radiating elements. A system of phase shifters, inserted in the feeder system exciting the radiators can be used for this purpose.

The major drawbacks to electrically controlled antennas with phase shifters, which provide for a continuous phase change in the electromagnetic oscillations (ferrite, semiconductor, ferroelectric phase shifters, etc.) are the instability (especially the temperature instability), the complexity of the control circuits and the high requirements placed on the stability of the phase shifter power supplies. These deficiencies also exist in digital control systems, when individual operating points on the characteristic of a continuous phase shifter are employed.

The indicated drawbacks are eliminated to a considerable extent with the switched technique of directional pattern control proposed by L.N. Deryugin in 1960. The essence of the switching method consists in dispensing with phase shifters having a continuous phase change and using switchers and switched phase shifters, at the output of which the phase of the electromagnetic oscillations takes on definite fixed values. The antenna beam control in this case reduces to the simplest operations of switching radiators or feeder system branches on and off.

The stability of switched antennas is due to the fact that the phase control elements (semiconductors, ferrites, ferroelectrics) operate in a mode in which only the extreme portions of their characteristics are used. Moreover, switched antennas can have a simpler controller than a conventional antenna with a parallel circuit configuration for the continuous phase shifters. The latter is related to the fact that the position of the beam in space is not governed by the control voltage, which is different for different antenna phase shifters, but only by its presence at particular switchers.

However, switched antennas also have a number of deficiencies, the most important of which is the presence of phase errors which arise because of the fact that the radiator excitation phases change in steps and can assume only definite values. This entails a reduction in antenna efficiency, an increase in the sidelobe radiation level and a jump-like motion of the beam.

Among the various methods of constructing switched antennas, one can single out the two most characteristic approaches. In the first, each radiator has a definite set of phases, from which the selection of the requisite phase is made by means of switching the switched phase shifter. With the second method, several radiators are placed in each section of the antenna with a length of λ/2, where these radiators are excited with different phases, and they are selectively turned on. Some of the aspects of designing switched antennas based on the first approach will be presented in § 2.10, since the realization of antennas with switched radiators encounters serious difficulties related to the necessity of placing a large number of radiating elements in a small portion of an antenna and considerably retarding the phase velocity of the electromagnetic waves in the feeder which excites the radiators.

2.9. Switched Phase Shifters

Switched phase shifters are the major component of phased antenna arrays. They can number up to several tens of thousands in highly directional scanning arrays. In this case, the spacing between the phase shifters usually falls in a range of 0.5 λ to λ.

Switched phase shifters should have a high efficiency, sufficient electrical strength, stability of the characteristics and consume the minimum power needed for controlling their operation.

Moreover, the following requirements are placed on the structural design of phase shifters: structural simplicity and suitability for production; small size and weight; high reliability.

So-called digital phase shifters are used in the majority of cases to control the excitation phase of the radiators in a phased array. A feed-through digital phase shifter is broken down into p stages, each of which can be in one of two states, characterized by the phase shift being introduced: 0 or $\pi/2^{m-1}$, where m is the number of the stage. It is sufficient to employ p control signals which take on values of 0 or 1 to select any of $M = 2^p$ possible states of the phase shifter. Then, for example, in a two place phase shifter, a signal of 00 corresponds to a zero phase shift, a phase shift of 90° has a control signal of 01, etc. A reflective phase shifter for reflecting arrays can be derived from a transmissive type by means of shorting the output. To preserve the phase shifts, it is obviously necessary to cut the phase shift realized by each stage in half, since the wave in a reflective phase shifter passes through each stage twice.

In ferrite phase shifters, the phase shift is due to the change in the magnetic permeability of the ferrite with the action of an external magnetic field. The switched elements of the majority of semiconductor phase shifters are PIN diodes. Since the diodes usually operate in the ultimate modes, the tolerances for the amplitude of the control signals are not stringent.

Merits of semiconductor phase shifters are the small size and weight, the fast switching speed, the simplicity of the control devices, their reciprocity and thermal stability. Semiconductor phase shifters are manufactured in stripline and microstripline variants to reduce the size and weight, and improve the stability, which makes it possible to use printed circuit technology. Advantages of ferrite phase shifters are the relatively high microwave power level, since a bulk ferrite medium is used to control the phase; lower losses, since waveguides are usually employed in making ferrite phase shifters, the losses in which are less than in lines using a T-mode, as well as a lower SWR. The switching speed of diode and ferrite phase shifters amounts to 0.1 psec--10 μsec and 0.1--30 μsec respectively.

None of the indicated types of phase shifters has an absolute advantage over the others and the use of a particular type depends on many factors: the power level, range of working temperatures, and requirements placed on switching speed and stability. It must be noted that the high cost of phased antenna arrays, as a consequency of the large number of microwave components used in them, limits the wide scale application of phased array systems. Information of phase shifters for phased antenna arrays is given in [2].

Semiconductor phase shifters have been developed at the present time which operate at a transmitted power level in a CW mode on the order of hundreds of watts and on the order of tens of kilowatts in a pulsed mode. In this case, the losses in a three place phase shifter in the ten cm band, for example, do not exceed 1 dB [2].

Ferrite phase shifters at wavelengths shorter than 5 cm have lower losses than semiconductor types. The losses per place amount to about 0.3 dB in the 3 cm band, while the pulsed and average transmitted powers are about 500 KW and 1,000 W respectively [2]. The advantage of ferrite phase shifters of some types is an internal memory, which makes it possible to control the phase by means of feeding in short pulses. In the intervals between pulses, the phase shifter remembers the phase shift, and no energy is expended to maintain it.

In contrast to ferrite phase shifters, semiconductor types using PIN diodes do not have such a property, and this is a drawback to them. To preserve the requisite phase shifts, it is necessary to expend considerable power: up to several kilowatts with a large number of phase shifters. In fact, according to [013], the control power for a diode phase shifter is 0.1 to 5 W, while the energy needed to switch a ferrite phase shifter is 20 to 2,000 microjoules.

Phase shifters using field effect diodes and resistive gates are being developed at the present time [2], the utilization of which will make it possible to reduce the control power for phase shifters from several kilowatts down to a few watts. The voltage provided by standard logic gates is altogether sufficient for the switching of these elements.

2.10. Discrete Phase Shifters and the Suppression of Switching Lobes

In the case of digital phasing, the phase distribution which can be realized in an array can be represented in the following form:

$$\Phi_{real} = \Phi_{initial} + \nu\Delta \qquad \Phi_{реал} = \Phi_{нач} + \nu\Delta, \tag{2.37}$$

where $\Phi_{initial}$ is the initial phase distribution corresponding to the case where all of the array phase shifters are in the same position, taken as the starting position; ν is the number of sequential switchings of a phase shifter with the minimal discrete step of a phase change; Δ is the minimal phase jump (discrete step) which can be realized by a phase shifter.

On the other hand, the feasible phase distribution differs from the requisite distribution because of the discrete nature of the phase shifter by the amount of the so-called switching phase errors:

$$\Phi_{real} = \Phi_{req} + \delta\Phi \qquad \Phi_{реал} = \Phi_{треб} + \delta\Phi. \tag{2.38}$$

In the majority of cases, the phasing is accomplished so that the phase errors are minimal. With such phasing, the maximum value of the phase errors does not exceed $\Delta/2$.

In accordance with the indicated phasing principle:

$$\nu = E\,[(\Phi_{треб} - \Phi_{нач})/\Delta + 0{,}5], \tag{2.39}$$

where E[X] is the integer part of X.

In the case of digital phasing, the directional pattern of an antenna array having N x Q radiators is:

$$f(\theta, \varphi) = F(\theta, \varphi) \sum_{n,\,q=1}^{N,\,Q} A_{nq}\, e^{j\left(\Phi_{треб} + \Phi^{п}_{nq} + \delta\Phi_{nq}\right)}, \tag{2.40}$$

where A_{nq} is the excitation amplitude of the nq-th radiator; Φ^{π}_{nq} is the spatial phase shift.

We shall make use of the Poisson summing formula and the Fourier expansion for the factor $e^{j\Phi\delta}$, treating it as a function of $u = \Phi_{req} - \Phi_{initial}$, which as it is easy to convince oneself, is periodic. If the phased antenna array takes the form of a system of radiators positioned at the nodes of a coordinate grid of a system of coordinates X, Y, then the directional pattern is [1]:

$$f(0,\varphi)=\frac{\sin\Delta/2}{\Delta/2}F(\theta,\varphi)\sum_{p,t,h=-\infty}^{+\infty}\frac{(-1)h}{Mh+1}\int_{X^{(1)}}^{X^{(2)}}\int_{Y^{(1)}}^{Y^{(2)}}\frac{A\,e^{j\Phi_{pth}}}{d_x d_y}d_x\,d_y, \tag{2.41}$$

where

$$X^{(1)}=-X^{(2)}=Nd_x/2;\,Y^{(1)}=-Y^{(2)}=Qd_y/2;$$

$$\Phi_{pth}=\Phi_{\text{треб}}+\Phi^{\text{п}}+Mh(\Phi_{\text{треб}}-\Phi_{\text{нач}})+2\pi p(X-X_1)/d_x+$$
$$+2\pi t(Y-Y_1)/d_y;$$

$A(X,Y)$ is a continuous function which satisfies the condition $A(X_nY_q) = A_{nq}$, where X_n and Y_q are the coordinates of the nq-th radiator; $M = 2\pi/\Delta$.

The sum of the terms of series (2.41) having a subscript of h = 0 defines the directional pattern of an equivalent array: an array without switching phase errors. The sum of the terms in (2.41) having a subscript of p = t = 0 represents the directional pattern of a switched antenna array with a continuous distribution of the radiators. The terms in the series having subscripts of p = t = h = 0 apply to the directional pattern of a continuously excited antenna without switching phase errors. The terms in the series with subscripts of t ≠ 0, p ≠ 0 and h = 0 correspond to the diffraction maxima of the directional pattern of an array without switching phase errors. The terms of the series with subscripts of h ≠ 0 and p = t = 0 define the additional lobes which arise in the directional pattern of the array because of the presence of switching errors. We shall call these lobes switching lobes in the following. Terms in the series having subscripts of h ≠ 0, p ≠ 0 or t ≠ 0 define the supplemental lobes in the directional pattern of the array due to both the discrete nature of the operation of the phase shifters as well as the discrete nature of the layout of the radiators. We shall call the indicated lobes combination lobes in the following. Because of the presence of switching phase errors, the directional gain of a switched antenna array is reduced:

$$D=D_0\left(\frac{\sin\Delta/2}{\Delta/2}\right), \tag{2.42}$$

where D_0 is the directional gain of an equivalent antenna array without switching phase errors (2.11).

One of the drawbacks to phased arrays with discrete phase shifters is the presence of switching and combination lobes, which in the case of discrete phase change steps of $\Delta = \pi/2 - \pi/4$ can be of a rather high level. For this reason, one of the problems of practical interest is the suppression of the indicated lobes.

The concept of switching and combination lobe suppression consists in the following. The configuration of these lobes, in accordance with (2.41), depends on $\Phi_{initial}$, where $\Phi_{initial}$, as can be seen from the given formulas, does not influence the directional pattern of an array without switching phase errors, defined by the sum of the terms of series (2.41) having a subscript of h = 0. Therefore, it is necessary to choose Φ_{initial} so that the switching and combination lobes have a minimal level. This is achieved with the uniform "erosion" of the indicated lobes in space, i.e., the optimal shape for lobe suppression is rectangular. In this case, the extent of the suppressed lobes should be such that they do not overlap one another, since when the lobes are superimposed in space, their total level is increased. It can be demonstrated that with such deformation of the combination lobes, their extent is proportional to the subscript h. Therefore, such a value of Φ_{initial} cannot be chosen so that the indicated condition is met simultaneously for all h. As a result, optimal suppression can be provided only for lobes with a definite value of the subscript h. Estimates of the level of additional sidelobe radiation, due to switched phase errors, show that with optimal suppression of the switching lobes with h = ± 1, the level of the overall sidelobe radiation due to the switched phase errors will be minimal.

If it is required that the absolute value of the integrals of (2.41) not depend on the angular coordinates, then in the case of a linear array, one of the equations for the determination of Φ_{initial} assumes the form [1]:

$$d^2\Phi_{\text{нач}}/dx^2 = 2\pi A^2/-\mathrm{j}f'^2_{ph}\,d^2_x\,Mh, \tag{2.43}$$

where f'_{ph} is the level of the uniformly washed-out lobe.

As has been demonstrated, maximum suppression of switching and combination lobes occurs in the case where the washed-out lobes are not superimposed on each other in space. By employing this condition, one can derive a second equation for the determination of the minimum value of f'_{ph} and the optimal function Φ_{initial} [1]:

$$Mh\left[\frac{d\Phi_{\text{нач}}(X^{(2)})}{dX} - \frac{d\Phi_{\text{нач}}(X^{(1)})}{dX}\right] = \frac{2\pi}{d_x}. \tag{2.44}$$

Equation (2.44) in conjunction with (2.43) completely defines the optimal initial phase distribution which assures the maximum suppression of the switching and combination lobes, as well as the level of the suppressed lobes.

Solving the system of equations (2.43) and (2.44), we derive the following for a uniform amplitude distribution (h = ± 1):

$$\Phi_{\text{нач}} = \kappa\gamma x^2; \quad q_{h=\pm 1} = 1/(M \pm 1)\sqrt{N}, \tag{2.45}$$

where

$$\gamma = \lambda/(2d_xNM); \tag{2.46}$$

$q_{h=\pm 1}$ is the level of the suppressed switching and combination lobes.

The overall sidelobe radiation level which is due to switching phase errors is:

$$q_\Sigma = 2/M\sqrt{N}. \tag{2.47}$$

In the case of a cosine amplitude distribution:

$$\Phi_{\text{нач}}=\frac{2\pi}{MNd_x^2}\left[\frac{X^2}{2}-\left(\frac{Nd_x}{2\pi}\right)^2\cos\frac{2\pi X}{Nd_x}\right], \tag{2.48}$$

$$q_\Sigma=\frac{\pi}{\sqrt{2}}\,\frac{1}{M\sqrt{N}}.$$

The results obtained for a linear array are easily extrapolated to two dimensional planar arrays. For example, for a planar rectangular array with the radiators arranged at the nodes of an orthogonal coordinate grid, with a uniform amplitude distribution:

$$\Phi_{\text{нач}}=\kappa\,(\gamma_x X^2+\gamma_y Y^2), \tag{2.49}$$

where $\gamma_x = \lambda/2d_x^2NM$; $\gamma_y = \lambda/2d_y^2QM$; N and Q are the number of rows and columns in the planar array respectively.

The level of the suppressed combination and switching lobes of the directional pattern of a planar array is:

$$q_\Sigma = 2/M\sqrt{NQ}. \tag{2.50}$$

Quite substantial suppression of the lobes due to the discrete change in the phase can be obtained in arrays with a large number of radiating elements. This makes it possible in some cases to employ coarser, and consequently, simpler and less expensive phase shifters with lower losses. The optimal initial phase distribution can be produced either by means of phase shifters with a fixed phase value, inserted at the output of the power divider, or by means of phase shifters for an array using a particular change in the phasing algorithm.

2.11. Beam Jumps in a Switched Array

The main lobe of the directional pattern of an equivalent array without switching phase errors is oriented precisely in a specified direction, θ_{main}. When switching lobes are present in the immediate vicinity of the main lobe, the maximum of their sum, i.e., the maximum of the array directional pattern, is slightly shifted relative to the direction θ_{main}. This shift, which is due to the switching phase errors, determines the error in setting the array beam in a specified direction. The error depends on the level of the switched beams, and consequently, on the discrete phase change step, Δ. Moreover, the position of the initial phase readout has an impact on the precision in setting the beam. Thus, if one of the end radiators of a linear array is chosen as the initial coordinate point, the beam steering precision proves to be four times higher than the precision with phase readout from the center of the array.

Beam steering precision is directly related to its jump-like motion, which is due to the discrete change in the phase. The average value of a jump change, when the readout origin is positioned in the center of the array, is:

$$\delta\theta = 2\theta_{0,5}\,\Delta/2N. \tag{2.51}$$

It is also necessary to note that with the same beam travel speed, the switching frequency of the end phase shifters will be different, depending on the position of the phase readout origin. This must be taken into account when assessing the operational speed of a phase shifter.

2.12. Design Procedure

The directional gain or directional pattern width, the scan sector, the sidelobe level and the beam steering precision are usually specified.

The specified sidelobe level and the requisite beam steering precision govern the discrete phase change step, i.e., the number of phase shifter positions and the amplitude distribution in an array.

The antenna dimensions are determined from the specified values of the directional gain or directional pattern width, the selected amplitude distribution, as well as the scan sector using the formulas of Table 2.1, as well as formulas (2.8) and (2.9). The spacing between the radiators and the number of phase shifters is found based on the specified scan sector by means of formulas (2.3) - (2.6).

It is expedient when determining the number of positions of the discretely switched phase shifters with respect to the maximum level of the sidelobes to represent the specified sidelobe level in the form of the sum of two terms, one of which is taken as the maximum switching lobe level, while the other is taken as the antenna sidelobe level without switching phase errors. Then one can determine Δ from the value of the first term of formulas (2.47) and (2.50) and the nature of the amplitude distribution in the array in accordance with the data of Table 2.1, based on the value of the second term.

The maximum level of the switching lobes is chosen so that the number of requisite positions of the phase shifter, $2\pi/\Delta$, is the least. This makes it possible to use phase shifters of the simplest structural designs. On the other hand, one cannot choose a second term which is too small, i.e., the level of the sidelobes of an ideal antenna, since this necessitates the use of amplitude distributions which fall off sharply towards the edges, something which leads to the necessity of increasing array dimensions to assure the specified directional pattern width or specified directional gain. A compromise solution is found, depending on the specific requirements based on the antenna array in each case.

Then the scheme is chosen for the energy distribution and the configuration of the phase shifters, the type of phase shifters, radiators, coupling elements, etc. and these assemblies are designed; the directional pattern is calculated and then the structural design is worked out.

3. FREQUENCY SCANNING ANTENNAS*

3.1. Fundamental Relationships for a Frequency Scanning Linear Radiator Array [07, 010, 1, 2]

Frequency control of an antenna beam is one of the techniques of electrical control and is based on changing the electrical spacing between radiators excited by a traveling wave with a change in the generator frequency. With this beam steering technique, a generator which is electrically tuned in a wide range of frequencies is needed to scan space in a rather large sector.

In microwave antennas with frequency beam control, the radiators are, as a rule, positioned directly in the exciting system. Linear arrays of radiators formed by slits cut in one of the walls of a rectangular waveguide are shown in Figure 3.1. A two-dimensional array of radiators is needed to obtain a controlled narrow directional pattern. Such an array can be created from linear arrays, arranged in a definite manner on a specified surface. Some of the possible variants of such antennas are shown in Figure 3.2.

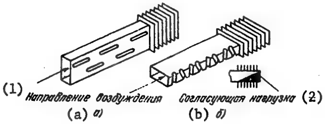

Figure 3.1. Slitted waveguide radiator arrays.

Key: 1. Direction of excitation;
2. Matching load.

In antennas which take the form of linear radiator arrays, the excitation is most often accomplished using series or parallel configurations (Figure 3.3). The direction of radiation of a linear array with an equally spaced arrangement of the radiators is determined by the equation:

$$\sin\theta = \gamma l_{\text{д}}/d - p\lambda/d, \qquad 3.1$$

where θ is the beam deflection angle from the normal to the axis of the array of radiators; $\gamma = c/v$ is the phase velocity retardation in the channelizing system exciting the radiators; $c = 3 \cdot 10^8$ m/sec; λ is the generator wavelength; $p = n + \Phi/2\pi$, $n = 0, \pm 1, +2, \ldots$, is the beam number; Φ is the fixed phase shift between adjacent radiators, due to the insertion of the supplemental phase shifters

---

* Questions of frequency scanning antenna design and theory were most completely treated for the first time by L.N. Deryugin [010].

(Figure 3.3c); l_d is the geometric difference in the lengths of the channelizing systems of two adjacent radiators; d is the spacing between the radiators; t is the period of the retarding interaction system.

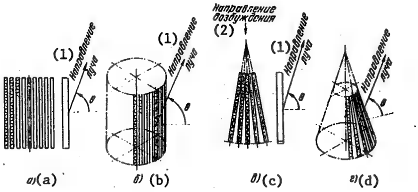
Направление возбуждения
(2)
(1)
Направление луча
θ
а)(a)
б) (b)
в)(c)
г)(d)

Figure 3.2. Antennas formed by linear two-dimensional arrays of radiators.

Key: a. Planar; b. Arranged on a cylindrical surface; c. Planar "fan-shaped"; d. Arranged on a conical surface.

1. Beam direction;
2. Direction of excitation.

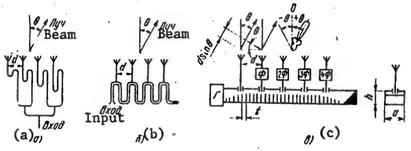
θ
Луч
Beam
d
Вход
Input
(a)а)
б)(b)
dsinθ
0
-θ
+θ
Φ
2Φ
3Φ
4Φ
Г
t
h
a
в) (c)

Figure 3.3. The excitation of a linear radiator array.

Key: a. Using a parallel configuration;
b. Using a series configuration;
c. With a periodic retarding interaction system.

When the generator frequency changes, because of the dependence of γ and λ/d on the frequency f, the radiation angle changes and the antenna beam moves in space.

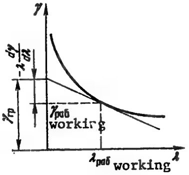

Figure 3.4. The dispersion characteristic $\gamma(\lambda)$ of a periodic interaction system.

The angular frequency sensitivity of the antenna is the term for the rate of change in the antenna beam position in space with a change in the frequency (the wavelength):

$$A=\frac{\partial\theta}{\partial\lambda/\lambda}=\frac{0{,}573}{\cos\theta}\left(-\frac{l_d}{d}\gamma_{rp}+\sin\theta\right), \qquad (3.2)$$

where $\gamma_{rp} = [\gamma_{gr}] = c/v_{gr}$ is the retardation of the group velocity of the wave propagating in the channelizing system; the coefficient of 0.573 is introduced when converting the angular frequency sensitivity from dimensionless units to degrees for the percentage change in frequency.

If follows from expression (3.2) that the angular frequency sensitivity depends on the beam direction, the dispersion properties of the system and the ratio l_d/d. The greater [illegible] and $(l_d/d)\gamma_{gr}$, the greater the angular frequency sensitivity.

The retarding of the group and phase velocities are related by the expression:

$$\gamma_{gr} = \gamma_{rp} = \gamma - \lambda d\gamma/d\lambda. \qquad (3.3)$$

If the dispersion characteristic of the channelizing system is known, $\gamma = \gamma(\lambda)$ (Figure 3.4), then γ_{gr} is determined graphically by the segment on the ordinate axis, intercepted by the tangent to the curve $\gamma(\lambda)$, run through the point corresponding to the value of γ in the system.

The slow-down in the group velocity γ_{gr} is also related to the power P flowing through the system and the per unit length electromagnetic energy W accumulated in the system:

$$\gamma_{gr} = cW/P \qquad (3.4)$$

where $P = v_{gr}W$.

To improve the angular frequency sensitivity of an antenna, it is necessary to employ channelizing systems with a large value of γ_{gr}, something which in turn can be achieved by increasing the ratio W/P.

The ultimate value of the power flowing along the channelizing system is:

$$P_{ult.} = W_{ult.} v_{gr} = cW_{ult.}/\gamma_{gr} = P_{\text{пред}} = W_{\text{пред}} v_{\text{гр}} = cW_{\text{пред}}/\gamma_{\text{гр}}, \quad (3.5)$$

where $W_{ult.}$ is the ultimate value of the per unit length electromagnetic energy of the system, which is limited by the effective cross-section of the system and the electrical strength.

Expression (3.5) makes it possible to establish the relationship of the power $P_{ult.}$ to the angular frequency sensitivity A, since both of these quantities depend on γ_{gr}, and to draw the conclusion that with an increase in A, the ultimate power always falls off. For a specified value of A, the increase in the ultimate power for any system can be achieved only by increasing W_{ult}. However, it must be stipulated that in a number of cases, the ultimate which can be passed is limited by the electrical strength of the radiators.

The thermal losses in the walls of the channelizing system are due to the attenuation of the wave propagating in it. The attenuation coefficient is:

$$\alpha = P_{loss}/2P = \alpha = P_{\text{пот}}/2P, \quad (3.6)$$

where P_{loss} is the power of the losses per unit length of the system.

The attenuation in the channelizing system at the distance of a wavelength taking expression (3.5) into account, is defined as:

$$\alpha\lambda = \gamma_{\text{гр}}\pi/Q, \quad (3.7)$$

where $Q = \omega W/P$ is the quality factor of the channelizing system ($\omega = 2\pi f$).

For retardive periodic structure type channelizing systems with a period of t, the Q does not exceed $Q_{max} = t/\delta$ (δ is the depth of field penetration into the metal). In actual structures, $Q = 0.3Q_{max}$, which makes it possible to estimate the anticipated losses in a system.

It is also not difficult to draw the conclusion from expressions (3.2) and (3.7) that an increase in the angular frequency sensitivity is always accompanied by a rise in the system losses. The presence of losses in a channelizing system places a limitation on the length of a radiator array, since with an increase in the length, its efficiency falls off, which in turn limits the generation of narrow directional patterns by an array of radiators.

The directional pattern width and the efficiency also depend on the distribution of the power radiated along the array. The exponential distribution has become widespread in practice (each element of the array radiates an identical fraction of the traveling wave power fed to it), as well as a uniform distribution (each element radiates the same power) and other special kinds of distributions (for example, symmetrical relative to the array center and falling off towards it edges).

In the case of uniform distribution, the efficiency of a radiator array is governed by an expression which is justified when $\alpha\lambda \ll 1$ (which is usually observed in practice):

$$\eta_A = \left[\exp(-2\alpha L) - \frac{P_L}{P_0}\right]\frac{2\alpha L}{1-\exp(-2\alpha L)}, \tag{3.8}$$

where P_0 is the power at the antenna input; P_L is the power at the end of the antenna; L is the antenna length.

The half power level directional pattern width for the case of radiation close to the normal to the axis of the array is determined from the formula:

$$2\theta_{0.5}\ [\text{degrees}] = 50.7\lambda/L \qquad 2\theta_{0,5}\ [\text{град}] = 50{,}7\lambda/L. \tag{3.9}$$

Taking expressions (3.8) and (3.9) into account, we derive the relationship between $2\theta_{0.5}$, α and η_A:

$$\eta_A = \left[\exp\left(-11{,}7\frac{\alpha\lambda}{2\theta_{0.5}}\right) - \frac{R_L}{P_0}\right]\frac{11{,}7\dfrac{\alpha\lambda}{2\theta_{0.5}}}{1-\exp\left(-11{,}7\dfrac{\alpha\lambda}{2\theta_{0.5}}\right)}. \tag{3.10}$$

In the case of an exponential distribution:

$$\eta_A = \left(1-\frac{P_L}{P_0}\right)\left(1+\frac{2\alpha L}{\ln(P_L/P_0)}\right). \tag{3.11}$$

The directional patttern width depends on the relative power getting through to the end of the antenna. When $P_L/P_0 = 0.05$ (the aperture utilization coefficient is 0.83 in this case):

$$2\theta_{0.5}\ [\text{degrees}] = 54.4\lambda/L \tag{3.12}$$

$$2\theta_{0,5}\ [\text{град}] = 54{,}4\lambda/L.$$

Taking expressions (3.11) and (3.12) into account, we obtain the following when $P_L/P_0 = 0.05$:

$$\eta_A = 0{,}95\,(1 - 4{,}17\alpha\lambda/2\theta_{0,5}). \tag{3.13}$$

(3.13)

When determining directional pattern width using formulas (3.9) and (3.12), the quantities λ and L have identical units of measurement.

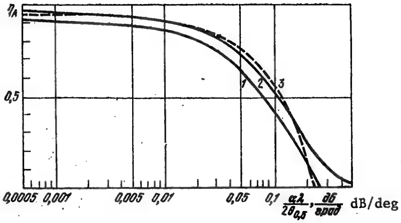

Figure 3.5. The antenna efficiency as a function of the ratio of attenuation times wavelength to the directional pattern width.

Curves for $\eta_A(\alpha\lambda/2\theta_{0.5})$, plotted using formulas (3.10) and (3.13), are shown in Figure 3.5. Curves 1 and 2 were obtained for radiator arrays with a uniform distribution where $P_L/P_0 = 0.05$ and $P_L/P_0 = 0$ respectively. Curve 3 was plotted for an exponential distribution where $P_L/P_0 = 0.05$. As follows from the graph, an array with an exponential distribution has a higher efficiency: from 0.9 to 0.4. Moreover, such an array permits switching the direction of excitation, something which makes it possible to increase the beam steering sector with the same frequency change and efficiency.

The working sector of space scanned by the beam of a radiator array can fall only within the bounds of the transmittance sector of the periodic structure used as the channelizing system (Figure 3.3c). All periodic structures used in frequency controlled antennas are bandpass filters, having frequency transmittance bands, to which the angular transmittance sectors correspond. The width and orientation of these sectors depend on the type of periodic structure, the specific features of the radiators and the number of cells in the interaction structure between the radiators.

As follows from expression (3.1), the beam direction for a radiator array in space depends on the supplemental fixed phase shift Φ in the exciter unit between the adjacent radiators. Phase shifts of the same angle when making the transition to each subsequent radiator are accomplished by fixed phase shifters. For example, in the form of line sections of equal length running to the radiators (see Figure 3.3a). An additional phase shift π can be realized rather simply. For example, when a rectangular H_{10} mode waveguide is used as the channelizing system, a phase shift of π can be obtained by using radiating slots, which are coupled in an alternating phase fashion to the waveguide field.

The shape of the main lobe of the directional pattern changes when the beam moves in space. As it approaches the axis of the array, the main lobe widens and becomes asymmetrical with respect to the direction θ. The change in the width of the main lobe will be small when scanning in an angular sector close to a normal to the axis of the array and increases sharply as it approaches the axis of the array. It is theoretically possible, but difficult in practice to preserve a constant width of the main lobe during wide angle scanning.

The half power level width of the main lobe, taking its asymmetry into account, for an array of length $L \gg \lambda$, with a uniform distribution of the radiated power, can be estimated from the expression:

$$2\theta_{0,5} = \arcsin(0{,}443\lambda/L + \sin\theta) + \arcsin(0{,}443\lambda/L - \sin\theta). \qquad (3.14)$$

In the case of axial radiation, the width of the main lobe proves to be $2.14\sqrt{L/\lambda}$ times greater than the width of the main lobe in the case of radiation along a normal.

The change in the width of the main lobe during its travel can be explained by the change in the effective length*, L_{eff}, of an array of radiators and the amplitude distribution along it. In a first approximation, for angles of $\theta < 70$-75 degrees (depending the length of the array L), L_{eff} can be determined as the projection of the array length L onto a direction perpendicular to the main lobe of the diredtional pattern:

$$L_{eff} \approx L\cos\theta \qquad (3.15)$$

When $L/\lambda \geq 10$, this assumption is quite well justified. Thus, the error in the determination of L_{eff} using formula (3.14) when $L/\lambda = 10$ and $\theta = 70$ degrees amounts to about 1.5 percent with respect to the value of L_{eff} determined from a more rigorous formula (see [07, p. 354]). In some cases, the scan sector can be limited by the permissible widening of the main lobe.

---

*The effective length is understood to be the length of a uniform in-phase linear array which yields a directional pattern at the half-power level of the same width as the array under consideration.

An integral part of a frequency scanning antenna is a frequency tunable generator. The precision in determining the beam position in space depends on the stability and precision in setting the generator frequency. There are centimeter and decimeter band generators at the present time, which can be electrically tuned in a rather wide range of frequencies (from ±10 percent up to an octave). The frequency tuning range of a generator depends to a considerable extent on its power and working frequency. Correspondingly, there are also wideband amplifiers which can be used in the receiving equipment.

In a number of cases, one can use exciters to excite an antenna which are designed in a complex circuit configuration and contain a comparatively low power generator with a wide frequency tuning range and broadband power amplifiers. When the requisite range of working frequencies is wider than the passband of a single amplifier, several amplifiers are employed; in this case, each of them operate in a band of working frequencies set aside for it. Such an approach can be used where it is necessary to change the beam direction in space while preserving its scanning sector.

However, when designing a frequency scanning antenna, one must remember that the use of a wide band of frequencies requires the use of radiators, transition and decoupling elements, etc., having a wide passband and possessing a low attenuation in this band. Otherwise, considerable changes may be observed in the power radiated by the antenna and the shape of the directional pattern when the frequency changes.

3.2. Channelizing Systems of Frequency Scanning Antennas [010]

In the structural designs of centimeter band frequency scanning antennas, the radiators, as a rule, are placed directly in the exciting channelizing systems (for example, a linear array of slotted radiators, with the slits cut in one of the walls of a rectangular waveguide), which can be designed around waveguides, coaxial lines, etc. The electrical properties of these channelizing systems are evaluated by the slow-down in the phase velocity γ, the dispersion characteristic $\gamma = \gamma(\lambda)$ and the attenuation factor α.

The major requirements placed on channelizing systems are as follows:

1. The retardation of the phase velocity γ should not be large, since with an increase in γ, the losses in the channelizing system increase, and greater accuracy is required in the manufacture of the system. The latter is related to the fact that minor relative changes can lead to the disruption of normal antenna operation in a number of cases.

2. The attenuation factor α should be as low as possible, since the antenna efficiency depends on its value, as well as the possible directional pattern width (for a specified efficiency).

3. The channelizing system should allow for the arrangement of radiators at a spacing of $d \simeq \lambda/2$ in an axial direction to avoid a multiple lobed directional pattern when the main lobe is deflected towards the axis of the array.

4. In a two-dimensional array, the transverse dimensions of the channelizing system should be such that the spacing between the radiators of adjacent linear arrays does not exceed . Otherwise, the directional pattern will have multiple lobes.

5. The channelizing system should have as small a size and weight as possible. This is especially important for aircraft antennas.

Waveguide Channelizing Systems (Figure 3.6).

H_{10} Mode Rectangular Waveguide. The retardation γ falls in a range of from 0 to 1. In practice, $\gamma = 0.36\text{--}0.86$. The angular frequency sensitivity of the waveguide is low and fluctuates on the average from tenths to units of degrees per percent change in frequency. The attenuation factor in the 3 cm band amounts to about 0.5 dB/m, which with an efficiency of $\eta_A = 90$ percent makes it possible to obtain a directional pattern width of about 1°.

Rectangular Waveguide Partially Filled with a Dielectric. The retardation γ can be regulated by changing the thickness of the dielectric and its dielectric permittivity ε. The slowdown usually falls in a range of 0.7 to 1.5. The attenuation factor is several times greater than for a regular waveguide (α is about 1.2 dB/m in the 3 cm band), and depends on the loss angle of the dielectric and its thickness h. A drawback to the system is the requirement that the dielectric properties of the dielectric employed be homogeneous.

Waveguide with a Finned Structure. The retardation is $\gamma > 1$, and can in practice be made close to unity and even considerably higher. The system has considerable dispersion and high angular frequency sensitivity. The attenuation factor in the 3 cm band for small values of γ ($\gamma = 1$--2) is about 2 dB/m. The system has a high weight as compared to a regular waveguide and requires a high fabrication precision.

Serpentine Waveguide. The retardation is $\gamma > 1$ and can be regulated in a considerable range by changing the length ($L + \Delta L_{equiv}$), and in this case, the angular frequency sensitivity is also adjusted in a wide range. The attenuation factor in this system in the 3 cm band is less than in systems with the same angular sensitivity, for example, in waveguide with an internal finned structure) and amounts to about 0.7 dB/m when $\gamma \approx 2.5$. The considerable weight, great length ($L + \Delta L_{equiv}$) and fabrication complexity must be numbered among the drawbacks to the system.

Helical Waveguide. The retardation is $\gamma > 1$ and is regulated by changing its geometric dimensions. The dispersion of the system is low. The attenuation factor in the 3 cm band is about 2.5 dB/m when $\gamma \approx 4$. A rectangular waveguide H plane bend is most frequently used, since this makes it possible to reduce the spacing between radiators.

Coaxial Channelizing Systems (Figure 3.7).

These are of interest in those cases where systems are needed having a poor dispersion and relatively simple control of the retardation. However, considerable attenuation is inherent in coaxial systems. Only a coaxial line partially filled with a dielectric (Figure 3.7b) represents an exception. A coaxial line with a finned structure on the inner conductor (Figure 3.7c) is distinguished from the remaining systems by the presence of sharply pronounced dispersion properties. The geometric dimensions of coaxial systems when they are used in the centimer band are small, which substantially limits the power they can carry.

When using periodic structures as channelizing systems, for example, a waveguide with a finned structure, a coaxial line with a disk-on-rod structure on the inner conductor, and serpentine and helical waveguides, one can obtain a high angular frequency sensitivity for an antenna. However, the considerable losses in such systems do not make it possible to design an antenna with a high efficiency and a narrow directional pattern. Moreover, these systems, as a rule, have considerable weight and are complex to manufacture, which limits the possibilities for their applications in a number of cases, especially in aircraft antennas.

A rectangular H_{10} mode waveguide channelizing system has a number of valuable qualities: low losses, relatively small size and weight, and a well mastered production technology. For this reason, linear arrays of radiators excited by this kind of channelizing system have become widespread in antenna engineering. The maximum theoretical scan sector of a waveguide antenna with radiators coupled to the waveguide field in an alternating phase fashion, without taking into account the frequency properties of the radiators and the elements used to couple to them, runs from -90° to +14° with a change in the retardation from 0.22 to 0.867 and a ratio of $\lambda/2a$ from 0.975 to 0.5. An average angular frequency sensitivity of -1.61° per percent and a change in the wavelength by a factor of 1.95 times correspond to the indicated scan sector. Switching the direction of the traveling wave in such an antenna makes it possible to cover a scan sector of 180°.

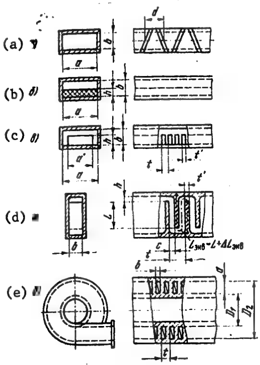

Figure 3.6. Waveguide channelizing system for frequency scanning antennas.

Key: a. Rectangular waveguide with slots, coupled to the H_{10} mode of the waveguide in an alternating phase fashion;
b. Rectangular waveguide, partially filled with a dielectric;
c. Rectangular waveguide with a finned structure placed in it;
d. Serpentine rectangular waveguide;
e. Helical rectangular waveguide.

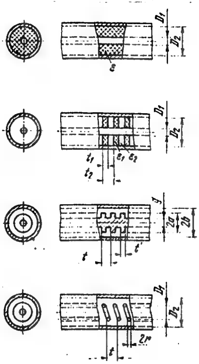

Figure 3.7. Coaxial channelizing systems for frequency scanning antennas.

Key: a. Filled with a dielectric;
b. With dielectric disks;
c. With a finned structure on the inner conductor;
d. Coaxial line with the inner conductor made in the form of a spiral.

We shall give the major relationships and design procedure for a frequency scanning slotted waveguide array, in which a regular rectangular H_{10} mode waveguide is used as the channelizing system. When other channelizing systems are employed, the design procedure will be somewhat different, since the expressions which characterize the relationship of the dispersion properties of systems to their geometric dimensions, as a rule, are rather complex. Moreover, the retardation in these systems is greater than unity, which, it goes without saying, is reflected in the recommendations for the choice of the antenna radiation zone.

3.3. The Frequency Scanning Slotted Waveguide Array [010, 2]

A slotted waveguide array (VShchR) is shown in Figure 3.1. A regular rectangular H_{10} mode waveguide is used as the channelizing system for such an antenna. The array radiators are slots cut in one of the waveguide walls. This antenna is excited from one end by a generator, and a matching load is connected to the other end to provide for antenna operation in a traveling wave mode.

We shall give the major characteristics of a regular waveguide with a H_{10} mode (see Figure 3.6a) as well as those which determine their relationship.

1. The phase velocity retardation is:

$$\gamma=\sqrt{1-(\lambda/2a)^2}, \tag{3.16}$$

where λ is the generator wavelength in cm; a is the cross-sectional dimension of the waveguide in the H plane in cm. The dispersion characteristic $\gamma = \gamma(\lambda/2a)$ is shown in Figure 3.8, plotted using formula (3.16).

2. The group velocity delay:

$$\gamma_{gr} = 1/\gamma \tag{3.17}$$

This follows from the well known relationship for a waveguide: $v_{gr}v = c^2$ or $\gamma_{gr}\gamma = 1$.

3. The ultimate transmitted power is:

$$\underset{\text{ultimate}}{P_{\text{пред}}}\overset{[\text{KW}]}{[\text{кВт}]}=\frac{abE^2_{\text{пред}}}{1{,}51}\sqrt{1-\left(\frac{\lambda}{2a}\right)^2}, \tag{3.18}$$

where b is the cross-sectional dimension of the waveguide in the E plane in cm; $E_{\text{пред}}$ $[E_{\text{ult}}]$ is the ultimately permissible electrical field intensity in the waveguide for the specified temperature, pressure and humidity, in KV/cm; a and λ are chosen in centimeters.

4. The attenuation factor is:

$$\alpha\underset{[\text{dB/m}]}{[\text{дБ/м}]}=793\left[1+2\frac{b}{a}\left(\frac{\lambda}{2a}\right)^2\right]\Big/ b\sqrt{\sigma\lambda\left[1-\left(\frac{\lambda}{2a}\right)^2\right]}\,. \tag{3.19}$$

Here σ is the conductance of the material of the waveguide walls in mhos/m; a, b and λ are chosen in centimeters.

5. The angular frequency sensitivity is:

$$A=\frac{\partial\theta}{\partial\lambda/\lambda}=\frac{0{,}573}{\cos\theta}(-\gamma_{\text{гр}}+\sin\theta)=\frac{0{,}573}{\cos\theta}\left(-\frac{1}{\gamma}+\sin\theta\right). \tag{3.20}$$

In accordance with formula (3.16), the retardation of the phase velocity can vary from 0 to 1, and it would seem that the angular frequency sensitivity can be made as great as desired. However, the range of change in γ which can be realized is considerably narrower. This is explained by the fact that when $\lambda \to \lambda_{cr} = 2a(\gamma \to 0)$, the losses increase sharply and the power P_{ult} falls off. The lower limit of γ can br found, if one assumes that the losses approximately double as compared to a conventional waveguide. In this case, $\lambda = 1.9a$ or $\lambda/2a = 0.95$ and $\gamma_{min} = 0.36$. The upper limit of λ is related to the requirement for H_{20} mode suppression, where this mode occurs when $\lambda = a$ or $\lambda/2a = 0.5$. Under these conditions, $\gamma_{max} = 0.867$. Thus, the retardation of the phase velocity γ is limited to values of $0.867 \geqq \gamma \geqq$ $\geqq 0.36$, while the retardation of the group velocity is limited to $2.77 \geqq \gamma_{gr} \geqq 1.15$.

The direction of radiation of a linear radiator array excited by a wave traveling along it is determined in accordance with equation (3.1) when $l_d = d$ using the formula:

$$\sin\theta=\gamma-n\lambda/d \tag{3.21}$$

for radiators coupled in phase to the waveguide field ($\Phi = 0$) and using the formula:

$$\sin\theta=\gamma-(n+0{,}5)\,\lambda/d \tag{3.22}$$

for radiators with alternate phase coupling to the waveguide field ($\Phi = \pi$).

The beam scanning with a change in frequency will occur by virtue of the change in γ and λ.

The curves for λ/d as a function of γ (the solid lines) are shown for convenience in analyzing and solving equations (3.21) and (3.22) in Figures 3.9 and 3.10 for various values of the parameter 2a/d, plotted from the relationship derived from the expression (3.16):

$$\lambda/d=\sqrt{1-\gamma^2}\,2a/d. \tag{3.23}$$

The grid of lines for λ/d is a function of γ is also shown in Figure 3.9 for various values of the beam inclination angle θ for $n = 0$ (the dashed lines). The values of

λ/d were calculated for $\gamma = 0.5$ and values of the parameter $2a/d$, corresponding to angles θ from 0 to 90° in steps of 5° and the slope of these lines was determined assuming that $\theta = \text{const.}$, since this function is represented by a straight line [see (3.22)], to construct the grid of lines.

In Figures 3.9 and 3.10, the radiation coverage zone for the corresponding numbers of beams are bounded by lines with different values of n. In Figure 3.10, a radiation zone to the left of the line $n = 0$, running vertically, corresponds to the beam with the number $n = 0$. The radiation regions for $n = 0$ (Figure 3.9) and $n = 1, 2$ (Figures 3.9 and 3.10) fall below the sloped lines corresponding to each n.

The choice of the spacing between adjacent radiators d, which should be such that during beam scanning in a specified sector, the possibility of the appearance of major sidelobes is precluded, is of considerable importance in an antenna design. This condition will be met if the spacing d satisfies the relationship:

$$d \leqslant d_{\max} = \lambda \frac{1 - 1/N}{1 + |\sin\theta|}, \tag{3.24}$$

where N is the number of radiators in the array.

When the condition $d = d_{\max}$ is met, the null of the nearest sidelobe maximum will coincide with the plane of the array, and consequently, the directional pattern will have only the main lobe.

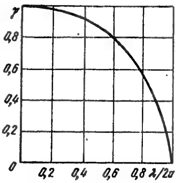

Figure 3.8. The dispersion characteristic of a regular H_{10} mode waveguide.

A graph of $d_{\max}/\lambda$ is given in Figure 3.11 as as a function of the scan angle θ for 10 and 100 radiators, plotted using formula (3.24). It follows from the graph that the maximum spacing between adjacent radiators of an array with tansverse radiation without beam scanning should be approximately equal to λ. If the beam scans in a range of ±90°, then $d_{\max} = \lambda/2$.

Thus, the condition for the existence of one main lobe of the direction pattern of a linear array of radiators during scanning requires that the spacing between the radiators be less than λ. On the other hand, in order for the direction of the main lobe to be close to the normal to the axis of the array, the excitation of the radiators should be close to in-phase. The latter is achieved in slotted waveguide arrays where $d = \lambda_B$ (λ_B is the wavelength in the waveguide, $\lambda_B > \lambda$). Alternating phase excitation of adjacent radiators is used to reduce the spacing between the radiators in slotted waveguide arrays. In this case, $d \simeq \lambda_V/2$. However, when all of the radiators are spaced at a distance of $d = \lambda_B/2$ from each other (so that the main lobe is directed along the normal to the axis of the array), the waves reflected from all

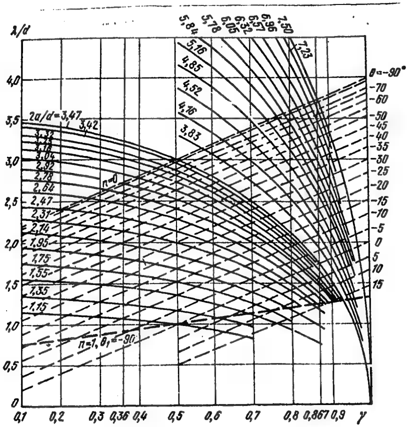

Figure 3.9. The radiation coverage zones and scan angles in the case of radiators with alternate phase coupling to the waveguide field.

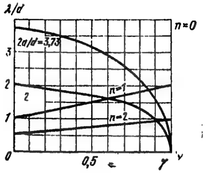

Figure 3.10. The radiation coverage zones ans scan angles in the case of radiators which are coupled in phase to the waveguide field.

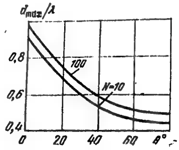

Figure 3.11. Curves for a_{max}/λ as a function of the scan angle θ. [sic]

of the radiators add in phase at the antenna input, something which sharply degrades its matching (the so-called "normal" effect is observed). In the case of beam deflection from the normal, values of d other than $\lambda_B/2$ and when the waves reflected from the radiators are mutually cancelling to a greater extent, $k_{vswr} \rightarrow 1$.

To determine the minimum spacing between radiators, d, which differs from $\lambda_B/2$ and for which the matching will be good throughout the entire working band of frequencies, one can employ the expression:

$$d<(1-1/N)\lambda_{\text{в min}}/2. \qquad (3.25)$$

To realize antenna radiation along the normal to its plane, it is necessary to match each slot radiator to the waveguide. The use of matched slots makes it possible to reduce the normal effect, i.e., avoid the sharp increase in k_{VSWR} when the main lobe direction coincides with the normal to the plane of the antenna.

A slotted waveguide array with alternatre phase excitation of the radiators can be designed with longitudinal slots in the wide wall of the waveguide (see Figure 3.1) on different sides of the center line or with the slots inclined in opposite directions in the narrow wall. The spacing between the slots d depends on the requisite direction of the main lobe of the directional pattern, θ, and the scan sector. When choosing the spacing, one can get a rough idea from expression (3.24). In actual antenna designs, d/λ is usually 0.3 to 0.7.

An analysis of equation (3.22) (see Figure 3.9) shows that when $\gamma = 0.36$--0.867 and when $\lambda/d > 1$, equation (3.22) makes sense only when $n = 0$, i.e., when the antenna operates with a null beam ($n = 0$), in which case, the beam was scanned primarily in the region of negative angles θ when the frequency changes (see Figure 3.3c).

3.4. The Design Procedure for a Frequency Scanning Linear Slotted Waveguide Array

It is assumed in the design procedure cited here that the retardation of the phase velocity in an excited waveguide slot is equal to the retardation in a regular waveguide in which there are no radiators. In an actual slotted waveguide array, because of the internal and external mutual coupling of the radiators, the retardation in the waveguide will differ somewhat from γ. In this case, the deviation in the delay from γ depends on the number of radiators, the spacing between them, and on the degree of their coupling to the waveguide field, etc.

Accounting for the influence of radiator mutual coupling on the operation of a slotted waveguide array is complicated and requires long and labor intensive calculations (see Chapter 6). Because of this, it is expedient in an approximate engineering calculation to neglect the mutual coupling of the radiators, assuming that the retardation is constant and equal to γ. In a number of practical problems, one can be limited to just such a design. However, when designing a pencil beam ($2\theta_{0.5} \leq 1°$) slotted waveguide array with high precision in the determination of its parameters and characteristics, following the preliminary approximate design of the antenna, a repeat design calculation is to be performed, using a more precisely specified value of the delay in the exciting waveguide slot, taking the mutual coupling of the radiators into account.

The design of a frequency scanning slotted waveguide array consists in determining the parameters of the waveguide which excite the slot radiators, as well as the spacing between the radiators, d, taking the beam scanning in the specified angular sector into account and the design of the radiators and their coupling to the waveguide to assure the requisite distribution of the radiated power along the array and then the calculation of the array directional pattern.

A specific feature of the determination of the waveguide parameters and the spacing d is the fact that the waveguide parameters γ and d for a specified scan sector $\Delta\theta$ and working wavelength λ are related together by a single equation (3.21) or (3.22). For this reason, to find one of the desired quantities, it is necessary to specify beforehand the remaining quantities incorporated in this equation. For example, in order to determine γ, the values of θ and d must be specified. By changing the values of θ and d, one can obtain several variants of the possible waveguide excitation system, and then choose that one of them which makes it possible to best satisfy the main requirements of the technical specifications (for example, minimal frequency variation during scanning, low attenuation factor in the waveguide, high angular frequency sensitivity of the array).

We shall introduce the following symbols: P is the power radiated by the antenna in KW; λ_{min}, λ_{cp} [λ_{avg}] and λ_{max} are the minimum, average and maximum wavelengths of the generator respectively, in cm:

$$\frac{\Delta\lambda}{\lambda_{cp}} = 2\frac{\lambda_{max}-\lambda_{min}}{\lambda_{max}+\lambda_{min}}\cdot 100\%$$

is the relative change in the generator wavelength, in percent; θ_{min}, θ_{cp} [θ_{avg}] and θ_{max} are the direction of the main lobe of the directional pattern for λ_{min}, λ_{avg} and λ_{max} respectively, in degrees; $2\theta_{0.5}$ is the width of the main lobe of the directional pattern at the half power level when $\lambda = \lambda_{avg}$, in degrees.

Equation (3.22) at the limits of the scan sector, which is bounded by the angles θ_{max} and θ_{min}, has the form:

$$\sin\theta_{max} = \gamma_{min} - 0{,}5\lambda_{max}/d; \quad (3.26)$$

$$\sin\theta_{min} = \gamma_{max} - 0{,}5\lambda_{min}/d. \quad (3.27)$$

Different variants of the problem can be encountered in design work. We shall cite a few of them.

Variant 1: P, λ_{avg}, $\Delta\lambda/\lambda_{avg}$, $2\theta_{0.5}$ and θ_{avg} are specified. Determine the possible scan sector $\Delta\theta$.

Variant 2: P, λ_{avg}, $\Delta\lambda/\lambda_{avg}$, $2\theta_{0.5}$ and $\Delta\theta$ are specified. Determine the possible beam direction θ_{avg}.

Variant 3: P, λ_{avg}, $\Delta\lambda/\lambda_{avg}$ and $2\theta_{0.5}$ are specified. Determine the beam direction θ_{avg} for which the scan sector $\Delta\theta$ will be the greatest.

Variant 4: P, λ_{avg}, $2\theta_{0.5}$, θ_{avg} and $\Delta\theta$ are specified. Assure the specified scan sector with as small as possible a relative change in the wavelength $\Delta\lambda/\lambda_{avg}$.

In doing the design calculations for any variant, it is recommended that one use the graphs of Figures 3.9--3.11 and the materials given in §3.1--3.3.

We shall consider an example of a procedure for the approximate design calculations in the case where P, λ_{avg}, $\Delta\lambda/\lambda_{avg}$, θ_{avg} and $2\theta_{0.5}$ are specified and it is necessary to determine the possible scan sector $\Delta\theta$.

1. We choose the type of radiators and the number of the working beam. Taking into account the considerations presented in §3.3, we choose slots with alternating phase coupling to the waveguide field as the radiators of the antenna array, and a beam number of $n = 0$.

2. By using the curves of Figures 3.9 and 3.12, we roughly calculate the possible beam directions θ_{avg}. Working from the specified values of λ_{avg} and $\Delta\lambda/\lambda_{avg}$, we find the wavelengths λ_{max} and λ_{min}. We start the calculation with the choice of the value of γ_{avg} corresponding to λ_{avg}. Considering the fact that the angular frequency sensitivity A (3.20) is larger for smaller values of γ, it is desirable to choose γ_{avg} less than 0.5, however, it must be remembered in this case that with a change in the frequency γ_{min} can prove to be less than 0.36 and the losses will rise in the waveguide. For this reason, it is not expedient to choose γ_{min} close to 0.36. Using the graphs of Figure 3.12, we approximate γ_{avg} for $\lambda_d > 1$ to obtain the requisite beam direction θ_{avg}. Based on the curves of Figure 3.9, we find the value of 2a/d for the known values of γ_{avg} and θ_{avg}; The value of 2a/d is a structural design parameter for the antenna being planned, and consequently, will stay constant during frequency scanning. We then determine γ_{max} and γ_{min}, preliminarily determining the waveguide dimension a corresponding to γ_{avg}. To determine a and the slow-down factors γ_{max} and γ_{min}, one can use formula (3.16) or the graphs of $\gamma = \gamma(\lambda/2a)$ shown in Figure 3.8.

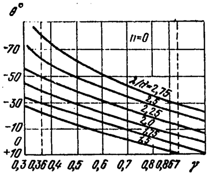

Figure 3.12. The scan angle θ as a function of γ for fixed values of λ/d when the antenna operates with a null beam.

To determine the angles θ_{max} and θ_{min}, we find the intersection points in the graphs of Figure 3.9 of the vertical lines corresponding to γ_{min} and γ_{max} with the line for $\lambda/d = \lambda/d(\gamma)$ when $2a/d$ = const. (the value of the parameter 2a/d has already been found). If the intersection point lies above the line $n = 0$, then such an operating mode is not feasible and the calculation is to be repeated, specifying another value of γ_{avg}. It is usually desirable to obtain the greatest scan sector $\Delta\theta$ for the specified relative change in the wavelength $\delta\lambda/\lambda_{avg}$. Therefore, one may specify two to three values of γ_{avg} in the calculations and find the maximum possible sector.

Considering the approximate nature of the performed calculations, related to the error in the determination of the design values from the graphs, we shall further specify these quantities precisely (paragraphs 3-6).

3. We specify the spacing between the radiators more precisely for the specified value of γ_{avg} based on equation (3.22):

$$d = 0{,}5\lambda_{cp}/(\gamma_{cp} - \sin\theta_{cp}).$$

Here, one must check to see that the condition $d \leq d_{max}$ is met when $\lambda = \lambda_{min}$ [see (3.24)] to avoid the appearance of major sidelobes.

4. We determine the size of the wide wall of the waveguide more precisely from the formula (3.16):

$$a = \lambda_{cp}/2\sqrt{1-\gamma_{cp}^2}.$$

5. We determine:

$$\gamma_{min} = \sqrt{1-(\lambda_{max}/2a)^2}, \quad \gamma_{max} = \sqrt{1-(\lambda_{min}/2a)^2}.$$

6. From equations (3.26) and (3.27), we find:

$$\theta_{max} = \arcsin(\gamma_{min} - 0{,}5\lambda_{max}/d),$$
$$\theta_{min} = \arcsin(\gamma_{max} - 0{,}5\lambda_{min}/d).$$

7. We determine the possible scanning sector:

$$\Delta\theta = \Delta_{max} - \Delta_{min}.$$

8. We find the angular frequency sensitivity at the average wavelength:

$$A = \frac{0{,}573}{\cos\theta_{cp}}\left(-\frac{1}{\gamma_{cp}} + \sin\theta_{cp}\right).$$

9. Using formula (3.22), we calculate the function $\theta = \theta(\lambda)$ in the working band and plot the graph.

10. We select the waveguide dimension b, being governed by considerations of electrical strength, the essence of higher modes and the possibility of cutting slots of widths $l_{slot} \approx \lambda_{avg}/2$.

11. We determine the ultimate transmission power P_{ult} from formula (3.18).

12. We choose the material for the waveguide walls and find the attenuation factor α from formula (3.19).

We select the distribution for the radiated power along the array of radiators, working from the requirements placed on the directional pattern and the gain of the slotted waveguide array. We determine the length of the antenna array L_A, its efficiency η_A, and the number of radiators in the array N. In the case where the simplest distributions are selected for the radiated power (uniform or exponential), the quantities L_A, η_A and N can be determined as indicated in paragraphs 13--15.

13. We select a uniform or exponential distribution for the radiated power along the array, and working from the specified width of the main lobe, $2\theta_{0.5}$, we find the approximate length of the antenna array from formula (3.15):

$$L_A = L_{eff}/\cos\theta_{avg}$$

L_{eff} is determined form formula (3.9) or (3.12) assuming that $L = L_{eff}$ when $\lambda = \lambda_{avg}$.

We shall determine L_A more precisely, checking to see that the condition $2\theta'_{0.5} \approx 2\theta_{0.5}$ is met, where $2\theta'_{0.5}$ is the width of the main lobe determined from formula (3.14).

14. We determine the efficiency of the slotted waveguide array using formula (3.8) or (3.11) at the boundaries of the working frequency band.

15. We find the number of radiators in the antenna array:

$$N = L_A/d + 1$$

16.* We choose the dimensions of the slotted radiators and their arrangement in the waveguide wall, taking into account the selected distribution for the radiated power along the array of radiators.

17. We calculate the directional pattern when $\lambda = \lambda_{min}$, λ_{avg} and λ_{max}. We determine the coformity of the width of the main directional pattern lobe to the requisite width and the change in it during scanning.

18. We find the directional gain of the antenna array.

19. We draw the electrical schematic of the slotted waveguide array.

---

*Points 16 through 18 are performed using the procedure set forth in Chapter 5.

20. We design the feeder channel coupling the transmitter to the slotted waveguide aray.

The structural design of the slotted waveguide array is accomplished taking its application into account.

The procedure is basically retained when doing the design calculations for variants 2-4; only paragraph 2 changes.

For variant 2, the rough calculation (paragraph 2) to determine the beam direction θ_{avg}, for which the requisite scan sector $\Delta\theta$ can be obtained, is carried out by means of the graphs of Figure 3.9. Since the angular frequency sensitivity is greater at small values of γ, then by specifying γ_{min} close to 0.36, we determine γ_{max} by the method indicated in paragraph 2. Drawing two vertical lines corresponding to the values of γ_{min} and γ_{max} and a horizontal line for $\lambda/d = 1$, we obtain a region in the graph for the choice of θ_{avg} in which the requisite scanning sector can be obtained. The calculation reduces to the determination the spacing between the radiators, d, which assures the requisite $\Delta\theta$ for the selected values of γ_{max} and γ_{min}. By using the curves $\lambda/d(\gamma)$ when $2a/\lambda$ = const., we find a curve on the graph in the resulting regions, which when we move along the curve from γ_{max} to γ_{min}, we obtain the requisite value of $\Delta\theta$. Then, having determined $\gamma_{avg} = \sqrt{1 - (\lambda/2a)^2}$, we find θ_{avg}.

For variant 3, the approximate calculations are performed in a manner similar to the calculations for variant 2, with the difference that θ_{avg} is determined for which $\Delta\theta$ will be a maximum.

For variant 4, the rough calculation reduces to obtaining the specified scan sector $\Delta\theta$ with a small a change as possible in the wavelength, i.e., it is desirable that $\Delta\lambda/\lambda_{avg}$ be small. For this purpose, we find the region of slow-down factors from the graph of Figure 3.12 for which one can obtain the specified direction θ_{avg}. We select two to three values of γ_{avg} corresponding to θ_{avg}. Based on the specified values of $\Delta\theta$ and θ_{avg}, we find the limits of the scan sector θ_{max} and θ_{min}. For each of the selected values of γ_{avg}, we perform the following calculations. Based on γ_{avg} and λ_{avg}, we find the waveguide dimension a and determine the parameter $2a/\lambda$. Then using the graphs of Figure 3.9, to determine the values of γ_{min} and γ_{max} corresponding to the intersection points of the straight lines $\theta = \theta_{max}$ = const. and $\theta = \theta_{min}$ = const., with the curve $(\lambda/d)(\gamma)$ for the found value of $2a/d$. The wavelengths λ_{max} and λ_{min} are determined from the formulas:

$$\lambda_{max} = 2a\sqrt{1-\gamma_{min}^2}, \quad \lambda_{min} = 2a\sqrt{1-\gamma_{max}^2},$$

while the range of change in the wavelengths is found using the formula $\Delta\lambda = \lambda_{max} - \lambda_{min}$. By repeating the same calculation for other values of γ_{avg} also, we will find new values of $\Delta\lambda$. As a result of the calculations, we determine the value of γ_{avg} corresponding to the least change in $\Delta\lambda$, which provides for the requisite sector $\Delta\theta$.

In doing the design calculations for variant 4, it can turn out that a considerable scan sector $\Delta\theta$ is required (for example, $\Delta\theta > 30°$). In this case, to reduce the requisite value of $\Delta\lambda/\lambda_{avg}$ during scanning, a system of parallel waveguides can be used which have different spacings between the radiators. Each waveguide, with the same change in $\Delta\lambda/\lambda_{avg}$ will provide for scanning in the corresponding sector, while the sum of these sectors should be equal to the total sector. The structural design of such an antenna will be more complex; it should consist of several waveguides, switched when making the transition from one scan sector to another. The design procedure for such an antenna is somewhat different than for a single slotted waveguide array, however, one can employ the procedure already considered in the design calculations for each waveguide. Breaking the total scan sector down into component parts and determining the number of requisite waveguides can be accomplished by using the graphs of Figure 3.9, as well as the book [010].

4. HIGHLY DIRECTIONAL CYLINDRICAL AND ARC ANTENNA ARRAYS

4.1. General Information

Cylindrical antenna arrays take the form of a system of radiators arranged on a cylindrical surface. A special case of cylindrical arrays is arc and ring antenna arrays, the radiators in which are arranged along an arc or circle of a particular radius.

Wire and slotted dipoles, open waveguide ends and horns, helical and dielectric rod antennas as well as director radiators can be used as the radiators in cylindrical arrays. The choice of the type of radiator depends on the working wavelength and the requisite passband, on the operational conditions and function, as well as on the structural design requirements placed on the array as a whole. In the centimeter band, the most convenient type of radiator for cylindrical arrays is so-called diffraction type radiators, which take the form of openings cut directly in the metal surface of a cylinder: a half-wave slot, an open waveguide end or a small horn.

A merit of such radiators is also the fact that they almost do not disrupt the aerodynamic properties of the cylindrical surface, something which is especially important when they are placed in aircraft. One of the important properties of pencil beam cylindrical arrays is the capability of electrical control of the beam position in a wide sector of space without changing its width and shape. For example, ring antenna arrays make it possible to have undistorted electrical beam scanning in the azimuthal plane. Cylindrical antenna arrays, as compared to linear ones, possess yet a series of useful properties. Numbered among them are a lower level of sidelobes (which are due to the discrete nature of the radiator arrangement and switching phase errors in the case of switched beam scanning), the possibility of expanding the working bandwidth, etc.

However, cylindrical antenna arrays also have a number of drawbacks as compared to linear and planar arrays, the chief of which is the increased complexity of the structural design of the antenna and its beam control system.

The Major Requirements Placed on Cylindrical Scanning Arrays. The main parameters of cylindrical antenna arrays are determined by working from their function, installation site and operating conditions. For pencil beam cylindrical scanning arrays, the main parameters specified during the design work are: the directional pattern width, level of the sidelobes, directional gain, scan sector and beam scanning rate, bandwidth properties, polarization of the radiated field, maximum radiated power, efficiency, reliability, climatic operating conditions and cost.

The optimal configuration for the cylindrical array and type of radiator should be selected during the planning process, the array dimensions should be determined (radius, length, angular sector) as well as the amplitude-phase distribution of the current in the radiators and the law governing the current change during scanning should be found, the directional pattern of the array calculated along with its directional gain, overall gain, bandwidth properties; the method of scanning is determined and a device is chosen to realize the scanning, and the structural design of the antenna array is worked out as a whole.

Structural Configurations of Cylindrical Arrays. Cylindrical antenna arrays can be broken down into three groups according to the method of microwave energy distribution among the individual radiators: arrays with series and parallel excitation, and arrays with a mixed feed circuit. Moreover, the array configurations in each of these groups can differ according to the method of energizing the phase shifters.

We shall treat the main features of the indicated circuit configurations using the example of ring and arc arrays [04, 09, 013, 1, 2]. A ring array with a parallel circuit for energy distribution between the radiators is shown in Figure 4.1a. A merit of this circuit is the fact that the antenna beam direction is only a slight function of the frequency and there is the possibility of controlling the amplitude distribution in the array by means of switching the inputs of the feeder lines in a switcher (S). A drawback to the parallel excitation configuration is the cumbersome feed system for energy distribution.

The variant of a ring array with spatial excitation (Figure 4.1b) is free of this deficiency. The operational principle of such an array consists in the following. The energy from the feed radiator is fed via a radial line to the receiving radiators, and then to the phase shifters and is radiated by the ring array in the requisite direction. The control of the antenna beam is accomplished within small sectors by means of phase shifters. In the case of wide angle scanning, it is necessary to change the amplitude distribution over the ring array, for example, by means of rotating the feed radiator or installing several feed radiators and switching them in turn.

One of the circuits for a series excited ring array is shown in Figure 4.1c. A merit of the circuit is the simplicity, as well as the fact that the volume inside the array remains free and can be occupied by other devices, something which is especially important when placing a ring array on the surface of an aircraft. However, arc arrays, designed in a series excitation configuration, also have a number of drawbacks, the main ones of which are the fact that the array beam direction is a function of frequency and it is difficult to control the amplitude distribution in the case of wide angle scanning.

A ring array formed from several arc arrays with a mixed circuit configuration for power distribution among the radiators is free of this latter drawback (Figure 4.1d). The use of mixed excitation makes it possible, on one hand, to preserve the advantages of parallel excited ring arrays, and on the other, to simplify the energy distribution system, especially for arrays with a large electrical radius.

The most promising structural configurations for cylindrical arrays are the mixed (Figure 4.2) and those with spatial excitation. The major properties of these cylindrical array configurations are the same as for the corresponding ring arrays.

When selecting the circuit configuration for the phase shifters, it is expedient to be governed by the following considerations. In the case of a series confi-

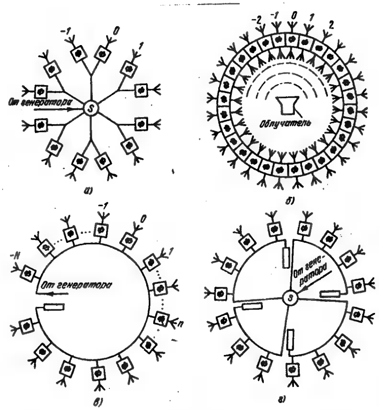

Figure 4.1. Structural configurations of ring antenna arrays.

Key: 1. From the generator.

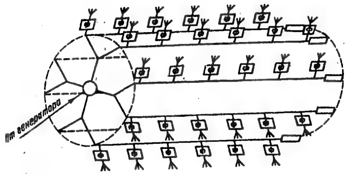

Figure 4.2. The structural configuration of a cylindrical antenna array.

guration of the phase shifters, the maximum carrying capacity and the efficiency are reduced, the dependence of the antenna directional pattern on the phase setting errors is increased and the bandwidth properties of the antenna are degraded. For this reason, the series configuration of the phase shifters is used rather rarely, primarily in linear antenna arrays, where such a circuit makes it possible to simplify the controller for the phase shifters. In cylindrical arrays, a series phase shifter circuit can be used in those portions of the feed-line which are arranged along the generatrix of the cylindrical surface, since this makes it possible to simplify the beam control unit in planes running through the axis of the cylindrical array. In the remaining cases, parallel phase shifter configurations are to be employed.

4.2. The Phase Distribution in Highly Directional Cylindrical Arrays

The amplitude distribution in cylindrical pencil beam arrays exerts a substantial influence on the shape of the directional pattern and is chosen depending on the requirements placed on the directional gain, the level of sidelobes and the bandwidth properties of the array. This question is treated in more detail in the following sections.

The phase distribution in cylindrical arrays is chosen by working from the requirement for beam formation in a specified direction. In this case, the phase distribution in the radiators placed on the surface of a cylinder is usually chosen so that the fields radiated by each radiator add together in phase in the direction θ_0, Φ_0 for highly directional arrays when generating a beam in the direction θ_0, Φ_0.

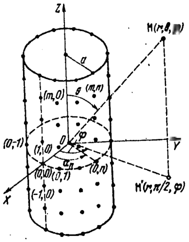

Figure 4.3. The coordinate system and scheme for the arrangement of radiators in a cylindrical array.

We shall number the radiators of a cylindrical array with a double subscript, mn. In this case, the phase center* of the 00-th radiator has cylindrical coordinates of z = 0 and $\alpha = 0$, while for the mn-th radiator, it has coordinates of $z = z_m$ and $\alpha = \alpha_n$ (Figure 4.3). The requisite phase distribution in this case $\Phi_{mn}(\theta_0, \varphi_0)$ of the current in the mn-th radiator of the cylindrical array has the form:

$$\Phi_{mn}(\theta_0, \varphi_0) = -[\kappa a \sin\theta_0 \cos(\varphi_0 - \alpha_n) + \kappa z_m \cos\theta_0 + 2\pi k], \quad k = 0, \pm 1, \pm 2, \ldots \tag{4.1}$$

In the special case of an arc array, arranged in the z = 0 plane, the requisite phase distribution is:

$$\Phi_{0n}(\theta_0, \varphi_0) = -[\kappa a \sin\theta_0 \cos(\varphi_0 - \alpha_n) + 2\pi k], \quad k = 0, \pm 1, \pm 2, \ldots \tag{4.2}$$

The requisite law governing the phase control of the mn-th phase shifter, $\Phi_{\text{фаз}\ mn}$ [$\Phi_{\text{phase}\ mn}$], depends on the circuit configuration of the antenna feeder channel and on the circuit configuration of the phase shifters themselves, and for a cylindrical array, can be found from the relationship:

$$\begin{aligned}\Phi_{\text{фаз}\ mn}(\theta_0 \varphi_0) = &-[\kappa a \sin\theta_0 \cos(\varphi_0 - \alpha_n) + \kappa z_m \cos\theta_0 - \\ &- \kappa a \sin\theta_0 \cos(\varphi_0 - \alpha_{n'}) - \kappa z_{m'} \cos\theta_0 - \Phi_{\text{фид}\ mn} + \Phi_{\text{фид}\ m'n'} + 2\pi k], \\ &k = 0, \pm 1, \pm 2, \ldots,\end{aligned} \tag{4.3}$$

---

*The proposal of the presence of a phase center for the mn-th radiator is justified for radiators arranged on a cylindrical surface of considerable radius: a >> λ.

where $\Phi_{\text{фид } mn}$ [$\Phi_{\text{feed } mn}$] designates the electrical length of the feedline from the generator to the input terminals of the mn-th radiator (without taking into account the electrical length of the phase shifter Φ_{mn} inserted in the feed channel for the mn-th radiator), while the subscripts m'n' designates the phase shifter, the phase of which is taken as zero.

Correspondingly, for an arc array:

$$\Phi_{\text{фаз } 0n}(\theta_0, \varphi_0) = -\{\kappa a \sin\theta_0 [\cos(\varphi_0 - \alpha_n) - \cos(\varphi_0 - \alpha_{n'})] - \\ - \Phi_{\text{фид } 0n} + \Phi_{\text{фид } 0n'} + 2\pi k\}, \quad k = 0, \pm 1, \pm 2, \ldots. \tag{4.4}$$

We shall cite the expressions for $\Phi_{\text{phase } mn}$ for several specific configurations of cylindrical and arc arrays.

1. A parallel excited arc array (Figure 4.1a). The electrical length of all of the feeder lines is the same, and the phase of the phase shifter of the radiator with the coordinate $\alpha_0 = 0$ is taken as the zero phase (n' = 0):

$$\Phi_{\text{фаз } 0n}(\theta_0 \varphi_0) = -\kappa a \sin\theta_0 [\cos(\varphi_0 - \alpha_n) - \cos\varphi_0] + 2\pi k, \\ k = 0, \pm 1, \pm 2, \ldots \tag{4.5}$$

Expression (4.5) is also justified for an arc array with spatial excitation (Figure 4.1b), if the phase center of the feed irradiator is placed in the geometric center of the arc array and n' = 0.

2. A series excited arc array. The phase shifters are inserted in a parallel circuit configuration (Figure 4.1c). The generator output is connected to the -N-th radiator, n' = -N:

$$\Phi_{\text{фаз } 0n}(\theta_0, \varphi_0) = -\kappa a \sin\theta_0 [\cos(\varphi_0 - \alpha_n) - \cos(\varphi_0 - \alpha_{-N})] + \\ + \kappa a \gamma (\alpha_n - \alpha_{-N}) + 2\pi k, \quad k = 0, \pm 1, \pm 2, \ldots, \tag{4.6}$$

where γ is the retardation in the supply feedline.

3. A series excited arc array. The phase shifters are connected in a series circuit configuration. The generator output is connected to the -N-th radiator, n' = -N:

$$\Phi_{\text{фаз } 0n}(\theta_0, \varphi_0) = -\kappa a \sin\theta_0 [\cos(\varphi_0 - \alpha_n) - \cos(\varphi_0 - \alpha_{-N})] + \\ + \kappa a \gamma (\alpha_n - \alpha_{-N}) + \sum_{p=-N}^{n-1} \Phi_{\text{фаз } 0p} + 2\pi k, \quad k = 0, \pm 1, \pm 2, \ldots \tag{4.7}$$

4. A cylindrical array with mixed excitation (Figure 4.2), n' = 0, m' = 0:

$$\Phi_{\text{фаз } mn}(\theta_0, \varphi_0) = -\kappa a \sin\theta_0 \cos(\varphi_0 - \alpha_n) - \\ - \kappa z_m \cos\theta_0 + \kappa a \sin\theta_0 \cos\varphi_0 + \kappa \gamma z_m + 2\pi k, \quad k = 0, \pm 1, \pm 2, \ldots, \tag{4.8}$$

where γ is the retardation of the wave in the feeders, arranged along the generatrix of the cylinder.

The value of the integer k in the expressions cited here depends on the type of phase shifter. Thus, if the phase shifter can change the phase continuously in a large range of phase values*, then k = 0 in expressions (4.3) - (4.8). However, so-called resetting phase shifters are used in electrically scanned antenna arrays, where the phase control range in such shifters is kept within a range of 0 to 2π radians. The advantage of such phase shifters consists in the smaller dimensions and losses, as well as in the greater precision in setting the phase as compared to phase shifters with large phase control ranges. When using resetting phase shifters, the value of k in the expressions cited here should be selected so that the following inequality is observed:

---

*The requisite range of continuous control of the phase of the wave in the phase shifters depends on the size of the cylindrical array and the scan sector, and for pencil beam arrays can reach several tens and even hundreds of thousands of degrees.

$$0 \leqslant \Phi_{\text{фаз}\,mn} \leqslant 2\pi. \tag{4.9}$$

The choice of the number of controlled phase shifters depends on the requisite scan sector, the directional pattern width and the amplitude distribution in the array. The minimum possible number of controlled phase shifters in the case of wide angle scanning is chosen equal to the number of radiators.

4.3. The Directional Patterns of Cylindrical Pencil Beam Arrays

The normalized complex vector directional pattern, $\vec{F}(\theta, \phi)$, of a cylindrical array when generating a beam in the direction θ_0, ϕ_0, can be written in the form:

$$\begin{gathered} \boldsymbol{F}(\theta, \varphi) = A \sum_{m=-M_1}^{M_2} \sum_{n=-N_1(m)}^{N_2(m)} |I_{mn}| \boldsymbol{F}_{mn}(\theta, \varphi) \sqrt{G_{mn}(1-|\Gamma_{mn}|)^2} \times \\ \times \exp\{-j[\kappa a \sin\theta_0 \cos(\varphi_0 - \alpha_n) + \kappa z_m \cos\theta_0 - \\ - \kappa a \sin\theta \cos(\varphi - \alpha_n) - \kappa z_m \cos\theta]\}, \end{gathered} \tag{4.10}$$

where $|I_{mn}|$ is the amplitude of the incident current (or voltage) waves in the feeder of the mn-th radiator; $\vec{F}_{mn}(\theta, \phi) = \vec{e}_{mn}(\theta, \phi) F_{mn}(\theta, \phi)$; $F_{mn}(\theta, \phi)$, $\vec{e}_{mn}(\theta, \phi)$ are the normalized amplitude and polarization patterns respectively of the mn-th radiator; G_{mn} is its gain; Γ_{mn} is the reflection factor from the input of the mn-th radiator; $-M_1$, M_2, $-N_1(m)$ and $N_2(m)$ are the numbers of the end radiators of the cylindrical array;

$$\frac{1}{A} = \sum_{m=-M_1}^{M_2} \sum_{n=-N_1(m)}^{N_2(m)} |I_{mn}| F_{mn}(\theta_0, \varphi_0) \sqrt{G_{mn}(1-|\Gamma_{mn}|)^2} \tag{4.11}$$

is the normalizing factor.

In the following, we shall assume that the quantities G_{mn} and Γ_{mn} do not depend on the number of a radiator, i.e. $G_{mn} = G_{00}$, $|\Gamma_{mn}| = |\Gamma_{00}|$.

Expression (4.10) can be represented as the directional pattern of an equivalent linear radiator:

$$\boldsymbol{F}(\theta, \varphi) = A \sum_{m=-M_1}^{M_2} |I_{m0}| \boldsymbol{F}_m(\theta, \varphi) \exp[-j\kappa z_m(\cos\theta_0 - \cos\theta)], \tag{4.12}$$

$$\begin{gathered} \text{где} \quad \boldsymbol{F}_m(\theta, \varphi) = \frac{\sqrt{G_{00}(1-|\Gamma_{00}|^2)}}{|I_{m0}|} \sum_{n=-N_1(m)}^{N_2(m)} |I_{mn}| \boldsymbol{F}(\theta, \varphi) \times \\ \times \exp\{-j\kappa a[\sin\theta_0 \cos(\varphi_0 - \alpha_n) - \sin\theta \cos(\varphi - \alpha_n)]\} \end{gathered} \tag{4.13}$$

is the complex vector directional pattern of the m-th arc array.

In a rather typical, although special case of a cylindrical array, formed by a set of identical arc arrays, and where the current amplitude distribution divided along the coordinates α and z is $|I_{mn}| = |I'_m||I_{0n}|$, the directional pattern of the cylindrical array is determined by the product of the directional pattern of the arc array, $\vec{F}_0(\theta, \phi)$, lying in the plane z = 0, times the factor for the linear system of radiators, $f_M(\theta)$:

$$F(\theta, \varphi) = F_0(\theta, \varphi) f_M(\theta), \tag{4.14}$$

где

$$f_M(\theta) = \frac{\sum_{m=-M_1}^{M_2} |I_{m0}| \exp[-j\kappa z_m(\cos\theta_0 - \cos\theta)]}{\sum_{m=-M_1}^{M_2} |I_{m0}|}, \tag{4.15}$$

$$F_0(\theta, \varphi) = \frac{\sum_{n=-N_1}^{N_2} |I_{0n}| F_{0n}(\theta, \varphi) \exp\{-j\kappa a[\sin\theta_0 \cos(\varphi_0 - \alpha_n) - \sin\theta \cos(\varphi - \alpha_n)]\}}{\sum_{n=-N_1}^{N_2} |I_{0n}| F_{0n}(\theta_0, \varphi_0)}. \tag{4.16}$$

Thus, the study of the directional pattern of a cylindrical antenna reduces basically to the study of the directional pattern of the corresponding arc array. Moreover, the directional pattern of the arc array is poorly directional in the plane passing through the direction of the beam and the z axis. For this reason, when generating a pencil beam, the shape of the directional pattern of a cylindrical array in the indicated plane in the region of the main lobe and the first sidelobes is governed primarily by the factor for the linear system of radiators, $f_M(\theta)$. However, the directional pattern completely matches the directional pattern of the arc array (4.16) in the orthogonal plane.

4.4. Directional Patterns of Arc and Cylindrical Arrays

When calculating the directional pattern of an arc array using expression (4.16), it is first of all necessary to determine the directional pattern of an individual radiator in the array, which is a rather complex and independent problem. The complexity of the problem consists in the necessity of taking into account both diffraction phenomena at the surface of the antenna and effects of radiator interaction in the arc and cylindrical arrays. The techniques for solving this problem can be partially found in the literature [1]. However, in the initial design stage, it is expedient to determine the directional pattern of an individual radiator by means of simpler approximation methods, without taking interaction into account and with an approximate accounting for diffraction phenomena. The essence of the approximation consists in the fact that the amplitude directional pattern of a radiator, $F_{0n}(\theta, \phi)$, in an array in a range of angles of $\alpha_n - \pi/2 < \phi < \alpha_n + \pi/2$ is computed just as for a single radiator in free space, while it is equated to zero in the range $\alpha_n + \pi/2 < \phi < 2\pi - \alpha_n$.

When determining the polarization pattern of a radiator, $\vec{e}_{0n}(\theta, \phi)$, one can make use of the following recommendations: the polarization pattern of linear radiators (dipole, slot, yagi type radiator) matches the polarization pattern of an elementary dipole sufficiently well, while the polarization pattern of aperture radiators (the open end of a waveguide, horn), matches the polarization pattern of a Huygens source.

For longitudinal linear radiators, arranged along the z axis on a cylindrical surface, at a point with an azimuth coordinate of α_n:

$$e_{0n}(\theta, \varphi) = \theta_0. \tag{4.17}$$

For similar transverse linear radiators:

$$e_{0n}(\theta, \varphi) = -\frac{\cos\theta \sin(\varphi-\alpha_n)}{\sqrt{1-\sin^2\theta \sin^2(\varphi-\alpha_n)}}\theta_0 - \frac{\cos(\varphi-\alpha_n)}{\sqrt{1-\sin^2\theta \sin^2(\varphi-\alpha_n)}}\varphi_0. \tag{4.18}$$

For aperture radiators with an azimuth coordinate of the phase center, α_n, and with an electrical field vector parallel to the XOY plane:

$$e_{0n}(\theta, \varphi) = \frac{\cos\theta \sin(\varphi-\alpha_n)}{1+\sin\theta\cos(\varphi-\alpha_n)}\theta_0 + \frac{\sin\theta+\cos(\varphi-\alpha_n)}{1+\sin\theta\cos(\varphi-\alpha_n)}\varphi_0. \tag{4.19}$$

For similar aperture radiators with an electrical field vector parallel to the z axis:

$$e_{0n}(\theta, \varphi) = \frac{\sin\theta+\cos(\varphi-\alpha_n)}{1+\sin\theta\cos(\varphi-\alpha_n)}\theta_0 - \frac{\cos\theta \sin(\varphi-\alpha_n)}{1+\sin\theta\cos(\varphi-\alpha_n)}\varphi_0. \tag{4.20}$$

In expressions (4.17) - (4.20), θ_0 and ϕ_0 are used to designated unit vectors in a spherical system of coordinates.

Taking the polarization patterns of individual radiators into account shows that in the general case, the directional patterns of arc arrays, besides the main polarization component of the radiated field, also have a parasitic (or cross polarization) component. The cross polarized component is absent only in arrays formed from longitudinal linear radiators, as well as in the case where the directional pattern of an array is considered in the plane of the arc ($\theta_0 = \pi/2$), when:

$$F_0 \doteq \left(\frac{\pi}{2}, \varphi\right) = F_0\left(\frac{\pi}{2}, \varphi\right) \begin{Bmatrix}\theta_0\\ \varphi_0\end{Bmatrix}^{*)}. \tag{4.21}$$

where: где

$$F_0\left(\frac{\pi}{2}, \varphi\right) = \tag{4.22}$$

$$= \frac{\sum_{n=-N_1}^{N_2} |I_{0n}|\, F_{0n}\left(\frac{\pi}{2}, \varphi\right) \exp\{-j\kappa a[\cos(\varphi_0-\alpha_n)-\cos(\varphi-\alpha_n)]\}}{\sum_{n=-N_1}^{N_2} |I_{0n}|\, F_{0n}\left(\frac{\pi}{2}, \varphi\right)}$$

Further design calculations of the directional pattern of an arc array can be performed in accordance with the following scheme:

---

*Writing the symbol $\begin{matrix}\theta_0\\ \phi_0\end{matrix}$ means that either the unit vector θ_0 or the unit vector ϕ_0 is chosen.

1. Direct calculation of the directional pattern of an individual radiator using formulas (4.14) - (4.16) and (4.22), taking into account the polarization patterns (4.17) - (4.20) and the calculated amplitude pattern. This computational work is cumbersome, absolutely requires the use of a computer and it is expedient in the concluding stage of the design work when specifying the characteristics more precisely for the selected array variant.

2. The introduction of reasonable assumptions, which make it possible to simplify the computational process in the initial design stage without substantial losses of precision. The essence of these assumptions consists in the following:

a) The directional pattern of the arc array is calculated only for the main planes, $\theta = \pi/2$ and $\phi = \phi_0$, and in the region of the main lobe and the first sidelobe;

b) The directional pattern of an individual radiator and the current distribution function in the arc array are approximated by elementary functions;

c) An arc radiator with a continuous current distribution, equal in value to the actual distribution at the points where the radiators are placed and with a sufficiently smooth current distribution among them is substituted for the discrete arc array.

Taking the assumptions enumerated above into account, the directional pattern of the array in the plane of the arc when generating a beam in the direction $\pi/2$, 0, with a precision of down to the normalizing factor A, is represented in the form:

$$F_0\left(\frac{\pi}{2}, \varphi\right) = A \int_{\alpha_{-N_1}}^{\alpha_{N_2}} I(\alpha) F\left(\frac{\pi}{2}, \varphi, \alpha\right) \exp\{-j\kappa a[\cos\alpha - \cos(\varphi-\alpha)]\}\, d\alpha, \tag{4.23}$$

where the term $F(\pi/2, \phi, \alpha)$ designates the directional pattern of an individual radiator having an azimuthal coordinate α. The equivalent linear radiator technique is the most convenient method for the approximate calculation of the directional pattern using expression (4.23). The essence of it consists in the fact that the directional pattern of an arc antenna is computed as the directional pattern of an in-phase linear antenna, the amplitude distribution in which corresponds to the projection of the amplitude distribution along the arc onto a linear antenna, positioned perpendicularly to the direction of the beam being generated. The amplitude distribution, $I_{equiv}(y)$ in the equivalent linear antenna can be determined from the expression:

$$I_{экв}(y) \simeq I\left(\arcsin\frac{y}{a}\right) F\left(\frac{\pi}{2}, 0, \arcsin\frac{y}{a}\right) \frac{1}{\sqrt{a^2-y^2}}, \tag{4.24}$$

and the directional pattern of the arc antenna from the following formula:

$$F_0\left(\frac{\pi}{2}, \varphi\right) = A \int_{y_1}^{y_2} I_{экв}(y) \exp(j\kappa y \sin\varphi)\, dy, \tag{4.25}$$

where

$$y_1 = a\sin\alpha_{-N_1};\quad y_2 = a\sin\alpha_{N_2}.$$

The range of permissible angles ϕ, within which one can use (4.25) for the calculations with an error not exceeding a few percent, is determined by the inequality:

$$|\varphi| \leqslant \arccos\left\{1 - \frac{\pi/2}{\kappa a\,[1-\cos(\max(|\alpha_{N_2}|, |\alpha_{-N_1}|))]}\right\}. \tag{4.26}$$

Based on the equivalent linear radiator technique, one can find (depending on the kind of amplitude distribution along the arc array and the directional pattern of an individual radiator) the relationships between the width and shape of the directional pattern of the array, the level of the first sidelobe and the projection $l_{equiv} = y_2 - y_1$ of the arc array onto the y axis. These functions are given in Table 4.1 for $y_2 = -y_1(\alpha_{-N_1} = \alpha_{N_2} = \beta)$. Values of the surface utilization coefficient for an arc antenna, ν, determined by the ratio of the directional gain of the arc antenna to the directional gain for the case of uniform amplitude distribution in the equivalent radiator, are given in the last column of Table 4.1.

During the design process, the requisite amplitude distribution in the equivalent linear radiator, $I_{equiv}(y)$ and its length are chosen from Table 4.1 based on the specified width and level of the first sidelobe. Then, the requisite amplitude distribution in the radiators of the arc array is determined from expression (4.24):

$$I(\alpha_n) = I_{\text{экв}}(a\sin\alpha_n)\,a\cos\alpha_n / F(\pi/2, 0, \alpha_n). \tag{4.27}$$

The directional pattern of an arc array in the region of the main lobe and the first sidelobes, which is governed by inequality (4.26), is calculated from the relevant expressions of Table 4.1.

When calculating the directional pattern of a scanning arc array with the main lobe deflected from the direction $\phi_0 = 0$, one can rotate the arc array through the angle $-\phi_0$ and employ the equivalent radiator technique. In this case, one must keep in mind the fact that an arc array, and consequently, the amplitude distribution and the equivalent radiator itself will no longer be symmetrical relative to the direction of the beam being generated, something which does not make it possible to fully utilize the results of Table 4.1. However, one can always choose an approximating amplitude distribution in the equivalent radiator from a set of functions which make it possible to calculate the integral in (4.25) in closed form.

It must be remembered when more precisely specifying the equivalent radiator technique that when the spacing between the radiators of the arc array, d, exceeds $\lambda/2$, additional parasitic lobes (higher order interference maxima) can appear in the pattern of the arc array, just as in the directional pattern of a linear array. Their level depends on ka and β, and falls off with an increase in ka and β.

The position of the interference maxima is practically independent of the dimensions of the arc array, and is determined primarily by the step of the antenna array. The individual radiator directional pattern and the form of the amplitude distribution in the array have a slight impact on the position of the interference

TABLE 4.1.

Распределение тока в эквивалентном раскрыве $I_{экв}(y)$	Соответствующее распределение тока в дуговой антенне $I(\alpha)$	ДН дуговой антенны $F_0\left(\frac{\pi}{2}, \varphi\right)$	Ширина ДН дуговой антенны, град	Уровень первого бокового лепестка, дБ	ν
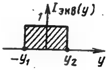	$\frac{a\cos\alpha}{F\left(\frac{\pi}{2}, 0, \alpha\right)}, \ -\beta < \alpha < \beta$	$\frac{\sin u^{*)}}{u}$	$50{,}5\lambda/l_{экв}$	$-13{,}2$	1
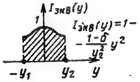 $I_{экв}(y)$ 1 $I_{экв}(y) = 1 - \frac{1-\delta}{y_2^2} y^2$ $-y_1$ y_2 y	$\left[1 - \frac{(1-\delta)\sin^2\alpha}{\sin^2\beta}\right] \times \cos\alpha \frac{a}{F\left(\frac{\pi}{2}, 0, \alpha\right)}, \ -\beta < \alpha < \beta$	$\frac{\sin u}{u} + (1-\delta)\left[\frac{(2-u)^2 \sin u}{u^3} - \frac{2u\cos u}{u^3}\right]$	$50{,}5\lambda/l_{экв}, \ \delta = 1$ $52{,}5\lambda/l_{экв}, \ \delta = 0{,}8$ $55{,}5\lambda/l_{экв}, \ \delta = 0{,}5$ $66\lambda/l_{экв}, \ \delta = 0$	$-13{,}2$ $-15{,}8$ $-17{,}1$ $-20{,}6$	1 0,994 0,97 0,833
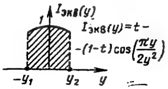 $I_{экв}(y)$ 1 $I_{экв}(y) = t - (1-t)\cos\left(\frac{\pi y}{2y^2}\right)$ $-y_1$ y_2 y	$\left[t - (1-t)\cos\left(\frac{\pi}{2}\frac{\sin\alpha}{\sin\beta}\right)\right] \times \cos\alpha \frac{a}{F\left(\frac{\pi}{2}, 0, \alpha\right)}; \ -\beta < \alpha < \beta$	$t\frac{\sin u}{u} + \frac{2}{\pi}(1-t)\frac{\cos u}{1 - 4\frac{u^2}{\pi^2}}$	$50{,}5\lambda/l_{экв}, \ t = 1$ $52\lambda/l_{экв}, \ t = 0{,}8$ $54\lambda/l_{экв}, \ t = 0{,}6$ $57{,}5\lambda/l_{экв}, \ t = 0{,}4$ $62\lambda/l_{экв}, \ t = 0{,}2$ $68{,}5\lambda/l_{экв}, \ t = 0$	$-13{,}2$ -14 -16 $-18{,}6$ $-21{,}5$ -23	1 0,99 0,975 0,95 0,915 0,81

---

*) $u = (\kappa l_{экв} \sin\varphi)/2$.

Key:
1. Current distribution in the equivalent aperture, $I_{equiv}(y)$;
2. The corresponding current distribution in the arc antenna, $I(\alpha)$;
3. Directional pattern of the arc antenna, $F_0(\pi/2, \phi)$;
4. Width of the arc antenna directional pattern, degrees;
5. Level of the first sidelobe, dB.

maxima. Thus, in the case of a uniform amplitude distribution and with isotropic radiators, the coordinate ϕ_p of the p-th order interference maximum when $\phi_0 = 0$, is approximately defined by the relationship:

$$\varphi_p \simeq 2 \arcsin (p\lambda/2d), \quad p = 1, 2, \ldots \tag{4.28}$$

With an amplitude distribution in an arc array, corresponding to the maximum of the directional gain, the position of the first order interference maxima is shifted in the direction of an increase in the coordinate ϕ by approximately 0.5 to 1.0 times the directional pattern width of $2\phi_{0.5}$. By knowing the direction of the interference maxima, their level $F_0(\pi/2, \phi_p)$ can be determined from expression (4.22). This same expression can be employed, if it is necessary to more precisely specify the directional pattern of the arc array in the requisite angular sector.

The directional pattern of a highly directional cylindrical array, $F(\theta, \phi)$, consisting of a system of identical arc arrays in a plane perpendicular to the axis of a cylinder, matches the directional pattern of a single arc array, and in the plane running through the axis of the cylinder and the direction of the array beam, it is represented in the form of the product of the arc array directional pattern (4.14) times the directivity factor for a linear antenna (4.15).

If the spacing between arc arrays along the z axis does not exceed $\lambda/2$, then in expression (4.15) the sum can be replaced by the integral:

$$f_L = A \int_{-L/2}^{L/2} I(z) \exp[j\kappa z (\cos\theta - \cos\theta_0)]\, dz, \tag{4.29}$$

where L is the length of the cylindrical antenna along the z axis.

The expression for $f_L(\theta)$, depending on the amplitude distribution, can be found in Table 4.1, if $I_{equiv}(y)$ is understood to be $I(z)$ and l_{equiv} is understood to be the quantity L.

If should be noted that when $l \gg \lambda$ and $l \gg a$, the following relationship obtains in the region of the main lobe and first sidelobes:

$$F(\theta, \varphi_0) \simeq f_L(\theta). \tag{4.30}$$

4.5. The Directional Gain of Cylindrical and Arc Arrays

The value of the directional gain of arc and cylindrical arrays depends on a number of factors, in particular, on the radiator directional pattern, the form of the amplitude-phase distribution over the radiators and the number of them.

The optimal phase distribution which assures a directional gain maximum in pencil beam cylindrical arrays is close to the distribution described by equation (4.1). The optimal amplitude distribution along the z coordinate is uniform, and along the ϕ coordinate, depends substantially on the step of the array. The general governing laws in the case where $ka \gg 10$ are as follows: for a step of $d/\lambda \simeq 0.5$, the optimal amplitude distribution approaches that distribution which, in being designed for an equivalent linear radiator in accordance with the distribution of (4.25), yields a uniform distribution in it:

$$I_{\text{opt}} \simeq \frac{\cos\alpha_n}{F(\pi/2,\,0,\,\alpha_n)}. \tag{4.31}$$

With an increase in the spacing between the radiators, the optimal amplitude distribution in the radiators approaches a function proportional to the amplitude pattern of the corresponding radiator in the direction of the beam being formed by the array:

$$I_{\text{opt}} \simeq F(\pi/2,\,0,\,\alpha_n). \tag{4.32}$$

Although expression (4.32) is justified only when the spacing between the radiators significantly exceeds the wavelength, it can be used as soon as d > λ.

The following relationships can be employed in estimating the maximum directional gain. For an arc array formed by a system of longitudinal half-wave slots, arranged in a cylinder,

$$D_{\max} \simeq \begin{cases} \dfrac{1{,}43\kappa a}{d/\lambda}\sin\beta & \text{при } d > \lambda/2, \\ & \text{when} \\ 2{,}86\kappa a\sin\beta & \text{при } d \leqslant \lambda/2, \end{cases} \tag{4.33}$$

where the angular sector occupied by the array is 2β, falls in a range of from 50 to 180°.

For a cylindrical array formed by a system of similar slots, which generates a pencil beam, directed perpendicular to the axis:

$$D_{\max} = \begin{cases} \dfrac{\pi S_{\text{экв}}}{d_1 d_2} & \text{при } d_1 > \dfrac{\lambda}{2},\ d_2 > \dfrac{\lambda}{2}. \\ & \text{when} \\ \dfrac{4\pi}{\lambda^2} S_{\text{экв}} & \text{при } d_1 \leqslant \dfrac{\lambda}{2},\ d_2 \leqslant \dfrac{\lambda}{2}. \end{cases} \tag{4.34}$$

where S_{equiv} is the equivalent aperture area; d_1 and d_2 are the spacings between adjacent slots in the plane passing through the axis of the cylinder and in the plane perpendicular to the axis of the cylinder respectively.

For the m-th arc array, the maximum directional gain can be approximated using the expression:

$$D_{\max} \simeq \sum_{n=-N_1}^{N_2} D_{mn} F_{mn}^2\left(\frac{\pi}{2},\,\varphi_0\right). \tag{4.35}$$

where D_{mn} is the directional gain of the mn-th radiator in the direction of the radiation maximum axis.

The summing in expression (4.35) can be approximately replaced by integration. In this case, for a system of identical radiators with D_{00}, we have:

$$D_{m\,\max} \simeq D_{00}\int_{\alpha_{-N_1}}^{\alpha_{N_2}} \frac{F_{mn}^2(\pi/2,\,\varphi_0)}{d/a}\,d\alpha_n = \\ = D_{00}\,\frac{\kappa a}{2\pi d/\lambda}\int_{-\beta_1}^{\beta_2} F_{mn}^2(\pi/2,\,\varphi_0)\,d\alpha_n. \tag{4.36}$$

Expressions are given for $D_{m\ max}$ in Table 4.2 for a few directional patterns, given the condition that $-\alpha_{-N1} = \alpha_{N2} = \beta$.

TABLE 4.2.

$F_{mn}\left(\frac{\pi}{2}, \varphi\right)$	$\cos(\varphi - \alpha_n)$	$\frac{\Delta + \cos(\varphi - \alpha_n)}{\Delta + 1}$
$D_{m\ max}$	$D_{00}\frac{a\beta}{d}\left[1 + \frac{\sin 2\beta}{2\beta}\right]$	$D_{00}\frac{a\beta}{d}\left[\frac{1 + 2\Delta^2 + 4\Delta\frac{\sin\beta}{\beta} + \frac{\sin 2\beta}{2\beta}}{(1+\Delta)^2}\right]$

The maximum directional gain of a cylindrical antenna formed from radiators of any type can be determined by summing the maximum directional gains of the corresponding arc arrays from which the cylindrical antenna is formed.

When the amplitude distribution differs from the optimal the array directional gain is reduced by a factor of ν times (ν is the surface utilization factor). For a cylindrical array with a shared current distribution of $|I_{mn}| = |I'_m|\ |I_{0n}|$:

$$\nu = \nu_1\nu_2 \tag{4.37}$$

where ν_1 is the antenna surface utilization factor for the z coordinate; ν_2 is the arc array surface utilization factor.

For an arc array with a spacing between the radiators of about $\lambda/2$, the coefficient ν_2 can be determined from Table 4.1 for the appropriate distribution in the equivalent linear radiator.

If the spacing between the radiators is approximately λ or more, then the coefficient ν_2 must be determined from the more complex formula:

$$\nu_2 = 1/(1 + \beta^2_{cp}), \tag{4.38}$$

$$\beta^2_{cp} = \sum_{n=-N_1}^{N^2} \left| I_n - \frac{I_{0n\ opt}\sum\limits_{p=-N_1}^{N_2} I_{0p} I_{0p\ opt}}{\sum\limits_{p=-N_1}^{N_2} I^2_{0p\ opt}} \right| \sum_{n=-N_1}^{N_2} \widetilde{I}^2_{0n},$$

$$\widetilde{I}^2_{0n} = \frac{\sum\limits_{p=-N_1}^{N^2} I_{0p} F_{0p}\left(\frac{\pi}{2}, \varphi_0\right)}{\sum\limits_{p=-N_1}^{N_2} \left| F_{0p}\left(\frac{\pi}{2}, \varphi_0\right)\right|^2} F^*_{0n}\left(\frac{\pi}{2}, \varphi_0\right). \tag{4.39}$$

$|I'_m|\ |I_{0n\ opt}|$ is the current amplitude in the mn-th radiator, having the maximum directional gain; $|I'_m|\ |I_{0n}|$ is the actual current amplitude in the mn-th radiator.

The coefficient ν_1 depends on the form of the amplitude distribution $|I'_m|$ with respect to the coordinate z and can be found as in the case of linear antennas.

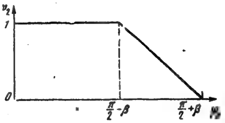

Figure 4.4. The surface utilization coefficient ν_2 as a function of the direction of the beam of a ring array.

We will note that in the case of electrical scanning in azimuth, it is necessary in the general case to control not just the phase, but also the amplitude distribution. The most effective method of amplitude distribution control is that of "shifting" it in azimuth through the scan angle without changing the shape. This technique is feasible in cylindrical and arc arrays with spatial excitation with electrically or mechanically driven motion of the array feed irradiator directional pattern.

However, it is frequently undesirable to control the amplitude distribution in cylindrical arrays during scanning for a number of reasons, in particular, because of the increased complexity of the circuitry and structural design of the antenna. With beam scanning of a cylindrical array in the azimuthal plane solely through the control of the phase distribution, the directional gain of the array changes. When the spacing between the radiators is about $\lambda/2$, the reduction in the directional gain during scanning can be determined from expression (4.38), where:

$$\beta_{\text{ср}}^2 = \frac{\int\limits_{l_{\text{экв}}} \left| I_{\text{экв}}(x) - \int\limits_{l_{\text{экв}}} I_{\text{экв}}(x)\, dx / l_{\text{экв}} \right|^2 dx}{\frac{1}{l_{\text{экв}}} \left| \int\limits_{l_{\text{экв}}} I_{\text{экв}}(x)\, dx \right|^2}, \tag{4.40}$$

$I_{\text{equiv}}(x)$ is the amplitude distribution in the equivalent radiator, perpendicular to the direction of the beam. This expression is to be used if the actual amplitude distribution in the equivalent radiator cannot successfully approximated by one of the functions in Table 4.1. Otherwise, it is simpler to choose the coefficient ν_2 from Table 4.1.

If the spacing between the radiators is approximately equal to λ, then the change in the directional gain during scanning is to be computed from formulas (4.38) and (4.39), taking into account the fact that:

$$I_{0n\ opt} = F^*_{0n}(\pi/2, \varphi_0), I_{0n} = F^*_{0n}(\pi/2, 0).$$

In two cases (radiators which are omnidirectional in azimuth and placed at a spacing of approximately λ or more, and radiators with a directional pattern of $F_{mn}(\pi/2, \phi) = \cos(\phi - \alpha_n)$, positioned at a spacing of about $\lambda/2$), the change in the directional gain during scanning and with a constant amplitude distribution is determined simply and shown graphically in Figure 4.4.

In both cases, the optimal amplitude distribution is uniform. So that the directional gain does not change during scanning, the beam direction ϕ_0 should not exceed an angle of $\pi/2 - \beta$.

The efficiency, η, of cylindrical (ring) antennas depends on the losses in the feeder channel and phase shifters, as well as the antenna circuit configuration. For this reason, the gain of cylindrical arrays should be computed in each specific case following the choice of the antenna circuit, the type of feedline and phase shifter. During the preliminary calculation of the gain of cylindrical scanning antennas, the efficiency of these antennas can be taken as 50 to 60%.

4.6. Bandwidth Properties of Arc Arrays

Arc antennas make it possible under certain conditions to obtain a poor dependence of the major directivity characteristics of the antennas on frequency (beam direction and width, sidelobe level, directional gain) in a wide band of frequencies. The bandwidth properties of arc arrays depend substantially on their circuit configuration, the type of radiators and control element.

Thus, in an arc array with spatial (or parallel) excitation (Figure 4.5), where broadband phase shifters are used [4], with a deviation of the frequency f from the center frequency f_0, with which the phasing is accomplished, a symmetrical phase error occurs in the aperture CD:

$$\Delta\Phi(y) = \kappa_0 \frac{\Delta f}{f} a \left[1 - \sqrt{1 - \left(\frac{y}{a}\right)^2}\,\right] \simeq \frac{1}{2} k_0 a \frac{\Delta f}{f_0} \left(\frac{y}{a}\right)^2, \qquad (4.41)$$

$$\text{when при } \frac{y}{a} < 0{,}6,$$

where $\Delta f = f - f_0$; $k_0 = 2\pi/\lambda_0$.

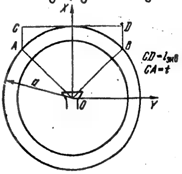

Figure 4.5. Configuration of a parallel excited arc array.

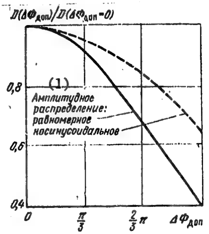

Figure 4.6. The reduction in the directional gain of an arc antenna as a function of the permissible phase error in the equivalent linear radiator.

Key: 1. Amplitude distribution: uniform, cosine.

The presence of a symmetrical phase error in the aperture CD leads to a reduction in the directional gain of an arc array, however, the direction of the pattern maximum remains as before, with a slight error.

The reduction in the arc array directional gain as a function of the value $\Delta\Phi_{доп}$ [$\Delta\Phi_{per}$] in the general case depends on the amplitude distribution in the equivalent aperture. In particular, graphs showing the drop in the directional gain for uniform and cosine amplitude distributions are presented in Figure 4.6 as a function of $\Delta\Phi_{per}$.

By using relationship (4.41) and the graph of Figure 4.6, one can always select the radius of an arc array a and the excitation sector, determined by the ratio $l_{equiv}/2a$, for which the reduction in the array directional gain in the specified passband will not exceed the permissible value. If the ratio is $l_{equiv}/2a$, then the requisite radius of the arc array, for which the phase error at the edges of the equivalent aperture does not exceed the permissible value $\Delta\Phi_{per}$ in a frequency range of $2\Delta f/f_0$, can be found from the approximate expression:

$$a \simeq \frac{\kappa_0 2\Delta f/f_0}{4\Delta\Phi_{доп}} \left(\frac{l_{экв}}{2}\right)^2. \qquad (4.42)$$

It should not be forgotten that the graphs of Figure 4.6 do not take into account the drop in the directional gain related to the frequency response of the phase shifters. For this reason, the phase shifters and radiators of the array should be chosen so that their working bandwidth is at least no less than the requisite bandwidth of the entire arc array as a whole, and the reduction in the array directional gain related to the phase shifter errors are insignificant within the requisite passband.

We shall consider the bandwidth properties of a series excited arc array. In this case, when the frequency changes, the phase error in the equivalent aperture will be composed of the error (4.41) and the error related to the frequency dependence of the phase change between the radiators in the feeder line. For this reason, the overall error is:

$$\Delta\Phi(y) = \kappa_0 a \frac{\Delta f}{f}\left[1 - \sqrt{1 - \left(\frac{y}{a}\right)^2}\right] + \kappa_0 a \gamma_0 \frac{\Delta\lambda_\Phi}{\lambda} \arcsin\left(\frac{y}{a}\right), \qquad (4.43)$$

where $\Delta\lambda_\Phi/\lambda$ is the relative change in the wavelength λ_Φ in the feedline; $\gamma_0 = \lambda_0/\lambda_{\Phi 0}$ is the retardation in the feedline at the center frequency.

Expanding $\Delta\Phi(y)$ in a Taylor's series in the vicinity of the point y = 0, and limiting ourselves to the first terms, we obtain [3]:

$$\Delta\Phi(y) \simeq \kappa_0 a \gamma_0 \frac{\Delta\lambda_\Phi}{\lambda}\frac{y}{a} + \frac{1}{2}\kappa_0 a \frac{\Delta f}{f}\left(\frac{y}{a}\right)^2 + \frac{1}{6}\kappa_0 a \gamma_0 \frac{\Delta\lambda_\Phi}{\lambda}\left(\frac{y}{a}\right)^3. \qquad (4.44)$$

The first term in (4.44) leads to the deflection of the beam of the arc array from the initial position by the amount:

$$\Delta\varphi_1 \simeq \arcsin\left(\frac{\kappa_0\gamma_0}{\kappa}\frac{\Delta\lambda_\Phi}{\lambda}\right). \qquad (4.45)$$

The second term in (4.44) leads to a reduction in the directional gain of the array according to the governing law defined by expression (4.41) and the graphs of Figure 4.6. The third term leads to beam asymmetry.

Thus, in a series excited arc array, the azimuthal plane position of the beam is frequency dependent. For this reason, such arrays can be used only in relatively narrow band systems. The displacement of the beam of an arc array in a small range (up to half of the width of the directional pattern, $2\phi_{0.5}$) is equivalent to an additional reduction in its directional gain.

During the preliminary calculations, when the law governing the amplitude distribution in the arrays has not yet been determined, the reduction in the direction 0, ϕ_0 when the beam position changes can be estimated from the formula:

$$\frac{D(0,\ \varphi_0 + \Delta\varphi)}{D(0,\ \varphi_0)} = \frac{\sin^3\left[\frac{\kappa_0 l_{\text{экв}}}{2}\sin\left(\frac{\kappa_0\gamma_0}{\kappa}\frac{\Delta\lambda_{\text{ф}}}{\lambda}\right)\right]}{\left(\kappa_0\frac{l_{\text{экв}}}{2}\right)^2\sin^3\left(\frac{\kappa_0\gamma_0}{\kappa}\frac{\Delta\lambda_{\text{ф}}}{\gamma}\right)}, \qquad (4.46)$$

which is justified for a uniform amplitude distribution in the equivalent aperture.

The bandwidth properties of a cylindrical array in azimuth are governed by the bandwidth properties of the corresponding arc arrays of which the cylindrical antenna is composed. In the $\phi = \phi_0$ plane though, the bandwidth properties of the cylindrical array directional pattern are governed by the bandwidth properties of the equivalent linear antenna array.

4.7. Some Structural and Circuit Design Variants for Arc and Cylindrical Arrays

A variant of an annular array with mechanical beam scanning in azimuth from 0 to 360° is shown schematically in Figure 4.7. The annular array is formed by two parallel metal disks (1) between which radiators are installed along the perimeter in the form of open rectangular waveguide ends (2) using a working H_{10} mode. Ferrite phase shifters (3) are installed in the waveguides, the phase in which changes as a result of the change in the bias magnetization current in winding (4) [5]. The length of a waveguide radiator should be the minimum possible, but such that the phase shifter installed in it is capable of assuring control of the electromagnetic field phase in a range of 0 to 2π radians.

A ring array is excited through a radial line from the feed radiator in the form of an open rectangular waveguide end or a horn (5). The aperture of this horn is chosen from the condition that the shape of its directional pattern corresponds to the shape of the requisite amplitude distribution in the ring array. To control the amplitude distribution during beam scanning, the feed horn is connected to a rotating coupling (6). The ring choke groove (7) serves for matching the feed radiator to the radial line and eliminating radiation through the slot between the rotating coupling and the radiating line.

The maximum electrical scan frequency in the given structural design is governed by the inertia of the rotating coupling, and in a circular scanning mode, can reach several tens of revolutions per second.

A drawback to the structural design considered here is the relatively low beam control speed, which is related to the presence of mechanical rotation of the feed radiator. A variant of an annular array is shown in Figure 4.8, which corresponds to the schematic of Figure 4.1a, with electrical beam scanning in a range of 0 to 360°. The energy is guided from the coaxial stub exciter (1) through the electrically controlled switch (2) to the requisite sector of the radial line (3), along the perimeter of which are the radiators in the form of waveguide sections with electrically controlled phase shifters installed in them. The beam scanning within the angular range determined by the angular spacing between two adjacent switcher channels is accomplished solely by virtue of the

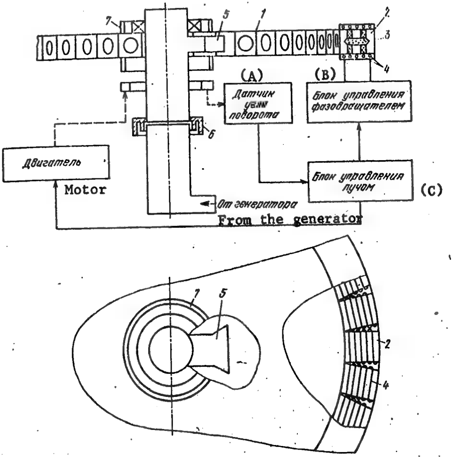
7
5
1
2
3
4
6
(A)
(B)
Датчик угла поворота
Блок управления фазовращателем
Двигатель
Motor
Блок управления лучом
(C)
От генератора
From the generator
7
5
2
4

Figure 4.7. A ring array with mechanical beam scanning.

Key: A. Rotation angle sensor;
B. Phase shifter control unit;
C. Beam control unit.

phase control at the output of the radiators. The number of switcher channels is chosen in accordance with the requirements placed on the permissible beam distortion during scanning (a six position switch is shown in Figure 4.8).

A multiposition switch can be designed around a reflective type isolator switch, which is depicted schematically in Figure 4.9. The operational principle of the switch is based on the dependence of the reflection factor on the magnetic field intensity. In such a switch, a thin metal partition (1), placed close to the ferrite (2), is soldered to the narrow wall of the waveguide perpendicular to the dominant mode electrical field lines of force. With a comparatively small bias magnetization field, the wave is almost completely reflected from the ferrite and energy does not float through the device. This occurs as a consequence of the conversion of the H_{10} mode to an E wave, which cannot propagate in a waveguide with metallic plates.

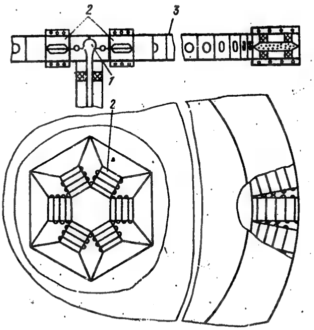

Figure 4.8. A ring array with electrical beam scanning by means of switching the feed irradiator.

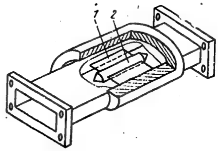

Figure 4.9. Schematic drawing of an isolator switch.

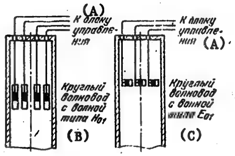
(A)
К блоку управления
Круглый волновод с волной типа H_{01}
(B)
К блоку управления
(A)
Круглый волновод с волной [illegible] E_{01}
(C)

Figure 4.10. Feed radiator for [illegible] ring array with switched outputs.

Key:
A. To the control unit;
B. Circular H_{01} mode waveguide;
C. Circular E_{01} mode waveguide.

In the absence of a magnetic field, the ferrite behaves like an isotropic dielectric and the microwave energy passes through to the device output with few losses. Such switches have a rather high K_{st} [SWR]. For this reason, when such switches are combined in an n-position switch, it is essential to provide matching elements. The speed of the switches amounts to tens of microseconds.

Other types of switchers designed around ferrites are also possible [5]. A system of resonant slots cut in a circular E_{10} or H_{01} mode waveguide (Figure 4.10) and switched with PIN diodes can also be used as switches. A drawback to such [illegible] system is the poor working bandwidth ±(2-3) % and the relatively small transmitted power (about 10 watts).

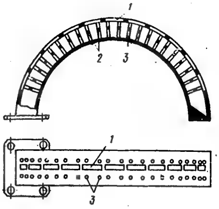

Figure 4.11. A series excited arc array.

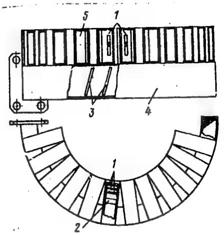

Figure 4.12. A series excited arc array with phase shifters using waveguide bridges.

An example of an annular array design in a series excitation configuration is shown in Figure 4.11. Half-wave slots (1) are cut along the center of the wide wall of the waveguide. Four diodes (2) inserted in the center of the metal stubs (3), installed between the wide walls of the waveguide, each on different sides of each slot, are used for independent control of the amplitude and phase of the field radiated through a slot. By changing the voltage applied to the diodes, one can change the phase of the field radiated through a slot from 0 to 360°. The amplitude control range is 35 dB [6] (the coupling of the field radiated by the slot to the waveguide field can vary from -50 to -15 dB). In particular, with a balanced circuit configuration for all four diodes, the slotted radiator treated here theoretically does not radiate (the coupling to the waveguide field is practically about -50 dB).

Another variant of the structural design of an arc array with series excitation and discretely switched phase shifters is shown in Figure 4.12. The electromagnetic wave energy from the feed waveguide 4 which is bent in an arc is fed through the coupling holes (3) sequentially to the input arms of the slotted waveguide bridges joined to the waveguide and passes through the coupling holes (2) to the two other arms of the bridge, each of which is loaded into slotted stops (1) which are switched by means of PIN diodes. In being reflected from the "turned-on" stops, i.e., from the stops to the PIN diodes of which a voltage is applied, the wave is then fed to the output channels of the bridges and the energy is radiated through the open ends of the waveguides. With a change in the position of "turned-on" stops, the phase of the field radiated by the waveguides 5 will change.

One of the beam scanning methods frequently used in practice in cylindrical antennas is the technique of phase-frequency scanning. The essence of it consists in the fact that the cylindrical array is built up using frequency scanning slotted waveguide antennas. The individual slotted waveguide antennas are joined together by means of a parallel excitation circuit, in the branches of which phase shifters are installed. The antenna beam is controlled in azimuth by means of these phase shifters, while the beam scanning is accomplished in the meridianal plane by changing the generator frequency.

Other circuits and structural designs are also possible for ring and cylindrical arrays [013, 1, 7].

4.8. The Design Procedure for Cylindrical Arrays

We shall consider a few variants for the design of cylindrical arrays.

Variant 1. Design an arc array with electrical beam scanning in the azimuthal plane in an angular sector of $(\phi_0 + \phi_{max}, \phi_0 - \phi_{max})$.

The main parameters are specified: the polarization of the radiated field, the width of the directional pattern in azimuth $2\phi_{0.5}$, the working bandwidth $2\Delta f/f_0$ and the permissible reduction in the directional gain at the edges of the band, the permissible level q of the first sidelobes, and the radiated power P. The additional parameters are: the precision in beam steering, the ultimate dimensions of the array, the scanning rate, etc.

The design calculation consists of the following steps.

1. Determine the amplitude distribution in the equivalent aperture and the length of the equivalent aperture l_{equiv} with the condition that the array beam is generated along the axis $\phi = \phi_0$ using the data of Table 4.1, based on a specified q and $2\phi_{0.5}$.

2. Select the circuit configuration for the arc array. For this purpose, if the precision in array beam steering is stipulated in the specifications, then ascertain by means of relationship (4.45) whether the requisite precision is realized in a series excited arc array. In this case, naturally, it is necessary to specify the type of feedline. If the answer is negative, then a parallel excitation configuration is chosen, and if it is positive, then by using expressions (4.41), (4.42) or (4.41), (4.45) and (4.46) and the graph in Figure 4.6, then based on the permissible reduction in the directional gain, it is necessary to find the minimum radius of the arc array for the case of parallel and series excitation respectively. If the radius found for the series excited arc array is not much greater than the radius of the same array with parallel excitation, and the array falls within permissible dimensional limits, then a series excited arc array is to be selected. Otherwise, it is necessary to choose a parallel excited array.

3. The angular size of the arc array is determined from the values found for a and l_{equiv} as well as the specified value of ϕ_{max}:

$$2\beta_{max} = 2(\beta + \varphi_{max}), \qquad (4.47)$$

where $\beta = \arcsin(l_{equiv}/2a)$.

4. The type of radiator is chosen and using expressions (4.17) - (4.20), its polarization and amplitude patterns are calculated. The minimal spacing between the radiators and the overall number of radiators is determined (from structural design considerations).

5. Using the working frequency and the requisite bandwidth, as well as the specified power, the type of feedline and the type of phase shifter are chosen.

6. The requisite electrical length of a phase shifter and the law governing the change in this length in the scan sector is found from formulas (4.3) - (4.7).

7. By means of expression (4.27) based on the chosen amplitude distribution $I_{equiv}(y)$ in the equivalent aperture and the calculated directional pattern of an individual radiator, the amplitude distribution is found in the array $I_n = I(\alpha_n)$.

8. The feed system for energy distribution among the radiators is designed using the amplitude distribution which has been found. The circuit configuration of the phase shifters is specified more precisely. If necessary, a device controlling the amplitude distribution during scanning is selected. For this purpose, the reduction in the directional gain in the scan sector with a constant amplitude distribution is determined beforehand from formulas (4.38), (4.40) or from the graphs of Figure 4.4. If this reduction exceeds the permissible value, then a provision is made for a device to control the amplitude distribution during scanning.

9. The shape of the main and first sidelobes of the directional pattern is computed using formula (4.25) or by means of Table 4.1. When using Table 4.1, it must be remembered that the design calculations can be carried out within limits governed by expression (4.26).

10. The level of the diffraction sidelobes is specified more precisely by means of formulas (4.22) and (4.28).

11. The directional gain of the array is determined from expressions (4.33), (4.35), (4.36), (4.37) - (4.39) or the data of Table 4.1 and 4.2.

12. The efficiency of the array and then the gain of the array is determined based on the known losses in the feedline, the switchers and in the phase shifters.

13. Taking into account the finally selected circuit, type of radiator and phase shifter feed system, the bandwidth properties of the arc array are found more precisely.

14. Where necessary, the shape of the directional pattern is found more precisely from formula (4.22) using a computer.

Variant 2. Design an arc array with electrical scanning in an angular sector of $(\phi_0 + \phi_{max}, \phi_0 - \phi_{max})$.

The main parameters are specified: the polarization of the radiated field, the directional gain, the working bandwidth, the radiated power and the level of the first sidelobes.

The design calculations consist of the following steps:

1. The amplitude distribution in the equivalent aperture is found from the specified level of the first sidelobes using Table 4.1.

2. In accordance with the specified bandwidth and installation site of the antenna array, the type of radiator is determined and its directional pattern is found. The minimum spacing d between adjacent radiators is determined based on structural design considerations.

3. The requisite number of radiators is determined based on the specified directional gain in the direction ϕ_0, using relationships (4.32) and (4.35) - (4.39).

The design calculations are then performed in accordance with the scheme for variant I in the following sequence: paragraph 2 is done, the angular size of the array $2\beta_{max}$ is determined and then paragraphs 5 - 10 and 12 - 14 are carried out.

Variant 3. Design an electrically scanning arc array for an angular sector of $(\phi_0 + \phi_{max}, \phi_0 - \phi_{max})$.

The main parameters are specified: the structural configuration of the array, its radius (or permissible boundaries, within the limits of which it can be chosen), the polarization of the radiated field, the directional gain (or beam width), the level of the first sidelobes, the radiated power and the average working frequency.

The design calculations are carried out in accordance with the scheme for variant 2 in the following sequence: paragraphs 1 - 3 are carried out, the angular dimension $2\beta_{max}$ and the radius of the array (if its permissible range of values is specified) are determined, and then paragraphs 5 - 10, 12 and 14 of variant 1 are carried, and finally, the working range of frequencies of the antenna is computed.

Variant 4. Design a cylindrical array with electrical scanning in azimuth in an angular sector of $(\phi_0 + \phi_{max}, \phi_0 - \phi_{max})$.

The main parameters of the array in the azimuthal plane are specified just as in variants 1 - 3; the width of the directional pattern and the level of the sidelobes in the plane $\phi = \phi_0$ are specified in addition, and the directional gain of the cylindrical array is specified instead of the directional gain of an arc array. The design calculations are performed in accordance with the procedure for variants 1 - 3, with the difference that the directional gain of the cylindrical array is determined using expressions (4.34), (4.37) - (4.39). The structural configuration of the cylindrical array is additional determined, as well as its dimension along the Z axis and the amplitude distribution along the z coordinate in the cylindrical array in accordance with the procedures for the design calculations for linear antenna arrays (the results of Table 4.1 can be used for this purpose, keeping in mind the note placed after formula (4.29)).

5. SLOTTED WAVEGUIDE ARRAYS

5.1. The Function and Specific Features of Slotted Waveguide Arrays

Slots are widely used in microwave engineering as radiating elements or as independent antennas. In this case, primarily slots in waveguides are used, although slots in metal plates or foil excited by means of striplines can also be employed [01].

Slotted waveguide linear arrays (VShchr) provide for a narrowing of the directional pattern in a plane running through the axis of the waveguide.

Slotted waveguide arrays with mechanical, electromechanical and electrical scanning are used along with slotted waveguide arrays having directional patterns which are stationary in space [01].

We will note the major merits of slotted waveguide arrays:

1) Because of the absence of protruding parts, the radiating surface of a slotted waveguide array can be co-located with the external surface of an aircraft fuselage, without introducing additional aerodynamic resistance in this case (an on-board antenna);
2) Optimal directional patterns can be realized in them, since the field distributions in the aperture can differ by virtue of changing the coupling of the radiators to the waveguide;
3) They have comparatively simple excitation and are simple to operate.

A drawback to slotted waveguide arrays is the limited bandwidth. With a change in frequency, there is a deviation of the beam in space from the specified position in a nonscanning slotted waveguide array, where this deviation is accompanied by a change in the width of the directional pattern as well as in the matching of the antenna to the feedline.

5.2. The Major Parameters of a Slot in a Waveguide

A slot in a waveguide is excited if it intersects the surface currents flowing through the inside walls with its own wide side.

When a slotted waveguide array is designed, for example, around a rectangular waveguide with a dominant H_{10} mode, it is necessary to take into account the fact that there are longitudinal and transverse surface currents in the waveguide in the wide walls and a transverse current in the narrow walls.

The four main types of radiating slots in a rectangular waveguide are shown in Figure 5.1. Slots I-III are located in the wide wall of the waveguide; slot IV is in the narrow wall. Longitudinal slot intersects the transverse current, if it is shifted relative to the center line of the wide wall of the waveguide. There is no radiation when $x_1 = 0$ and the radiation increases with an increase in the displacement x_1. Transverse slot II is excited by the longitudinal currents. The intensity of the excitation decreases with increasing displacement from the center line. When $x_1 = 0$, the radiation is a maximum. The oblique displaced slot III intersects both the longitudinal and the transverse currents. When $x_1 = 0$ and the inclination angle of the slot is $\delta = 0$, there is no radiation. Slot IV, which is cut in the side wall, is not excited when $\delta = 0$. When $\delta = 90°$, the radiation is a maximum. By means of combining slots I and II, one can obtain a cross-shaped slot. With a certain positioning of the center of the cross-shaped slot, it radiates a circularly polarized field [01].

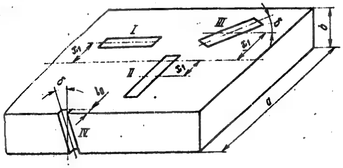

Figure 5.1. The main types of slots used in slotted waveguide arrays.

As has already been indicated, a longitudinal slot running along the center line of the waveguide ($x_1 = 0$) and an oblique slot in the side wall (when $\delta = 0$) do not radiate. However, currents flowing in the waveguide walls close to these slots can produce such changes that radiation takes place. So-called reactive dipoles are used for this: metallic rods, screwed into the waveguide alongside the slot, which disrupt the symmetry of the current in the waveguide wall.

Oblique slots in the narrow wall usually stick a little bit into the wide walls of the waveguide. When such slots are cut in a waveguide, it turns out that susceptance of the slot is low and has an insignificant influence on the propagation constant of the waveguide [01], practically regardless of the inclination angle of the slot δ (if $\delta \leq 15°$) for a fixed value of the cutout depth l_0. Moreover, the slot susceptance changes considerably less with a change in the frequency than in the case of slots cut in the wide wall of a waveguide. For this reason, oblique slots in the narrow wall of a waveguide are preferable (both from electrical and structural viewpoints), especially in large antenna systems.

External and Internal Radiation Admittances of a Slot. The Equivalent Normalized Admittance of a Slot in a Waveguide. When a slot in a waveguide is excited by the currents flowing through its interior walls, it radiates electromagnetic energy both into the external space and into the waveguide. The slot radiation admittance, which is determined by the external radiation, is called the external radiation admittance: $Y_{(e)} = G_\Sigma + jB^{(e)}$. The radiation admittance determined by the radiation of energy into the waveguide is called the internal radiation admittance of the slot: $Y^{(i)} = G^{(i)} + jB^{(i)}$.

It can be demonstrated by means of the duality principle [1], that the external radiation admittance of a resonant slot, cut in the wall of a waveguide, and having an infinite flange is:

$$Y^{(e)} = G_\Sigma = 0{,}5R_\Sigma/(60\pi)^2,$$

where R_Σ is the radiation resistance of an equivalent symmetrical dipole.

The radiation admittance of actual slot antennas, cut in a shield of finite dimensions, is always 10 to 15% less [2] than the admittance of a slot in an infinite shield. Consequently, one can assume that the external radiation admittance of a slot in a waveguide is:

$$G_\Sigma \simeq 0{,}9R_\Sigma/2\,(60\pi)^2. \tag{5.1}$$

Knowledge of the internal admittances of the slots, $Y^{(i)}$, along with the external values, makes it possible to determine the resonant frequency of slots of different lengths and to trace this as a function of the position in the wall of the waveguide [3].

As is well known, a slot cut in a waveguide disrupts the operational conditions of the waveguide, causing the reflection of electromagnetic energy: a portion of the energy is radiated, while the remainder travels further along the waveguide. Thus, a slot is a load for the waveguide, in which a portion of the power is dissipated, equivalent to the radiation power.

For this reason, an idea of the influence of a slot on the field in a waveguide, and correspondingly, of the equivalent circuit of a slot, can be obtained by replacing the waveguide with an equivalent two wire line, in which impedances are inserted in parallel (g + jb) or in series (r + jx) depending on the type of slot. Thus, a longitudinal slot is equivalent to an impedance inserted in parallel with the line, while a transverse one corresponds to a series connected impedance [07]. When doing design calculations for slotted waveguide arrays, a series resistance r, normalized for the characteristic impedance of the waveguide, is usually employed, as well as a parallel conductance, normalized with respect to the characteristic conductance of the waveguide. Both r and g are uniquely related to the external and internal radiation admittances of a slot and can be found from the power balance condition in the slot cross-section in the waveguide [2, 07].

An equivalent circuit of a resonant slot (Figure 5.8a), cut arbitrarily in a waveguide (III in Figure 5.1) can be represented by two sections of a two wire line with an electrical length of Δ_1 and Δ_2 with a shunting conductance g [4]. The equality $\Delta_1 = -\Delta_2$ is justified in this case, i.e., an arbitrary resonant slot in a waveguide does not change the phase of the wave passing through.

The major types of slots which can be cut in waveguides and their equivalent circuits are shown in Table 5.1; relations are also given for the equivalent normalized resistances and conductances of half-wave slots in a waveguide. The following symbols are introduced in Table 5.1: λ is the generator wavelength; λ_B is the wavelength in the waveguide; a and b are the internal dimensions of the waveguide.

The Resonant Length of a Slot. The formulas given in Table 5.1 for the equivalent conductances and equivalent resistances of slots in a waveguide were derived for half-wave slots. This length is close to the resonant length of a

TABLE 5.1.

Расположение щели (1)	Эквивалентная схема (2)	Эквивалентная проводимость или сопротивление (3)
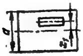	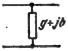	$g=2{,}09\frac{a}{b}\frac{\lambda_в}{\lambda}\cos^2\left(\frac{\pi}{2}\frac{\lambda}{\lambda_в}\right)\sin^2\left(\frac{\pi x_1}{a}\right)$
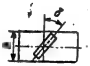	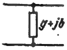	$g=\frac{30}{73\pi}\frac{\lambda_в}{\lambda}\frac{\lambda^4}{a^3b}\times$ $\times\left[\frac{\sin\delta\cos\left(\frac{\pi}{2}\frac{\lambda}{\lambda_в}\sin\delta\right)}{1-\left(\frac{\lambda}{\lambda_в}\right)^2\sin^2\delta}\right]^2$
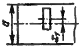	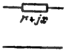	$r=0{,}523\left(\frac{\lambda_в}{\lambda}\right)^2\frac{\lambda^2}{ab}\cos^2\left(\frac{\pi}{2}\frac{\lambda}{2a}\right)\times$ $\times\cos^2\left(\frac{\pi x_1}{a}\right)$
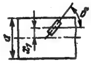	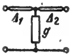	$g=0{,}82\lambda(a_1^2+b_1^2),\ \Delta_1=\frac{\pi}{2}-$ $-\operatorname{arctg}\frac{b_1}{x_1},\ \Delta_2=-\Delta_1$

Key: 1. Arrangement of the slot;
2. Equivalent circuit;
3. Equivalent conductance or resistance.

slot for which the equivalent susceptance b and the equivalent reactance x are zero. Since g and r change little close to resonance, the expressions for g and r can also be used for resonant slots. The resonant length of a slot is slightly less than λ/2, and is smaller, the wider the slot is. Moreover, the resonant length of a slot depends on the displacement of the slot relative to the center of the wide wall of the waveguide.

One can employ the calculated curves [07] shown in Figure 5.2 in a form convenient for direct determination of the resonant length of slots, $2l$, to determine the resonant length of a longitudinal slot in the wide wall of a waveguide. The data are given for a waveguide with a retardation factor of $\gamma = \lambda/\lambda_B = 0.67$ for three values of the slot width d_1. It can be seen that the wider the slot is, the greater the resonant length of the slot differs from λ/2. For a fixed slot width and a slight increase in the displacement x_1 of a longitudinal slot relative to the center of the wide wall of a waveguide, the resonance length increases, approaching λ/2. With a further increase in the displacement of the slot, its resonant length decreases.

The resonant length of a transverse slot in the wide wall of a rectangular 3 cm band waveguide when $x_1 = 0$ is equal to $2l = 0.488\ \lambda$ [3], i.e., differs insigni-

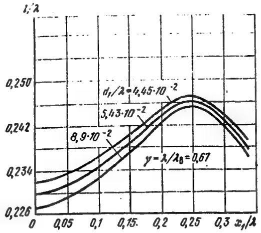

Figure 5.2. The resonant length of a longitudinal slot as a function of its displacement x_1.

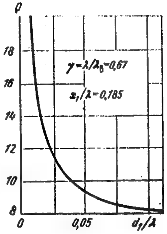

Figure 5.3. The Q of a slot as a function of its relative width d_1/λ.

ficantly from a generator half-wavelength. Inclined slots in the narrow wall have a resonant length equal to approximately half of the wavelength in free space [01] (its precise value is usually chosen experimentally).

In design calculations for slotted waveguide arrays, it is important to know the slot passband, which is characterized by the quality factor Q. The Q of a longitudinal slot is shown in Figure 5.3 as a function of its relative width d_1/λ for a waveguide with a phase velocity retardation of $\gamma = 0.67$ when the center of the slot is shifted relative to the center line of the wide wall of the waveguide by $x_1/\lambda - 0.185$. It follows from the figure that with a slot width of $d_1/\lambda = 0.05 - 0.1$, its Q changes insignificantly and does not exceed 10, which with a high carrier frequency in the microwave band corresponds to a considerable bandwidth ($2\Delta f/f \approx 10\%$).

The graph for the Q of a longitudinal slot as a function of its relative width can also be used for a transverse slot in a roughly estimating its bandwidth.

The slot width in a slotted waveguide array is chosen by working from the conditions for assuring the requisite electrical strength and the necessary passband. When a slotted antenna operates only in a receive mode, the major factor in the selection of the slot width is the bandwidth of the signals being received.

When selecting the slot width d_1, a safety margin of two or three times with respect to the breakdown field intensity for the center of the slot should be provided, where the field intensity, E_{slot}, is a maximum ($2l = \lambda/2$). This safety margin is chosen by working from the structural design requirements and the operational conditions of the slotted antenna:

$$E_{slot} = \qquad E_m = \frac{U_m}{d_1} \leqslant \left(\frac{1}{2} - \frac{1}{3}\right) E_{\text{пр}}, \tag{5.2}$$

where U_m is the voltage amplitude at the antinode; $E_{\text{пр}}$ [E_{ult}] is the ultimate value of the field intensity at which electrical breakdown begins (for air under normal atmospheric conditions, E_{ult} = 30 KV/cm).

In the case of a uniform amplitude distribution over the antenna aperture, when the power radiated by the antenna is divided equally among the slots:

$$U_m = \sqrt{\frac{2P}{N}\frac{1}{G_\Sigma}}, \qquad (5.3)$$

where P is the power delivered to the antenna; G_Σ is the radiation conductance of the slot; N is the number of slots.

If the amplitude distribution over the aperture differs from a uniform distribution, the slot which radiates the greatest power is to be determined for the specified amplitude distribution. Knowing the distribution of the radiated power over the antenna slots and the delivered power, it is not difficult to calculate what fraction of the total power goes for a given slot. Substituting the value found in formula (5.3) in place of P/N, one can find U_m.

Finally, the slot width is determined from (5.2):

$$d_1 \geqslant (2-3)\, U_m / E_{\text{пред.}\ \text{ult.}} \qquad (5.4)$$

If the slot is filled with a dielectric or covered with a dielectric plate, its electrical strength is increased [9].

5.3. The Types of Slotted Waveguide Arrays

Distinctions are drawn between resonant antennas, nonresonant ones and antennas with matched slots.

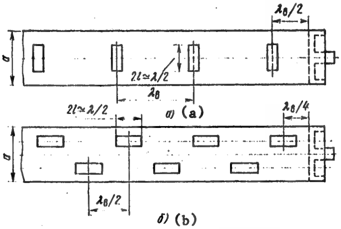

Figure 5.4. A resonant antenna with transverse (a) and longitudinal (b) slots.

In resonant antennas, the spacing between adjacent slots is equal to λ_B (Figure 5.4a: the slots are coupled in-phase to the waveguide field), or $\lambda_B/2$ (Figure 5.4b: the slots are coupled in an alternating phase fashion to the waveguide field). Thus, resonant antennas are in-phase antennas, and consequently, the direction of maximum radiation coincides with a normal to the longitudinal axis of the antenna. In-phase excitation of longitudinal slots placed on different sides of the center line at a spacing of $\lambda_B/2$ is assured by virtue of an additional phase shift of 180°, due to transverse currents in opposite directions on both sides of the center line of the wide wall of the waveguide. In the case of inclined slots in the side wall, the additional 180° shift is obtained by virtue of changing the direction of slot inclination ($\pm\delta$). Consequently, the resulting phase shift for adjacent radiators in both cases proves to be 360° or 0°, regardless of the type of load at the end of the antenna.

A resonant antenna can be quite well matched to the feedline in an extremely narrow band of frequencies. In fact, since each slot is not individually matched to the waveguide, all of the waves reflected from the slots are added together in-phase at the antenna input and the reflection factor of the system becomes large. It is obvious that this mismatching can be compensated at the antenna input by means of any tuning element, but since the matching is disrupted with even small changes in the frequency, the antenna remains a very narrow band type. For this reason, in the majority of cases one dispenses with in-phase excitation of individual slots and the spacing between them is chosen as $d \gtrless \lambda_B/2$.

A characteristic feature of the nonresonant antenna obtained in this fashion is the greater bandwidth within which there is good matching, since individual reflections are almost completely cancelled with the large number of radiators.

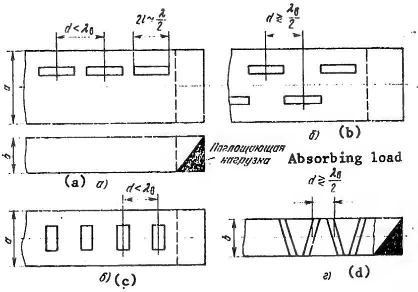

Figure 5.5. Configurations of nonresonant slotted waveguide antennas with longitudinal (a, b), and transverse (c) slots in the wide wall of a waveguide, as well as with oblique (d) slots in the narrow wall of a waveguide.

However, when the spacing between the slots differs from $\lambda_B/2$, this leads to out-of-phase excitation of the slots by the incident wave and the direction of the main radiation lobe is deflected from the normal to the antenna axis. This deflection is most often small (with the exception of special cases) and changes in the shape of the main lobe and the level of the sidelobes caused by the deflection of the beam are still not noticeable. For this reason, the directional properties of such an antenna can also be determined as in the case of in-phase excitation, with subsequent accounting for the beam inclination angle.

A terminal absorbing load is usually installed to eliminate reflections from the end of a waveguide. Circuits of nonresonant antennas with in-phase coupling of the slots are shown in Figure 5.5 (Figure 5.5a, c) as well as with alternate phase coupling (Figure 5.5b, d) to the waveguide field, where the slots are cut in both the wide and in the narrow walls of the waveguide. In all cases, the phase distribution in the antenna can be considered linear if the mutual coupling of the radiators via both the internal and external space is not taken into account.

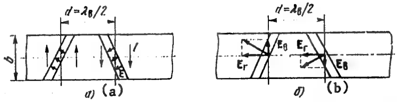

Figure 5.6. Inclined slots in the narrow wall of a waveguide.

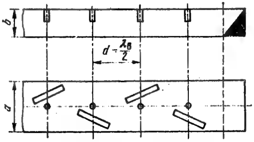

Figure 5.7. A slotted antenna with obliquely displaced matched slots.

While the slotted waveguide arrays shown in Figure 5.5a-c have a radiation field with only the dominant polarization, antennas with oblique slots in the narrow wall (Figure 5.5d) also have a field with parasitic polarization.

The direction of the transverse currents in the narrow wall of a waveguide and the field intensity vectors for the electrical field excited in two oppositely inclined slots ($\pm\delta$) where the spacing between them is $\lambda_B/2$ is shown in Figure 5.6a with the arrows. The radiation of such slots is determined by the horizontal components of the field intensity vector of the slots (Figure 5.6b). The vertical components produce a parasitically polarized field. To reduce the parasitic component of the radiation field, the inclination angles of the slots must be made $\delta \leq 15°$, for which the power lost to parasitic polarization amounts to less than 1%. However, this limits the possibility of obtaining the requisite normalized conductances of the slots, g. For this reason, special steps are taken in practice [01] to suppress the parasitic polarization field.

In antennas with matched slots, each slot (longitudinal, transverse or obliquely displaced) is matched to the waveguide by means of a reactive dipole or a stop and does not produce any reflections. Consequently, a traveling wave mode is established in such antennas with a terminal absorbing load. A schematic of an antenna with obliquely displaced matched slots is shown as an example in Figure 5.7. In such antennas, good matching to the feed waveguide is obtained in a wide passband (5 to 10%). In the case of obliquely displaced slots in the wide wall of a waveguide, through the choice of the inclination angle δ and the displacement x_1, the normalized conductance of the waveguide in the cross-section of the slot is made equal to unity and the susceptance existing in this cross-section is cancelled out by means of a reactive stub. Since the stub is installed in the waveguide section, passing through the center of the slot, with a change in the frequency there is a simultaneous change in the susceptances of the stub and the slot and their mutual compensation takes place in a certain range of frequencies. With a substantial change in frequency, the antenna likewise remains matched to the feed waveguide, since it becomes a nonresonant one.

The spacing between matched radiators in an array with alternate phase coupling of the slots is usually taken equal to $\lambda_B/2$ at the nominal frequency. The direction of the maximum radiation in this case is perpendicular to the axis of the waveguide.

5.4. Methods of Designing Slotted Waveguide Arrays

There are several methods of designing slotted waveguide arrays. Strict design techniques entail considerable mathematical difficulties, and for this reason they are not used in engineering calculations and in synthesis problems. Approximate methods are usually employed in engineering calculations.

Approximate design calculations can be performed for slotted waveguide arrays by means of the energy technique of [07], which does not take into account the mutual coupling of the slots via the internal and external spaces. It is assumed that the phase shift between adjacent radiators through the feed waveguide is equal to the electrical spacing between them of $2\pi d/\lambda_B$, while the phase distribution in the antenna aperture is linear. However, because of the external and internal mutual coupling of the slots in the waveguide, there is a substantial deviation of the amplitude-phase distribution from the requisite distribution, while the attainable directional pattern deviates from the specified one, which is primarily due to the cross coupling of the slots via the dominant mode [5].

The method of recurrent relationships of [6] takes mutual coupling of the slots via the dominant mode in the feed waveguide into account and provides for a better approximation of the specified distribution in the antenna aperture by the feasible distribution as compared to the energy technique.

The most precise design calculations for slotted waveguide arrays can be performed using the method of successive approximations of [07], which takes into account both external and internal interaction of the slots in the waveguide (via the dominant and higher modes). However, the design calculations are more complicated in this case.

We shall consider the method of recurrent relationships and the energy technique for design calculations of slotted waveguide arrays.

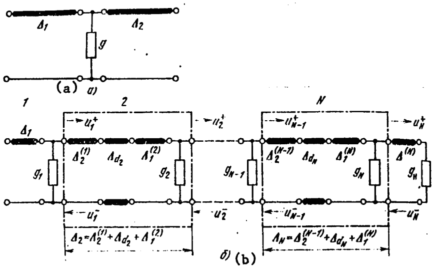

Figure 5.8. The equivalent circuits of a resonant slot, arbitrarily cut in the wall of a waveguide (a), and a slotted waveguide array (b).

The Method of Recurrent Relationships [6]. The equivalent circuit of a slotted waveguide array with arbitrary resonant slots in the form of a two wire line with shunting conductances is shown in Figure 5.8b. The spacing between adjacent conductances is composed of the distance between the slots and the two wire line sections incorporated in the equivalent circuit of the slots. We designate the complex amplitudes of the incident and reflected wave voltages at the input as u^+_{n-1} and u^-_{n-1}, and use the symbols u^+_n and u^-_n for the complex amplitudes of the incident and reflected waves at the output of the n-th four-pole network, into which the equivalent circuit of the antenna is broken down:

$$u^+_{n-1} = A_{n-1} + j B_{n-1},\ u^+_n = A_n + j B_n,$$
$$u^-_{n-1} = C_{n-1} + j D_{n-1},\ u^-_n = C_n + j D_n. \qquad (5.5)$$

By using four-pole network theory, one can establish the fact that the real components A_{n-1} and C_{n-1} and the imaginary component B_{n-1} and D_{n-1} of the complex amplitudes of the incident and reflected voltages at the input of the n-th four-pole network are expressed as follows in terms of the real A_n, C_n and imaginary B_n and D_n components of the complex amplitudes of the incident and reflected voltages at the output of the same four-pole network:

$$A_{n-1} = \left(1 + \frac{g_n}{2}\right)(A_n \cos \Delta_n - B_n \sin \Delta_n) + \frac{g_n}{2}(C_n \cos \Delta_n - D_n \sin \Delta_n),$$
$$B_{n-1} = \left(1 + \frac{g_n}{2}\right)(A_n \sin \Delta_n + B_n \cos \Delta_n) + \frac{g_n}{2}(C_n \sin \Delta_n + D_n \cos \Delta_n), \qquad (5.6)$$
$$C_{n-1} = \left(1 - \frac{g_n}{2}\right)(C_n \cos \Delta_n + D_n \sin \Delta_n) - \frac{g_n}{2}(A_n \cos \Delta_n + B_n \sin \Delta_n),$$
$$D_{n-1} = \left(1 - \frac{g_n}{2}\right)(D_n \cos \Delta_n - C_n \sin \Delta_n) + \frac{g_n}{2}(A_n \sin \Delta_n - B_n \cos \Delta_n). \qquad (5.6)$$

Here, g_n is the normalized conductance of the n-th slot; $\Delta_n = \Delta_{d_n} + \Delta_2^{(n-1)} + \Delta_1^{(n)}$ is the electrical spacing between the (n-1)th and the n-th conductances in the equivalent circuit; Δ_{d_n} is the electrical spacing between the slots along the waveguide; $\Delta_1^{(n)}$ and $\Delta_2^{(n-1)}$ are the electrical lengths which are due to the equivalent circuit of the n-th and (n-1)th slots.

Taking into account the symbols which have been introduced, the radiation power and phase of the field radiated by the n-th slot are as follows respectively:

$$P_n = |u_n^+ + u_n^-|^2 g_n = [(A_n + C_n)^2 + (B_n + D_n)^2]\, g_n; \qquad (5.7)$$

$$\Phi_n = \arg(u_n^+ + u_n^-) = \operatorname{arctg} \frac{B_n + D_n}{A_n + C_n} \pm k\pi, \qquad (5.8)$$

where k = 0, 1, 2, ...

Using formulas (5.6) - (5.8), one can perform the design calculations for a slotted waveguide array taking into account the mutual coupling of the slots via the dominant mode and without taking their interaction into account via the external space or via higher order modes.

The distributions of the radiated powers P_n or the amplitudes $F(z_n)$ (z_n is the coordinate of the n-th radiator) as well as the phases Φ_n of the fields radiated by each slot are usually specified in the design of slotted waveguide arrays. The distribution of the radiated powers should be normalized so that:

$$\sum_{n=1}^{N} P_n = 1 - \varkappa, \qquad (5.9)$$

where the power at the input to the antenna is taken equal to unity ($P_0 = 1$); $\kappa = P_L/P_0$ is the ratio of the power absorbed in the load P_L to the power at the antenna input P_0.

Since the amplitude distribution $f(z_n)$ is related to the distribution of the powers P_n by a certain normalizing factor σ:

$$P_n = \sigma f^2(z_n), \qquad (5.10)$$

then by substituting the value of P_n from (5.10) in formula (5.9) instead of P_n, we obtain:

$$\sigma = (1 - \varkappa) \Big/ \sum_{n=1}^{N} f^2(z_n). \qquad (5.11)$$

After determining $\sum_{n=1}^{N} f^2(z_n)$ from the specified distribution and the known relative value of the power absorbed in the load (usually, $\kappa = 0.05 - 0.1$ to obtain the maximum antenna gain), the normalizing factor σ is found, and consequently also the power radiated by any slot P_n [formula (5.10)], given the condition that the power at the antenna input is taken equal to unity.

The design of an antenna in the case of a specified amplitude distribution (antenna synthesis) is managed using an equivalent circuit (Figure 5.8) from the antenna end, i.e., from the last N-th four-pole network. The electrical spacing between the slots is considered to be specified and constant in this case.

If there is a matched load ($g_H = [g_{load}] = 1$, $u_N^- = 0$) following the last N-th slot in a nonresonant antenna, then in expressions (5.6) $B_N = C_N = D_N = 0$ and $A_N = \sqrt{\kappa}$. Then we obtain for the normalized conductance of the last N-th slot from formula (5.7):

$$g_N = P_N / \kappa. \tag{5.12}$$

The phase of the field radiated by the last slot is taken equal to zero (see equation (5.8)). The quantities P_N and κ included in formula (5.12) are known: the power P_N is determined by expression (5.10) while $\kappa = 0.05 - 0.1$ in the usually employed antennas of the type considered here.

Then, by using expressions (5.5) - (5.7), the real and imaginary components of the complex amplitudes of the incident and reflected waves are calculated: A_{N-1}, B_{N-1}, C_{N-1} and D_{N-1} at the input to the N-th four-pole network, and consequently also the conductance of the (N-1)th slot:

$$g_{N-1} = \frac{P_{N-1}}{(A_{N-1} + C_{N-1})^2 + (B_{N-1} + D_{N-1})^2}. \tag{5.13}$$

By sequentially applying formulas (5.6) and (5.13) with the preliminary substitution of the current subscript n in the last formula for the subscript N-1, we determine the parameters of the equivalent circuit of the antenna.

The quantity $\Delta_n = \Delta_2^{(n-1)} + \Delta_{dn} + \Delta_1^{(n)}$ takes on a simpler form, $\Delta_n = \Delta_{dn}$, if longitudinal slots are used in the wide wall of the waveguide for which $\Delta_1^{(n)} = -\Delta_2^{(n)} = 0$ (Figure 5.8a) [4] or transverse slots in the wide wall, for which $\Delta_1^{(n)} = \pi/2$ and $\Delta_2^{(n)} = -\pi/2$. In the case of more complex slots (for example, obliquely displaced slots in the wide wall of a waveguide), the quantities $\Delta_1^{(n)}$ and $\Delta_2^{(n)}$ are determined by the expressions given in [4].

The deviation of the phase distribution in the antenna aperture from a linear distribution, which is caused by the mutual coupling of the slots via the dominant mode in the waveguide, is calculated from the formulas:

$$\delta\Phi = \frac{2\pi}{\lambda_n} d(N-n) - \Phi_n \tag{5.14}$$

in the case of slots coupled in phase to the waveguide field, and

$$\delta\Phi = \left(\frac{2\pi}{\lambda_n} d + \pi\right)(N-n) - \Phi_n \tag{5.14a}$$

in the case of alternate phase coupled slots, where Φ_n is the phase of the field radiated by the n-th slot [formula (5.8)].

In calculations using formulas (5.14) and (5.14a), the number k in expression (5.8) is chosen so that the difference between the quantities appearing on the right sides of formulas (5.14) and (5.14a) will be the least.

One can correct the phase distribution in the aperture by changing the spacing between the radiators d or by using more complex slots, but there no need for this, since in the given design method, the external mutual coupling of the slots and mutual coupling via higher modes have not been taken into account.

The method of designing slotted waveguide antennas using the recurrent relationships (5.6) is applicable for any number of radiators in nonresonant antennas and for any amplitude distribution over the aperture.

However, with a large number of radiators in an antenna, i.e., in a long* antenna, its design is simplified. In fact, with a large number of slots, their coupling to the waveguide proves to be rather weak and the reflections from the slots are neglectably small. Moreover, since in a nonresonant antenna, the adjacent radiators are excited with a slight phase shift, then at the antenna input, practically all of the waves reflected from the slots cancel each other out and the input impedance of the antenna remains close to the characteristic impedance of the feed waveguide in which a mode is established which is close to the traveling wave mode.

In this case, one can use the energy technique to calculate the parameters of the antenna. We shall indicate the approximate limit of applicability of this technique for nonresonant antennas.

The design calculations for a slotted waveguide array where N = 12 for a specified amplitude distribution [6] using the energy technique and the method of recurrent relationships have shown that in the case of short antennas (N = 12), the energy technique yields too rough an estimate: the error in the feasible distribution of the powers relative to the specified value in some radiators reaches ±30%. Moreover, the amplitude distribution proves to be asymmetrical. For this reason, in an approximate design of an antenna for a specified amplitude-phase distribution using the energy technique, one should roughly take the number of radiators as $N \geq 15$, if the power absorbed in the matched load is $\kappa = P_L/P_0 = 0.05 - 0.1$. In the case of a greater power dissipated in the load, the number of radiators N is correspondingly reduced.

The Energy Method for Design Calculations.

Nonresonant Antennas. Formula (5.10) determines the relative radiation power of any n-th slot (i.e., the radiation power P_N referenced to the power delivered to the antenna P_0, which is taken as unity):

$$P_n = \sigma f^2(z_n) = \frac{1-\varkappa}{\sum\limits_{n=1}^{N} f^2(z_n)} f^2(z_n).$$

The factor 1-κ in the numerator of this expression, without taking into account the losses in the walls of the waveguide, is the antenna efficiency η_A; therefore:

$$P_n = \frac{\eta_A}{\sum\limits_{n=1}^{N} f^2(z_n)} f^2(z_n). \tag{5.15}$$

Considering the relationship [07] between the relative radiation power P_n, the slot coupling factor to the waveguide, α_n, and the slot conductance g_n:

---

*We will conditionally understand a long antenna to be one in which the per unit length radiation power is low.

$$\alpha_1 = P_1, \alpha_2 = \frac{P_2}{1-P_1}, \ldots, \alpha_n = \frac{P_n}{1-(P_1+P_2+\ldots P_{n-1})}, \tag{5.16}$$

$$g_n \simeq \alpha_n/(1-\alpha_n), \tag{5.17}$$

One can initially determine the relative radiation powers P_n of all of the slots based on the specified amplitude distribution as well as the antenna efficiency by means of iterative conversion calculations from the last N-th slot to the first, and then the coupling factors α_n, and finally, the equivalent normalized slot conductances, g_n (5.17). Based on the known slot conductances, the coupling elements are determined, i.e., the displacements of the slots relative to the waveguide axis, x_1, or their inclination angle, δ [see § 5.2, Table 5.1].

In the case of identical slot radiators (an exponential distribution of the field amplitudes over the antenna), when the equivalent conductances (or resistances) of all of the slots are equal, formula (5.17) can be used to determine them from the specified η_A, where:

$$\alpha = 1 - \sqrt[N]{1-\eta_A}. \tag{5.18}$$

Resonant Antennas. A resonant antenna with arbitrary resonant slots and a spacing of $d = \lambda_B/2$ between them (or $d = \lambda_B$) is designed by the energy technique, which consists in the following. If the amplitude distribution is designated as $f(z_n)$, just as before, and one takes into account the fact that all of the slots are resonant, then the equivalent normalized conductance of the n-th slot is [05]:

$$g_n = g_{вх} f^2(z_n) \Big/ \sum_{n=1}^{N} f^2(z_n). \tag{5.19}$$

The antenna conductance g_{BX} [g_{in}] incorporated in the formula is chosen so as to assure good matching of the antenna to the feed waveguide. Thus, the value g_{in} can be chosen equal to unity.

Antennas with Matched Slots. As was indicated in § 5.3, obliquely displaced slots in the wide wall of a waveguide are used along with simple slots, where the former slots are characterized by two geometric parameters: the displacement x_1 and the rotation angle δ, by means of which one can independently adjust the amplitude and phase of the field radiated by the slot. Matched obliquely displaced slots for which there is no mutual coupling of the radiators via the dominant mode are of the greatest practical interest, since there are no reflections from the radiators and a traveling wave mode is established in the antenna, the designing of the antenna for a specified distribution is accomplished by the energy technique using the formulas for nonresonant antennas.

The methods set forth for designing slotted waveguide arrays with slots equivalent to parallel conductances, g_n, inserted in a line equivalent to the waveguide, also remain valid for slots equivalent to resistances r_n, which are inserted in series in the line. For this reason, the design calculations for an antenna are performed in a similar manner, with the condition that the normalized resistances r_n are substituted for the normalized conductances g_n in the appropriate expressions.

5.5. Matching a Slotted Waveguide Array to a Feed Waveguide

The matching of a slotted waveguide array to the waveguide feeder is usually judged based on the value of the reflection factor from the antenna input. In the case of a nonresonant antenna with a terminal matched load, the reflection factor from the antenna input is [05]:

$$\Gamma = \frac{-\sum_{n=1}^{N} \frac{1}{2}(g_n + j b_n)\exp\left(-j\frac{2\pi}{\lambda_{\text{в}}}2nd\right)}{1+\sum_{n=1}^{N}\frac{1}{2}(g_n + j b_n)}, \tag{5.20}$$

where $g_n + jb_n$ is the total equivalent normalized admittance of the n-th slot.

In the case of identical slot radiators, where the admittances of all of the slots are identical, this expression assumes the form:

$$\Gamma = \frac{\frac{N}{2}(g + j b)\exp\left[-j\frac{2\pi}{\lambda_{\text{в}}}(N+1)d\right]}{1+\frac{1}{2}N(g+jb)} \, \frac{\sin\left(\frac{2\pi}{\lambda_{\text{в}}}Nd\right)}{N\sin\left(\frac{2\pi}{\lambda_{\text{в}}}d\right)}. \tag{5.21}$$

It follows from formula (5.21) that the reflection factor takes on a value of zero (K_{st} = [SWR] = 1) when $2\pi Nd/\lambda_B = \pi(N \pm 1)$. The spacing between the slots, d, is determined from this so that throughout the entire range of change in λ, there is no resonant excitation of the antenna and higher order major lobes do not appear in the directional pattern:

$$d \leqslant (N-1)\lambda_{\text{в}\,\min}/2N. \tag{5.22}$$

Formula (5.22) was derived for the special case where the admittances of all of the slots are equal. If the admittances of the slots in the slotted waveguide array are not equal, then the formula cited here can nonetheless be used for a rough determination of the spacing between the radiators.

In the case of a multiple slot resonant antenna, a short circuiting piston at its end is frequently employed to assure its matching to the feed waveguide (SWR = 1) for any amplitude distribution in the aperture. When the spacing between the radiators is $\lambda_B/2$ (or λ_B) and the spacing from the center of the last slot to the piston is $\lambda_B(2p - 1)/4$ in the case of longitudinal slots and $\lambda_B p/2$ in the case of transverse slots (p = 1, 2, ...), the reflection factor at the antenna input is zero, if the sum of the admittances of all of the slots is $\sum_{n=1}^{N}(g_n + jb_n) = 1$.

5.6. The Influence of a Change in Frequency on Antenna Characteristics

A consideration of the expression for the reflection factor (5.20) from the antenna input shows that when the frequency changes, both the quantity $(2\pi/\lambda_B)$ 2nd and the total admittance of each slot $g_n + jb_n$ also change.

Calculations and experiments show that with slight changes in the frequency, the deviations of the slot admittances from the nominal values are small and a change in the electrical spacing between them ($2\pi d/\lambda_B$) exerts the main influence on the change in the reflection factor, and consequently also on the SWR. The SWR of a slotted waveguide array [05] is shown in Figure 5.9 as a function of the change in the electrical spacing between the radiators when the frequency changes. When selecting the spacing between slots using formula (5.22), the working band of the antenna falls outside the "main lobe" of the SWR, defined by the value K_{st} = [SWR] = 1, and the matching is good. The working band of resonant antennas falls in the region of the "main lobe" of the SWR (Figure 5.9), something which determines the sharp change in the reflection factor when the frequency changes.

A frequency change has an impact not only on the antenna matching, but also on the directional characteristics. When estimating the influence of a frequency change on the radiation, the radiative properties of individual elements can be considered to be independent of frequency in a first approximation [01], just as when investigating questions of matching. In this case, a frequency change leads to beam rotation in space, because of the change in the phase change along the waveguide, and this deflection of the beam can be calculated from formula (5.26).

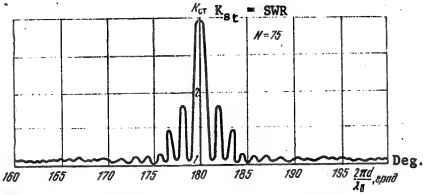

Figure 5.9. The standing wave ratio in the waveguide feeder for a slotted waveguide array as a function of the electrical spacing between the slots.

5.7. The Directional Properties of Slotted Waveguide Arrays

The same methods are used to calculate the directional patterns of slotted waveguide arrays as for the calculation of the directional patterns of multiple dipole antennas. In this case, the shape of the directional pattern is governed by the amplitude-phase distribution in the antenna aperture.

The following kinds of amplitude distributions are the ones most frequently used in practice: uniform, symmetrically decaying relative to the antenna center and exponential. The phase distribution is most often linear.

The normalized directional pattern of a linear array of radiators can be written in the form:

$$F(0, \varphi) = F_1(0, \varphi) F_n(0, \varphi), \qquad (5.23)$$

where $f_1(\theta, \phi)$ is the directional pattern of a single radiator; $F_n(\theta, \phi)$ is the antenna array factor, which depends on the number of slots in the antenna.

We shall give expressions for the antenna factor for various amplitude distributions in the antenna. In the case of a uniform amplitude and linear phase distribution over the length of the array:

$$F_n(0) = \frac{\sin (N\psi/2)}{N \sin (\psi/2)}, \qquad (5.24)$$

where $\psi = k_0 d \sin \theta - \psi_1$ is the phase shift between the fields produced at the observation point by adjacent radiators; $k_0 = 2\pi/\lambda$ is the phase constant of free space; θ is the angle read out from the normal to the line of position of the slots (Figure 5.10); ψ_1 is the phase difference between adjacent radiators along the feed system; N is the number of slots. In an in-phase antenna, $\psi_1 = 0$; in a nonresonant antenna with in-phase coupling of the slots to the waveguide, $\psi_1 = 2\pi d/\lambda_B$; and in the case of alternate phase coupling, $\psi_1 = 2\pi d/\lambda_B - \pi$.

If the field distribution in the aperture of a discrete linear array of radiators is exponential, then:

$$F_n(0) = \frac{\operatorname{sh}(\xi/N)}{\operatorname{sh}\xi} \sqrt{\frac{\sin^2 u + \operatorname{sh}^2 \xi}{\sin^2 (u/N) + \operatorname{sh}^2 (\xi/N)}}, \qquad (5.25)^*$$

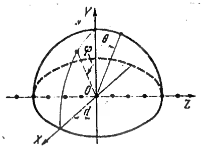

Figure 5.10. The readout of the angles in calculating the directional pattern of slotted waveguide arrays.

where $\xi = \alpha L/2$ is a quantity which characterizes the nonuniformity of the amplitude distribution in the aperture; $\alpha = \alpha_\Sigma + \alpha_{CT}$ is the attenuation constant, due to radiation losses as well as losses in the waveguide walls, Np/m; in a waveguide with low losses, $\alpha_{ST} \ll \alpha_\Sigma$ and $\alpha \approx \alpha_\Sigma$; $L \approx Nd$ is the length of the antenna array; $u = 0.5\, k_0 L(\sin \theta - \sin \theta_{main})$ is the generalized coordinate; θ_{main} is the direction of the main lobe of the antenna directional pattern.

The deflection of the main lobe of the directional pattern from the normal to the line of position of the radiators is determined from the formula:

$$\sin \theta_{\underset{\text{main}}{\text{гл}}} = \gamma - p\lambda/d, \qquad (5.26)$$

where $\gamma = \lambda/\lambda_B$ is the retardation of the phase velocity in the waveguide; p = 0 applies to slots coupled to the waveguide field in phase, and p = 0.5 is for alternate phase coupled slots.

The following obvious relationship can be employed to determine the attenuation constant α_Σ:

---

*The formula was derived by G.A. Yevstropov and G.K. Fridman.

$$\alpha_{\Sigma} = \frac{1}{2Nd}\ln\frac{P_0}{P_L}.$$

In the case of antennas with a symmetrical amplitude distribution relative to the center which falls off towards the edges (for example, a cosine distribution), the calculation of the directional pattern in the case of a large number of radiators involves labor intensive computations. In this case, one can use the factor for an antenna with a continuous distribution of omnidirectional radiators, $F_L(\theta)$ [7], since the directional pattern of a discrete array and a continuous one practically coincide when $N \geq 6$ ($d \approx \lambda/2$):

$$F_n(\theta) \simeq F_L(\theta) = \frac{1}{A_{10}+2A_1/\pi}\left\{A_0\frac{\sin u}{u} + \frac{A_1}{2}\left[\frac{\sin(u-\pi/2)}{u-\pi/2} + \frac{\sin(u+\pi/2)}{u+\pi/2}\right]\right\}, \tag{5.27}$$

where A_0 is the amplitude of the field at the edges of the antenna.

When the amplitude distribution over the antenna is referenced to unity: $A_1 = 1 - A_0$. The directional pattern of a single slot $F_1(\theta)$ in the YOZ plane, which passes through the line of position of the radiators (Figure 5.10), can be determined from the formulas for the directional pattern of a slot in an infinite shield in the case of engineering calculations: for a longitudinal slot, $F_1(\theta) = [\cos((\pi/2) \cdot \sin\theta)]/\cos\theta$, and for a transverse slot, $F_1(\theta) \approx 1$, since the antenna length is usually great (several wavelengths), and moreover, the directional properties of an antenna in this plane are determined primarily by the array factor $F_n(\theta)$.

When determining the directional pattern in the transverse plane (YOX in Figure 5.10) for an antenna with longitudinal slots in the wide wall of a waveguide, one must consider the fact that the finite dimensions of the shield (the transverse dimensions of the waveguide) have a substantial impact on the shape of the directional pattern [07]: the limited nature of the shield imparts a directional nature to the radiation: the field in the direction of the shield is reduced to approximately 40 to 50% relative to the value of the field in the direction of the directional pattern maximum.

In order to simplify the determination of the directional pattern of a slot in the plane normal to its longitudinal axis (the YOX plane), it is convenient to replace the waveguide with a flat strip of the same width [06]. It then turns out that for a waveguide width of $a = (0.7 - 0.8)\lambda$, the directional pattern will be close to any of the patterns depicted in Figure 5.11.

In the case of transverse slots in the wide wall of a waveguide or slots which are inclined in the narrow wall, the directional pattern in the YOX plane can be approximated from the formulas for the directional pattern of a slot in an infinite shield, since the shield dimensions in the direction of the slot axis have little influence on the directional pattern in either the E-plane or the H-plane of the slot [07].

Formulas are given in Table 5.2 for the determination of the width of the directional pattern of in-phase slotted waveguide arrays and the levels of the

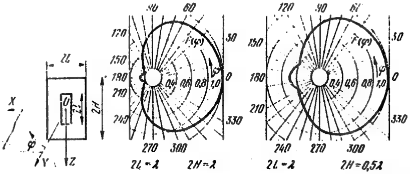

Figure 5.11. Calculated directional patterns of a half-wave slot in the E-plane for various dimensions of the rectangular shield.

first sidelobes are indicated for various amplitude distributions in the antenna. One can also use the indicated formulas in the case of nonresonant antennas, since the spacing between the radiators in such antennas (5.22) differs insignificantly from the spacing in in-phase arrays and the angle of beam deflection from the normal to the array is small.

TABLE 5.2.

Амплитудное распределение Amplitude Distribution	$2\theta^0_{0,5}$	Уровень первого бокового лепестка, дБ (1)
Равномерное Uniform	$51\lambda/Nd$	−13,5
Экспоненциальное ($\varkappa = P_L/P_0 = 0{,}05$) Exponential	$54{,}4\ \lambda/Nd$	−12,1
Косинусоидальное; амплитуда поля на краях антенны: (2) $A_0=0{,}5$ ($A_1=0{,}5$) $A_0=0$ ($A_1=1$)	 $56\ \lambda/Nd$ $68\ \lambda/Nd$	 −17,8 −23,6

Key: 1. Level of the first sidelobe, dB;
2. Cosine; the amplitude of the field at the antenna edges.

In those special cases where it is necessary to deflect the beam considerably from the normal to the array, the effective length of the aperture $L_{eff} \approx Nd\cos\theta_{main}$ is to be substituted in the formulas for the directional pattern width, $2\theta_{0.5}$, in place of the antenna length $L \approx Nd$.

The directional gain of an antenna with alternate phase slots in the wide or narrow walls of a waveguide when $\gamma = \lambda/\lambda_B < 1$ and $d = \lambda_B/2 \approx (0.6 - 0.9)\lambda$ is determined by the approximate formula:

$$D_0 \simeq g_0 (3 + \nu N/\lambda), \qquad (5.28)$$

where $\nu = 2$ for longitudinal slots in the wide wall and $\nu = 4$ for oblique slots in the narrow wall of a waveguide (when $\delta \leqq 15°$).

The aperture utilization coefficient, g_0, incorporated in formula (5.28) depends on the amplitude distribution in the antenna: in the case of a uniform distribution, $g_0 = 1$; with an exponential distribution $g_0 = 0.85$ and 0.92 respectively for $\varepsilon = P_L/P_0 = 5\%$ and 10%; with a cosine distribution, $g_0 = 0.81$ and 0.965 for $A_0 = 0$ and $A_0 = 0.5$ respectively.

The directional gain of an antenna can be estimated using formula (5.28) during scanning, if the beam deflection angle $\theta_{main} \leqq 40\%$, $d/\lambda \leq 0.6$ and the antenna length is $L = Nd \gg \lambda$, since a change in the antenna directional gain during scanning in the indicated range, because of the change in the effective length of the aperture, is compensated in that a linear antenna becomes directional in two planes when $\theta_{main} \to 90°$, while for $\theta_{main} = 0$, the antenna is directional in one plane [03].

In contrast to a linear array, a planar array of radiators is directional in both main planes, and for this reason, its directional gain during scanning begins to fall off immediately because of the reduction in the effective aperture of the array.

The efficiency of a nonresonant slotted waveguide radiator, η_A, can be computed from formulas (3.8) or (3.11).

Since a short-circuiting piston is usually installed in a resonant antenna instead of an absorbing load, its efficiency is higher than the efficiency of a nonresonant antenna of the same dimensions. With known values for the efficiency and directional gain of an antenna, the overall gain is $G = D_0\eta_A$.

5.8. Possible Structural Configurations for Slotted Waveguide Arrays and Structural Design Examples

Depending on the function of an antenna, it can be constructed in the form of a linear or planar slotted waveguide array or consist of a set of linear slotted arrays, arranged along the generatrices of the surface of an aircraft (Figures 5.12 - 5.16). A schematic depiction of a portion of a linear antenna with oblique slots in the narrow wall of the waveguide, which is used in marine radars, is shown in Figure 5.12. To attenuate the parasitic component of the radiation field of such an antenna, which is polarized perpendicular to the axis of the waveguide, metal isolation projections [01] are installed between adjacent slots. By utilizing the basic concepts of wave

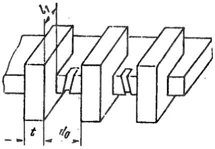

Figure 5.12. Inclined slots in the narrow wall of a waveguide with isolating metal projections between the radiators.

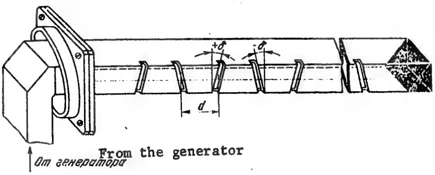
+δ
δ
d
From the generator
От генератора

Figure 5.13. A nonresonant slotted waveguide array with slots in the side wall of the waveguide.

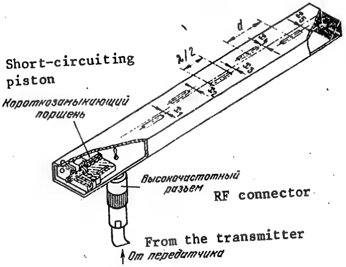
d
λ/2
Short-circuiting piston
Короткозамыкающий поршень
Высокочастотный разъем
RF connector
From the transmitter
От передатчика

Figure 5.14. A nonresonant slotted waveguide array with longitudinal slots in the wide wall of the waveguide.

attenuation in an overmoded waveguide in the case of propagation between parallel metal plates [8] and knowing the spacing between the slots, one can determine the spacing between the projections d_0 (Figure 5.12), their length l_1 and thickness t.

Examples of the structural design of nonresonant slotted waveguide antennas with oblique slots in the narrow wall of the waveguide when they are excited from a rectangular waveguide (Figure 5.13) as well as with longitudinal slots in the wide wall when fed by a coaxial cable (Figure 5.14) are shown in Figures 5.13 and 5.14.

An example of the structural design of a slotted waveguide array with electromechanical scanning (with a removable upper slotted wall) is shown in Figure 5.15.

One of the variants of a two dimensional slotted waveguide array [9] consisting of eight parallel waveguides, in each of which ten dumb-bell slots are cut is shown in Figure 5.16a. As compared to conventional rectangulars slots, dumb-bell slots have a greater bandwidth [07]. A specific feature of the antenna is the

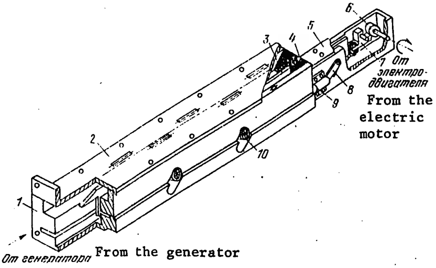

Figure 5.15. An electromechanically scanned slotted waveguide array.

Key:
1. Housing;
2. Upper wall with the slots;
3. Moving metal projection - "knife";
4. Absorbing load;
5. Cover for the beam steering mechanism;
6. Cam;
7. Push rod;
8. Return mechanism link;
9. Return spring housing;
10. "Knife" guide bearing.

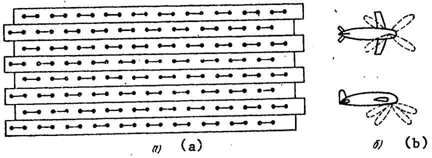

Figure 5.16. The antenna of an aircraft navigation system (a) and its directional patterns (dashed lines) (b).

fact that the even and odd waveguides are fed from different sides by means of power dividers and the entire aperture is used to generate four beams (Figure 5.16b). Such antennas are used, for example, in aircraft independent Doppler navigation radars, intended for determining the speed and drift angle of an aircraft.

For protection against atmospheric precipitation and dust, the aperture of the slotted waveguide array is covered with a dielectric plate or the entire radiating system should be housed in a radiotransparent fairing.

5.9. A Sample Design Calculation Procedure for Slotted Waveguide Arrays

When developing or planning slotted waveguide arrays, the starting data, for example, can be the width of the directional pattern in the two main planes or in one of them ($2\theta_{0.5}$) and the level of the sidelobes; and the directional gain D_0.

We shall deal with the design procedure for the following variant: the directional pattern width is specified in one or two main planes as well as the sidelobe radiation level.

The type of slotted waveguide antenna is chosen at the outset. If the angular position of the main lobe of the directional pattern, θ_{main}, is specified and the antenna should provide for operation in a band of frequencies, a nonresonant antenna is chosen. However, if according to the design specifications, the antenna is a narrow band one, but should have a high efficiency, a resonant antenna is preferable. Then the spacing between the radiators is found in the waveguide selected for the construction of the antenna and the specified band of frequencies. In a resonant antenna with alternating phase slots, $d = \lambda_B/2$. In a nonresonant antenna, the quantity d can be chosen in two ways. If the position of the main lobe of the directional pattern in space, θ_{main} is specified, then the requisite value of d is found from formula (5.26). If the angle θ_{main} is not specified though, then the spacing between the radiators is chosen from the condition that $d \lessgtr \lambda_B/2$, as well as to assure that there is no resonant excitation of the antenna at the edge frequencies of the specified band (5.22). Then, the amplitude distribution for the antenna is selected which assures a directional pattern with a specified sidelobe level. Based on the now known amplitude distribution, the length of the antenna is found (and correspondingly, the number of radiators), which assures the requisite half-power level directional pattern width (see the formulas in Table 5.2).

Then the design calculations are carried out in the following order:

1. Based on the overall equivalent circuit for the antenna (Figure 5.8b), the equivalent normalized conductances, g_n (or resistances r_n), are computed for all N slots of the antenna (see § 5.4);

2. Knowing g_n or r_n, the displacement of the center of the slots relative to the center of the wide wall of the waveguide, x_1, or their inclination angle in the side wall, δ, is determined from the formulas of Table 5.1.

3. Having calculated the radiation conductance of the slot in the waveguide, G_Σ (i.e., the external conductance), the voltage at the antinode U_m (5.3), and consequently also the slot width d_1 (5.4) are determined from the known value of the power at the input (in the case of a transmitting antenna).

4. With a known position of the slots in the waveguide wall and their width, the resonant length of the slots in the waveguide is found from the data of § 5.2.

5. The directional pattern (see § 5.7), the directional gain and overall gain of the antenna are calculated.

Besides the electrical design of the antenna itself, design calculations are also performed for the feedline and exciter; when called for by the design specifications, the requisite type of rotating joint is selected and its main characteristics are determined.

6. ACCOUNTING FOR MUTUAL COUPLING EFFECTS IN SLOTTED WAVEGUIDE ARRAYS

As has already been noted in Chapter 5, the energy and recurrent techniques of design calculations for slotted waveguide arrays (VShchR) do not assure the practical veasibility of antennas with the anticipated parameters in many cases. This applies primarily to arrays with a low sidelobe level in the directional pattern and is explained by the fact that in the indicated techniques, many electrodynamic factors are not taken into account which occur in the actual antenna structure. It has been determined as a result of specific calculations and experiments that the limit of applicability of these methods for arrays with a comparatively small number of radiators (up to 30) in each waveguide [1, 2] can be considered a directional pattern level of roughly* -15 dB.

To illustrate this fact, experimentally measured directional patterns and directional patterns calculated by the energy and recurrent techniques for typical nonresonant alternating phase slotted waveguide arrays with different numbers N_1 of longitudinal slots in the wide wall of the waveguide are shown in Figure 6.1. In these antennas, the identical amplitude-phase distribution of the field in the aperture of the arrays, V_n, was specified as:

$$V_n = \left[1 - 0{,}95\cos\left(2\pi\frac{n-1}{N_1-1}\right)\right]\exp\left[-j\kappa d\,(n-1)\sin\theta_{\text{гл}}\right],\quad 1 \leqslant n \leqslant N_1, \qquad (6.1)$$

where $\theta_{\text{гл}}$ [θ_{main}] is the angular direction of the main beam of the directional pattern; $d = 0.575\lambda$ is the step of the array; $k = 2\pi/\lambda$ is the wave number.

An analysis of the calculated and experimental results makes it possible to conclude that it is necessary to study and take into account electrodynamic factors which are significant in the practical realization of directional patterns with a low sidelobe level.

The work which has been done at the present time shows that such factors include [1-5] nonresonance of the slots, internal mutual coupling of the slots via higher modes, finite thickness of the waveguide walls, and external mutual coupling of the radiators. It is apparent that all of these factors influence the directional pattern in different ways. For this reason, before working out an engineering procedure for taking them into account, it makes sense to conduct a differential analysis of these effects and to compare the results obtained with the experimental data.

It is procedurally expedient for the further presentation of the material to adduce the example of antennas with slots in the wide wall of the waveguide, which are widely used in practice.

---

*Roughly, because it depends on the form of the amplitude distribution of the field in the array aperture.

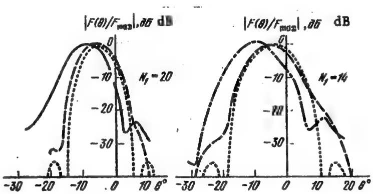

Figure 6.1. The directional patterns of slotted waveguide arrays.

Key: The solid curves are for experimental data;
The dashed curves were calculated using the recurrent method;
The dotted curves were computed using the energy technique;
The dashed-and-dotted curves were computed taking into account the nonresonance of the slots and their mutual coupling via higher modes.

6.1. Basic Relationships

Initial Equations. Let a system of N_1 arbitrarily oriented narrow slots be cut in the wide wall of a rectangular waveguide, excited by sources located inside it. As shown in Figure 6.2, we shall introduce in each of them a local system of cartesian coordinates with the OY_n axis directed along the normal to the surface of the wide wall of the waveguide. Then the complex amplitudes of the voltages V_n in the slots, for the case of known distributions of these voltages $\psi_n(z_n)$ can be found from the following system of linear equations, which take into account electrodynamic effects of external mutual coupling [6]:

$$\sum_{n=1}^{N_1} V_n Y_{mn} = F_m, \quad 1 \leqslant m \leqslant N_1, \tag{6.2}$$

where $Y_{mn} = Y_{mn}^{(e)} + Y_{mn}^{(i)}$; $Y_{mn}^{(e)}$ and $Y_{mn}^{(i)}$ are the external and internal mutual admittances of the m-th and n-th slots respectively; F_m is the internal magnetomotive force, applied to the m-th slot. The general formulas for $Y_{mn}^{(e)}$, $Y_{mn}^{(i)}$ and F_m are known [6]:

$$Y_{mn}^{(e)} = \int_{-l_m}^{l_m} \psi_m(z_m) H_n^{(e)}(z_m)\, dz_m; \tag{6.3}$$

$$Y_{mn}^{(i)} = -\int_{-l_m}^{l_m} \psi_m(z_m) H_n^{(i)}(z_m)\, dz_m; \tag{6.4}$$

$$F_m = \int_{-l_m}^{l} \psi_m(z_m)\, H_m^{(0)}(z_m)\, dz_m, \qquad (6.5)$$

where $2l_m$ is the length of the m-th slot; $H_m^{(0)}(z_m)$, $H_n^{(e)}(z_m)$ and $H_n^{(i)}(z_m)$ are the tangents to this slot of the components of the magnetic vectors of the unperturbed field of the sources and the fields radiated into the external space and into the waveguide of the n-th slot respectively, where these have a unit amplitude.

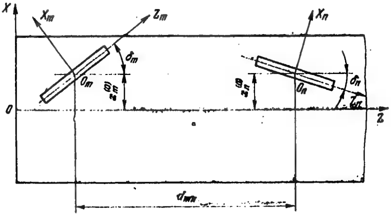

Figure 6.2. An array with obliquely displaced slots in the wide wall of a waveguide.

The major difficulty in practical calculations of V_n consist in determining the matrices for the external and internal admittances for a specific arrangement of the slots.

The Internal and External Admittances. The external admittances $Y_{mn}^{(e)}$ are, as a rule, determined approximately, but with sufficient precision for practical purposes by means of the duality principle [01]. It is enormously more complicated to calculate the internal admittances $Y_{mn}^{(i)}$. As can be seen from formula (6.4), for this it is primarily necessary to find the electromagnetic field vector H in the waveguide, which is excited by the arbitrarily oriented n-th slot. To solve this problem, one can employ the concept of vector potential, given in the literature [7]. Substituting in it the distribution of the magnetic current in the slot, using generally known formulas, we find the components of the magnetic field and consequently, the component $H_n^{(i)}(z_m)$ tangential to the slot. Substituting it in expression (6.4), following integration in explicit form, we derive the formula for calculating the internal mutual admittance of the slot, $Y_{mn}^{(i)}$.

Resonant or slightly mistuned slots are most frequently used in practice, where the voltage distribution in the slots is described by the function:

$$\psi_m(z_m)=\cos(\pi z_m/2l_m), \qquad -l_m\leqslant z_m\leqslant l_m. \tag{6.6}$$

As the calculations performed using the scheme described here, taking (6.6) into account, the following expression is derived for the determination of the internal admittances [1]:

$$Y_{mn}^{(I)}=\frac{j}{2\omega\mu ab}\sum_{p=0}^{\infty}\sum_{q=0}^{\infty}(-1)^p\frac{e^{-\gamma_{pq}d_{mn}}}{\gamma_{pq}\cos\delta_n}\times$$

$$\times\left\{\left[\mathcal{F}_{1\delta_n}\left(\frac{a_q^{(1)}}{\cos\delta_n}\right)+\mathcal{F}_{1\delta_n}\left(\frac{a_q^{(2)}}{\cos\delta_n}\right)\right]\left(A_{pq}\cos\frac{\pi q}{a}y_n^{(0)}+B_{pq}\sin\frac{\pi q}{a}y_n^{(0)}\right)+\right.$$

$$+\left[\left(\mathcal{F}_{2\delta_n}\left(\frac{a_q^{(1)}}{\cos\delta_n}\right)+\mathcal{F}_{2\delta_n}\left(\frac{a_q^{(2)}}{\cos\delta_n}\right)\right]\times\right.$$

$$\left.\times\left(B_{pq}\cos\frac{\pi q}{a}y_n^{(0)}-A_{pq}\sin\frac{\pi q}{a}y_n^{(0)}\right)\right\}, \qquad (6.7) \qquad (6.7)$$

где

where

$$A_{pq}=(k^2+\gamma_{pq}^{(2)})\,\varepsilon_{pq}^{(1)}\varepsilon_{qp}^{(2)}\cos\delta_n\,T_{2pq}+\gamma_{pq}\varepsilon_{pq}^{(1)}\sin\left(\delta_n\frac{\pi q}{a}\right)T_{1pq};$$

$$B_{pq}=\left[k^2-\left(\frac{pq}{a}\right)^2\right]\varepsilon_{pq}^{(1)}\sin\delta_n\,T_{1pq}-\gamma_{pq}\varepsilon_{pq}^{(1)}\varepsilon_{qp}^{(2)}\cos\left(\delta_n\frac{\pi q}{a}\right)T_{2pq};$$

$x_n^{(0)}$ is the displacement of the center of the n-th slot relative to the center line of the wide wall of the waveguide; d_{mn} is the distance along the Z axis between the centers of the m-th and n-th slots:

$$T_{\frac{1}{2}pq}=\frac{(-1)^p}{2}\begin{matrix}\cos\\ \sin\end{matrix}(\delta_m)\left\{\begin{matrix}\cos\\ \sin\end{matrix}\left(\frac{\pi q}{a}y_n^{(0)}\right)\left[\mathcal{F}_{1\delta_m}(a_q^{(1)})+\mathcal{F}_{1\delta_m}(a_q^{(2)})\right]+\right.$$

$$\left.+\begin{matrix}\sin\\ \cos\end{matrix}\left(-\frac{\pi q}{a}y_n^{(0)}\right)\left[\mathcal{F}_{2\delta_m}(a_q^{(1)})+\mathcal{F}_{2\delta_m}(a_q^{(2)})\right]\right\};$$

$$\mathcal{F}_{\frac{1}{2}\delta_m}(a_q^{\beta})\frac{1}{1+(\gamma_{pq}/a_q^{(\alpha)})^2}\left[\frac{2}{a_q^{(\alpha)}}\begin{matrix}\mathrm{ch}\\ \mathrm{sh}\end{matrix}(\gamma_{pq}s_m)\begin{matrix}\sin\\ \cos\end{matrix}(a_q^{(\alpha)}s_m)+\right.$$

$$\left.+\frac{2\gamma_{pq}}{(a_q^{(\alpha)})^2}\begin{matrix}\mathrm{sh}\\ \mathrm{ch}\end{matrix}(\gamma_{pq}s_m)\begin{matrix}\cos\\ \sin\end{matrix}(-a_q^{(\alpha)}s_m)\right];$$

$$a_q^{(\alpha)}=\frac{\pi q}{a}\sin\delta_n+(-1)^{\alpha}\frac{\pi}{2l_n}, \quad \alpha=1,2;$$

$$\gamma_{pq}=\sqrt{(\pi p/b)^2+(\pi q/a)^2-\kappa^2};$$

$$s_m=l_m\cos\delta_m;$$

$$\varepsilon_{pq}^{(1)}=\begin{cases}0, & p=0,\quad q=0,\\ 1, & p=0,\quad q>0,\\ 2, & p>0;\end{cases} \qquad \varepsilon_{pq}^{(2)}=\begin{cases}0, & q=0,\quad p=0,\\ 1, & q=0,\quad p>0,\\ 2, & q>0.\end{cases}$$

By using the procedure for calculating the mutual impedances of electrical dipoles [01], following a series of cumbersome mathematical derivations from expression (6.3), we obtain the following formula for the calculation of the external mutual admittances of the slot:

$$
\begin{aligned}
Y^{(e)}_{mn} = {} & -30j\,\frac{l_n}{l_m}\Big\{\cos(\delta_m-\delta_n)\Big[\int_{-1}^{0}\Big(\frac{\exp -j\kappa_m r_{-1mn}}{r_{-1mn}}+\frac{\exp -j\kappa_m r_{1mn}}{r_{1mn}} - \\
& -2\cos\kappa_m\frac{\exp -j\kappa_m r_{0mn}}{r_{0mn}}\Big)\sin[\kappa_n(1+\xi)]\,d\xi + \\
& +\int_{0}^{1}\Big(\frac{\exp -j\kappa_m r_{-1mn}}{r_{-1mn}}+\frac{\exp -j\kappa_m r_{1mn}}{r_{1mn}}-2\cos\kappa_m\frac{\exp -j\kappa_m r_{0mn}}{r_{0mn}}\Big)\sin\kappa_n(1-\xi)\,d\xi\Big] + \\
& +\sin(\delta_m-\delta_n)\Big[\int_{-1}^{0}(\sigma_{mn}-1)\frac{\exp -j\kappa_m r_{-1mn}}{r_{-1mn}} + \\
& +(\sigma_{mn}+1)\frac{\exp -j\kappa_m r_{1mn}}{r_{1mn}}-2\sigma_{mn}\cos\kappa_m\frac{\exp -j\kappa_m r_{0mn}}{r_{0mn}}\Big)\frac{\sin\kappa_n(1+\xi)}{\delta_{mn}}\,d\xi - \\
& -\int_{0}^{1}\Big((\sigma_{mn}-1)\frac{\exp -j\kappa_m r_{-1mn}}{r_{-1mn}}+(\sigma_{mn}+1)\frac{\exp -j\kappa_m r_{1mn}}{r_{1mn}} - \\
& -2\sigma_{mn}\cos\kappa_m\frac{\exp -j\kappa_m r_{0mn}}{r_{0mn}}\Big)\frac{\sin\kappa_n(1-\xi)}{\delta_{mn}}\,d\xi\Big]\Big\}. \qquad (6.8) \qquad (6.8)
\end{aligned}
$$

где

where

$$r_{\alpha mn} = \sqrt{\delta^2_{mn} + (\sigma_{mn}+\alpha)^2}, \quad \alpha = -1;\ 0;\ 1;$$

$$\delta_{mn} = \frac{y^{(0)}_m - y^{(0)}_n}{l_m} + \xi\sin(\delta_m-\delta_n)\,\frac{l_n}{l_m};$$

$$\sigma_{mn} = \frac{d_{mn}}{l_m} + \xi\cos(\delta_m-\delta_n)\,\frac{l_n}{l_m};\ \kappa_s = \kappa l_s\ (s = m,\ n).$$

6.2. Planar Slotted Waveguide Array

We shall now consider a planar array composed of N_2 waveguides, in each of which N_1 slots are cut. It is apparent that with a known excitation of the waveguides, the complex voltage amplitudes in the slots can be theoretically determined from system (6.2). But when the overal number of slots $N_1N_2 > 100$ (this is the most real case in practice), the solution of system (6.2) is problematical, even using modern computers. An analysis which has been made [1, 3] shows that to solve this problem, it is expedient to employ the technique of iterative approximations, in each step of which the voltage amplitudes in the slots cut only in one waveguide are determined.

We rewrite system (6.2) as follows for a planar array:

$$\sum_{n_2=1}^{N_2}\sum_{n_1=1}^{N_1} V_{n_1 n_2} Y_{m_1 m_2 n_1 n_2} = F_{m_1 m_2}, \quad 1 \leqslant m_1 \leqslant N_1, \quad 1 \leqslant m_2 \leqslant N_2, \tag{6.9}$$

where all of the symbols are clear from a comparison with expressions (6.2) - (6.5).

We shall consider an arbitrary waveguide with the number $m_2^{(0)}$; then it is not difficult to transform (6.9) as follows:

$$\sum_{n_1=1}^{N_1} V_{n_1 m_2^{(0)}} \left[Y^{(e)}_{m_1 m_2^{(0)} n_1 m_2^{(0)}} + Y^{(i)}_{m_1 m_2^{(0)} n_1 m_2^{(0)}}\right] = F_{m_1 m_2^{(0)}} - \sum_{\substack{n_2=1 \\ n_2 \neq m_2}}^{N_2} \sum_{n_1=1}^{N_1} V_{n_1 n_2} Y^{(e)}_{m_1 m_2^{(0)} n_1 n_2}, \tag{6.10}$$

since when $n_2 \neq m_2^{(0)}$, the internal admittances $Y^{(i)}_{m_1 m_2^{(0)} n_1 n_2} = 0$.

System (6.10) can be solved by iterative approximations. In fact, for a fixed value of $m_2^{(0)}$ and known values of $V_{n_1 n_2}$ from the preceding step in the calculations, by solving the N_1-th (and not $N_1 N_2$) order system of (6.10), we find the amplitudes $V_{n_1 m_2^{(0)}}$. By successively varying $n_2^{(0)}$ from 1 to N_2, we determine the distribution of the complex voltage amplitudes over the entire aperture of the array. One can take $V_{n_1 n_2} = 0$ ($n_2 \neq m_2^{(0)}$) as the initial approximation of the amplitude values, which as can be seen from (6.10), is equivalent in this set to dispensing with the accounting for the external mutual coupling of the array waveguides for the $m_2^{(0)}$ waveguide. It is clear from physical considerations that the computational method considered here converges. This is also confirmed by the large number of specific calculations performed on computers.

The external admittances $Y^{(e)}_{m_1 m_2 n_1 n_2}$ are determined from formula (6.8) when the geometric parameters which characterize the mutual arrangement of the slots in the planar array are substituted in them.

6.3. An Analysis of Mutual Coupling Effects on the Directional Pattern of an Array

It is obvious that it is difficult to theoretically study in general form the influence of introducing the electrodynamic factors enumerated above on the directional pattern of an array because of the complexity of formula (6.7)--(6.10). Therefore, the only possible approach is the utilization of computers. The degree of influence of each factor on the directional pattern can be illustrated with an example of analyzing a specific slotted waveguide array.

For the sake of simplicity, we shall consider a slotted waveguide array formed by slots cut in the wide wall. The directional pattern of this array in the vertical plane is:

$$F(0) = \sum_{n=1}^{N_1} f_n(0) V_n \exp[j\kappa z_n^{(0)} \sin 0], \tag{6.11}$$

where $f_n(\theta)$ is the individual directional pattern of a slot in this plane; θ is the angle read out from a normal to the array; $z_n^{(0)}$ is the coordinate of the center of the n-th slot.

The experimentally measured directional pattern of an equally spaced, alternate phase coupled traveling wave slotted waveguide array, as well as the patterns computed using formula (6.11) with the recurrent technique are shown in Figure 6.3 for the following parameters: $N_1 = 20$, $l_n = 0.48\lambda$, $d = 0.445\lambda_B$, $a = 0.78\lambda$, $b = 0.344\lambda$, $P_H = [P_{load}] = 0.1$ and values of V_n determined from (6.1).

We shall perform a differential analysis of the impact of the various electrodynamic factors on the directional pattern. For this, we first of all determine the external and internal mutual admittances. Since $d \approx 0.5\lambda$ in this example, then, as follows from formulas (6.8) and [01], one can assume in a first approximation* that the mutual external admittances are:

$$Y_{mn}^{(e)} = \begin{cases} 1{,}028 \cdot 10^{-3}\ \text{Ом}^{-1}, \\ \qquad m = n, \qquad (6.12) \\ 0, \quad m \neq n. \end{cases} \tag{6.12}$$

The inherent internal admittances $Y_{nn}^{(i)}$ were determined in the literature [5], while the mutual admittances $Y_{mn}^{(i)}$ are computed from formula (6.7) when $\delta_n = \delta_m = 0$ is substituted in them, since the slot in the slotted waveguide array are longitudinal:

$$Y_{mn}^{(i)} = \begin{cases} j\sqrt{\dfrac{\varepsilon}{\mu}} \displaystyle\sum_{p=0}^{\infty} \sum_{q=0}^{\infty} \frac{\varepsilon_{pq}^{(1)} \varepsilon_{qp}^{(2)}}{\kappa^3 ab\,[(\pi/2\kappa l)^2 + \beta_{pq}^2]} \times \\ \quad \times \left[\dfrac{\sin(\pi q d_1/2a)}{\pi q d_1/2a}\right]^2 \cos^2\left(\dfrac{\pi p}{a}\, y_n^{(0)}\right) \times \\ \quad \times \left\{\dfrac{1 + e^{-2\beta_{pq}\kappa l}}{\beta_{pq}}\, \dfrac{1 + \beta_{pq}^2}{(\pi/2\kappa l)^2 + \beta_{pq}^2} \left(\dfrac{\pi}{2\kappa l}\right)^2 + \kappa l\left[1 - \left(\dfrac{\pi}{2\kappa l}\right)^2\right]\right\}, \\ \qquad\qquad m = n; \ (6.13) \\ j\sqrt{\dfrac{\varepsilon}{\mu}} \displaystyle\sum_{p=0}^{\infty} \sum_{q=0}^{\infty} \frac{\varepsilon_{pq}^{(1)} \varepsilon_{qp}^{(2)}}{2\kappa ab\beta_{pq}} \left[\left(\dfrac{\pi q}{\kappa a}\right)^2 + \left(\dfrac{\pi p}{\kappa b}\right)^2\right] \cos\left(\dfrac{\pi q}{a}\, y_n^{(0)}\right) \times \\ \quad \times \cos\left(\dfrac{\pi q}{a}\, y_m^{(0)}\right) \dfrac{\pi^2}{4\kappa^2 l_n l_m}\, \dfrac{e^{\kappa l_n \beta_{pq}} + e^{-\kappa l_n \beta_{pq}}}{(\pi/2\kappa l_n)^2 + \beta_{pq}^2} \times \\ \quad \times \dfrac{e^{\kappa l_m \beta_{pq}} + e^{-\kappa l_m \beta_{pq}}}{(\pi/2\kappa l_m)^2 + \beta_{pq}^2}\, e^{-\kappa|m-n| d\beta_{pq}}, \quad m \neq n, \end{cases} \tag{6.13}$$

---

*Where necessary, the mutual admittances can be computed precisely from formula (6.8).

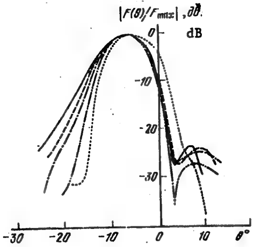

Figure 6.3. The influence of various factors on the shape of the directional pattern of a slotted waveguide array.

Key: The dotted curve is for the method of recurrent relationships; The curve with two dots between dashes takes nonresonant slots into account; The curve with a single dot between dashes takes nonresonance of the slot and mutual coupling via higher modes into account; The dashed curve accounts for the thickness of the waveguide wall; The solid curve is the experimental directional pattern.

where d_1 is the slot width; $\beta_{pq} = [(\pi q/ka)^2 + (\pi p/kb)^2 - 1]^{0.5}$; ; ε and μ are the dielectric permittivity and magnetic permeability of the ambient space.

As can be seen from (6.13), the slot width d_1 is included in the expression for the inherent admittance. It has been shown in the literature [8] that a slot in a real waveguide with a wall thickness t is equivalent in terms of its electrodynamic parameters to a slot of width d_1^*, cut in an infinitely thin wall. The relationship between d_1^* and d_1 is shown in Figure 6.4. It follows from what has been presented here that in order to take the waveguide wall thickness into account, it is necessary to substitute d_1^* for d_1 in formula (6.13).

Thus, system (6.2) with the matrix of mutual admittances, determined by expressions (6.12) and (6.13), makes it possible to find the amplitudes V_n, taking into account both all and individual electrodynamic factors. An analysis of the directional patterns calculated from these values of V_n makes it possible to more precisely specify which factors are the most significant.

a. Slot Nonresonance. We shall note two special features of formula (6.13) for the calculation of the internal admittance of a slot $Y_{nn}^{(i)}$: 1) Each term in (6.13), which is assigned the subscripts p, q, is a partial internal admittance of the for a H_{qp} mode; 2) The partial admittances depend on three geometric parameters of a slot (the length, $2l_n$; the width d_1 and the displacement $x_n^{(0)}$). Consequently, the resonant length of a slot also depends on the number of modes H_{qp} taken into account (6.13), the slot width and its displacement relative to the edge line of the wide wall of the waveguide. The nature of the resonant slot length as a function of d_1 and $x_n^{(0)}$ is the same as that shown in Figure 5.2.

It is apparent that when just slot nonresonance is taken into account, the amplitudes V_n are determined from a system of equations (6.2), in which it is necessary to set the internal and external mutual admittances $Y_{mn}^{(i)}$ and $Y_{mn}^{(e)}$ equal to zero. A computer was used to study the influence of higher modes on the shaping of the directional pattern. Calculations demonstrated that for a relative error in determining the active and reactive components of the internal admittance of no more than one percent, it is sufficient to take only the first seven modes: H_{10}, H_{01}, H_{02}, H_{20}, H_{21}, H_{12} and H_{22} [1, 3].

The directional pattern of an array calculated under these conditions is shown in Figure 6.3. A comparison of the curves shows that accounting for just slot nonresonance, although it is important, does not lead to satisfactory results. Consequently, it is also necessary to take other electrodynamic factors into account.

b. Internal Mutual Coupling of Slots Via Higher Modes. In order to also take this into account, it is necessary to take into account the mutual admittances $Y_{mn}^{(i)}$, which are calculated from formula (6.13), in the matrix of system (6.2). The directional pattern which takes into account slot nonresonance and internal mutual coupling via higher modes is shown in Figure 6.3, from which the rather good correlation between the experimental and theoretical results can be seen.

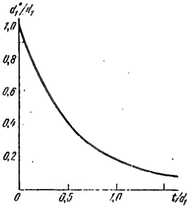

Figure 6.4. The equivalent slot width as a function of the thickness of the waveguide wall.

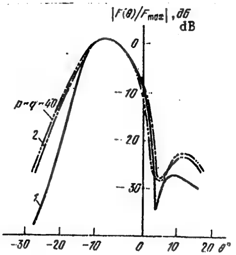

Figure 6.5. The influence of the modal composition of the higher modes on the shaping of the directional pattern of a slotted waveguide array.

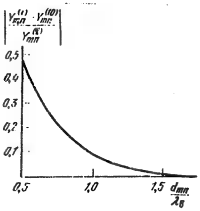

Figure 6.6. The mutual admittance of slots due to higher modes as a function of the spacing between them ($Y_{mn}^{(10)}$ is the part of the mutual admittance $Y_{mn}^{(i)}$, which is due to interaction via the dominant H_{10} mode).

The data of mathematical modeling of the influence of higher modes (up to $p = q = 40$) on the shape of the directional pattern [1, 3] are shown in Figure 6.5, from which it follows that the major contribution is made by the H_{10}, H_{01}, H_{02}, H_{20}, H_{21}, H_{12} and H_{22} modes. Figure 6.6 illustrates the rapid decrease in the mutual coupling of slots via higher modes when the spacing between them increases: in particular, when $d > 1.5\lambda_B$, the contribution of higher modes to the mutual admittance $Y_{pq}^{(i)}$ is less than 0.1 percent, and for this reason, one can assume that under these conditions, mutual coupling is due only to the dominant H_{10} mode.

c. Finite Thickness of Waveguide Walls. In order to take into account the dependence of the equivalent slot width d_1^* on the thickness of the waveguide wall t, it is sufficient to introduce in place of the actual width d_1 of the slot, its equivalent width d_1^* in formula (6.13) for the calculation of the inherent internal admittance $Y_{nn}^{(i)}$. It follows from Figure 6.4 that with an increase in t, the equivalent width of the slot decreases, by virtue of which the value of the factor $\left[\sin\left(\frac{\pi q d_1^*}{2a}\right) \Big/ \frac{\pi q d_1^*}{2a}\right]^2$ increases. This leads to the fact that to obtain a specified precision in the determination of $Y_{nn}^{(i)}$, it is necessary to take into account a larger number of modes than in paragraphs a and b. Computer calculations have shown that with the same relative error of one percent as in paragraph a for the calculation of $Y_{nn}^{(i)}$, it is sufficient to use the first 14 higher modes.

The directional patterns of an array calculated for the cases of the actual slot width d_1 and the equivalent width d_1^* are shown in Figure 6.3. A comparison of the dashed-and-dotted and the dashed curves attests to the necessity of taking the finite thickness of waveguide walls into account.

d. External Mutual Coupling of Radiators. The necessity of taking this factor into account in planar slotted waveguide arrays is obvious, since at least the nearest slots of adjacent waveguides have a substantial influence on each radiator. The conductance and susceptance components of the external mutual admittances $Y_{mn}^{(e)}$ can amount to up to 40 percent of the inherent external admittances $Y_{nn}^{(e)}$ of the slot. In order to take the external mutual coupling into account, it is sufficient to substitute the values of $Y_{mn}^{(e)}$, computed from formula (6.8), in the matrix for the mutual admittances of the system of equations (6.2).

In those cases where the spacing between the slots, d_{mn}, is no less than 0.5λ, one can use the following formula to calculate the external mutual admittances [01]:

$$Y_{mn}^{(e)}=j\,\frac{1{,}64\lambda}{\pi d_{mn}}\,\frac{\cos\left(\frac{\pi}{2}\cos\theta_m\right)}{\sin\theta_m}\,\frac{\cos\left(\frac{\pi}{2}\cos\theta_n\right)}{\sin\theta_n}\,e^{-j\frac{2\pi}{\lambda}d_{mn}}, \tag{6.14}$$

where Θ_m and Θ_n are the angles between the radius vector from one slot to another and the longitudinal axes of the m-th and n-th slots respectively. In this case, since the slots are longintudinal, $\theta_n = \theta_m = 0$, and therefore $Y_{mn}^{(e)} = 0$.

Similar results are also obtained for other amplitude-phase distributions of the field in the aperture of the array.

Thus, when synthesizing planar slotted waveguide arrays, it is necessary to take into account all four electrodynamic factors, and when calculating the internal admittances, to consider only the first 14 higher modes. For this reason, the superscripts in the twin summation signs of (6.13) are to be set equal to p = q = = 3:

$$Y_{mn}^{(i)}=\begin{cases}\sqrt{\frac{\varepsilon}{\mu}}\sum\limits_{p=0}^{3}\sum\limits_{q=0}^{3}\frac{\varepsilon_{pq}^{(1)}\varepsilon_{qp}^{2}}{ab\kappa^{3}\left[(\pi/2\kappa l)^{2}+\beta_{pq}^{2}\right]}\left[\frac{\sin(\pi q d_1/2a)}{\pi q d_1/2a}\right]^{2}\cos^{2}\left(\frac{\pi p}{a}y_n^{(0)}\right)\times\\ \times\left\{\frac{1+e^{-2\kappa l\beta_{pq}}}{\beta_{pq}}\frac{1+\beta_{pq}^{2}}{(\pi/2\kappa l)^{2}+\beta_{pq}^{2}}\left(\frac{\pi}{2kl}\right)^{2}+\kappa l\left[1-\left(\frac{\pi}{2\kappa l}\right)^{2}\right]\right\},\quad m=n, \qquad (6.15a)\\ j\sqrt{\frac{\varepsilon}{\mu}}\sum\limits_{p=0}^{3}\sum\limits_{q=0}^{3}\frac{\varepsilon_{pq}^{(1)}\varepsilon_{qp}^{(2)}}{2ab\kappa\beta_{pq}}\left[\left(\frac{\pi q}{\kappa b}\right)^{2}+\left(\frac{\pi p}{\kappa a}\right)^{2}\right]\cos\left(\frac{\pi q}{a}y_n^{(0)}\right)\times\\ \times\cos\left(\frac{\pi q}{a}y_m^{(0)}\right)\frac{\pi^{2}}{4\kappa^{2}l_n l_m}\frac{e^{\kappa l_m\beta_{pq}}+e^{-\kappa l_m\beta_{pq}}}{(\pi/2\kappa l_m)^{2}+\beta_{pc}^{2}}\times\\ \times\frac{e^{\kappa l_n\beta_{pq}}+e^{-\kappa l_n\beta_{pq}}}{(\pi/2\kappa l_n)^{2}+\beta_{pq}^{2}}\,e^{-\kappa|m-n|d\beta_{pq}},\quad m\neq n. \qquad (6.15б)\end{cases}$$

(6.15a)

(6.15b)

6.4. A Procedure for Synthesizing a Linear Slotted Waveguide Array Taking Electrodynamic Mutual Coupling Effects Into Account

The General Scheme. In order to design a slotted waveguide array, taking mutual coupling effects into account, it is necessary, as follows from equations (6.2), to find the internal and external admittances of the slots for a specified number and type of array radiators, as well as the geometry for their arrangement, which realize the requisite distribution of the complex voltage amplitudes V_n. Since this is a rather complicated nonlinear mathematical problem, it is expedient to approach its solution from physical considerations.

We shall first treat the case of [illegible] linear slotted waveguide array. It is obvious that the magnetomotive force in an arbitrary m-th slot can be represented as:

$$F_m = V_m^{(1)} \left(Y_{mn}^{(i)} + Y_{mn}^{(e)} \right), \tag{6.16}$$

where $V_m^{(I)}$ is the voltage in the slot without taking the mutual coupling effect into account.

Then we rewrite system (6.2) in the following manner:

$$\sum_{n=1}^{N_1} V_n \left(Y_{mn}^{(i)} + Y_{mn}^{(e)} \right) = V_m^{(1)} \left(Y_{mm}^{(i)} + Y_{mm}^{(e)} \right), \quad 1 \leqslant m < N_1. \tag{6.17}$$

It can be solved by an iteration technique, by employing certain physical considerations. It has been shown in paper [3] that for this, it is sufficient to employ the following procedures:

1. Based on the known values of V_n (the requisite distribution) using one of the known methods, which do not take into account all of the mutual coupling factors, the array geometry is determined (the displacement of the slots $x_n^{(0)}$ and the spacing between them).

2. Using formulas (6.8) and (6.7) (or (6.14)) the matrix of the internal $Y_{mn}^{(i)}$ and external $Y_{mn}^{(e)}$ admittances is calculated, where these admittances are due to factors not taken into account in paragraph 1.

3. The complex voltage amplitudes $Y_m^{(1)}$ are determined from the known values of V_n, $Y_{mn}^{(i)}$ and $Y_{mn}^{(e)}$ from expression (6.17).

4. Based on the computed values of $V_m^{(1)}$, just as in paragraph 1, the next approximation of the array geometry is determined, and then paragraph 2, 3, etc. are carried out.

It is clear from physical considerations that this iterative process converges. As a result of the calculation, that array geometry will be found which assures the realization of the requisite distribution in the antenna aperture, taking all of the electrodynamic mutual coupling factors into account.

The Initial Approximation. As can be seen from the synthesis scheme proposed here, the most complex procedure in a computational sense is procedure 1, all the more since the known computational methods cannot be used (the energy or recurrent methods), since the complex distribution of $V_m^{(1)}$ in the general case has [illegible] non-linear phase characteristic. To carry out the procedure, a special method has been proposed in a number of papers [2, 9-11], which is based on the representation of the slotted waveguide radiator in the form of a long line of four-pole networks, which are characterized by the equivalent circuits of the slots.

The equivalent circuits of various slots of length $l_n = 0.5\lambda$, cut in the wide wall of a waveguide and their equivalent normalized admittances (or impedances) are presented in Table 6.1, in which the same symbols are used as in Chapter 5. All of the parameters of these circuits are uniquely related to the external $Y_{nn}^{(e)}$ and internal $Y_{nn}^{(i)}$ admittances and are found from the balance condition for the complex powers in the waveguide slot cross-section [12].

Thus, a dominant mode slotted waveguide array can be represented in the form of series connected four-pole networks.

It can shown by employing four-pole network theory that the normalized incident and reflected voltage waves, U_n^+ and U_n^-, at the input and output of the n-th four-pole network are interrelated by the following expressions:

$$\begin{pmatrix} U_{n-1}^+ \\ U_{n-1}^- \end{pmatrix} = \begin{pmatrix} a_1 e^{\Delta_n} + a_2 e^{-\Delta_n} & a_3 e^{\Delta_n} + a_4 e^{-\Delta_n} \\ b_1 e^{\Delta_n} + b_2 e^{-\Delta_n} & b_3 e^{\Delta_n} + b_4 e^{-\Delta_n} \end{pmatrix} \begin{pmatrix} U_n^+ \\ U_n^- \end{pmatrix}, \tag{6.18}$$

where:

$$a_1 = (1+\xi_3)\,[1+\xi_1+\xi_2+2\xi_1\xi_2]; \qquad a_2 = \xi_3\,[\xi_1-\xi_2+2\xi_1\xi_2];$$
$$a_3 = q\,(1+\xi_3)\,[\xi_1-\xi_2-2\xi_1\xi_2]; \qquad a_4 = -q\xi_3\,[1-\xi_1-\xi_2+2\xi_1\xi_2];$$
$$b_1 = q\xi_3\,[1+\xi_1+\xi_2+2\xi_1\xi_2]; \qquad b_2 = -q\,(1-\xi_3)\,[\xi_1-\xi_2+2\xi_1\xi_2];$$
$$b_3 = \xi_3\,[\xi_1-\xi_2-2\xi_1\xi_2]; \qquad b_4 = (1-\xi_3)\,[1-\xi_1-\xi_2+2\xi_1\xi_2];$$

$\Lambda_n = (2\pi/\lambda_n)\,d_n$; $q = 1$, $\xi_1 = y_a^{(n)}$, $\xi_2 = z_n$; $\xi_3 = y_b^{n-1}$ for the equivalent circuit of Figure 6.7a; $q = -1$, $\xi_1 = z_a^{(n)}$, $\xi_2 - y_n$, $\xi_3 = z_b^{(n-1)}$ for the equivalent circuit of Figure 6.7b; d_n is the spacing between the n-th and (n-1)-th radiators.

All of the equivalent conductances $g_n = \mathrm{Re}\,\xi_2$, $b_n = \mathrm{Im}\,\xi_2$ and d_n can be found based on the specified amplitude $f_n = |V_n|$ and phase $\phi_n = \arg V_n$ distributions, with the initial values of $d_n^{(0)}$ and the fractions of the power absorbed in the load P_H specified from physical considerations.

For this, the auxiliary normalized coefficient is determined initially:

$$s_{N_1} = \frac{P_H}{1-P_H}\sum_{n=1}^{N_1}|V_n|^2. \tag{6.19}$$

If the incident voltage wave to the slotted waveguide array load is normalized to unity, i.e., we set $U_{N_1}^+ = 1$, then the reflected wave amplitude will be $U_{N_1}^- = q\Gamma$, where Γ is the reflection factor, while $q = \pm 1$ for the equivalent circuits of Figures 6.7a and 6.7b respectively. Then, as shown in the literature [10, 11], the

TABLE 6.1

(1) Положение и эквивалентная схема щели	(2) Внутренняя проводимость щели $Y^{(i)}=G^{(i)}+jB^{(i)}$	Эквивалентные проводимость или сопротивление (3)
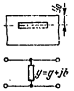	(6.15a)	$Y=\frac{2G^{(i)}}{Y_{\Sigma}+jB^{(i)}}$
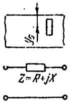	$Y^{(i)}=j\sqrt{\frac{\varepsilon}{\mu}}\times$ $\times\sum_{p=1}^{3}\sum_{q=0}^{3}\frac{8\varepsilon_{pq}^{(2)}\left[1-\left(\frac{\pi p}{2\kappa a}\right)^2\right]}{\kappa^3 ab}\times$ $\times\left(\frac{2l}{\pi d_1}\right)^2\left[\frac{\cos\left(\frac{2\pi pl}{2a}\right)}{1-\left(\frac{2\pi pl}{b}\right)^2}\right]^2\times$ $\times\sin^2\left(\frac{\pi p}{b}y_0\right)\frac{1}{\beta_{pq}^2}\times$ $\times\left[\kappa d_1-\frac{1-\exp(-\beta_{pq}\kappa d_1)}{\beta_{pq}}\right]$	$Z=\frac{2G^{(i)}}{Y_{\Sigma}+jB^{(i)}}$
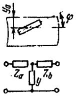	(6.7)	$Y=\sqrt{1-\left(\frac{\pi}{\kappa a}\right)^2}\times$ $\times\frac{D_2^2}{Y_{\Sigma}+jB^{(i)}}$; $Z_a=-j\frac{D_1}{D_2}$; $Z_b=j\frac{D_1}{D_2}$

Примечание. Величины D_1 и D_2 определены в [12].

Note: The quantities D_1 and D_2 are determined in [12].

Key:
1. Position and equivalent circuit of the slot;
2. Internal admittance of the slot, $Y(i) = G^{(i)} + jB(i)$;
3. Equivalent admittance or impedance.

conductance (or resistance) of the slots is computed from the formula:

$$g_n = |V_n|^2 / s_{N_1} |U_n^+ - qU_n^-|^2. \tag{6.20}$$

from expression [13]:

$$g_n = 2\mathrm{Re}\left\{\frac{\mathrm{Re}\left[Y_{nn}^{(i)}\left(x_n^{(0)}\right)\right]}{Y_{nn}^{(e)} + j\mathrm{Im}\left[Y_{nn}^{(i)}\left(x_n^{(0)}\right)\right]}\right\} \tag{6.21}$$

We determine the displacement $x_{n_0}^{(0)}$ of the n-th slot relative to the center line of the wide wall of the waveguide by any gradient technique, in particular in the following manner:

$$x_{n_\nu}^{(0)} = x_{n_{\nu-1}}^{(0)} + \delta_\nu \,\mathrm{sign}\,(g_n - g_{n_\nu}), \tag{6.22}$$

where

$$g_{n_\nu} = 2\mathrm{Re}\left\{\frac{\mathrm{Re}\left[Y_{nn}^{(i)}\left(x_{n_\nu}^{(0)}\right)\right]}{Y_{nn}^{(e)} + j\mathrm{Im}\left[Y_{nn}^{(i)}\left(x_{n_\nu}^{(0)}\right)\right]}\right\},$$

$$\delta_\nu = \begin{cases} \delta_{\nu-1}; & \nu = 1 \;\text{или}\; \mathrm{sign}\,(g_n - g_{n_{\nu-1}}) = \mathrm{sign}\,(g_n - g_{n_{\nu-2}}), \\ \delta_{\nu-1}/2, & \overset{\text{or}}{\mathrm{sign}}\,(g_n - g_{n_{\nu-1}}) \neq \mathrm{sign}\,(g_n - g_{n_{\nu-2}}). \end{cases}$$

It is natural to take the following [7] as the initial value of $x_{n_0}^{(0)}$:

$$x_n^* = (-1)^n \left[\frac{a}{\pi} \arcsin \sqrt{\frac{b}{a}\frac{\lambda_0}{\lambda_B}\frac{g_n}{2{,}09\cos^2\left(\frac{\pi}{2}\frac{\lambda_0}{\lambda_B}\right)}}\right], \tag{6.23}$$

which realizes the requisite value of g_n given the condition of slot resonance. The initial step δ_0 is chosen in a range of a/20 = a/10.

We determine the equivalent susceptance of the slot from the value found for $x_n^{(0)}$:

$$b_n = 2\mathrm{Im}\left\{\frac{\mathrm{Re}\left[Y_{nn}^{(i)}\left(x_n^{(0)}\right)\right]}{Y_{nn}^{(e)} + j\mathrm{Im}\left[Y_{nn}^{(i)}\left(x_n^{(0)}\right)\right]}\right\}. \tag{6.24}$$

The amplitude and phase of the field radiated by the n-th slot are:

$$|\overline{V}_n| = \sqrt{g_n}\,|U_n^+ - qU_n^-|; \tag{6.25}$$

$$\overline{\Phi}_n = \arg\,(U_n^+ - qU_n^-). \tag{6.26}$$

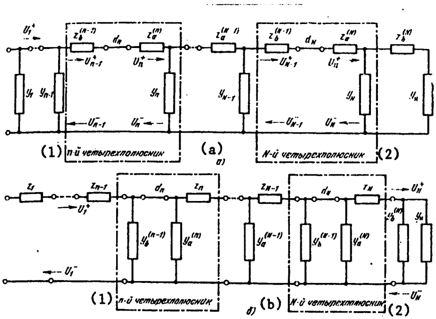
U_1^+
$Z_б^{(n-1)}$
d_n
$Z_a^{(n)}$
$Z_a^{(N-1)}$
$Z_б^{(N-1)}$
d_N
$Z_a^{(N)}$
$Z_б^{(N)}$
U_{n-1}^+
U_n^+
U_{N-1}^+
U_N^+
y_1
y_{n-1}
y_n
y_{N-1}
y_N
U_{n-1}^-
U_n^-
U_{N-1}^-
U_N^-
(1)
n-й четырехполюсник
(a)
а)
N-й четырехполюсник
(2)
z_1
z_{n-1}
d_n
z_n
z_{N-1}
d_N
z_N
U_N^+
U_1^+
$y_б^{(n-1)}$
$y_a^{(n)}$
$y_a^{(N-1)}$
$y_б^{(N-1)}$
$y_a^{(N)}$
$y_б^{(N)}$
y_N
U_1^-
(1)
n-й четырехполюсник
б)
(b)
N-й четырехполюсник
(2)
U_N^-

Figure 6.7. Equivalent circuits of slotted waveguide arrays.

Key: 1. The n-th four-pole network;
2. The N-th four-pole network.

To realize the specified phase distribution for each n, the following conditions should obviously be met: $\overline{\Phi}_n - \overline{\Phi}_{n-1} = \Phi_n - \Phi_{n-1}$. Taking (6.26) into account, we have:

$$\Phi_n - \Phi_{n-1} = \arg \frac{U_n^+ + qU_n^-}{U_{n-1}^+ + qU_{n-1}^-}. \tag{6.27}$$

Expression (6.27) can be the starting one when selecting the spacing d_n between the slots for the realization of the specified phase distribution. We transform the right side of (6.27):

$$\frac{U_{n-1}^+ - qU_{n-1}^-}{U_n^+ - qU_n^-} = \operatorname{ch} \Delta_n + \hat{\xi}_n \operatorname{sh} \Delta_n, \tag{6.28}$$

where

$$\hat{\xi}_n = \hat{a}_n + j\hat{b}_n = \frac{U_n^+ + qU_n^-}{U_n^+ - qU_n^-} + \frac{[(a_1 - qb_1 - 1)U_n^+ + (a_3 - qb_3)U_n^-]\, e^{\Delta_n} + [(a_2 - qb_2)U_n^+ + (1 - a_4 + qb_4)U_n^-]\, e^{\Delta_n}}{(U_n^+ - qU_n^-)\operatorname{sh} \Delta_n}. \tag{6.29}$$

Taking these symbol designations into account, following some uncomplicated transformations, expression (6.29) reduces to the form:

$$d_n = \begin{cases} \frac{\lambda_в}{2\pi} \operatorname{arctg} Q_n, & d_0 < \frac{\lambda_в}{4}; \\ \frac{\lambda_в}{2} + \frac{\lambda_в}{2\pi} \operatorname{arctg} Q_n, & Q_n \geqslant 0, \ \frac{\lambda_в}{4} < d_0 \leqslant 3\frac{\lambda_в}{4}; \\ \lambda_в + \frac{\lambda_в}{2\pi} \operatorname{arctg} Q_n, & Q_n < 0, \ \frac{\lambda_в}{4} < d_0 \leqslant 3\frac{\lambda_в}{4}; \ d > \frac{3}{4}\lambda_в, \end{cases} \quad (6.30)$$

where: где

$$Q_n = \frac{\operatorname{tg}(\Phi_{n-1} - \Phi_n)}{\hat{a}_n + \hat{b}_n \operatorname{tg}(\Phi_{n-1} - \Phi_n)}; \quad d_в = \frac{\lambda_0 \lambda_в}{2(\lambda_0 - \lambda_в \sin \theta_{гл})};$$

$\theta_{гл}$ [θ_{main}] is the direction of the main lobe of the directional pattern.

By sequentially applying relationships (6.18) and (6.20), we find all of the values g_n, b_n and d_n. We will note that the calculations using these formulas yield the same results for the equivalent circuits of Figures 6.7a and 6.7b [11].

Taking equalities (6.20) and (6.25) into account, we obtain $|\overline{V}_n| = |\overline{V}_n|$, i.e., with the found conductances g_n, the specified amplitude distribution is actually realized in the aperture of the array.

The spacing computed from formula (6.30) realize the specified phase distribution. For example, if it is necessary to realize a linear phase front in the antenna aperture, then it is necessary to substitute the value $(2\pi/\lambda_0)d_n \sin\theta_{main}$ in formula (6.30) instead of $\Phi_{n-1} - \Theta_n$.

Equation (6.27) is satisfied only for definite values of the spacing d_n^*. Physically, this means that in the aperture of an array with a spacing of d_n between the radiators, the specified phase distribution is realized, taking into account the dominant mode mutual coupling of the radiators. In practice, d_n^* is determined by iteration using formula (6.30), where the original values of the spacings d_n are substituted in the right side. If equation (6.27) is not satisfied in this case, new values $d_n^{(1)}$ are substituted in the right side, and the entire cycle is repeated. It can be demonstrated that this process converges.

Thus, the method described here makes it possible to realize a specified amplitude-phase distribution in a linear array, taking into account all of the electrodynamic mutual coupling factors.

The results of such a synthesis for the 20 element slotted waveguide array treated earlier where $\lambda_0 = 3.66$ cm are presented in Figure 6.8 and in Table 6.2. The directional pattern synthesized using this procedure (Figure 6.8, the solid curve) has a sidelobe level of less than -30 dB, and shows a good correlation prior to these values with the requisite directional pattern (Figure 6.8, the dashed curve), while the directional pattern computed without accounting for the mutual coupling

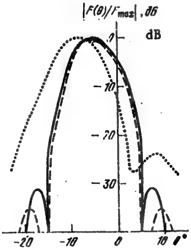

Figure 6.8. The results of calculating the directional patterns of slotted waveguide arrays.

Key: The dashed curve is the theoretical directional pattern;
The solid curve takes into account mutual coupling effects;
The dotted curve is where the mutual coupling of the radiators is not taken into account.

effect (Figure 6.8, the dotted curve), correlates with the desired directional pattern down to only about the -15 dB level. It must be noted that there is no precise correspondence between the synthesized and specified directional patterns because the spacings between the slots changed and the slotted waveguide array changed from an equally spaced one to an unequally spaced array.

TABLE 6

N_1	(1) С учетом взаимовлияния			(2) Без учета взаимовлияния		
	$x_n^{(0)}$, мм mm	d_n, мм mm	g_n	$x_n^{(0)}$, мм mm	d_n, мм mm	g_n
1	0,14	24,44	$0{,}95\cdot10^{-4}$	0,12	21,0	$0{,}32\cdot10^{-4}$
2	—0,13	21,72	$0{,}43\cdot10^{-3}$	—0,16	21,0	$0{,}17\cdot10^{-3}$
3	0,68	22,16	$0{,}18\cdot10^{-2}$	0,50	21,0	$0{,}11\cdot10^{-3}$
4	—0,87	21,81	$0{,}52\cdot10^{-2}$	—0,83	21,0	$0{,}40\cdot10^{-2}$
5	1,18	21,17	$0{,}11\cdot10^{-1}$	1,48	21,0	$0{,}10\cdot10^{-1}$
6	—2,73	21,11	$0{,}19\cdot10^{-1}$	—1,98	21,0	$0{,}19\cdot10^{-1}$
7	2,91	21,02	$0{,}33\cdot10^{-1}$	2,60	21,0	$0{,}31\cdot10^{-1}$
8	—3,86	21,38	$0{,}55\cdot10^{-1}$	—3,10	21,0	$0{,}45\cdot10^{-1}$
9	4,70	21,76	$0{,}83\cdot10^{-1}$	3,77	21,0	$0{,}64\cdot10^{-1}$
10	—5,52	22,03	0,119	—4,41	21,0	$0{,}875\cdot10^{-1}$
11	6,51	22,16	0,160	5,30	21,0	0,153
12	—7,29	22,18	0,195	—6,20	21,0	0,159
13	8,00	22,18	0,205	7,14	21,0	0,197
14	—7,43	22,08	0,182	—7,27	21,0	0,205
15	6,04	21,74	0,134	6,31	21,0	0,161
16	—4,82	21,31	$0{,}09\cdot10^{-1}$	—4,52	21,0	$0{,}92\cdot10^{-1}$
17	3,66	21,28	$0{,}47\cdot10^{-1}$	2,86	21,0	$0{,}37\cdot10^{-1}$
18	—2,61	21,33	$0{,}19\cdot10^{-1}$	—1,43	21,0	$0{,}10\cdot10^{-1}$
19	0,86	21,36	$0{,}46\cdot10^{-2}$	0,62	21,0	$0{,}17\cdot10^{-2}$
20	—0,93	22,21	$0{,}87\cdot10^{-3}$	—0,27	21,0	$0{,}41\cdot10^{-3}$

Key: 1. Taking mutual coupling into account;
2. Without taking mutual coupling into account.

6.5. A Procedure for Synthesizing a Planar Slotted Waveguide Array Taking Mutual Coupling Into Account

We shall now briefly consider a synthesis procedure for a planar slotted waveguide array. As was shown in §6.2, with a known law for the excitation of the waveguides, the complex voltage amplitudes $V_{n_1 n_2}$ in the slots are determined from the system of equations (6.9). In accordance with (6.16), the magnetomotive force is:

$$F_{m_1 m_2} = V^{(1)}_{m_1 m_2} \left(Y^{(i)}_{m_1 m_2,\ m_1 m_2} + Y^{(e)}_{m_1 m_2,\ m_1 m_2} \right), \tag{6.31}$$

where $V^{(1)}_{m_1 m_2}$ is the voltage in a slot without taking mutual influence into account.

By substituting (6.31) in (6.9), we obtain a system of equations which makes it possible to synthesize a slotted waveguide array by the methods described in §6.4. In fact, by asigning an arbitrary waveguide the number $m_2^{(0)}$ and knowing the matrix for the internal and external mutual and inherent admittances of the planar slotted waveguide array from the preceding set in the calculations, we arrive at the linear array synthesis problem treated in §6.4:

$$\sum_{n_1=1}^{N_1} V_{n_1 m_2^{(0)}} \left[Y^{(e)}_{m_1 m_2^{(0)}\ n_1 m_2^{(0)}} + Y^{(i)}_{m_1 m_2^{(0)}\ n_1 m_2^{(0)}} \right] = V^{(1)}_{m_1 m_2^{(0)}} \left[Y^{(e)}_{m_1 m_2^{(0)}\ m_1 m_2^{(0)}} + Y^{(i)}_{m_1 m_2^{(0)}\ m_1 m_2^{(0)}} \right] - \sum_{\substack{n_2=1 \\ n_2 \neq m_2^0}}^{N_2} \sum_{n_1=1}^{N_1} V_{n_1 n_2} Y^{(e)}_{m_1 m_2^{(0)} n_1 n_2}. \tag{6.32}$$

By successively varying $n_2^{(0)}$ from 1 to N_2, we find all of the internal admittances of the slots, and consequently, their (the slots') arrangement in the wide wall of each waveguide.

Thus, the following procedure for the design of a planar slotted waveguide array can be recommended [3]:

1. We determine the external and internal inherent and mutual admittances of the slots and their (the slots') arrangement based on the amplitude-phase distribution of $V_{m_1 m_2^{(0)}}$ specified for each waveguide having a number $1 \leq m_2^{(0)} \leq N_2$ by means of the procedure of §6.4.

2. Using the geometry for the slot configuration found in paragraph 1 and employing formulas (6.7) and (6.8), we find the external mutual admittance matrix.

3. By substituting the matrix of the external and internal admittances, calculated in paragraphs 1 and 2 in the system of equations (6.32), based on the procedure of §6.4 we determine the next approximation of the array geometry and its admittance matrices, etc.

This process usually converges after a few steps. Just as in the case of linear array, that geometry of the planar array will be found as a result of the calculation which provides for the realization of the requisite amplitude-phase distribution in the antenna aperture, taking into account all of the electrodynamic mutual influence factors.

6.6. Design Calculation Recommendations

The starting data in the design of planar nonresonant slotted waveguide arrays, as a rule, are the following: the direction of the main beam of the directional pattern; the width of the directional pattern in the main planes at the half-power level; the permissible level of directional pattern sidelobes; the gain; the fraction of the power lost in the load, and the permissible aperture size.

Depending on the purpose of the slotted waveguide array, particular groups of initial requirements will be the major ones. Examples of such groups of requirements (variants) are cited in Chapter 5. In all of these variants, one of the intermediate steps has to be the calculation of the amplitude-phase distribution of the field in the antenna aperture, the calculation of the spacings d_n between the slots as well as the number of waveguides N_2 and slots N_1 in each of them. Based on these data, using the procedures of §6.4 and §6.5, we determine the arrangement of the slots in the wide walls of the waveguides, which realizes the requisite amplitude-phase distribution of the field in the slotted waveguide array aperture, taking mutual coupling into account.

The calculation of the remaining parameters of the array is accomplished just as described in §5.9.

In performing the calculations, one specific feature revealed in §6.4 must be remembered: taking into account all of the mutual coupling factors leads to an unequally spaced configuration of the slots, because of which, the theoretical level of the first sidelobes of the directional pattern may not be achieved. For this reason, it is necessary in practical calculations to set standards which are several decibels more stringent for the requisite sidelobe level.

7. PHASED ANTENNA ARRAYS WITH A HEMISPHERICAL SCAN SPACE

7.1. General Governing Laws

The Classification of Phased Antenna Arrays with a Hemispherical Scan Field. Operational Principle. Planar phased arrays provide for a rather high gain in scanning sectors not exceeding 40° to 50° from the normal to the plane of the antenna. The scanning sector of a planar phased antenna array is bounded by the main lobe of the directional pattern of a radiating element of the array and is determined by the dimensions of the radiating elements as well as the mutual coupling between them. However, for some radars (ground based and marine long range radars, on-board multifunction radars in aircraft and space vehicles, etc.), phased arrays are needed having a scan sector of more than a hemisphere (including circular scanning in the horizontal plane). These requirements can be met in phased arrays of a special structural design, which employ spatial (aplanar) systems of radiators:

1. Hybrid phased antenna arrays, which take the form of a combination of a planar phased array which scans in a comparatively small sector and an uncontrolled locking system, which makes it possible to extend the scan sector. One of the most suitable structural designs for a hemispherical scan space is a planar phased array with an axially symmetric lens, which is called a shell or dome shaped lens (see § 7.2) [1]. For a definite functional relationship between the index of refraction of the lens and the central angle θ, the scan sector of a planar phased array can be increased by 1.5 to 2 times.

2. Conformal phased arrays, the radiators of which are arranged on aplanar surfaces (usually convex axially symmetric surfaces) [1 - 3]: cylindrical, conical, spherical, etc. Besides conventional scanning conformal scanning is also used, i.e., scanning which provides for a constant shape of the directional pattern and a constant gain in the direction of the main lobe. Conformal scanning is accomplished through the switching of the radiators in such a way that the shape and dimensions of the radiating region, moved around the axis or the center of symmetry of the phased array, are preserved.

Conformal phased antenna arrays make it possible to obtain undistorted scanning in azimuth (cylindrical and conical phased antenna arrays) or over the entire hemisphere (spherical phased arrays). However, because of the simultaneous utilization of only a small portion of the overall number of radiators (10 to 50%), conformal phased arrays will contain a very large number of controlled modules (about 10^4 to 10^5) and have a high cost.

3. Polyhedral phased antenna arrays, which take the form of a spatial system of planar phased arrays (subarrays), arranged on the faces of convex polyhedra (pyramids, prisms, regular polyhedra, etc.) and which can be phased either independently or jointly [013]. Polyhedral phased arrays with hemispherical scanning have fluctuations in the gain and changes in the shape of the directional pattern, which decrease with an increasing number of subarrays.

Requirements Placed on Radiating Elements. The in-phase addition of fields having the same polarization of all of the radiators included in the radiating region in necessary to generate the main lobe of a convex conformal phased antenna array in a specified direction. The movement of the radiating region over the convex surface requires changes in the plane of polarization of the fields of the radiators included in it. For this reason, it is expedient to use radiators with either circular or controlled polarization in certain phased arrays with hemispherical scanning (spherical, conical, etc.).

The same types of poorly directional radiators with axial symmetry are used as the radiating elements of phased arrays with hemispherical scanning as for planar phased antenna arrays [05]. The following types of radiators have become the most widespread for the generation of the requisite polarization characteristics: cross-shaped dipoles, cylindrical helical antennas, frequency independent antennas in the decimeter band; open ends of waveguides (horns), dielectric rods, helical and frequency independent antennas as well slot radiators in the centimeter band.

The Directional Pattern and Gain of Hemispherical Scan Phased Antenna Arrays. The Scan Pattern. The calculation of the directional pattern and the gain for various phased array structural configurations have their own special features, however, some of the basic governing laws can be utilized in all variants.

For pyramidal phased arrays, consisting of three to five planar subarrays, which execute independent scanning in adjacent spatial sectors, the calculation of the directional pattern and the gain is accomplished using the same methods as for planar phased antenna arrays.

For large convex conformal and polyhedral phased arrays, the approximate computation of the directional pattern and the gain, with the condition that the main lobe is unique [01], can be carried out using the technique of an equivalent plane aperture (EPR) [EPA] [3]. The projection of the radiating region of the convex phased antenna array onto a plane normal to the direction of the maximum of the main lobe (Figure 7.1) is taken as the equivalent plane aperture. The equivalent plane aperture is made in-phase by phase leads in the radiators with respect to the central radiator:

$$\Delta\Phi_\nu = k(r_\nu - r_0), \tag{7.1}$$

where $k = 2\pi/\lambda$; r_ν is the spacing of the ν-th radiator from the equivalent plane aperture; r_0 is the spacing of the central radiator from the equivalent plane aperture.

The amplitude distribution in the equivalent plane aperture $A(\rho)$ can be approximately represented in terms of the directional patterns of the radiating elements $F_{\text{И}}(\theta)$ $[F_{\text{rad}}(\theta)]$ in the direction of the main lobe maximum of the phased antenna array (Figure 7.1):

$$A(\rho) \pm F_{\text{и}}(\vartheta). \tag{7.2}$$

The differing density in the placement of the radiators in the equivalent plane aperture when they are projected from the convex surface leads to a change in the amplitude distribution $A(\rho)$. This correction for the change in the amplitude distribution can be found using the methods of geometric optics.

One can approximately determine the directional pattern and directional gain of an equivalent plane aperture by the conventional aperture method [01] for the value found for $A(\rho)$. The approximate nature of the equivalent plane aperture technique must be kept in mind, which when $\theta_0 = 30° - 60°$ yields a satisfactory precision in the calculation of the directional pattern of a convex phased array in a sector of $\theta_{main} \pm \theta'$, where:

$$\theta'/2\theta_{0,5} \leqslant (R/\lambda)^{1/2}. \tag{7.3}$$

($2\theta_{0.5}$ is the width of the main lobe of the directional pattern of the phased antenna array). A more precise calculation of the directional pattern and directional gain of convex antennas is set forth in paper [2].

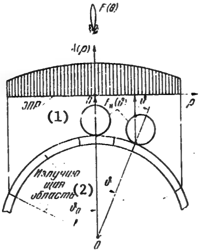

Figure 7.1. Explanation of the equivalent plane aperture technique.

Key: 1. Equivalent plane aperture;
2. Radiating surface.

The function $G(\theta_{main}, \phi_{main})$ normalized with respect to the maximum value of the gain G_0 is called the scan pattern:

$$F^2_{\text{ск}}(\theta_{\text{гл}}, \varphi_{\text{гл}}) = G(\theta_{\text{гл}}, \varphi_{\text{гл}})/G_0; \tag{7.4}$$

and the losses in the gain are defined by the expression:

$$\Delta G(\theta_{\text{гл}}, \varphi_{\text{гл}}) = 10 \lg F^2_{\text{ск}}(\theta_{\text{гл}}, \varphi_{\text{гл}}). \tag{7.5}$$

The most reasonable placement of the radiators on the surface of a phased array (in the sense of minimal area and gain losses) is achieved in the case where the geometric area of a cell $S_{\text{иг}}$ is equal to its effective area $S_{\text{и эфф}} = (\gamma^2/4\pi)D_{\text{и0}}$:

$$S_{\text{иг}} \simeq S_{\text{и эф}}, \tag{7.6}$$

where $D_{\text{и0}}$ is the maximum directional gain of an elementary radiator of the phased array. In this case:

$$G_0 = K_{\text{ип}} \eta S_{\text{г}} (4\pi/\lambda^2), \tag{7.7}$$

where $K_{\text{ип}}$ is the surface utilization coefficient of the equivalent aperture; η is the efficiency of the phased array elements; $S_{\text{г}}$ is the geometric area of the equivalent plane aperture.

7.2. A Hybrid Phased Antenna Array with a Hemispherical Scan Space. Operational Principle. Specific Structural Design Features of a Phased Array with a Dome Shaped Lens.

We shall consider one of the promising systems: a planar phased array with a hemispherical dome shaped lens (Figure 7.2) [1]. A merit of this structural design is the comparatively low cost, which exceeds the cost of the planar phased array by 1.5 to 2 times in all. During hemispherical scanning, the effective antenna area amounts to 0.3 to 0.4 times the geometric area of a planar phased array.

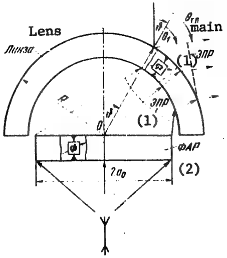

Figure 7.2. Hybrid phased antenna array with a dome shaped lens.

Key: 1. Effective plane surface;
2. Phased antenna array.

A planar phased antenna array with a circular radiating aperture scans in a sector not exceeding 50 to 60° from the normal to the antenna, irradiating a dome shaped lens with a variable index of refraction from the inside (when transmitting). The lens, usually in the form of a spherical shell (dome) of constant thickness, consists of transmissive elements, which include internal and exterior radiators and waveguides which couple them to uncontrolled phased shifters, which produce fixed phase shifts. These phase shifts are figured so that the main lobe of the directional pattern receives an additional deflection from the axis of symmetry (the normal to the planar phased array), while the scan sector is extended out to a hemisphere.

The axial symmetry of the system assures conformal scanning with respect to the coordinate ϕ (the directional pattern parameters and the gain do not depend on the direction of the main lobe, ϕ_{main}). When the radiating region moves from the "pole" of the lens ($\theta_{main} = 0$) to the "equator" ($\theta_{main} = \pi/2$), the directional pattern changes from a pencil beam to a fan-shaped one, while the gain changes, since the dimensions and shape of the radiating region change.

Basic Design Expressions. The parameters of the phased antenna array and dome-shaped lens depend on the distribution of the phase shift $\Phi(\theta)$, introduced by the lens and which causes an additional deflection of the main lobe of the directional pattern, $\Theta_{main}(\theta)$ (Figure 7.2).

In the case of a linear function:

$$\Theta_{main} = q_1\theta, \qquad \theta_{\text{гл}} = q_1\vartheta, \quad q_1 > 1. \tag{7.8}$$

The retardation factor along the surface of the lens (along the "meridian", see Figure 7.2) is:

$$\gamma = -\frac{1}{\kappa R}\,\frac{d\Phi(\vartheta)}{d\vartheta} = \sin[(q_1-1)\vartheta], \tag{7.9}$$

where R is the radius of the lens; and:

$$\Phi(\vartheta) = -\frac{2\kappa R}{q_1-1}\sin^2\frac{(q_1-1)\vartheta}{2} \tag{7.10}$$

is the phase distribution.

To reduce the lens thickness, it should have a zonal configuration, so that the following condition is met: $0 \leq \Phi(\theta) \leq 2\pi$.

The boundaries of the zones, θ_n, are determined from the condition $\Phi(\theta_n) = -2\pi n$:

$$\vartheta_n = \frac{2}{q_1-1}\arcsin\sqrt{n\frac{(q_1-1)\lambda}{2R}}\,. \tag{7.11}$$

The specified phase distribution $\Phi(\theta)$ (7.10) is assured through the appropriate design of the uncontrolled phase shifters and determines the nature of the change in the system gain when the main lobe is defracted from the axis of symmetry.

An approximate estimate of the gain of a phased antenna array with a dome-shaped lens can be made on the basis of the following considerations. Neglecting the change in the amplitude distribution introduced by the lens, we find:

$$G(\theta_{\text{гл}}) \simeq G_0 F^2_{\text{цр}}(\vartheta) F^2_{\text{нл}}(\theta_1)\,\frac{S_{\text{эпр}}}{S_0}\,, \tag{7.12}$$

$$G(\Theta_{main}) \approx G_0 F^2_{cent}(\theta) F^2_{out}(\Theta_1)\,[S_{epa}/S_0]$$

where G is the maximum gain of the phased antenna array (in the direction of the normal); $F_{cent}(\theta)$ is the directional pattern of the central radiator of the planar phased array (in the direction of the beam OA); $F_{out}(\theta)$ is the directional pattern of the outside radiator of the lens, corresponding to the beam OA, in the direction of the deflected beam of the antenna directional pattern; $\Theta_1 = (q_1 - 1)\theta$ is the deflection of the main lobe of the antenna from the central ray OA; S_{epa} is the area of the equivalent plane aperture, normal to the direction of the main maximum of the antenna directional pattern; S_0 is the area of the planar phased antenna array.

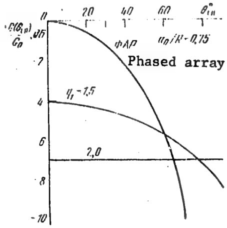

Figure 7.3
Graphs of $G(\theta_{main})/G_0$ as a function of θ_{main}.

The equivalent plane aperture of the radiating region has a circular shape when $\Theta_{main} = 0$ and the shape of an asymmetrical oval when $\Theta_{main} > 0$. The dimensions of the equivalent plane aperture can be approximately determined by solving transcendental equations, derived on the basis of geometric optics. Graphs for the function $G(\Theta_{main})/G_0$ are shown in Figure 7.3 for $F^2_{cent}(\theta_0) \approx \cos\theta_0$ and $F^2_{out}(\Theta_1) \approx \cos\Theta_1$. It can be seen from the graphs that depending on the requirements placed on the function $G(\Theta_{main})$, an optimal value of the parameter q_1 can be chosen. In the majority of cases, expedient values are $q_1 \approx 1.5 - 2.0$.

The relationships for the gain were derived with the assumption that the equivalent plane aperture is in phase. To meet this condition, the phase distribution in the aperture of the phased antenna array should be nonlinear. The wave front between the lens and the planar phased array should be convex facing the phased array.

According to existing data [1], a hybrid phased antenna array with a dome-shaped lens provides for hemispherical scanning even in large sectors. The gain reduction during scanning for $q_1 = 1.5 - 2.0$ reaches 4 to 5 dB. The level of the sidelobes does not exceed -18 to -20 dB.

The main advantage of the structural design is the cost which is lower than the cost of other phased antenna arrays with hemispherical scanning.

7.3. Conformal Phased Antenna Arrays.

Classification and Excitation Techniques. The radiators of conformal phased arrays are arranged on aplanar (usually convex, axially symmetric) surfaces. Cylindrical, conical and spherical phased arrays have become the most widespread. Conformal phased arrays provide for a hemispherical scan space with the least fluctuations in the gain and are the most expensive among systems of this class, which is due to the large number of controlled phase shifters and the complex phasing system.

Small fluctuations in the gain are achieved by scanning without changing the shape of the directional pattern by means of moving the radiating region of the array around the axis or the center of symmetry by means of electrical switching. In this case, the size, shape, and number of elements in the radiating region remain approximately the same (conformal scanning).

To realize conformal scanning, the feed distribution of the radiating elements of the phased array should be the same, regardless of the direction of the main lobe. Feeder systems (parallel or mixed) and active systems (amplifiers, generators or frequency multipliers in each element) are used to feed conformal phased arrays.

Besides switching the radiators, the phase distribution and the focusing system for the radiators in the direction of the main lobe are controlled in conformal phased arrays. The convex shape of the surface of conformal arrays leads to the necessity of producing nonlinear phase distributions. The control is accomplished, just as in planar phased arrays, by means of specialized computers or matrix configurations (Butler matrices, etc.).

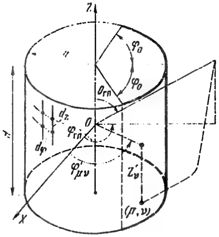

Figure 7.4. A cylindrical phased antenna array.

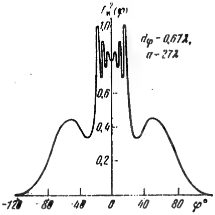

Figure 7.5. The directional pattern of a cylindrical phased antenna array radiator.

Cylindrical Phased Antenna Arrays*. Cylindrical phased arrays (Figure 7.4) do not provide for complete hemispherical scanning (they are not effective in a sector of out to 30 to 40° from the system axis) and are used in those cases where it is necessary to have circular conformal scanning with maximum gain in a plane normal to the axis of symmetry. Effective scanning of the "axial" sector can be accomplished by a planar phased array, placed on the upper base of the cylinder (this variant is not treated here).

Since a cylindrical surface unwraps into a plane, the placement of the radiators on it is the same as on planar phased arrays (a triangular or rectangular grid can be used). Conformal scanning is accomplished in a plane normal to the axis of symmetry of cylindrical phased arrays by moving the radiating region; in the plane of the generatrix of the cylinder, conventional sector scanning is employed using a linear phase distribution. Cylindrical phased arrays can produce radiation of any polarization (including linear).

The elementary radiators of cylindrical phased arrays are chosen from the usual considerations (see § 7.1). The directional patterns of the isolated radiators are close in the majority of cases in shape to a cosinusoidal form:

$$F_{и}(\theta, \varphi) \simeq \sin\theta \cos(\varphi - \varphi'_{\mu\nu}), \qquad (7.13)$$

where $\phi'_{\mu\nu}$ are the coordinates of an element with the number $\mu\nu$.

The influence of mutual coupling of the radiators via the dominant and higher modes is manifest in the greatly indented nature of the directional pattern of an element in the plane normal to the system axis (Figure 7.5), and in the sharp drop in the gain in the case where the radiating region encompasses a sector greater than $2\pi_0$, where:

$$\sin\varphi_0 \simeq \lambda/d_\varphi - 1, \qquad (7.14)$$

---

*Additional information on cylindrical phased arrays is contained in Chapter 4.

d_ϕ is the array step in a plane normal to the system axis. The drop in the gain is related to the violation of the uniqueness condition (the appearance of additional main lobes) and the mismatching of the array because of mutual coupling of the element. Since similar phenomena also occur during sector scanning in the plane of the generatrix if the scan sector $2\theta_{CK}$ does not satisfy the main lobe uniqueness condition, the steps of the array d_ϕ and d_z should satisfy the following conditions (see 2.3):

$$d_\varphi/\lambda \leqslant (1+\sin\varphi_0)^{-1}, \tag{7.15}$$

$$d_z/\lambda \leqslant (1+\sin\theta_{\text{ск}})^{-1}, \tag{7.16}$$

To focus the radiation in the direction (θ_{main}, ϕ_{main}), a phase distribution should be created in the radiating portion of the surface of the cylindrical phased array which assures that the distribution in the equivalent plane aperture is in phase; the phase of the $\mu\nu$-th radiator is:

$$\Phi_{\mu\nu} = -\kappa\,[a\sin\theta_{\text{гл}}\cos(\varphi_{\text{гл}}-\varphi'_{\mu\nu}) + Z_\nu\cos\theta_{\text{гл}}], \tag{7.17}$$

where $k = 2\pi/\lambda$; a is the radius of the cylinder; Z'_ν and $\phi'_{\mu\nu}$ are the coordinates of the $\mu\nu$ radiator of the phased antenna array.

When the main lobe uniqueness condition is met, the techniques of an equivalent plane aperture and an equivalent linear antenna can be used to calculate the directional pattern of the cylindrical phased array, while the concept of the effective length of a linear antenna can be used to calculate the width of the main lobe. The requisite level of the aperture sidelobes q can be achieved by switching off a portion of the radiators (thinning the array).

To assure minimal cost of a cylindrical phased array, the aperture angle ϕ_0 is optimized. The optimization criteria are a minimum number of controlled radiators and minimal antenna dimensions. Minimal dimensions (the antenna diameter 2a) are achieved when $\phi_0 = 60 - 90°$ (when $\phi_0 > 60°$, the requisite number of radiators practically does not change). Since an increase in ϕ_0 leads to a decrease in d_ϕ/λ (when $\phi_0 = 60$ to $90°$, $d_\phi/\lambda = 0.54 - 0.50$), something which is frequently undesirable because of structural design considerations, values of $\phi_0 = 50 - 60°$ are expedient.

The overall number of controlled radiators, in the case of dimensions of the radiating region of $H \cdot 2a\phi_0$ and a rectangular grid is:

$$N_{\square} = N_z N_\varphi, \tag{7.18}$$

and in the case of a triangular grid:

$$N_\wedge = (\sqrt{3}/2)\,N_{\square}; \tag{7.19}$$

Here, the requisite number of radiators along the generatrix is:

$$N_z = H/d_z = C_{0,5}/2\theta_{0,5z}\,(1+\sin\theta_{\text{ск}}), \tag{7.20}$$

$2\theta_{0.5Z} = C_{0.5}\lambda/H$ is the width of the main lobe in the plane of the generatrix; the requisite number of elements about the periphery of the cylinder is:

(7.21)

$2\Theta_{0.5\phi}$ is the width of the main lobe in a plane normal to the axis of the cylinder (the directional pattern of an element of the phased array is taken as cosinusoidal).

Circular conformal scanning is achieved in a cylindrical phased array while at the same time using a comparatively small fraction of the overall number of radiators (30 to 40%).

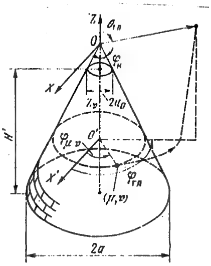

Figure 7.6. A conical phased antenna array.

Conical phased arrays (Figure 7.6) provide for a hemispherical scan (with fluctuations in the gain of several decibels). They are used in cases where it is necessary to place a hemispherical scanning phased array in a conical (or ogive) housing of an aircraft, as well as when the maximum gain should be achieved in an axial direction or a direction inclined to the axis of the cone.

Conformal scanning (movement of the radiating region) is realized in conical phased arrays in the plane of the base, as well as conventional sector scanning in the plane of the generatrix. The radiating region occupies a sector, the size of which depends on the direction of the main lobe, Θ_{main}.

In the case of hemispherical scanning, some portions of the conical surface radiate at large angles, and for this reason, it is expedient to take the step of the array close to 0.5λ (d/λ = 0.50 - 0.55), although in a number of cases, it must be increased up to 0.6λ to 0.75λ because of structural design considerations.

It is expedient to use radiators, the main directional pattern lobe of which is not directed along a normal to the generatrix of the cone, but rather in the direction of the requisite maximum gain. The influence of mutual coupling between the radiators of a conical phased array on the directional pattern of a radiator in the plane of the base is manifest, just as in cylindrical phased arrays, in an indented central portion of the directional pattern of a radiator. However, in contrast to cylindrical phased arrays, the deep nulls in the directional pattern related to the appearance of additional interference maxima, are nearly absent because of the conical shape of the surface (Figure 7.7). The width of the main lobe, $2\Theta_{0.5}$, and the gain, G_{max}, of a conical phased array are determined by the dimensions of the equivalent plane aperture of the radiating region.

$$N_\varphi = 2\pi a/d_\varphi \approx 4\pi \frac{C_{0.6}}{2\Theta_{0.5\varphi}} \frac{1+\sin\varphi_0}{\sin 2\varphi_0 + 2\varphi_0},$$

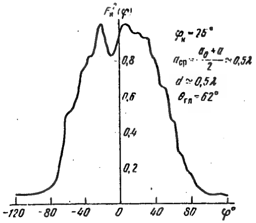

Figure 7.7. The directional pattern of a conical phased antenna array radiator.

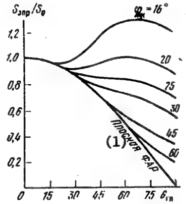

Figure 7.8. S_{epa}/S_0 as a function of Θ_{main}.

Key: 1. Planar phase antenna array.

The graphs of Figure 7.8 make it possible to estimate the change in the equivalent plane aperture area of a conical phased array, S_{epa}/S_0 ($S_0 = \pi a^2$ is the area of the base) with a change in the direction of focusing of Θ_{main} and the vertex angle of the cone ϕ_k (the angle between the axis and the generatrix). As a rule, radiators are not placed at the vertex of the cone, however, this area is small and was not taken into account in the given case. An analysis of the graphs shows that to reduce variations in the gain during scanning, it is expedient to employ conical surfaces having ϕ_k = 18 to 20°.

The impossibility of placing controlled radiators at the vertex of the cone leads to the appearance of a nonradiating region in the equivalent plane aperture. In the case of axial radiation, it has the shape of a circle with a radius of $a_0 << a$. The dimensions of the nonradiating region, when $a_0/a = 0.1 - 0.3$, have little impact on the gain, but can substantially increase the level of the aperture sidelobes q. The level of the sidelobes q as a function of the ratio a_0/a with a axial radiation for uniform ($A(r) = 1$) and optimal $A_{opt}(r)$ amplitude distributions are shown in Figure 7.9 [4].

The following phase distribution should be produced to focus the radiation in the direction Θ_{main}, ϕ_{main} on the radiating portion of a conical phased antenna array:

$$\Phi_{\mu\nu} = \kappa Z_\nu [\operatorname{tg} \varphi_к \sin \theta_{гл} \cos(\varphi_{гл} - \varphi'_{\mu\nu}) - \cos \theta_{гл}], \tag{7.22}$$

where the coordinates of the elements $Z_\nu < 0$. The requisite number of radiators is:

$$N = S_к/S_{пр}, \tag{7.23}$$

where:

$$S_к = \pi a^2 [1 - (a_0/a)^2] \operatorname{cosec} \varphi_к \tag{7.24}$$

is the area of the conical surface; and:

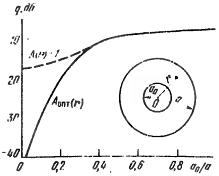

Figure 7.9. The level of sidelobes where a nonradiating region is present.

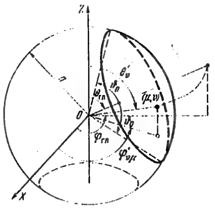

Figure 7.10. A spherical phased antenna array.

$$S_{\text{яч}} = \begin{cases} d^2 & \text{in the case of a square grid,} \\ 2d^2/\sqrt{3} & \text{in the case of a triangular grid.} \end{cases} \qquad (7.25)$$

is the geometric area of a cell; d is the step of the array.

To obtain narrow directional patterns, the overall number of controlled radiators in conical phased arrays should be of the same order of magnitude (10^4) as for cylindrical arrays. A hemispherical scan with gain variations of no more than 1 to 2 dB can be provided using a conical phased array.

Spherical phased arrays (Figure 7.10) provide for a hemispherical scan with minimal changes in the directional pattern and gain variations (0.1 to 1.0 dB). This is accomplished by arranging the radiators with a nearly uniform density over the surface of the sphere and employing conformal scanning, i.e, maintaining the shape and dimensions of the radiating region during scanning. The center of the radiating region in usually located in the direction of the main lobe (or the equal signal direction). The radiating region is moved by switching the feed for the radiators, while the phasing (identical within the limits of the radiating region for any position of the region) serves to compensate for phase errors (focusing). Disconnecting some of the radiators and controlling the shape of the radiating region make it possible to obtain directional patterns with different parameters.

The most uniform filling of a spherical surface with radiators is obtained with a triangular grid for the radiator layout.

To preclude large losses in the gain, the step of the array d/λ when generating an axially symmetric main lobe is to be chosen based on the condition (in a manner similar to a cylindrical phased array):

$$d/\lambda \leqslant (1+\sin\vartheta_0)^{-1}, \qquad (7.26)$$

where $2\theta_0$ is the central angle of the radiating segment (Figure 7.10). The type and dimensions of a radiating element are chosen based on the same considerations as for other convex phased antenna arrays. The influence of mutual coupling of the elements of a spherical phased array on the directional pattern of a radiator is less pronounced than for other types. In the case of spheres with large radii ($a/\lambda > 10$), the directional pattern of a radiator is close to the directional pattern of an element of a planar array having the same period. When condition (7.26) is met, the directional pattern of a radiator of a spherical phased antenna array is:

$$F_{и}(\theta, \varphi) \simeq \cos(\theta - \theta'_{\nu}) \cos(\varphi - \varphi'_{\mu\nu}), \qquad (7.27)$$

where θ'_{ν} and $\phi'_{\mu\nu}$ are the spherical coordinates of the $\mu\nu$-th radiator.

The radiators of a spherical phased array should have either circular or controlled polarization.

The central angle of the radiating region, θ_0, can be optimized based on the criterion of a minimum overall number of radiators to obtain the specified width of the main lobe of the directional pattern or a specified gain [5]. Calculations show that the minimum number of controlled radiators is obtained when $\theta = 50°$ to $90°$, but because of the poor radiation efficiency of elements having a directional pattern of the type of (7.27) at large angles, it is expedient in practice to use phased arrays where $\theta_0 = 45°$ to $60°$.

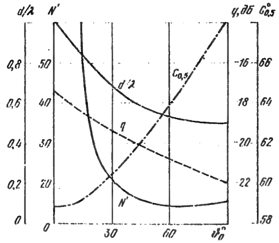

Figure 7.11. The parameters of a spherical phased array as a function of θ_0.

A surface covered with radiators should encompass the portion of the sphere bounded by the angles:

$$0 \leqslant \theta' \leqslant \pi/2 + \theta_0, \qquad (7.28)$$

where the spherical surface in the region $\theta' > \pi/2$ can be replaced by a cylindrical one because of structural design considerations (a spherocylindrical phased array). The total radiating area of the surface does not change in this case. The following phase distribution [04] is produced to focus the radiation in the direction Θ_{main}, ϕ_{main} on the radiating segment of the spherical phased array:

$$\Phi_{\mu\nu} = -ka[\cos\theta_{гл} \cos\theta'_{\nu} + \sin\theta_{гл} \sin\theta'_{\nu} \cos(\varphi_{гл} - \varphi'_{\mu\nu})]. \qquad (7.29)$$

The overall dimensions and requisite number of radiators in a spherical (or spherocylindrical) phased array are calculated using the following procedure.

1. The radius of the circular equivalent planar aperture of the radiating segment, a_{epa}, is determined:

$$2a_{эпр}/\lambda = C_{0,5}/2\theta_{0,5}, \qquad (7.30)$$

where in the case of a cosine directional pattern of a radiator (see (7.27)) and $\nu_0 = 45 - 60°$, the coefficient $C_{0.5} \approx 62 - 64°$, while the level of the aperture sidelobes is $q \approx -20$ to -21 dB (see Figure 7.11).

2. The radius of the spherical surface is determined:

$$a = a_{epa}/\sin\theta_0 \tag{7.31}$$

3. The step of the array is determined (see (7.26)); when $\nu_0 = 45 - 60°$, the step is $d/\lambda = 0.59 - 0.54$ (see Figure 7.11).

4. The requisite number of radiators N in the case of a triangular layout grid, taking formulas (7.25) and (7.28) into account, is found from the expression:

$$N = N'/(20_{0,5})^2, \tag{7.32}$$

where

$$N' = \frac{\pi}{\sqrt{3}} C_{0,5}^2 \frac{(1+\sin\vartheta_0)^3}{\sin^2\vartheta_0} \tag{7.33}$$

(see Figure 7.11). The overall number of radiators in a spherical phased array in the case of narrow directional patterns is $N \approx 10^4 - 10^5$.

7.4. Polyhedral Phased Antenna Arrays.

Classification. Excitation Techniques. Polyhedral phased antenna arrays take the form of a system of planar phased arrays (subarrays), arranged on the faces of a convex polyhedron.

Where the number of subarrays is $N_{sub} \leq 10$, they are usually arranged on the faces of a regular or truncated pyramid. Such polyhedral phased arrays are called pyramidal. In the case of a large number of subarrays, they are placed on the faces of a regular polyhedron (for example, an icosahedron) on inscribed in the sphere of a polyhedron derived from an icosahedron by the sequential fractionization of its faces. The overall number of subarrays can reach $N_{sub} \approx 10^2 - 10^3$, while the overall number of radiators runs to $N \approx 10^4 - 10^5$.

In terms of the directional pattern parameters, pyramidal phased arrays are close to planar arrays, while polyhedral phased arrays where $N_{sub} \approx 10^2$ are close to conformal phased arrays (such phased arrays can be called quasiconformal). A spatial excitation technique (in a transmissive variant) can also be used to excite the subarrays, in addition to feeder and active excitation methods.

Polyhedral phased arrays have the following advantages over planar and hybrid phased antenna arrays: the possibility of realizing hemispherical scanning with smaller fluctuations in the gain and better utilization of the surface taken up by the radiators. As compared to conformal phased arrays, they are better suited for production, something which is related to the use of not just modules of the same type, but also subarrays of the same type, as well as the utilization of a spatial feed system for the subarrays and the simplification of the phase distribution control system.

In pyramidal phased arrays, the planar subarrays are placed on the faces of regular or truncated pyramids where the number of side faces is M = 3 - 6 (Figure 7.12). Two phasing modes are possible for the subarrays: independent and combined. In the first mode, each subarray scans independently of the others in a definite spatial sector; in the second, several subarrays scan as a single system. It is expedient to employ both modes in combination.

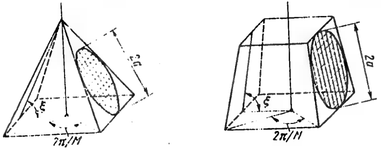

Figure 7.12. Pyramidal phased antenna arrays.

In the case of independent phasing, the design procedure for the structural and radio engineering parameters of planar subarrays does not differ from the procedure used for planar phased arrays.

The optimal slope angle for the side face of a pyramid, ξ_{opt}, can be determined by working from one of the following requirements:

1) Maximum gain in a definite direction, Θ_{max}, and in this case:

$$\xi_{opt} = \Theta_{max} \qquad (7.34)$$

$$\xi_{опт} = \theta_{max};$$

2) Minimum variations in the gain in the hemisphere, in this case:

$$\xi_{опт} = \operatorname{arctg}\left(\cos\frac{\pi}{M}\right). \qquad (7.35)$$

For a truncated pyramid (using the upper face, where a subarray can be placed):

$$\xi_{opt} = \arccos\left(\operatorname{cosec}^2\frac{\pi}{M} - \sqrt{\operatorname{cosec}^4\frac{\pi}{M} - \operatorname{cosec}^2\frac{\pi}{M} + 1}\right). \qquad (7.36)$$

The minimum gain G_{min} is obtained with maximum beam deflection from the normal to the subarray:

$$\theta_{ск} = \arccos(\sin\xi\cos\pi/M). \qquad (7.37)$$

The drop in the gain at the boundary of the scan sectors of the subarrays in the case of a cosine directional pattern of a radiator is:

$$\Delta G\,[дБ] \simeq 10\lg(\cos^2\theta_{ск}). \qquad (7.38)$$

The main lobe uniqueness condition requires limiting the step of the subarrays:

$$d/\lambda \leqslant (1 + \sin\theta_{ск})^{-1}, \qquad (7.39)$$

and therefore, the overall number of radiators in a pyramidal phased array with a circular configuration for the subarrays $N = AN'$ arranged on the faces of the pyramid, where:

$$A = \begin{cases} \frac{\pi}{4}\left(\frac{C_{0,5}}{2\theta_{0,5}}\right)^2 & \text{in the case of a square grid,} \\ \frac{\pi\sqrt{3}}{8}\left(\frac{C_{0,5}}{2\theta_{0,5}}\right)^2 & \text{in the case of a triangular grid.} \end{cases}$$

$C_{0.5}$ = 62--67 when q = -20 -- -25 dB and with a quasioptimal amplitude distribution (or the equivalent thinning of the subarrays);

$$N' = \begin{cases} M(1+\sin\theta_{\text{ск}})^2 & \text{for a pyramid,} \\ (M+1)(1+\sin\theta_{\text{ск}})^2 & \text{for a truncated pyramid.} \end{cases}$$

Comparative data are given in Table 7.1 for pyramidal phased arrays where M = 3--6. An analysis of the data of Table 7.1 shows that pyramidal systems with four sides have the best combination of parameters. In this case, a truncated pyramid (five subarrays) has the least fluctuations in the gain, while a four sided pyramid without a top face has the fewest number of radiators.

TABLE 7.1.

Параметр	Пирамида				Усеченная пирамида			
M	3	4	5	6	3	4	5	6
ξ°_{opt}	63,5	54,7	51,0	49,1	82,5	74,5	69,6	66,8
$\theta^\circ_{\text{ск}}$	63,5	54,7	51,0	49,1	60,3	47,1	40,7	37,3
$-\Delta G$, дБ	7,0	4,8	4,0	3,7	6,1	3,3	2,4	2,0
N'	10,8	13,2	15,8	18,5	14,0	15,0	16,4	18,1

The joint phasing of several adjacent subarrays of pyramidal phased arrays is expedient to reduce the drop in the gain in the region of the boundaries of adjacent sectors. Thus, for a pyramidal phased array where M = 4, the joint phasing of two subarrays in a range of ± 20 to ± 25° from the boundaries of adjacent sectors leads to a drop in the gain from 4.8 down to 1.0 to 1.5 dB. In this case, the considerable spacing between the centers of the subarrays leads to the appearance of additional diffraction lobes, having a level of -10 to -13 dB.

Pyramidal phased arrays are the simplest in terms of structural design among phased arrays with hemispherical scanning, but have considerable fluctuations in gain within the hemisphere.

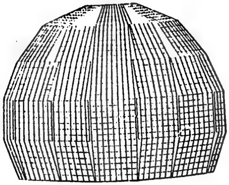

Figure 7.13. A strip structure of a polyhedral phased antenna array.

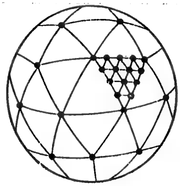

Figure 7.14. An icosahedral structure for a polyhedral phased antenna array.

It is expedient to use quasiconformal phased arrays in the form of polyhedra inscribed in a sphere, where the polyhedra have a large number of almost identical faces (20 to 400), on which identical planar subarrays are arranged, to reduce fluctuations in the gain within the scan sector. The subarrays can be realized in the form of strip (Figure 7.13) or icosahedral structures (Figure 7.14). The number of radiators in one subarray (10 to 100) is governed by the requisite overall number of radiators in the phased array, N, the minimum permissible number of subarrays, N_{sub}, and the operational convenience of the system.

When $N_{sub} \approx 10^2$, estimates of the main structural design and radio engineering parameters of a quasiconformal polyhedral phased array can be derived just as for a spherical phased array (see § 3.4). However, breaking the radiating system down into subarrays and the polyhedral shape of the radiating surface cause a certain change in the parameters, primarily in the gain and the directional pattern.

We shall use the number of subarrays N_0 arranged about the periphery of a great circle of the sphere as an independent parameter. When $N_0 > 10$, the overall number of subarrays N_{sub}, placed on the faces of a polyhedron inscribed in a spherical segment, bounded by the angles $0 \leq \theta' \leq \pi/2 + \theta_0$, can be approximated by the expression:

$$N_{\text{пр}} \simeq (1 + \sin(\vartheta_0)\, n_0^2/2\pi. \qquad (7.41)$$

The overall number of subarrays in the case of strip and icosahedral structures of a polyhedron is shown in the graphs of Figure 7.15.

Since when $n_0 > 10$, the faces cannot be the same, while it is expedient to standardize the form and dimensions of the subarrays, the entire area of the faces cannot be utilized. The losses in area lead to gain losses of:

$$\Delta G_S\ [\text{dB}] = 10 \log (N_C S_c/S_{sph}) \qquad \Delta G_S\,[\text{дБ}] = 10\,\lg (N_c S_c/S_{\text{сф}}), \qquad (7.42)$$

where S_c is the area of one subarray; S_{sph} is the truncated area of the sphere, circumscribed around the polyhedron.

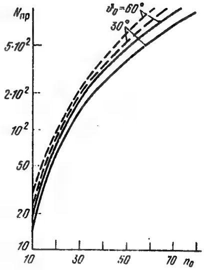

Figure 7.15. N_c as a function of n_0 (the solid curves are for an icosahedral structure; the dashed curves are for a strip structure).

The gain losses ΔG_{loss} for strip and icosahedral structures of a polyhedral phased array fall off with an increase in n_0; when $n_0 = 10$--10^2, $\Delta G_S = -1.5$ to -0.5 dB.

The control of the phase distribution and the motion of the radiating region in quasiconformal polyhedral phased arrays have some special features.

1. The steering of the radiating region is accomplished by turning not individual radiators on and off, but rather entire subarrays; since 10 to 100 subarrays are incorporated in the radiating region (sometimes less than 10), this causes jumps in the gain, which fall off with an increase in n_0; when $n_0 = 10$--10^2 and $\theta_0 = 45$--$60°$, the jumps in the gain when switching the subarrays amount to from 2 to 0.1 dB; when $n_0 > 30$, they do not exceed 0.5 dB.

2. Multistage phase control is usually employed in polyhedral phased arrays: a special computer specifies the phase distribution relative to the centers of the subarrays included in the radiating region (see (7.29)); each planar subarray is focused by conventional means in the common direction (θ_{main}, ϕ_{main}).

The calculation of the directional pattern, the gain and the overall structural design parameters can be carried out just as in the case of spherical phased arrays, while the design calculations for each subarray (structure, excitation, matching, phasing) can be performed in accordance with the procedure used for planar phased arrays.

8. BEAM STEERING SYSTEMS FOR PHASED ANTENNA ARRAYS

8.1. Phased Antenna Array Control Problems.

Various electronically controlled radiofrequency devices are used for control of the phase distribution of phased antenna array: phase shifters, switchers, splitters and attenuators. Phase shifters are used in modern phased arrays in which the phase shift can be varied discretely: in quantum steps, where the number of quanta is equal to 2^v, $v = 3, 4, 5$, while the quantum step is $\Delta = 360° \cdot 2^{-v}$, i.e., 45°, 22°30', 11°15' respectively.

The phase shifting elements in phase shifters can be ferrites and semiconductor devices, in particular, PIN diodes. The structural design of the phase shifters also differs correspondingly. The operation of phase shifting elements is assured by actuating amplifiers, which are an integral part of the phase shifters. The control signal is fed to the input of the actuating amplifiers from the phase shifter control unit.

Phase shifters also have such a configuration of the phase shifting elements that the number of its inputs is equal to the digit capacity (ν) of the phase shifter. A binary quantized signal is fed to each input. Consequently, a ν-place parallel binary code is fed to the phase shifter.

High frequency switchers provide for the connection of the input RF channel to one of the two output channels in accordance with the binary control signal which is fed in. Consequently, the signal controlling the switcher is a single place binary code.

Attenuators are RF devices, the gain or the attenuation of which depends on the control signal level. This control signal can be either continuous (analog) or quantized.

The problems of beam steering in phased antenna arrays can be treated the most completely using the example of a circular scan receiving phased array, for which a generalized structural configuration of the control system is shown in Figure 8.1. To provide electronic scanning in a wide scan sector (for example, in the hemisphere above a ground surface), it is necessary to employ phased arrays with a convex structure, for example, a spherical configuration.

The receiving elements and phase shifters are combined in subarrays, most frequently planar arrays. The number of phased array elements can run up to 10^5 and more and the number of subarrays can reach several hundreds. The combining of the components in subarrays is necessary to reduce the number of input channels of the switcher and simplify its design. Moreover, the packing of the spherical surface with planar subarrays makes it possible to use the very simplest row and column algorithms and control devices.

Only the working region of a phased array surface participates in generating a directional pattern in a specified direction. The smaller the number of subarrays incorporated in the working region, the fewer the possibilities for adaptation: spatial filtering of interference. The greater the number of subarrays incorporated in the working region, the more complicated the switcher is. Taking these contradictory requirements into account, the number of subarrays in the working region can fluctuate in a wide range (5 to 50).

The number of possible working zones is limited to several tens (depending on the structural design of the phased array). Each working zone provides for scanning in a definite sector of space, usually not exceeding ± 15 to ± 30° from the center direction.

The switcher serves to connect the subarrays participating in the formation of the working zone to the subsequent processing channels. The number of RF inputs to the switcher is equal to the total number of subarrays on the surface of the phased antenna array, while the number of outputs is equal to the number of subarrays included in the working zone. The switcher consists of a set of RF switches, connected in accordance with a truth table and controlled by signals generated in the switcher control unit (BUK).

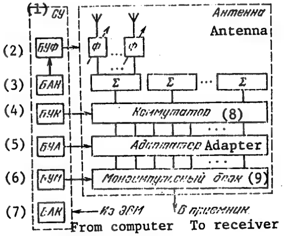

Figure 8.1. Structural configuration of a receiving phased antenna array.

Key:
1. Beam steering system;
2. Phase shifter controller;
3. Automatic tuning unit;
4. Switcher control unit;
5. Adaptation control unit;
6. Monopulse signal processing controller;
7. Automatic monitor;
8. Switcher;
9. Monopulse unit.

The phasing direction code (direction cosines of the main lobe of the directional pattern) is fed to the input of the phase shifter controller (BUF) from the central computer. The codes which are fed to the phase shifters are generated in accordance with this code. For this reason, it is most expedient to design the phase shifter controllers in the form of a special digital computer. The phase shifter controller is the most complex and most important assembly of the beam steering system (SU) and will be treated in more detail in subsequent sections.

Modern circular scan phased arrays take the form of extremely large and complex structures. These structures undergo deformations, both elastic and irreversible when exposed to external factors (temperature changes, wind, rain, snow, etc.). As a result, the position of the direction of the main lobe of the directional pattern in space changes. If the errors caused by these deformations exceed the specified aiming precision, it becomes necessary to have tuning and automatic fine tuning. Information on the phased array geometry, external factors, true coordinates of the targets or aiming points, based on which the tuning is accomplished, is fed to the input of the automatic tuning unit (BAN). The correction signals generated by the automatic tuning unit are fed to the phase shifter controller, eliminating or reducing the phase distribution errors.

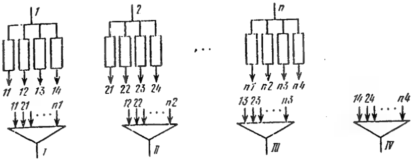

Figure 8.2. The principle of monopulse signal processing.

Modern radar is unthinkable without interference filtering (natural and artificial). Spatial filtration is also used along with frequency and time filtration. Any directional antenna realizes spatial filtration. However, even with spatial filtering of interference from different directions, falling on the sidelobes of the directional pattern, reception is disrupted if the interference power is much greater than the power of the useful received signal.

Adaptation systems have been developed to attenuate the impact of interference in modern phased arrays. The amplitude-phase distribution on the surface of a phased array is changed in such a manner as a consequence of adaptation that reception is substantially attenuated from interference source directions, retaining in this case a sufficient level of the useful received signal in the direction of the main lobe of the directional pattern. As a result of adaptation, "nulls" or "dips" are formed in the directional pattern in the directions of the interference.

Adaptation is all the more effective, the more the parameters of the amplitude-phase distribution change and the greater the number of channels in the adaptation system. Usually, the gains and phase shift (amplitude-phase adaptation) or only the phase shift (phase adaptation) change in each channel during adaptation. In the case of amplitude-phase adaptation, each channel is split into two quadrature channels (with a phase shift of $\pi/2$), and a controlled attenuator with a gain which varies from -1 to +1 is inserted in each subchannel. Thus, the amplitude can be varied from 0 to $\sqrt{2}$ and the phase varied from 0 to 2π. In the case of phase adaptation, a controlled phase shifter is used in each channel.

The adaptation controller (BUA) generates control signals for the attenuators and phase shifters. The algorithms in accordance with which these control signals are generated depend on the presence and completeness of the data on the interference sources, as well as on the choice of the adaptation quality indicator.

In the case of a multichannel antenna and monopulse signal processing, it becomes possible to simultaneously generate four directional patterns, which are shifted in pairs by approximately half of the 0.5 power level directional pattern width. For this, four splitting phase shifters each are installed in each channel, as shown in Figure 8.2. The phase shifts in these phase shifters must be changed when the direction of phasing changes within one working zone and when changing the working zones. Consequently, the splitting phase shifters are controllable, and a monopulse signal processing control unit (BUM) is provided to control them.

An automatic monitor unit (BAK) for both the operability of the control system itself and the antenna complex as a whole is included in the phased array control system in addition to the units enumerated above (phase shifter controller, automatic tuning unit, switcher control unit, adaptation controller and monopulse signal processing controller). It should be noted that the monitoring of the operational status of the phased array requires a clear cut definition of entire antenna failure. Experiments show that the failure of up to 10% of all of the elements does not lead to the failure of the entire antenna. In this case, the shape of the directional pattern changes somewhat, but the antenna remains operable.

The structural configuration of a phased array described here, of course, is not the only one. The control system is somewhat simpler in transmitting phase arrays: there is no adaptation control unit, no monopulse processing, there can be many fewer modules and the switcher can be altogether absent or substantially simplified. The control system for a phased array with a small scan sector is simplified a great deal, when one can use an antenna with a planar configuration.

8.2. Control Algorithms for Phase Shifters.

The major task of controlling phase shifters is the generation of a plane phase front, perpendicular to the specified phasing direction.

The phasing direction is a unit vector r_m, having coordinates of ξ_{xm}, ξ_{ym} and ξ_{zm}, which are direction cosines. The phasing direction can also be specified by two angles Θ and ϕ, however, the algorithms for computing the control codes prove to be considerably more complicated in this case.

We shall consider the i-th radiating element with phase center coordinates of $R_i(x_i, y_i, z_i)$. In order to produce a plane wave front, perpendicular to r_m and passing through the origin, it is necessary to compensate for the spatial phase change at a distance of d_i with the phase shifter (Figure 8.3). This distance is determined by the scalar product:

$$d_i = (\mathrm{R}_i \mathrm{r}_m) = x_i \xi_{xm} + y_i \xi_{ym} + z_i \xi_{zm}. \tag{8.1}$$

For a specified wavelength λ, at this distance the phase change (in radians) is defined as follows:

$$\Phi_{\Sigma i} = \frac{2\pi}{\lambda} d_i = \frac{2\pi}{\lambda} (x_i \xi_{xm} + y_i \xi_{ym} + z_i \xi_{zm}). \tag{8.2}$$

The phase change can contain a definite number of whole periods and an additional phase shift Φ_i:

$$\Phi_{\Sigma i} = 2\pi\kappa + \Phi_i, \tag{8.3}$$

where k is an integer.

Since a phase shift of 2πk does not have any influence when combining harmonics, the phase shifter should compensate for the phase shift of Φ_i, determined from (8.2):

$$\Phi_i = 2\pi\left\{\frac{x_i}{\lambda}\xi_{xm} + \frac{y_i}{\lambda}\xi_{ym} + \frac{z_i}{\lambda}\xi_{zm}\right\}_{\text{др}}, \tag{8.4}$$

where $\{\cdot\}_{\text{др}}$ is the operation of isolating the fractional part of the number.

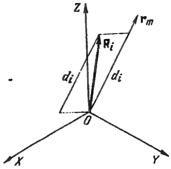

Figure 8.3. On the determination of the spatial phase change.

As has already been noted, phase shifters with a quantum step of $\Delta + 2\pi \cdot 2^{-\nu}$ rad are used at the present time for controlling the beam of phased arrays. The value of the quantized phase shift is found by quantizing Φ_i, i.e., by performing a nonlinear transformation, defined by the graphs shown in Figure 8.4 for ν = 2. In these graphs, the phase shifts are plotted on the ordinate, where these shifts can be produced by the phase shifter, while the continuous value of Φ_i is plotted along the abscissa. The quantization operation is essentially one of rounding-off: in Figure 8.4a, in the direction of the least, and in Figure 8.4b, in the direction of the nearest permitted (quantized) value. A definite binary ν-digit code, n_i, corresponds to each permitted value of the phase shift. It is convenient, and so it is usually done, for this code to numerically determine the number of quanta included in $\Phi_{i\ \text{qu}}$ or to determine a quantity proportional to this number.

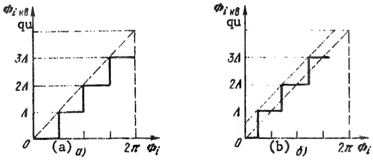

Figure 8.4. Rounding off to the least (a) and to the nearest (b) value.

To determine the control code when rounding-off in the direction of the least value of n_i, the phase shift Φ_i is not to be expressed in radians, but rather in quanta by working from the fact that 2π radians correspond to 2^ν quanta, and after this, the lower order digits following the decimal point are rejected, i.e., the integer part of the following number is singled out:

$$n_i = \left\{\frac{\Phi_i}{2\pi}\cdot 2^\nu\right\} = \left\{2^\nu\left\{\frac{x_i}{\lambda}\xi_{xm} + \frac{y_i}{\lambda}\xi_{ym} + \frac{z_i}{\lambda}\xi_{zm}\right\}_{\text{др}}\right\}_{\text{ц}}, \tag{8.5}$$

where $\{\cdot\}_{\text{ц}}$ is the isolation of the integer portion of the number.

If all of the numbers included in (8.5) are expressed in binary notation, then multiplying by 2^v is simply shifting the number over by v places. This operation can be performed by a separation method, not feeding the integer part of $2^v\Phi_i/2\pi$ to the control inputs of the phase shifter, but rather the v high order digits of the number $\Phi_i/2\pi$. Then the algorithm for computing the code for the i-th phase shifter can be written in the following manner:

$$n_i = s_i - [s_i]_1 -]\, s_i\, [_{v+1}, \tag{8.6}$$

where:

$$s_i = x_i\,\xi_{xm} + y_i\,\xi_{ym} + z_i\,\xi_{zm}; \tag{8.7}$$

$x_i = x_i/\lambda$; $y_i = y_i/\lambda$; and $z_i = z_i/\lambda$ are the coordinates expressed in wavelengths; $[\cdot]$ are the digits to the left of the decimal point, beginning with the first; $]\cdot[_{v+1}$ are the digits to the right of the decimal point, starting with v + 1.

Thus, to calculate the control code for a v-place capacity phase shifter, it is necessary to perform three multiplication and two addition (8.7) operations, after which the ν digits to the right of the decimal point are isolated. Element coordinates are stored in a read only memory; the codes for the direction cosines are fed to the input of the beam control system.

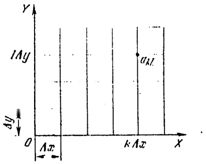

Figure 8.5. A planar orthogonal phased antenna array.

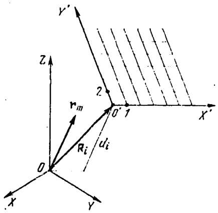

Figure 8.6. On the beam steering of a modular phased array.

When rounding off to the nearest side, as can be seen from Figure 8.4b, prior to rounding off it is necessary to add $2^{-(v+1)}$ to the number s_i, which corresponds to adding half of a quantum step to Φ_i. Adding $2^{-(v+1)}$ corresponds to feeding a carry to the (v + 1)th digit following the decimal point after finishing the computation of the unit place.

The algorithm (8.6), (8.7) provides for calculating the code for any phase shifter and is therefore applicable to any phased array design, however, its realization requires either that an individual computer (and then the speed of the control system will be a maximum) be installed at each phase shifter, or that the phase codes be computed sequentially for a group of phase shifters.

In the latter case, it is necessary to provide a switcher which connects the computer sequentially to the requisite elements. The control circuitry can be simplified in the special of a planar phased array with an equally spaced configuration of the elements.

As can be seen from Figure 8.5, each element has its own column and row number, a_{kl}. The coordinates of an element are $x_{kl} = k\Delta x$, $y_{kl} = l\Delta y$ and $z_{kl} = 0$. Consequently, algorithm (8.7) reduces to the form:

$$s_{kl} = k\Delta x\xi_{xm} + l\Delta y\xi_{ym} = k\varepsilon_x + l\varepsilon_y. \qquad (8.8)$$

This is the so-called row and column control algorithm. It is necessary to compute the phase changes for the array step along the x and y axes to realize this algorithm: $\varepsilon_x = \Delta x\xi_{xm}$ and $\varepsilon_y = \Delta y\xi_{ym}$, after which, by using expression (8.8), the total phase shift s_{kl} is computed, and finally, the quantization is performed in accordance with (8.6).

The calculation of $k\varepsilon_x$ and $l\varepsilon_y$ can be simplified if one considers that k and l are integers. Thus, if k, l = 2, 4, 8, 16, etc., then multiplication is accomplished by simply shifting by one, two and three places respectively. Multiplication by 3, 5, 6, ... reduces to the addition of the two numbers already obtained for the corresponding cells (2 + 1 = 3, 4 + 1 = 5, 4 + 2 = 6, etc.). In a similar manner, multiplication by other integers can also be realized, for example, 7 = 6 + 1 = 4 + 2 + 1, 11 = 8 + 2 + 1.

If the working zone of an antenna consists of several planar modules, then the phasing is accomplished in a single system of coordinates. In this case, the reference phase s_{00} is calculated for each module, which is determined by the spatial phase change of the i-th module (d_i) relative to the phase at the origin of the central system of coordinates XYZ, as shown in Figure 8.6. The phase change in accordance with an expression similar to (8.8), but which takes into account the position and orientation of the module, is added to this reference phase.

Thus:

$$s_{kl} = s_{00} + k\varepsilon_{x'} + l\varepsilon_{y'}. \qquad (8.9)$$

The further generation of the control code is carried out in accordance with (8.6).

To calculate the phase changes for the array step $\varepsilon_{x'}$ and $\varepsilon_{y'}$, it is necessary to determine the spatial phase changes in a single system of coordinates for two points on the X' axis and two points on the Y' axis (for example, for the points 0, 1 and 2 in Figure 8.6), and then to determine the difference in the phase changes:

$$\begin{gathered}\varepsilon_{x'} = s_{10} - s_{00} = x_{10}\xi_{xm} + y\xi_{ym} + z_{10}\xi_{zm} - (x_{00}\xi_{xm} + y_{00}\xi_{ym} + z\xi_{zm}) = \\ = \Delta x'\xi_{xm} + \Delta y'\xi_{ym} + \Delta z'\xi_{zm}, \\ \varepsilon_{y'} = \Delta x''\xi_{xm} + \Delta y''\xi_{ym} + \Delta z''\xi_{zm}, \\ \begin{array}{ll} \Delta x' = x_{10} - x_{00}, & \Delta x'' = x_{01} - x_{00}, \\ \Delta y' = y_{10} - y_{00}, & \Delta y' = y_{01} - y_{00}, \\ \Delta z' = z_{10} - z_{00} & \Delta z'' = z_{01} - z_{00}; \end{array}\end{gathered} \qquad (8.10)$$

x_{00}, y_{00} and z_{00} are the coordinates of the point O'; x_{10}, y_{10} and z_{10} are the coordinates of point 1; x_{01}, y_{01} and z_{01} are the coordinates of point 2 in Figure 8.6:

$$s_{00} = x_{00}\xi_{ym} + z_{00}\xi_{zm}. \tag{8.11}$$

Row and column algorithms are applicable in the case of equally spaced modules in a planar phased array. However, to reduce the directional pattern sidelobes, it is expedient to introduced random components into the configuration of the modules. In this case, the application of row and column algorithms proves to be impossible in the general case. A quasirandom arrangement of the modules at the nodes of a rather thick equally spaced array is sometimes used, the majority of the nodes of which remain unfilled. Individual control with the calculation of the code independently for each cell remains a universal approach.

8.3. Algorithms for Generating Directional Patterns of Special Shapes.

When generating a directional pattern of a special shape (cosiecant, beavertail pattern, etc.), the wave front in the direction of the radiation differs from a plane front. A small deviation from a plane front is achieved by changing the geometry of conventional parabolic antennas, for example, using special cosecant hoods.

The requisite deviations from a plane front can be realized in phased arrays by feeding the appropriate control codes to the phase shifters. This makes it possible to change the shape of the directional pattern during operation by electronic means.

The shape of the directional is specified relative to the direction of radiation by a functional relationship in the vertical and horizontal planes. For this reason, the deviation in the phase distribution is specified relative to a plane front, perpendicular to the phasing direction in the x', y' coordinates. The OY' and OZ' coordinate axes and the phasing direction vector, r_m, fall in one plane, and the OX' axis os perpendicular to OY' (Figure 8.7).

It can be shown that the unit vectors of the new system of system of coordinates (i, j, k) are expressed in terms of the unit vectors of the main system of coordinates and the phasing vector r_m:

$$\begin{gathered}
\mathbf{k}' = \mathbf{r}_m = \mathbf{i}\xi_{xm} + \mathbf{j}\xi_{ym} + \mathbf{k}\xi_{zm},\\
\mathbf{i}' = \frac{\mathbf{k}\mathbf{k}'}{|[\mathbf{k}\mathbf{k}']|} = \frac{\begin{vmatrix} \mathbf{i} & \mathbf{j} & \mathbf{k} \\ 1 & 0 & 0 \\ \xi_{xm} & \xi_{ym} & \xi_{zm} \end{vmatrix}}{|[\mathbf{k}\mathbf{k}']|} = \frac{-\mathbf{i}\xi_{ym} + \mathbf{j}\xi_{xm}}{\sqrt{\xi_{xm}^2 + \xi_{ym}^2}},\\
\mathbf{j}' = [\mathbf{k}\mathbf{k}'] = \frac{-\mathbf{i}\xi_{xm}\xi_{zm} - \mathbf{j}\xi_{ym}\xi_{zm} + \mathbf{k}(\xi_{xm}^2 + \xi_{ym}^2)}{\sqrt{\xi_{xm}^2 + \xi_{ym}^2}},
\end{gathered} \tag{8.12}$$

where [A B] is the vector product of the vectors A and B.

$$x' = (\mathbf{R}\mathbf{i}) = \frac{-x\xi_{ym} + y\xi_{xm}}{\sqrt{\xi_{xm}^2 + \xi_{ym}^2}},$$

$$y' = (\mathbf{R}\mathbf{j}') = \frac{-x\xi_{xm}\xi_{zm} - y\xi_{zm} + z(\xi_{xm}^2 - \xi_{ym}^2)}{\sqrt{\xi_{xm}^2 + \xi_{ym}^2}}. \qquad (8.13)$$

The additional phase shift, which changes the direction of the directional pattern beam, is given in general form by the function:

$$\Phi_{add} = \Phi_{add}(x', y') = \qquad \Phi_{доп} = \Phi_{доп}(x', y'). \qquad (8.14)$$

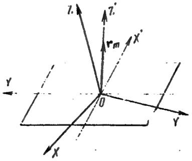

Figure 8.7. Rotation of the system of coordinates.

Consequently, the phase shift calculation algorithm for the i-th cell consists of the following operation: 1) The calculation of the phase shift to produce a plane front in accordance with (8.7); 2) The determination of the new coordinates of the cell in accordance with (8.13); 3) The calculation of the additional phase shift for the i-th cell in accordance with (8.14); 4) The determination of the overall phase shift for the i-th cell:

$$s_i' = s_i + \Phi_{i\,доп}; \qquad (8.15)$$

and 5) The determination of the code generated for the control of the i-th phase shifter, in accordance with (8.6).

The algorith for generating directional patterns of a special shape includes extremely complex expressions for coordinate transformation (8.13), functional transformation (8.14), supplemental addition (8.15), and moreover, there remain all of the procedures for calculating the plane front (8.6) and (8.7).

Different ways of simplifying the computational algorithm are possible by means of approximating the requisite phase distribution. Thus, with a modular configuration of a phased array, one can calculate the supplemental phase angles only for the reference phase of the modules, defined by relationship (8.11). In this case, the phase distribution in the antenna aperture is of a piecewise plane-parallel nature: each module produces a plane front, perpendicular to the direction of radiation, while there are phase jumps between these plane sections, which also produce the total approximation of the phase distribution.

The phase distributions can be more precisely approximated by the plane sections if these sections are not made mutually parallel, but tangential to the requisite phase distribution. In this case, it is necessary to calculate the column for each module using the complex algorithm of (8.13).

8.4. Switcher Control Algorithms

A switcher serves to generate the working area from the set of subarrays. The output channels of the switcher are connected to the subarrays of the working zone in a strictly defined order, for example, the first channel to the center subarray, the second to the next one up, etc. A possible variant for the generation of the working area from seven subarrays is shown in Figure 8.8. When the phasing direction is changed and the working area is changed, the same subarray can appear in a different place in the working zone. Thus, when producing the working area, which is shown with the dashed line, the subarray which was designated with the number *1*, is now designated number 7. This same subarray can appear in any other location in the working zone. Consequently, the switcher should provide for the capability of connecting each antenna subarray to any output of the switcher.

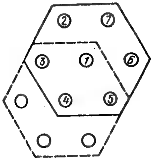

Figure 8.8. Shifting the working zone.

If the number of input channels (number of antenna subarrays) is N, while the number of subarrays including the working zone M, then the number of switches is:

$$S_n = M \log_2 N \qquad (8.16)$$

A single digit control code (0 or 1) is fed to each switch. Consequently, the control unit for the switcher has S_n outputs. The direction code (of the direction cosines of the vector r_m) is fed to the input of this device. The operational algorithm for the control device for the switcher is broken down into two parts: the determination of the number of the working area which will generate the directional pattern in the requisite direction, and the generation of the control signals for the switches of the switcher. The first task is handled by a decoder and the second by an encoder.

Each working zone provides for scanning space in a rather narrow sector of ±15 to ±20° relative to the central direction of the given working zone. When the target leaves this sector, the next working zone is switched on. For this reason, the task of selecting the working zone consists in determining whether the specified direction belongs to the scan sector of a working zone. This task is simplest to solve by determing the angle between the central direction of the working zone and the specified phasing direction.

That working zone is selected for which this angle is the least. To curtail the calculations, one can determine the cosine of this angle and select that working

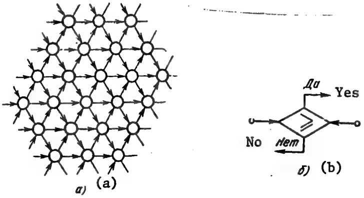

Figure 8.9. Priority coupling configuration.

zone for which this cosine is the greatest. The calculation of the cosine of an angle is the determination of the scalar product of two unit vectors:

$$\cos v=(r_m r_ц)=\xi_{xm}\xi_{xц}+\xi_{ym}\xi_{yц}+\xi_{zm}\xi_{zц}, \qquad (8.17)$$

where ν is the angle between the phasing direction and the central direction of the working zone; $r(\xi_x, \xi_y, \xi_z)$ is the unit vector of the center direction of the working zone.

The coordinates of the working zone center in spherical antennas are proportional to the direction cosines of the center direction of the working zone:

$$R_ц(x_ц, y_ц, z_ц)=Rr_ц(\xi_{xц}, \xi_{yц}, \xi_{zц}). \qquad (8.18)$$

For this reason, (8.17) may not be computed, but the quantites s_i determined by (8.7) compared in calculating the reference phase of a module.

The algorthims for selecting the greatest from a set of values can differ. The simplest is a sequential elimination of the least values, however, it requires the performance of hundreds (based on the number of working areas) of sequential comparisons, and for this reason, it is the worst in terms of operational speed. Since the function (8.17) is monotonic with respect to v, there is no need to compare the value of this function for a given working zone with the values for all other zones; it is sufficient to compare it with the nearest zones on the surface of the phased array. That working zone is selected for which the value of cos v is the greatest as compared to the nearest one, but not with all of them.

It can be seen from Figure 8.8 that the nearest working zones can number no more than six. Consequently, the choice of the working zone is made by an AND gate with six inputs. When the value of cos(v) is equal for two or even three working zones, it is necessary to give priority to a particular circuit. A schematic showing priority based on a given direction (axial priority) is shown as an example in Figure 8.9. Each arrow in this figure is a priority comparison gate, the operational principle of which is shown in Figure 8.9b. When cos(v) is equal for the right and left working zones, a "1" will be fed to AND gate of the right side working zone; this zone enjoys the priority in this case.

Thus, the switcher control unit consists of two units: a decoder and an encoder. The phasing direction code is fed to the decoder input. A "1" signal appears at one of the $N_{w.z.}$ outputs of the decoder, which corresponds to the selected working zone, while a "zero" appears at the remaining ones ($N_{w.z.}$ is the number of working zones, which can be less than the number of subarrays, since not every subarray can be the center of a working zone.

The encoder has $N_{w.z.}$ inputs and S_n outputs (S_n is the number of binary switches in the RF switcher). When a "1" is fed to one of the encoder inputs, a S-digit code is produced at its output, which provides for the connection of the requisite subarrays into a working zone in accordance with the truth table.

For convex phased arrays, the truth table is drawn up manually. This is explained by the fact that convex surfaces (sphere, ellipsoid of rotation, etc.) cannot be packed regularly with a rather large number of points. It is known from geometry that no more than 12 points (an icosahedron) can be regularly arranged [equidistantly spaced] on a complete sphere. For this reason, when packing a sphere with a large number of subarrays, it is impossible to provide for an identical configuration of the working zones and to define a single phasing algorithm. This leads to the necessity of composing the truth table for the switcher manually.

The circuit configuration for encoders are determined by the component base and are described in the considerable literature on digital device design.

8.5. Adaptation Control Algorithms

Phased array adaptation is the generation of such a directional pattern that an improvement is assured in the quality indicators for antenna functioning. Optimal adaptation provides for the extremum of the generalized quality indicator.

Adaptation of receiving phased arrays is accomplished for the spatial filtering of interference, i.e., to suppress the gain in the directions of incoming interference while retaining adequate gain in the requisite direction. In this case, the quality indicator is either the signal power to noise power ratio at the output of the phased array, or the mean square error between the requisite and actual output signals. Adaptation is realized by changing the complex frequency response in the channels of the modules included in the working zone. Each channel is split into two: a phase shift of π/2 is realized in one of the subchannels; an electronically controlled amplifier or attenuator is inserted in each subchannel. The signals in all the channels are then added. Thus, the output signal:

$$y = \sum_i x_i w_i = X^{\tau} W = W^{\tau} X,$$

where $X = [x_i]$ is the column vector of the signals; $W = [w_i]$ is the column vector of the weighting coefficients; W^T and X^T are transposed vectors.

If the requisite signal is y_0, then the mean square error is defined by the expression:

$$\overline{e^2(t)} = \overline{(y-y_0)^2} = \overline{y^2} - 2\overline{yy_0} + \overline{y_0^2} = W^T\overline{XX^T} - 2W^T\overline{Xy_0} + \overline{y_0^2}, \tag{8.19}$$

where $\overline{(\cdot)}$ is averaging with respect to time. The product $\overline{XX^T}$ is the square matrix for the interchannel cross-correlation coefficients $R_{xx} = [x_i x_k]$, while $\overline{X}_{y_0} = X_{xy_0}$ is the correlation vector between the input signals and the requisite output signal. Taking this into account, expression (8.19) can be written as follows:

$$\overline{e^2(t)} = \sigma^2 = W^T R_{xx} W - 2W^T S_{xy_0} + \overline{y_0^2}. \tag{8.20}$$

The optimal value of the vector for the coefficients W^* correspond to the minimal mean square error $e^2(t)_{min}$. Any variation μU

$$W = W^* + \mu U \tag{8.21}$$

for an arbitrary vector U and a small coefficient of variation increases the mean square error. By substituting (8.21) in (8.20), we obtain the function $\sigma^2(\mu)$. This function is minimal when $\mu = 0$. Consequently, the following equation is observed (the extremum condition):

$$\left.\frac{\partial\delta^2(\mu)}{\partial\mu}\right|_{\mu=0} = 0. \tag{8.22}$$

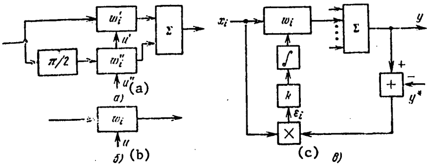

Figure 8.10. Multichannel adaptation.

By substituting (8.21) in (8.20), (8.22) can be written in the following form:

$$\left.\frac{\partial\sigma^2(\mu)}{\partial\mu}\right|_{\mu=0} = 2U^T(R_{xx}W^* - S_{xy_0}) = 0. \tag{8.23}$$

Since U is an arbitrary vector, then (8.23) can be satisfied only when the expression in parentheses is equal to zero, i.e., when $R_{xx}W^* = S_{xy_0}$. The vector of the optimal coefficient is also determined from this equation:

$$W^* = R_{xx}^{-1} S_{xy_0} = R_{xx}^{-1} \overline{X y_0}. \tag{8.24}$$

This is the equation for optimal Wiener multichannel filtration.

We determine the requisite output signal by the transform W_0 on the useful output signal X_0, so that:

$$y_0 = X_0^T W_0 = W_0^T X_0. \tag{8.25}$$

By virtue of this, expression (8.24) is reduced to the form:

$$W^* = R_{xx}^{-1} \overline{X (X_0^T W_0)} = R_{xx}^{-1} R_{xx_0} W_0. \tag{8.26}$$

In particular, if the input signal contains the expected signal X_0 and interference X_Π, then:

$$W^* = (R_{X_0 X_0} + R_{X_0 X_\Pi} + R_{X_\Pi X_0} + R_{X_\Pi X_\Pi})^{-1} (R_{X_0 X_0} + R_{X_0 X_\Pi}) W_0. \tag{8.27}$$

When the signal X_0 and the interference X_Π are independent:

$$W^* = (R_{X_0 X_0} + R_{X_\Pi X_\Pi})^{-1} R_{X_0 X_0} W_0. \tag{8.28}$$

It is completely obvious in the absence of interference:

$$W^* = R_{X_0 X_0}^{-1} R_{X_0 X_0} W_0 = W_0 \tag{8.29}$$

and those coefficients W_0 are established in system for which $y = y_0$ and there is no error.

One of the most widespread adaptation control circuit configurations is shown in Figure 8.10, where the control circuitry for a module and for the argument of the complex frequency response w_i is shown (Figure 8.10a), as well as its schematic representation (Figure 8.10b). In the case of a linear control characteristic for the weighting coefficients:

$$w_i = au_i \tag{8.30}$$

The behavior of the system depicted in Figure 8.10c is described by the expressions:

$$\frac{du_i}{dt} = ke_i, \quad e_i = ex_i; \; e = y - y_0; \; y = \sum_m w_m x_m. \tag{8.31}$$

Eliminating all of the intermediate variables from these expressions and taking into account the averaging narrow band response of the control system, we obtain the system of equations:

$$\frac{dw_m}{dt} = -ak\left(\sum_l \overline{x_l x_m} w_l - \overline{y_0 x_m}\right), \; m=1, 2, \ldots, M. \tag{8.32}$$

We write this equation as follows in vector form:

$$\frac{d\mathbf{W}}{dt} = -ak(\mathbf{R}_{XX}\mathbf{W} - \mathbf{S}_{Xy_0}) = -ak(\mathbf{R}_{XX}\mathbf{W} - \mathbf{X}y_0). \tag{8.33}$$

It follows from (8.33) that in the steady-state mode, the weighting coefficients are:

$$W_{\text{s.s.}} = \mathbf{W}_{\text{уст}} = \mathbf{R}_{XX}^{-1}\mathbf{X}y_0. \tag{8.34}$$

In this case, as can be seen from a comparison with (8.24), the mean square error $e^2(t)$ is minimal and the entire system provides for optimal Wiener filtration.

The adaptation circuit described here was proposed for the first time by Widrow. The main drawback to this configuration is the necessity of apriori knowledge of the form of the useful (requisite) signal y_0. However, if it is knonw, then adaptation is not necessary.

In the case of signals which are weak relative to the noise, the useful signal power can be disregarded ($y_0 = 0$). In this case, adaptation is realized, however, in accordance with (8.34) all of the channels are blocked, $W \to 0$ and the antenna ceases to respond not only to the interfence, but also to any other signals.

Various methods have been proposed for eliminating this deficiency. One of the techniques is dual mode adaptation. In the first mode, it is assumed that the useful signal is absent and that the interference is suppressed (along with the useful signal, if it is present!). In the second mode, the inputs of all of the channels are switched to a useful signal simulator for X_0. In this case, the known output signal y_0 for the input signal being simulated is fed to the control circuit.

If prior to the start of the first mode, the coefficient vector is designated as W[n], then by the end of the first mode of duration τ_1, we obtain the increment of the coefficients in a first approximation determined from (8.33) when $y_0 = 0$:

$$\Delta\mathbf{W}[n]_1 \simeq \left.\frac{\tau_1 d\mathbf{W}}{dt}\right|_{\substack{\mathbf{W}[n] \\ y_0=0}} = -ak\tau_1\mathbf{R}_{XX}\mathbf{W}[n], \; n=1, 2, \ldots \tag{8.35}$$

Similarly, when $R_{XX} = R_{X_0X_0}$ we determine from (8.33) the increment of the coefficient vector during the second mode which is of duration τ_2:

$$\Delta W[n] = \tau_2 \frac{dW}{dt}\Bigg|_{\substack{W[n]\\ R_{X_0X_0}\\ x_n}} = -ak\tau_2 (R_{X_0X_0} W[n] - \overline{X_0 y_0}). \qquad (8.36)$$

Thus, by the start of the next first mode, the coefficient vector W[n+1] is determined from (8.35) and (8.36) by the recurrent equation:

$$\begin{aligned} W[n+1] &= W[n] - ak\{(\tau_1 R_{XX} + \tau_2 R_{X_0X_0}) W[n] - \tau_2 \overline{X_0 y_0}\} = \\ &= W[n] - ak\{(\tau_1 R_{XX} + \tau_2 R_{X_0X_0}) W[n] - \tau_2 R_{X_0X_0} W_0\}. \end{aligned} \qquad (8.36a)$$

After completing the transition modes W[n+1] = W[n] = W[∞] and using (8.36a), we find:

$$W[\infty] = (\tau_1 R_{XX} + \tau_2 R_{X_0X_0})^{-1} \tau_2 R_{X_0X_0} W_0. \qquad (8.37)$$

It follows from (8.37) that with an increase in the signal level, adaptation approaches optimal Wiener filtration when the interference and the useful signal are independent, and in the absence of interference ($X_\pi = 0$), the adaptation system provides for the requisite directional pattern.

Various circuits are possible which assure a compromise pattern between that needed without interference and the optimal one in the presence of interference. Some of them are shown in Figure 8.11.

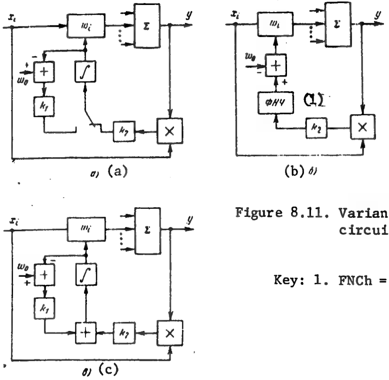

Figure 8.11. Variants of adaptation circuits.

Key: 1. FNCh = low pass filter.

The circuit configuration described here with mode switching is shown in Figure 8.11a; open loop and closed loop single mode feed circuits for the desired distributions, w_0, in the form of low frequency control signals are shown in Figures 8.11b and 8.11c.

8.6. The Design of Beam Steering Systems for a Specified Precision of the Directional Pattern Orientation in Space

For the correct choice of the parameters for the beam steering system of a phased array it is necessary to analyze the errors produced by the control unit and their impact on the directional pattern. Some three types of control errors can be singled out according to the point of occurrence: input errors, computer errors and output quantization errors. In this case, the phase error element of a phased array can be represented by the expression:

$$\mu_i=\mu_{im}+\mu_{ir}+\mu_{i\Delta}, \tag{8.38}$$

where μ_{im} is the phase distortion caused by the input errors; μ_{ir} is the phase distortion caused by computational errors; $\mu_{i\Delta}$ are the phase shifter quantization errors.

If the input data in expression (8.1) are specified with errors of $\delta\vec{R}_i = R_i\delta r_i$, δr_m, then the resulting error in the computations will be:

$$\delta d_i = (R_i\,\delta r_m) + (\delta R_i\,r_m) = \mu_{im} + R_{ir}. \tag{8.39}$$

The quantity

$$\mu_{im} = R_i\,(r_i\,\delta r_m) \tag{8.40}$$

is the function for each element of the error in the representation of the vector r_m by a digital code, where the argument of this function, δr_m, which is common to all elements is determined only the direction of r_m.

The second component

$$\mu_{ir} = R_i\,(r_m\,\delta r_i) \tag{8.41}$$

is determined by the errors in the digital code representation of the vector $\vec{R}_i$. The quantity δr_i differs for each element in the general case.

The quantization error $\varepsilon_{i\Delta}$ is distributed over the set of elements uniformly in a range of $\pm\Delta/2$, where Δ is the phase shifter quantum step.

Thus, the phase distortion ε_{im} is functionally distributed over the elements of the phased array. The quantities μ_{ir} and μ_Δ in the case of a large number of phased array elements not mutually correlated and are randomly distributed over the elements of the phased array. The mathematical expectations of the errors ε_{ir} and $\varepsilon_{i\Delta}$ are equal to zero by virtue of the symmetry of the distribution of these quantities.

The dispersion of these errors is:

$$\mathcal{D}[\mu_{ir}+\mu_{i\Delta}]=\mathcal{D}[\mu_{ir}]+\mathcal{D}[\mu_{i\Delta}]=K_i^2 q_r^2/12+\Delta^2/12=\mathcal{D}_r+\mathcal{D}_\Delta, \tag{8.42}$$

where $q_r = 2^{-p_r}$; p_r is the number of digit places in the computer.

In analyzing the impact of control errrors on the shifting of the directional pattern maximum with deviations in the phase direction r_m from the axis of symmetry of a convex phased array through an angle of $\theta \leq 15$--20°, the vector for the displacement in the directional pattern maximum can be represented as the vector sum of two orthogonal components.

It has been demonstrated that in a first approximation the position of a directional pattern maximum in space is defined by the normal to the plane of regression of the phase distribution. Taking this displacement of the directional pattern maximum into account, h_x and h_y are defined by the following ratios:

$$h_x=\frac{\sum\limits_i^N x_i(\mu_{ir}+\mu_{i\Delta})}{\sum\limits_i^N x_i^2},\qquad h_y=\frac{\sum\limits_i^N y_i(\mu_{ir}+\mu_{i\Delta})}{\Sigma y_i^2}; \tag{8.43}$$

$$\mathcal{D}[h_x]=\sum_i^N x^2(\mathcal{D}_r+\mathcal{D}_\Delta)\Big/\left(\sum_i^N x_i^2\right)^2=\mathcal{D}[h_y]=C_h(\mathcal{D}_r+\mathcal{D}_\Delta); \tag{8.44}$$

$$M[h_x]=M[h_y]=0. \tag{8.45}$$

In a rectangular planar array of m x m cells, the displacements of the directional pattern maxima in the XOZ and YOZ planes are independent and are determined by the errors in the calculation of the phase change over an array step, x_0, y_0, and by the quantization errors of the cells, μ_{kl}:

$$h_x=\sum_{k=1}^m\sum_{l=1}^m k\mu_{kl}/mx_0\sum_{k=1}^m k^2+\mu_0/x_0; \tag{8.46}$$

$$\mathcal{D}[hx]=\mathcal{D}_0/x_0^2+\mathcal{D}_\Delta/mx_0^2\sum_{k=1}^m k^2, \tag{8.47}$$

where μ_0 is the error in calculating the phase shift for one step of the planar array; μ_{kl} is the quantization error of the kl-th cell; kl are the numbers of the cells with respect to rows and columns.

The shift in the directional pattern maximum because of the functional error is defined similarly:

$$f_x = \sum_{i}^{N} x_i \mu_{im} \Big/ \sum_{i}^{N} x_i^2; \quad f_y = \sum_{i}^{N} y_i \mu_{im} \Big/ \sum_{i}^{N} y_i^2. \tag{8.48}$$

Since the following condition is met for an axially symmetric phased array:

$$\sum_{i=1}^{N} x_i y_i = \sum_{i=1}^{N} x_i z_i = 0, \tag{8.49}$$

Then expression (8.48) can be represented in the form:

$$f_x = \frac{\delta \mathbf{r}_m}{\sum_{i=1}^{N} x_i^2} \sum_{i=1}^{N} x_i \mathbf{R}_i = \frac{\delta \mathbf{r}_m}{\sum_{i=1}^{N} x_i^2} \left[\mathbf{i} \left(\sum_{i=1}^{N} x_i x_i \right) + \mathbf{j} \left(\sum_{i=1}^{N} x_i y_i \right) + \mathbf{k} \left(\sum_{i=1}^{N} x_i z_i \right) \right], \tag{8.50}$$

$$\delta \mathbf{r}_m \mathbf{i} = \delta x_m, \tag{8.51}$$

where $q_m = 2^{-p_m}$; p_m is the number of digits which specify the components of a unit vector.

An analysis of the random quantities h_x and h_y shows that they have a two-dimensional gaussian distribution while the correlation coefficient between the quantities h_x and h_y is equal to zero. In this case, the scalar value of $h = \sqrt{h_x^2 + h_y^2}$ has a Rayleigh distribution.

$$\varphi(h) = \frac{h}{\sigma_h^2} \exp\left(-\frac{h^2}{2\sigma_h^2} \right), \tag{8.52}$$

where $\sigma^2 = \sigma_x^2 = \sigma_y^2 = \mathcal{D}[h_x] = \mathcal{D}[h_y]$.

The distribution of the system of random quantities f_x and f_y is uniform in a range of:

$$-q_m/2 \leqslant f_x < q_m/2, \quad -q_m/2 \leqslant f_y < q_m/2;$$
$$-q_m \sqrt{2}/2 \leqslant f = \sqrt{f_x^2 + f_y^2} \leqslant \sqrt{q_m^2/4 + q_m^2/4} = q_m \sqrt{2}/2. \tag{8.53}$$

Thus, the input errors determine the discrete positions of a phased array beam in space. Its displacement, which is caused by these errors, depends only on the number of digits in the code which specifies the direction cosines of the vector r_m.

Computational errors and output quantization errors lead to a random shifting of the beam from its discrete positions. The shift depends on the phased array geometry, the number of elements in the array, the word length of the computer and the word length of the phase shifters which are used.

We shall consider the procedure for calculating the parameters of the control system computer by a phased array. Let the discrete step for beam steering, $f_{\max}$ (radians) and the ultimate permissible steering error, $h_{\max}$, be specified, where $f_{\max} > h_{\max}$.

We determine the number of digits p_m in the input code from expression (8.53):

$$q_m \sqrt{2}/2 \leqslant f_{\max}. \tag{8.54}$$

Considering the fact that $q_m = 2^{-p_m}$, we obtain:

$$p_m \geqslant -(\log_2 f_{\max} + 0{,}5). \tag{8.55}$$

We determine thw word step p_r by means of relationships (8.42) or (8.44) given the condition:

$$h^2_{\max} \geqslant 0{,}9\,\mathscr{D}[h] = 9C_h(\mathscr{D}_r + \mathscr{D}_\Delta). \tag{8.56}$$

For this, we express the permissible dispersion D_r:

$$\mathscr{D}_r \leqslant h^2_{\max}/9C_h - \mathscr{D}_\Delta. \tag{8.57}$$

For a known value of the quantum step of the phase shifter and a known phased array geometry, we find:

$$\mathscr{D}_\Delta \leqslant \frac{\Delta^2}{12}; \qquad \frac{1}{C_R} = \sum_i^N x_i^2 = \sum_i^N y_i^2. \tag{8.58}$$

Taking (8.42) into account, we obtain:

$$q_r \leqslant \frac{1}{R}\sqrt{12\left(\frac{h_{\max}}{9C_R} D_\Lambda\right)}, \tag{8.59}$$

whence:

$$p_r \geqq -\log_2 q_r \tag{8.60}$$

The computation sequence established here makes it possible to determine the word length of the input data code and the word length of the computer based on the requisite discrete step and precision of phased array beam steering, given the condition that the coordinates of the phased array elements and the phase shifter quantum step are specified.

Sample Calculation. 1. The planar array $m \times m$, $m = 11$, $x_0 = y_0 = 2\pi$ and $\Delta = \pi/4$ is specified. The requisite discrete step for the beam is 1° and the beam steering precision is 10'.

We express the angular quantities in radians:

$$f_{max} = 1.75 \cdot 10^{-2} \text{ rad}; \qquad h_{max} = 0.292 \cdot 10^{-2} \text{ rad}.$$

Substituting the value f_{max} in (8.47), we obtain:

$$p_m \geqq -(\log_2 1.75 \cdot 10^{-2} + 0.5) = 55 \text{ [sic]}.$$

We choose $p_m = 6$ digits.

We determine the square of the permissible beam deflection:

$$h^2_{max}(0.292 \cdot 10^{-2})^2 = 8.5 \cdot 10^{-6} \text{ rad}^2.$$

The second term in equation (8.47) is:

$$\frac{\mathcal{D}_\Delta}{m x_0^2 \sum\limits_m p^2} = \frac{(\pi/4)^2 (1/12)}{11 (2\pi)^2 2 (1+2^2+3^2+4^2+5^2)} = \frac{1{,}63 \cdot 10^{-1}}{4{,}77 \cdot 10^4} = 0{,}3410^{-6} \text{рад}^2.$$

The first term in equation (8.47) is:

$$\frac{\mathcal{D}_r}{x_0^2} = \frac{h^2_{max}}{9} - 0{,}34 \cdot 10^{-6} = \frac{8{,}5 \cdot 10^{-6}}{9} - 0{,}34 \cdot 10^{-6} = 0{,}6 \cdot 10^{-6} \text{ рад}^2.$$

We determine the computer word:

$$\mathcal{D}_r = x_0^2 q_r^2/12, \quad \mathcal{D}_r/x_0^2 = p_r^2/12 = 0{,}6 \cdot 10^{-6}.$$

whence:

$$q_r^2 = 7{,}2 \cdot 10^{-6}, \quad q_r = 2^{-p_r} = 2{,}68 \cdot 10^{-3}.$$

From the last expression, we have the following:

$$-p_r \log 2 = -3 + 0.43 = -2.57; \quad p_r \geqq 2.57/0.3 = 8.6$$

We choose p_2 = 9 digits.

2. A hemispherical array has a radius $p_1 = 25 \cdot 2\pi$, $\Delta = \pi/4$ and $C_1 = 0.2 \cdot 10^{-4}$. The digit capacity of the input code p_m has already been determined. We substitute the initial data in equation (8.58):

$$\mathcal{D}_r \leqslant \frac{8,5 \cdot 10^{-6}}{9,02 \cdot 10^{-4}} - \frac{(\pi/4)^2}{12} = 4,72 \cdot 10^{-2} - 1,63 \cdot 10^{-2} = 3,09 \cdot 10^{-2} \text{ рад}^2.$$

We obtain the following from formula (8.59):

$$q_r \leqslant \frac{1}{25 \cdot 2\pi} \sqrt{12 \cdot 3,09 \cdot 10^{-2}} = \frac{6,09 \cdot 10^{-1}}{1,57 \cdot 10^{2}} = 3,87 \cdot 10^{-3}.$$

From this we obtain p_r = 8 digits.

RADIATING ELEMENTS OF AN ANTENNA ARRAY

SECTION II

9. PRINTED CIRCUIT ANTENNA

9.1. The Function and Specific Features of Printed Circuit Antennas

Printed circuit antennas differ in their structural design from other types of microwave antennas. Not only radiators, but also transmission lines, matching elements, etc. can be made using the techniques of printed circuit technology. More than other antennas, these meet the requirement of miniaturization, one of the major requirements for aircraft equipment. This explains the increasingly widespread use of printed circuit antennas.

We shall note the major advantages of printed circuit antennas:

--Structural simplicity, small volume, weight and cost;

--Convenience in combining antennas with printed circuit feed lines and devices;

--High fabrication precision, because of which good reproducibility of antenna characteristics is achieved;

--The ability to design antenna structures for aircraft which protrude little or not at all, in particular, structural designs which do not change their strength characteristics.

The drawbacks to printed circuit antennas include poor electrical strength, the difficulty of designing tunable devices and measuring the parameters of printed circuit components.

Printed circuit antennas are used in a frequency range of from 100 MHz to 30 GHz at low and moderate power levels. At very low frequencies, the size and weight of antennas which are comparable to the wavelength become quite considerable. At higher frequencies, these antennas have no advantages as compared to others. Printed circuit antennas are poorly directional and for this reason, they are used primarily as constituents of antenna arrays.

9.2. The Major Types of Printed Circuit Antennas and Their Operational Principles

The major elements which form an antenna are the radiator (the antenna itself) and the excitation device. Printed circuit antennas correspondingly differ in the operational principle of the radiator and the manner of its excitation, as well as in the type of transmission line. Moreover, the radiation characteristics of the antennas and their structural parameters can also be distinctive attributes. Primarily the first group of attributes is treated in this chapter. The radiation characteristics of the antennas are of the topic treated in this chapter.

Striplines are most frequently used as the transmission lines. As a rule, the type of striplines governs the structural design of the other antenna elements. In the low frequency portion of the band, the excitation is accomplished by means of coaxial lines. It is also possible to use a waveguide transmission line.

Resonator type printed circuit radiators designed around asymmetrical striplines (see Chapter 2) also find widescale application. Another more traditional type of printed circuit antenna is dipoles of various configurations and slots cut in the metal wall of a symmetrical type transmission stripline. Developmental modifications of these antennas are stripline spirals and curvilinear radiators.

An example of a resonator printed circuit radiator is shown in Figure 9.1. This radiator is used most often [1, 2]. It consists of a rectangular strip conductor [1], placed on a thin dielectric layer (2) with a conducting substrate (3). The radiator is excited by a strip transmission line. This system is a flat lossy resonator filled with a dielectric for the transmission line, where the losses are due to radiation. The edges of the resonator form two radiating slots A and B, which are spaced l apart, approximately equal to $\lambda_d/2$, where λ_d is the wavelength in the dielectric. At the edges of the resonator, the components of the field which are normal to the conducting substrate are out of phase. The field components parallel to the conducting substrate add together in phase and form a linearly polarized radiation field having a direction of maximum radiation along to the normal to the plane of the substrate. The dimension b of the radiator can differ.

To obtain a rotating polarization field, two pairs of radiating slots are needed which are arranged perpendicular to each other and are excited with a phase shift of 90° each. For this, a square radiator is chosen which is excited at two points in the center of adjacent sides of a strip conductor. The excitation is realized most readily by a rectangular radiator with a single feed point, which is shown in Figure 9.2. One side of the strip conductor of the radiator is greater than $\lambda_d/2$ by the amount Δ, while the other is smaller by the same amount, something which provides for the 90° phase shift for each. The quantity Δ is chosen experimentally. The radiator is excited by astripline. A possible excitation variant for this radiator is a coaxial line perpendicular to the conducting substrate. The center conductor of the coax line is connected to the strip conductor of the radiator.

Other types are discrete radiators in the form of printed circuit dipoles and slots. The current in the strip conductor of the radiator serves as the radiation source in this case. Slot antennas, excited by a stripline, are a direct analog of slotted waveguide antennas. They are widely used as the radiating elements of scanning antennas arrays. With the appropriate excitation, one can use such radiators to design antenna systems which realize extremely arbitrary directional characteristics.

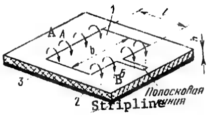

Figure 9.1. A printed circuit resonator antenna with linear polarization.

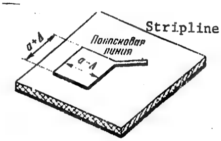

Figure 9.2. A printed circuit resonator antenna with a rotating polarization field.

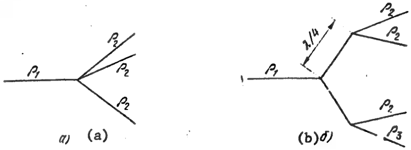

Figure 9.3. Antenna excitation circuits.

One of the methods of exciting radiating elements is excitation using a system of branched lines of the same electrical length (Figure 9.3). If the excitation is realized using a line with a characteristic impedance ρ_1, then with N branches having a characteristic impedance of ρ_2 (Figure 9.3), the relationship $\rho_1 = N\rho_2$ is observed. With a large number of radiators, it is expedient to insert a transformer ahead of each branch (Figure 9.3b). Such an excitation techniques is realized especially conveniently using striplines.

In another approach, the traveling wave excites the radiating elements which are arranged along the transmission line. This technique is also realized quite well using strip transmission lines. A drawback to it is the great dependence on frequency. Other excitation methods are also possible, but they are used comparatively rarely.

Almost all of the elements of a feed line channel which are used for coaxial and waveguide transmission lines, as well as the feeder channel as a whole can be constructed in a printed circuit design. However, as a rule, only individual printed circuit assemblies are used in a feeder channel. For printed circuit antennas, coaxial or waveguide lines are most frequently used as the main feed line. Because of this, it becomes necessary to have elements for joining striplines to waveguide and coaxial lines. The major components of striplines, including coaxial to stripline and waveguide to stripline junctions, as well as stripline connectors and splitters, are described in [07, 014, 02].

9.3. The Major Characteristics and Design of Printed Circuit Resonator Antennas.

We shall single out among antennas of this type the antenna which is shown in Figure 9.1 as the basic antenna. The linearly polarized field is produced by the radiation of two slots, which form the walls of the resonator, which represents a half-wave section of an asymmetrical stripline. Antennas of this type are usually employed as receiving antennas.

It is assumed in the antenna design that the dimension h(Figure 9.1) satisfies the condition $kh << 1$, where $k = 2\pi/\lambda$, λ is the working wavelength. It is also assumed that the field distribution in the radiating slot corresponds to a T mode field distribution in the cross-section of a regular stripline. In this way, the influence of higher modes on the radiation of the slot is neglected.

These presuppositions make it possible to represent the radiating slot of a resonator as a linear radiator, similar to a narrow slot in a conducting shield Figure 9.4). Thus, the analysis of a resonator antenna reduces to the analysis of ordinary slot antennas. The field in the radiating slot of the antenna has the form $\vec{E} = \vec{x}_0 E_x$, $|x| \leq h/2$. This field determines the magnetic current of an equivalent linear radiator as $\vec{I}_M = \vec{z}_0 2E_x$, $|z| \leq b/2$, where $\vec{x}_0$ and $\vec{z}_0$ are unit vectors of the coordinate system of Figure 9.4.

The Antenna Directional Pattern. The field of a linear magnetic radiator is known (for example, see 01). The electrical field of the radiator has components of E_θ and E_θ in the spherical system of coordinates of Figure 9.4. The antenna polarization is determined by the projection of the E_θ component on the normal to the plane of the slots (the Y axis). Then for the indicated polarization, the directional pattern (DN) of the antenna as a system of two equivalent linear radiators, which are excited in phase, has the form:

$$F(0, \varphi) = \frac{\sin(\pi b \lambda^{-1} \cos\varphi)}{\pi b \lambda^{-1} \cos\varphi} \cos\theta \cos\left(\frac{\pi l}{\lambda} \sin\theta\right). \quad (9.1)$$

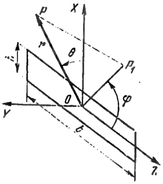

Figure 9.4. The coordinate system for the radiating slot of a printed circuit antenna.

The first two factors in expression (9.1) define the directional pattern of an equivalent linear radiator for the indicated polarization, while the last term is the directivity characteristic of a system of two identical radiators, spaced a distance l from each other.

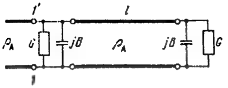

Figure 9.5. The equivalent circuit of a printed circuit resonator type antenna.

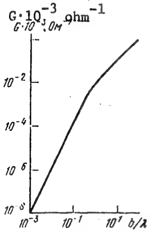

Figure 9.6. Antenna slot conductance G as a function of the quantity b/λ.

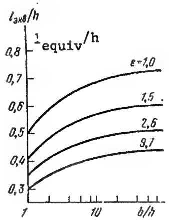

Figure 9.7. The quantity l_{equiv}/h as a function of the ratio of the dimensions b/h and the dielectric permittivity ε of a printed circuit antenna.

The Antenna Input Admittance. The equivalent circuit of the antenna as a transmission load is shown in Figure 9.5. The two radiating slots of the antenna, having an input admittance of $Y = G + jB$ are separated by a line section of length l with a low characteristic impedance of ρ_A. The input admittance of the antenna Y_{in} is the result of combining the slot admittance at the antenna input (the terminals 1-1') and of the slot which is transformed to the input through the line section l so that:

$$Y_{in} \qquad Y_{\text{вх}} = G + jB + Y_A \frac{(G+jB) + jY_A \operatorname{tg} \beta l}{Y_A + j(G+jB) \operatorname{tg} \beta l}, \tag{9.2}$$

where β is the line propagation constant; $Y_A = 1 - \rho_A$.

The radiation conductance G is calculated by the method usually employed in slotted antenna theory. The conductance G is shown in Figure 9.6 as a function of b/λ. For b/λ > 1, we have [2]:

$$G\ [\text{Ohms}^{-1}] \simeq b/120\lambda \tag{9.3}$$

The reactive component B of the slot admittance is due to its capacitance and is computed from the formula:

$$B\ [\text{Ohms}^{-1}] = l_{\text{equiv}}/60\Lambda \qquad (9.4)$$

where l_{equiv} is a quantity equivalent to the length of a stripline open at the end having the same input admittance; $\Lambda = \lambda/\sqrt{\varepsilon_{\text{eff}}}$ where Λ is the wavelength in the stripline; ε_{eff} is the effective dielectric permittivity of the substrate, which is determined in [014, p 62]. The curves for l_{equiv}/h for various values of ε are plotted in Figure 9.7 as a function of b/h.

An antenna is tuned to resonance if its input admittance is a real quantity. The resonance condition follows from expression (9.2):

$$\operatorname{tg} \beta l = 2Y_{\Lambda} B/(G^2 + B^2 - Y_{\Lambda}^2). \qquad (9.5)$$

Expression (9.5) defines the resonant length of a line section l having a low characteristic impedance ρ_A. In this case, the input admittance of the antenna is $Y_{in} = 2G$. The quantity l computed in this fashion is somewhat less than half of a wavelength in the stripline.

The design of an antenna consists in computing the dimensions of its resonator and selecting a stripline to obtain the specified width of the main lobe of the directional pattern (or directional gain) of the antenna. Additional requirements are set which are related to the conditions for the placement and operation of the antenna on board the vehicle. These requirements are important when selecting the dimensions of the strip conductor and the dielectric substrate of the antenna which are its major structural components. The design of an antenna is most easily accomplished by means of trial-and-error selection of its parameters.

The selection of antenna dimensions consists in the following. Based on a specified directivity characteristic, the dimension b is determined for the strip conductor of the antenna (Figure 9.1). In this case, the dimension l is assumed to be equal to 0.4λ to 0.5λ. The stripline conductor can have either a square or a rectangular shape. The characteristic impedance ρ_A of an asymmetrical stripline depends on the value of b (Figure 9.5), where this impedance should not be too low and usually amounts to 10 to 15 ohms. Then the h dimension of the antenna is chosen, usually $h < 0.1\lambda$, as well as the material of the dielectric substrate [014]. The dielectric permittivity of the substrate is most frequently chosen equal to $\varepsilon = 2.25$--2.5. In individual cases, a ceramic ($\varepsilon \simeq 10$) can be chosen as the substrate.

The selected antenna parameters make it possible to calculate the characteristic impedance ρ_A of a low impedance asymmetrical stripline as well as the input admittance of the radiating slot of the antenna $Y = G + jB$ using formulas (9.3) and (9.4), taking into account the function shown in Figure 9.7. The propagation constant β of a low impedance line is determined from [014]. The resonant length of a low impedance stripline section l and the input admittance of the antenna Y_{in} are determined from formula (9.5). An asymmetrical stripline with a characteristic impedance of $\rho_\phi = 50$ ohms is usually chosen as the transmission line. A matching element in the form of a quarter-wave transformer is used to match the

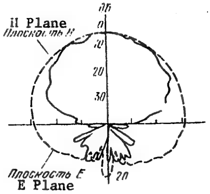

Figure 9.8. The directional pattern of a printed circuit resonator type antenna.

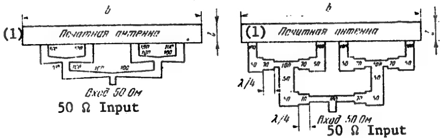

Figure 9.9. Excitation configurations for a printec circuit resonator type antenna having a large value of the dimension b.

Key: 1. Printed circuit antenna.

antenna to the stripline. Matching is an extremely labor intensive operation. It is accomplished by the trial and error design of the matching element and is more successful, the closer the characteristic impedance of the antenna is to the characteristic impedance of the line. Where there is a substantial difference in these values, the antenna design procedure is repeated for its other parameters.

A linearly polarized antenna (Figure 9.1) with a sqare stripline conductor designed for a frequency of 9 GHz, has the following characteristics. The radiating slot admittance of the antenna is $Y = (0.922 + j7.45) \cdot 10^{-3}$ ohms^{-1}. The resonant length of the antenna is $l = 0.46\lambda$ when $\rho_A = 15$ ohms. The antenna is matched to the stripline having a characteristic impedance of $\rho_\phi = 50$ ohms by means of a quarter-wave transformer. In a passband of $\Delta f/f_0 = 2\%$, the SWR is less than two. The measured gain is 7.6 dB with losses in the line of 0.3 dB. The typical directional pattern of the antenna in the E and H planes is shown in Figure 9.8.

The antenna is extremely narrow band. To improve the bandwidth performance it is recommended that the characteristic impedance ρ_A of the low impedance stripline be increased, a dielectric substrate with a greater value of ε be selected to reduce the resonator length, the inductance of the antenna be increased by means of making holes or slotted cuts in the stripline conductor of the antenna, as well as that broadband techniques for matching the antenna to the transmission line be employed. All of this will make it possible to increase the passband of the antenna $\Delta f/f_0$ up to 50%.

For an antenna with a rectangular strip conductor and dimensions of $d > \lambda$, the excitation system is built for the condition of equal electrical paths of the branched transmission lines (see §9.2). Several points are excited in the strip conductor in this case. Two excitation configurations are shown in Figure 9.9 for an antenna with a dimension $b = 2\lambda$ for a line with a characteristic impedance $\rho_\phi = 50$ ohms. The proposed technique is also applicable to the design of rotationally polarized antennas.

9.4. Antenna Arrays with Resonator Elements

Antenna arrays with radiating resonator type elements are constructed in the form of strings of radiators and sets of these strings. When designing a linear antenna array, it is usually assumed that the radiators are arranged at equal spacings d from each other and are excited in-phase or with a constant and small phase difference. The analysis of such arrays is performed as an analysis of in-phase arrays, with subsequent accounting for the inclination of the main lobe of the directional pattern if this is necessary. Such excitatin presupposes a single transmission line for a linear array. It is also possible to excite array elements where the electrical length of the transmission lines are equal (see §9.2).

Basic Relationships for a Linear Array. The directional pattern of a linear system of identical radiators with in-phase excitation has the form (see Chapter 2):

$$F_N = \sum_{n=1}^{N} A_n \exp\left[j\kappa (n-1) d \cos\theta\right], \tag{9.6}$$

where A_n is the amplitude of the n-th radiator; θ is the angle read out from the axis of the array; N is the number of radiators. It is assumed in this case that the number of resonator type elements is N/2. If the spacing between the radiators of the array is $d = \lambda/2$, then the directional gain of the array is:

$$D = \left(\sum_{n=1}^{N} A_n\right)^2 \Big/ \sum_{n=1}^{N} A_n^2. \tag{9.7}$$

The greatest directivity of an array is achieved when all of the amplitudes are equal: $A_n = A$. Then the directional gain of the array is $D = N$. This is the case of uniform excitation of a linear array and it is of the greatest practical interest.

The directional pattern of a uniform array, using the principle of directional pattern multiplication of [01], can be written in the form:

$$F(\theta, \varphi) = F_1(\theta, \varphi) F_N(\theta), \tag{9.8}$$

where $F_1(\theta, \phi)$ is the directional pattern of a single radiator; F_N is the group directional pattern of the array. The directional pattern of a resonator type element is described by expression (9.1). In the case of N/2 elements in the array, the group directional pattern is:

$$F_N = \sin(N\Phi/4)/(N/2)\sin\Phi, \qquad (9.9)$$

where $\Phi = (kd\cos\theta - \Phi_0)$ is the phase shift between the fields produced by adjacent elements; Φ_0 is the phase difference in the excitation of the adjacent elements. In the case of in-phase excitation of the elements of the array, $\Phi_0 = 0$.

Ways of Exciting Array Elements. In the case of in-phase excitation of resonator type elements, one speaks of resonant excitation of an array. In order to avoid the appearance of secondary main lobes in the directional pattern, the spacing between array elements (taking the directional pattern of an element into account) (Figure 9.8) should not exceed $\lambda/2$. Resonant excitation of an array is characterized by the fact that the main radiation is directed along a normal to the plane of the array. The major drawback to such excitation is the poor matching of the array to the transmission line. For an array of four series connected resonator elements, designed for a frequency of 9 GHz, the matching passband for a SWR level of no more than two amounts to 1.7 %. The resonant frequency, the input admittance of the array, as follows from the schematic shown in Figure 9.10, is $Y_{in} = NG$, where $Y = G + jB$ is the input admittance of the radiating slot of a resonator element (see §9.3); N is the number of slots. An antenna array with the elements excited "off of resonance" in a traveling wave mode is free of this deficiency. With a large number of elements, the reflections from each of them "on the average" cancel out, which provides for good matching of the antenna array. A drawback to this excitation technique is the deviation of the direction of the main lobe from a normal to the plane of the array, which changes with a change in frequency. However, with a small phase difference for the excitation of adjacent elements "close to resonance", this deviation is small.

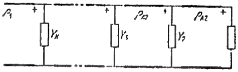

Figure 9.10. The equivalent circuit of a linear in-phase array using printed circuit resonator type elements.

An example of an array excited in a traveling wave mode is shown in Figure 9.10. One end of the array is connected to a coaxial feed line, while the other is loaded into an absorbing load. The angle of inclination θ of the main lobe of the directional pattern to the antenna axis is computed from formula [3]:

$$\cos\theta = [\lambda - (l + 0{,}5b)]/l, \qquad (9.10)$$

where l and b are the dimensions of the array. It follows from formula (9.10) that the inclination angle θ changes with a change in frequency, where the main radiation is directed in a direction opposite to the direction of wave propagation in the transmission line. It follows from the theory of periodic structures that this is explained by the choice of the propagation constant $\beta = k \cos\theta$ for the spatial harmonic which is responsible for the primary radiation.

The characteristic features of antenna arrays with resonator type elements, when they are excited in resonance and traveling wave modes are similar to the features of slotted waveguide arrays which were treated in Chapter 5, with the same excitation modes.

The design of an antenna array consists in selecting the number of elements in it and designing the elements for a specified directivity, i.e., main lobe width of the directional pattern or directional gain. A uniform in-phase array is taken as the basis for the design calculations, for which expressions (9.7) - (9.9) apply. The calculation of array gain is extremely approximate, since it is necessary to take transmission losses into account, and the calculation of the gain can serve only as a qualitative estimate of the selected antenna circuit. The design procedure for a linear array is as follows.

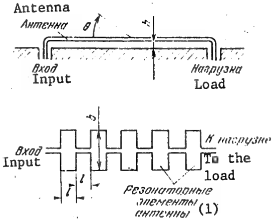

Figure 9.11. A linear traveling wave array with printed circuit resonator type elements.

Key: 1. Resonator antenna elements.

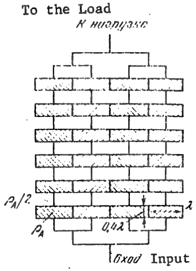

Figure 9.12. A printed circuit antenna in the form of a composition of linear traveling wave arrays.

The number of resonator type array elements, N/2, is chosen for a specified directivity. This number is taken equal to the directional gain of the array. Then the radiating element is designed using the procedure given in §9.3. The spacing between the array elements d is chosen equal to the dimension l, which is the resonant dimension of an element. The dimension b of a radiating element is chosen equal to either l or λ for a rectangular stripline conductor. In the case of a large value of b, the excitation of an element is complicated and takes on the form shown in Figure 9.9. With in-phase excitation of the antenna array, the directional pattern is computed using formulas (9.8) and (9.9) for $\Phi_0 = 0$.

When an array is excited in a traveling wave mode, the angle of inclination of the main lobe of the directional pattern is calculated using formula (9.10). This makes it possible to determine the phase shift, Φ_0, and to employ formulas (9.8) and (9.9) to calculate the directional pattern as well as the directional gain of the antenna array. The gain of the array is determined by the value of the efficiency, which under conditions of weak coupling of the radiators to the transmission line may be less than 50 percent. The radiation losses in a line loaded with an antenna array are taken at a level of 10 dB, which makes the results of analyzing traveling wave antnnas reliable and makes it possible to obtain the optimal gain.

The coupling of the radiators of a yagi antenna to a transmission line is governed by the h dimension (Figure 9.11) and the characteristic impedance of the line ρ. The smaller h is, the smaller the attenuation constant α for the traveling wave in the line. It is assumed in this case that the propagation constant β does not change over the length of the line. The longer the antenna array, the smaller the height h. For an antenna structure with a length of 20λ, the height h reaches 0.025λ.

If the yagi antenna designed in this manner does not have the requisite directivity, then its design calculations are repeated for a different number of radiating elements. A traveling wave array, designed for a frequency of 635 MHz, has dimensions of: $l = 0.4\lambda$, $b = \lambda$ and $h = 0.075\lambda$ [3]. A set of strips is used to improve the directivity. An example of an antenna of four strips is shown in Figure 9.12.

9.5. Printed Circuit Dipole Antennas

Dipole antennas and modifications of them are some of the most used radiators in antenna engineering. They are used particularly as the radiating elements of large antenna arrays. This explains the ever greater use of printed circuit dipole antennas. A stripline dipole takes the form of a strip conductor on a thin dielectric layer (Figure 9.13). When used as a part of an antenna array, a printed circuit dipole is usually positioned above a flat conducting shield.

The design calculations for a printed circuit dipole can be performed as the calculations of a strip dipole, with the subsequent accounting for the impact of the thin dielectric layer. In turn, a correspondence can be established between the strip dipole and a dipole with a circular cross-section (a wire dipole), which has the same directional pattern and input impedance. In this case, the cross-sectional dimension of the wire dipole is half as great (Figure 9.13). Such a comparison is experimentally confirmed given the condition that the length of the strip dipole 2L is substantially greater than its cross-sectional size 2d where $2d \ll \lambda$. In this case, to calculate the characteristics of a strip dipole, one an use the results of numerical and experimental studies of fine wire antennas. The influence of a dielectric layer consists in changing the length of a strip dipole, in particular, in shortening the resonant length of the dipole.

The Current Distribution and Overall Input Impedance of a Strip Dipole. The surface current, $\mathcal{J}(x, y) = \mathbf{X}_0 \mathcal{J}(x, y)$, induced in a narrow strip conductor of a dipole where $-d \leq y \leq d$ and $-L \leq x \leq L$, can be characterized by the quantity:

$$I(x) = \frac{1}{\pi} \int_{-d}^{d} \mathcal{J}(x, y)\, dy, \qquad (9.11)$$

which is used in calculating the total input impedance of a strip dipole. The surface current $\mathcal{J}(x, y)$ has a singularity at the corner edges of the strip conductor, which is of a local nature and constant over its length. Taking this singularity and expression (9.11) into account, the current $\mathcal{J}(x, y)$ has the representation:

$$\mathcal{J}(x, y) = I(x)/\sqrt{d^2 - y^2}. \qquad (9.12)$$

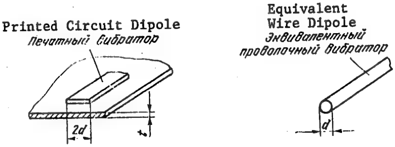

Figure 9.13. A comparison of a printed circuit dipole with a wire one.

Taken as the current I(x) in this expression is the current of an equivalent wire dipole (Figure 9.13).

The results of a numerical investigation show that the current distribution over the length of the dipole approaches a sine distribution, as is adopted in approximate dipole theory [01], only for a dipole length of $2L \leq 0.5\lambda$. Examples of the current distribution for other values of L are given in [01]. Resonant length dipoles find the most widescale practical applications.

The resistive and reactive components of the input impedance, $Z_{in} = R_{in} + JX_{in}$, of a strip dipole are shown as a function of its length L for various values of d in Figure 9.14. The value of the input impedance of a strip dipole differs from the input impedance of the infinitely fine wire dipole which is treated in approximate dipole antenna theory. We will also note that the resonant length of a strip dipole is close to 0.23λ, and practically does not change with a change in the d dimension of a narrow strip.

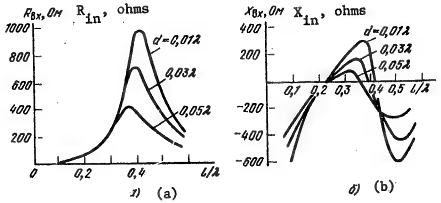

а) (a) б) (b)

Figure 9.14. The input impedance of a strip dipole as a function of the arm length L/λ and the dimension d.

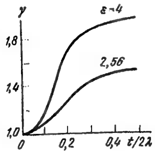

Figure 9.15. The retardation of the surface wave as a function of the dielectric layer thickness.

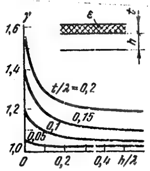

Figure 9.16. The retardation γ of a surface wave as a function of the height h/λ of a dielectric layer of thickness t above the surface of a shield.

The directional pattern of a strip dipole where $L/d > 5$ is taken to be the same as for an infinitely fine wire dipole. The dipole directional pattern is shown in [01]. However, when $L/d \leq 5$, instead of nulls, minima at a level of approximately 12 dB appear. Such "swelling" of the directional pattern nulls is undesirable when a dipole is used as an element in an antenna array, primarily because of the increase in the coupling between elements, the appearance of cross-polarization of the radiation and the reduction in the gain. The design method described here for a strip dipole is applicable to a conductor with a dimension of $2d \leq 0.1\lambda$.

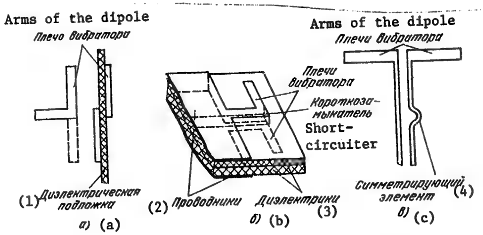

Figure 9.17. Excitation configurations for a printed circuit dipole using a balanced (a), balanced three-plate (b) and a two-wire (c) stripline.

Key:
1. Dielectric substrate;
2. Conductors;
3. Dielectrics;
4. Balancing element.

The Influence of the Dielectric Layer. The dielectric layer of a printed circuit dipole is chosen to be extremely thin $t < 0.1\lambda$, since it is only a structural component with low losses. For this reason, as a rule, it does not influence the directional pattern of a dipole and is considered primarily when calculating its resonant length. The shortening of a dipole depends on the retardation of the electrical wave propagating in the planar dielectric layer with a thickness t. When $t \to 0$, these waves degenerate into a free space T-type mode.

The retardation $\gamma = c/u_{\phi}$ of a lower mode is shown in Figure 9.15 as a function of the layer thickness t [4]. The retardation γ of the indicated mode is shown in Figure 9.16 as the function of the thickness t of a dielectric layer positioned above a conducting shield at a distance of h from the shield where the dielectric permittivity of the layer is $\varepsilon = 4$ [4]. The resonant length of the dipole is taken equal to $L_{res} \simeq 0.23\lambda/\gamma$.

Excitation of a Printed Circuit Dipole. The transmission line can be tied into a printed circuit dipole both perpendicularly to the strip conductor of the dipole, and in the plane of the conductor. In the first case, a coax line with a balancing device is usually employed, just as in the case of a wire dipole. In the second, excitation by means of balanced stripline finds the widest applications (Figure 9.17a, b). Sometimes the excitation is accomplished by means of a two conductor stripline (Figure 9.17c). As a rule, striplines connected to the input of a dipole by means of transition couplers [07, 014] are connected to other types of transmission lines (stripline and coaxial transmission lines, as well as waveguides), which are more convenient in structural terms and have better characteristics.

9.6. Antenna Arrays with Printed Circuit Dipole Elements

Printed circuit dipole radiators are successfully used as phased array elements both for transmission and reception. The basic mode for the study of large planar arrays is an infinite array, the radiating elements of which are excited by a current having the same amplitude and a linearly changing phase. Such a model can yield satisfactory results for a dipole array over a plane shield where the number of dipole elements is just 10 x 10. The analysis of a dipole antenna array consists in analyzing the input impedances as a function of the scan angle. Knowing these impedances, the influence of the latter on mismatching in the feed system of the antenna array can be minimized.

Printed circuit dipoles in a periodic antenna array are placed at its nodes, usually above a conducting shield. Printed circuit dipoles incorporated in an antenna array can be combined in quadrupole elements (quadrupoles), as shown in Figure 9.18. By changing the interconnection of the dipoles in a quadrupole, one can substantially change the characteristics of the antenna array. Printed circuit dipoles are usually assumed to be resonant and have a size of 2d << λ. Under these conditions, the analysis of an array with dipole elements can be carried out based on the existing literature [03, Vol 2; 6]. For dipoles of arbitrary length, a study of dipole arrays using integral equations is given in [7].

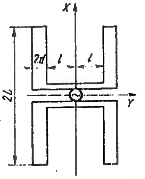

Figure 9.18. Quadrupole elements of an antenna array.

The Total Input Impedance of a Dipole Element of an Array Positioned Above a Shield. A printed circuit dipole as an element in an infinite array, depending on the numbers m, n, has an exciting voltage at the input which varies in accordance with the following law.

$$U_{mn} = U_0 e^{-jm\beta d_x} e^{-jn\alpha d_y}, \qquad (9.13)$$

where $\beta = \kappa \sin\theta \cos\varphi$; $\alpha = \kappa \sin\theta \sin\varphi$, $\kappa = 2\pi/\lambda$; d_x and d_y are the periods of the array.

Since an array is a periodic structure, the surface current induced with such excitation in the strip conductors of the dipoles, can be represented by a Fourier series expansion:

$$\mathcal{J}^{(i)} = \sum_{m=-\infty}^{\infty} \sum_{n=-\infty}^{\infty} \mathcal{J}_{mn}^{(i)} e^{-j\beta_m x} e^{-j\alpha_n y}, \qquad (9.14)$$

where $\beta_m = \beta + 2\pi m/d_x$, $\alpha_n = \alpha + 2\pi n/d_y$; i is the number of the dipole which combines the subscripts m' and n'. The coefficients $\mathcal{J}_{mn}^{(i)}$ can be calculated if the current distribution in the dipole is specified. This distribution is known for a resonant length dipole. Taking (9.12) into account, the surface current of the i-th dipole is defined as:

$$\mathcal{J}^{(i)} = \frac{I_0^{(i)}}{\sqrt{d^2-y^2}} \cos\frac{\pi x}{2L}, \tag{9.15}$$

where $I_0^{(i)}$ is the current at the input to the i-th dipole. Then the Fourier coefficients in expansion (9.14) have the form:

$$\mathcal{J}_{mn}^{(i)} = 2\frac{I_0^{(i)}\,2L}{d_x d_y} J_0(\alpha_n d) \frac{\cos\beta_m L}{1-(2\beta_m L/\pi)^2}, \tag{9.16}$$

where J_0 is a zero order Bessel function.

The input impedance of a dipole is defined as the ratio of twice the complex power P at the surface of the array within the bounds of its elementary cell to the square of the absolute value of the current at the dipole input:

$$\begin{gathered} Z = \frac{2P}{|I_0|^2} = 2\rho_0 \frac{(2L)^2}{d_x d_y} \sum_{m=-\infty}^{\infty} \sum_{n=-\infty}^{\infty} (\mathcal{J}_{mn}\mathcal{J}_{mn}^{*}) \times \\ \times \frac{1-(\beta_m/\kappa)^2}{\gamma_{mn}/\kappa} [1-\exp(-j\gamma_{mn}2h)], \end{gathered} \tag{9.17}$$

where $\gamma_{mn}^2 + \beta_m^2 + \alpha_n^2 = k^2$; $\rho_0 = 120\pi$ ohms; h is the spacing from the array to the shield.

The series (9.17) converges, and when calculating the value of Z, one can limit oneself to a finite number of terms in the series. Knowing the input impedance of the dipole, it is not difficult to calculate the reflection factor in the transmission line which couples the dipole to the generator. It depends on the scan angle and is determined from the formula:

$$\Gamma(\theta, \varphi) = [\rho_\phi - Z(\theta, \varphi)]/[\rho_\phi + Z(\theta, \varphi)], \tag{9.18}$$

where ρ_ϕ is the characteristic impedance of the feed line.

Formulas (9.17) and (9.18) are easily subjected to numerical study.

When studying the influence of the input impedance of a dipole on the reflection factor, which determines the conditions in the transmission line, a distinction must be drawn between the behavior of the resistive R and the reactive X components of the impedance. As studies of dipole arrays shown, these components are different functions of the scan angle. For this reason, the convergence of series (9.17) when calculating the quantities R and X requires separate treatment. When additional main lobes are absent in the directional pattern of an array, one can limit oneself to one term of the series (9.17), which corresponds to the number m = 0 and n = 0, to calculate the resistive component R. The calculation of the reactive component X requires taking a large number of terms of this series into account [03, Vol. 2]. The detailed analysis of the quantities R and X depends on the specific dimensions of the antenna array. However, there is no need in many cases to know the true value of the total input impedance Z, since the array elements are matched for a certain scan angle, usually normal to the plane of the array. In this case, it is of interest to change the input impedance when changing the scan angle, which reduces the volume of computational work.

The Total Input Impedance of a Quadrupole Element of an Array. A system of two coupled dipoles, which form a quadrupole element of an array (Figure 9.18), is excited by the voltage U_0 of a generator which is connected to its center point. Depending on the number m, n of the quadrupole element, the exciting voltage varies in accordance with (9.13). By representing the surface current induced in the strip conductors of the dipoles with expansion (9.14), where i = 1, 2, we obtain the expansion factors for the current in the following form on analogy with (9.16):

$$\begin{aligned} \mathcal{J}_{mn}^{(1)} &= 2\,\frac{I_0^{(1)}\,2L}{d_x\,d_y}\,J_0(\alpha_n d)\,\frac{\cos(\beta_m L)}{1-(2\beta_m L/\pi)^2}, \\ \mathcal{J}_{mn}^{(2)} &= 2\,\frac{I_0^{(2)}\,2L}{d_x\,d_y}\,J_0(\alpha_n d)\,\frac{\cos(\beta_m L)}{1-(2\beta_m L/\pi)^2}. \end{aligned} \tag{9.19}$$

Taking (9.19) into account, the internal and mutual impedances of the dipoles comprising the quadrupole, Z_{uv}, where u, v = 1,2, are determined by expression [5]:

$$\begin{aligned} Z_{uv} = &-\frac{d_x\,d_y}{2I_0^{(u)*}\,I_0^{(v)}}\,\rho_0 \sum_{m=-\infty}^{\infty}\sum_{n=-\infty}^{\infty} \mathcal{J}_{mn}^{(u)*}\times \\ &\times \mathcal{J}_{mn}^{(v)}\,\frac{d_n^2-\kappa^2}{\mathcal{J}\gamma_{mn}}\left(1-e^{-2j\gamma_{mn}h}\right), \end{aligned} \tag{9.20}$$

where $\rho_0 = 120\pi$

Because of the identical nature of the dipoles, we write $Z_{11} = Z_{22}$. The series (9.20) converges, and when calculating the quantity Z_{uv}, one can limit oneself to a finite number of terms in the series.

The input impedance of a quadrupole, $Z = R + jX$, as a generator load, is composed of the input impedances of the dipoles under conditions of their mutual coupling, transformed to the point where the generator is connected. Then, taking (9.20) into account, we have [5]:

$$\begin{aligned} Z = \frac{U_0}{I_0^{(1)}+I_0^{(2)}} = &[(Z_{12}Z_{21}-Z_{11}^2)\cos^2\gamma l-\rho_\Lambda^2\sin^2\gamma l- \\ &-2jZ_{11}\rho_\Lambda\cos\gamma l\sin\gamma l]/[Z_{12}+Z_{21}+2Z_{11}(\sin^2\gamma l-\cos^2\gamma l)+ \\ &+2j\rho_\Lambda^{-1}(Z_{12}Z_{21}-Z_{11}^2-\rho_\Lambda^2)\cos\gamma l\sin\gamma l], \end{aligned} \tag{9.21}$$

where ρ_A, γ and l are the characteristic impedance, propagation constant and length of the transmission line segment respectively (Figure 9.18).

Knowing the input impedance of a quadrupole, Z, we calculate the reflection factor $\Gamma(\theta, \phi)$ from formula (9.18), where this factor determines the conditions in the quadrupole transmission line as a function of the scan angle. The remarks made for a dipole element of an array also apply to the calculation of the quantities Z_{uv} and Z.

The design calculations for a printed circuit dipole array are carried out using the procedure indicated in Chapter 2. The design of a dipole and a quadrupole as elements of an array with a selected cell size for the array, consists in choosing prined circuit dipoles at the resonant length (see §9.6) and the quadrupole dimensions, with the subsequent calculation of the input impedances using formulas (9.17) and (9.21) respectively, as well as the reflection factor Γ in the transmission line using formula (9.18). The array gain can be determined based on Γ (see Chapter 2). If the gain is less than the requisite value, the design calculations are performed for other array dimensions.

The study of dipole arrays has shown that the size of an array cell is one of the major parameters governing the input impedance of a dipole. Cell dimensions should be chosen somewhat less than follows from the condition for the lack of additional main lobes in the directional pattern. This makes it possible to match the input impedances of the dipoles in the array in a wider scan sector. Moreover, an important parameter is the spacing of the array dipoles, h, from the shield. It has been determined that one can select a value of h such that the dipole mismatching in the scan sector is the same in the E and H planes. In this case, the maximum value of the SWR in the transmission line is minimized and the best matching results are obtained within the scanning sector. The initial value is $h = 0.25\lambda$. As a result of matching, one can obtain a SWR of no more than two in a scan sector of 45°.

9.7. Other Printed Circuit Radiating Systems

Also to be singled out among printed circuit antennas are planar spirals (detailed data on them are given in [03, Vol. 2], as well as other types of antennas, the major difference in which is the manner of excitation. We shall consider a few of them.

Dipoles Systems With In-Phase Excitation. Dipole arrays with in-phase excitation find practical applications. The connection of the dipoles in a quadrupole (see §9.7) makes it possible to produce in-phase apertures, the effective area of which is practically the same as the geometric area of the aperture. For this reason, in composing apertures of different areas, the width of the antenna beam directed along the normal to its surface can change. An example of a quadrupole composed of triangular dipoles is shown in Figure 9.19. Another method of in-phase excitation of dipoles is their series connection to the transmission line, similar to the excitation of a system of resonator type radiators (see §9.4). Series excitation is extremely narrow band.

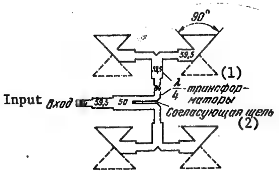

Figure 9.19. An in-phase antenna array of four printed circuit dipoles.

Key: 1. Quarter-wavelength transformers;
2. Matching slot.

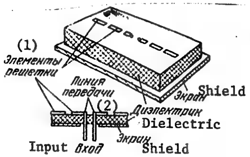

Figure 9.20. A five element dipole array with resonant excitation.

Key: 1. Array elements;
2. Transmission line.

Dipole Systems with Resonance Excitation. Series excitation of dipole systems can also be accomplished by the method realized in a Franklin antenna [02]. In this case, each dipole of the antenna system excites the next dipole so that an in--phase radiating system is formed. An example of the structural design of such an antenna with five dipole elements which are capacitively coupled is shown in Figure 9.40. Planar arrays are put together using the same principle. Radiating systems with resonant exciation are narrow band systems. The direction of the radiation depends on the frequency.

Traveling Wave Radiating Systems. The principles employed in the design of antennas for the long wave band are used in printed circuit radiating systems made in the form of traveling wave antennas [Yagi antennas]. An example of such an antenna (a "sandwich" type) is shown in Figure 9.21. The radiating structure takes the form of zig-zag strip conductor (wave shaped), through which the traveling current wave propagates. The conductor is placed above the conducting shield, which can be replaced by a resonator. The main radiation direction θ_0 is computed from the formula:

$$\sin\theta_0 = \frac{L/\lambda - 1}{d/\lambda},$$

where L is the length of the conductor from point A to point B; d is the period of the structure. For $L/\lambda = 1$, the angle $\theta = 0$, and we obtain a transverse radiation antenna. If $L/\lambda = 2$, then the angle $\theta_0 = 90°$, i.e., the antenna radiates longitudinally.

Slotted Antennas, Excited by a Strip Transmission Line, are used in the same band of frequencies as slotted waveguide antennas. In contrast to the latter, slotted antennas have the advantage that the transmission has practically no dispersion. For this reason, the frequency dependence of the characteristics of these slotted antennas is less than for slotted waveguide antennas. Drawbacks to the slot antennas are the increased requirements placed on the transmission stripline for antennas of great length and the necessity of experimentally working out its dimensions.

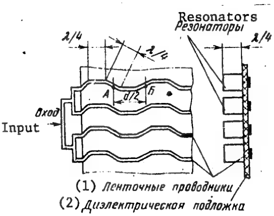
Resonators
Резонаторы
λ/4
λ/4
λ/4
A
d/2
Б
Вход
Input
(1) Ленточные проводники
(2) Диэлектрическая подложка

Figure 9.21. A sandwich type traveling wave antenna array.

Key: 1. Strip conductors;
2. Dielectric substrate.

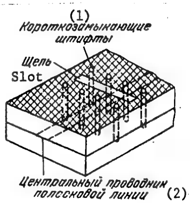
(1)
Короткозамыкающие штифты
Щель
Slot
Центральный проводник полосковой линии
(2)

Figure 9.22. A slot antenna in a symmetrical stripline.

Key: 1. Short circuiting pins;
2. Center conductor of the stripline.

Slot radiators for an antenna are cut in the outer conductor of a balanced stripline. The presence of the slot causes higher modes to appear in the stripline, where a combination of pins is used to suppress these modes (Figure 9.22). The slot length is computed from the formula $l = 0.5\lambda\sqrt{(\varepsilon + 1)}$ [08] and is made more precise

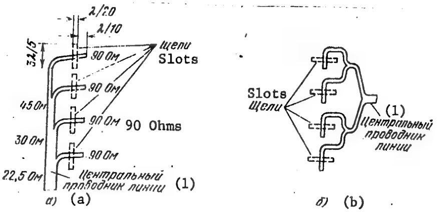
λ/20
λ/10
3λ/5
щели
Slots
90 Ом
90 Ом
90 Ом
90 Ohms
90 Ом
45 Ом
30 Ом
22,5 Ом
Центральный проводник линии
(1)
а) (a)
Slots
Щели
(1)
Центральный проводник линии
б) (b)

Figure 9.23. Excitation configurations for a multislot antenna using a three-plate symmetrical stripline.

Key: 1. Center conductor of the stripline.

experimentally. The coupling of the slot to the transmission stripline is adjusted by shifting the slot relative to the center conductor of the line.

Two excitation circuits, which are shown in Figure 9.23, are used for comparatively small slot arrays. The circuit which realizes series excitation of the slot is shown in Figure 9.23a. The dimensions indicated in the schematic were worked out experimentally. The circuit which provides for excitation of the slots with identical electrical paths is shown in Figure 9.23b. In long arrays, the slots are excited by traveling waves in the feed line. It is also possible to have slot excitation in a standing wave mode. The directional characteristics of slot arrays are determined just as for slotted waveguide antennas (see Chapter 5).

A slot antenna excited by a stripline is convenient for frequency scanning. To increase the phase difference between adjacent slots with a change in frequency, one can place devices in the stripline which increase its electrical length, in particular, employ a zigzag center conductor for the stripline. The electrical length between the slots can amount to several wavelengths. Thus, one can obtain wide angle scanning. A scanning angle of up to 60° has been obtained in the 3-cm band when the frequency is changed by 5%.

10. YAGI RADIATORS FOR PLANAR PHASED ANTENNA ARRAYS

10.1. Phased Arrays of Yagi Radiators

A design procedure is given in this chapter for antenna arrays of radiators in the form of director antennas, or as they are still called, "wave channel" antennas [yagi antennas] [05] (Figure 10.1). The technique is realized in the form of a computer program which makes it possible to calculate the main characteristics and optimal geometric dimensions of the array radiators.

The set of the directors of the antenna array radiators form an interacting structure, which can be treated as a layer of an artificial dielectric, covering the array [08]. By varying the parameters of this dielectric, one can improve the matching of the array radiators to the exciting feedlines in a specified scan sector, which is an important merit of yagi radiators [2]. Such antenna arrays can be used in the traditional meter and decimeter bands for yagi antennas. The development of stripline technology has made it possible to use yagi radiators in the centimeter band.

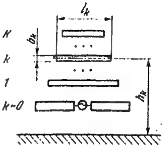

Figure 10.1. Schematic of a yagi radiator.

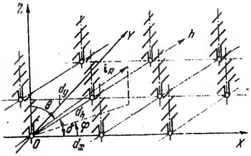

Figure 10.2. The geometry of a phased yagi array.

During antenna array beam scanning, because of the interaction of the radiators, there is a change in the input impedances which leads to their mismatching. Therefore, when designing antenna arrays, it is necessary to assure those geometric dimensions of the radiators, shape and dimensions of a cell in the array [03] and parameters of the radiator input circuit for which the best matching of the radiators of the array to the exciting feedlines is provided in the specified scan sector in the working band of frequencies. Since mismatching during scanning is due to the interaction of the radiators, which occurs only in arrays, the design of a yagi radiator should be based on the analysis of its characteristics as a part of an array of identical elements.

10.2. Analysis of the Electromagnetic Field of a Phased Antenna Array of Yagi Radiators

The properties of an antenna array of yagi radiators (Figure 10.2) can be described most completely by means of solving the electrodynamic boundary problem for Maxwell's equations in the case of boundary conditions for the tangential components of the field vectors at the separation boundary of the different media.

In the case of phased arrays with large dimensions (more than 10 x 10 radiators), the mismatching of the majority of its radiators, located in the central region of the array, can be studied using a simpler model in the form of an infinite antenna array with a uniform amplitude distribution [08].

An infinite planar array is a periodic structure, the study of the electromagnetic field of which can be reduced to the solution of the electrodynamic boundary problem in one cell of the structure [08]. This boundary problem is solved based on the formulation of an integral equation for the currents in the dipoles of a yagi radiator and solving it by the method of moments [2]. As a result, the following expressions are derived for the directional pattern of a radiator in the array when the dipoles are oriented along the y axis (Figure 10.2):

$$F_\varphi(\theta, \varphi) = \cos\varphi I(\gamma, u) \sum_{k=0}^{K} \sum_{m=0}^{M} b_{mk}(\gamma, u) g_{mk}(\gamma, u) \xi_k(\vartheta) \sin \vartheta h_k;$$

$$F_\theta(\theta, \varphi) = \cos\theta \sin\varphi I(\gamma, u) \sum_{k=0}^{K} \sum_{m=1}^{M} b_{mk}(\gamma, u) g_{mk} \xi_k(\vartheta) \sin \vartheta h_k, \tag{10.1}$$

where $b_{mk} = x_{mk} / \sum_{m=1}^{M} I_m x_{m0}$ are the expansion coefficients for the current distribution in the k-th dipole of a yagi radiator for the sinusoidal harmonics of the current:

$$\psi_m^{(k)}(y) = \sin\left[\frac{\pi m}{l_k}\left(\frac{l_k}{2} - y\right)\right], \quad m = 1, 2, \ldots, M$$

(l_k is the length and h_k is the mounting height of the k-th dipole) (Figure 10.1). The quantities x_{mk} are determined from the solution of a system of linear algebraic equations:

$$\sum_{k'=0}^{K} \sum_{m'=1}^{M} x_{m'k'} Z_{m'k'mk}(\gamma, u) = I_m \delta_{k0}, \tag{10.2}$$

where $Z_{m'k'mk}$ are the mutual impedances for the m'-th current harmonic in the k'-th dipole and the m-th current harmonic in the k-th dipole of a radiator when the entire array is excited. Expressions for the mutual impedances are given in [2]:

$$I_m = \begin{cases} (-1)^{(m-1)/2}, & m \text{ нечетное, odd} \\ 0, & m \text{ четное, even} \end{cases}$$

where $\delta_{kk'}$ is Kronecker's delta: $\delta_{kk} = 1$, $\delta_{kk'} = 0$ when $k \neq k'$; $I(\gamma, u)$ is the current in the gap of the active dipole;

$$\gamma = \kappa \sin\theta \cos\varphi; \; u = \kappa \sin\theta \sin\varphi; \; \vartheta = \kappa \cos\theta. \tag{10.3}$$

The directional pattern of a radiator in an array is influenced by the parameters of the equivalent circuit of its input circuit (Figure 10.3). In this circuit, the characteristic impedance of the transmission feedline ρ, the transformation ratio of the ideal transformer n and the reactive component jX are the equivalent parameters of its input four-pole network;

$$Z_{\text{вх}}(\gamma, u) = \sum_{k'=0}^{K} \sum_{m=1}^{M} \sum_{m'=1}^{M} b_{m'k'} b_{m0}^{*} Z_{m'k',m0}(\gamma, u) \tag{10.4}$$

is the input impedance of the active dipole, taking into account the influence of the directors and the adjacent radiators (when the entire array is excited with a uniform amplitude and a linear phase distribution).

This impedance (in contrast to the input impedance of an individually excited radiator) is frequently called the effective input impedance. It follows from the equivalent circuit that the dipole current is:

$$I(\gamma, u) = 2n\sqrt{2\rho}/[Z_{\underset{\text{in}}{\text{вх}}}(\gamma, u) + Z_l], \qquad (10.5)$$

where $Z_l = n^2\rho + jX$.

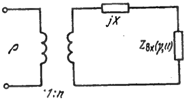

Figure 10.3. The equivalent circuit of a yagi radiator.

It is usually necessary in practice to turn to the experimental alignment of the input circuit for good matching of the radiators, for example, using a waveguide model of the phased array [08], which corresponds to matching of the phased array for radiation in a certain direction θ_0, ϕ_0. It is not difficult to determine from the equivalent circuit that for the condition of matching, the equivalent parameters of the input four-pole network are defined by the expressions:

$$n = \sqrt{\operatorname{Re} Z_{\text{вх}}(\gamma_0, u_0)/\rho}; \quad X = -\operatorname{Im} Z_{\text{вх}}(\gamma_0, u_0), \qquad (10.6)$$

where $\gamma_0 = \kappa \sin\theta_0 \cos\varphi_0$; $u_0 = \kappa \sin\theta_0 \sin\varphi_0$.

For this reason, when calculating the characteristics of phased arrays, it is expedient to assume that the equivalent parameters of the input circuit correspond to (10.6), and when designing the circuit, it is necessary to provide for the selection of its equivalent parameters in accordance with the calculated or measured value of the effective input impedance $Z_{in}(\gamma_0, u_0)$.

Based on the effective input impedance of a radiator, one can determine the effective reflection factor from the radiator input. We have from the equivalent circuit and formulas (10.6):

$$\Gamma_{\text{д}} = \frac{Z_{\text{вх}}(\gamma, u) - Z_{\text{вх}}(\gamma_0, u_0)}{Z_{\text{вх}}(\gamma, u) + Z^{*}_{\text{вх}}(\gamma_0, u_0)}. \qquad (10.7)$$

$[Z_{BX} = Z_{in}]$

Information on a program written in the algorithmic Fortran language which realizes the calculation of the indicated characteristics of a yagi radiator in an array using the BESM-6 computer is given in [1].

10.3. The Characteristics of a Yagi Radiator in a Planar Phased Antenna Array

It is essential to know the number of the current harmonics in the dipoles, M, and the number of spatial Floquet harmonics [08], which must be taken into account when calculating the mutual impedances in (10.2) to obtain satisfactory precision in practice in calculations of the characteristics of a radiator in an array. Computations show that for a dipole length of 0.2 to 0.7 λ, to assure a precision of 0.5 to 1% it is sufficient to retain three to five harmonics when calculating the E-plane directional pattern and one to three harmonics when calculating the H-plane directional pattern. In this case, the requisite number of Floquet spatial harmonics amounts 60--100 [2]. A slightly greater error, running up to a few percent, will be observed in this case in a narrow region of sharp resonance changes in the directional pattern. To illustrate the convergence of the solution, the directional patterns of a yagi radiator in an array are shown in Figure 10.4a in the E-plane where the different numbers of current harmonics considered are M = 1, 3, 5.

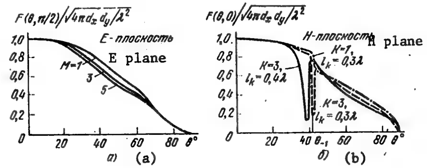

Figure 10.4. The directional pattern of a yagi radiator in an array with a rectangular grid.

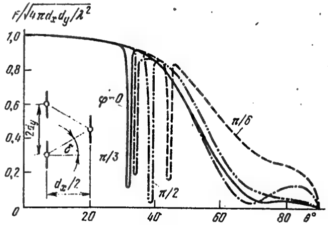

Figure 10.5. The directional pattern of a yagi radiator in an array with a triangular grid.

An important feature of a yagi radiator is the possible presence of sharp resonance "dips" of a finite depth in its directional pattern in the H-plane (and in other close planes where $|\phi| \leq 30$--$45°$) (Figure 10.4b). In particular, in an array with a rectangular grid, a dip occurs in the H-plane in directions close to the angle θ, $\theta_{-1} = \arcsin(\lambda/d_x - 1)$ on the part of the smaller values. The angle θ_{-1} is frequently called the "grazing" diffraction lobe occurrence angle. In the general case, the directions of the dips are also close to the directions of the "grazing" diffraction lobes, which are determined from the equation:

$$\left(\sin\theta\cos\varphi + \frac{\lambda}{d_x}p\right)^2 + \left(\sin\theta\sin\varphi + \frac{\lambda}{d_y}q - \frac{\lambda}{d_x}p\operatorname{ctg}\delta\right)^2 = 1, \qquad (10.8)$$

where p, q = 0, ± 1 are the numbers of the diffraction lobes ($p^2 + q^2 \neq 0$). The dip in the directional pattern of a yagi radiator is due to the retarding properties of the aggregate of array directors where the dipole length is less than resonant (about $\lambda/2$) [3]. If the retarding interacting director structure is treated as a layer of an artificial dielectric [07], then as follows from a comparison with an array covered with a dielectric plate [08, 09], the existence of a dip is to be anticipated if the retardation of the yagi structure is sufficiently great. The greater this retardation and the coating thickness, the closer the dip should be shifted to the transverse direction to the array. This shift actually occurs when the retardation increases in a director structure, in particular, with a reduction in the spacing between the directors and with an increase in their length (but no greater than the resonance length) [3], and amounts to a few degrees (Figure 10.4b).

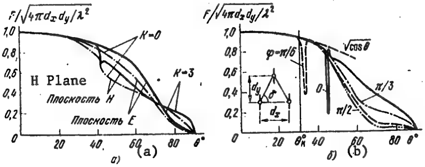

Figure 10.6. The directional pattern of an optimized yagi radiator in an array.

a. Rectangular grid:

b. Triangular grid:

Since the analogy with the case of an array covered with a dielectric layer is not complete, there can also be no dip in the directional pattern of a yagi radiator at certain values of the radiator parameters (for K = 1 in Figure 10.4b). In this case, there is a sharp rolloff in the directional pattern at angles of $\theta > \theta_{-1}$.

Since with an increase in the wavelength, the direction of a dip moves away from the transverse direction to the array, then the array step in the H-plane, d_x, is to be chosen from the condition for single beam scanning at the upper working frequency in an angular sector which exceeds the specified scan sector by the width of the dip region in the directional pattern of a radiator in the array.

By virtue of the fact that dipoles do not radiate along their own axis, a dip does not occur in the directional pattern of a radiator, as a rule, in the E-plane and in planes close to it ($|\phi| = \pi/2$) (Figure 10.4a). Since the directional pattern of a yagi radiator in the E-plane is of a smooth monotonic nature and takes on small values at angles of θ close to 90°, then the spacing between radiators in the E-plane, d_y, can be chosen somewhat greater than the value which follows from the condition for single beam scanning. The step d_y is chosen depending on the permissible decrease in the gain at the edge of the scan sector and the permissible diffraction lobe level at the highest frequency.

Arrays with a triangular grid and the dipoles oriented along one of the sides of a triangular cell are an exception. In this case, a dip also occurs in the E-plane (Figure 10.5). For this reason, the use of such a grid is not expedient in a number of cases. A grid with an orthogonal orientation of the dipoles is preferable, in which there is no dip in the E-plane (Figure 10.6b).

However, it must be remembered that all of the directional patterns cited here belong to an infinite array.

The finite dimensions of an actual antenna array has an impact first of all on the directional pattern of a radiator in the region of the dip. The finite nature of a phased array is not felt if the dimensions of an array are so great that the beam width does not exceed the region of the dip. With a decrease in array dimensions, the depth of the dip will fall off, while its width will increase in proportion to the beam width of the array. With a further reduction in antenna dimensions, the dip completely disappears. In this case, a model in the form of an infinite array can be considered justified only for directions falling outside the region of the dip in an infinite antenna array.

10.4. The Optimization of a Yagi Radiator in an Array

We shall now consider questions of designing the geometry of a yagi radiator: the choice of the number of directors, the length, the mounting height, etc. The existence of a program for calculating radiator characteristics on a computer makes it possible to automate this portion of the design work to a certain extent. The mathematical tools for this are numerical optimization techniques [4]. Where these techniques are used, by working from the requirements placed on the antenna array characteristics, a so-called quality indicator is put together, which depends on the radiator parameters. Numerical optimization algorithms provide for searching out the optimal values of the parameters which attain the extremal value of the quality indicator.

The average array gain in the scanning sector can frequently be chosen as the quality indicator for the phased array, which by virtue of (2.13), is proportional to the quantity:

$$f = \iint\limits_{\Omega_{\text{ск scan}}} |F(\theta, \varphi)|^2 \sin\theta \, d\theta \, d\varphi, \qquad (10.9)$$

where Ω_{CK} is the scan sector.

The optimization of a yagi radiator based on this quality indicator is carried out in accordance with the program of [1]. Computation of the double integral of (10.9) in the program is replaced by summing using Gauss' formula ($n = 4$) for the inner integral with respect to θ and using the rectangle formula for the outside integral with respect to ϕ. Since the range of variation in the radiator parameters is limited: the spacing between the dipoles is always greater than their width, the length of the dipoles is always positive, etc., it is necessary to employ optimization techniques with limitations [4]. Since the quality indicator (10.9) is always positive, one can employ the following variant of the external penalty function technique: set $f = 0$ outside the range of permissible values of the parameters. To find the extremum of the resulting function f, defined in an unlimited range of values of the arguments, the method of local variations is employed in the program [4].

The major parameters which characterize the properties of the yagi structure (Figure 10.1) are taken as the parameters to be optimized in the program. These are the mounting height for the layer of directors h_1, the spacing between the dipoles $\Delta h = h_{k+1} - h_k$ ($k = 1, 2, \dots K - 1$) which is assumed to be constant, the length of the first director $_1$ and the shortening of the directors Δ = $_{k+1} - {}_k$ ($k = 1, 2, \dots K - 1$), which is also taken to be constant. As a result of this, the number of variables is curtailed so much that it is now possible to optimize a radiator in a comparatively small amount of machine time. In this case, the following approach to the design of a yagi radiator can be proposed. The optimization with respect to the selected main parameters is carried out in a first approximation ($M = 1$) in the first stage. Then, treating the resulting geometry of a radiator as the starting point, a more precise selection of these parameters is made for $M = 3 \dots 5$. In the third stage, the radiator can be optimized with respect to the remaining parameters, for example, one can choose the best θ_0, ϕ_0 matching direction. Such an approach to the solution makes it possible to choose parameters for a yagi radiator, expending no more than a few hours of BESM-6 computer time on each step. Results of calculations show that even after the first optimization step, sufficiently good matching of the radiator to space is achieved, so that the subsequent steps may prove to be superfluous.

Since a quality indicator usually has several local extrema, the choice of the starting point for the optimization program is of considerable importance. Calculations show that such parameters as the mounting height h_1 and the length of the first dipole l_1, can be arbitrarily chosen in a range of $h_1 = 0.25$--$0.4\ \lambda$ and $l_1 = 0.3$--$0.4\ \lambda$. At the same time, depending on the choice of the initial values of the parameters Δh and Δl, one can obtain different "optimal" values of the parameters. For this reason, it is necessary to take somewhat different starting sets of values for Δh and Δl. Usually, these quantities fall in a range of $\Delta h = 0.1$--$0.35\ \lambda$ and $\Delta l = -0.05$--$0.15\ \lambda$. The initial direction for the matching can be arbitrary, just so the condition $\theta_0 < \theta_{-1}$ is met, for example, $\theta_0 = 0$. Experience with the calculations shows that the number of directors in a radiator is expediently chosen larger than $K = 2$--3.

The directional patterns of an optimized yagi radiator with three directors in a scan sector of ± 40° in the H-plane and ± 60° in the E-plane are shown in Figure 10.6a for a rectangular grid with steps of $d_x = 0.6\ \lambda$ and $d_y = 0.54\ \lambda$.

The directional patterns of a dipole radiator (K = 0) are also shown in this same figure for comparison. As can be seen from these curves, the reduction in the gain of the array for optimized radiators as compared to the maximum possible value amounts to 0.3 dB overall in the scan sector. This is considerably less than for an array of radiators consisting only of one active dipole (K = 0).

Better matching to space in the main planes can be achieved in an antenna array with a triangular grid for the configuration of the radiators, since in this case, the dip in the directional pattern of a radiator in the H-plane is removed considerably from the transverse direction. However, the dip in the plane $|\phi| = 30°$ is brought closer to the direction of the normal in this case. The directional patterns of an optimized yagi radiator in an array with an equilateral triangular grid for a specified scan sector of $|\theta| \leq 32°$ and array steps of $d_x = 0.7453\ \lambda$ and $d_y = 0.6415\ \lambda$ are shown in Figure 10.6b. As can be seen, practically ideal matching of the phased array in the single beam sector is achieved, with the exception of a narrow dip region.

It must be noted that the quality indicator in the cases cited here has yet another maximum at $\Delta h = 0.03$--$0.05\ \lambda$ and $\Delta 1 = -0.05$--$-0.06\ \lambda$, which corresponds to a more compact structural design of the yagi radiator. However, the maximum gain losses of the phased array in this case because of mismatching amount to about 0.5 dB.

The calculation of the characteristics of optimized radiators in a band of frequencies shows that an array matched to space at the high frequency remains well matched with a reduction of 20% and more in the frequency, given the condition that the parameters of the input circuit conform to (10.6).

10.5. Designing the Input Circuit of a Yagi Radiator

The conditions for matching the radiators of an array during scanning in a chosen direction θ_0, ϕ_0 (10.6) mean that the input circuit accomplishes the matching of the characteristic impedance of the transmission line ρ to the impedance of the load $Z_{in}(\gamma_0, u_0)$ in a specified frequency band. Such an input circuit is designed using the methods of microwave network theory.

We shall consider the procedure for designing the simplest input circuit. The structural design of a linear array of yagi radiators for the centimeter band using striplines is shown in Figure 10.7a [6]. In this figure: 1 are the directors of the radiator; 2 is the active dipole; 3-5 are the balancing device elements for the excitation of the dipole; 6 is the exciting stripline radiator; 7 is a phase shifter; 8 is a directional coupler; 9 is the matched load for the free arm of the coupler; 10 is the distribution stripline exciting the phased array; 11 is the dielectric substrate. The dashed lines show the configuration of the conductors on the back side of the substrate.

The strip transmission line section 4 is a quarter-wave transformer [06] which matches the load impedance connected to the balancing device in the active dipole gap to the characteristic impedance of exciting line 6. The short circuited loop 5 using a slotted transmission line provides for symmetrical excitation of the dipole. At the center frequency, its length is $= \lambda_5/4$, where λ_5 is the wavelength in the slotted line. In the case of a purely resistive load, the length of an open-circuited section of stripline 3 is also equal to $\lambda_4/4$ (λ_4 is the wavelength in the stripline). In the general case, the length l_3 is chosen from the condition for the compensation of the reactive component of the input impedance of the radiator:

$$\operatorname{ctg}(2\pi l_3/\lambda_3) = X_{\text{вх}}(\gamma_0, u_0)/\rho_3. \qquad (10.10)$$

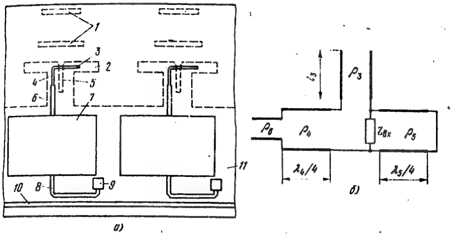

Figure 10.7. The structural design of a linear stripline array of yagi radiators (a) and the equivalent circuit of the exciter (b).

The characteristic impedance of the quarter-wave transformer $\rho_4 = \rho_3$ is determined by the values of the impedances being matched [06]:

$$\rho_4 = \sqrt{R_{\text{вх}}(\gamma_0, u_0)\,\rho_6}. \qquad (10.11)$$

The calculation of the wavelength in stripline and slotted line, as well as the calculation of the geometric dimensions of the lines based on a specified value of the characteristic impedance can be carried out using the techniques given in [5].

Since the input circuit configuration cited here can provide for only narrow band matching of the radiator to the transmission line, the entire calculation is carried out at the center frequency. The passband of such a radiator amounts to a few percent. Since the methods of calculating the input circuitry are rather approximate, while the mathematical model for the yagi array considered here is idealized, the results obtained from calculating the parameters of the input network require an experimental improvement in the precision. As has already been noted, this is conveniently done using a waveguide model of the phased array, which simulates the radiation in the direction θ_0, ϕ_0.

If the requisite passband of a radiator is more than 10%, then a more complex microwave network is to be used instead of the quarter-wave transformer (4), where broadband matching techniques must be used for the design of this network [7].

10.6. A Design Procedure for a Yagi Radiator for Phased Antenna Arrays

Various sets of initial data are possible for the design of a yagi radiator. Typical is the specification of the scan sector, the permissible reduction in the gain during scanning and the permissible level of the sidelobes of the phased array. The parameters of a unit cell in the array d_x, d_y and γ can be chosen based on these initial data (see Chapter 2). In particular, with a rectangular grid for the layout of the radiators, the steps are chosen in accordance with the specified scan sector using formula (2.3), and in the case of a triangular grid, using formula (2.4).

The mounting height of the active dipole, h_0, is ordinarily chosen equal 0.2--0.25 λ and the length l_0 = 0.45--0.5 λ. The thickness of the dipoles is chosen in a range of 0.02 to 0.05 λ and the matching direction $\theta_0 < \theta_{-1}$. The number of directors of a radiator is chosen as K = 1 and the initial values of the radiator parameters being varied, l_1 and h_1 are chosen in accordance with the recommendations given in § 10.4; the initial optimization of the radiator parameters is accomplished on a computer for the case where M = 1. It is necessary for the optimization program to specify the precision in the determination of the extremum and the error in the determination of the optimal dimensions of the dipoles. It is usually sufficient to take the former as 0.005 - 0.01, and the precision in the determination of the geometric dimensions as 0.005 - 0.01 λ. The optimization results are evaluated in the sense of attaining the specified radiator characteristics. The array steps are made more precise in accordance with the recommendations given in § 10.3. In particular, the array step can be slightly increased in the E-plane, given the condition of assuring a specified gain and diffraction lobe level. Where necessary, the number of directors is increased and the the initial value of the parameters Δl and Δh is specified (see § 10.4). The optimal dimensions of an array cell and the radiators are found as a result of several trial and error calculations, which are then made more precise using optimization programs where M = 3--5.

Based on the value of the input impedance $Z_{in}(\gamma_0, u_0)$ obtained with the computer, the input network is designed and the structural design of the antenna array is worked out.

The calculation of the directional pattern characteristics of the antenna array is then carried out on the whole in accordance with the general procedure (see Chapter 2).

11. APPROXIMATE DESIGN CALCULATIONS FOR PHASED WAVEGUIDE ANTENNA ARRAYS TAKING MUTUAL COUPLING INTO ACCOUNT

11.1. General Considerations

The open ends of waveguides are the most widespread radiators for antenna arrays in the centimeter band. Various modifications of waveguide radiators, realized by means of dielectric inserts, stops and other devices, are described in Chapter 12. A design procedure for phased array geometry is given in § 2.12 without taking mutual coupling into account. The results of such design calculations can be used as the initial approximation in drawing up the mathematical model of a phased array, in which the interaction between radiators, edge effect, excitation circuit configuration, etc. should be taken into account in the general case.

An approximate design procedure for phased arrays is proposed in this chapter using graphs, calculated taking mutual coupling into effect. The graphs are plotted for planar waveguide arrays with a rectangular grid for the arrangement of the radiators in the case of small cross-sections of the waveguide radiators and small thickness of their walls. In such arrays, the mutual coupling is due primarily to the dominant mode, however, the majority of the graphs in this chapter were plotted taking into account the existence of higher modes also. Thus, the material of this chapter makes it possible to improve on the precision of the design procedure adopted in Chapter 2.

11.2. Design Graphs

The concept of the gain of an element in an array was introduced in Chapter 2 (formula (2.16)). The power transmission gain of $1 - \Gamma^2(\theta, \phi)$, incorporated in (2.16) is a function of the position of the main lobe of the directional pattern (θ_{max}, ϕ_{max}), since as is well known, the input admittance of the radiators and the reflection factor $\Gamma(\theta, \phi)$ change during the scanning process.

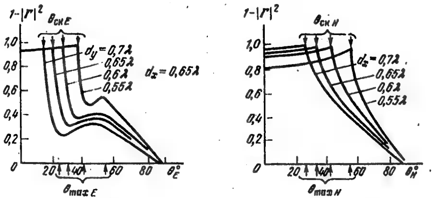

а) (a) б) (b)

Figure 11.1. The power transmission gain in the case of E-plane (a) and H-plane (b) scanning for various spacings between the array radiators.

Curves are plotted in Figure 11.1 which characterize the change in the power transmission gain during scanning in the E and H-planes for an infinite waveguide array with a rectangular grid for the radiator layout with various spacings d_x and d_y between the radiators (see Figure 2.1) [1]. The curves in the E-plane were obtained experimentally; they were calculated for the H-plane assuming infinitely thin walls ($a = d_x$ and $b = d_y$). The arrows on the abscissa indicate the values of the angles θ_{max}, which when the main lobe deviates by these amounts, a grazing (at an angle of 90°) diffraction maximum appears. Corresponding to each spacing between the radiators (d_x or d_y), as is well known, is its own value of θ_{max}. With the deflection of the main lobe through an angle approximately equal to θ_{max}, a sharp mismatching of the radiators to the feeders is observed, the reflection increases while the power transmission gain falls off. The sharp drop in the power transmission gain limits the scan sector θ_{scan}. In the case of E-plane scanning, the permissible scan sector is less than the ultimate angle θ_{maxE}:

$$\theta_{scan\ E} = 0.7\theta_{maxE} \qquad \theta_{\text{сн}E} \simeq 0{,}7\theta_{maxE}. \tag{11.1}$$

When scanning in the H-plane, $\theta_{max\ H}$ practically coincides with the angle $\theta_{scan\ H}$.

When taking only dominant mode mutual coupling into account, the reflection factor changes monotonically within the bounds of the scan sector θ_{scan}.

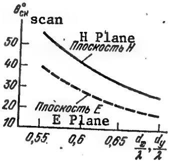

Figure 11.2. The permissible scan sector as a function of the spacing between array radiators.

The maximum permissible beam deflection angles $\theta_{scan\ H}$ and $\theta_{scan\ E}$ is shown in Figure 11.2 as a function of the spacing between the array radiators for the dominant mode.

The reflection factor can be determined as a function of the aperture dimensions of the radiators and the spacings between them taking mutual coupling via higher modes into account using the results found in the literature [08]. Also studied there is the reflection factor as a function of the waveguide wall thickness t in an infinite array. It is shown that changing the thickness of the waveguide walls with a constant spacing between waveguides has no impact on the position of the minimum gain in the scan sector which is due to the considerable mismatching at the moment of the appearance of the highest, the first maximum in the array factor; on the other hand, changing the thickness of the walls has a substantial influence on the absolute value of the reflection factor.

The change in the absolute value and phase of the reflection factor in the E and H-planes for various thicknesses of the waveguide walls is shown in Figures 11.3 and 11.4 by way of example. In accordance with these figures, as well as based on similar curves available in the literature [08] for other array dimensions, one can plot generalizing graphs for the maximum possible reflection factor in the scan sector as a function of the dimensions of one radiator, a and b, for the case of a constant spacing between radiators (Figure 11.5). One can draw the following conclusions based on what has been presented.

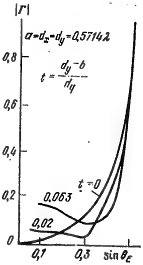

Figure 11.3. The absolute value of the reflection factor for E-plane scanning as a function of waveguide wall thickness.

1. The maximum value of the absolute value of the reflection factor occurs with radiation along a normal when scanning in the H-plane in a planar array of rectangular smooth waveguides with a small cross-section, which are placed at the junction nodes of a rectangular grid. The absolute value of the reflection factor $|\Gamma|$ is greater, the smaller the radiator aperture a for a constant d_x, or what is the same thing, the thicker the waveguide wall.

Using the curves of Figure 11.5b, one can approximate the absolute value of the reflection factor for the case of radiation along the normal based on the selected spacing between the radiators d_x/λ and the aperture dimensions of a single radiator.

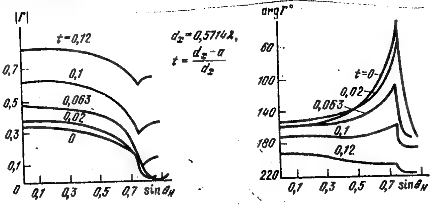

Figure 11.4. The absolute value of Γ and the phase, argΓ, of the reflection factor for the case of H-plane scanning as a function of waveguide wall thickness.

2. In the case of E-plane scanning, the reflection factor function is more comples. Its absolute value in the case of radiation along the normal depends not only on b and d_y, but also on the a and d_x dimensions of the array in the H-plane. When the main lobe of the direction pattern is deflected from the normal, $|\Gamma|$ initially falls off to a certain minimum value, and then rises rather sharply. Corresponding to each waveguide wall thickness is its own main lobe deflection angle for which $|\Gamma|$ is minimal. The maximum value of $|\Gamma|_{max}$

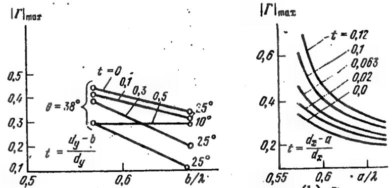

(a) а) (b) б)

Figure 11.5. The maximum reflection factor of a radiating waveguide for various wall thicknesses in the case of E-plane (a) and H-plane (b) scanning.

(Figure 11.5a) is obtained in the majority of cases at the edge of the scan sector (thus, for example, for $b/\lambda = 0.5714$ when $\theta = 38°$ and $b/\lambda = 0.6724$ when $\theta = 25°$, where the angles 38° and 25° bound the scan sector for the corresponding array dimensions), and $|\Gamma|$ rises considerably outside the bounds of the scan sector.

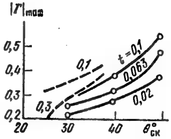

Figure 11.6. The maximum reflection factor as a function of the selected scan sector, θ_{CK} [θ_{scan}] in the H-plane (solid curves) and E-plane (dashed curves).

The graphs of Figure 11.5a were plotted with respect to two points, and can therefore be used only in rough calculations. The resulting graph (Figure 11.6) was plotted based on the curves of Figure 11.5, which shows what maximum mismatch can be anticipated in an array when scanning throughout the entire permissible sector θ_{scan} in the E and H-planes.

The maximum permissible mismatching in the exciting waveguides $|\Gamma_{max}|$ may be stipulated in the technical specifications when designing the antenna array. Then the permissible scan sector will be limited by the specified value of $|\Gamma|_{max}$ and can be determined for the waveguide array without the matching devices using the graph of Figure 11.6. As can be seen from Figure 11.6, the reflection factor cannot be less than 0.2 for any wall thickness or dimensions of the waveguide aperture when scanning in a sector of more than 30°.

If the requisite values of the maximum permissible reflection factor and scan sector are not assured, then a provision should be made for matching the radiators to the exciting waveguides. Impedance transformers, dielectric inserts inside the waveguides and dielectric coatings in the antenna aperture can be employed [illegible] the matching devices. The presence of a dielectric can substantially improve the matching thoughout the entire scan sector, but at the same time, it leads to the appearance of anomalous nulls in the gain.

Questions of matching waveguide radiators in scanning arrays are treated in detail in Chapter 12.

The graphs shown in Figures 11.2--11.6 can be successfully used to determine the reflection factor in waveguide phased arrays where the waveguide wall thickness is small and where their cross-section dimensions satisfy the conditions:

$$a < 0{,}75\lambda;\quad b < 0{,}5\lambda. \tag{11.2}$$

In this case, the interaction of higher modes changes the reflection factor by no more than 10% as compared to the value calculated when taking only the dominant mode into account.

The direct method of determining the reflection factor $\Gamma(\theta, \phi)$, taking mutual coupling via higher modes into account for any array structure, consists in the following. By treating a large multielement phased array as a infinite periodic structure, the field in the exterior region (where $z \geq 0$) can be broken down in terms of the spatial harmonics of this structure. The field in the interior region (where $z \leq 0$) can be represented in the form of the superposition of the dominant mode and higher modes, of which only the H_{10} mode may propagate through the waveguide [3 - 5].

The condition of field equality at the boundary of the internal and external regions (when $z = 0$) leads to an integral Fredholm equation of the first (or second) kind. For the numerical solution of a Fredholm equation, it is necessary to make a transition from the integral equation to a system of linear algebraic equations, by selecting the appropriate system of base functions. In the case of a waveguide phased array, it is convenient to take the set of modes in the waveguide as the base functions. Only a limited number of modes in the waveguide and spatial harmonics in the external space, needed to obtain a good approximation, are used in the calculations. The computational program, compiled using the algorithm described here, is given in Chapter 12.

11.3. Design Recommendations

1. When designing phased waveguide arrays, it must be kept in mind that mutual coupling of the radiators can have a substantial impact on their matching to the exciting waveguides and on the antenna gain in the scan sector.

2. The geometric dimensions of the array and its elements can be roughly determined without taking mutual coupling into account using the formulas given in Chapter 2.

The initial values for the design calculations are the width of the main lobe of the directional pattern, the level of the first sidelobe, the scan sectors $\theta_{\text{scan E}}$ and $\theta_{\text{scan H}}$, the permissible reflection factor $|\Gamma|_{\max}$ and the permissible nonuniformity in the antenna gain within the scan sector. In accordance with the design procedure recommended in § 2.12, the overall dimensions of the array L_x and L_y are determined, as well as the amplitude distribution (see Table 2.1) and the spacing between the radiators and the number of them.

The results obtained are to be treated only as an initial approximation.

3. Taking the mutual coupling of the radiators in the array into account makes it possible to specify its dimensions more precisely. In particular, the spacing between the radiators is to be chosen from the graphs of Figure 11.2, taking into account the fact that in the E-plane, the angle $\theta_{max\ E}$ included in formulas (2.3)--(2.6) must be determined using formula (11.1). Increasing the spacing between the radiators to a value greater than the design figure is not permissible, since this leads to the appearance of a dip in the gain within the scan sector. Reducing the spacing between the radiators as compared to the calculated value is not expedient in the majority of cases, since this leads to an increase in the reflection factor $|\Gamma_{max}|$ when scanning in the H-plane, although $|\Gamma|_{max}$ [sic] decreases slightly in the case of E-plane scanning. Moreover, with a decrease in the spacing between the radiators, it is necessary to increase the overall number of them in the array to maintain the previous overall dimensions L_x and L_y.

The anticipated maximum value of the absolute value of the reflection factor in a given scan sector can be roughly determined from the curves of Figure 11.6. If $|\Gamma|_{max}$ exceeds the reflection factor permitted by the operational conditions of the entire antenna and feed system, then the scan sector should be reduced or provisions should be made for matching devices in the structural design of the radiators.

4. The maximum aperture size of a single radiator is determined by the permissible spacing between the radiators in the array; the minimum size $a_{min} > \lambda/2$ is limited by the propagation conditions of the H_{10} mode. Moreover, it is necessary to keep the following in mind when selecting the dimensions of the aperture of a radiator. With a decrease in the dimensions a and b, the reflection factor $|\Gamma|_{max}$ increases. The value of $|\Gamma|_{max}$ can be estimated by means of Figure 11.5. On the other hand, an increase in the a and b dimensions can lead to the appearance of anomalous nulls in the scan sector [3]. If the aperture dimensions do not exceed those recommended by the conditions of § 11.2, then anomalous nulls will not appear in the entire sector of ± 90°; if the indicated conditions are not met, then it is necessary to completely calculated the input admittances and reflection factors.

5. The recommended procedure, which was drawn up based on the results of analyzing infinite arrays, can also be used to choose all of the dimensions of sufficient large finite arrays. This is justified by the fact that the directions in which there are dips in the gain do not depend on the overall dimensions of the array. However, with a decrease in the array dimensions, a dip becomes wider (occupies a greater angle) while its depth decreases. If it is assumed that the edge effect is manifest in five radiators on each side of the array, then arrays where the number of radiators is more than a thousand may be considered large.

6. The electrical parameters of a phased array can be calculated after its geometric dimensions have been selected.

To precisely determine such antenna parameters as the directional pattern, gain and reflection factor, it is necessary to obtain a complete solution of the problem, i.e., find the input admittances of all the radiators (the central and edge ones) as well as the amplitude-phase distribution of the fields in the aperture. This calculation is extremely cumbersome and requires the use of high speed computers.

The electrical parameters of antennas are approximately estimated as follows.

The normalized curves for the change in the gain

$$g/g_{\max}=\cos\theta\,[1-\Gamma^2(\theta,\varphi)] \tag{11.3}$$

(see (2.16)) for various values of d_x/λ approxmately match each other up to angles at which diffraction maxima appear, and within this range of angles, are well approximated by the function:

$$f(\theta_H)=(\cos\theta_H+\sqrt{\cos\theta_H})/2. \tag{11.4}$$

The gain along the normal is determined with respect to the width of the main lobe of the directional patterns in the two planes $2\theta_H$ and $2\theta_E$:

$$G_{\max}=33\,000\eta/(2\theta_H\cdot 2\theta_E), \tag{11.5}$$

(where η is the efficiency of the array), or based on the radiating surface of the array:

$$G_{\max}=2\pi L_x L_y \nu\eta/\lambda^2, \tag{11.6}$$

where ν is the surface utilization factor for the array, which depends on the amplitude distribution in the array.

The directional pattern is approximately calculated from the formulas for a continuous radiating aperture as a function of the amplitude distribution of the field in the aperture (see Table 2.1).

Mutual coupling of the radiators somewhat changes the structure of the sidelobes of the directional pattern, which in this case, cannot be described by a sufficiently simple analytical expression.

7. The procedure considered here can be used for the approximate design of phased antenna arrays. It yields more precise results than calculations without considering mutual coupling of the radiators using the formulas of Chapter 2. Using this same procedure, the initial approximation can be calculated when constructing an algorithm for the more precise computer design of phased antenna arrays.

12. WIDE ANGLE MATCHING OF THE WAVEGUIDE RADIATORS OF PLANAR PHASED ANTENNA ARRAYS

In a multi-element planar phased array, the radiators, in the form of open ends of rectangular waveguides, are placed at the intersection points of a generalized triangular coordinate grid (Figure 12.1). The following symbols are used in the figure: a and b are the waveguide dimensions; a' and b' are the dimensions of the window of a stop, placed in the radiator aperture; d_x and d_y are the spacings between the rows of radiators in an array along the X and Y axes respectively; α is an angle which defines the mutual arrangement of the rows of radiators in the array. In particular, when α = 90°, we obtain a rectangular grid and when α = 60°, a hexagonal grid.

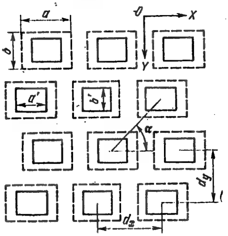

Figure 12.1. The layout of radiators in an array with a generalized triangular grid.

The end goal of designing the radiating element of a phased array is the wide angle matching of the radiator, i.e., finding those geometric dimensions of the array and characteristics of the matching devices for which the maximum reflection factor in the feeders does not exceed a certain specified value within the scan sector.

The most effective method of designing waveguide radiators for phased arrays, matched in a wide range of angles, is a technique based on the calculation of the radiator characteristics taking into account the matching devices both within the feeder elements and outside of them, with the subsequent variation of the parameters in the problem of designing phased arrays until obtaining the requisite results [013]. The time and cost for the development of multi-element phased arrays with this method are significantly curtailed as compared to methods based on the experimental development of the radiators. The utilization of this method presupposes the presence of computer programs with which one can calculate the characteristics of a radiator based on the solution of the corresponding electrodynamic problem for a waveguide array with the matching devices for subsequent system optimization.

12.1. Methods of Matching Waveguide Radiators in Planar Phased Antenna Arrays

We shall treat the most widespread methods of matching the radiators of planar waveguide phased arrays.

The Utilization of Dielectrics [08]. The use of dielectrics in antenna arrays leads to the appearance of additional parameters in the design problem. The presence of dielectric elements exerts a substantial influence on the distribution of the fields in the waveguide apertures. For this reason, the choice of the parameters of dielectric elements such as the dielectric permittivity and the thickness of the dielectric has a strong influence on the characteristics of an antenna array.

For optimal matching, the choice of the parameters in an antenna array with dielectrics is best of all accomplished using the method of parameter variation. In this case, all of the parameters, with the exception of one, are fixed and the calculations are performed while changing this parameter in a specified range. The method of parameter variation is most effectively realized in a "man--computer" system, which makes it possible to narrow the range of values of several parameters.

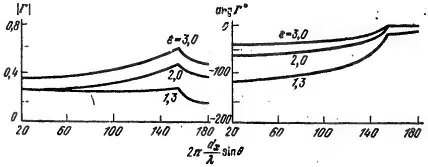

Figure 12.2. The absolute value and the phase of the reflection factor as a function of the scan angle in the H-plane for an array of waveguides completely filled with a dielectric (d_x = 0.5714 λ; a = 0.5354 λ).

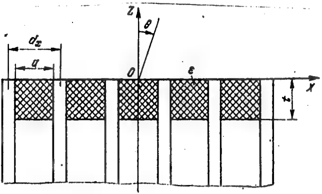

Figure 12.3. A phased waveguide array with dielectric inserts.

We shall consider some design data to illustrate the influence of dielectrics on antenna array characteristics.

Typical results are given in Figure 12.2 for a waveguide array in the case of H-plane scanning when the waveguides are filled with a dielectric. We will note that the absolute value |Γ| and the phase arg Γ of the reflection factor change little with a change in the scan angle, which makes it possible to have good matching of the antenna array in a wide range of angles (at least at one frequency), even in those cases where considerable reflection is present. The break in the curves considered here is due to the occurrence of a diffraction beam.

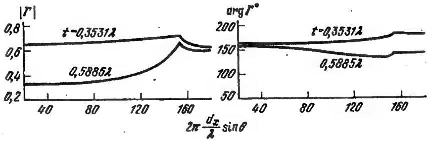

Figure 12.4. The absolute value and phase of the reflection factor as a function of the H-plane scan angle for an array of waveguides with dielectric inserts ($\varepsilon = 2$; $d_x = 0.5714\ \lambda$; $a = 0.5354\ \lambda$).

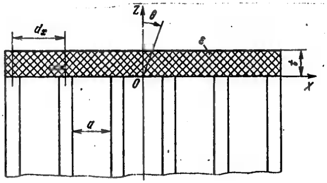

Figure 12.5. A phased waveguide antenna array with a dielectric coating.

In the case where the antenna array waveguides have dielectric inserts (Figure 12.3), an additional air--dielectric separation boundary appears. In this case, to control the characteristics of the radiators, two new parameters are added: the dielectric permittivity of the dielectric ε and the insert thickness t. For each value of the dielectric permittivity, one can find that insert thickness for which the absolute value and phase of the reflection factor change little practically throughout the entire working scan range, i.e., in the region where only one main beam exists (Figure 12.4). However, the presence of a supplemental separation boundary leads to the fact that the dependence of the reflection factor on the scan angle becomes more sensitive to a change in frequency. Moreover, if the absolute value of the reflection factor has greater values (see, for example, the curves for $t = 0.3531\ \lambda$), then the problem of matching the antenna array in the passband becomes complicated. With an increase in the dielectric permittivity of the insert, the task of broadband matching becomes even more difficult. Moreover, the presence of dielectric inserts can lead to the propagation of higher modes in the region of the waveguide filled with the dielectric, where these modes are excited in the antenna aperture and disappear in a region not filled with the dielectric, something which at certain values of t can produce resonance peaks in the curves of the reflection factor.

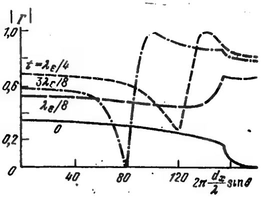

Figure 12.6. The absolute value of the the reflection factor as a function of the scan angle for an array with a single layer dielectric coating.

$d_x = a = 0.5714\lambda$; $\varepsilon = 3.0625$; λ_ε is the wavelength in the dielectric.

In the case where a dielectric coating is used in the aperture of a phased array (Figure 12.5), the reflection from the "coating--free space" separation boundary is used to partially eliminate the reflection from the aperture. Just as in the case of an antenna array with dielectric inserts, with the appropriate choice of coating parameters, one can make the reflection factor in the working band only slightly dependent on the scan angles. However, because of the fact that at rather large values of ε, the beam deflection from the normal leads to the occurrence of a wave in the antenna array similar to a surface wave, which propagates inside the dielectric, but decays in free space; an increase in the dielectric coating thickness above a certain critical value causes a resonance peak to appear in the curve of the reflection factor, the maximum value of which is practically equal to 1 and which, with an increase in the coating thickness, shifts in the direction of the normal to the array. A further increase in the coating thickness leads to the appearance of two and more peaks in the reflection factor curve (Figure 12.6).

We will note that the curves of the reflection factor plotted as a function of the scan angle for an antenna array with dielectric inserts usually are of a more continuous nature than the corresponding characteristics of an antenna array with a dielectric coating. This is of considerable practical importance when matching an array.

Thus, the use of dielectrics makes it possible to improve the antenna array matching during scanning. However, wide angle matching by means of dielectric inserts or coatings degrades the frequency response of the phased antenna array parameters as the result of the appearance of an additional separation surface. It was shown in the literature [08] that matching can be improved in a wide range of scanning angles at a single frequency. The use of multilayer dielectric inserts or coatings makes it possible to improve the frequency properties of an element.

Stops in a Waveguide Aperture [1]. An advantage of matching by means of a stop is the lack of a finite spacing between it and the radiating aperture, which leads to a lower frequency sensitivity of the array.

A waveguide radiator loaded with a stop is shown in Figure 12.7, in which a dielectric is incorporated to improve the matching. Here, ε' is the dielectric permittivity of the material filling the waveguide; ε_1 is the dielectric permittivity of the insert material; ε_2 and ε_3 are the dielectric constants of the dielectric coating of the array surface; c_1 and c_2 are the distances from the center of the waveguide to the edges of the stop along the X axis: d_1 and d_2 are the distances from the center of the waveguide to the edges of the stop along the Y axis.

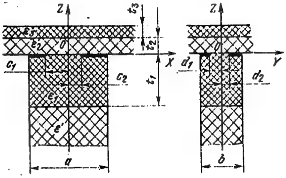

Figure 12.7. A waveguide radiator loaded with a dielectric and a stop in the aperture.

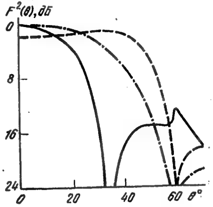

Figure 12.8. The power directional pattern in the H-plane for a waveguide radiator loaded with a stop.

The power directional pattern of the waveguide radiator depicted in Figure 12.7 and arranged in a triangular grid is shown in Figure 12.8 for the following parameter values: $d_x = 1.008\ \lambda$, $d_y = 0.504\ \lambda$, $\alpha = 45°$, $a = 0.905\ \lambda$, $b = 0.4\ \lambda$, $\varepsilon' = \varepsilon_1 = \varepsilon_2 = \varepsilon_3 = 1$ (the radiator is not loaded with a dielectric), $d_1 = d_2 = 0.2\ \lambda$, the parameters c_1 and c_2 are equal to each other and vary from $0.4525\ \lambda$ to $0.226\ \lambda$ (the stop covers half of the waveguide aperture). The solid curve corresponds to the lack of a stop, while the dashed and dotted as well as the dashed curves correspond to the presence of stops which cover 25 and 50% of the aperture area of the waveguide respectively. In the absence of a stop, a sharp dip is observed in the directional pattern at an angle of $\theta = 34°$ (although the diffraction beam appearance angle is approximately 60°). The introduction of a stop shifts the dip from the direction normal to the antenna aperture. A further increase in the area occupied by the stop leads to a reduction in the radiation along the normal to the surface and to overcompensation for the mismatching of the array. In this case, the presence of the stop does not degrade the characteristics of the array in the E-plane and D-plane (diagonal plane, i.e., at an angle of 45° to the E and H planes).

Eliminating the dip in the directional pattern of an element is an important feature of the method of matching by means of stops, which makes it possible to simply and effectively solve the problem of combatting anomalous "blinding" of the array.

The reflection factor is shown in Figure 12.9 as a function of the scanning angle in the H, E and D planes for the waveguide radiator depicted in Figure 12.7 and arranged in a triangular grid, for the following parameter values:

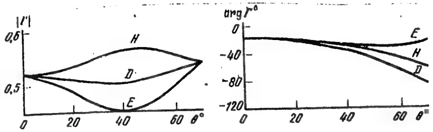

Figure 12.9. The reflection factor as a function of the scan angle for a waveguide radiator loaded with a stop and a dielectric.

$d_x = 0.9225\ \lambda$, $d_y = 0.27\ \lambda$, $\alpha = 30°$, $a = 0.905\ \lambda$, $b = 0.187\ \lambda$, $\varepsilon' = 1$, $\varepsilon_1 = 2.56$, $\varepsilon_2 = 1$, $\varepsilon_3 = 2.6$, $t_1 = 0.984\ \lambda$, $t_2 = 0.061\ \lambda$, $t_3 = 0.101\ \lambda$, $d_1 = d_2 = 0.0935\ \lambda$ and $c_1 = c_2 = 0.2715\ \lambda$.

One can note slight deviations of the reflection factor in the scan sector, which makes it possible to effectively match the antenna array.

Thus, the use of stops as matching elements can substantially improve phased array matching in a wide sector of scan angles in a rather broad bandwidth, as well as significantly shift the resonance dip in the directional pattern of a radiating element from the direction normal to the array aperture, or even eliminate it. The simplicity of fabricating stops is also to be noted.

12.2. Matching With a Fixed Scanning Angle

The radiating aperture of a waveguide element in a phased array represents a complex load for the exciting waveguide where this load changes during scanning. The conventional matching four-pole network inserted in the feed channel for each element can match the feeder to the load for a certain scanning angle, however, a considerable mismatch will be retained for the other angles because of the fact that the conventional matching four-pole network does not change its parameters with a change in the scanning angle. However, if one can beforehand manage to have the reflection factor change in a relative small range within the scan sector (for example, by using a dielectric or stops in the waveguide aperture), then the use of matching for some of the scan angles will make it possible to achieve better matching of the phased array throughout the entire sector. As a rule, matching consists in introducing an additional inhomogeneity into the radiator waveguide, where this inhomogeneity creates a reflected wave equal in amplitude and opposite in sign to the wave existing in the line which is reflected from the load.

An equivalent circuit for the connection of a feeder to the waveguide radiator of a phased array is shown in Figure 12.10 [2]. The insertion admittance of the radiating aperture which depends on the scanning angles is expressed in terms of the reflection factor Γ in a given cross-section by the well known-relationship:

$$\overline{Y}_a(\theta, \varphi) = G_a(\theta, \varphi) + jB_a(\theta, \varphi) = \frac{1-\Gamma(\theta, \varphi)}{1+\Gamma(\theta, \varphi)}\,\frac{1}{\rho_0}; \tag{12.1}$$

where $B_a(\theta_0, \phi_0)$ is the reactance of the matching device which compensates for the reactance introduced by the radiating aperture at the specified scan angle; n_0 is the transformation ratio of the ideal transformer which serves for matching the characteristic impedance of the feeder to the resistive component of the radiator input impedance; ρ_1 and ρ_0 are the characteristic impedances of the feeder and the waveguide radiator respectively.

Inductive and capacitive stops as well as inductive rods are used most often as the compensating reactances in waveguides.

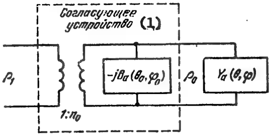

Figure 12.10. The equivalent circuit for matching ■ feedline to a radiator.

Key: 1. Matching device.

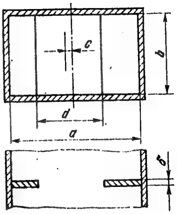

Figure 12.11. An inductive stop in a waveguide.

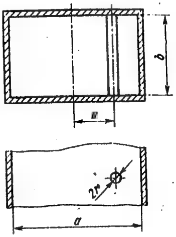

Figure 12.12. An inductive rod in a waveguide.

An inductive stop (Figure 12.11) can be asymmetrical in the general case and is characterized by the width of the window d and the thickness b, as well as the spacing between the centers of the waveguide and the stop window, c.

The following approximate formula can be used for the calculation of the normalized susceptance of a very thin (δ << d) stop:

$$\grave{B} \simeq -\frac{\Lambda}{a}\operatorname{ctg}^2\frac{\pi d}{2a}\left(1+\sec^2\frac{\pi d}{2a}\operatorname{tg}^2\frac{\pi c}{a}\right), \tag{12.2}$$

where:

$$\Lambda=\frac{\lambda}{\sqrt{1-(\lambda/2a)^2}} \tag{12.3}$$

is the wavelength in the waveguide.

For a symmetrical stop (c = 0):

$$B \simeq -\frac{\Lambda}{a}\operatorname{ctg}^2\frac{\pi d}{2a}, \tag{12.4}$$

while for a one-sided stop [c = (a - d)/2]:

$$B \simeq -\frac{\Lambda}{a}\operatorname{ctg}^2\frac{\pi d}{2a}\left(1+\sec^2\frac{\pi d}{2a}\operatorname{tg}^2\pi\frac{a-d}{2a}\right). \tag{12.5}$$

The finite thickness of a stop can be approximately taken into account by substituting the quantity d - δ in place of the quantity d. For inductive stops, the influence of the finite thickness is comparatively small.

The Inductive Rod (Figure 12.12). The normalized susceptance of an inductive rod is calculated from the approximate formula:

$$B \simeq -\frac{2\Lambda}{a}\left[\sec^2\left(\frac{\pi c}{a}\right)\ln\left(\frac{2a}{r}\cos\frac{\pi c}{2}\right)-2\right]^{-1}, \tag{12.6}$$

which yields adequate precision in the cases of practical importance.

The Capacitive Stop (Figure 12.13). An approximate formula for the calculation of the normalized susceptance of a capacitive stop, assuming that its thickness is infinitely small, has the form:

$$B \simeq \frac{4b}{\Lambda}\ln\left(\operatorname{cosec}\frac{\pi d}{2b}\sec\frac{\pi c}{b}\right). \tag{12.7}$$

Taking the finite thickness into account is accomplished by adding the following correction factor to B:

$$\Delta B = \frac{2\pi\delta}{\Lambda}\left(\frac{b}{d}-\frac{d}{b}\right). \tag{12.8}$$

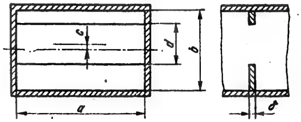

Figure 12.13. A capacitive stop in a waveguide.

Capacitive stops reduce the electrical strength of the waveguide channel and thereby decrease the power which can be transmitted through the waveguide. For this reason, they are rarely used as matching elements.

A more precise calculation of the matching reactances can be made using the graphs given in [3].

Quarter-wave transformers, continuous or stepped transitions, etc. can be used as the ideal transformers, the detailed design procedure for which is also given in [3].

Thus, the design of a waveguide radiator for a planar phased antenna array, matched in a wide range of scan angles, is carried out in the following order:

1. The array geometry and dimensions of a radiator are selected (see Chapters 2 and 11).

2. The matching device in the radiator aperture (dielectric, stops, etc.) is selected using the method of parameter variation on a computer to obtain the minimum change in the reflection factor within the scan sector. In this case, a certain correction of the array geometry and radiator dimensions is possible.

3. The matching device in the radiator waveguide is selected to obtain a reflection factor in the feeder for all scanning directions no greater than the permissible factor.

There are a program and description of an algorithm for the calculation of the directional pattern and reflection factor for a waveguide radiator in a planar array in the library of algorithms and programs of Moscow Aviation Institute, where this program and algorithm can be used to calculate the characteristics of a waveguide radiator for a specified array geometry and parameters of the matching devices as well as to optimize the radiator characteristics by means of dynamic programming.

CHAPTER 13. SLOTTED RESONATOR RADIATORS FOR PLANAR ANTENNA ARRAYS

Slotted resonator antennas are used in the microwave band as independent antennas as well as in the form of radiators for antenna arrays (AR) with linear, elliptical and controlled polarization of the radiated field. It is most expedient to use them at wavelengths of 10 to 60 cm.

A merit of slotted resonator radiators is the possibility of combining them with the metallic surface of the objects in which they are installed.

A single slotted resonator radiator takes the form of a slot cut in a conducting shield, where the slot closes a metal cavity (the resonator) and is excited at one or more points by means of coaxial or striplines. Excitation directly in the plane of the slot makes it possible to not only tune to resonance with a small resonator depth, but to match the input impedance of the slot in a structurally simple manner to the characteristic impedance of the exciting feedline, by displacing the connection point of the feeder relative to the center of the slot.

The major characteristics in the design of antenna arrays made of slotted resonator radiators are: the input impedance of the radiator incorporated in the antenna array as a function of the scanning direction; the geometry of the array and radiator; the partial directional pattern of a radiator; the polarization characteristics (for elliptically polarized radiators). In the case where a slotted resonator radiator is used as an independent antenna (for example, in telemetry, communications, etc.), the major characteristics are: the input admittance within the passband [as a function of frequency], the directional pattern and the polarization characteristic.

A complete analysis and the optimization of the indicated characteristics can be made only by means of mathematical models close to the actual devices and the study of these models by rigorous methods of electrodynamics.

13.1. Analysis of the Characteristics of a Slotted Resonator Radiator

The analysis is based on the solution of Maxwell's equation taking into account the boundary conditions at the appropriate surfaces.

The following model has been adopted for the antenna arrays (Figure 13.1). Each radiator is excited by a system of N sources at the points η_i (i = 1, 2, ...). Each source takes the form of an electrical current sheet with a density of $j^e_{\eta_i}(\eta_i - y)$, directed along the OX axis. With the action of the field produced by the sources, such a distribution of the magnetic current density $j^{\mu}(x, y)$ arises in the slot that the tangential component of the electrical field intensity vector is equal to zero at the surface of the shield and is continuous in the slot, while the tangential component of the magnetic vector in the slot satisfies the condition [1]:

$$[\mathbf{n}, (\mathbf{H}^{(I)} - \mathbf{H}^{(II)})] = \left\{ \sum_{i=1}^{N} j^e_{\eta_i} (\eta_i - y) \right\} \mathbf{x}_0, \qquad (13.1)$$

where $H^{(I)}$ and $H^{(II)}$ are the magnetic field intensity vectors for the regions under consideration; region I is the dielectric coating $(0 \leq z \leq x_s)$, region II is the resonator $(-h \leq z < 0)$ (see Figure 13.1); n is a unit normal; x_0 is a unit vector along the OX axis.

Taking (13.1) into account, one can derive the following integral equation for the unknown electrical field distribution $E_x(x, y)$ in the slot [2] both in the case of an antenna array [4, 6] and in the case of an individual radiator [3, 5]:

$$\begin{aligned}&\int\limits_{S_{\text{щ}}} E_x(x', y')\left[G_y^{\mu\,(I)} + G_y^{\mu\,(II)} + \frac{\partial g^{\mu\,(I)}}{\partial z}\right]_{z=z'=0} dx'\,dy' + \\ &+ \frac{1}{2k_2}\int\limits_{-l}^{l} \Phi\,|_{y=\xi} \sin\kappa_2|y-\xi|\,d\xi = C_1\cos\kappa_2 y + C_2\sin\kappa_2 y - \\ &-\frac{j}{2}\sqrt{\frac{\mu_0}{\varepsilon_2}}\left\{\sum_{i=1}^{N} I^e_{\eta_i}\int\limits_{-l}^{l} f(\eta_i - y')\sin\kappa_2|y-y'|\,dy'\right\}. \end{aligned} \tag{13.2}$$

Here:

$$G_y^{\mu\,(I)} = \begin{cases} \dfrac{\exp(-j\kappa_1 r)}{r}, \quad r = \sqrt{(x-x')^2 + (y-y')^2 + (z-z')^2}, \\ \qquad\qquad \text{для одиночного излучателя,} \\ \displaystyle\sum_{m=-\infty}^{\infty}\sum_{n=-\infty}^{\infty} \frac{\exp\{j[\kappa_{xm}(x-x') + k_{yn}(y-y')]\}}{j\cdot 2d_x d_y \sin\alpha\gamma_{mn}^{(I)}} \times \\ \times[f_{mn}(z, z') + 2A_{mn}\cos\gamma_{mn}^{(I)} z] \quad \text{для излучателя в АР} \end{cases}$$

for an individual radiator,

for a radiator in an antenna array

are the diagonal elements of Green's tensor function;

$$g^{\mu\,(I)} = \begin{cases} 0 \qquad\qquad \text{для одиночного излучателя,} \\ \displaystyle\sum_{m=-\infty}^{\infty}\sum_{n=-\infty}^{\infty}\left\{\left(\frac{\varepsilon_1}{\varepsilon_3} - 1\right)\frac{\exp(j[\kappa_{xm}(x-x') + \kappa_{yn}(y-y')])}{2d_x d_y \sin\alpha\gamma_{mn}^{(I)}} \times \right. \\ \left. \times\sin\gamma_{mn}^{(I)} z\left[\dfrac{f_{mn}(x_s, z') + 2A_{mn}\cos\gamma_{mn}^{(I)} x_s}{\gamma_{mn}^{(I)}\cos\gamma_{mn}^{(I)} x_s + j\gamma_{mn}^{(III)}\sin\gamma_{mn}^{(III)} x_s}\right]\right\} \quad \text{для излуча-} \\ \qquad\qquad \text{теля в АР} \end{cases}$$

for an individual radiator

for a radiator in an antenna array

are the nondiagonal elements of Green's tensor function,

$$f_{mn}(z, z') = \exp(-j\gamma_{mn}^{(I)}|z - z'|) + \exp(j\gamma_{mn}^{(I)}[z + z']);$$

$$\kappa_1 = \omega\sqrt{\varepsilon_0\varepsilon_1\mu_0};\quad \kappa_2 = \omega\sqrt{\varepsilon_0\varepsilon_2\mu_0};\quad \gamma_{mn}^{(I)} = \sqrt{\kappa_1^2 - \kappa_{xm}^2 - \kappa_{yn}^2};$$

$$A_{mn} = f_{mn}(x_s, z')\,\frac{\varepsilon_3\gamma_{mn}^{(I)} - \varepsilon_1\gamma_{mn}^{(III)}}{2(\varepsilon_1\gamma_{mn}^{(III)}\cos\gamma_{mn}^{(III)} x_s + j\varepsilon_3\gamma_{mn}^{(I)}\sin\gamma_{mn}^{(I)} x_s)};$$

$$\kappa_{xm}=\frac{2\pi m-\psi_x}{d_x};\quad \kappa_{yn}=2\pi\left(\frac{n}{d_y\sin\alpha}-\frac{m}{d_x\operatorname{tg}\alpha}\right)-\frac{\psi_y}{d_y},\quad n=0,\ \pm1,$$

$$\pm2,\ldots;\quad m=0,\ \pm1,\ \pm2,\ldots;$$

$$\psi_x=\kappa_0 d_x\sin\theta\cos\varphi;\quad \psi_y=\kappa_0 d_y\sin\theta\sin\varphi,\quad \kappa_0=\omega\sqrt{\varepsilon_0\mu_0};$$

$$\gamma_{mn}^{(III)}=\sqrt{\kappa_3^2-\kappa_{xm}^2-\kappa_{yn}^2};\quad \kappa_3=\omega\sqrt{\varepsilon_0\varepsilon_3\mu_0};$$

$$G_y^{\mu(II)}=\sum_{m=0}^{\infty}\sum_{n=1}^{\infty}\frac{2\varepsilon_m}{ab}v_{mn}(x,y)\,v_{mn}(x',y')\times$$

$$\times\begin{cases}\cos\gamma_{mn}^{(II)}z\cos\gamma_{mn}^{(II)}(h-z'), & z<z',\\ \cos\gamma_{mn}^{(II)}z'\cos\gamma_{mn}^{(II)}(h-z), & z>z';\end{cases}$$

$$v_{mn}(x,y)=\cos\beta_x\left(x+\frac{a}{2}\right)\sin\beta_y\left(y+\frac{b}{2}\right),\quad \beta_x=\frac{\pi m}{a},\quad \beta_y=\frac{\pi n}{b};$$

$$\varepsilon_m=\begin{cases}1, & m=0,\\ 2, & m\neq0,\end{cases}\quad \gamma_{mn}^{(II)}=\sqrt{\kappa_2^2-\beta_x^2-\beta_y^2};$$

where $S_{\text{Ш}}$ is the slot area; (x, y) and (x', y') are the coordinates of the observation point and the integration point respectively; θ, ϕ are the angles in spherical coordinates; ε_0 is the absolute dielectric permittivity; ε_1, ε_2 and ε_3 are the relative dielectric permittivity of the dielectric coating, the resonator and the space above the coating respectively; C_1 and C_2 are complex constants of integration; $f(\eta_i - y)$ is a function which takes into account the specified features of the excitation of the antenna (one usually takes $f(\eta_i - y) = \delta(\eta_i - y)$, where $\delta(\eta_i - y)$ is a [illegible] function); $I_{\eta i}^{e}$ is the complex amplitude of the exciting current;

$$\Phi=\begin{cases}0 & \text{for a single radiator}\\ (\kappa_2^2-\kappa_1^2)A_y^{\mu(I)}+\kappa_2^2A_z'^{\mu(I)} & \text{for a radiator in an antenna array}\end{cases}$$

$$A_y^{\mu(I)}=\int\limits_{S_{\text{Ш}}}E_x(x',y')\,G_y^{\mu(I)}\,dx'\,dy';$$

$$A_z'^{\mu(I)}=\int\limits_{S_{\text{Ш}}}E_x(x',y')\frac{\partial g^{\mu(I)}}{\partial z}\,dx'\,dy'.$$

To find $E_x(x', y')$ from integral equation (13.2), it is necessary to employ regularizing methods. This is related to the fact that the solution of equation (13.2) is an improper problem: as great a change in the solution as desired can correspond to a small change in the right side of (13.2). One of the regularizing methods which makes it possible to obtain a solution of (13.2) with a sufficient degree of precision is the autoregularization technique of [2]. The basis for the method is the hypothesis of the smoothness of the solution and apriori information on the type $1/4\pi r$ integrable singularity in the nucleus of equation (13.2). By employing a piecewise constant approximation

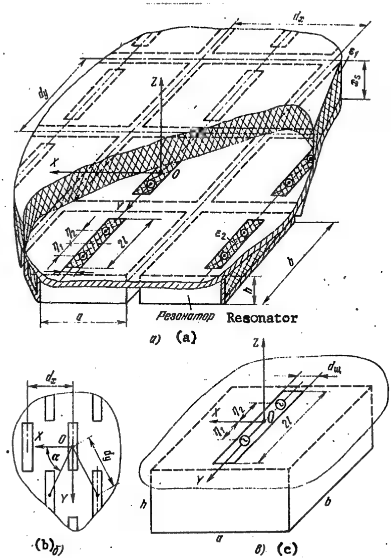
d_x
d_y
ε_1
a_3
Z
X
0
Y
η_1
η_2
$2l$
ε_2
b
h
a
Резонатор Resonator
а) (a)
d_x
X
0
α
Y
d_p
(b) б)
Z
$d_ш$
X
η_2
0
η_1
$2l$
Y
h
b
a
в) (c)

Figure 13.1. Slotted resonator structures.

Key: a. Antenna array with a dielectric coating (rectangular grid);
b. Triangular grid for radiator layout;
c. Single radiator.

for the desired function and segregating the singularity from the nucleus of (13.2) when the observation (x, y) and integration (x', y') points coincide, one can derive a system of linear algebraic equations which have a stable solution.

Equation (13.2) was reduced to an algorithm on a computer in papers [3-6] by the autoregularizing technique and the distribution $E_x(x', y')$ was found which is needed to determine the characteristics of a single radiator and a radiator incorporated in an antenna array. The program written in Algol-60 is in the library of algorithms and programs of Moscow Aviation Institute. The input admittance $Y_{\eta i}$ is defined as the ratio of the current $I^e_{\eta i}$ to the voltage at the points η_i:

$$U_{\eta_i}=\int\limits_{-d/2}^{d/2} E_x(x,\,y)\Big|_{y=\eta_i} dx,$$

$$Y_{\eta_i}=G+jB=I^e_{\eta_i}/U_{\eta_i}. \qquad (13.3)$$

The directivity function $g(\theta,\ \phi)$ of a slotted resonator radiator incorporated in an antenna array, in a single beam scanning mode, which coincides with the normalized partial directional pattern of a radiator with respect to power, $F^2(\theta,\ \phi)$, with a precision of within the constant factor $4\pi S/\lambda^2$, is defined as:

$$g(\theta,\ \varphi)=\frac{4\pi S}{\lambda^2}\cos\theta\,[1-|\Gamma(\theta,\ \varphi)|^2]. \qquad (13.4)$$

Here, $S = d_x d_y \sin\alpha$;

$$\Gamma(\theta,\ \varphi)=[1+Y(\theta,\ \varphi)]/[1-Y(\theta,\ \varphi)] \qquad (13.5)$$

is the reflection factor, $Y(\theta,\ \phi)$ is the input admittance at the excitation point normalized with respect to the exciting feeder. When a radiator is excited at several points:

$$Y(\theta,\ \varphi)=\sum_{i=1}^{N} Y_{\eta_i}(\theta,\ \varphi).$$

The directional pattern of a slotted resonator radiator, used as an independent antenna, is found from the known field distribution in the slot $E_x(x',\ y')$.

13.2. The Characteristics of a Slotted Resonator Radiator as a Independent Antenna

Functions were derived based on the program for the solution of integral equation (13.2), where these functions are recommended for the calculation of the resonant* operating mode of an antenna. The results of the numerical calculation are given in Figures 13.2--13.4.

Figure 13.2 illustrates the conductance component G of the input admittance Y as a function of the position of the antenna excitation point relative to the center of the slot in the resonant operating mode (B = 0) for various relative widths ($d_{Щ}/\lambda$) [(d_{slot}/λ)] and lengths ($2l/\lambda$) of the slot. Curves for the relative width of the resonator (a/λ) are shown in Figure 13.3 as a function of its relative depth (h/λ) when B = 0. The voltage standing wave ratio $K_{st\ U}$ [VSWR] curves for the antenna as a function of frequency are shown in Figure 13.4 for various slot widths.

---

*The resonant operating mode of an antenna is understood to be that mode in which the reactive component of the input admittance of the antenna is $Y_{\eta_0} = 0$.

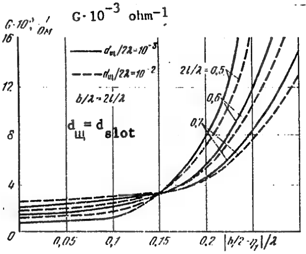

Figure 13.2. The conductance of a slot (B = 0) as a function of the position of the excitation point relative to the center of the slot.

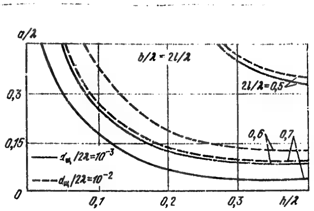

Figure 13.3. Resonator width a/λ as ■ function of the depth h/λ when $B = 0$.

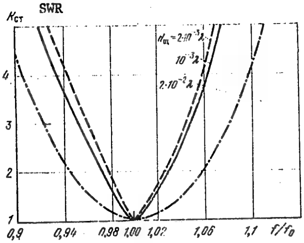

Figure 13.4. The SWR as a function of frequency for various slot widths.

We shall consider a specific example of the determination of antenna parameters which assure a matched operating mode of ■ slotted resonator antenna with an exciting feeder having a characteristic impedance of $\rho = 100$ ohms with a bandwidth of about 12% for a VSWR of 2 with slot dimensions of $2l/\lambda = 0.6$ and $d_{slot}/2\lambda = 10^{-2}$. Since the antenna and the feeder are matched when $G = 1/\rho$, we find the point corresponding to $G = 10 \cdot 10^{-3}$ $ohms^{-1}$ on the curve for the specified slot dimensions ($2l/\lambda = 0.6$ and $d_{slot}/2\lambda = 10^{-2}$). The abscissa of this point, which defines the displacement of the excitation point relative to the center of the slot is equal to $0.249\ \lambda$. The resonator dimensions which assure a resonant operating mode of the antenna are chosen from the graphs of Figure 13.3. For example, if it is important because of structural considerations to keep the depth of the resonator h small (approximately $0.1\ \lambda$), then for a slot of the same dimensions, the width a and length b of the resonator should be $0.375\ \lambda$ and $0.6\ \lambda$ respectively.

13.3. The Characteristics of ■ Slotted Resonator Radiator in a Planar Antenna Array

Curves for the conductance component G and susceptance component B of the input admittance Y of ■ slot antenna incorporated in an antenna array with various dielectric coatings ($\varepsilon_1 = 3, 2.35$) are shown in Figure 13.5 as a function of the

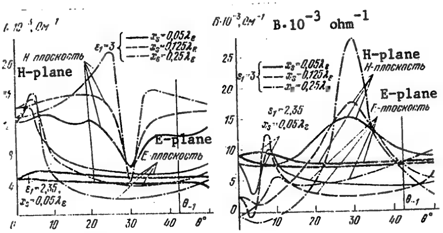

Figure 13.5. The conductance and reactive component of the input admittance of a radiator incorporated in an antenna array as a function of the scan angle in the E and H planes: rectangular grid, $d_y = 0.6\lambda$ and $2l/\lambda = 0.5$.

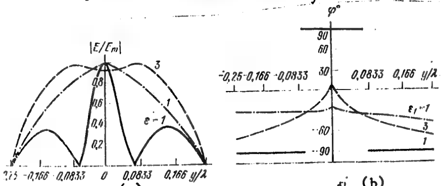

а) (a)

б) (b)

Figure 13.6. The amplitude (a) and phase (b) distributions of the electrical field over the slot.

$d_x = d_y = 0.6\lambda$; $2l/\lambda = 0.5$; the dashed curves are for E-plane scanning; $\theta \simeq 42°$; the dashed and dotted curves are for H-plane scanning, $\theta \simeq 40°$; the solid curves are the characteristic distribution.

scanning angle in the E and H planes when each radiator is excited at a single point ($\eta_1 = 0$). The dielectric coatings have a substantial influence on the distribution of the fields and the mutual coupling of the radiators in the array. For this reason, the correct selection of the parameters ε_1 and x_s is quite important in the design work. It can be seen from Figure 13.5 that with an increase in ε_1, the absolute values of G and B change significantly, and with an increase in the thickness of the dielectric coating, the range of variation in these parameters increases (the angle θ_{-1} for the occurrence of the first diffraction lobe is noted).

Curves for the amplitude and phase distributions of the electrical field in the plane of the slot are shown in Figure 13.6 for various operating modes of a radiator incorporated in an antenna array. As can be seen from Figure 13.6, when

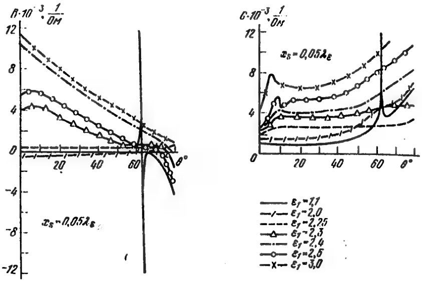

Figure 13.7. The influence of the quantity ε_1 on the total input admittance.

$\theta = 42°$ (the occurrence of the first diffraction lobe), the field distribution along the slot differs sharply from a sinusoidal distribution when scanning in the E-plane and is asymmetrical and out-of-phase in the H-plane. The most characteristic amplitude-phase distribution of the field in an array with a dielectric coating where $\varepsilon_1 = 3$ is shown in Figure 13.6 with the dashed curve.

Figure 13.7 illustrates the influence of the relative dielectric permittivity ε_1 on the components of the input admittance of a slotted resonator radiator incorporated in an antenna array with a triangular grid where the coating thickness is $x_s = 0.05\lambda_\varepsilon$ and for the case of E-plane scanning.

13.4. The Optimization of the Characteristics of a Slotted Resonator Radiator in an Antenna Array

When designing a phased antenna array, it is necessary to assure a minimal reflection factor $\Gamma(\theta, \phi)$ in the specified scan sector and frequency band. The optimization of a radiator incorporated in an antenna array at a fixed frequency is accomplished by means of minimizing the function [08]:

$$I = \iint_{\theta_{CK}} |\Gamma(\theta)|^2 d\theta = \iint_{\theta_{CK}} \left| \frac{1 - Y(\theta)}{1 + Y(\theta)} \right|^2 d\theta, \qquad (13.6)$$

where θ_{CK} [θ_{scan}] is the specified scanning sector.

The optimization was carried out using the method of local variations in a "user -- computer" dialog mode, which made it possible to narrow the range of values of the parameters needed to obtain the requisite characteristics. The calculation of the double integral in formula (13.6) was carried out for three sections: $\phi = 0$, $\pi/2$ and $\pi/4$. The optimization was accomplished in the specified sector θ_{scan} through the choice of the geometry of the array and radiator, and the parameters of the dielectric coating ε_1 and x_s.

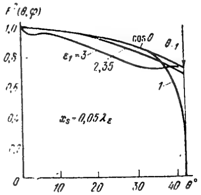

Figure 13.8. Optimization of the E-plane directional pattern of a radiator.

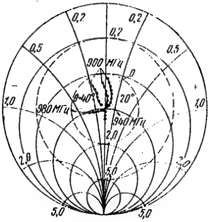

Figure 13.9. The frequency curves for a radiator within the sector of scan angles.

Curves for $G(\theta)$ and $B(\theta)$ in the E and H planes of an optimized radiator for a rectangular grid are shown in Figure 13.5. It can be seen that by selecting the parameters ε_1 and s, one can achieve a smooth change in these curves in an angular sector of $\theta = 0$ to 45° ($\varepsilon_1 = 2.35$; $x_s = 0.05\lambda_g$). Similar optimization results in the E-plane for an arrangement of the radiators in a triangular grid are shown in Figure 13.7 (see the curves for $\varepsilon_1 = 2.25$).

The normalized power directional pattern of a radiator $F^2(\theta, \phi) = (\lambda^2/4\pi S)g(\theta, \phi)$ is shown in Figure 13.8 for a nonoptimized ($\varepsilon_1 = 1$ and $\varepsilon_1 = 3$ and an optimized ($\varepsilon_1 = 2.35$) slotted resonator radiator incorporated in an antenna array.

The frequency characteristics of $Y(\theta)$ for a rectangular grid in the E-plane of a radiator optimized at the center frequency f_0 are shown in Figure 13.9. The working bandwidth at a level where the SWR is 2 is about 10 percent. We will note that for complete optimization of the radiator, working from the specified sector and frequency coverage, it is necessary to minimize (13.6) within the passband.

Matching of the radiators incorporated in an antenna array to the excited device is usually achieved for $\theta = 0$. This can be achieved for the radiators considered here by means of shifting the excitation point relative to the center of the slot (see Figure 13.2) for each radiator. To find the precise position of the excitation point η_i in the plane of the slot, it is necessary to use the program for calculating the characteristics of a radiator by the autoregularization method;

during the design stage, one can use the functions shown in Figure 13.2 with a high degree of confidence.

13.5. Examples of the Realization of Slotted Resonator Radiators

Structural designs of slotted resonator radiators excited by a miniature coaxial cable (Figure 13.10a) or by a stripline or a system of striplines in the case of excitation at several points (Figure 13.10b) are shown in Figure 13.10.

The stripline conductor (3) is run inside the resonator until it intersets the slot 1 and is shorted at a certain spacing from the slot by the jumper 4. The stripline conductor is coupled to the exciting feeder by means of the coaxial to stripline transition (5). The choice of the dimensions of components 3--5 for matching is accomplished experimentally. The structure shown in Figure 13.10b is used to obtain radiation with circular polarization. A schematic of the excitation is shown in Figure 13.11a and its stripline realization is shown in Figure 13.11b. The circuit provides for the excitation of each slot at two points and a phase shift of 90° between the slots. Radiator inputs 1--4 in Figure 13.10b are connected directly to outputs 1--4 of the excitation circuit (see Figure 3.11c [sic]) by means of the coaxial to stripline transitions (5). The stripline excitation device consists of a 3 dB divider and two 3 dB directional couplers; the characteristics and parameters of the directional couplers can be determined using the procedure set forth in Chapter 22 and 23. The excitation of each slot at two points provides for 20 to 25 dB of isolation between the slots with respect to the feed.

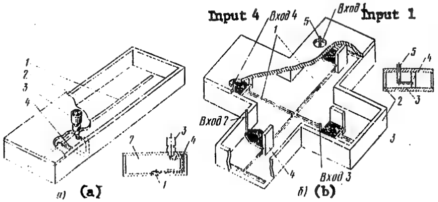

Figure 13.10. Ways of exciting a slotted resonator radiator with a coaxial cable (a):

Key:
1. Rectangular slot;
2. Resonator;
3. RF connector;
4. Coaxial cable;

With a stripline (b):
1. Orthogonal slots;
2. Cross-shaped resonator;

[Key to Figure 13.10, continued]:

3. Stripline;
4. Shorting jumper;
5. Coaxial transition.

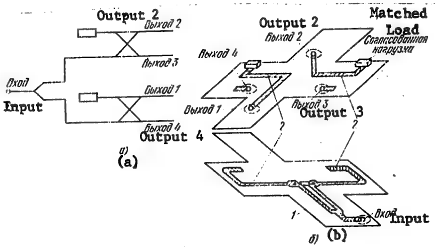

Figure 13.11. Circuit configuration for the excitation of a slotted resonator with rotating polarization of the field.

Key: a. Electrical circuit;
b. Topology; 1. 3 dB divider;
1. 3 dB divider;
2. Directional couplers with front coupling.

13.6. The Design Procedure

The design procedure for a slotted resonator radiator as an independent antenna where the characteristic impedance of the exciting feeder, the dimensions and the bandwidth are specified is accomplished using the functions shown in Figures 13.2 to 13.4. The directional pattern and gain of the antenna are found from the formulas derived, for example, in [0.1, 02].

The design procedure for phased arrays of slotted resonator radiators is similar to the general procedure for the design of antenna arrays based on specified technical requirements (see Chapter 2).

The characteristics of an individual radiator as part of an antenna array can be computed using the program which makes it possible to assure a resonant mode (the selection of the dimensions a, b, h and $2l$), achieve matching (the choice of ε_i when $\theta = 0$) and optimize the radiator characteristics within the scan sector. However, the following procedure for working with the program in a user--computer dialog mode is expedient for the efficient utilization of the machine time:

1. Working from the value found for the array step h, determined by θscan (see Chapter 2), we choose the slot length $2l$ and the resonator $b \geq 2l$ (Figure 13.1).

2. Working from the specified value ε_1 for the dielectric coating and the structural requirements for the dimensions a, h and x_s, we find the resonator operating mode of the radiator ($B = 0$) and optimize it (the most expedient range of change for a/2 and h/λ are respectively: $0.1 \leq a/\lambda \leq 0.5$ and $0.1 < h/\lambda$).

3. We achieve matching to the radiator excitation circuit by shifting the point ε_i (in a first approximation, this displacement can be determined from the graph in Figure 13.2).

4. The gain of a radiator incorporated in an antenna array, $g(\theta, \phi)$ is determined from (13.4), while the radiator directional pattern is determined using the formula: $F(\beta, \phi) = (\lambda^2/4\pi S)g(\theta, \phi)$.

5. Where necessary, the bandwidth is calculated for the radiator incorporated in the antenna array (see Figure 13.9). The bandwidth of an optimized radiator is approximately 10 percent for a VSWR of 2.

14. RADIATING WAVEGUIDE MODULES WITH REFLECTIVE PHASE SHIFTERS

14.1. The Modular Design of a Phased Antenna Array

Regardless of the structural configuration of a phased array, homogeneous units can be singled out in it which consist of a number of microwave elements and devices. These units are joined together by a distribution feeder. Units of a modular design are employed to provide for production suitability of phased antenna arrays and to standardize their structural design.

The basic elements of a module are the radiator (or a group of them), phase shifter and an element for coupling the distribution feed line. The presence of isolation, tuning and other auxiliary assemblies is also possible.

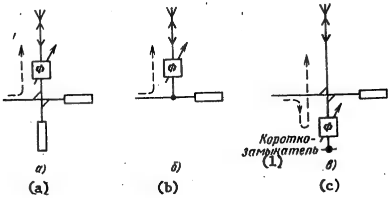

Figure 14.1. Configurations of radiating modules.
a. With a feedthrough phase shifter and a matched load;
b. Without it;
c. With a reflective phase shifter.

Key: 1. Short-circuiter.

The basic configurations of modules are depicted in Figure 14.1. A module with a coupling element in the form of directional coupler is depicted in Figure 14.1a, where arm of the coupler forms a distribution feeder section, while the other is loaded into a feedthrough phase shifter with a radiator and an absorbing load. The absorbing load is provided to compensate for re-reflections which occur in the module. A module is depicted in Figure 14.1b in which the coupling element is a tee. A module is depicted in Figure 14.1c which contains a radiator and a directional coupler with a reflective phase shifter in one of the arms. The paths for the distribution of the electromagnetic wave to the radiator are indicated by the dashed arrow lines in these figures.

The greateest value of the directional gain of an array is achieved in the phased array shown in Figure 14.2. The impact of various kinds of distortions and mismatching on the directional gain is substantially attenuated in this circuit because of the use of directional coupler with absorbing loads.

Variants of waveguide modules have been considered, however, the theoretical results and circuits of the modules are also applicable to other types of microwave lines.

14.2. Multiposition Phase Shifter for a Module

The basis for a multiposition phase shifter is an extremely simple series produced phase shifter using semiconductor n-i-p-i-n diodes with four phase positions (Figure 14.3) [1]. It has the following main parameters: working frequency of 7.7 GHz, Discrete phase step of $\Delta = \pi/2$, average thermal losses of from 1.2 to 1.6 dB, switching current of 100 ± 10 mA, switching voltage of 1 volt and an ultimate microwave through power of from 10 to 15 KW and an average power of up to 10 watts.

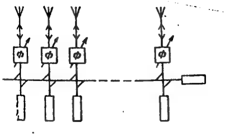

Figure 14.2. Schematic of an antenna array with a series distribution of the energy.

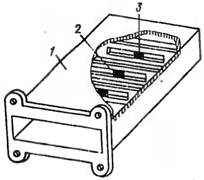

Figure 14.3. A reflective phase shifter with n-i-p-i-n diodes.

Key: 1. Waveguide; 2. Partition with the switched slot;
3. n-i-p-i-n doide.

The thermal losses introduced by phase shifters govern the efficiency of an antenna and its gain. These losses are determined by the quality of the diodes used in the phase shifters [1]:

$$K = r_{\text{rev loss}}/r_{\text{for loss}},$$

where $r_{\text{rev loss}}$ is the reverse loss resistance of the diode; $r_{\text{for loss}}$ is the forward loss resistance of the diode. The relative gain of an antenna, G, is plotted in Figure 14.4 as a function of thd discrete phase control step, Δ. The quality of the switchers is the parameter in these graphs. In centimer band series produced diodes, the quality figure fluctuates from 300 to 1,000. In the case of large values of the discrete phase control step ($\Delta \geq \pi/2$), the antenna gain is low because of the large switching errors in beam steering, i.e., because of the low directional gain. With a decrease in Δ, the thermal losses increase, but the directional gain rises more rapidly, right up to a certain value of Δ, which depends on the quality of the switchers.

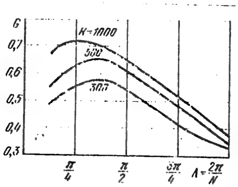

Figure 14.4. The antenna gain as a function of the discrete step of the phase shifter and the quality of the n-i-n-i-n diode.

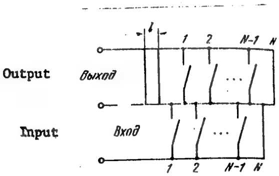

Figure 14.5. Schematic of a through transfer bridge phase shifter with N and 2N discrete phase state steps.

Thus, the maximum value of the coefficient is achieved when $\pi/4 \leq \Delta \leq \pi 2$, and as follows from the graphs of Figure 14.4, circuits with four and eight phase states have the same gain. However, the fewer the number of discrete steps $N \doteq 2\pi/\Delta$, the higher the sidelobe level and the lower the beam steering precision. Moreover, the line--column method of controlling the phase distribution which is widely used at the present time leads to a doubling of the phase errors in the aperture and correspondingly requires a reduction in Δ. For this reason, phase shifters with eight phase states are to be prefered.

One of the widespread and simple circuit designs for through transfer phase shifters based on reflective configurations is a circuit which employs a slotted waveguide bridge (Figure 14.5). The operational principle of a slotted bridge is described in the literature [2]. Such a through transfer phase shifter, in the case of sequential switching of the switching elements synchronously in two reflective phase shifters provides for a number of phase states equal to the number of phases of a single reflective phase shifter N.

TABLE 14.1

	1	2	3	4	5	...	p	$p+1$	...	$2N$
q	1	1	2	2	3	...	i	i	...	N
m	0	1	1	2	2	...	$i-1$	i	...	N

The doubling of the number of discrete phase states (2N) is achieved by inserting a static Δ/4 phase shifter in one of the arms of the bridge (opposite the input), which is equivalent to lengthening this arm by the amount:

$$l = \lambda_B/4N, \tag{14.1}$$

where λ_B is the wavelength in the waveguide.

The switching of the switching elements in a through transfer phase shifter takes place sequentially: first in one reflective phase shifter, then in the other.

The switching sequence for reflective phase shifters to obtain a through transfer phase shifter with two N phase states is shown in Table 14.1. The following symbols are used in the table: n = q + m is the number of the phase state of the feedthrough phase shifter with two 2N phase states; q and m are the phase state numbers of the upper and lower reflective phase shifters respectively (Figure 14.5).

Such a circuit configuration for reflective phase shifters is called a circuit with double the number of discrete phase values. The scattering matrix of an ideal phase shifter has the following form with a precision of down to the common phase multiplying factor:

$$[S]=e^{j\pi/2}\begin{vmatrix}\Gamma_\phi & K_\phi\\ K_\phi & -\Gamma_\phi\end{vmatrix}, \qquad (14.2)$$

where

$$\Gamma_\phi=\sin\left[(q-m)\frac{\Delta}{2}-\frac{\Delta}{4}\right]\exp\left[-j\left(n\Delta_1+\frac{\Delta}{4}\right)\right];$$

$$K_\phi=\cos\left[(q-m)\frac{\Delta}{2}-\frac{\Delta}{4}\right]\exp\left[-j\left(n\Delta_1+\frac{\Delta}{4}\right)\right],$$

where Δ = 2π/N is the discrete phase step of the reflective phase shifter; Δ_1 = = π/N = Δ/2 is the discrete phase step of the feedthrough phase shifter.

The constancy of the absolute values of the coefficients K_ϕ and Γ_ϕ is achieved through the selection of the phase shift Δ/4 and the switching algorithm for the diodes, which is given in Table 14.1, from which the follows the condition:

$$q-m=\begin{cases}0 & \text{при четном } n, \text{ for even } n;\\ 1 & \text{при нечетном } n. \text{ for odd } n.\end{cases} \qquad (14.3)$$

When condition (14.3) is met, the absolute value of the transmission gain is constant and equal to cosΔ/4.

By adducing similar arguments concerning the absolute value of the reflection factor, we find that it is also constant and equal to sinΔ/4.

The errors in slotted bridge operation and the thermal losses in the switchers have an influence on phase shifter characteristics. The transmission and reflection factors for an ideal feedthrough phase shifter with two N states are expressed as follows:

$$K_\phi'=j2\varkappa Q^{-1}\left(\frac{1}{1+\varkappa^2}-c^2\right)\exp\left[-j\left(n\frac{\Delta}{2}+\frac{\Delta}{4}\right)\right]\cos\frac{\Delta}{4}+$$

$$+c+2Q^{-2}\Gamma\varkappa\left(\frac{1}{1+\varkappa^2}-c^2\right)\exp\left[-j2\left(n\frac{\Delta}{2}+\frac{\Delta}{4}\right)\right]\cos\frac{\Delta}{2}; \qquad (14.4)$$

$$\Gamma'_{\phi}=-j2\varkappa^{3}Q^{-1}\left(\frac{1}{1+\varkappa^{2}}-c^{2}\right)\exp\left[-j\left(n\frac{\Delta}{2}+\frac{\Delta}{4}\right)\right]\sin\frac{\Delta}{4}+$$
$$+c\varkappa e^{j\pi/2}+2Q^{-2}c\varkappa^{3}\left(\frac{1}{1+\varkappa^{2}}-c^{2}\right)\exp\left[-j2\left(n\frac{\Delta}{2}+\frac{\Delta}{4}\right)\right]\sin\frac{\Delta}{2},\qquad(14.5)$$

where Q is are the power losses in the phase shifter which are due to the quality of the switchers K; Γ is the reflection factor from the input of the slotted waveguide bridge; c is the decoupling of the slotted bridge; κ = /b/d/ is the division factor with respect to the field between the output arms of the slotted waveguide bridge (for an ideal 3 dB bridge, κ = 1).

The relationship between these coefficients is determined by the equation:

$$\Gamma|^{2}+|b|^{2}+|c|^{2}+|d|^{2}=1.$$

In series produced slotted waveguide bridges:

$\Gamma \approx 0.1$ to 0.15; $c \approx -20$ to -25 dB; $b \approx d$.

For feedthrough and reflective phase shifters [1]:

$$Q=\left(1+2\sqrt{\frac{2N-1}{K}}\right)^{2},\quad Q=\left(1+\sqrt{\frac{N-1}{K}}\right)^{4}.\qquad(14.6)$$

The first term in (14.4) for the transmission gain K'_{ϕ} determines the amplitude and phase at the output of a feedthrough phase shifter, while the second and third terms determine the amplitude and phase errors of the phase shifter which are due to the error in the parameters of its components.

The maximum relative amplitude error σ_m and the maximum phase error ν are determined by the expressions:

$$\sigma_m=\frac{c+2Q^{-2}\Gamma\varkappa\left(\frac{1}{1+\varkappa^{2}}-c^{3}\right)\cos\frac{\Lambda}{2}}{2Q^{-1}\varkappa\left(\frac{1}{1+\varkappa^{2}}-c^{3}\right)\cos\frac{\Lambda}{4}};$$
$$\nu=\arcsin\frac{c+2Q^{-2}\Gamma\varkappa\left(\frac{1}{1+\varkappa^{2}}-c^{2}\right)\cos\frac{\Lambda}{2}}{2Q^{-1}\varkappa\left(\frac{1}{1+\varkappa^{3}}-c^{3}\right)\cos\frac{\Lambda}{4}}.\qquad(14.7)$$

The mean square value of the efficiency of a feedthrough phase shifter with respect to all of the phase states is:

$$\eta_{cp}=\frac{1}{2N}\sum_{n=1}^{2N}|K'_{\phi}|^2_n. \qquad (14.8)$$

14.3. Microwave Bridge Devices for Feedthrough Phase Shifters

There are two types of bridges which are the most widely used in a waveguide design: H-plane bridge, which takes the form of the connection of two rectangular waveguides at the narrow wall (Figure 14.6a) and an E-plane bridge, which takes the form of the connection of two waveguides at the wide wall (Figure 14.6b). These bridges are called forward directivity devices. The wave incoming to the one of the arms (1 and 2) of the bridge (Figure 14.6) is divided equally between the arms which are opposite each other (3 and 4), without changing the direction of propagation.

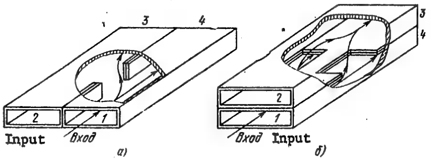

Figure 14.6. H-plane (a) and E-plane (b) slotted waveguide bridges.

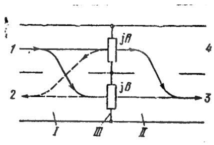

Figure 14.7. Schematic of an inverse directivity slotted waveguide bridge.

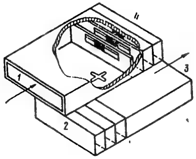

Figure 14.8. A through transfer phase shifter with a reverse directivity bridge.

The input and output of a through transmission phase shifter using these bridges prove to be arranged in a row, something which is structurally inconvenient. For this reason, reverse directivity slotted bridges are used (Figure 14.7) [3], in which the opposite inputs are separated. They consist of two series connected slotted waveguide bridges I and II (Figure 14.7), which are coupled to each other by identical reactances III with identical susceptances jB.

The effect of the reactances reduces to the reflection of the incident wave. The reactances are chosen so that the reflection and transmission gains are equal. When a wave is incident at input 1 of bridge I, it does not pass through to arm 2 by virtue of the cancelling effect of the wave reflected from reactance III. In this case, the waves passing through the reactances add in arm 3 of bridge II.

A schematic drawing of the wave motion inside the bridge is shown in Figure 14.7. The dashed lines indicate the motion of the reflected wave while the solid lines show the wave passing through.

When reflective phase shifters are connected to arms 2 and 3, the device is converted to a feedthrough phase shifter, the input and output of which are diametrically opposite. Such phase shifters using an E-plane slotted waveguide bridge has extremely small transverse dimensions, which are determined by the size of the wide wall of the waveguide and a doubled dimension for the narrow wall, because of which they are used in transmissive phased arrays with wide angle scanning.

A variant of a reverse directivity bridge is a directional coupler, consisting of two rectangular waveguides which are coupled by a cross-shaped coupling hole (Figure 14.8). The waveguides are laid on each other and offset by half of the wide wall width. With 50 percent coupling between them, a directional coupler is a waveguide bridge with reverse directivity. When a wave impinges on arm 1, it is divided equally between arms 2 and 4. Arm 3 proves to be decoupled from arm 1.

By connecting reflective phase shifters to arms 2 and 4, we realize a transmissive phase shifter (Figure 14.8). The resulting structural design proves to be rather compact, since its vertical dimension is determined by twice the height of the waveguide, while the transverse dimension is approximately equal to γ.

14.4. The Design of a Radiating Module of an Antenna Array

A module with an absorbing load (Figure 14.9, also see Figure 14.1a) takes the structural form of two waveguides (1 and 2) arranged orthogonally one on top of the other, and coupled via the wide wall with a coupling hole (3). An absorbing load (4) and feedthrough phase shifter (5) (see §14.2) are connected to the upper waveguide, where the radiator (6) is connected to the output of the phase shifter.

The power coupling factor β^2 through the coupling element is chosen depending on the amplitude distribution in the aperture of the phased array. The coefficient γ characterizes the energy which passes into the absorbing load because of the nonideal nature of the coupling element. The portion of the energy which flows through waveguide 1 to excite the subsequent modules is characterized by the through transmission factor α. We designate the reflection factor from the module input as δ. These coefficients are related by the expression:

$$|\alpha|^2+|\delta|^2+|\gamma|^2+|\beta|^2=1. \qquad (14.9)$$

Actual absorbing loads have a finite absorption and introduce small reflections, which we shall designate as Γ_N.

When modules operate in a phased array, there are reflections, Γ_p, from its radiators because of their mutual coupling.

Taking (14.4) and (14.5) into account, the module transmission gain is defined by the expression:

$$|K_{\text{м}}|=\beta K'_{\text{ф}}(1-\gamma\Gamma_{\text{н}}\alpha-\delta\Gamma'_{\text{ф}}-\Gamma_{\text{p}}\Gamma'_{\text{ф}}-\alpha^2\Gamma_{\text{н}}\Gamma'_{\text{ф}}), \qquad (14.10)$$

while the module reflection factor is:

$$|\Gamma_{\text{м}}|=\delta+\beta^2[\Gamma'_{\text{ф}}+\delta\Gamma'^2_{\text{ф}}+K'^2_{\text{ф}}\Gamma_{\text{p}}]+2\alpha\beta\gamma\Gamma'_{\text{ф}}. \qquad (14.11)$$

The amplitude and phase errors of a module are maximum when all of the re-reflections and distortions add together with unfavorable phases. Since the phase of the field in equations (14.10) and (14.11) changes in accordance with a complex law and depends on a large number of factors, the maximum errors determine the minimum possible gain of a phased array in the scan sector.

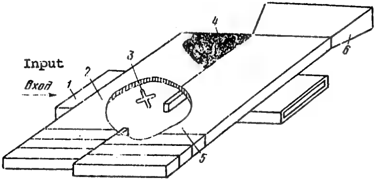

Figure 14.9. A radiating module with an absorbing load.

To estimate the maximum amplitude error in the excitation of the radiators of a module, the following expression is justified:

$$\begin{aligned}|\Delta A| = {} & [\alpha\gamma\Gamma_n c + \beta c + (\alpha^2\beta\Gamma_n c + \\ & + \beta\Gamma_p c + \delta c\beta)\sin(\Delta/4) + \\ & + \alpha\gamma\Gamma_n\cos(\Delta/4) + (\beta\Gamma_p + \\ & + \alpha^2\beta\Gamma_n)\sin(\Delta/4)\cos(\Delta/4)] : \\ & : \beta\cos(\Delta/4).\end{aligned} \tag{14.12}$$

The maximum phase error in the excitation is:

$$|\delta\Phi| = \arcsin|\Delta A|. \tag{14.13}$$

Knowing the relative amplitude and phase errors of a module makes it possible to determine the minimal values of the directional gain and gain G in a real phased array (the inverse problem also frequently occurs in practice: having specified the minimal directional and gain G of a phased array, determine the permissible scatter in the module parameters). The efficiency of a module is:

$$\eta = |K_M/K_{M\ id}|^2 \tag{14.14}$$

In order to obtain $K_{M\ id}$, it is necessary to substitute K_M for the case of ideal elements of a module in expression (14.10).

A module without an absorbing load (Figure 14.10) is structurally simpler than that depicted in Figure 14.9. It consists of two orthogonally arranged waveguides (1 and 2), which are directionally coupled together by whole (3) in the wide wall. A reflective phase shifter (4) with a discrete step of Δ and a radiator (5) are connected to the upper waveguide. In such a module, the coefficient γ characterizes the energy passing through the coupling element from the input of waveguide 1 to the radiator, bypassing the phase shifter.

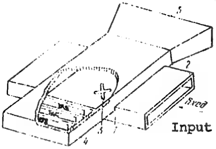

Figure 14.10. A radiating module without an absorbing load.

The resulting transmission gain from the input of waveguide 1 to the aperture of the radiator is defined by the expression:

$$|K_M| = \frac{\alpha\beta Q^{-1}\sqrt{1-\Gamma_p^2}\,e^{-jn\Delta}}{1+\alpha^2 Q^{-1}\Gamma_p e^{-jn\Delta}}\left(1-\frac{\gamma}{\beta}\,\frac{1}{\alpha Q^{-1}e^{-jn\Delta}}-\delta\right). \tag{14.15}$$

In this module, even in the case of ideal elements, the input of waveguide 1 is always mismatched because of the presence of a wave which propagates through the coupling pole of the phase shifter to the radiator.

The reflection factor of the radiating module without an absorbing load, taking into account the nonideal nature of the elements incorporated in it, is:

$$|\Gamma_M| = \delta - \frac{\beta^2 Q^{-1} e^{-jn\Delta}}{1+\alpha^2 Q^{-1}\Gamma_p e^{-jn\Delta}}\left(1-\frac{2\alpha\gamma\Gamma_p}{\beta}\right). \tag{14.16}$$

The maximum amplitude and phase errors of a module without an absorbing load are:

$$|\Delta A| = \frac{1}{1+\alpha^2 Q^{-1}\Gamma_p}\left(\alpha^2\Gamma_p + \frac{\gamma}{\alpha\beta Q^{-1}} - \delta\right); \tag{14.17}$$

$$|\delta\varphi| = \arcsin\left|\frac{1}{1+\alpha^2 Q^{-1}\Gamma_p}\left(\alpha^2\Gamma_p + \frac{\gamma}{\alpha\beta Q^{-1}} - \delta\right)\right|. \tag{14.18}$$

When designing a module, by specifying definite values of its amplitude and phase errors, a module circuit configuration is chosen which governs its structural design.

14.5. Waveguide Directional Couplers

One of the elements of a radiating module is a directional coupler, on the properties of which the characteristics of the module itself substantially depend. Directional couplers using coupled striplines are treated in Chapter 23. The major parameters of couplers cited there (the cross-talk attenuation C_{12}, directivity C_{24}, etc.) are also characteristic of waveguide directional couplers. In this chapter, C_{12} and C_{24} are defined by the following expression:

$$C_{12} = -10\lg(1/\beta)^2,\ \ C_{24} = -10\lg(\beta/\gamma)^2. \tag{14.19}$$

The waveguides in couplers are frequently arranged perpendicularly to each other (Figure 14.11). One or two coupling holes are used depending on the requisite cross-talk attenuation C_{12} [6]. The spacing from the waveguide walls to the center of a hole is $x \approx a/4$.

Experimental gaphs of C_{12} and C_{24} are given in Figures 14.14--14.17 as a function of the slot dimensions for directional couplers with orthogonal configuration of the waveguide. We will note that for crosstalk attenuations of less than -20 dB,

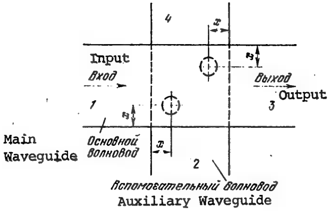
4
x
Input
Вход
Выход
Output
1
3
Main
Waveguide
Основной
волновод
x
2
Вспомогательный волновод
Auxiliary Waveguide

Figure 14.11. Configuration of a crossed waveguide directional coupler.

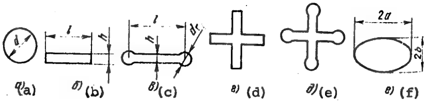
d
l
h
l
h
2a
2b
а)(a)
б)(b)
в)(c)
г)(d)
д)(e)
е)(f)

Figure 14.12. Configuration of coupling holes.
a. Circular;
b,c. Rectangular with and without dumbbells;
d,e. Cross-shaped with and without dumbbells;
f. Ellipsoidal.

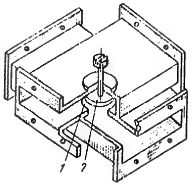

Figure 14.13. A directional coupler with variable crosstalk attenuation.

Key: 1. Circular coupling hole;
2. Moving metal disk.

the dimensions of the slots are calculated from the formulas given in [7], however, for a greater attenuation (right up to C_{12} = 13 dB), these formulas yield considerable errors and it is better in practice to employ the experimental graphs (Figures 14.14--14.17).

The configurations of the coupling elements which are most frequently employed in practice are shown in Figure 14.12. It is impossible to obtain a crosstalk attenuation of $C_{12} > -16...-18$ dB for a single circular opening. Either two holes made in opposite angles of the common wall of the waveguides (Figure 14.11) or directional couplers with variable coupling (Figure 14.13) are used to increase C_{12}.

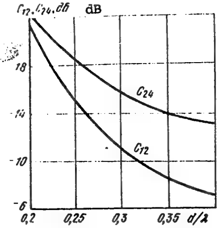

Figure 14.14. The crosstalk attenuation C_{12} and directivity C_{24} of a coupler with two circular coupling holes as a function of the hole diameter.

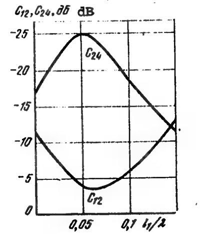

Figure 14.15. The crosstalk attenuation C_{12} and the directivity C_{24} as a function of the disk.

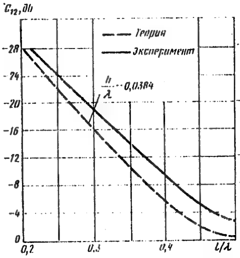

Figure 14.16. The crosstalk attenuation for a cross-shaped coupling hole (Figure 14.12d) as a function of the slot length. [The dashed curves are from theory and the solid curves are experimental].

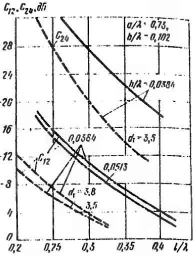

Figure 14.17. The crosstalk attenuation C_{12} and directivity C_{24} of a coupler with two cross-shaped coupling holes as a function of the slot length.

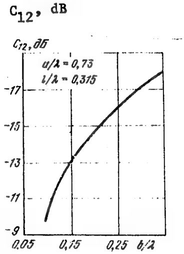

Figure 14.18. The crosstalk attenuation of a coupler with two cross-shaped coupling holes as a function the waveguide height.

Curves for C_{12} and C_{24} are spotted in Figure 14.14 as a function of the change in the diameter d of the opening. The crosstalk attenuation of $C_{12} = -8$ dB corresponds to the maximum diameters of the two openings.

Experimental curves for the crosstalk attenuation C_{12} and the directivity C_{24} are plotted in Figure 14.15 as a function of the depth of disk immersion, l_1.

Crossed coupling slots (Figures 14.12d, e) make it possible to provide a crosstalk attenuation of down to -3 dB while retaining a high directivity. The theoretical and experimental curves for the crosstalk attenuation C_{12} are shown in Figure 14.16 for a change in the slot length for a cross-shaped opening (Figure 14.12d).

Experimental curves for the crosstalk attenuation and directivity as a function of the slot length as shown in Figure 14.17 for a directional coupler with two cross-shaped coupling poles of the dumbbell type (the dashed curves) as well as those without dumbbells (the solid curves). It can well seen from this figure that the dumbbell and its size has a considerable impact on the crosstalk attenuation for the same slot length l. The directivity of such couplers, right up to $C_{12} = -3$ dB, is no worse than -20 to -25 dB. For a greater increase in the crosstalk attenuation, it is necessary to improve the precision in the fabrication of the coupling holes.

The crosstalk attenuation of directional couplers changes substantially as a function of the waveguide height. The crosstalk attenuation is shown in Figure 14.18 as a function of the b dimension of the narrow wall of a waveguide. C_{12} changes especially sharply at small values of b.

14.6. An Approximate Design Calculation Procedure for a Radiating Module

When designing a radiating module, one takes into account the fact that it is an element of a phased waveguide array. Then the initial data are:

--The width of the directional pattern of a single module at the half-power level, $2\theta_{0.5}$;

--The discrete step of the phase shifter, Δ;

--The permissible values of the amplitude and phase errors of the phase shifter (σ_m, ν) and the radiating module (ΔA, $\delta\Phi$);

--The parameters of the slotted bridge (the decoupling c, the reflection factor at the bridge input Γ and the division ratio between the output arms, κ);

--The parameters of the directional coupler (crosstalk attenuation $C12$ or the branching of the incident wave β, the directivity C_{24}, the reflection factor δ);

--The reflection factor from the absorbing load Γ_H;

--The module efficiency η.

We shall consider an approximate procedure for the design of a radiating module for two possible variants.

Variant 1. The following are specified: Δ, $2\theta_{0.5}$, σ_m, ν, ΔA, $\sigma\Phi$, Γ_H, Γ, C_{24}, C_{12}, κ, δ and c. Determine the efficiency of the module.

1. It is expedient to start the design with the choice of the module circuit configuration (see Figure 14.1), working from the specified directional pattern width of the module, $2\theta_{0.5}$, and its amplitude ΔA and phase $\delta\Phi$ errors.

2. Knowing Δ, determine the type and circuit configuration of the phase shifter (see § 14.2). Then, the coefficients K_{Φ}' and Γ_{Φ}' of the selected phase shifter are found using formulas (14.4) and (14.5). The losses in the n-i-p-i-n diodes of the phase shifter are determined from formula (14.6).

3. After this, the amplitude σ_m and phase ν errors in the phase shifter are found and they are compared with the specified values. If σ_m and ν exceed the specified values, then it is necessary to more precisely specify the type and circuit of the phase shifter and repeat all of the calculations.

4. Horns, dielectric rods and spirals find the greatest application as radiators. The type of radiator is chosen from [0.5] and its dimensions and electrical characteristics are calculated.

5. Knowing C12 for β, we determine γ from expression (14.19), and the number of coupling holes in the coupler and their dimensions are chosen from the graph of Figures 14.14 - 14.18.

6. Then, based on the values found fro the parameters of the module and phase shifter, the transmission gain K_M and the reflection factor Γ_M of the module are determined from formulas (14.10) and (14.11). The maximum values of the amplitude error ΔA and the phase error $\delta\Phi$ of the module are found from formula (14.12) and (14.13).

7. Then the module efficiency is determined (see (14.14)).

Variant 2. The following are specified: Δ, $2\theta_{0.5}$, σ_m, ν, Γ, ϕ, κ, δ, Γ_H, $C12$, $C24$ and η. Determine the maximum values of the amplitude ΔA and phase $\delta\Phi$ errors of the module.

It is first of all necessary to perform the design calculations for the module as indicated in paragraph 1--5 for variant 1. Then the coefficients K_M (14.10) and Γ_M (14.11) are determined. We find η from formula (14.14).

If η is less than the specified value, then it is necessary to moreprecisely specify the coefficients in formulas (14.16), (14.10) and (14.11) which influence the efficiency of the module, and then determine K_M, Γ_M and η over again. Then, ΔA and $\delta\Phi$ are to be determined from equations (14.12) and (14.13).

If the design calculations are performed for a module with an absorbing load, then the procedure for the calculations remains as before, only instead of expressions (14.10) - (14.13), the corresponding formulas are used: (14.15) - (14.18).

In both variants, it is necessary during the module design process to determine which of its parameters (κ, Γ, c, δ, γ, β, Γ_H, Γ_p) have the greatest influence on the module characteristics (K_M, Γ_M, ΔA, $\delta\Phi$, η). For this, some of the elements are assumed to be ideal or their parameters are fixed in the appropriate formulas (14.10) - (14.14) or (14.15) - (14.18), and in the calculations, one must change the parameter, the influence of which on the resulting characteristics of the module must be ascertained.

The structural design of a module is accomplished taking its use in a phased array into account.

15. MODULES OF TRANSMITTING PHASED ANTENNA ARRAYS USING SEMICONDUCTOR DEVICES

The use of semiconductor active elements, microwave generators of various types, which make it possible to boost the operational speed and reliability of radio electronic systems, as well as improve their size and weight characteristics, is promising for aircraft transmitting actve phased antenna arrays (AFAR).

A transmitting active phased array takes the form of a system of radiators, arranged on some surface, each of which is excited by a separate generator, which makes it possible to reduce the losses in the distribution device of the array, and consequently, improve the overall system efficiency.

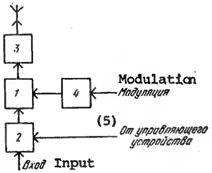

Figure 15.1. Block diagram of a module.

Key:
1. Microwave generator;
2. Controlled phase shifter;
3. Matching device;
4. Modulator;
5. From the controller.

We shall call a device consisting of a radiator, active elements as well as the signal control elements, an active phased antenna array module in the following. A block diagram of a module is shown in Figure 15.1. The microwave generator in this module can be realized using various active elements: power amplifiers with a tuned or bandpass response, combination of a power amplifier and a frequency converter (for example, a multiplier), and it is also possible to use a power self-excited oscillator. In the latter case, the oscillators in the modules in all of the radiators should be synchronized to assure coherency. The output signals of the modules can be modulated using a modulator or the modulted signals can be amplified. To provide for the optimal operating conditions of the active element, it is necessary to have a device for matching the radiator. Finally, to obtain directional radiation and the capability of scanning, a definite phase distribution of the output signals of the modules is produced by means of controlled phase shifters. The array modules are excited by a distribution system. The main techniques of exciting the modules of active phased arrays are shown in Figure 15.2. The excitation circuit shown in Figure 15.2a includes a power divider and a microwave channel, which produce specified amplitude and phase relationships at the inputs to the modules. Using a frequency multiplier in an active phased array module makes it possible to operate the excitation distribution system at a reduced frequency, something which can additionally reduce the losses in it. In those cases where the power of the exciter proves to be inadequate to excite all of the modules of an array, stepped excitation is employed (Figure 15.2b). A transmissive spatial excitation configuration of the modules is shown in Figure 15.2c, while a reflective circuit is shown in Figure 15.2d. It is expedient to use the two latter excitation circuits in the case of modules with frequency conversion (or multiplication), since in this case, the portion of the exciter power radiated beyond the edge of the array does not participate in the formation of sidelobes in the array directional pattern at the working frequency.

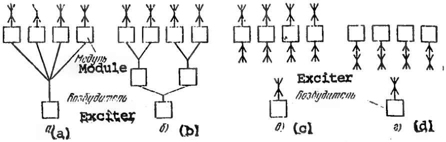

Figure 15.2. Excitation configurations for modules in active phased arrays.

We shall also note the possibility in principle of using mutual coupling between the radiators to excite an active phased array. In this case, there is no need to use a cumbersome distribution device. Thus, using two pole active devices, one can provide for a synchronous self-oscillating mode in the array modules.

15.1. The Major Characteristics of the Active Elements of Modules

A transmitting active phased array can be treated as a device which sums the radiation power of several modules in a specific direction.

We shall consider the major requirements placed on the characteristics of the active elements of active phased array modules, the meeting of which assures effective summing. The output power of a module is governed by the requirements placed on the radiation power level and can be defined as the ratio $P_M = P_\Sigma/N$, where P_Σ is the total radiation power; N is the number of modules in the array.

The gain of the generator of a module is defined as the ratio of the input power to the module to the excitation power. Increasing the gain makes it possible to reduce the excitation power for a set radiation power, and consequently, the power losses in the distribution device in which the bulk of the radio frequency losses occur. With an increase in the number of modules with a constant array step, its directional pattern narrows and the losses in the distribution system increase. For this reason, modules with a high gain should be used for arrays with narrow directional patterns.

The gain of a generator which provides for complete compensation of the losses in the excitation system is $K_p = 1/\eta_\Phi$, where η_Φ is the overall efficiency of the distribution system, taking into account the losses in the phase shifters and the matching elements at the inputs to the modules. The maximum value of K_p is limited by the amplifier stability margin or the synchronous operational mode margin of a self-excited oscillator. Moreover, there are possible limitations related to the increase in the phase instability in the modules with an increase in K_p because of the rise in the slope of the generator phase characteristic.

The efficiency of a generator governs the overall efficiency of an active phased array to a considerable extent, which is equal to the ratio of the total radiation power to the power of the primary power supplies for the array, including the exciter power supply. Moreover, generator efficiency governs the thermal mode of the array modules. A poor efficiency of the active elements can lead to severe thermal conditions and limit the maximum radiation power.

The load characteristic of a generator (the output power and phase of the output signals as a function of the total input impedance of the radiator Z_{in}) is one of the most important characteristics of a generator when it is used in array modules with wide angle scanning. In these arrays, the total input impedance of a radiator during scanning changes considerably because of the mutual coupling of the radiators, where the laws governing the change in Z_{in} prove to be different for the central and peripheral radiators. Because of the change in Z_{in}, there is a change in the resistive component of the load impedance of the generator output stage, something which leads to a change in the output power and the electronic operating conditions, in particular, to a change in the power losses in the generator. The reactive component of the load impedance determines the mistuning of the output microwave circuit of the generator relative to the excitation frequency as well as the corresponding change in the output phase. Thus, a change in the input impedance of a radiator during scanning leads to the appearance of amplitude and phase errors at the output of a module, and as a result, to a reduction in the directional gain for specific radiation directions. The maximum scan angle in this case can prove to be limited by the permissible reduction in the array directional gain.

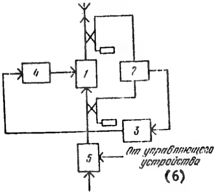

Figure 15.3. Block diagram of an active phased array module having a generator with a phase locked loop.

Key:
1. Microwave oscillator;
2. Phase detector;
3. Direct current amplifier;
4. Phase controller for the oscillator output;
5. Phase shifter;
6. From the controller.

One of the ways of reducing the impact of the input impedance of a radiator on the parameters of a module in a transmitting active phased array is the use of nonreciprocal elements, for example, ferrite isolators and circulators, inserted between the generator and radiator.

Besides the requirements treated above, others are also placed on modules which are common to generators operating as part of radio transmitting systems, for example, on the passband, level of harmonic filtration, etc.

We will note that the inconstancy of not only the load but also the supply voltages and temperature have a destabilizing effect on the phase of the output signals of a module. The overall phase error at the output of a module, taking into account the effect of all of the destabilizing factors, can prove to be impermissibly high. In this case, phase locked loop tuning systems can be used to eliminate the phase error. An example of the structural configuration of a module having an oscillator using a phase locked loop is shown in Figure 15.3.

15.2. Major Structural Design Requirements

The overall dimensions of active phased array modules are governed by the possibility of placing them in an antenna array. To eliminate spurious radiation maxima during scanning, the array step should not be significantly greater than $\lambda/2$. For this reason, when designing active phased array modules, especially for the centimeter band, there arises the problem of their miniaturization. This task is complicated in the case of transceiving arrays in which the module should also contain a receiving section and a device for separating the transmitted and received waves.

These requirements can be satified with a hybrid integrated circuit design of the modules. However, the small dimensions of active semiconductor devices and their limited electron efficiency leads to excessive localization of the heat emissions and the necessity of using effective heat sinks and cooling devices, which limit the miniaturization possibilities.

The range of miniaturization of electromagnetic systems in a film integrated circuit design is limited. The major component of a microwave circuit is the asymmetrical microstrip transmission line. The microwave networks of oscillators and amplifiers should contain line sections, the length of which is commensurate with a half-wavelength. Thin (units and tenths of a millimeter) dielectric substrates with a high relative dielectric permittivity (about ten) are used to reduce the wavelength in a line as well as the transverse dimensions of a line, where these substrates make it possible to reduce the wavelength in a line by a factor of about 2.5 times, while the transverse dimension of the conducting strip is reduced to tenths of a millimeter. However, such small transverse dimensions lead to an increase in the losses in the conductors. Moreover, elevated losses occur in dielectrics with a large dielectric permittivity. As a result, the Q of microstrip oscillating systems falls off an average of 5 to 10 times as compared to waveguide and coaxial oscillatory systems, something which leads to a reduction in the efficiency of the microwave circuits of high power oscillators.

In the decimeter band, one can employ oscillating systems using lumped inductances made with film technology and lumped capacitances, both outboard types and film technology capacitors, which makes it possible to additionally reduce the size of the microwave circuitry as compared to the wavelength, but which leads to an even greater increase in conductance losses.

15.3. Active Semiconductor Devices for Active Phased Antenna Array Modules

At the present time, transistors and various diodes with negative resistance are used in active phased array modules. Moreover, diodes with a nonlinear capacitance of the p-n junction (parametric diodes, varactors and charge storage diodes) are also used. With the exception of parametric amplifiers and oscillators, nonlinear capacitance devices are not active ones and are used as passive microwave frequency multipliers, as well as for amplitude, frequency and phase modulation.

We shall briefly consider the properties of microwave devices in which the semiconductor devices enumerated above are employed.

Microwave power amplifiers using transistors are employed in the decimeter and centimeter bands at output powers of from tens to a few watts in the long wave portion of the centimeter band. These amplifiers have a relative bandwidth of up to 10 to 15%. Their gain amounts to 15 to 25 in the long wave portion of the decimeter band and 2 to 3 in the short wave portion of this band, as well as in the centimeter band. The efficiency of transistor amplifiers ranges from 15 to 25%, which is markedly greater than the efficiency of power amplifiers using other semiconductor devices. Microwave self-excited oscillators are also designed around transistors, both with mechanical and electronic frequency tuning. In such self-excited oscillators, as a rule, external feedback circuits are employed, which, of course, complicates their structural design as compared to diode oscillators and amplifiers. An advantage of transistorized microwave amplifiers is also the unidirectional nature (without additional decoupling components).

Generators and amplifiers using negative resistance diodes are employed primarily in the centimeter and millimeter bands. The operational principle of such devices is based on the compensation of the resistance of the resonant system, taking into account the resistance introduced by the load: by the negative resistance of the impedance of the diode. With total compensation for the losses, as self-excited oscillator mode is established in the generator. With partial compensation of the losses, there is regenerative amplification of external signals. As specific feature of self-excited diode oscillators is the absence of external feedback circuits, which simplifies their design as compared to the design of three-terminal generators. Regenerative amplifiers do no have unidirectional properties and require the use of isolating elements.

Diodes with various negative resistance mechanisms are used in microwave diode oscillators and amplifiers: avalanche-transit diodes (LPD's) [IMPATT diodes] and diodes with electron transport between valleys (DPE's) [tunnel diodes]. IMPATT diodes are used primarily in generators with an output power of a few watts in the centimeter band and hundreds of milliwatts in the millimeter band. The wide scale use of IMPATT diode amplifiers is precluded by the high noise level, which is related to the avalanche nature of the generation of charge carriers in these diodes. Tunnel diode oscillators are three to ten times inferior in terms of power to IMPATT diode oscillators, however, they have somewhat better noise characteristics. The efficiency of diode oscillators does not exceed 10% at the present time in the centimeter band.

Frequency multipliers using varactors and charge storage diodes (DNZ's) are usually employed for frequency multiplication in transistor power amplifiers, which makes it possible to obtain outputs with power levels suitable for many practical applications as well as acceptable efficiencies in the shortwave portion of the decimeter and centimeter bands. The output frequencies of varactor multipliers with a blocked junction can attain 30 to 50 GHz. As has already been noted, diode multipliers with a nonlinear capacitance of the p-n junction do not have any gain and the microwave power conversion gain for them is always less than unity, and becomes less, the greater the multiplication factor.

We will note that each of the semiconductor devices treated here can operate using parametric effects. For example, an amplification mode in a transistor can be combined with parametric frequency multiplication of the amplified signals across a nonlinear collector capacitance. Autoparametric modes are employed in diode oscillators.

15.4. The Radiation Power of Active Semiconductor Phased Antenna Arrays

We shall estimate the radiation power of a planar active phased array designed using the configuration of Figure 15.2a, for the following types of active devices: transistors, IMPATT diodes and tunnel diodes. The power capabilities of these devices are illustrated by the graphs in Figure 15.4. In the active phased array configuration considered here, the devices enumerated above can be used both as amplifiers and self-excited oscillators. In the latter case, the exciter synchronizes the oscillations in all of the modules of the active array.

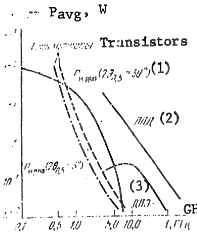

Figure 15.4. The power of semiconductor devices as a function of the working frequency.

Key:
1. Permissible radiation power for a single element in an array $(2\theta_{0.5} = 30°)$;
2. IMPATT diodes;
3. Tunnel diodes.

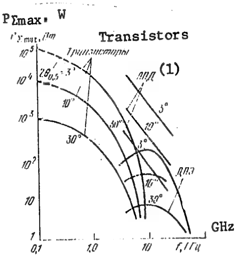

Figure 15.5. The total radiated power as a function of frequency.

Key:
1. IMPATT diodes;
2. Tunnel diodes.

The total radiation power of an active phased array is governed by the output power of a module, the layout density of the radiators and the size of the array. In turn, the array size depends on the width of its directional pattern, $2\theta_{0.5}$ and can be defined as $L \simeq 60\lambda/2\theta_{0.5}$.

As has already been noted, the array step is approximately $\lambda/2$. It is difficult in practice to reduce the step, since the transverse dimensions of the radiators are usually close to a half-wavelength (for example, $\lambda/3$ for spirals, about $\lambda/2$ for symmetrical dipoles, etc.).

Thus, the maximum number of radiators in, for example, a square array is $N^2 = (2L/\lambda)^2$ or taking into account the relationship between L and $2\theta_{0.5}$, $N^2 = 1.44 \cdot 10^4/2\theta^2_{0.5}$.

Then the maximum value of the total radiation power is:

$$P_{\Sigma\,\max} = 1,44\cdot10^4\,P_M/2\theta^2_{0.5},$$

where P_M is the radiation power of a single array element.

An estimate of the total radiation power for arrays built using transistors, IMPATT diodes and tunnel diodes which was obtained in this fashion in shown in Figure 15.5. The dashed lines show the possible limitation of the power in the long wave region because of the unacceptably large array dimensions.

The problem of minimizing the number of radiators for the purpose of simplifying and reducing the cost of the structural design of an array and the control devices usually comes up when developing a phased array. The same problem can also occur in the case of active phased antenna arrays. We shall determine the reduction in the radiation power with such minimization.

The maximum array step for which there are no spurious maxima is:

$$d = \lambda/(1+\sin\theta_{\max}),$$

where $\theta_{\max}$ is the maximum beam deflection angle from the normal.

Correspondingly, the number of radiators in a square array is:

$$N^2 = L^2(1+\sin\theta_{\max})/\lambda^2,$$

and the total radiation power is:

$$P_\Sigma = 3,6\cdot10^3\,P_M\left(\frac{1+\sin\theta_{\max}}{2\theta_{0.5}}\right).$$

The reduction in the power as compared to the maximum value is:

$$\frac{P_\Sigma}{P_{\Sigma\max}} = \left(\frac{1+\sin\theta_{\max}}{2}\right)^2.$$

This ratio is shown in Figure 15.6 as a function of a specified scan angle θ. It can be seen from this figure, for example, that with the minimization of the

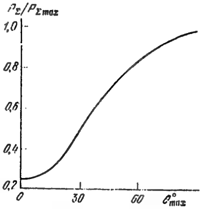

Figure 15.6. The relative reduction in power as a function of the scanning angle.

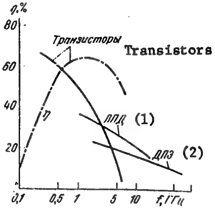

Figure 15.7. The efficiency of semiconductor oscillators as a function of frequency.

Key: 1. IMPATT diodes;
2. Tunnel diodes.

number of radiators, and consequently also the number of array modules, for a scan sector of $\theta_{max} < 15°$, the total radiated power amounts to approximately a quarter of the maximum value determined by the graphs of Figure 15.5.

The Efficiency of Active Elements and the Thermal Conditions in an Array. The maximum values of the efficiency which can be attained at the present time for the semiconductor devices considered here are shown in Figure 15.7 for various frequencies, from which it can be seen that the efficiency of the active devices falls off with a rise in frequency, and at frequencies above 5 GHz, can drop down to 10 to 25%. Along with this, the average radiofrequency power flux density through the radiating surface of the array, S, for an array step close to λ/2, is:

$$P_{\Sigma}/S = P_{M} N^{2} \Big/ \left(\frac{\lambda}{2} N\right)^{2} = 4P_{M}/\lambda^{2}$$

and, as can be seen, increases for a set power of an array element in proportion to the square of the frequency. The thermal flux density through the surfaces bounding the array structure, by virtue of the decrease in the efficiency with increasing frequency, rises even more rapidly, something which can lead to the establishing of severe and even unacceptable thermal conditions in the modules. The use of effective forced cooling methods though detracts to some extent from one of the advantages of a semiconductor active phased array: its compactness.

We shall estimate the thermal limitations in the case of natural cooling of a structure by the ambient air, keeping in mind that the thermal mode of an array depends on the specific features of its structural design, and for this reason, a preliminary estimate can only be a very approximate one.

We shall represent the structural design of an array in simplified terms: in the form of a compact planar unit with solid walls. We shall initially treat the case where the area S of the radiating surface is considerably greater than the area of the side surfaces of the structure, while the heat output through the surface opposite to the radiating surface is made difficult because of the presence of the distribution device which is close to it. It can be assumed that the thermal output in this case, which occurs with the generation of narrow directional patterns, takes place primarily through the radiating surface of the array, i.e., the heat output surface can be considered as coinciding with the radiating surface S.

Then, in a steady-state thermal mode, the heat flux density is:

$$P_{M\ loss}/S_M = \frac{P_{\text{М пот}}}{S_{\text{М}}} = \frac{P_{\text{М}}}{S_{\text{М}}}\left(\frac{1}{\eta_{\text{М}}}-1\right) = 4\frac{P_{\text{М}}}{\lambda^2}\left(\frac{1}{\eta_{\text{М}}}-1\right),$$

where $P_{M\ loss}$ is the power loss in the module; η_M is the module efficiency; S_M is the array area allocated for one module.

The heat flux density determines the temperature gradient between the cooled surface and the air in accordance with the relationship:

$$\frac{P_{\text{М пот}}}{S} = \alpha\Delta t \text{ или } 4\frac{P_{\text{М}}}{\lambda^2}\left(\frac{1}{\eta_{\text{М}}}-1\right) = \alpha\Delta t,$$

where α is the heat transfer coefficient.

We shall set a permissible temperature gradient of $\Delta t_{per} = 50°$ C, for which in the case of cooling by natural air convection and thermal radiation, $\alpha = 8\ \text{W}\cdot\text{m}^{-2}\cdot\text{deg}^{-1}$. The minimum permissible value of the module efficiency is:

$$1/\eta_{M\ per} = 0.25\ \alpha\Delta t_{per}\lambda^2/P_M + 1 \qquad 1/\eta_{\text{М доп}} = 0{,}25\alpha\Delta t_{\text{доп}}\lambda^2/P_{\text{М}}+1,$$

and for the values adopted for α and Δt:

$$1/\eta_{M\ per} = 100\lambda^2/P_M + 1. \qquad 1/\eta_{\text{М доп}} = 100\lambda^2/P_{\text{М}}+1.$$

The calculation performed with this formula for a transistor module shows that the quantity $\eta_{M\ per}$ changes with frequency, as shown in Figure 15.7. It can be seen that at frequencies above 0.6 GHz, the actual efficiencies of devices is less than the minimum permissible, and this means (for the assumed value of α), that the use of transistors in this frequency range in maximum power modes, determined by the corresponding curve (Figure 15.4), leads to unacceptable thermal conditions in the array.

Also shown in Figure 15.7 are the attainable values of the efficiency for IMPATT and tunnel diodes. For IMPATT diode modules, the minimum permissible efficiency amounts to no less than 90%, which significantly exceeds the actual efficiency throughout the entire range of utilization of these devices. For modules using tunnel diodes, the values of $\eta_{M\ per}$ approximately coincide with the feasible values. Consequently, these devices can be used in maximum power modes.

To establish the permissible thermal mode of an array in frequency regions where the actual efficiencies of a module are less than the minimum permissible values, the power of an array element should be reduced down to:

$$P_{M\ per} = \eta_M \alpha \Delta t_{per} \lambda^2/4(1 - \eta_M), \qquad P_{\text{м доп}} = \eta_{\text{м}} \alpha \Delta t_{\text{доп}} \lambda^2/4(1 - \eta_{\text{м}}),$$

while for the values adopted for α and Δt, it should be reduced down to:

$$P_{M\ per} = 100\eta_M \lambda^2 (1 - \eta_M).$$

In some usage ranges for transistors, the permissible power is more than an order of magnitude lower than the possible power of the device (see the curve for $P_{M\ per}$ for $2\theta_{0.5} = 3°$ in Figure 15.4. The maximum value of the total radiated power because of thermal limitations does not exceed:

$$P_{\Sigma\max} = 1{,}44 \cdot 10^6 \frac{\eta_{\text{м}}}{1 - \eta_{\text{м}}} \left(\frac{\lambda}{2\theta_{0,5}}\right)^2.$$

In the case of a broad directional pattern, the radiating surface of the array proves to be reduced and the structural configuration of the array approaches a cube. The cooling conditions are significantly improved in this case by virtue of heat transfer from the side surfaces of the structure. Assuming the shape of the structure to be close to a cube, one can figure that the thermal flux density is reduced by a factor of three to five. Then, we obtain the following for the minimum permissible efficiency and power:

$$1/\eta_{\text{м доп}} = 400\lambda^2/P_\Sigma + 1;$$
$$P_{\text{м доп}} = 400\eta_{\text{м}} \lambda^2/(1 - \eta_{\text{м}}).$$

In this case, the gap between the maximum possible module power and the permissible power proves to be smaller (see the curve for $P_{M\ per}$ for $2\theta_{0.5} = 30°$ in Figure 15.4).

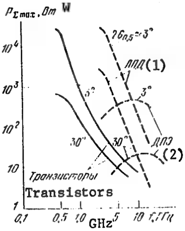

Figure 15.8. The total radiated power as a function of frequency, taking thermal limitations into account.

Key: 1. IMPATT diodes;
2. Tunnel diodes.

Graphs of the maximum values $P_{\Sigma\ max}$ are shown in Figure 15.8 for values of $\eta_{M\ per}$ determined from the graphs of Figure 15.7 for narrow ($2\theta_{0.5} \approx 3°$) and wide ($2\theta_{0.5} \approx 30°$) array directional patterns for three types of active devices used in modules. It can be seen from Figure 15.8 in particular that when using tunnel diodes, because of the absence of thermal limitations, the radiated power is increased while the directional pattern narrows much more rapidly than, for example, when using IMPATT diodes, for which there are thermal limitations.

The estimate made here for the powers and working frequencies of active phased arrays with microwave amplifiers or oscillators using semiconductor active devices is approximate. The limitations which have been ascertained are not to be treated as the impossibility of of designing active phased arrays for certain values of transmitted powers and frequencies. These limitations point only towards certain difficulties in constructing an array. The thermal limitations which arise because of the necessity of a rather dense layout of the modules, as well as because of the insufficient efficiency of semiconductor oscillators and amplifiers in certain frequency bands are obviously the most important.

There are the following possibilities for reducing or eliminating thermal limitations: increasing the efficiency of the active devices or developing effective methods of cooling them, which do not substantially increase the size and weight of the array structure.

15.5. Active Phased Antenna Array Efficiency

As has already been noted, an active antenna array can have a greater efficiency than a passive one as a result of the decrease in the losses in the distribution system. The possibility of realizing a gain in the efficiency depends on the efficiency of the array distribution system, the efficiency of a module and its active element gain.

We shall estimate the efficiency of an active array designed in the configuration of Figure 15.2a, and determine the advantage gained in the efficiency as compared to a passive array. We shall introduce the following symbols: η_Γ is the overall efficiency of the transmitter working into a passive array; η_Φ and η'_Φ are the efficiencies of the distribution units for the passive and active arrays [respectively]; η_B and η_M are the efficiencies of the exciter and a module of the active array; K_{P_M} is the power gain of an active array module; P is the RF power delivered to a radiator; we assume the efficiencies of the radiators to be close to unity in both systems.

The efficiency of an array is $\eta_A = 1 - P_\pi/P_0$, where P_0 is the power consumed from the active element power supplies; $P_\pi = P'_\pi + P''_\pi$ are the total power losses in the array, which are composed of the RF losses P'_π in the distribution device and the conversion losses P''_π in the active elements.

For an active array, when figured on a per radiator basis, we have a conversion loss power in the generator $P''_{\Gamma\pi}$ and the exciter $P''_{B\pi}$:

$$P''_{\Gamma\text{п}} = (1-\eta'_\Gamma)\,P/\eta'_\Gamma;\quad P''_{\text{вп}} = (1-\eta_\text{в})\,P/K_{P_\text{м}}\,\eta'_\Phi\,\eta_\text{в}.$$

The power losses in the distribution unit are:

$$P' = (1-\eta'_\Phi)\,P/K_{P_\text{м}}\,\eta'_\Phi.$$

The power of the power supplies for the modules $P_{0\Gamma}$ and the exciter P_{0B}, when figured on a per module basis, amount to $P_0 = P_{0\Gamma} + P_{0B} = P/\eta_M + P'K_{P_M}\eta'_\Phi\eta_B$.

By summing all of the losses, in accordance with the definition introduced for the efficiency, we obtain the expression for the efficiency of an active array:

$$\eta_{\text{Aa}} = \eta'_\Phi\,\eta_\text{м}\,\eta_\text{в}\,(K_{P_\text{м}}+1)/(\eta_\text{м}+K_{P_\text{м}}\,\eta'_\Phi\,\eta_\text{в}).$$

The efficiency of a passive array is $\eta_{A\pi} = \eta_\Gamma \eta_\Phi$. Thus, the gain in the efficiency of an active array as compared to a passive one is:

$$M = \frac{\eta_{Aa}}{\eta_{A\Pi}} = \frac{\eta_M \eta'_\Phi}{\eta_\Gamma \eta_\Phi} = \frac{K_{P_M}+1}{\eta_M/\eta_B + K_{P_M}\eta'_\Phi}.$$

The graphs of the advantage gained as a function of η_Φ plotted from the formula:

$$M = (K_{P_M}+1)/(1+K_{P_M}\eta_\Phi),$$

are justified for $\eta_\Phi = \eta'_\Phi$; $\eta_\Gamma = \eta_M = \eta_B$, are shown in Figure 15.9. To determine the advantage gained, M, using these graphs, the scale on the ordinate is to be changed by a factor of η_M/η_Γ times in the case where $\eta_M \neq \eta_\Gamma$, which is frequently encountered in practice.

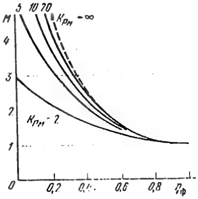

Figure 15.9. The amount of the gain in the efficiency of an active array as a function of the feed channel efficiency.

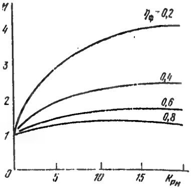

Figure 15.10. The amount of the gain in active array efficiency as a function of module gain.

The graphs show that it is expedient to use active phased arrays in the case of large losses in the distribution system. For example, when $\eta_\Phi = 0.2 M = 3.7$, for $K_{P_M} = 10$. The advantage gained in the efficiency depends on the number of radiators: with an increase in the number of radiators (when the directional pattern is narrowed), the advantage gained in the efficiency of an active array increases as compared to a passive array.

The advantage gained in the efficiency also increases when modules are used which have a high power gain. Curves of the advantage gained M are shown in Figure 15.10 as a function of the gain K_{P_M}. As follows from the graphs, a substantial rise in the advantage occurs with an increase in K_{P_M} up to approximately 10. A further increase in the gain does not lead to a marked rise in the advantage, if the efficiency of the distribution system is no lower than 0.2.

The expression derived for the advantage gained in the efficiency makes it possible to evaluate the expediency in power terms of using an active antenna array in place of a passive one. An advantage of M > 1 obtains if the efficiency of the modules used in the active array satisfy the condition:

$$\eta_M > \frac{K_{P_M}\eta_\Gamma\eta_\Phi}{K_{P_M}+1-\eta_\Gamma\eta_\Phi/\eta_\Pi\eta'_\Phi}$$

or when $K_{P_M} \gg 1$, the condition $\eta_M > \eta_\Gamma\eta_\Phi$. For example, if in a passive array $\eta_\Phi \approx 0.3\eta_\Gamma \approx 0.5$, then a transition to an active array is expedient in power terms where the efficiency of a module in such an array is no less than 0.15.

It should be noted that the increase in the radiation power in the direction of the main lobe of the directional pattern when changing over from a passive to an active array, with a constant power of the power supplies, will be less than the advantage gained in the efficiency. This is due to the presence of additional amplitude, and primarily phase errors in the active elements of the modules. The influence of amplitude errors in the output signals of the modules can be disregarded, however, the appearance of additional phase errors leads to a reduction in the directional gain of an active as compared to a passive array.

15.6. Recommendations for the Selection of Module Circuits and Parameters

The circuit configuration of a module is selected by working from the necessity of obtaining the requisite microwave power level at its output, assuring as high an efficiency as possible for a module as well as a power gain sufficient to reduce the power in the distribution system (for example, by an order of magnitude as compared to the radiated power) for the purpose of increasing the efficiency of the active array. Moreover, the point of insertion of the phase shifter and the modulation method are to be determined, if modulation is provided for the signals specifically in an array module.

The selection of the structural configuration of an active antenna array module should start with the estimate of the module output power. For a known value of the total radiated power P_Σ and a specified directional pattern width of the array, the power required for each radiator, for a square array with a step close to $\lambda/2$, is $P_M \approx 7 \cdot 10^{-5}(2\theta_{0.5})^2P_\Sigma$.

The power of the output stage of a module is $P = 1.2P_1$. By knowing P, we choose the semiconductor device for the output stage, which, in providing the requisite power at the working frequency, has the greatest efficiency. For a comparative estimate of the power and efficiency of various semiconductor devices, one can make use of the graphs of Figures 15.4 and 15.7. In accordance with these graphs, it is preferable to employ transistors in the decimeter band up to frequencies below 1 - 3 GHz. We will note that in this band, the output power of a module can be increased as compared to the values defined by the graphs of Figure 15.4 through adding the powers of several transistors in a module.

At frequencies of 1 - 3 GHz, one can recommend the use of a multiplier stage using a varactor with a multiplication factor of 2 to 4, excited by a transistor oscillator, at the output of a module. The output power of such a transistor--varactor network runs to a few watts with an overall efficiency of 20 to 40%.

At frequencies of 1 - 3 GHz, one can also use TRAPATT diode amplifiers and self-excited oscillators.

Both transistor--varactor chains as well as microwave diode oscillators, IMPATT self-excited oscillators and tunnel diodes can be used in a frequency range of 3 - 10 GHz.

One can obtain powers of units and fractions of a watt with efficiencies of up to 10% in the output stages of a module. Additional considerations may be taken into account in the final selection of the module output stage. For example, the use of transistor--varactor chains makes it possible have phase control at a reduced frequency, which makes it possible in a number of cases to reduce the losses in the phase shifters. On the other hand, diode oscillators and amplifiers are simpler and more compact.

The choice of the semiconductor device for the module output stage determines the entire structural configuration of the module to a considerable extent, since all of the remaining module stages are chosen by working from the necessity of obtaining a definite module power gain.

Transistorized oscillators and amplifiers in the decimeter band, as a rule, have low power gains (2 to 4), and for this reason, to obtain an overall module gain of about 10, it is necessary to use 2 to 3 stages of amplification.

Then one can estimate the overall module efficiency, taking into account the fact that at low gains per stage, it is determined by not just the efficiency of the output stage, but also the preceding stages. Assuming the efficiency and gains of all of the stages to be approximately the same, the overall efficiency of a module can be estimated from the following formula:

$$\eta \simeq \sum_{m=1}^{m=n} \frac{1}{K_{PK}^{m} \eta_1},$$

where η_1 is the efficiency of a stage; K_{P_K} is the stage power gain; n is the number of stages in a module. The losses in the phase shifter have not been taken into account in the formula cited here, assuming that the phase shifter is inserted at the input to the module. The insertion of the phase shifter at another point leads to a drop in the efficiency, and this becomes greater, the higher the power level at which the phase shifter operates. The value of the module efficiency obtained in this manner can be taken as the basis for the estimation of the thermal mode of the array (see § 15.4). Such an estimate should ascertain the necessity of forced cooling of a module.

In the case of active phased arrays using diode generators in a module, as a rule, is a single stage design and consists of an amplifier or a self-excited oscillator and a phase shifter separated by an isolating element. The output of the diode generator is fed to the input of the phase shifter, where the generator is of the same type as the module generator. Taking into account the fact that to obtain a stable gain mode or reliable synchronization of a diode generator, the ratio of its output power to the excitation or synchronization power should be approximately 10, the oscillator or amplifier of the preceding stage can drive

5 to 10 modules. Thus, in the case where diode amplifiers or oscillators are used, an active phased array is designed in the circuit configuration of Figure 15.2b, which makes it possible to standardize the active elements of the array.

When choosing the modulation method, as well as the modulated stage and number of stages, one is to be governed by the same considerations as for multistage transmitters. Here, we shall only note some of the special features which are related to the fact that a large number of modules are modulated simultaneously. Two techniques can be used for the simultaneous modulation of the modules. The first, incorporated in each module is its own modulator, while the modulating signal is fed to the inputs of the modulators at a low power level. In the second, one rather high power modulator services all of the array modules. With the second approach, the modulator power proves to be increased, since a portion of it is lost in the distribution device for the modulating signal. In the first, the module size is increased and its thermal conditions can be degraded because of unavoidable losses in the modulator. In both cases, the distribution unit for the modulating signals should be carefully designed, since with broadband modulation (for example, using short pulses), various modulation distortions can appear in a complex channelizing system.

We shall also note that any amplitude modulation in an active phased array using synchronized diode amplifiers or oscillators is possible only in the output stages, while frequency modulation is possible only by means of synchronizing the output stages with frequency modulated signals. In all cases, the spectral width of the modulating signals should not exceed the synchronization bandwidth.

CHAPTER 16. EXTERNALLY EXCITED OSCILLATORS AND AMPLIFIERS USING POWER TRANSISTORS

16.1. General Information

Microwave power transistors are widely used in externally excited oscillators and amplifiers (Figure 16.1), used in the modules of transmitting active phased antenna arrays as the driver or the output stages, where these have been given the name of power amplifiers. A specific feature of these amplifiers is the comparatively high output power level (more than a watt) with a relatively high efficiency (more than 30 to 40 percent). The power gain K_p is of no less importance for preamplifier stages. Power amplifier usually operate in a transistor collector current cutoff mode. They are frequently structured in the form of hybrid integrated circuits (GIS). Questions of the theory and design of microwave power amplifiers are treated in the literature [1-5].

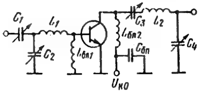

Figure 16.1. Basic schematic of a microwave transistor power amplifier.

A number of problems must be solved when designing a microwave power amplifier, one of which is assuring a transistor operating mode which makes it possible to obtain sufficiently high values of the efficiency and K_p for a specified output power. Because of the difficulty of an analytical solution of such a problem, experimental techniques are frequently used in practice to determine the optimum operational mode of a transistor [6].

The procedure presented here for the design calculations of a microwave power amplifier is based on the utilization of the "piecewise-linear" transistor model. This thoery makes it possible to analyze the major processes in a transistor in a collector current cutoff mode, ascertain the influence of transistor equivalent circuit parameters of its operational mode, develop an engineer procedure for design calculations of high power amplifier stages and compare two transistor circuit configurations: common emitter (OE) and common base (OB).

The amplifier mode depends in many respects on the proper design of its external microwave circuits. In this regard, questions of the electrical and structural design of microwave circuits for transistor power amplifiers are treated in Chapters 17 and 20.

16.2. The Equivalent Circuit of a Microwave Transistor

The equivalent circuit of a microwave power transistor is shown in Figure 16.2 for the collector current cutoff mode. Taken as its basis is the physical equivalent circuit of Giacoletto, supplemented with certain elements of importance for the microwave band. We shall explain the elements of the circuit of Figure 16.2: L_{b2}, L_{e2} and L_{c2} are the external lead inductances of the base, emitter and collector [respectively], usually made in the form of strips or stubs; L_{b1}, L_{e1} and L_{c1} are the corresponding inductances of the internal leads; C_{b0}, C_{e0} and C_{c0} are the transistor lead capacitances to the package; C_{KK} is the collector metallization capacitance to the package; r'_b, r'_c and r'_e are the resistances of the base, collector and emitter material (r'_e also incorporates stabilizing reistance which is a structural component of a number of microwave transistors); r is the recombination resistance; C_e is the barrier capacitance of a cutoff emitter junction; C_{dif} is the diffusion capacitance of a turned-on emitter junction; C_{ca} and C_{cp} are the components of the collector junction capacitance, called the active and passive component capacitances respectively of C_c; C_{ce} is the through capacitance of the emitter contact region;

$$i_g = i_{\text{г}} = \begin{cases} S_{\text{п}}(u_{\text{п}} - U'), & u_{\text{п}} > U', \\ 0, & u_{\text{п}} \leqslant U' \end{cases}$$

is the equivalent controlled current generator. The junction transconductance is a complex quantity: $S_{\text{п}} = \dot{S}_{\text{п}} \exp - j\omega\tau_{\text{п}}$, , where $\omega\tau_{\pi} \simeq 0.4\omega/\omega_{ult}$ is the phase determined by the charge carrier transit time ($\omega_{ult} = 2\pi f_{ult}$, where f_{ult} is the ultimate current gain frequency in a common emitter configuration); u_{π} is the instantaneous voltage across the emitter junction; U' is the voltage shift for the approximated static characteristic i_c (u_v) of the transistor with the piecewise linear approximation. The capacitances between the leads of the transistor are not shown in the schematic of Figure 16.2, which can be neglected in the case of power devices.

The use of the relatively cumbersome equivalent circuit of Figure 16.2 is justified for practical calculations at frequencies ω for which $1/\omega C_{V0} < 10\omega L_{B2}$. At lower frequencies, one may disregard the capacitance between the leads and the package C_{v0} (C_{b0}, C_{e0} and C_{c0}) and the capacitance C_{KK}, while the inductances of leads L_{v1} (L_{b1}, L_{e1} and L_{c1}) and L_{v2} (L_{b2}, L_{e2}, L_{c2}) are replaced by their sum $L_v = L_{v1} + L_{v2}$.

The parameters of the equivalent circuit depend on the currents flowing through it and the applied voltages. Because of this, a rigorous calculation of a transistor operating mode is difficult, even on a computer. However, one can make a rather simple analysis of the processes in a transistor, taking into account the major phenomenon in a cutoff mode, if a simplified model is employed. The parameters of this model are the result of linearization of the actual transistor parameters individually for the active operating regions and the cutoff region. Linearized parameters depend on the transistor operating conditions, for a selected mode, they are considered constant within the range of each region.

Reference data, which are usually the following quantities, can be used to estimate the parameters of a transistor equivalent circuit. h_{21e} is the static current gain in a common emitter configuration, τ_k is the time constant of the internal feedback circuit, also designated as "r_b, C_c, where C_c is the capacitance

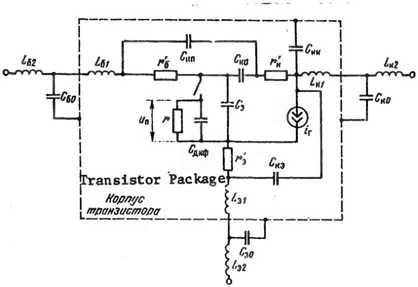

Figure 16.2. The equivalent circuit of a microwave transistor.

(The closed position of the switch corresponds to the turned-on state of the transistor; an open switch corresponds to the cutoff state).

of the collector junction, C_e is the capacitance of the emitter junction, f_{ult} is the ultimate current gain frequency in a common emitter configuration. Moreover, the collector current at which the value of f_{ult} decreases by $\sqrt{2}$ as compared to the maximum value f_{ult} at a certain frequency f for a specified collector voltage is also indicated for power transistors. This current is called the critical current i_{cr} [1].

The following relationships exist between the data sheet parameters for a transistor and the equivalent circuit parameters:

$$C_d = C_e + C_{dif};\ C_c = C_{ca} + C_{cp},\ C_{ca} = C_c/(2\ldots4);$$

$$\tau_k = r'_b C_{ca};\quad h_{21e} = S_\pi r;\quad f_{ult} = S_\pi/2\pi C_d. \tag{16.1}$$

$$C_{\text{д}} = C_{\text{э}} + C_{\text{диф}};\ C_{\text{к}} = C_{\text{ка}} + C_{\text{кп}},\ C_{\text{ка}} = C_{\text{к}}/(2\ldots4);$$

$$\tau_{\text{к}} = r'_{\text{б}} C_{\text{ка}};\ h_{21\text{э}} = S_{\text{п}} r;\ f_{\text{гр}} = S_{\text{п}}/2\pi C_{\text{д}},$$

$$S_\pi = qi_c/kT_j = 42.5i_c/(1 + 3.66 \cdot 10^{-3} t_j). \tag{16.2}$$

$$S_{\text{п}} = qi_{\text{к}}/kT_{\text{п}} = 42{,}5i_{\text{к}}/(1 + 3{,}66 \cdot 10^{-3}\, t_{\text{п}}),$$

TABLE 16.1

Тип транзистора[1] Transistor Type	Корпус[2] Package	Предельные эксплуатационные данные Ultimate Operational Data								
		$U_{КЭ}$, В 1.	$U_{ЭБ}$, [illegible] 2.	$I_{Ки}$, А 3.	$I_К$, А 4.	$I_{кр}$, А 5.	$R_{пк}$ °С/Вт[3] 6	$t_п$, °С 7	$t_к$, °С 8	P, Вт, при $t_к = 25$° С (9)
ГТ387	И	12				0,16	160[3]	100		0,3
КТ606	И I	60	4	0,8	0,4	>0,1	44	120	85	2,5
КТ610Б	И	26	4		0,3	~0,4		150		1,5
КТ904А	И	60	4	1,5	0,8	0,8	16	120	85	5
КТ907А	Э	60	4	3	1	1,8	7,5	120	85	13,5
КТ909А	Э	60	3,5	4	2	4	3,8	120	85	25
КТ909Б	Э E	60	3,5	[illegible]	4	8	1,9	120	85	50
КТ913А	И	55	3,5	1	0,5	0,6	20	150	125	4,7
КТ913Б	И	55	3,5	2	1	1,2	10	150	125	8
КТ913В	И I	55	3,5	2	1	[illegible]	10	150	125	12
КТ918Б	Б	30	2,5		0,2	0,2	50	150	85	2,5
КТ919А	Б	45	3,5	1,5	0,7	1,5	12	150		10
КТ919Б	Б B	45	3,5	0,7	0,35	0,8	25	150		5,3
КТ919В	Б	45	3,5	0,4	0,2	0,4	40	150		3
КТ937А-2	Б		2,5		0,25	0,2	34,5	150		3,6

Параметры типового режима Typical Mode Parameters					Электрические параметры и параметры эквивалентной схемы (20)				
10. f, МГц	11. $U_{к0}$, В	12 $P_{вых}$, Вт	13. K_P	14. η, %	15. $h_{21Э}$	16. U', В	$S'_{гр}$, См 17	$f_{гр}$, МГц 18.	$C_к$, пФ 19.
3000	7	0,090	3	30	50	0,3	0,035	3000	1,7
400	28	0,8	3	40	20	0,7	0,018	400	4
400	12,6	1	10	45	70	0,7	0,1	1000	3,8
400	28	3,2	3,2	40	30	0,6	0,06	500	6
400	28	10	3	65	50	0,6	0,19	600	15
500	28	24	2,4	60	15	0,6	0,46	650	24
500	28	42	2,1	60	20	0,6	0,92	650	40
1000	28	3,3	3,3	50	40	0,7	0,065	1100	4
1000	28	6	3	50	50	0,7	0,11	1100	7,5
1000	28	11	2,8	50	50	0,7	0,20	1100	7,5
3000	20	0,5	3,5	35		0,7	0,02	2000	2
2000	28	4,4	4,4	33		0,7	0,13	1800	7,5
2000	28	2	4	30		0,7	0,06	2100	4,1
2000	28	1	5	25		0,7	0,03	2100	2,8
5000	21	2	⩾2	35	80	0,7	0,11	3000 при $I_к = 0,6$ А (22)	$C_к = 0,9$, $C_{к0} = 0,8$

TABLE 16.1 [continued]:

Тип транзистора Transistor Type	Корпус Package	(20) Электрические параметры и параметры эквивалентной схемы							
		$C_{ка}$, пФ (21)	$C_э$, пФ	$r'_б$, Ом	$r'_э$, Ом	$r'_к$, Ом	$L_б$, нГн	$L_э$, нГн nHy	$L_к$, нГн nHy
ГТ387	И	0,3	4	10	—	3	0,5	0,9	0,9
КТ606	И	1,5	30	4	0,2	6	3	3	3
КТ610Б	И	1,3	15	6	2	—	2,5	0,7	2,5
КТ904А	И	2	65	2	0,1	3	3	3	3
КТ907А	Э	5	110	1	0,4	1,5	3	0,8	3
КТ909А	Э	8	150	2	0,1	1	1,7	0,45	2
КТ909Б	Э	13	300	0,5	0,05	0,5	1,7	0,35	[illegible]
КТ913А	И	1,3	25	2	0,15	2	3	0,52	3
КТ913Б	И	2,5	50	1	0,2	1	2,5	0,25	2,5
КТ913В	И	2,5	80	1	0,2	1	2,3	0,23	2,5
КТ918Б	Б	0,7	10	1,3	—	0,7	0,15	0,8	0,8
КТ919А	Б	2,5	50	0,5	0,14	0,7	0,14	0,4	0,7
КТ919Б	Б	1,5	20	1	—	1,4	0,25	0,5	0,6
КТ919В	Б	0,7	10	2	—	3	0,35	1,3	0,7
КТ937А-2	Б	$C_{ка}=0,3$ $C_{кк}=0,8$ $C_{кэ}=0,2$	$C_э=10$ $C_{эо}=2,5$	2	—	[illegible]	0,25	$L_{э1}=0,7$ $L_{э2}=0,5$	$L_{к1}=0,7$ $L_{к2}=0,6$

[1] Все транзисторы $n-p-n$.
[2] И—все выводы изолированы от корпуса, Э—с корпусом соединен эмиттер, Б—база.
[3] Тепловое сопротивление переход—среда.
[4] При отсутствии значения $h_{21э}$ взять его равным 15...50.
[5] При прочерке в графе считать параметр равным нулю.

---

[1] All of the transistors are n-p-n.
[2] I: all of the leads are insulated from the package; E: with the package connected to the emitter; B: to the base.
[3] The junction to environment thermal resistance.
[4] When there is no value for h_{21e}, take it as equal to 15 - 50.
[5] When drawn in a graph, the parameter is considered equal to zero.

Key:
1. U_{ce}, volts;
2. U_{eb}, volts;
3. $I_{c.i}$, amps;
4. I_c, amps;
5. I_{cr}. amps;
6. $R_{junc.coll.}$, °C/W[3];
7. t_j, °C;
8. t_c, °C;
9. P, watts at t_c = 25 °C;
10. f, MHz;
11. U_{c0}, V;
12. P_{out}, watts;
13. Power gain;
14. Efficiency, %;
15. h_{21e}[4];
16. U', volts;
17. S'_{ult}, mhos;
18. f_{ult}, MHz;
19. C_c, pFd;
20. Electrical parameters and equivalent circuit parameters;
21. C_{ca}, pFd;
22. 3,000 at i_c = 0.6 amps.

where q is the charge on an electron; k is Boltzmann's constant; T_j and t_j are the junction temperatures in °K and °C; i_c is the collector current, amps; S_π is in mhos.

Moreover, the static transconductance $i_c(u_v)$ is used in the calculations, which is equal to the ratio of the small increments in the collector current and the base to emitter voltage in the case of a short-circuited load:

$$S = h_{21e}/[r_b' + r + (1+h_{21e})r_e'] \qquad (16.3)$$

$$S = h_{21э}/[r_б' + r + (1 + h_{21э})r_э'].$$

When averaging the parameter S_π, it is recommended that a value of the current i_c, equal to half of the height of a current pulse of the equivalent generator i_{cm} or the amplitude of its fundamental I_{g1}, be subsituted in formual (16.2), which in typical modes is close to $0.5i_{cm}$.

The junction capacitances C_c and C_e depend on the voltages applied to them. When averaging the junction capacitance over a radio frequency period, one can take the collector capacitance in the case of a voltage across it of U_{c0} as C_c. The averaged value of C_e falls in a range between C_e ($u_{eb} = 0$) and C_e ($u_{eb} = U_{eb\ max}$). When calculating transistor operating conditions, the averaged parameters of C_c and C_e are taken from Table 16.1.

16.3. A Time and Harmonic Analysis of Transistor Currents and Voltages

In the general case, the voltage and current at the input to a transistor in a cutoff mode have a nonharmonic waveform and this complicates the calculation. In the microwave band, the input current of power transistors proves to be close to a harmonic waveform though because of the suppression of the higher harmonics of the current by the inductance of the input lead. The current waveform is even closer to a harmonic one when coupling networks are used which contain an inductance inserted in series with the input transistors (Figure 16.1). The collector voltage waveform is also different from a harmonic waveform because of the nonlinearity of the collector capacitance, as well as because of the nonzero resistance of the collector circuit for higher harmonics. However, practice shows that the assumption of a harmonic voltage waveform does not lead to large errors when determining the major power indicators of amplifiers. In accordance with this, in the following analysis we shall assume that the input current and the collector voltage do not contain higher harmonics.

At frequencies of $f \geq 3f_{ult}/h_{21e}$, the resistance R (Figure 16.2) is a poor shunt of the capacitance C_d, and it can be disregarded. This inequality also governs the lower cutoff frequency for the analysis given here.

At low frequencies, with a harmonic voltage across the collector, the optimal condition in terms of the set of parameters (power delivered by the transistor,

P_{out}, the efficiency and K_p [power gain]) is the limiting mode, which is characterized by the slope of the limiting mode line, S_{limit}, determined from the static characteristics. At microwave frequencies, the residual voltage across the collector exceeds the value found from the static characteristics for the specified pulse height [2], and therefore the quantity $S'_{limit} < S_{limit}$ is used in the calculations.

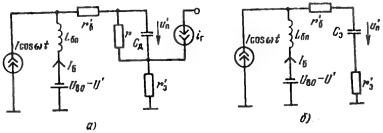

Figure 16.3. The equivalent circuit of the input circuit of an amplifier for the calculation of the voltage across the emitter junction for the on (a) and off (b) states.

To assure the maximum efficiency with a harmonic collector voltage, the load resistance, R_g, of the equivalent generator with respect to the first harmonic should be resistive. The resistive nature of this load and its value are assured through the tuning of the collector circuit.

We shall now move on to the time analysis of the voltages and currents in the circuits of Figure 16.3. We shall initially treat the voltage waveform across the emitter junction of the transistor in the common emitter configuration. It is governed by the control current i, which takes the form of the difference between the base current and the current flowing through the collector capacitance. The base current contains a small constant component I_b and a harmonic component, equal to the input current of the stage. We shall consider the current through C_c ti be harmonic, since it is primarily determined by the sinusoidal voltage at the collector. For this reason, one can assume that the alternating component of the control current contains only the primary frequency component with an amplitude of $\hat{I}$, which governs the voltage across the junction $u_п$ [u_j].

The voltage u_j can be calculated by employing the equivalent circuit of Figure 16.3, which reflects the processes in the emitter junction and is a part of the equivalent circuit of Figure 16.2. The voltage across the transistor emitter junction for the active range, $u_{j\,on}$ and for the cutoff range, $u_{j\,off}$, is determined by the following differential equations respectively:

$$C_д \frac{d\,(u_{п\,откр} - U')}{dt} \simeq I\cos\omega t \quad при \quad u_п > U'; \qquad (16.4)$$

$$C_э \frac{d\,(u_{п\,закр} - U')}{dt} \simeq I\cos\omega t \quad при \quad u_п \leqslant U'. \qquad (16.5)$$

TABLE 16.2

θ°	$\cos\theta$	$\gamma_0(\theta)$	$\gamma_1(\theta)$	$g_1(\theta)$	θ°	$\cos\theta$	$\gamma_0(\theta)$	$\gamma_1(\theta)$	$g_1(\theta)$
60	0,500	0,109	0,196	1,80	93	—0,052	0,345	0,532	1,54
65	0,423	0,136	0,239	1,76	94	—0,070	0,354	0,543	1,53
70	0,342	0,166	0,288	1,73	95	—0,087	0,363	0,554	1,53
71	0,326	0,172	0,298	1,72	96	—0,105	0,372	0,566	1,52
72	0,309	0,179	0,307	1,71	97	—0,122	0,381	0,577	1,51
73	0,292	0,186	0,316	1,70	98	—0,139	0,391	0,588	1,50
74	0,276	0,192	0,326	1,70	99	—0,156	0,401	0,599	1,49
75	0,259	0,199	0,337	1,69	100	—0,174	0;411	0,611	1,49
76	0,242	0,208	0,348	1,68	101	—0,191	0,420	0,622	1,48
77	0,225	0,214	0,359	1,68	102	—0,208	0,429	0,631	1,47
78	0,208	0,221	0,368	1,67	103	—0,225	0,438	0,642	1,46
79	0,191	0,229	0,380	1,66	104	—0,242	0,449	0,652	1,45
80	0,174	0,236	0,390	1,65	105	—0,259	0,458	0,662	1,45
81	0,156	0,244	0,400	1,64	106	—0,276	0,467	0,674	1,44
82	0,139	0,253	0,413	1,63	107	—0,292	0,477	0,682	1,43
83	0,122	0,259	0,422	1,62	108	—0,309	0,488	0,692	1,42
84	0,105	0,267	0,434	1,61	109	—0,326	0,498	0,701	1,41
85	0,087	0,276	0,445	1,61	110	—0,342	0,509	0,713	1,40
86	0,070	0,284	0,456	1,61	111	—0,358	0,519	0,722	1,39
87	0,052	0,293	0,467	1,60	112	—0,375	0,528	0,731	1,38
88	0,035	0,301	0,479	1,59	113	—0,391	0,538	0,741	1,38
89	0,017	0,309	0,489	1,58	114	—0,407	0,548	0,751	1,37
90	0,000	0,319	0,500	1,57	115	—0,423	0,558	0,760	1,36
91	—0,017	0,328	0,511	1,56	118	—0,469	0,589	0,786	1,33
92	—0,035	0,337	0,522	1,55	120	—0,500	0,609	0,805	1,32

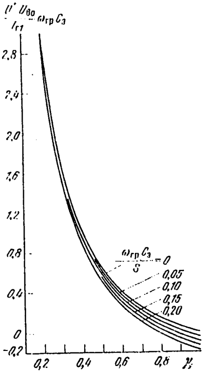

← Figure 16.4. A graph for calculating the coefficients γ_1 from equation (16.11).

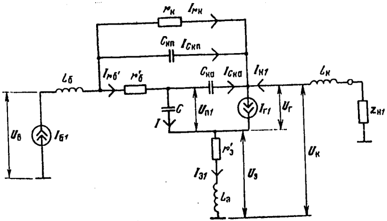

↑

Figure 16.5. The equivalent circuit of a common emitter amplifier for the fundamental frequency currents and voltages.

The solution of equations (16.4) and (16.5) has the form:

$$U_{j\ \text{on}} - U' = \quad u_{\text{п отпр}} - U' = (I/\omega C_{\text{п}})(\sin\omega t - \cos\theta) \quad \text{при } u_{\text{п}} > U'; \quad (16.6) \qquad (16.6)$$

when $u_j > U'$

$$u_{j\ \text{off}} - U' = \quad u_{\text{п закр}} - U' = (I/\omega C_{\text{п}})(\sin\omega t - \cos\theta) \quad \text{при } u_{\text{п}} \leqslant U', \quad (16.7) \qquad (16.7)$$

when $u_j \leqq U'$

where θ is the equivalent generator (EG) current cutoff angle.

The equivalent generator current, i_g, is proportional to the voltage ($u_{j\ \text{on}} - U'$) and has a cosine pulse waveform. Taking (16.1) into account:

$$i_g = \quad i_{\text{г}} = (I\omega_{\text{гр}}/\omega)[\sin(\omega t - \omega\tau_{\text{п}}) - \cos\theta] \quad \text{при } u_{\text{п}} > U'. \quad (16.8) \qquad (16.8)$$

when $u_j > U'$

The complex amplitude of the first harmonic I_{g1} and the constant component of the equivalent generator current, I_c, can be found using the expasion coefficients for the cosine pulse γ_1 and γ_0 (see Table 16.2):

$$I_{g1} = \quad I_{\text{г1}} = -j(I\omega_{\text{гр}}/\omega)\gamma_1 \exp(-j\omega\tau_{\text{п}}); \qquad (16.9)$$

$$I_c = \quad I_{\text{К}} = I_{\text{г0}} = I\omega_{\text{гр}}\gamma_0/\omega. \qquad (16.10)$$

The cutoff angle is governed by the balance equation for the DC voltages at the transistor input, which taking expressions (16.6), (16.7) and (16.9) into account as well as the relationships between the transistor parameters, can be reduced to the form:

$$-(U_{v0} - U')\omega_{ult}C_e/I_{g1} = \cos\theta/\gamma_1 + (1-\omega_{ult}C_e/S)\gamma_0/\gamma_1 = \qquad (16.11)$$

$$= \quad -(U_{\text{б0}} - U')\omega_{\text{гр}}C_{\text{э}}/I_{\text{г1}} = \cos\theta/\gamma_1 + (1 - \omega_{\text{гр}}C_{\text{э}}/S)\gamma_0/\gamma_1.$$

Here, U_{v0} is the base--emitter bias voltage.

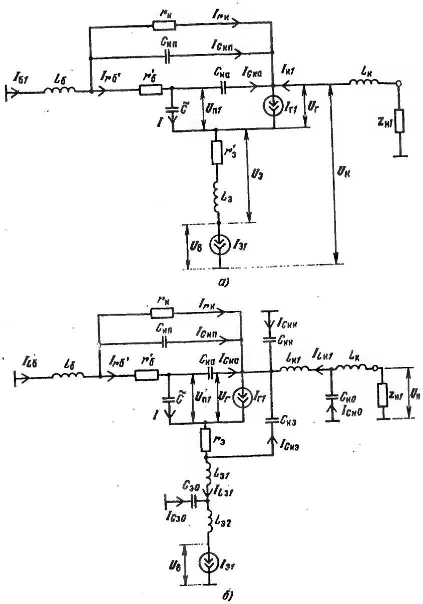
rк
Irк
Cкп
Icкп
Iб1
Lб
Irб'
r'б
Cка
Icка
Iк1
Lк
C̃
I
Uп1
Ir1
Ur
Zн1
r'э
Uэ
Uк
Lэ
Uб
Iэ1
a)
Icкк
Cкк
Lк1
ILк1
Cк0
Icк0
Uн
Cкэ
Icкэ
rэ
Lэ1
Cэ0
ILэ1
Icэ0
Lэ2
б)

Figure 16.6. The equivalent circuit of a common base amplifier for the first harmonic current and voltages without taking the package capacitances into account (a) and taking them into account (b).

Knowing the transistor parameters S, ω_{ult}, C_e and U', one can determine the expansion coefficient γ_1 for the specified current I_{g1} and the bias U_{v0} using the graph of Figure 16.4, which is plotted in accordance with equation (16.11).

The peak inverse voltage across the emitter junction, in accordance with (16.7) and (16.9), is equal to:

$$u_{eb\ peak} = u_{\text{ЭБ пик}} = -I_{\text{г1}}(1+\cos 0)/\omega_{\text{гр}} C_{\text{э}} \gamma_1 + U'. \qquad (16.12)$$

The first harmonic of the voltage at the emitter junction, averaged over one high frequency period, in accordance with (16.7), is equal to:

$$U_{junction\ 1} \approx U_{junction\ 1\ off} = U_{\text{п1}} \simeq U_{\text{п 1 закр}} = -jI(1-\gamma_1)/\omega C_{\text{э}}. \qquad (16.13)$$

In a common base circuit configuration, the voltage across a cutoff emitter junction and the collector current pulse are somewhat asymmetrical in the general case with excitation by a harmonic emitter current. This leads primarily to a change in the phase of the fundamental of the emitter output current relative to the input current. However, at the higher operating frequencies of a transistor (above $f_{\text{Гр}}$ [f_{cutoff}]), this change is comparatively small (about a few degrees) and it can be disregarded because of the small gain in the calculation precision.

The harmonic analysis made here makes it possible to move on from the transistor model shown in Figure 16.2 to the equivalent circuits of generators with common emitter and common base configurations for the fundamental current and voltages. For frequencies at the which the capacitance C_{BO} can be disregarded, these circuits are shown in Figures 16.5 and 16.6a, while for higher frequencies at which a common emitter circuit is usually employed, see the circuit of Figure 16.6b. An equivalent current generator with a switch is replaced with a fundamental harmonic current generator $I_{\text{Г}}$ [$I_{gn\ 1}$], defined by formula (16.9), while the emitter junction is represented by a capacitance averaged over a period of the radio frequency, which in accordance with (16.13) is equal to $\tilde{C} = C_e(1 - \gamma_1)^{-1}$. The resistance r_K represents the losses in the material of the collector in the parallel equivalent circuit.

The system of equations which relate the complexing amplitudes of the currents and voltages in the circuits of Figures 16.5 and 16.6a is given in §16.5.

16.4. The Properties of Common Emitter and Common Base Generator Configurations

In analyzing and comparing the main properties of common emitter and common base oscillators/amplifiers, it is expedient to treat two cases separately:

1. A low inductive reactance for the common lead ωL_{com}, for which the fundamental harmonic voltage across the inductance L_{com} does not exceed 3 to 5 percent of the voltage amplitude across the collector. The following inequality corresponds to this case: for a common emitter circuit:

$$\omega L_e = \omega L_{\text{э}} \leqslant 0{,}03 R_{\text{к}}, \qquad (16.14)$$

while for a common base configuration:

$$\omega L_b = \quad \omega L_{\text{б}} \leqslant 0{,}1\,(\omega_{\text{гр}}\gamma_1/\omega)\,R_{\text{к}}\,(1+\omega_{\text{гр}}\,C_{\text{к}}\,R_{\text{к}}\,\gamma_1)^{-1}, \tag{16.15}$$

where $R_K = [R_c] \approx (0.25\ldots0.35)U_{K0}^2/P_{out}$, $\gamma_1 = 0.3\ldots0.6$.

2. A large inductive reactance of the common electrode lead.

In the first case, all of the design calculation equations prove to be simpler and they can be used to easily illustrate and explain the basic properties of amplifiers and simply execute the design of an oscillator/amplifier for a specified power in a load. For this reason, we initially turn to the first case. We shall assume that $f \leq f_{cutoff}$. Then, as a rule, one can disregard the resistance r'_k and consider the junction transconductance to be a real quantity. Moreover, in this case, one can neglect the capacitances C_{KE} $[C_{ce}]$ and C_{kk} $[C_{cc}]$.

By solving the system of equations which relate the complex amplitudes of the voltages and currents introduced in the equivalent circuits of Figures 16.5 and 16.6a, we find the current transmission gain:

$$K_{i\ \text{com.em.}} = I_{\text{gen1}}/I_{b1} = \quad K_{i\text{ОЭ}} = I_{\text{г}1}/I_{\text{Б}1} = -j\omega_{\text{гр}}\gamma_1/\omega\,(1+\omega_{\text{гр}}\,C_{\text{к}}\,R_{\text{к}}\,\gamma_1), \tag{16.16}$$

$$K_{i\ \text{com. base}} = \quad K_{i\text{ОБ}} = I_{\text{г}1}/I_{\text{Э}1} = (1+j\omega/\omega_{\text{гр}}\gamma_1)^{-1}; \tag{16.17}$$

And the input impedance for the fundamental frequency current is:

$$z_{\text{вх}1} = r_{\text{вх}1} + jx_{\text{вх}1};\quad z_{\text{вх}1\,\text{ОЭ}} = U_{\text{в}}/I_{\text{Б}1};\quad z_{\text{вх}1\text{ОБ}} = U_{\text{в}}/I_{\text{Э}1},$$

where

$$r_{\text{вх ОЭ}} = \frac{r'_{\text{б}}(1+\omega_{\text{гр}}\,C_{\text{ка}}\,R_{\text{к}}\,\gamma_1)+\omega_{\text{гр}}\,L_{\text{э}}\,\gamma_1+r'_{\text{э}}}{1+\omega_{\text{гр}}\,C_{\text{к}}\,R_{\text{к}}\,\gamma_1}; \tag{16.18}$$

$$x_{\text{вх}1\,\text{ОЭ}} = \omega L_{\text{б}} + \frac{\omega L_{\text{э}}-(1-\gamma_1)/\omega C_{\text{э}}-r'_{\text{э}}\,\omega_{\text{гр}}\,\gamma_1/\omega}{1+\omega_{\text{гр}}\,C_{\text{к}}\,R_{\text{к}}\,\gamma_1}; \tag{16.19}$$

$$r_{\text{вх}1\,\text{ОБ}} = r'_{\text{э}} + \frac{r'_{\text{б}}(1+\omega_{\text{гр}}\,C_{\text{ка}}\,R_{\text{к}}\,\gamma_1)-\omega_{\text{гр}}\,L_{\text{б}}\,\gamma_1\,(1+\omega_{\text{гр}}\,C_{\text{к}}\,R_{\text{к}}\,\gamma_1)+\dfrac{1-\gamma_1}{\omega C_{\text{э}}}\,\dfrac{\omega_{\text{гр}}\,\gamma_1}{\omega}}{1+(\omega_{\text{гр}}\,\gamma_1/\omega)^2}; \tag{16.20}$$

$$x_{\text{вх}1\,\text{ОБ}} = \omega L_{\text{э}} + \frac{\omega L_{\text{б}}(1+\omega_{\text{гр}}\,C_{\text{к}}\,R_{\text{к}}\,\gamma_1)+r'_{\text{б}}(1+\omega_{\text{гр}}\,C_{\text{ка}}\,R_{\text{к}}\,\gamma_1)\,\dfrac{\omega_{\text{гр}}\,\gamma_1}{\omega}-\dfrac{1-\gamma_1}{\omega C_{\text{э}}}}{1+(\omega_{\text{гр}}\,\gamma_1/\omega)^2}; \tag{16.21}$$

and the power gains are:

$$K_{P\,\text{ОЭ}} = \left(\frac{\omega_{\text{гр}}\,\gamma_1}{\omega}\right)^2 \frac{R_{\text{к}}}{[\,r'_{\text{б}}(1+\omega_{\text{гр}}\,C_{\text{ка}}\,R_{\text{к}}\,\gamma_1)+\omega_{\text{гр}}\,L_{\text{э}}\,\gamma_1+r'_{\text{э}}]\,(1+\omega_{\text{гр}}\,C_{\text{к}}\,R_{\text{к}}\,\gamma_1)}, \tag{16.22}$$

(16.22)

$$K_{P\,\text{ОБ}} = (\omega_{\text{гр}}\gamma_1/\omega)^2 R_{\text{к}} \{r_{\text{б}}'(1 + \omega_{\text{гр}} C_{\text{ка}} R_{\text{к}}\gamma_1) - \\ - \omega_{\text{гр}} L_{\text{б}}\gamma_1 (1 + \omega_{\text{гр}} C_{\text{к}} R_{\text{к}}\gamma_1) + (1 - \gamma_1)\omega_{\text{гр}}\gamma_1/\omega^2 C_{\text{э}} + \\ + r_{\text{э}}'[1 + (\omega_{\text{гр}}\gamma_1/\omega)^2]\}^{-1}. \qquad (16.23)$$

The properties of microwave transistor oscillators/amplifiers are determined to a significant extent by the high level internal feedback loops in the transistors, the nature of which differs for the common emitter and common base configurations. In a common base generator configuration with a resistive load, these are negative feedback loops through the inductance of the emitter lead L_e and the collector C_k.

The governing factor in a common base configuration oscillator/amplifier is the positive feedback through the base lead inductance.

It follows from formula 16.16 that in a common emitter circuit, the coupling through C_k leads to a reduction in the current transmission gain by a factor of $(1 + \omega_{cut}C_kR_k\gamma_1)$ as compared to a short-circuited load. In accordance with (16.17), the transmission gain $K_{i\ com.base}$ depends on the load impedance. In both circuits, the current transmission gain at microwave frequencies is usually less than unity. Only at freuencies several times lower than f_{cut} in a common emitter configuration does $K_i > 1$.

In a common emitter circuit, the real part of the input impedance $r_{in1\ OE}$ (16.18) is positive in the case of a resistive load and is independent of frequency. The quantity $r_{in\ OB}$ [common base input resistance] (16.20) depends greatly on the frequency and with an increase in the inductance L_b can become negative. This means that an externally excited generator is potentially unstable because of the positive coupling through L_b.

For both configurations, the quantity r_{in1} proves to be small: units or fractions of an ohm. An increase in the maximum power of a single transistor up to hundreds of watts is accompanied by a reduction in r_{in1} down to hundredths of an ohm. In this case, the efficiency of the input matching circuit proves to be poor and this is one of the reasons which limit the increase in transistor power.

The reactive component of the input impedance, x_{in1}, close to the upper cutoff frequency of a transistor, is, as a rule, of an inductive nature which is due to the inductances of the base and emitter leads. Usually, x_{in1} component is considerably greater than r_{in1} and is a component part of the input matching network of an amplifier.

It follows from formula (16.22) that the power gain in a common emitter configuration is inversely proportional to the square of the working frequency. It is governed to a considerable extent by the values of C_k [C_{coll}] and L_e. It can be shown that if $\omega_{cut}L_e\gamma_1 > 3r_b'$ and $\omega_{cut}C_{col}R_{col}\gamma_1 > 3$, then:

$$K_{P\ com.em.} \simeq 1/\omega^2 C_c L_e \quad = \quad K_{P\,\text{ОЭ}} \simeq 1/\omega^2 C_{\text{к}} L_{\text{э}}.$$

An amplifier/oscillator is little sensitive in this case to the scatter in the transistor parameters and the change in the cutoff angle, but the gain proves to be low. The upper working frequency of a common emitter amplifier, corresponding to a reduction K_p down to 2 to 3 usually does not exceed f_{cut}.

Positive feedback loops act through the inductance L_b and the capacitance C_{ce} in a common base amplifier. The feedback through C_{ke} is of secondary importance for power transistors, just as the feedback through the capacitances C_{ka} and $C_{k\pi}$. The positive feedback through L_b explains the comparatively high sensitivity of a common base configuration to changes in transistor parameters and cutoff angle. This coupling can cause parasitic oscillation or strong gain in stability. It is necessary to take special steps to prevent this: incorporate emitter degeneration bias, insert neutralizing capacitances in the base circuit, or use an unblocked resistance in the emitter circuit. A special resistor can be used for this resistance, and sometimes, the internal resistance of the exciting generator, the output resistance of the power divider bridge, etc.

The upper working frequency in a common base configuration can run to approximately $3f_{cutoff}$.

Formulas (16.16) - (16.23) were derived with the assumption that $\omega L_{com.}$ is small. This assumption leads to a marked understatement of the output power and efficiency in a common emitter configuration with large values of ωL_{com} and to an exaggeration of these quantities in the common base configuration. Because of this, we shall consider the impact of L_{com} on the power relationships in an amplifier/ /oscillator.

In studying an externally excited generator, we are dealing with a system of two generators (the input signal generator and the equivalent controlled generator of the active device), which are connected through the elements of the equivalent circuit of the transistor to its load. It is well known from the theory of the joint operation of generators driving the common load that depending on the amplitude and phase relationships in the circuit, both power addition in the load as well as the transition of any of the generators to a power consumption mode are possible.

In the common emitter configuration, the voltage across the load, U_k, and consequently also the power are determined by the voltage difference between U_g and U_e. The voltage U_e is partially produced by the excitation generator current. The phase relationships for the currents and voltages are such that there is an increase in the power in the load as compared to the case where $L_e = 0$ ("straight-through"). With a short circuit of the output or with a low load resistance, the portion of the excitation generator power related to the voltage U_e is dissipated in the collector of the transistor.

If the generator efficiency is defined as the ratio of the power in the load, P_{out}, to the power consumed from the collector supply, P_0, because of the straight-through flow, the generator efficiency increases simultaneously with the increase in P_{out}. It should be noted that with this definition, the efficiency can prove to be greater than unity.

In a common base configuration, the voltage across the load is primarily determined by the sum of U_g and U_{Lb}, since the voltage across the capacitance $\check{C}$ is extremely small. Just as in the preceding case, the voltage across the inductance of the common electrode is produced partially by the input current, however, in contrast to the common emitter circuit, the phase relationships in a common base configuration are such that a portion of the power P_g is transmitted to the input network. Because of this, the useful power in the load of an externally excited generator and the generator efficiency are reduced as compared to the case where $L_b = 0$, but nonetheless, less power is required from the excitation generator and consequently the gain is increased and self-excitation can even occur.

16.5. The Procedure and Sequence for the Design Calculations of the Operating Mode of an Oscillator/Amplifier

In the course of designing a generator with external excitation, one is to first choose the transistor and determine its circuit configuration based on the specified power and frequency. If the requisite transistor type is not present in Table 16.1, one can estimate the parameters of its equivalent circuit, using reference data and the estimates given in this section. Then the design calculations are performed for the electrical and thermal operating conditions of the transistor.

The type of transistor is selected taking into account the specified requirements for the output power and frequency from the reference handbook data. The parameters of the typical operating condition, corresponding to the maximum utilization of the device both with respect to power and frequency are specified in the reference data for microwave power devices. The indicated output power corresponds to a transistor package temperature of about 20 °C. The useful power falls off with an increase in temperature, since the permissible power dissipation is reduced. With a reduction in frequency, the maximum useful power of a transistor increases.

It is expedient to use microwave power transistors at powers of no less than 40 to 50% of the power in the typical mode indicated in the handbook. Considerable underutilization of a device with respect to power leads to a substantial degradation of its amplification properties.

The range of operating frequencies recommended for a given transistor is also frequently indicated in the handbook. The lower working frequency is usually recommended at no less than 20 to 30 percent of f_{cutoff}, while the upper frequency is close to f_{cutoff} for a common emitter circuit and reaches 2 to 3 times f_{cutoff} for a common base configuration. At the lower operating frequency of this range, the maximum output power can be approximately twice as great as the power at the upper frequency limit.

It sometimes turns out that the requisite power at a specified frequency can be obtained with different transistors. Where a choice is possible, it is preferable to use transistors with a higher gain, however, it is not desirable to use devices, the lower frequency limit of which is higher than the specified working frequency, since in this case, operational reliability will be reduced, and the probability of self-excitation will increase. Moreover, higher frequency devices also cost more.

The circuit configuration (common emitter or common base) is determined in a number of cases by the package structure of the selected transistor. For example, KT907 and KT909 transistors can be used only in a common emitter configuration, since they have the emitter connected to the package. The KT918 and KT919 transistors, on the other hand, are used only in a common base configuration: they have the package connected to the base. The KT606 and KT904 devices can operate in either configuration, since they have leads which are insulated from the package. The KT911, KT913 and KT916 devices, although they also have leads insulated from the package, are more conveniently used in a common emitter configuration, since two of their emitter leads should be inserted in the circuit in a balanced fashion because of structural design considerations. The common base configuration is a higher frequency circuit and is used considerably more often frequencies above 1 GHz.

The parameters of transistors needed for operational mode design are given in Table 16.1. If the selected transistor is not present in Table 16.1, its parameters may be estimated by knowing the data sheet values for f_{cutoff}, $r'_b C_k$ and C_k. Moreover, one must know the inductance of the common lead. Transistors which are specially intended for common emitter or common base circuits have a minimal common lead inductance (0.1 to 0.4 nHy) while the inductance of the collector and input leads are several times higher. The capacitance C_e is usually 5 to 10 times greater than C_k; the resistance r'_k is close to r'_b and r'_e does not exceed $0.3r'_b$. The data sheet value of f_{cutoff} is usually 1.5 to 2 times less than the actual value, while the data sheet value of C_k is overstated by a few tens of percent.

The time constant $r'_b C_k$, which is indicated in the data sheet, can sometimes exceed the actual value by an order of magnitude. It must be kept in mind that the parameter $r'_b C_k$ is the product of r'_b times C_{ka}, and not times C_k. The parameter h_{21e} is not critical in the design calculations for microwave amplifiers and oscillators. The static characteristic shift voltage U' for silicon transistors falls in a range of 0.6 to 0.9 volts. The parameter $S'_{\text{гп}}$ [S'_{cutoff}] can be taken as approximately equal to $15P_{out}/U^2_{k0}$, where U_{k0} and P_{out} correspond to the typical mode (P_{out} in watts and U_{k0} is in volts).

If the design calculations using the typical mode power and frequency yield a value of K_p which differs from the data sheet value by no more than $\pm 20\%$ for a common emitter cnfiguration, one can assume that the equivalent circuit parameters have been correctly estimated. If the absolute value of the peak inverse voltage at the emitter $|u_{eb\ peak}|$ is greater than the permissible value or almost equal to it according to the design calculations, this means that the calculated value of C_e is understated.

We shall move on the design procedure for the transistor operating mode at a specified power into a load P_{out}. The initial data for the design calculations are: power delivered by the transistor, P_{out}; the working frequency f; the ambient temperature, t_{cp}; the transistor type and the circuit configuration (common emitter or common base).

If the requisite power is close to the level which the transistor can deliver (but does not exceed it), then the standard supply voltage for this transistor is to be used: most often 28 volts. When a transistor is underutilized in terms of power, it it expedient to lower the supply voltage to improve the reliability. However, one must take into account the fact that cutting U_{k0} in half leads to a reduction in f_{cutoff} by approximately 5 to 15% and to an increase in C_k by approximately 20 to 25%. The bias voltage U_{B0} in power stages is usually taken as zero. This simplifies the circuit and makes it possible to obtain a cutoff angle close to 90°, for which the ratio between P_{out}, the efficiency and Kp is close to optimal.

The transistor package temperature can be taken equal to $p_k = t_{ambient} + (10...20)$ °C, taking into account the extra heating of the heat sink relative to the ambient medium.

If the influence of ωL_{com} can be disregarded in accordance with inequality (16.14) and (16.15), then in the design calculations one can employ the simplified equations (16.16)-(16.23). The procedure for such design calculations is set forth in [5-6].

We shall give a design calculation procedure for the more general case, where inequalities (16.14) and (16.15) may not be observed. In this case, however, it is difficult to accomplish the calculations directly for the specified power in the load. If is considerably easier to carry out the calculations by specifying the power P_g developed by an equivalent generator. This power in a common emitter configuration is to be taken as 10 to 20 percent less than P_{out}, since in this circuit, the transistor output power has an increment because of the straight flow through of a portion of the input power. On the other hand, P_g is to be taken greater than P_{out} in a common base configuration, since a considerable portion of the power developed by the current generator, I_{g1}, is fed to the input circuit of the amplifier. At frequencies above f_{cutoff}, P_g is to be taken at 20 to 20% higher than P_{out} in a common base configuration; at frequencies below f_{cutoff}, this difference is less.

Initially, the calculation is carried out in the following order regardless of the circuit configuration (common emitter or common base).

1. We determine the collector voltage utilization factor, specifying P_g and U_{k0} taking what has been presented above into account:

$$\xi_{cutoff} = \qquad \xi_{\text{гр}} = 0{,}5\left[1 + \sqrt{1 - 16P_{\text{г}}/(S'_{\text{гр}}U^2_{\text{к0}})}\,\right].$$

2. We find the current and voltage amplitude of the fundamental frequency of the equivalent generator:

$$U_{\text{г}} \quad \xi_{\text{гр}} U_{\text{к0}}, \quad I_{\text{г1}} = 2P_{\text{г}}/U_{\text{г}}.$$

3. The peak collector voltage, uk peak, should not exceed the permissible value of $U_{KE\ max}$:

$$u_{coll.peak} = U_{c0} + U_{gen} < U_{CE\ max} = \qquad u_{\text{К пик}} = U_{\text{к}0} + U_{\text{г}} < U_{\text{КЭ max}}.$$

This inequality is not observed, the operational mode is to be changes or another type of transistor is to be selected.

4. We determine the transistor parameters:

$$S_{\text{п}} = 42{,}5 I_{\text{к}1}/(1 + 3{,}66\cdot 10^{-3}\, t_{\text{п}}), \quad r = h_{21\text{э}}/S_{\text{п}},\ S = h_{21\text{э}}[r'_{\text{б}} + r + r'_{\text{э}}(1 + h_{21\text{э}})]^{-1}.$$

The value of t_{π} [$t_{junction}$] can be taken equal to the ultimate permissible value (see Table 16.1).

5. Having calculated the values of the parameters $-(U_{B0} - U')\omega_{cut}C_e/I_{gen1}$ and $\omega_{cut}C_e/S$, we find the expansion coefficient γ_1 from the graphs of Figures 16.4 for the fundamental frequency of the equivalent generator current. Then, for the value found for γ_1, we determine the values of $\cos\theta$ and the coefficient of the form $g_1 = \gamma_1/\gamma_0$ from Table 16.2.

6. We determine the peak inverse voltage at the emitter, ueb peak, from formula (16.12). The absolute value of ueb peak should not exceed $U_{eb\ max}$.

Then in paragraphs 7 through 22 we calculate the complex amplitudes of the currents and voltages in the elements of the equivalent circuit of Figures 16.5 and 16.6a. The current I_{g1} is taken as the vector with the zero phase. In this case, the vector I_{g1} is equal to its own scalar value I_{g1} found in paragraph 2.

7. $I = jI_{\text{г}1}\dfrac{\omega}{\omega_{\text{гр}}\gamma_1}(\cos\omega\tau_{\text{п}} + j\sin\omega\tau_{\text{п}})$, где $\omega\tau_{\text{п}} = 0{,}4\omega/\omega_{\text{гр}}$.
8. $U_{\text{п}1} = -jI(1-\gamma_1)/\omega C_{\text{э}}$.
9. $U_{\text{Cка}} = U_{\text{г}} + U_{\text{п}1}$.
10. $I_{\text{Cка}} = j\omega C_{\text{ка}} U_{\text{Cка}}$.
11. $I_{r\text{б}'} = I + I_{\text{Cка}}$.
12. $U_{r\text{б}'} = r'_{\text{б}} I_{r'\text{б}}$.
13. $U_{\text{Cкп}} = U_{r\text{б}'} + U_{\text{Cка}}$.
14. $I_{\text{Cкп}} = j\omega C_{\text{кп}} U_{\text{Cкп}}$.
15. $r_{\text{к}} = [(\omega C_{\text{к}})^2 r'_{\text{к}}]^{-1}$.
16. $I_{r\text{к}} = U_{\text{Cкп}}/r_{\text{к}}$.
17. $I_{\text{Б}1} = I_{r\text{б}'} + I_{\text{Cкп}} + I_{r\text{к}}$.
18. $U_{L\text{б}} = j\omega L_{\text{б}} I_{\text{Б}1}$.
19. $I_{\text{Э}1} = I + I_{\text{г}1}$.
20. $U_{\text{Э}} = I_{\text{Э}1}(r'_{\text{э}} + j\omega L_{\text{э}})$.
21. $U_{\text{в}} = U_{\text{Э}} + U_{L\text{б}} + U_{r\text{б}'} + U_{\text{п}1}$.
22. $I_{\text{К}1} = I_{\text{г}1} - I_{\text{Cка}} - I_{\text{Cкп}} - I_{r\text{к}}$.

23. We calculate the voltage amplitude across the load and the input impedance of the transistor for the fundamental frequency: $U_{col\ com.em.} = U_{gen} - U_e$; $Z_{in\ 1\ com.em.} = U_B/I_{base\ 1}$; $U_{c\ com.base} = U_{C\ col.\ gen.} + U_{L\ base}$; $Z_{in\ 1\ com.base} = U_B/I_{c\,1}$.

$$U_{\text{К ОЭ}} = U_{\text{г}} - U_{\text{Э}};\ z_{\text{вх 1 ОЭ}} = U_{\text{в}}/I_{\text{Б}1},\ U_{\text{К ОБ}} = U_{\text{Cкп}} + U_{L\text{б}};\ z_{\text{вх 1 ОБ}} = U_{\text{в}}/I_{\text{Э}1}.$$

24. The excitation power and the power delivered to the load are:

$$P_{exc} = \qquad P_{\text{в}} = 0{,}5\,[\operatorname{Re} U_{\text{в}} \operatorname{Re} I_{\text{вх1}} + \operatorname{Im} U_{\text{в}} \operatorname{Im} I_{\text{вх1}}];$$

$$P_{out} = \qquad P_{\text{вых}} = 0{,}5\,[\operatorname{Re} U_{\text{К}} \operatorname{Re} I_{\text{К1}} + \operatorname{Im} U_{\text{К}} \operatorname{Im} I_{\text{К1}}].$$

For the common emitter configuration, $I_{in\ 1}$ = Ibase 1; $U_{col} = U_{col\ com.em.}$; and for the common base configuration, $I_{in\ 1} = I_{e1}$, $U_{col} = U_{col\ com.base}$.

If the power in the load P_{out} found as a result of the calculations differs considerably from the specified value, the calculations are to be repeated, correcting the value of P_{gen}, taking the deviation into account.

25. The DC component of the collector current, the power consumed from the supply and the efficiency are equal to the following regardless of the circuit configuration:

$$I_{\text{К}} = I_{\text{г1}}/g_1(\Theta); \quad P_0 = I_{\text{К}} U_{\text{к0}}; \quad \eta = P_{\text{вых}}/P_0.$$

26. The power gain, the power dissipated by the transistor, and the permissible power dissipation for a given transistor package temperature are determined from the following formulas, regardless of the circuit configuration:

$$K_P = P_{\text{вых}}/P_{\text{в}}; \quad P_{\text{рас}} = P_0 - P_{\text{вых}} + P_{\text{в}};$$
$$P_{\max} = (t_{\text{п}\max} - t_{\text{к}})/R_{\text{пк}}.$$

The maximum value of $t_{\pi\ max}$ [maximum junction temperature] is the maximum permissible value of t_{π} from Table 16.1.

It must be demonstrated that P_{pac} [Pdiss] < P_{max}.

27. The equivalent load impedance at the external leads of the transistor is:

$$Z_{load\ 1} = U_{col}/I_{col\ 1} - j\omega L_{col}, \qquad z_{\text{н1}} = U_{\text{К}}/I_{\text{К1}} - j\omega L_{\text{к}},$$

where $U_{col} = U_{col\ com.em.}$ for a common emitter circuit and $U_{col} = U_{col\ com.base}$ for a common base circuit.

In some cases, zero bias is not optimal. For example, when a transistor is considerably underutilized in terms of power, the cutoff angle in a zero bias mode is too small as compared to the optimal value. On the other hand, in a common base amplifier, a reduction in the cutoff angles may be needed to stabilize the operating mode. For this reason, it is necessary in the first case to introduce unblocking bias to increase the cutoff angle, and in the second case, to use blocking bias, for example, self-biasing to reduce the cutoff angle. In these cases, the design calculations should be performed for the specified cutoff angle. The procedure for such design calculations differs somewhat from that given in paragraphs 1 and 5.

A more precise formula is used in paragraph 1:

$$\xi_{\text{cutoff}} = \quad \xi_{\text{гр}} = 0{,}5\left[1 + \sqrt{1 - 8P_{\text{г}}/(S_{\text{гр}}\alpha_1(\Theta)U_{\text{к}0}^2)}\right],$$

where $\alpha_1(\Theta)$ is determined for the specified angle Θ from Table 16.2. The bias voltage U_{B0} is found in paragraph 5 from formula (16.11), where this bias assures the specified cutoff angle. If the bias is blocking bias, it can be realized by means of a resistance $R_e = -U_{B0}/I_c$, which is bypassed with a capacitor.

The calculation procedure cited here for power amplifiers is given for frequencies at which one can disregard the capacitance C_{B0}. For the 3 to 5 GHz band, a more complete equivalent circuit of a transistor is to be used (Figure 16.2). Common base amplifiers operate in this band. The equivalent circuit of a common base amplifier is shown in Figure 16.6b. The design calculations are carried out initially in accordance with paragraphs 1--18. Then, the following currents, voltages and resistances are calculated in paragraphs 19--37:

19. $I_{C\,\text{кэ}} = j\omega C_{\text{кэ}} U_{\text{г}}$, 20. $I_{L\text{э}1} = I + I_{\text{г}1} - I_{C\text{кэ}}$,
21. $U_{L\text{э}1} = j\omega L_{\text{э}1} I_{L\text{э}1}$, 22. $U_{C\text{э}0} = U_{L\text{б}} + U_{r\text{б}} + U_{\text{п}1} + U_{L\text{э}1}$

(We neglect the voltage across r_e' because it is small).

23. $I_{C\text{э}0} = j\omega C_{\text{э}0} U_{C\text{э}0}$. 24. $I_{\text{э}1} = I_{L\text{э}1} + I_{C\text{э}0}$.
25. $U_{L\text{э}2} = j\omega L_{\text{э}2} I_{\text{э}1}$. 26. $U_{\text{Э}} = U_{C\text{э}0} + U_{L\text{э}2}$.
27. $z_{\text{вх}} = U_{\text{Э}}/I_{\text{Э}1}$. 28. $U_{C\text{кк}} = U_{C\text{кп}} + U_{L\text{б}}$. 29. $I_{C\text{кк}} = j\omega C_{\text{кк}} U_{C\text{кк}}$.
30. $I_{L\text{к}1} = I_{\text{г}1} - I_{r\text{к}} - I_{C\text{кп}} - I_{C\text{ка}} - I_{C\text{кэ}} - I_{C\text{кк}}$. 31. $U_{L\text{к}1} = j\omega L_{\text{к}1} I_{L\text{к}1}$.
32. $U_{C\text{к}0} = U_{C\text{кк}} - U_{L\text{к}1}$. 33. $I_{C\text{к}0} = j\omega C_{\text{к}0} U_{C\text{к}0}$. 34. $I_{\text{н}} = -I_{C\text{к}0} + I_{L\text{к}1}$.
35. $U_{L\text{к}2} = j\omega L_{\text{к}2} I_{\text{н}}$. 36. $U_{\text{н}} = U_{C\text{к}0} - U_{L\text{к}2}$. 37. $z_{\text{н}} = U_{\text{н}}/I_{\text{н}}$.

38. The excitation power and the power delivered to the load are:

$$P_{\text{exc}} = \quad P_{\text{в}} = 0{,}5\,(\operatorname{Re} U_{\text{в}} \operatorname{Re} I_{\text{Э}1} + \operatorname{Im} U_{\text{в}} \operatorname{Im} I_{\text{Э}1});$$

$$P_{\text{out}} = \quad P_{\text{вых}} = 0{,}5\,(\operatorname{Re} U_{\text{н}} \operatorname{Re} I_{\text{н}} + \operatorname{Im} U_{\text{н}} \operatorname{Im} I_{\text{н}}).$$

The quantities I_c, P_0, η, K_p and P_{diss} are found just as in paragraphs 25 and 26 of the preceding design procedure.

As experience shows, at frequencies on the order of hundreds of megahertz the experimental and calculated results for the averaged parameters of a given type of transistor are sufficiently close, and for this reason, there is no necessity of a substantial reworking of the circuitry and structural design as compared to the calculated values. The influence of the imprecision in the knowledge of the transistor parameters and their scatter is easily eliminated by means of using fine tuning elements without changing the circuitry.

The design of amplifiers for frequencies on the order of several gigahertz based on the handbook data for transistors can apparently not be accomplished at the present time without experimental breadboarding to realize possible changes in the circuitry and structural design. This is explained by the approximate nature and complexity of the equivalent circuits of transistors and the inadequate precision in determining their parameters. The latter is related, on one hand, to measurement difficulties, and on the other, to the scatter in the parameters. In a wavelength range of 10 cm and shorter, even a comparatively slight scatter in the inductances of the leads and capacitances of the package can lead to sharp changes in the input impedance of a transistor because of resonance phenomena. This is explained by the fact that the input circuit of a transistor, which includes these reactive elements, forms a resonant system with a high Q (of about 10), which resonates within the working passband of the transistor. For example, in a range of 3 to 5 GHz, the calculated values of the resistive and reactive components of the input impedance of a KT937 transistor change by two orders of magnitude. The resonator nature of the input circuit is also responsible for the high sensitivity of the input impedance at a fixed frequency to small changes in the input circuit parameters. For example, an error of 20% in determining the inductance L_{e1} close to resonance changes the values of the resistive and reactive components of the input impedance of KT937 transistor by an order of magnitude. Imprecision in the fabrication of passive networks can have similar consequences. Moreover, when designing coupling networks, certain parasitic coupling circuits which influence the operating mode of an amplifier are not taken into account. Many of these factors can be disregarded at lower frequencies.

The measurement of the matrix parameters of a transistor does not eliminate the indicated difficult. Such measurements are also have a great deal of ambiguity, since a slight change in the length of transistor leads can greatly change the measurement result.

The conclusion that calculations where one fixed set of any parameters are used, either "physical" or matrix, are inadequate follows from what has been said above. It is recommended that calculations be performed with variations in the parameters. A series of such calculations will assist in ascertaining the most critical parameters, predicting possible changes in the operating mode of a transistor which are related to the scatter in different specimens of the transistor, the change in frequency, etc., as well as in selecting the kind of coupling network and providing for the requisite means of fine tuning.

17. EXTERNALLY EXCITED MICROWAVE CIRCUITS FOR TRANSISTOR OSCILLATORS AND AMPLIFIERS

17.1. General Information

In externally excited generators, designed in common emitter (Figure 17.1a) or common base (Figure 17.1b) configurations, the microwave networks can be represented in the form of four-pole networks of linear reactive elements, the power losses in which are neglectably small.

To obtain a selected power operating mode for a transistor, it is necessary to provide the requisite impedances with respect to the fundamental frequency, $Z_{in\ 1}$ and $Z_{load\ 1}$ (Figure 17.1), at its input and output. These impedances can in principle be determined by calculating the operational mode of the transistor based on its physical equivalent circuit (see Chapter 16 or [1 - 5]). At the present time, the calculation of the operational mode of a microwave power transistor is an approximate calculation, and as a rule, requires in addition that the electrical parameters of the transistor be found more precisely experimentally. Because of this, the method of experimentally determining the total input $Z_{in\ 1}$ and output $Z^*_{out\ 1}$ impedances of the transistor with respect to the first harmonic at some specified frequency and a definite electrical operating mode has become widespread in practice along with the analytical technique. A generalized schematic of a generator in which the transistor is replaced by the equivalent circuit taking these impedances into account is shown in Figure 17.2.

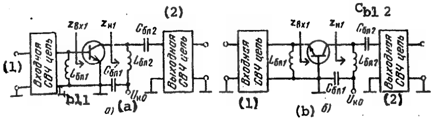

Figure 17.1. General schematic of an amplifier/oscillator with external excitation.

Key: 1. Input microwave network;
2. Output microwave network.

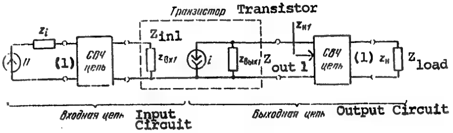

Figure 17.2. Generalized radiofrequency circuit of an amplifier/oscillator with the transistor equivalent circuit.

---

*It is presupposed that $Z_{out\ 1}$ corresponds to the complex conjugate of the load impedance of the transistor $Z_{load\ 1}$, i.e., $Z_{out\ 1} \approx Z^*_{load\ 1}$.

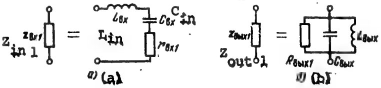

Figure 17.3. The equivalent circuits of transistor input (a) and output (b) networks.

TABLE 17.1.

Таблица 17.1

Transistor Тип транзистора Type	(1) $r_{вх1}$, Ом	2. $L_{вх}$, нГн	(3) $R_{вых1}$, Ом	(4) $C_{вых}$, пФ	(5) $f_{раб}$, ГГц	(6) $P_{вых}$, Вт	(7) K_P	η, %	$U_{к0}$, В (8)
KT607	6	1,3	120	1,2	1	1	3	45	28
KT612	4,2	0,9	180	2,2	1	0,3	6	60	7
KT904	5,5	6,5	85	8	0,4	3	3	50	28
KT904*	4,5	3	105	4,9	0,4	3	4	60	28
KT911A	8	5	36	6	1	1,5	4	40	28
KT911A*	5	3	35	5	1	1,5	5	40	28
KT913A	3	3,19	52,5	2,7	1	3	3	45	28
KT913Б	1,2	2,55	32,9	4	1	5	2,8...3	55...60	28
KT913B	1,2	2,23	16,0	4,4	1	10	2,6...2,8	60...65	28
KT918	6,5	1,5	200	2,4	2	1	4	40	28
KT919A	1,6	1,11	25,0	12,7	1	4	3	45...50	25
KT919Б B	2,3	1,27	64,1	7,1	1	2,5	5	45	20
KT919B V	4,5	0,955	118,6	5,8	1	2,6	10	55	22

---

* Бескорпусная конструкция

---

*Unpackaged structure.

Key:
1. $r_{in\ 1}$, ohms;
2. L_{in}, nanohenries;
3. $R_{out\ 1}$, ohms;
4. C_{out}, picofarads;
5. Working frequency, GHz;
6. P_{out}, watts;
7. Power gain;
8. $U_{coll.\ 0}$, volts.

Calculations and measurements of the impedances $Z_{in\ 1}$ and $Z_{out\ 1}$ have shown [3, 6, 8] that the input circuit impedance of a transistor can be approximated by the overall impedance of a series circuit consisting of a resistance $r_{in\ 1}$, an inductance L_{in} and a capacitance C_{in} (Figure 17.3a), the resonant frequency of which can be higher or lower than the working frequency of the amplifier/oscillator, while the impedance of the output circuit is quite well approximated by the impedance of a parallel circuit consisting of $R_{out\ 1}$, L_{out} and C_{out}, which is shown in Figure 17.3b. The parameters of the transistor input and output circuits depend on its operating power conditions and frequency. For this reason, the impedances $Z_{in\ 1}$ and $Z_{out\ 1}$ are determined at the working frequency for the selected operating mode. When an amplifier or oscillator operates in a certain band of frequencies, it is necessary to determine $Z_{in\ 1}$ and $Z_{out\ 1}$ for the transistor, taking its power operating mode throughout the entire specified bandwidth into account. The reactive component of the impedance $Z_{in\ 1}$ or $Z_{out\ 1}$ can be of in inductive or capacitive nature, depending on the working frequency of the transistor. Experimental values are given in Table 17.1 for the elements of the equivalent circuit of the input and output networks of some microwave transistors, with the operating mode parameters indicated for which they were measured.

When designing microwave circuits for oscillators/amplifiers, we shall assume that the impedances Z_{in} and $Z_{load\ 1}$ (or $Z_{out\ 1}$) are known. Then the four-pole network in the input circuit of a generator (Figure 17.2) should transform the impedance at the generator input Z_i to the impedance $Z_{in\ 1}$, while the four-pole network in the output circuit should transform the load impedance Z_{load} to the impedance $Z_{load\ 1}$ (or $Z_{out\ 1}$). Consequently, the microwave four-pole network in this case plays the part of an impedance transformer and for this reason is called a transforming network. Since the transformation of the impedances in the input (or output) microwave network is usually accomplished for matching in this circuit, the four-pole network is also called a matching circuit. It is understood in this case that when matching is achieved in the microwave input circuit of a generator, the greatest power will be transmitted from the stage driving the generator to the input circuit of the transistor. In this case, the impedance $Z_{in\ 1}$ and the impedance of the four-pole network at the connection points, $Z_{in\ 1}$, will be complex conjugate quantities. In the output microwave network when matched, $Z_{out\ 1}$ is the complex conjugate of the input impedance $Z_{load\ 1}$ of the four-pole network on the transistor side, which will deliver the specified power to the load. Taking that presented above into account, we shall call the microwave network formed by the transforming four-pole network of linear reactive elements a matching network [7].

The major electrical requirements placed on the microwave networks of an externally excited generator are providing for the requisite impedance transformation, as low as possible power losses during power transmission, the specified bandwidth, the requisite filtration level of the higher harmonics and suppression of spurious frequencies.

A specific feature of high power amplifier transistors as compared to low and intermediate power transistors is the small values of the resistive components $r_{in\ 1}$ and $R_{out\ 1}$ of the impedances $Z_{in\ 1}$ and $Z_{out\ 1}$ respectively, which are frequently substantially less than the resistive components of the impedances at the generator input and output. In this regard, a microwave network should provide a relatively high transformation ratio (from a few units up to 10). In this case, the power losses increase markedly in the networks and the passband is narrowed.

The efficiency of power transmission to the load is estimated in terms of the circuit efficiency, η_{cir}, defined as the ratio of the power P_{load}, dissipated in in the load, to the oscillatory power P delivered to the microwave network:

$$\eta_{cir} = P_{load}/P \tag{17.1}$$

In modern transistorized transmitters, including integrated circuit stages, externally excited generators are usually not tuned. The requisite bandwidth of the amplifier stage is governed by the conditions necessary for normal transmitter operation (for example, the kind of modulation, the range of frequencies covered without tuning the stage, the requisite phase stability of the signals at the output).

The requirement of filtration of the higher harmonics basically applies to the output microwave circuit of an amplifier/oscillator. This is explained by the fact that microwave power transistors usually operate in modes in which the voltage waveform at the collector differs substantially from a sine wave. For this reason, to obtain a voltage close to a sine wave at the output of an amplifier/oscillator, the output microwave circuit should filter out the higher harmonics as much as possible.

Matching microwave four-pole networks of the coupled resonant parallel circuit type or individual Γ, T and Π section filters (or two to three series stages of such filters) meet the electrical requirements considered here to a sufficient extent. The use of one to two such sections makes it possible to obtain a rather high impedance transformation ratio, provide for a comparatively wide passband and filter the higher harmonics. In the case of elevated requirements placed on the passband and the suppression of spurious and out-of-band signals, complex filters are employed.

When designing the microwave networks for amplifier/oscillators used in the modules of active phased arrays, it is desirable to use the simplest microwave circuits which are convenient for integrated circuit technology.

Microwave circuits for transistorized amplifier/oscillators using integrated circuit technology can be constructed from elements with lumped parameters, such as inductance coils, capacitors and resistors. These components have small dimensions and a sufficiently high Q in a frequency range of from hundreds of megahertz up to 1 GHz*. In circuits intended for operation at frequencies above 1 GHz, elements with distributed parameters are used in the form of sections of unbalanced striplines. Making a stripline on a substrate of a dielectric material with a high relative dielectric permittivity ($\varepsilon > 7$) makes it possible to substantially reduce the dimensions of a circuit. With the present state of the art in microwave microelectronics technology, integrated circuits with distributed and to a greater extent, with lumped parameters have relatively high losses, which are primarily due to the significant reduction in the perimeter of the conductors in step with the decrease in the element size. Because of this, microwave circuits should not be especially complex and contain a large number of elements.

---

*See Chapter 20 of this book.

17.2. The Design of the Microwave Networks of Amplifiers and Oscillators

The Input Microwave Matching Network (Figure 17.2). If the excitation power is delivered to the generator input by means of a matched transmission line with a characteristic impedance of ρ, then one can assume that the internal impedance of the driving source Z_i is equal to ρ.

In accordance with the equivalent circuit of the input circuit of a transistor, shown in Figure 17.3a:

$$Z_{in\ 1} = \quad z_{\text{вх}1}=r_{\text{вх}1}+j\,(\omega L_{\text{вх}}-1/\omega C_{\text{вх}})=r_{\text{вх}1}+jx_{\text{вх}1}.$$

The reactive component $x_{in\ 1}$ of this impedance can be both of an inductive nature (at a working frequency higher than the resonant frequency of the transistor input circuit), and a capacitive nature (at a working frequency lower than the resonant frequency of the input circuit). For many modern intermediate and high power transistors, operating in the decimeter band, the values $1/\omega C_{in}$ are substantially less than ωL_{in} [3.6], and in this case, one can approximately assume that:

$$Z_{in\ 1} \simeq r_{in\ 1} + j\omega L_{in} \qquad z_{\text{вх}1}\simeq r_{\text{вх}1}+j\omega L_{\text{вх}}.$$

Because of the fact that the inductance L_{in} cannot be less than a certain value governed by the dimensions and structural design of the package and length of the leads (where a package is absent) of a transistor, while $r_{in\ 1}$ decreases with increasing transistor power [3.8], the quality factor Q_{in} of its equivalent input circuit at the working frequency f, which is defined as:

$$Q_{\text{вх}}=2\pi f L_{\text{вх}}/r_{\text{вх}1},$$

proves to be rather high, something which makes it considerably more difficult to design broadband input microwave circuits for an amplifier or oscillator.

An input microwave circuit using lumped elements is simplest when a Γ-section reactive four-pole network is used. Examples of such networks are shown in Figures 17.4a and b. These circuits are feasible if the resistance ρ (or the resistive component of the impedance Z_i) is greater than $r_{in\ 1}$. In the circuit of Figure 17.4a, the inductance L_{in} can be incorporated in the inductance L_1, and then the total series inductance of the Γ-network is $L_{series} = L_1 + L_{in}$. In the circuit of Figure 17.4b, the inductive reactance ωL_{in} can be partially compensated by the reactance $1/\omega C_2$, if L_{in} is greater than the requisite value of L_{series} of the Γ-network. The T and Π section networks (Figure 17.4, c-e) make it possible to provide for impedance transformations in greater ranges for a specified frequency band than does a Γ section circuit. Moreover, with rather large parallel capacitances of these circuits, the filtering of the higher harmonics at the generator input is improved.

When it is necessary to match impedances which differ significantly in value in a certain range of frequencies, stepped transformation is employed. Circuits are used for this which consist of several Γ or Π sections with low transformation ratios.

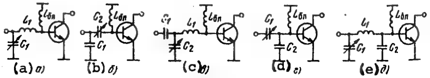

Figure 17.4. Circuit configurations of input microwave matching networks for an amplifier/oscillator using lumped elements.

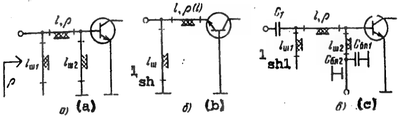

Figure 17.5. Circuit configurations for input microwave matching networks of an oscillator/amplifier using asymmetrical stripline sections.

[1_{sh} = shunt inductance].

At frequencies above 1 GHz, microwave networks are designed around asymmetrical stripline sections (Figure 17.5), in which lumped noninductive capacitors are frequently inserted, which make it possible to additionally create an isolating capacitance in the circuit for the DC. In the circuit of Figure 17.5a, matching is achieved by using a single loop transformer (1, $1_{sh\ 1}$). In the circuit of Figure 17.5b, the matching network is made in the form of an irregular stripline 1 with a changing characteristic impedance $\rho(1)$. The circuit of Figure 17.5c differs from the circuit of Figure 17.5a only in the presence of capacitance C_1. The loops $1_{sh\ 2}$ in the circuits of Figures 17.5a and c and 1_{sh} in the circuit of Figure 17.5b play the part of RF blocking chokes. The loops are structurally made in the form of short circuited line sections with a length close to $\lambda/4$ (where λ is the working wavelength in the line), having a high characteristic impedance (of about 100 ohms). The radiofrequency short circuiting of the loop $1_{sh\ 2}$ in the circuit of Figure 17.5c is achieved by connecting capacitor $C_{bl.1}$ to it which has a rather high capacitance.

Naturally, the examples cited here do not exhaust the possible circuit configurations for these networks. When selecting a microwave network configuration which meets the electrical requirements placed on it, one must remember that the use of simpler circuits with low power losses makes it possible to simplify the structural execution of the microwave network and reduce the overall area occupied by the circuit on the substrate of a hybrid IC.

The Output Matching Microwave Network (Figure 17.2). In the general case, the load impedance is $Z_H = r_H + jx_H$, where r_H and x_H are the resistive and reactive components of this impedance respectively. In the case where the generator load is the input impedance of a matched transmission line with a characteristic impedance of ρ, $Z_H = \rho$.

In the design calculations of a generator output circuit, it is more convenient to use the admittance instead of the impedance $Z_{out\ 1}$ (see Figure 17.3b):

$$y_{\text{вых1}} = \frac{1}{z_{\text{вых1}}} = g_{\text{вых1}} + jb_{\text{вых1}} = \frac{1}{R_{\text{вых1}}} + j\left(\omega C_{\text{вых}} - \frac{1}{\omega L_{\text{вых}}}\right).$$

Here $g_{out\ 1}$ and $b_{out\ 1}$ are the conductance and the reactive components of the admittance $Y_{out\ 1}$.

For the majority of modern transistors in the decimeter band, the reactive component of the output admittance has a capacitive character (see Table 17.1) and:

$$Y_{out\ 1} = 1/R_{out\ 1} + j\omega C_{out}. \qquad y_{\text{вых1}} \simeq 1/R_{\text{вых1}} + j\omega C_{\text{вых}}.$$

The Q of the equivalent output circuit of a transistor in this case is:

$$Q_{\text{вых}} = R_{\text{вых1}}\,\omega C_{\text{вых}} = R_{\text{н1}}\,\omega C_{\text{вых}}.$$

Here, $\omega = 2\pi f$ (f is the working frequency of the generator); $R_{H\ 1}$ is the resistive component of the impedance $Z_{H\ 1}$ of a parallel circuit consisting of $R_{H\ 1}$ and $X_{H\ 1}$.

Microwave power transistors usually have a low quality factor Q_{out}, which is substantially less than the quality factor of their input circuit Q_{in}. In this respect, it is easier to design a generator output microwave network of sufficient bandwidth than an input circuit.

Besides the impedance transformation, requirements are also placed on a matching four-pole network in the output microwave circuit of a generator to provide for a high efficiency, η_c , a definite bandwidth and a requisite higher harmonic filtration level. The meeting of these requirements depends in many on the correct choice of the microwave network output circuit, the electrical characteristics of which are governed to a considerable extent by its quality factor Q, taking the load into account. With a small Q in the circuit, it is easier to obtain a high efficiency and a relatively wide passband, but in this case, it is more difficult to meet the requirement for good filtration of the higher harmonics. For this reason, such a value of Q should be assured in the design of a microwave output network that certain compromise requirements are satisfied.

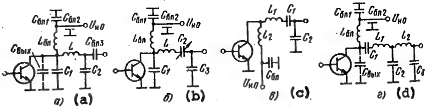

Figure 17.6. Circuit configurations of output microwave matching networks of an amplifier/oscillator using lumped elements.

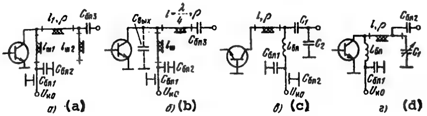

Figure 17.7. Circuit configurations for the output microwave matching networks of an amplifier/oscillator using asymmetrical stripline sections.

Γ and Π section networks are frequently used in the matching output microwave circuit of transistor amplifier/oscillators. The simplest of them (the Γ section) can be used in cases where increased requirements are not placed on the filtering of higher harmonics at the generator output and it is necessary to match impedances which are close in value in a narrow band of frequencies. It is expedient to have a Q of such a circuit of no more than two to three.

Π-networks have become widespread in the circuit configurations of output microwave networks. To improve the filtering properties of microwave networks with respect to the higher harmonics, capacitances are inserted in the parallel branches of the Π-network. For this purpose, Π-networks are used which contain an additional series tuned circuit in the series branch, which is tuned to the fundamental frequency of the oscillator/amplifier (Figure 17.6b-d). The presence of such a filter makes it possible to substantially reduce the impedance of the series circuit (L_1, C_1 in Figure 17.6c, d) for the fundamental as compared to its impedance for higher harmonics, and thereby improve the filtering properties of the microwave network. Π-networks which start with an inductance are used in a number of cases to improve transistor efficiency. Such microwave networks, because of the presence of the inductance, create a considerable resistance to higher harmonics, and a relatively large voltage level of these harmonics appears at the transistor collector, something which produces a substantially nonsinusoidal waveform of the collector voltage. The collector voltage is small during that portion of the signal period when the majority of the resistive collector current is flowing, something which leads to an improvement in transistor efficiency.

The circuit configurations for the output microwave network of an oscillator/amplifier, depending on their operating frequency and structural requirements, are designed around components with either lumped or distributed parameters.

Examples of output microwave circuit designs for a transistor oscillator/amplifier with external excitation and using lumped elements are shown in Figure 17.6. The circuit of 17.6a contains a Π-network, starting with a capacitor C_1. Frequently, capacitor C_1 is absent from the circuit and its role is played by the capacitance C_{out} of the transistor. Capacitor $C_{bl\ 3}$ is a blocking capacitor. The circuit of Figure 17.6b with a series resonant circuit, the inductances of which are a part of the inductance L, has better filtering properties with respect to higher harmonics. In the circuit of Figure 17.6c, the Π-network starts with the inductance L_2, the function of which has already been stated. The circuit of Figure 17.6d makes it possible to satisfy higher requirements placed on the matching of impedances in a rather wide band of frequencies as well as the filtering of higher harmonics at the generator output.

Examples of output microwave network configurations are given in Figure 17.7 using asymmetrical stripline elements. Lumped isolating and blocking noninductive capacitors are also used in these circuits.

In the circuit of Figure 17.7a, matching is achieved by a single loop transformer (l_1, $l_{sh\ 2}$). The characteristic impedance ρ of the line l_1 is equal to the load impedance. The short-circuited loop $l_{sh\ 1}$ with a length of $\lambda/4$ performs the function of a radiofrequency blocking choke. A quarter-wave transformer is used in the circuit of Figure 17.7b which matches the resistances $R_{out\ 1}$ of the transistor and ρ of the load. The reactive component of the output impedance of the transistor output circuit is compensated by the impedance of the short-circuited loop l_{sh}. In the circuit of Figure 17.7c, line section l, capacitance C_{out} and capacitors C_1 and C_2 form a microwave network close to a Π-network. In the circuit of Figure 17.7d, the microwave network consisting of line section , loaded into capacitance C_1, is tuned to resonance at the fundamental frequency. The necessary coupling to the load is assured by connecting the load resistance ρ through an isolating capacitor C_2 to a part of the line section l.

When designing the circuit configuration for a microwave output network which meets the electrical requirements placed on it, one must strive to see that the circuit is as simple and as convenient as possible for its execution in the form of a hybrid integrated circuit.

17.3. Oscillator/Amplifier Power Supply Circuits

The power supply circuit for an oscillator/amplifier should be designed so that it does not disrupt the operation of its microwave circuitry. A parallel supply circuit is most frequently used (Figure 17.8), since the usual microwave circuit configuration does not allow for the use of a series supply circuit. In the case of a parallel supply circuit, the DC source is connected to the transistor terminals through a blocking choke, $L_{bl\ 1}$, which has a high resistance to the alternating component of the amplifier/oscillator current, so that the supply source has no influence on the operation of the microwave circuitry. Improved blocking of the voltage supply is achieved by inserting a capacitor which has a low resistance to alternating current (capacitors $C_{bl\ 3}$ and $C_{bl\ 4}$ in Figure 17.8a and b). To prevent the direct current component of the oscillator/amplifier from flowing into the load networks (or into the network of the preceding stage), isolating capacitors are inserted in the circuit ($C_{bl\ 1}$ and $C_{bl\ 2}$ in Figure 17.8a and b). A series inserted microwave circuit capacitor (C_1 in Figure 17.6c, d) frequently performs the function of an isolating capacitor. The choice of the choke inductance and capacitance of the blocking capacitors is made by working from the requirements for normal operation of the oscillator/amplifier circuit and the possibilities for realizing the blocking elements.

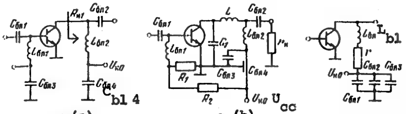

а) (a) б) (b) в) (c)

Figure 17.8. Parallel power supply configurations for an amplifier/oscillator.

In order that the blocking choke (Figure 17.8a) does not exert any marked influence on the operation of the transistor output circuit, its inductance $L_{bl\ 2}$ is chosen by using the approximate relationship:

$$\omega L_{bl\ 2} \geqq 10R_{load\ 1} \qquad \omega L_{бл2} \geqslant 10R_{н1}. \tag{17.2}$$

The capacitance of capacitor $C_{bl\ 4}$ is determined from the relationship:

$$C_{бл4} \geqslant 50\cdot 10^3/\omega^2 L_{бл2}, \tag{17.3}$$

derived from the condition that the resonant frequency for series resonance of the circuit $L_{bl\ 2}$, $C_{bl\ 4}$ (Figure 17.8a) should be considerably lower than the working frequency of the oscillator or amplifier*.

The upper limit for the values of the inductance L_{bl} and the capacitance C_{bl} is basically limited by the production process capabilities. To reduce the requisite value of L_{bl} in the case where $R_{load\ 1} > r_{load}$, it is expedient to connect the power supply circuit closer to the load, for example, as shown in Figure 17.8b. The value of L_{bl} with this circuit configuration can be chosen from the condition $\omega L_{bl\ 2} \geqq 10r_{load}$.

To estimate the approximate values of the parameters of the blocking elements inserted in the input circuit of an amplifier/oscillator (Figure 17.8a), one can derive relationships similar to (17.2) and (17.3):

$$\omega L_{бл1} \geqslant 10 z_{nx1}; \quad C_{бл3} \geqslant 50\cdot 10^3/\omega^2 L_{бл1},$$

where $z_{nx1} = \sqrt{r_{nx1}^2 + x_{nx1}^2}$.

The capacitance of the isolating capacitor (if it is not a component of the microwave circuit) is determined from the condition that the voltage be small as compared to the voltage across the resistance $R_{load\ 1}$ (Figure 17.8a) or r_{load} (Figure 17.8b) when the fundamental frequency flows through the capacitor, i.e.,

---

*In expressions (17.2) and (17.3) and in those given in the following, it is assumed that $\omega = 2\pi f$, the working frequency is taken in gigahertz, the capacitance is in picofarads, the inductance is in nanohenries and the resistance is in ohms.

$C_{bl\ 2} \geqq 10 \cdot 10^3/\omega R$, where R is either $R_{load\ 1}$ or r_{load} depending on the point where $C_{bl\ 2}$ is inserted.

When designing power supply circuits for an amplifier/oscillator, one must keep in mind the fact that the blocking chokes and capacitors form tuned systems, which not infrequently lead to the appearance of parasitics in the amplifier or oscillator at a frequency considerably lower than the working frequency. This promotes an increase in the transistor current gain with a reduction in its working frequency. To prevent the appearance of these oscillations, it is necessary to reduce the Q of the blocking chokes, something which can be achieved, for example, by inserting a resistor with a small resistance r (a few ohms) in series with the choke (Figure 17.8c), or by fabricating the coil L_{bl} from a conductor with a high ohmic resistance. Another method of breaking up oscillations at low frequencies is inserting capacitors of various values in series with L_{bl}, which creates series resonances at definite frequencies substantially lower than the working frequency in the power supply circuitry ($C_{bl\ 1}$, $C_{bl\ 2}$ and $C_{bl\ 3}$ in the circuit of Figure 17.8c). These recommendations should be taken into account when designing an automatic bias network.

17.4. The Design of Microwave Matching Transformer Networks Using Lumped Elements

As has already been noted, linear reactive four-pole networks in the form of Γ, T and Π section networks and combinations of them made from lumped elements are widely used as microwave networks. Complex impedances can be inserted in practical circuits in the general case at the input and output of the matching four-pole networks. When designing a microwave network, the reactive components of these impedances can be incorporated in the four-pole network. Then there will be only resistive components* at the input and output of the four-pole network.

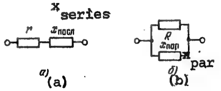

Figure 17.9. Equivalent series (a) and parallel (b) networks.

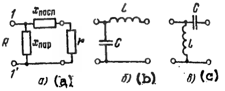

Figure 17.10. A Γ section network.

The property of four-pole Γ, T and Π networks of transforming an impedance is based on the principle of converting a series circuit of resistive and reactive impedance components at a definite frequency to an equivalent parallel circuit, which has the same impedance as the series circuit (Figure 17.9). We shall give the basic relationships for such equivalent circuits [9, 10], by introducing the concept of circuit Q: $Q = x_{ser}/r$ for a series circuit and $Q = R/x_{par}$ for a parallel circuit.

---

*The solution of the problem of matching arbitrary complex impedances by means of very simple matching networks is treated in the literature [11].

By equating the impedances of these circuits, we obtain:

$$r + jx_{ser} = Rjx_{par}/(R + jx_{par}) \quad r + j\,x_{\text{посл}} = R\,j\,x_{\text{пар}}/(R + j\,x_{\text{пар}}). \qquad (17.4)$$

Assuming that the quality factor of a circuit Q does not change during transformation, and by using expression (17.4), we find the relationship between the impedances of the series and parallel circuits:

$$r = Rx^2_{\text{пар}}/(R^2 + x^2_{\text{пар}}) = R/(1 + Q^2), \qquad (17.5)$$

$$x_{\text{посл}} = x_{\text{пар}}\,R^2/(R^2 + x^2_{\text{пар}}) = x_{\text{пар}}\,Q^2/(1 + Q^2), \qquad (17.6)$$

$$R = (r^2 + x^2_{\text{посл}})/r = r\,(1 + Q)^2, \qquad (17.7)$$

$$x_{\text{пар}} = (r^2 + x^2_{\text{посл}})/x_{\text{посл}} = x_{\text{посл}}\,(1 + Q^2)/Q^2. \qquad (17.8)$$

In the case where the resistances r and R are known, the reactances x_{ser} and x_{par} can be found from the formulas:

$$x_{\text{посл}} = \sqrt{(R-r)\,r}, \; x_{\text{пар}} = R\,[(R-r)/r]^{-1/2}. \qquad (17.9)$$

If follows from expression (17.5) that:

$$R/r = (1 + Q^2). \qquad (17.10)$$

Thus, by varying the Q with the appropriate choice of values for x_{ser} and x_{par}, one can obtain the requisite resistance transformation.

The relationships obtained here make it possible to design Γ, Π and T transforming networks, assuming that they match the resistances for a definite working frequency. The simplest of these circuits is a Γ-network, containing two reactive elements.

The Γ-Network. The equivalent circuit of a Γ-network is shown in Figure 17.10a, while two of its possible practical variants for matching resistances of r and R are shown in Figure 17.10b, c (where R > r). The impedances of the series and parallel circuit components have different kinds of reactance to obtain a purely resistive impedance at the input and output. The circuits of Figures 17.10b and c are identical in terms of their transforming properties, however, the circuit of Figure 17.10b has better filtering properties as regards the higher harmonics, thanks to the insertion of a parallel capacitance.

We shall give an approximate procedure for the design calculations of Γ-network elements for two cases, which are encountered most frequently during design work.

1. The resistances r and R, which must be matched, are specified. In this case, the resistances x_{ser} and x_{par} can be determined from formulas (17.9). It is

frequently convenient during calculations to make use of the quality factor of the circuit, Q, which makes it possible to estimate such circuit parameters as the efficiency and filtration factor. For specified values of r and R:

$$Q = \sqrt{R/r - 1}. \qquad (17.11)$$

2. The quality factor Q and one of the resistances are specified. By employing the formulas for the Q and expression (17.10), we find:

for known values of Q and r:

$$x_{\text{посл}} = Qr, \quad R = r(1+Q^2), \quad x_{\text{пар}} = R/Q,$$

for known values of Q and R:

$$x_{\text{пар}} = R/Q, \; r = R/(1+Q^2), \; x_{\text{посл}} = Qr.$$

The nature of the reactances x_{ser} and x_{par} should be different and determined by the specific Γ-network configuration. In the case of known reactances x_{ser} and x_{par}:

$$L = x_L/2\pi f; \; C = 10^3/2\pi f x_C. \qquad (17.12)$$

A specific feature of a Γ-network is the fact that its requisite Q is determined by the impedances which must be matched. For this reason, if the impedances being matched differ substantially in their value, then the Q proves to be rather high, which leads to a narrowing of the circuit bandwidth. With values of the impedances which are close, the requisite circuit Q proves to be low and the filtering capability of the circuit is degraded. Calculations show that for a Q of about 3, the attenuation of the second harmonic at the circuit output will be about 20 dB.

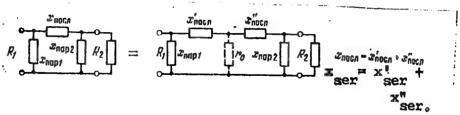

Figure 17.11. The equivalent circuit of a Π-network.

Π and T-Networks. The equivalent circuits of Π and T-networks are shown in Figures 17.11 and 17.13 respectively. The variants of these circuits which are most frequently used in oscillator and amplifier circuits are shown in Figures 17.12 and 17.14.

We shall consider that Π and T-networks consist of two Γ-networks, which we call sections. Consequently, when calculating the parameters of the elements of Π and T-networks, one can employ the formulas derived for the Γ-network. For this, each Γ-network should be supplemented with a second resistance, which in the case of a Π-network will appear in the Γ section as a series r_0, and in the T-network as a parallel R_0 (the same for both sections, since it acts at the points where they are connected). The resistances r_0 and R_0 (see Figures 17.11 and 17.13) should satisfy the conditions:

$$r_0 < R_1,\ R_2;\ R_0 > r_1,\ r_2.$$

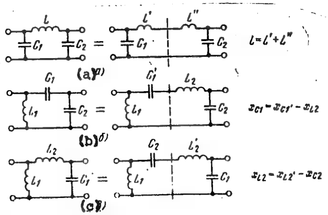
L
C1
C2
L'
L''
L=L'+L''
(a) а)
C1
L1
C2
C1'
L2
x_C1 = x_C1' - x_L2
(b) б)
L2
L1
C1
C2
L2'
x_L2 = x_L2' - x_C2
(c) в)

Figure 17.12. П-networks.

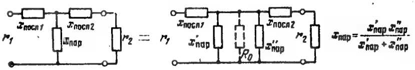
x_посл1
x_посл2
r1
x_пар
r2
x'_пар
R0
x''_пар
x_пар = x'_пар x''_пар / (x'_пар + x''_пар)

Figure 17.13. The equivalent circuit of a T-network.

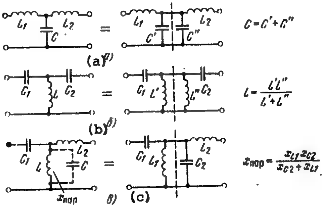
L1
L2
C
C'
C''
C=C'+C''
(a) а)
C1
L
C2
L'
L''
L = L'L''/(L'+L'')
(b) б)
C1
L
L2
C
x_пар
L1
C2
x_пар = x_L1 x_C2 / (x_C2 + x_L1)
в) (c)

Figure 17.14. T-networks.

To find the resistance r_0 (or R_0), the quality factor Q of one of the Г sections is to be specified beforehand, and then, knowing the resistance being matched R (or r), the following is calculated from formula (17.10):

$$r_0 = R/(1 + Q^2) \quad \text{or} \quad R_0 = r(1 + Q^2).$$

$$r_0 = R/(1 + Q^2)$$
либо $R_0 = r(1 + Q^2)$.

TABLE 17.2.

A Π-Network (Figure 17.11)	A Π-Network with a Supplemental Filter (Figure 17.15b)	A T-Network (Figure 17.13)
The values of R_1, R_2, Q_1 and f_0 are known.	The values of R_1, R_2, Q_1, Q_0 and f_0 are known.	The values of r_1, r_2, Q_1 and f_0 are known.
1. $r_0 = R_1/(1+Q_1^2)$	1. $r_0 = R_1/(1+Q_1^2)$	1. $R_0 = r_1(1+Q_1^2)$
2. Check for the condition $r_0 < R_2$.	2. Check for the condition $r_0 < R_2$.	2. Check for the condition $R_0 > r_2$.
3. $x_{par\ 1} = R_1/Q_1$, $x'_{ser} = Q_1 r_0$	3. $x_{L1'} = Q_1 r_0$, $x_{C\ 1} = R_1/Q_1$	3. $x_{ser\ 1} = Q_1 r_1$, $x'_{par} = R_0/Q_1$
4. $Q_2 = \sqrt{R_2/r_0 - 1}$	4. $X_{L\ 0} = X_{C\ 0} = Q_0 r_0$	4. $Q_2 = \sqrt{R_0/r_2 - 1}$
5. $x''_{ser} = Q_2 r_0$, $x_{par\ 2} = R_2/Q_2$	5. $Q_2 = \sqrt{R_2/r_0 - 1}$	5. $x''_{par} = R_0/Q_2$, $x_{ser\ 2} = Q_2 r_2$
6. $x_{ser} = x'_{ser} + x''_{ser}$	6. $x_{L\ 1''} = Q_2 r_0$, $x_{C\ 2} = R_2/Q_2$	6. $x_{par} = (x'_{par} x''_{par})/(x'_{par} + x''_{par})$
7. Calculate L and C from formulas (17.12).	7. $x_L = x_{L\ 1'} + x_{L\ 1''} + x_{L\ 0}$	7. Calculate L and C from formulas (17.12).
	8. Calculate L and C from formulas (17.12).	

Notes: 1. If $r_0 > R_2$ (a Π-network) or $R_0 < r_2$ (a T-network), then matching is impossible. 2. The impedances x_{ser} and x_{par} should have different signs. 3. Take the sign of the reactances into account during summing.

Here $R = R_1$ or $R = R_2$, while $r = r_1$ or $r = r_2$ depending on the Q of which section is known. The parameters of the Γ section components are calculated sequentially from one section to the other using the procedure given for a Γ-network. The design calculation procedure for Π and T-networks, in the case of known resistances which are being matched and a known Q_1 of the first Γ section of the network at the working frequency f_0, is given in Table 17.2.

In contrast to a Γ-network, in which the resistances being matched, r and R, should satisfy the condition $r < R$, in a Π-network, we can have both $R_1 > R_2$ and $R_1 < R_2$ (similarly, for a T-network, there can be both $r_1 > r_2$ and $r_1 < r_2$), something which is important when designing the microwave circuit of an amplifier or oscillator. A drawback to the given calculation procedure is the ambiguity in the parameters of the circuit elements which depend on the value of Q_1, which can be chosen with different values in the design calculations. It is expedient to take the quantity Q as no more than 2 to 5 [1].

A Π-Network with Improved Filtering of Higher Harmonics. To improve the filtering properties of the microwave network, the circuit of which is shown in Figure 17.12a, a filter in the form of a series tuned circuit L_0 and C_0, which resonates at the working frequency (Figure 17.15), is additionally inserted in the inductive branch of the circuit. The inductance and capacitance of the resonant circuit are related by the relationship $\omega_0 L_0 = 1/\omega_0 C_0$, where $\omega_0 = 2\pi f_0$. The procedure for the design calculations for a П-network configuration with an additional filter is given in Table 17.2.

The Г, П and T-networks treated here do not always make it possible to match the specified resistances within the requisite frequency passband with an easily realized quality factor Q. Then one can use a more complex four-pole network consisting of several П and T sections in the matching network, where this four-pole network is also represented in the form of joined Г sections in the calculations.

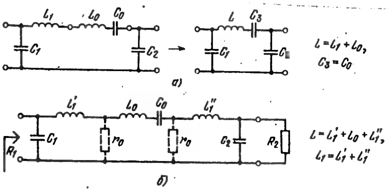

Figure 17.15. A П-network with an additional filter L_0, C_0 (a) and its representation in the form of three sections.

The efficiency of a microwave circuit, in accordance with formula (17.1) is:

$$\eta_{\text{ц}} = P_{\text{н}}/P = 1 - P_{\text{п}}/(P_{\text{н}} + P_{\text{п}}).$$

Here $P = P_H + P_\Pi$ [$P = P_{load} + P_{con}$]; P_{con} is the power lost in the elements of the network and the connecting conductors.

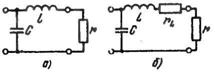

Figure 17.16. On the calculation of the efficiency of a Г-network.

One of the powers (P_{load} or P) is usually known when designing a network. To find the power P_{con}, it is necessary to determine the power losses in each element of the network as well as the connecting conductors, and then to sum them. When using a hybrid integrated circuit, the length of the connecting conductors is to be kept to a minimum. For this reason, one can assume that the losses in the connecting conductors are neglectably small and disregard them when calculating the efficiency.

We shall initially consider the procedure for determining the efficiency of the simplest microwave network: the Г section shown in Figure 17.16a. The power losses in such a network are composed of the losses in the inductance coil and the capacitor. In many practical circuits, the losses in the capacitor are substantially less than the losses in the coil, since the Q of the capacitors used in microwave circuits is an order of magnitude higher than the Q of the coils, Q_L. Consequently, the losses in a capacitor can be disregarded and then the equivalent circuit of a Γ section, taking into account only the losses in the coil (r_L), will assume the form shown in Figure 17.16b, while its efficiency can be determined from the approximate formula:

$$\eta_ц \simeq 1 - r_L/(r_L + r) = 1 - Q/Q'. \qquad (17.13)$$

Here $Q = x_L/(r + r_L)$; $Q' \simeq Q_L = x_L/r_L$ is the Q of the Γ section taking the resistance r of the load into account and without this resistance respectively.

TABLE 17.3.

Тип цепи Type of Network	when & $\eta_ц$ при $Q'_k \gg Q_k$ и $Q'_k = Q' \gg 1$ c
Г-цепь рис. (17.10) Gamma Network, Fig. 17.10	$1 - Q_1/Q'$
П-цепь (рис. 17.12) Pi Network (Fig. 17.12)	$\left(1 - \frac{Q_1}{Q'_1}\right)\left(1 - \frac{Q_2}{Q'_2}\right) \simeq 1 - \frac{Q_1 + Q_2}{Q'}$
(1) П-цепь с дополнительным фильтром (рис. 17.15)	$\left(1 - \frac{Q_1}{Q'_1}\right)\left(1 - \frac{Q_2}{Q'_2}\right)\left(1 - \frac{Q_0}{Q'_0}\right) \simeq$ $\simeq 1 - \frac{Q_1 + Q_2 + Q_0}{Q'}$
Т-цепь (рис. 17.14) T Network (Fig. 17.14)	$\left(1 - \frac{Q_1}{Q'_1}\right)\left(1 - \frac{Q_2}{Q'_2}\right) \simeq 1 - \frac{Q_1 + Q_2}{Q'}$

Key: 1. П-network with additional filter (Figure 17.15).

It follows from formula (17.13) that to obtain a high efficiency, the quality factor Q' should be considerably greater than Q, which becomes difficult to accomplish when the load resistance is low and can become even commensurate with the loss resistance in the microwave network elements. The actual Q of inductance coils using film technology amounts to 50 to 100. For this reason, to achieve a high efficiency (about 0.9), the Q of a Γ section should be no less than 5 to 8.

A Γ section is an integral part of П and T-networks, and for this reason, the efficiency of such networks can be found as the product of the efficiencies of the individual Γ sections comprising these networks. For a network consisting of k Γ sections, $\eta_c = \eta_1 \eta_2 \ldots \eta_k$. Here, $\eta_k = 1 - Q_k/Q'_k$ (Q_k is the quality factor of the k-th Γ section, taking the load impedance into account; Q'_k is the quality factor of the k-th Γ section, due solely to the losses in it).

The calculation of the efficiency requires knowledge of the true values of the quality factors Q_k and Q'_k. However, in the majority of practical cases, the values Q_k and Q'_k are known approximately, since they considerably dependent on the specific realization of the entire network circuitry. For this reason, to estimate the efficiency of a Γ section is $Q_k = x_{ser}/r$, while the quality factor of the coil is found from the approximate formulas (see Chapter 20) or is taken from practical data. Approximate formulas for determining the efficiency of Π and T section microwave circuits, assuming that $Q'_k >> Q_k$, while the quality factors Q'_k of each of the sections are approximately the same, are given in Table 17.3.

Estimating the Frequency Passband. When designing microwave networks in the form of four-pole networks which match resistances, we worked from the condition for complete network matching at a specified frequency f_0. When the frequency deviates from f_0, mismatching occurs in the network. Under actual operational conditions of a microwave network, some mismatching is permissible. Consequently, one can determine the passband of a network, within which mismatching will be acceptable. The passband is frequently estimated based on the change in the microwave circuit transmission gain [12] which is related to the absolute value of the voltage reflection factor, Γ, at the input to this circuit*. For this reason, to determine the passband, we employ the condition for obtaining a specified permissible value Γ_{per} at the limits of the passband for the case of complete circuit matching at the frequency f_0.

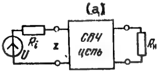

Figure 17.17. On the determination of the reflection factor at the input to a microwave four-pole network.

Key: a. Microwave network.

The absolute value of the reflection factor at the input of a linear reactive four-pole microwave network, loaded into a resistance R_{load} (Figure 17.17) [12], is:

$$\Gamma = |z - R_i| / |z + R_i|.$$

Here, R_i is the resistance at the microwave network input; z is the input impedance of the four-pole network at the frequency f.

At a frequency of f_0, $Z = R_i$ and $\Gamma = 0$. When the frequency changes in the vicinity of f_0, the impedance Z becomes different from R_i and $\Gamma \neq 0$. Having specified the value of Γ_{per} and finding the frequencies for which $\Gamma = \Gamma_{per}$, we define the bandwidth within the limits of which $\Gamma(f) \leq \Gamma_{per}$.

A possible approach to the determination of the passband from a specified value of Γ_{per}, for example, the Γ-network shown in Figure 17.10b, can be the following. We initially calculate the parameters of the L and C components of the Γ-network for the condition of complete matching at a specified frequency f_0 for which $z = R_i$. Then, assuming that the parameters of the L, C and r circuit components are independent of frequency, we find the impedance Z at the points 1 - 1' at a frequency f which differs slightly from the specified frequency.

---

*Where there are no losses in a microwave network, the absolute value of the reflection factor at its input and output is the same.

Having accomplished the necessary transformations, we derive a formula for the absolute value of the reflection factor, expressed in terms of the resistances R' and x'_{par} of a parallel circuit equivalent to a series circuit of r and x_{ser}:

$$\Gamma^2 = \left(\frac{|z - R_l|}{|z + R_l|}\right)^2 = \frac{(R_l R')^2 + \left(x''_{\text{пар}}\right)^2 (R' - R_l)^2}{(R_l R')^2 + \left(x''_{\text{пар}}\right)^2 (R' + R_l)^2}.$$

Here: $X''_{par} = x_{par} x'_{par} / (x_{par} + x'_{par})$. $x''_{\text{пар}} = x_{\text{пар}} x'_{\text{пар}} / (x_{\text{пар}} + x'_{\text{пар}})$.

The frequencies in the vicinity of f_0 for which $\Gamma = \Gamma_{per}$ determine the boundaries of the passband. The calculation of the frequency passband is substantially facilitated when a computer is used.

A Procedure and Examples of the Design Calculations for the Microwave Circuit of a Transistor Amplifier/Oscillator. We shall consider an approximate design procedure for the input and output microwave circuits of transistor amplifiers/oscillators which are frequently encountered. Some practical circuits for these networks are shown in Figures 17.4 and 17.6. The procedure for the determination of the component parameters of microwave networks can be as follows:

1. We compose the total equivalent circuit for the microwave network being designed, taking into account the requisite impedance with respect to the fundamental at the input (or output) of the transistor, the impedance at the amplifier/oscillator input (or the load impedance at the output of the amplifier/oscillator). Assuming that the blocking elements (L_{b1}, C_{b1}) have no substantial impact on the operation of the microwave circuitry, we do not include them in the circuits. However, if these elements perform definite functions in the microwave network circuitry, then they must be taken into account.

2. We represent the total equivalent circuit in the form of series connected Γ sections (as was done in the calculation of Π and T-networks, etc.), in which the series and parallel reactances should be of a different nature (if an inductance is inserted in series, then a capacitance is to be inserted in parallel).

3. We calculate the parameters of the components of the Γ sections using the procedure given.

4. We determine the parameters of the equivalent circuit components, and in the case where the inductances and capacitances which are obtained can be realized conveniently, we conclude the calculations. However, if the requisite nominal values of the reactive elements make it difficult to execute the microwave network in the form of a desirable type of structure, for example, in the form of a hybrid IC, then the calculation of the component parameters of the network is to be repeated, specifying other values for the Q of the Γ sections or by slightly changing the circuit of the network, for example, by adding one or two Γ sections to it. It is recommended that during the course of the electrical design calculations, an approximate structural design of the circuit elements be carried out so as to get an idea of their overall dimensions and degree of complexity.

5. We determine the parameters of the electrical circuit components more precisely for the network being designed.

6. We determine the passband of the microwave network based on the specified permissible value of the absolute value of the reflection factor at the network input.

7. We structurally design the circuit components (inductance coils, capacitors) or choose them from catalogs of ready-made products; we determine the Q of these elements.

8. We calculate the efficiency of the circuit being designed.

During design calculations of microwave network configurations, it must be kept in mind that each of their structural components (inductance coils, capacitors, connecting wires) is a complex electromagnetic circuit in the general case. For this reason, when designing a circuit around hybrid IC's, one is to take into account the impedance of each element. However, this is possible only after the preliminary breadboarding of the circuit.

Microwave network design is facilitated when computers are used.

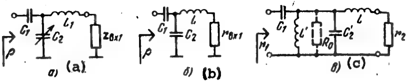

Figure 17.18. The equivalent circuit for the input microwave network of an amplifier/oscillator (Figure 17.4c) and its representation in the form of two Γ sections.

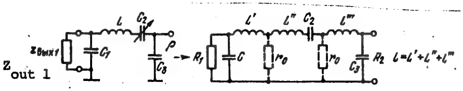

Figure 17.19. The equivalent circuit of the output microwave network of an amplifier/oscillator (Figure 17.6b) and its representation in the form of two Γ sections and an additional filter.

We shall give the procedure for the electrical design of some microwave network circuit configurations for transistor amplifiers/oscillators as an example.

Example 1. We shall consider the circuit of the input microwave network for the amplifier/oscillator depicted in Figure 17.4c. Taking into account the connection of a transmission line having a characteristic impedance of ρ to the input of this circuit and the replacement of the input circuit of the transistor with its equivalent impedance $Z_{in\ 1} = r_{in\ 1} + j\omega L_{in}$ and the subsequent combining of the inductances L_1 and L_{in} into a single inductance L to obtain a pure resistance, connected to the network on the transistor side, we obtain an equivalent circuit in the form of a T-network (Figure 17.18b). We then represent this circuit as a connection of two Γ sections (Figure 17.18c). Assuming the resistances $r_1 = \rho$ and $r_2 = r_{in\ 1}$ and the working frequency f_0 to be known, we calculate the parameters of the circuit elements (see Table 17.2). After determining the capacitances C_1 and C_2, we find the inductance of the circuit being designed $L_1 = L - L_{in}$.

We estimate the efficiency of the network from the formula given in Table 17.3. We then determine the passband of the circuit.

Example 2. The circuit of the output microwave network of the transistor amplifier/oscillator shown in Figure 17.6b. We represent the impedance of the transistor output network at the fundamental frequency, $Z_{out\ 1} = Z^*_{load\ 1}$, in the form of the impedance of a parallel network consisting of a resistance $R_{out\ 1}$ and a capacitance C_{out}, while we take the load impedance equal to the characteristic impedance of the transmission line ρ which is connected to the output of the amplifier/oscillator. Taking this into account, we draw the equivalent circuit in the form of a Π-network with an additional filter and then we represent it as the connection of two Γ sections, between which the additional filter is inserted (see Figure 17.19). Assuming that $R_1 = R_{out\ 1}$ and $R_2 = \rho$, C_{out}, and the working frequency f_0 are specified, we determine the component parameters of the circuit depicted in Figure 17.19 using the procedure given in Table 17.2. The Q of one of the Γ sections and the filter is to be specified beforehand. Then, we find the capacitance of the capacitor $C_1 = C - C_{out}$. We calculate the network efficiency from the appropriate formula in Table 17.3. Then we determine the passband of the network.

17.5. The Design of A Microwave Matching and Transforming Network Using Elements with Distributed Parameters

Components with distributed parameters, which take the form of asymmetrical transmission stripline sections, and which are often called stripline elements, are widely used in the microwave networks of integrated circuit transistor amplifiers and oscillators. These elements make it possible to transform impedances, attain a specified level of matching in the microwave network, create the requisite reactances, assure the filtering of higher harmonics, realize a radio-frequency blocking choke in the power supply circuit for the amplifier/oscillator, etc.

Stripline elements are usually made in the form of regular unbalanced transmission lines of various lengths. Quarter-wave resistance transformers are widely used. It is expedient in a number of practical cases to employ sections of an irregular transmission line, the characteristic impedance of which changes along its length, for example, either linearly or exponentially. This makes it possible to provide for impedance transformation with a shorter geometric line length and to obtain a broader passband for the network than with a regular line section. A stepped network of two and more quarter-wave regular line sections with different characteristic impedances can also serve as an example of an irregular transmission line.

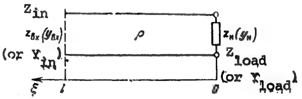

Figure 17.20. The equivalent circuit of a regular transmission line with a length l.

To match a transmission line, line sections are connected to it which are short-circuited or open-circuited at the end, which make it possible to create different resistances to the radio-frequency current at a certain point in the line. Such elements have been given the name of loops. Loops with a length of $l \leq \lambda/4$ (λ is the wavelength in the line) are the most frequently used. Loops longer than $\lambda/4$ are rarely used because of their considerable geometric length and narrow bandwidth. Loops with a length of $l < \lambda/4$ are used to produce reactances. Quarter-wave loops, open-circuited at the end, serve to produce a low RF resistance, for example, to improve the filtering of undesirable harmonics, while short-circuited loops are used to create a high RF resistance, for example, to realize a blocking choke in an amplifier or oscillator circuit. The most widespread matching network is a single loop transformer, which takes the form of a transmission line section with a loop connected to it.

TABLE 17.4.

$z_{\text{н}}, y_{\text{н}}$	$z_{\text{вх}}, y_{\text{вх}}$	(A) Активные и реактивные составляющие
$z_{\text{н}} = r_{\text{н}} + j\,x_{\text{н}}$	$z_{\text{вх}} = r_{\text{вх}} + j\,x_{\text{вх}}$	$r_{\text{вх}} = \dfrac{\rho^2 r_{\text{н}}(1+\operatorname{tg}^2 \kappa l)}{(\rho - x_{\text{н}} \operatorname{tg} \kappa l)^2 + (r_{\text{н}} \operatorname{tg} \kappa l)^2}$ $x_{\text{вх}} = \dfrac{\rho^2 x_{\text{н}}(1-\operatorname{tg}^2 \kappa l) + \rho(\rho^2 - r_{\text{н}}^2 - x_{\text{н}}^2)\operatorname{tg} \kappa l}{(\rho - x_{\text{н}} \operatorname{tg} \kappa l)^2 + (r_{\text{н}} \operatorname{tg} \kappa l)^2}$
	$y_{\text{вх}} = g_{\text{вх}} - j\,b_{\text{вх}}$	$g_{\text{вх}} = \dfrac{r_{\text{н}}(1+\operatorname{tg}^2 \kappa l)}{r_{\text{н}}^2 + (x_{\text{н}} + \rho \operatorname{tg} \kappa l)^2},$ $b_{\text{вх}} = \dfrac{x_{\text{н}}(1-\operatorname{tg}^2 \kappa l) + \rho^{-1}(\rho^2 - r_{\text{н}}^2 - x_{\text{н}}^2)\operatorname{tg} \kappa l}{r_{\text{н}}^2 + (x_{\text{н}} + \rho \operatorname{tg} \kappa l)^2}$
$y_{\text{н}} = g_{\text{н}} + j\,b_{\text{н}}$	$y_{\text{вх}} = g_{\text{вх}} + j\,b_{\text{вх}}$	$g_{\text{вх}} = \dfrac{g_{\text{н}}(1+\operatorname{tg}^2 \kappa l)}{(1-\rho b_{\text{н}} \operatorname{tg} \kappa l)^2 + (\rho g_{\text{н}} \operatorname{tg} \kappa l)^2}$ $b_{\text{вх}} = \dfrac{b_{\text{н}}(1-\operatorname{tg}^2 \kappa l) + \rho(\rho^{-2} - g_{\text{н}}^2 - b_{\text{н}}^2)\operatorname{tg} \kappa l}{(1-\rho b_{\text{н}} \operatorname{tg} \kappa l)^2 + (\rho g_{\text{н}} \operatorname{tg} \kappa l)^2}$

Notes: 1. If $Z_H = r_H - jx_H$ [$Z_{load} = r_{load} - jx_{load}$], the sign in front of x_H in the formulas for r_{in}, g_{in}, x_{in} and b_{in} must be changed. 2. If $Y_H = g_H - jb_H$, then the sign in front of b_H in the formulas for g_{in} and b_{in} must be changed.

Key: A. Resistive and reactive components.

The design procedure for stripline elements is based on the relationships which follow from the theory of long lines. When drawing up the equivalent circuit of a microwave network for an amplifier/oscillator, the line section of length 1 is replaced by an impedance equal to its input impedance.

The input impedance Z_{in} and the input admittance Y_{in} of a lossless* line at a distance from its end, loaded into a complex impedance Z_H [Z_{load}] (Figure 17.20) are defined by the relationships:

$$z_{\text{вх}} = \rho\,(z_{\text{н}} + j\rho\,\text{tg}\,\kappa l)/(\rho + j z_{\text{н}}\,\text{tg}\,\kappa l); \tag{17.14}$$

$$y_{\text{вх}} = (\rho + j z_{\text{н}}\,\text{tg}\,\kappa l)/\rho\,(z_{\text{н}} + j\rho\,\text{tg}\,\kappa l). \tag{17.15}$$

Here, ρ is the characteristic impedance of the line; $k = 2\pi/\lambda$.

Taking the load impedance to be $Z_H = r_H + jx_H$, we represent Z_{BX} [Z_{in}] and Y_{BX} [Y_{in}] in the form of two components also:

$$z_{\text{вх}} = r_{\text{вх}} + j\,x_{\text{вх}};\ y_{\text{вх}} = g_{\text{вх}} - j\,b_{\text{вх}}.$$

The formulas for the determination of the components of the input impedance or admittance of a line loaded into Z_{load} or Y_{load}, derived from expressions (17.14) and (17.15), are given in Table 17.4.

The input impedance of a regular line section with a length of $\lambda/4$, loaded into a resistance r_{load}, is purely resistive: $Z_{in} = r_{in} = \rho^2/r_{load}$.

In the case where a line section with a length of $1 \leq \lambda/4$ is short-circuited (s.c.) or open-circuited (o.c.) at one end, its input impedance and input admittance are defined by the relationships:

$$Z_{in\ s.c.} = j\rho \tan kl,\ Y_{in\ s.c.} = -j\rho^{-1}\cot kl \qquad z_{\text{вх кз}} = j\rho\,\text{tg}\,\kappa l,\ \ y_{\text{вх кз}} = -j\rho^{-1}\,\text{ctg}\,\kappa l; \tag{17.16}$$

$$Z_{in\ o.c.} = -j\rho \cot kl,\ Y_{in\ o.c.} = j\rho^{-1}\tan kl \qquad z_{\text{вх хх}} = -j\rho\,\text{ctg}\,\kappa l,\ \ y_{\text{вх хх}} = j\rho^{-1}\,\text{tg}\,\kappa l. \tag{17.17}$$

By changing the length 1 of the line sections, one can change the nature of the reactance in the input impedance. The quantity Z_{in} also depends on the characteristic impedance of the line ρ. When $1 = \lambda/4$, $Z_{in\ s.c.} \to \infty$ and $Z_{in\ o.c.} \to 0$ with a decrease in the losses in the line.

Estimating the Bandwidth. As has already been noted in § 17.4, an estimate of the bandwidth of a microwave network can be made based on the permissible voltage reflection factor, Γ_{per}, at the input of the microwave network or based on the voltage standing wave ratio (SWR) which is related to it. Let's say that a microwave network is formed by a line section having an input impedance of $Z_{in} = r_{in} + jx_{in}$ and is loaded into an impedance Z_{load}. A transmission line with a characteristic impedance ρ is connected to the input to this circuit. The absolute value of the reflection factor at the input of such a microwave network is:

---

*The assumption of low losses is justified for a large number of practical problems without a substantial error, since the length of the line sections used is $1 < \lambda/4$.

$$\Gamma = \left| \frac{z_{\text{вх}}-\rho}{z_{\text{вх}}+\rho} \right| = \frac{\sqrt{(r_{\text{вх}}-\rho)^2+x_{\text{вх}}^2}}{\sqrt{(r_{\text{вх}}+\rho)^2+x_{\text{вх}}^2}}.$$

By specifying the permissible value of Γ_{per} (or the SWR) at the circuit input, one can determine the passband within which Γ (or the SWR) will not exceed a specified value.

By way of example, we shall give a procedure for determining the passband of a quarter-wave transformer, which matches two resistances R_1 and R_2. We shall also assume that the frequency f_0 and the permissible reflection factor Γ_{per} are specified. At the frequency f_0, the transformer length is $l = \lambda_0/4$ and the characteristic impedance of the line is $\rho = \sqrt{R_1R_2}$. The reflection factor at the transformer input (at the point of connection of the resistance R_1) is:

$$\Gamma = (z_{\text{вх}} - R_1)/(z_{\text{вх}} + R_1). \tag{17.18}$$

Since at the frequency f_0, the impedance is $Z_{in} = R_1$, then $\Gamma = 0$. When the frequency deviates from f_0, the impedance Z_{in} becomes different from R_1. We shall determine the impedance Z_{in} using formula (17.14), and by employing expression (17.18), we shall find the reflection factor Γ, and then we derive the formula to calculate its absolute value:

$$\Gamma = \sqrt{\frac{(r-1)^2}{(r+1)^2+4r\,\text{tg}^2\,0{,}5\,\pi f/f_0}}.$$

Here, $r = R_2/R_1$; the argument of the tangent is converted to the form $(2\pi/\lambda)(\lambda_0/4) = 0.5\pi f/f_0$.

By equating $\Gamma = \Gamma_{per}$, we find the values for the relative frequencies f_1/f_0 and f_2/f_0 at the limits of the passband:

$$\frac{f_{1,2}}{f_0} = \frac{2}{\pi}\,\text{arctg}\left[\pm\sqrt{\frac{(r-1)^2}{4r\Gamma_{\text{доп}}^2} - \frac{(r+1)^2}{4r}}\,\right].$$

Thus, within the passband $(f_2 - f_1)/f_0$ $\Gamma \leqq \Gamma_{per}$.

The Single Loop Transformer. Two circuits of a single loop transformer are shown in Figure 17.21, which differ in the type of loop (short-circuited or open-circuited) and the point of its connection to the line. One can obtain an input impedance of a transformer loaded into an impedance Z_2, close or equal to the requisite impedance Z_1 in the general case by changing the length of the line l, the length of the loop l_{sh} and the characteristic impedances of the line ρ and the loop ρ_{sh}. The solution of such a problem is not unique. For this reason, one can search out a certain optimal circuit variant when solving the problem. In this case, the optimization can be carried out using different parameters, which are the most important ones in each specific problem, for example, a minimal overall line length, or requisite passband. In those cases, where the optimization is not obligatory, the requisite input impedance can be obtained through the choice of l and l_{sh}. The characteristic impedances ρ and ρ_{sh} are chosen based on structural design considerations or by working from the convenience of connecting them to other microwave networks. In some cases, it is more convenient to specify the line length l and to determine the requisite characteristic impedance of the line ρ and the loop parameters. However, it can turn out that the value obtained for ρ is difficult to realize structurally.

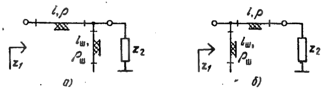

Figure 17.21. The circuit of a matching microwave network in the form of a stripline with a loop for the load impedance (a) and at the network input (b).

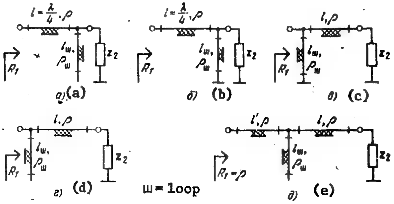

Figure 17.22. Circuit configurations for a microwave network in the form of a stripline with a single loop, which match a complex impedance to a resistance.

In practical circuits of transistor oscillators/amplifiers, frequently one of the impedances being matched is purely resistive and equal to the characteristic impedance of the transmission line connected at the input or output of the oscillator/amplifier. Circuit variants of a single loop transformer which make it possible to match a complex impedance to a resistance are shown in Figure 17.22. In this case, the loop (short-circuited or open) serves to compensate for the reactive component or the load impedance Z_2 (Figure 17.22a and b), or the input impedance (Figure 17.22c - e) of the transformer. In the realization of the configurations of Figures 17.22 a and b, structural difficulties are frequently encountered which are related to the necessity of placing the loop directly at the input (or output) of the transistor or the realization of a quarter-wave line with the requisite characteristic impedance. In such cases, the circuits of Figures 17.22c - e are more convenient, where the characteristic impedance of the line can be selected based on structural design considerations or chosen equal to the characteristic impedance ρ of the transmission line connected to the input (Figure 17.22e).

A Design Procedure for the Circuits Shown in Figures 17.22a and b. The loop in these circuits serves to compensate for the reactive component x_2 of the impedance Z_2. The resistive component r_2 of this impedance is transformed to the requisite resistance R_2 by the line section of $l = \lambda/4$. We choose the type of loop by working from the requisite nature of the compensating reactance, assuming that the loop length should be less than $\lambda/4$. We specify the characteristic impedance ρ_{sh} of the line section forming the loop based on structural considerations (from 50 to 100 ohms).

We then proceed as follows for the subsequent design calculations:

1. We transform the impedance $Z_2 = r_2 + jx_2$ to a parallel circuit consisting of the resistive R_2 and reactive x_2 components, which are found from formulas (17.7) and (17.8).

2. We find the length of the compensating loop l_{sh} from the condition that the input impedance of the loop Z_{sh} should be equal to the reactance x_2 and be of the opposite kind of reactance (in the formulas, one must take into account the sign of the reactance x_2). It is expedient in this case that $l_{sh} < \lambda/4$. By using expressions (17.16) and (17.17), we determine l_{sh}.

3. We calculate the characteristic impedance of the transforming $\lambda/4$ line: $\rho = \sqrt{R_1 R_2}$.

The Design Calculation Procedure for the Circuits Shown in Figure 17.22c - e. In the circuits considered here, matching can be achieved if the input admittance of the line l, loaded into the impedance Z_2, has a conductance component equal to $1/R_1$, while its susceptance component is compensated by the input admittance of the loop. We choose the characteristic impedances of the line ρ and the loop ρ_{sh} in this case solely from structural design considerations. We assume that the load impedance is $Z_2 = r_2 + jx_2$.

We proceed as follows with the calculations:

1. We find the length of the line section l from the condition that the conductance component of the input admittance of the line g_{in} is equal to the quantity $1/R_1$. Designating $1/R_1 = G_1$ and equating it to g_{in}, we obtain $g_{in} = G_1$. By using the formula from Table 17.4 for g_{in}, we solve this equation for tan(kl):

$$\mathrm{tg}_{1,2}(\kappa l) = T_{1,2} = \frac{G_1 x_2 \rho \pm \sqrt{G_1 r_2^3 + G_1 r_2 x_2^2 + G_1 \rho^2 r_2 - r_2^2 - G_1^2 \rho^2 r_2^2}}{r_2 - G_1 \rho^2}.$$

We then determine the possible length of the line sections:

$$l_1 = \frac{\lambda}{2\pi}(\mathrm{arctg}\, T_1 + m\pi),\ l_2 = \frac{\lambda}{2\pi}(\mathrm{arctg}\, T_2 + m\pi),\ m = 0, 1, 2, \ldots$$

We choose the shortest most structurally feasible section.

2. We calculate the reactive component of its input admittance b_{in} for the length 1 which is found (see Table 17.4).

3. We select the type of loop which compensates for the component b_{in}. By employing the condition $y_{sh} = -jb_{in}$ (the sign of the susceptance b_{in} is to be taken into account in the formulas), we determine the loop length from formulas (17.16) and (17.17).

In the circuit depicted in Figure 17.22e, the characteristic impedance of the line and the resistance R_1 at the circuit input are the same and equal to ρ. For this case, the calculation is carried out in a manner similar to that just considered taking into account the fact that $R_1 = \rho$. The line section length 1' can be arbitrary and can be chosen from the considerations of the convenience of connection to the feed power transmission line. After determining the parameters of the microwave network components, it is expedient to estimate the passband of this network. The estimation of the passband of the circuits shown in Figures 17.22a - e is a rather cumbersome and labor intensive process, and for this reason it is better performed on computers.

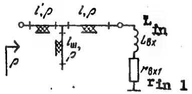

Figure 17.23. The equivalent circuit of the microwave input network for a transistor oscillator or amplifier (Figure 17.5a).

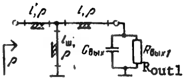

Figure 17.24. The equivalent circuit of the output microwave network of a transistor oscillator or amplifier (Figure 17.7b).

The Procedure and Examples of Design Calculations for the Microwave Networks of Transistor Oscillators/Amplifiers Using Stripline Elements. We shall treat a possible design procedure for some practical circuit configurations of microwave networks for transistor amplifiers/oscillators using a single loop transformer. We shall assume that the working frequency, the input and output circuit impedances of the transistor at the working frequency, the impedance at the input to the amplifier/oscillator and the load impedance are known. It is also assumed that the microwave network configuration has been selected.

1. We draw up the complete equivalent circuit of the microwave network, without taking into account the blocking elements in the amplifier/oscillator power supply circuitry, assuming that they have no marked influence on circuit operation. However, if the blocking elements perform definite functions in the circuit, then they are incorporated in the equivalent circuit.

2. We select the type of loop, as well as the characteristic impedances of the stripline and loop. One can also choose the type of loop after determining the lengths of short-circuited and open circuit loops which provide for matching in the microwave network, taking the loop of the least length.

3. We determine the length of the stripline and the length of the compensating loop from the condition for complete matching in the microwave network at the working frequency.

4. We calculate the bandwidth of the microwave network from the specified permissible SWR or reflection factor Γ.

5. We carry out the structural design calculations for the stripline elements (see Chapter 20 of this book).

We shall give as an example the procedure for design calculations for the microwave amplifier/oscillator networks shown in Figures 17.5a and 17.7a.

Example 1. The circuit configuration of the input microwave network for a transistor amplifier/oscillator is shown in Figure 17.5a. Assuming that the impedance of the transistor input network at the working frequency is $Z_{in\ 1} = r_{in\ 1} + j\omega L_{in}$, the impedance at the output of the amplifier/oscillator is equal to the characteristic impedance ρ of the transmission line which is connected to its input, we draw up the equivalent circuit of the microwave network (see Figure 17.23). We take the characteristic impedance of the stripline equal to ρ for convenience in connecting to the transmission line at the input. We carry out the design calculations for the circuit components using the procedure given for the circuit of a single loop transformer, depicted in Figure 17.22e. The loop length (Figure 17.5a), which is a radiofrequency choke, is chosen equal to $\lambda/4$. It is expedient to choose the characteristic impedance of this loop at a high value (up to 100 ohms).

Example 2. The output microwave network of a transistor amplifier/oscillator is shown in Figure 17.7a. The equivalent circuit of this network, taking into account the impedance of the transistor output network at the working frequency, which is represented in the form of a parallel resistance $R_{out\ 1}$ and capacitance C_{out} and load impedance, equal to the characteristic impedance ρ of the transmission line which is connected to the amplifier/oscillator output, is shown in Figure 17.24. The design procedure for this circuit is similar to that which was used when designing the circuit of a single loop transformer which is shown in Figure 17.22e. The short-circuited loop $l_{sh\ 1}$ (Figure 17.7a) performs the function of a radiofrequency choke and has a length of $\lambda/4$.

18. FREQUENCY MULTIPLIERS USING NONLINEAR CAPACITANCE DIODES

18.1. General Information

In microwave band active phased antenna array modules, because of the fact that the working frequencies of the transistor power amplifiers do not exceed a few gigahertz at the present time, it is necessary to use frequency multipliers as the output stages [1].

Despite the fact that frequency multiplication can be accomplished using any nonlinear elements, diodes with a nonlinear p-n junction capacitance are used as the nonlinear elements in the microwave band: varactors and charge storage diodes (DNZ) [CSD's] [2]. These frequency multipliers are distinguished by a rather high power conversion efficiency, good reliability, small size and weight, the capability of operating at frequencies right up to submillimeter wavelengths and a low power consumption.

Any frequency conversion (including multiplication) is accompanied by the appearance of parasitic harmonic components in the output signal spectrum in addition to the working frequency. For this reason, a filter must be installed at the output of a frequency multiplier, where this filter segregates out the working frequency and suppresses the parasitic harmonics. A filter which passes the input frequency and prevents the output frequencies from getting through to the input should also be installed at the multiplier input of diode multipliers. Optimum power transmission from the signal source to the multiplier input and from its output to the load is assured by the appropriate matching of the diode impedance to the power source at the input and the load at the output respectively. Thus, each multiplier with a nonlinear capacitance diode should contain filter and matching networks at the input and output.

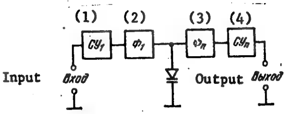

Figure 18.1. Block diagram of a parallel type frequency multiplier.

Key:
1. Input matching network;
2. Input filter network;
3. Output filter network;
4. Output matching network.

A distinction is drawn between parallel and series type frequency multipliers according to the type of circuit configuration of the diode with the input and output circuits [3]. A block diagram of a parallel multiplier circuit is shown in Figure 18.1, where SU_1 [1], Φ_1 [2], SU_n [4] and Φ_n [3] are the matching and filtering circuits at the input and output respectively. In multipliers designed in this circuit configuration, the heat sinking of the diode is facilitated, since one of the diode electrodes can be connected to the package. This makes it preferable to use parallel frequency multipliers in the high power output stages of transmitters and active phased array modules. Because of this, only parallel frequency multipliers are treated in the following.

A specific feature of parallel multipliers is frequency conversion by virtue of the nonlinearity of the volt-coulomb characteristic of the p-n junction capacitance. For this reason, the filter networks of the multipliers should provide for passing only two current harmonics through the diode and segregate the requisite harmonic from the spectrum.

The following are usually known when designing frequency multipliers: the requisite output power level, P_{out}, the output frequency $f_{out} = nf_{in}$ (n is the multiplication factor; f_{in} is the input frequency), the level of suppression of adjacent harmonic components, the working bandwidth Δf and the overall dimensions of the structure.

The choice of a nonlinear capacitance diode and its operating conditions are made based on these data and the multiplication factor for one or more multiplier stages is determined as well as the type of matching and filter networks; the efficiencies of the input (η_{in}) and the output (η_{out}) multiplier networks are found approximately or specified.

Then the power design calculations are performed for the diode operating mode based on the specified power at the output frequency $P_{dn} = P_{out}/\eta_{out}$, as a result of which, the following are determined: the diode conversion gain $\eta_d = P_{dn}/P_{d\ 1}$ (where $P_{d\ 1}$ is the input power to the diode), the input power to the multiplier $P_{in} = P_{d\ 1}/\eta_{in}$, the multiplier conversion gain $\eta_{mul} = P_{out}/P_{in} = \eta_{in}\eta_d\eta_{out}$, the diode impedance at the input (Z_{in}) and output (Z_{out}) frequencies. Then the matching and filter networks of the multiplier are designed. The multiplier design work is completed with working out of the structure with the requisite overall dimensions.

18.2. The Selection of the Multiplication Factor for the Frequency Multiplier of an Active Phased Antenna Array Module

The multiplication factor of a frequency multiplier intended for use in active phased array modules [1] is governed by the requisite values of the output power P_{out} and output frequency f_{out} of the multiplier, as well as the working frequency f_w and power P_w of the existing amplifiers preceding the frequency multiplier.

In this case, the multiplication factor is:

$$n = f_{out}/f_w = f_{out}/f_{in} \qquad n = f_{\text{вых}}/f_{\text{у}} = f_{\text{вых}}/f_{\text{вх}}. \tag{18.1}$$

Since the operating frequency range of transistor amplifiers is limited (at the present time, to frequencies in the decimeter band), then there is also a limitation on the minimal value of the multiplication factor in a module for a fixed frequency f_{out}. This minimum value of n can be estimated based on the following considerations. The power distribution of transistor amplifiers over a frequency band can always be expressed in the form of some function:

$$P_w = \phi(f_x) \qquad P_{\text{у}} = \varphi(f_x). \tag{18.2}$$

Assuming that the conversion factor of the frequency multiplier is inversely proportional to the multiplication factor, taking (18.1) and (18.2) into account, we derive an expression which makes it possible to estimate the multiplication factor and make a preliminary choice of the final amplifier stage:

$$\frac{m}{n}\varphi\left(\frac{f_{\text{вых}}}{n}\right)\geqslant P_{\text{вых}}, \tag{18.3}$$

where m is the number of amplifier stages operating off of one multiplier input. It is obviously expedient to choose $m \leq 2$ for the module of an active phased array because of considerations of structural simplicity and small size.

It can be roughly assumed that the efficiency of an active phased antenna array module with frequency multiplication of η_m is determined by the electronic efficiency of the output stage of the transistor amplifier η_w and the conversion gain of the multiplier η_{mul}. Since we have assumed that $\eta_{mul} \simeq 1/n$, then $\eta_m \simeq \eta_w/n$.

If $n \leq 3$, then in making the transition from $n = 2$ to $n = 3$, a slight increase in η_m is possible which is related to the increase in the electron efficiency of the amplifier, η_w, because of the reduction in its working frequency. When $n > 3$, the efficiency of the module falls off with an increase in the multiplication factor.

The overall multiplication factor n, chosen from condition (18.3) when $n \geq 4$, can be realized in one multiplier or in several series connected multipliers, since $n = n_1, n_2 \ldots, n_k$, where $n_1, n_2, \ldots, n_k$ are the multiplication factors of the individual multipliers.

It is of course preferable to use a single multiplier to reduce the size. However, it is expedient in a number of cases to use several multipliers. This is due to the fact that the utilization of individual multipliers with a low multiplication factor ($n \leq 3$) makes it possible to obtain greater values of the output powers, as well as to substantially expand the working bandwidths of the multipliers, something which is quite important when modules operate with wideband signals.

In fact, the ultimate passband which can be achieved in single diode frequency multipliers is governed by the values of the adjacent harmonics in the output signal spectrum of the multiplier and amounts to:

$$\Delta f_{ult} = f_{in}/(n + 0.5). \qquad \Delta f_{\text{пред}} = f_{\text{вх}}/(n+0{,}5). \tag{18.4}$$

It should be noted that in multipliers with small values of n, passbands can be realized which are greater than those determined by formula (18.4) if a combination configuration of two diodes is used in them. Thus, for balanced multipliers and multipliers with opposing-parallel or opposing-series diodes:

$$\Delta f_{ult} = 2f_{in}/(1 + n).$$

Moreover, multipliers with diodes connected in combination make it possible to approximately double the output power.

Drawbacks to these multipliers are a slight increase in circuit complexity (especially for the balanced multiplier), multiplication only by an odd factor (multipliers with diodes connected in opposition) or by an even factor (the balanced circuit), as well increased requirements placed on the identical nature of the parameters of the diodes which are used.

Since the working frequency range of a multiplier should be less than the ultimate, with an increase in the multiplication factor, its working band decreases. This leads to an increase in the requirements placed on the frequency filters (especially on the output filter), and as a consequence, to increased complexity of their structural design.

It is also necessary to take into account the fact that with an increase in the multiplication factor, the influence of the phase errors of the preceding stages on parameters which characterize the directional properties of an active phased array also increases [1] as well as the influence of the instability of the source of the bias applied to the nonlinear capacitance diode to establish its initial operating point on the phase of the output signals and their power [4].

The change in the phase of a multiplier output when the bias voltage deviates from the working voltage in frequency multipliers using varactors in a blocked p-n junction is:

$$\Delta\Phi = \frac{1}{2} n\nu Q_{д} \left(\frac{1-\eta_{д}}{1+\eta_{д}}\right) \frac{\Delta U_0}{U_0}, \qquad (18.5)$$

where ν is a coefficient which characterizes the degree of nonlinearity of the blocked p-n junction capacitance and depends on the type of p-n junction (for a sharp junction, $\nu = 1/2$; for a smooth junction, $\nu = 1/3$); η_d is determined for the working bias voltage U_0; ΔU_0 is the deviation of the bias from the operating value; Q_d is the diode quality factor at the operating bias voltage. The quality factor can be calculated from the data sheet for a diode [6]:

$$Q_d = \frac{f_{ult}}{f_{in}} (U_0/U_\pi)^\nu \qquad Q_{д} = \frac{f_{пред}}{f_{вх}} \left(\frac{U_0}{U_{п}}\right)^\nu, \qquad (18.6)$$

where the frequency f_{ult} is the parameter of the diode measured when determining the bias voltage U_π and which designates the input frequency for which $Q_d = 1$.

In frequency multipliers using charge storage diodes:

$$\Delta\Phi = \frac{nQ_{д}}{\pi} \left(\frac{1-\eta_{д}}{1+\eta_{д}}\right) \frac{\sin\Theta\,(\sin\Theta - \Theta\cos\Theta)}{\Theta} \frac{\Delta U}{U_0}, \qquad (18.7)$$

where Θ is the charge cut-off angle, which characterizes that portion of the oscillation period during which the p-n junction is blocked, and which determines to a considerable extent the conversion gain and output power [7].

Expressions (18.5) and (18.7) can not only be suitable for the analysis of the stability of the phase characteristics of frequency multipliers, but also for the estimation of the possibility of employing frequency multipliers as phase equalizers to reduce the systematic phase error in active phased array modules, or as phase shifters.

The change in the output power which is due to the mistuning of the multiplier microwave circuits can be found from the approximate expression:

$$\frac{P'_{\text{вых}}}{P_{\text{вых}}} = \frac{4(1+\eta_{\text{д}})}{\left(4+\operatorname{tg}^2\frac{\Delta\Phi}{n}\right)\left[2\eta_{\text{д}}+(1-\eta_{\text{л}})\left(1+0,25\operatorname{tg}^2\frac{\Delta\Phi}{n}\right)^{n-1}\right]}, \tag{18.8}$$

where P'_{out} is the output power in the case of untuned microwave circuits ($\Delta\Phi = 0$).

It follows from (18.8) that with an increase in $\Delta\Phi$, the output power falls off more quickly, the smaller η_d is.

If a frequency multiplier is used as a phase shifter, then the maximum deviation of the output signal phase is $|\Delta\Phi| = 180°$. In this case, as follows from (18.8), to reduce the range of variation in the output power when controlling the phase, it is necessary that the multiplication factor be as great as possible. However, with an increase in n the conversion gain falls off and the phase instability rises. For this reason, it is recommended that n be taken as n = 3...5 in phase shifter multipliers.

18.3. The Selection of Nonlinear Capacitance Diode and Its Operating Mode

Nonlinear capacitance diodes can operate in two basic modes: in a cutoff p-n junction mode and in a partially turned-on mode.

In the cutoff p-n junction mode, multiplication is possible at frequencies of $f_{in} < f_{ult}$. Since f_{ult} reaches 400 GHz and more in modern varactors, it is possible in this mode to multiply any frequencies, right down to submillimeter wavelengths.

In the partially turned-on mode, multiplication is possible only in a limited range of frequencies [6]:

$$f_{lower} < f_{in} < f_{upper}.$$

The lower limit of the frequency range is governed by the minority carrier recombination time: $f_{lower} \simeq 1/t_r$; the upper limit is governed by the recovery time of the cut off p-n junction: $f_{upper} = 1/t_{rec}$. When $f_{in} < f_{upper}$, a turned-on p-n junction introduces considerable losses and substantially reduces the conversion gain. When $f_{in} > f_{upper}$, the nonlinear properties of the diode are manifest only weakly, something which also leads to a substantial reduction of the conversion gain. For diodes being produced by our industry, f_{upper} does not exceed GHz. For this reason, in multipliers with an output frequency below

10 GHz, a diode can operate in both modes, while multipliers where $f_{out} > 10$ GHz, it can operate only in a cutoff p-n junction mode.

In a block p-n junction mode, the instantaneous voltage, u, across it in the absence of a breakdown and with cutoff should satisfy the condition:

$$0 \leqq u \leqq U_{per} \qquad 0 \leqslant u \leqslant U_{доп}. \tag{18.9}$$

However, in a partial cutoff mode, the voltage u should satisfy only the condition for the absence of junction breakdown:

$$u \leqq U_{per} \qquad u \leqslant U_{доп}. \tag{18.10}$$

It follows from (18.9) and (18.10) that in a cutoff p-n junction mode, in contrast to the partially turned-on state, limitations are placed on the maximum amplitude of the oscillations. This is also due to the greater working powers of frequency multipliers using nonlinear capacitance diodes which operate in a partial cutoff mode [7]. An advantage of partial cutoff is also the higher multiplier conversion gain given the same multiplication factor and diode Q. In this case, when operating in a junction cutoff mode, the conversion gain falls off so sharply with an increase in the multiplication factor n, that n > 3 is not used in practice.

It follows from what has been presented here that in multipliers with an output frequency of $f_{out} < 10$ GHz, it is most expedient to employ varactors in a partial junction cutoff mode, and especially, charge storage diodes, the nonlinear properties of which are manifest to the greatest extent in this mode.

The power parameters of diodes are the following: the normalized power P_{norm} and the permissible diode power dissipation P_{per}. The power P_{norm} characterizes the maximum output power without breakdown [2]: $P_{norm} = U^2_{per}/R_S$, where:

$$R_S = 1/2\pi f_{ult} C(U_n) \qquad R_S = 1/2\pi f_{пред} C(U_п) \tag{18.11}$$

is the diode loss resistance.

The power P_{per} characterizes the maximum output power without thermal breakdown of the junction, since

$$R_{dp} \leqq P_{per} \eta_d/(1 - \eta_d). \qquad P_{дп} \leqslant P_{доп} \eta_д/(1 - \eta_д). \tag{18.12}$$

It is well known [6, 7] that with an increase in the diode Q, the conversion gain increases, tending to unity, while the output power of the multiplier falls off, tending to zero. For this reason, when selecting a diode, one must be governed by the conditions for assuring the specified power with a relatively high conversion gain.

For a parallel varactor type multiplier operating in a cutoff p-n junction mode, a preliminary selection can be made by means of the expression:

$$P_{dp}/P_{norm} < 1/4\alpha$$

where α is a certain coefficient which depends on the type of the p-n junction and the multiplication factor. A number of values of α are given in Table 18.1.

TABLE 18.1

n	[illegible]	(1) $\frac{U_{0max}}{U_{доп}}$	β	α	[illegible]
2	0,65	0,44	$16,25\cdot10^{-3}$	231	1/2
[illegible]	0,732	0,466	$9,15\cdot10^{-2}$	927	1/3
3	0,82	0,476	$0,7\cdot10^{-3}$	$1,2\cdot10^{5}$	1/3

Key: 1. $U_{0\,max}/U_{per}$.

The parameters of the selected varactor should satisfy the expressions:

$$Q_{min} < f_{ult}/f_{in} < Q_{max} \qquad Q_{min} < f_{пред}/f_{вх} < Q_{max}, \tag{18.13}$$

where:

$$Q_{max} = \frac{1}{\beta}\sqrt{\frac{1-2\alpha P_{дп} + \sqrt{1-4\,\alpha_{дп}/P_{норм}}}{4\,[\alpha P_{дп}/P_{норм}]^2} - 1}; \tag{18.14}$$

$$Q_{min} = 2\sqrt{\eta_{д\,min}}\,/\beta\,(1-\eta_{д\,min}), \tag{18.15}$$

β is a certain coefficient, the value of which is given in Table 18.1; $\eta_{d\,min}$ is the minimum value of the diode conversion gain.

A charge storage diode is initially selected with respect to frequency in accordance with the condition $f_{lower} < f_{in}f < f_{upper}$, and then with respect to power [6]:

$$P_{норм}/P_{дп} > 8\,(1-\cos\Theta)/\gamma_n^2(\Theta). \tag{18.16}$$

Here:

$$\gamma_n(\Theta) = \frac{1}{n\pi}\left[\frac{\sin(n-1)\,\Theta}{n-1} - \frac{\sin(n+1)\,\Theta}{n+1}\right]$$

is a coefficient which takes into account the nonlinear properties of the charge storage diode capacitance [8, 10]. At optimal cutoff angles of $\theta_0 = k\pi/n$, it takes on the maximum values:

$$\gamma_n(\Theta_0) = \frac{2\sin\frac{k\pi\,(n-1)}{\pi}}{\pi\,(n^2-1)}, \quad k = 1, 2, \ldots, n-1 \tag{18.17}$$

Since maximum values of the conversion gain can be obtained at optimal cutoff angles [7], then taking (18.17) into account, condition (18.16) is represented in the following form with the realization of elevated conversion gains:

$$\frac{P_{\text{порм}}}{P_{\text{дп}}} > \left[\frac{\sqrt{2\pi}\,(n^2-1)\left(1-\cos\frac{k\pi}{n}\right)}{\sin\frac{k\pi(n-1)}{n}} \right]^2, \quad k=1, 2, \ldots, n-1.$$

It is well known that with the same Q in a charge storage diode multiplier, the greatest conversion gain is realized at cutoff angles of $\theta_{max} = \pi/2$ in the case of even values of n, and:

$$\Theta_{\max} = \frac{\pi}{2}\left(\frac{n-1}{n}\right) \text{ или } \Theta_{\max} = \frac{\pi}{2}\left(\frac{n+1}{n}\right)$$

in the case of odd values of n. It follows from (18.17) that for cutoff angles of $\theta < \theta_{max}$, greater powers can be obtained at the multiplier output than when $\theta = \theta_{max}$, but in this case, the conversion gains are lower.

Increasing the working powers and increasing the conversion gain can lead to a substantial rise in the power dissipation, and for this reason, it is necessary to check the condition of the permissible power dissipation, which is more conveniently represented in the following form taking (18.12) into account:

$$\frac{f_{max}}{f_{in}} = \frac{f_{\max}}{f_{\text{вх}}} > \frac{2}{\gamma_n(\Theta)} \frac{\sqrt{1+P_{\text{доп}}/P_{\text{дп}}}}{P_{\text{доп}}/P_{\text{дп}}}.$$

The final choice of a diode is also made using formulas (18.13) - (18.15), in which the value of $\gamma_n(\theta)$ is to be substituted instead of β. We will note that when selecting the type of charge storage diode, one must also specify the cutoff angle θ at the same time.

Thus, the following parameters become known with the choice of the diode: the breakdown or permissible inverse voltage U_{br}, the varactor nonlinearity exponent, the recombination time t_r and the recovery time t_{rec}, the maximum frequency f_{ult}, the permissible power dissipation P_{per}, the p-n junction capacitance for a definite bias voltage $C(U_\pi)$, the bias voltage U_π at which $C(U_\pi)$ and f_{ult} were measured as well as the loss resistance r_{ser} (18.11) and the cutoff angle θ.

18.4. The Power Design Calculation Procedure for the Operational Mode of a Diode in a Parallel Type Multiplier

The design calculations for a diode operating mode are carried out based on the output power for it:

$$P_{dn} = P_{out}/\eta_{out}. \qquad P_{\text{дп}} = P_{\text{вых}}/\eta_{\text{вых}}.$$

Here, η_{out} is roughly specified in a range of 0.8 to 0.95. The type of diode is selected based on the known values of P_{dn}, f_{out} and n.

The power design procedure for a diode for both modes is practically the same, however, because of the difference in the volt-coulomb characteristics of the p-n junction in these modes, the computational relationships are different.

The Cutoff p-n Junction Mode. 1. We calculate the operating bias voltage U_0 with which the specified diode output power P_{dn} can be obtained based on the following expression:

$$P_{\text{дп}} = \left(\frac{U}{U_{0\,\max}}\right)^2 \frac{U^2_{\text{доп}}}{\alpha R_S} \frac{\sqrt{1+a}}{(1+\sqrt{1+a})^2}, \tag{18.18}$$

where $a = \left[\beta \frac{f_{\text{пред}}}{f_{\text{вх}}} \left(\frac{U_0}{U_{\text{п}}}\right)^{\nu}\right]^2$ is the conversion parameter; the values of α and β are taken from Table 18.1; $U_{0\,\max}$ is the maximum permissible bias voltage, which satisfies the condition for no junction breakdown (18.9). The values of $U_{0\,\max}$ for different values of n and ν are also given in Table 18.1.

The equation for P_{dn} (18.18) is uniquely related to U_0, however, it does not resolve in explicit form in the general case with respect to U_0 and U_0 can be found either graphically or with a computer.

In the special cases where a < 2, which occurs when $\eta_d < 0.25$:

$$U_0 = \frac{2U_{0\,\max}}{U_{\text{доп}}} \sqrt{R_S \alpha P_{\text{вых}}};$$

When $a > 10 - \eta_d > 0.5$:

$$U_0 = U_{0\,\max} \left[\alpha\beta \frac{f_{\text{пред}}}{f_{\text{вх}}} \left(\frac{U_{0\,\max}}{U_{\text{п}}}\right)^{\nu} \frac{P_{\text{вых}} R_s}{U^2_{\text{доп}}}\right]^{\frac{1}{2\nu}}.$$

2. We calculate the varactor quality factor Q_d for the voltage U_0 using formula (18.6).

3. We determine the conversion gain:

$$\eta_{\text{д}} = \beta Q^2_{\text{д}} / \left[1 + \sqrt{1 + (\beta Q_{\text{д}})^2}\right]^2.$$

4. We calculate the input power:

$$P_{in} = P_{dn}/\eta_{in}\eta_d \qquad P_{\text{вх}} = P_{\text{дп}}/\eta_{\text{вх}}\,\eta_{\text{д}}. \tag{18.19}$$

Here, η_{in} just as η_{out} is specified by working from the frequency range and the proposed type of multiplier circuit.

5. We check the condition of permissible power dissipation in the diode using formula (18.12). If this condition is not met, then it is necessary to either choose a diode with a greater value of f_{ult} or P_{per}, or to use addition circuits or a multiplication circuit with two diodes [3].

6. We determine the varactor capacitance for the bias voltage U_0:

$$C(U_0) = C(U_{\text{п}})(U_{\text{п}}/U_0)^{\nu}.$$

7. We calculate the overall impedance of the p-n junction at the input frequency:

$Z_{\text{total in}} = r_{\text{total in}} + jx_{\text{total in}}$. $z_{\text{п вх}} = r_{\text{п вх}} + jx_{\text{п вх}}$.

Here:

$$r_{\text{п вх}} = r_{\text{посл}} \sqrt{1 + (\beta Q_{\text{д}})^2};$$

$$x_{\text{п вх}} = -\frac{1}{2\pi f_{\text{вх}} C(U_0)} \sqrt{1 - \left(\frac{\nu}{1-\nu}\right)^2 q^2 \left(1 + \frac{\eta_{\text{д}}}{n}\right)^2},$$

where q is a certain parameter which characterizes the ratio of the maximum permissible value of the amplitude of charge oscillations to the constant charge across the nonlinear capacitance (see Table 18.1).

8. We calculate the total impedance of the p-n junction at the output frequency $Z_{\text{tot out}} = r_{\text{tot out}} + jx_{\text{tot out}}$. Here, $r_{\text{tot out}} = r_{\text{tot in}}$ and $x_{\text{tot out}} = x_{\text{tot in}}/n$.

The Partial Cutoff Mode Using a Charge Storage Diode. 1. We determine the cutoff angle θ more precisely. Since it is practically always necessary in a frequency multiplier to obtain the greatest conversion gain, then one must choose cutoff angles corresponding to the maximum values of the conversion gain:

$$\Theta_0 = \begin{cases} \frac{\pi}{2} & \text{for even } n; \ \text{при четных } n, \\ \left(\frac{n \pm 1}{n}\right)\frac{\pi}{2} & \text{при нечетных } n. \ \text{for odd } n. \end{cases}$$

2. We calculate:

$$\gamma_n(\Theta) = \frac{1}{\pi n}\left[\frac{\sin(n-1)\Theta}{n-1} - \frac{\sin(n+1)\Theta}{n+1}\right].$$

To facilitate the calculations, some of the values of γ_n when $\theta = \theta_0$ are given in Table 18.2.

TABLE 18.2.

n	2	3	3	4	4	5	5	5	6	6	6
θ_0°	90	120	60	90	45	108	72	36	90	60	30
$\gamma_n(\theta_0)\cdot 10^2$	21,1	6,9	6,9	4,24	3	2,52	2,52	1,56	1,82	1,57	0,91

3. We determine the conversion parameter:

$$a = \left[\frac{f_{\text{пред}}}{f_{\text{вх}}} \gamma_n(\Theta)\right]^2.$$

4. We calculate the amplitude of the charge fundamental frequency:

$$q_1 = \frac{1+\sqrt{1+a}}{2\pi f_{\text{вх}}}\sqrt{\frac{2P_{\text{дп}}}{R_S a\sqrt{1+a}}}.$$

5. We calculate the maximum permissible value of the charge amplitude which satisfies condition (18.10):

$$q_{1\max} = C(U_{\text{п}})U_{\text{per}}[1/(1-\cos\Theta)]. \quad q_{1\max} = C(U_{\text{п}})\,U_{\text{доп}}\frac{1}{1-\cos\Theta}.$$

6. We check for the condition of no diode breakdown: $q_1 < q_{1\max}$. If this condition is not met, then it is necessary to choose a diode with a greater value of U_{per}. If there are no diodes with a greater value of U_{per} in the specified frequency range, then one can reduce the cutoff angle Θ down to a value which satisfies the no breakdown condition. However, the conversion gain in this case will be less than at the optimum cutoff angle.

7. We calculate the conversion gain:

$$\eta_{\text{д}} = a/(1+\sqrt{1+a})^2.$$

8. We determine the input power from (18.19).

9. We check the condition of the permissible power dissipation using (18.12).

10. We calculate the bias voltage:

$$U_0 = \frac{q_1}{C(U_{\text{п}})}\,\frac{\sin\Theta-\Theta\cos\Theta}{\pi}.$$

11. We calculate the total impedance of the p-n junction at the input frequency $z_{\text{п вх}} = r_{\text{п вх}} + jx_{\text{п вх}}$. [$Z_{\text{tot in}} = r_{\text{tot in}} + jx_{\text{tot in}}$]. Here:

$$r_{\text{п вх}} = R_S\sqrt{1+a}\,;\; x_{\text{п вх}} = -\frac{1}{2\pi f_{\text{вх}}C(U_{\text{п}})}\,\frac{\Theta-\sin\Theta\cos\Theta}{\pi}.$$

12. We calculate the total impedance of the p-n junction at the output frequency: $z_{\text{п вых}} = r_{\text{п вых}} + jx_{\text{п вых}}$. [$Z_{\text{tot out}} = r_{\text{tot out}} + jx_{\text{tot out}}$]. Here:

$$r_{\text{п вых}} = r_{\text{п вх}};\; x_{\text{п вых}} = -\frac{1}{2\pi f_{\text{вых}}C(U_{\text{п}})}\,\frac{\Theta}{\pi}.$$

18.5. The Design of the Microwave Input and Output Networks of a Multiplier

The structural design of a frequency multiplier depends on the range of working frequencies and the electrical requirements.

Since the cross-sectional dimensions of the structure of an active phased array module are limited by the spacing between the radiators, the input and output microwave networks in microwave band multipliers are frequently made using microstrip lines. In this case, the matching devices provide for the matching of the diode impedance at the input frequency to the characteristic impedance of the line at the multiplier input and the diode impedance at the output frequency to the characteristic impedance of the line at the multiplier output. The characteristic impedances of these lines are usually 50 or 75 ohms.

The filters of frequency multipliers are made with either open-circuited or short-circuited loops, or with low pass filters (FNCh) and bandpass filters (PPF). The filters in the input and output microwave networks of narrow band frequency multipliers with an odd value of the multiplication factor, the working bandwidth of which is considerably less than the maximum, can be made from quarter-wavelength open or short-circuited line sections [8]. In narrow band frequency multipliers with an even value of the multiplication factor, there can be a filter using line sections in the input microwave circuit, while there can be a bandpass filter in the output circuit. Low pass filters are used in the microwave input circuit of broadband frequency multipliers with any multiplication factor, while bandpass filters are used in the output circuit.

The insertion points of matching and filter networks relative to the diode are chosen so that the impedance of the output microwave circuit at the input frequency f_{in} is considerably greater than the diode impedance Z_{in}, while the impedance of the input microwave network at the output frequency is the diode impedance Z_{out}.

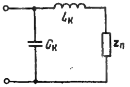

Figure 18.2. The equivalent circuit of a diode in a package.

The diode impedance is determined not only by the the p-n junction impedance, but also by the reactive parameters of the package: the inductance of the leads L_k and the package capacitance C_k. The diode equivalent circuit is depicted in Figure 18.2, where Z_π is the impedance of the p-n junction at the input or output frequency. In accordance with Figure 18.2, the diode impedance at the input frequency, taking into account the package parameters, is $Z_{BX} = r_{BX} + jx_{BX}$ [$Z_{in} = r_{in} + jx_{in}$], where:

$$\begin{aligned} r_{\text{вх}} &= \frac{r_{\text{п вх}}}{[1-2\pi f_{\text{вх}} C_{\text{к}}(x_{\text{п вх}}+2\pi f_{\text{вх}} L_{\text{к}})]^2+(2\pi f_{\text{вх}} C_{\text{к}} r_{\text{п вх}})^2}; \\ x_{\text{вх}} &= \frac{(x_{\text{п вх}}+2\pi f_{\text{вх}} L_{\text{к}})[1-2\pi f_{\text{вх}} C_{\text{к}}(x_{\text{п вх}}+2\pi f_{\text{вх}} L_{\text{к}})]-r^2_{\text{п вх}}\, 2\pi f_{\text{вх}} C_{\text{к}}}{[1-2\pi f_{\text{вх}} C_{\text{к}}(x_{\text{п вх}}+2\pi f_{\text{вх}} L_{\text{к}})]^2+(2\pi f_{\text{вх}} C_{\text{к}} r_{\text{п вх}})^2}. \end{aligned} \tag{18.20}$$

(18.20)

In the expressions cited here for an unpackaged diode with wire or tab leads, one can assume that $C_k = 0$, and for a diode with a beam type chip structure (where there are no wire or tab leads), $C_k = 0$ and $L_k = 0$.

Expressions (18.20) can be used to calculate the diode impedance at the output frequency, if the subscript "BX" ["in"] is replaced with the subscript "вых" ["out"].

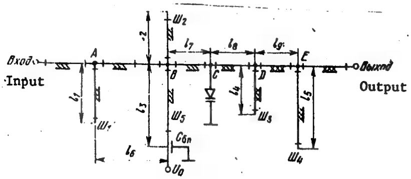

Figure 18.3. Schematic of a parallel type frequency multiplier with loops using microstrip lines.

One of the possible circuit configurations for a parallel type multiplier with open loops is shown in Figure 18.3. The loop Sh_1 compensates for the reactive component of the diode impedance at the frequency f_{in}, figured from the point of diode insertion (point C) to point A of the line.

The insertion point of the loop Sh_1 in the input circuit is calculated by means of the relationship:

$$\operatorname{tg}\frac{2\pi}{\lambda_1}l_6=\frac{B}{B^2\rho+G^2\rho G}\left(1\pm\sqrt{1-\frac{(1-G\rho)(B^2\rho+G^2\rho-G)}{\rho B^2}}\right). \qquad (18.21)$$

Loop Sh_2 provides for filtering the output frequency from the input microwave network and decoupling the input circuit from the output circuit at the output frequency f_{out}. The length of the loop Sh_2 is $l_2 = \lambda_1/4n$, where λ_1 is the wavelength of the output frequency in the line, while its point of insertion is found at a distance of $l_7 = l_2$ from the diode. In this case, loop Sh_2, in shorting the main line connecting the input of the multiplier to the diode at the point B prevents this frequency from getting through to the multiplier input and provides for a close to infinite resistance of the input microwave circuit on the diode side at the output frequency f_{out}.

Here:

$$G=\frac{r_{вх}\left(1+\operatorname{tg}^2\frac{\pi}{2n}\right)}{r_{вх}^2+\left(x_{вх}+\rho\operatorname{tg}\frac{\pi}{2n}\right)^2},$$

$$\frac{2r_{вх}^2\operatorname{tg}\frac{\pi}{2n}-\left(\rho-x_{вх}\operatorname{tg}\frac{\pi}{2n}\right)\left(x_{вх}+\rho\operatorname{tg}\frac{\pi}{2n}\right)+\operatorname{tg}\frac{\pi}{2n}\left(x_{вх}+\rho\operatorname{tg}\frac{\pi}{2n}\right)^2}{\rho\left[r_{вх}^2+\left(x_{вх}+\rho\operatorname{tg}\frac{\pi}{2n}\right)^2\right]} \qquad (18.22)$$

are the conductance and reactive components of the admittance of the line at point B.

The fact that the characteristic impedances of all of the line sections are the same and equal to the characteristic impedance ρ of the input line was taken into account in deriving this relationship.

The length l_1 of the loop Sh_1 is determined from the expression:

$$\operatorname{tg}\frac{2\pi}{\lambda_1}l_1=\frac{\rho^2G^2\operatorname{tg}\frac{2\pi}{\lambda_1}l_6-\left(B\rho+\operatorname{tg}\frac{2\pi}{\lambda_1}l_6\right)\left(1-B\rho\operatorname{tg}\frac{2\pi}{\lambda_1}l_6\right)}{\left(1-B\rho\operatorname{tg}\frac{2\pi}{\lambda_1}l_6\right)^2+\left(G\rho\operatorname{tg}\frac{2\pi}{\lambda_1}l_6\right)^2}.$$

The values of B and G are computed from formulas (18.22).

The loop Sh_3 and line section l_8 in the multiplier output circuit provide for matching of the diode impedance at the output frequency to the characteristic impedance of the line connected to the multiplier output. The connection point of the loop and its length when the characteristic impedances of all the sections are equal are chosen by means of the following relationships:

$$\operatorname{tg}\frac{2\pi n}{\lambda_1}l_8=\frac{-x_{\text{вых}}\rho\pm\sqrt{-2r^2_{\text{вых}}\rho^2+r_{\text{вых}}(x^2_{\text{вых}}+\rho^2)+r^2_{\text{вых}}\rho}}{\rho(\rho-R_{\text{вых}})};\quad(18.23)$$

$$\operatorname{tg}\frac{2\pi n}{\lambda_1}l_4=\frac{-r^2_{\text{вых}}\operatorname{tg}\frac{2\pi n}{\lambda_1}l_8+\left(\rho-x_{\text{вых}}\operatorname{tg}\frac{2\pi n}{\lambda_1}l_8\right)\left(x_{\text{вых}}+\rho\operatorname{tg}\frac{2\pi n}{\lambda_1}l_8\right)}{r^2_{\text{вых}}+\left(x_{\text{вых}}+\rho\operatorname{tg}\frac{2\pi n}{\lambda_1}l_8\right)^2}.\qquad(18.23)$$

The length of open loop Sh_4 is $l_5 = \lambda_1/4$, which blocks the input frequency at the multiplier output. The point of connection of the loop Sh_4 relative to loop Sh_3 is determined from the condition for obtaining a close to infinite impedance of the output microwave network on the diode side at the input frequency. If the characteristic impedances of all of the lines of the microwave network are equal to the impedance of the line at the multiplier output, the length of the section l_9 is determined from the relationship:

$$\operatorname{tg}\frac{2\pi}{\lambda_1}l_9=\frac{1}{\operatorname{tg}\frac{2\pi}{\lambda_1}l_8+\operatorname{tg}\frac{2\pi}{\lambda_1}l_4}.$$

Note: In expressions (18.21) and (18.23), the sign in front of the square root is chosen from the condition for obtaining the smallest microwave circuitry dimensions.

Loop Sh_5 with a length of $l_3 = \lambda_1/4$ is short-circuited for radiofrequencies through the blocking capacitor (C_{b1}) and serves to decouple the microwave circuits from the DC supply circuitry for the bias voltage U_0 fed to the diode through line sections l_3 and l_7. To expand the range of working frequencies of the circuit which contains loop Sh_5 and the blocking capacitor, the characteristic impedance ρ_{sh} [ρ_{loop}] of loop Sh_5 is to chosen substantially greater (by a factor of three to five times) than the characteristic impedance of the main line ρ. The maximum value of ρ_{sh} is limited by the technological capabilities of fabricating lines of small width and amounts to 150 to 200 ohms. The capacitance of the blocking capacitor is chosen from the relationship:

$C_{b1} \approx (20...50)/2\pi f_{in}\rho_{loop}$. $C_{\text{бл}}\simeq(20\ldots50)/2\pi f_{\text{вх}}\rho_{\text{ш}}$.

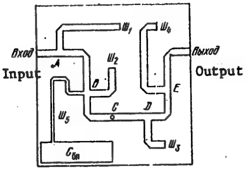

Figure 18.4. Multiplier circuit board.

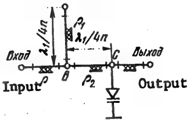

Figure 18.5. Schematic of a simplified input microwave network for a frequency multiplier.

One of the layout variants for a printed circuit board of the multiplier networks designed in the configuration of Figure 18.3 is shown in Figure 18.4. To reduce the dimensions of the circuit board, it is recommended that the conducting strips of the microstrip lines be bent at an angle of 90° and brought close to each other, but no closer than three substrate thicknesses to preclude parasitic coupling between them.

In a number of cases, the input microwave network of a multiplier is simplified by providing matching of the diode impedance at the input frequency through the choice of the characteristic impedances of the filter loop Sh_2 and the section l_7 which connects the loop to the diode. A schematic of a simplified microwave input circuit is shown in Figure 18.5. The characteristic impedances of the sections ρ_1 and ρ_2 are calculated from the formulas:

$$\rho_1=\frac{\rho_2\,\mathrm{tg}\,\frac{\pi}{2n}\left[r_{\text{вх}}^2+\left(x_{\text{вх}}+\rho_2\,\mathrm{tg}\,\frac{\pi}{2n}\right)^2\right]}{\left(\rho_2-\underset{\text{in}}{x_{\text{вх}}}\,\mathrm{tg}\,\frac{\pi}{2n}\right)\left(\underset{\text{in}}{x_{\text{вх}}}+\rho_2\,\mathrm{tg}\,\frac{\pi}{2n}\right)-\underset{\text{in}}{r_{\text{вх}}^2}\,\mathrm{tg}\,\frac{\pi}{2n}},$$

where

$$\rho_2=\frac{1}{\mathrm{tg}\,\frac{\pi}{2n}}\left(-x_{\text{вх}}\pm\sqrt{r_{\text{вх}}\rho\left(1+\mathrm{tg}^2\frac{\pi}{2n}\right)-r_{\text{вх}}^2}\right).$$

When $x_{in} > 0$, a plus sign is used, and when $x_{in} < 0$, that sign which provides for an acceptable value of ρ_2 in terms of the structural design. If the values obtained for ρ_1 or ρ_2 are difficult to achieve in practice, then matching must be accomplished using the configuration of Figure 18.3.

CHAPTER 19. MICROWAVE AMPLIFIERS AND OSCILLATORS USING AVALANCHE TRANSIT TIME DIODES

19.1. Basic Characteristics

Avalanche transit time diodes (LPD's) [IMPATT diodes] can be used to construct the oscillator and amplifier stages of transmitting active phased array modules in a frequency range from a few up to hundreds of gigahertz. As compared to other microwave semiconductor devices, IMPATT diodes provide for a high output power in a CW mode at frequencies above 10 GHz and greater efficiency in a pulsed mode at frequencies on the order of a few GHz.

The parameters and technical characteristics of microwave IMPATT devices such as the output power, working frequency, efficiency, etc., depends substantially on the diode operating conditions. No less than five operational modes of IMPATT diodes have been experimentally observed, which are realized depending on the parameters of the diode oscillatory circuitry and the power supply networks. For the practical application of IMPATT diodes in microwave power oscillators and amplifiers, there are two modes of significance which differ in the rate of drift of the current carrier in the blocking p-n junction layer: the fast drift mode, in which the rate of travel of the carriers is equal to the saturation rate for the given semiconductor material, called the avalanche transit mode (LPR), and the slow drift mode, in which the rate of motion of the carriers is significantly less than the saturation rate, called the trapped plasma mode (RZP). (In the foreign literature, these modes are called IMPATT and TRAPATT modes respectively).

The working frequency for TRAPATT devices falls in the decimeter band. In this band, when a single diode is used, the pulsed power with an efficiency of 25 to 30 percent at frequencies around 1 GHz usually amounts to 100 to 400 watts, and with CW operation, 10 to 40 watts.

The IMPATT mode is a higher frequency mode. Its operating frequencies fall in the centimeter and millimeter bands. The power delivered by a single diode in the centimeter band amounts to a few watts with an efficiency of about 10 percent in a CW mode and tens of watts in a pulsed mode. In the millimeter band, IMPATT diodes make it possible to obtain a CW output power on the order of a few watts at a frequency of 50 GHZ with an efficiency of 14 percent and 0.38 watts a frequency of 90 GHz with an efficiency of 12.5 percent.

It can be anticipated that in upcoming years, the power of a single IMPATT diode in a CW mode will reach 30 watts at a frequency of 10 GHz, 2 to 3 watts at a frequency of 50 GHz (avalanche and transit time mode) and 50 watts at 1 GHz (TRAPATT). The indicated powers can be increased by approximately an order of magnitude when various methods of power additions are employed.

It must be noted that because of the technical difficulties in realizing a TRAPATT mode, it was discovered and studied considerably later than avalanche and transit diode operation, and its theory is incompletely developed at the present time. The lack of a simple mathematical model which permits the calculation of the diode impedance makes it difficult to design a TRAPATT diode module, and the design of such modules is accomplished at the present time by primarily an empirical approach. Because of this, the fundamentals of the engineering design of microwave stages are set forth in this chapter for IMPATT diodes and only some of the major features of TRAPATT design are treated.

The use of IMPATT diodes is most expedient in the output stages of modules where poor noise characteristics are not of substantial importance and the governing parameters are the output power and the efficiency. Since output stages, as a rule, operate with a power gain, the characteristics of IMPATT power amplifiers are of the main practical significance.

The properties of IMPATT amplifiers (ULPD) are qualitatively similar to the properties of the well known amplifiers using negative resistance diodes (parametric and tunnel diodes) as well as electron transport diodes (DPE's). In generalizing the results of theoretical studies of such amplifiers, one can formulate the major properties of IMPATT diode amplifiers.

1. The maximum value of the gain is limited by the amplifier stability conditions (the instability in the diode resistance, the nonideal nature of load matching, etc.) and under actual operating conditions for an amplifier, should not exceed 20 dB in the case of low input signal levels.

2. The maximum output power and efficiency are realized at a certain definite input signal level; in this case, the gain falls off by a factor of several times relative to its small signal value, so that the actual values of the gain in a maximum output power mode do not exceed 10 dB.

3. The maximum output power and efficiency of an amplifier are approximately equal to the corresponding parameters of an optimally tuned self-excited oscillator using the same diode.

4. The bandwidth of an IMPATT diode amplifier is limited by the diode Q in accordance with Fanno's relationship:

$$\left(\frac{\Delta f}{f_0}\right)_{\text{пред}} \approx \frac{\pi}{Q_{\text{д}}} \frac{1}{\ln \sqrt{K_p}},$$

where $(\Delta f/f_0)_{\text{ult}}$ is the ultimate bandwidth; K_p is the power gain; Q_d is the diode quality factor. It follows from this that for the actual values of $Q_d \approx 6$--15 and $K_p \leq 10$ dB, the ultimate passband does not exceed 15 percent.

5. The nonlinear distortions at the output of an IMPATT amplifier increase with an increase in the gain and for small gains ($K_p < 10$ dB) do not exceed the distortions in traveling wave tube amplifiers.

Thus, the output amplifier an IMPATT diode module can provide an output power on the order of a few watts in a CW mode in the centimeter band and of several tens of watts in the decimeter band with a gain of around 10 dB. in a passband of approximately 15 percent.

In staructural terms, the IMPATT diode amplifier or oscillator is made in the form of a microwave resonator (cylindrical, rectangular, toroidal, coaxial, stripline, etc.), coupled to the load and the input signal source (in the case of an amplifier) with the diode mounted in it. An external view of an amplifier is shown in Figure 19.1.

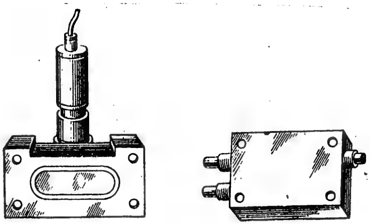

Figure 19.1. External view of an IMPATT diode amplifier.

19.2. The Parameters of IMPATT diodes and Specific Features of Their Applications in the Modules of Active Phased Transmitting Antenna Arrays

An avalanche transit time diode (Figure 19.2) is a complex semiconductor structure (1), which is mounted on a heat sink (2), housed in a hermetically sealed package.

The distribution of the electric field intensity E(x) in the diode is shown in Figure 19.3, where x is the distance figured from the plane of the junction. Such a distribution is characteristic of all of the known types of IMPATT diodes [1-5], and for this reason, the essence of the physical processes occurringin IMPATT diodes is described by the same mathematical model regardless of the nature of the internal structure of the diodes.

The major contents of this model reduced to the fact that when the inverse bias voltage is equal to the breakdown value U_{br}, the electrical field intensity exceeds the critical value $E = E_{cr}$, corresponding to the onset of avalanche breakdown, only in a small region of the barrier layer with a width of δ (Figure 19.3), because of which, the entire barrier layer of the p-n junction with a width W is broken down into two regions: a narrow region of width δ ($\delta << W$), in which the process of impact ionization and avalanche like multiplication of the number of carriers takes place: the so-called multiplication layer (SU) and a region of carrier drift of width $W - \delta$, where the carriers formed in the multiplication layer move at a velocity V. It is assumed that the electric field intensity in the barrier layer during the time of carrier drift does not fall below a certain value E_S, corresponding to the saturation velocity V_S, so that the drift speed is constant and equal to the saturation velocity $V = V_S$.

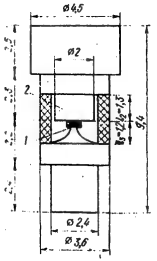

Figure 19.2. The structural design of an IMPATT diode in a package.

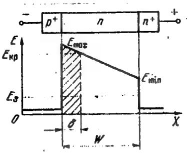

Figure 19.3. The distribution of the electric field intensity E(x) in an IMPATT diode.

Based on the model considered here for a harmonic voltage of low amplitude applied to the diode, the impedance of the p-n junction is determined by the following expressions [1]:

$$z_{p\text{-}n} = R_{p\text{-}n} + j\,X_{p\text{-}n};$$

$$R_{p\text{-}n} = -\frac{1}{\omega C}\,\frac{\beta^2}{1-\beta^2}\,\frac{1-\cos\omega\tau}{\omega\tau}; \qquad (19.1)$$

$$X_{p\text{-}n} = \frac{1}{\omega C}\left(\frac{\beta^2}{1-\beta^2}\,\frac{\omega\tau-\sin\omega\tau}{\omega\tau} - \frac{1}{1-\beta^2}\right). \qquad (19.2)$$

Here, $C = \varepsilon S/W$ is the barrier layer capacitance of the p-n junction; S is the junction area; $\omega = 2\pi f$ is the frequency of the harmonic voltage applied to the diode; $\tau = (W - \delta)/V_S$ is the drift region transit time by the carriers;

$$\beta^2 = \omega_л^2/\omega^2 \qquad (19.3)$$

is a parameter which characterizes the diode operating mode; $\omega_л$ is the avalanche frequency which characterizes the resonant frequency of the electron-hole plasma in the multiplication layer. The avalanche frequency is determined by the properties of the semiconductor material and the technological and structural parameters of the p-n junction, in accordance with the expression [1]:

$$\omega_{\text{л}} = \left[\frac{2I_0(m+\gamma)Y_S}{\varepsilon S\delta E_{\text{кр}}}\right]^{1/2}, \tag{19.4}$$

where I_0 is the DC current flowing through the junction; m is a coefficient which determines the dependence of the impact ionization coefficient of the majority carriers on the electrical field intensity for an approximation of this function with a power function of the type E^m; γ is a coefficient which characterizes the sharpness of the p-n junction.

When developing a circuit for an IMPATT diode oscillator, it is convenient to treat as a two-pole network characterized the impedance $Z_d = r_d + jX_d$, the resistive r_d and reactive X_d components of which can be determined on the basis of the simplified equivalent circuit [1] shown in Figure 19.4:

$$r_{\text{д}} = \frac{X_C^2(R_{p\text{-}n} - R_S)}{(R_{p\text{-}n} - R_S)^2 + (X_{p\text{-}n} + X_L - X_C)^2}; \tag{19.5}$$

$$X_{\text{д}} = \frac{-X_C[(R_{p\text{-}n} - R_S)^2 + (X_{p\text{-}n} + X_L)(X_{p\text{-}n} + X_L - X_C)]}{(R_{p\text{-}n} - R_S)^2 + (X_{p\text{-}n} - X_L + X_C)^2}, \tag{19.6}$$

where

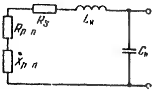

Figure 19.4. The equivalent circuit of an avalanche transit time diode.

The expressions given here make it possible to ascertain the major properties of an IMPATT diode which govern the specifics of its applications in the design of oscillator and amplifier stages in active phased antenna array modules.

The resistance of an IMPATT diode is negative when $\beta^2 < 1$, i.e., at frequencies of:

$$\omega > \omega_l. \tag{19.7}$$

Physically, this means that when condition (19.7) is met, the alternating current $i(t) = \mathrm{Re}\, I_m e^{j\omega t \pm \phi}$ flowing through the diode is shifted in phase relative to the applied harmonic voltage $u(t) = \mathrm{Re}\, U_m e^{j\omega t}$ by an angle of 90° < ϕ < 270°. In this case, the diode can be treated as a source of oscillatory power. The average power delivered by the diode to an external circuit over an oscillation period T is proportional to the negative resistance of the diode $r_d = U_m/I_m$.

The negative resistance (NR) of a diode for given structural and production process parameters depends, as follows from (19.1) - (19.5), on the frequency and direct current of the diode. The nature of the frequency dependence of the negative resistance of a p-n junction is determined by the factor $(1 - \cos\omega\tau)/\omega\tau$ in accordance with (19.1), where this factor has a maximum at a certain optimal value of the transit angle $\theta_{opt} = (\omega\tau)_{opt} = 2.2$ rad. It follows from this that for a specified carrier drift time, a definite frequency f_{tr}, called the transit frequency, corresponds to the maximum negative resistance of a p-n junction:

$$f_{tr} = f_{\text{пр}} = 0{,}35 V_S/(W-\delta). \qquad (19.8)$$

Thus, the width of the depleted region of an IMPATT diode, intended for operation at a specified frequency, should have a definite value, depending on the properties of the semiconductor material. If the diode is intended for operating in a range of frequencies, then the depletion region width is usually selected so that the average frequency of the band is equal to the optimal frequency:

$$f_{opt} = (f_{min} + f_{max})/2. \qquad (19.9)$$

In this case, the power delivered by the diode to the axternal circuit is a maximum at the center frequency of the band and falls off towards its boundaries.

The negative resistance of an IMPATT diode increases with an increase in the direct current I_0, as follows from (19.1) - (19.5). However, the working current I_0 at a specified frequency should always be less than the characteristic current I_x, for which the avalanche frequency becomes equal to the working frequency, since in this case, $\beta^2 = 1$ and $|R_{p-n}| \to \infty$. The characteristic current is frequently used as the IMPATT diode parameter in place of the avalanche frequency. In this case:

$$\beta^2 = I_0/I_x \qquad (19.10)$$

and as follows from (19.4):

$$I_x = \omega^2 \varepsilon S \delta E_{\text{кр}}/2(m+\gamma) V_S. \qquad (19.11)$$

The maximum permissible diode working current $I_{0\,per}$ is limited in the case of a specified ultimate temperature for the p-n junction, $T_{p-n\,per}$ by the temperature of the heat sink T_0 in accordance with the expression [1]:

$$I_{0\ per} = I_{0\ \text{доп}} = (T_{p\text{-}n\ \text{доп}} - T_0)/R_{\text{т}} U_0, \qquad (19.12)$$

where R_T is the thermal resistance of the diode; U_0 is the DC voltage.

Thus, the diode power depends substantially on its structural design (R_T) and the configuration of the microwave network (T_0). For modern IMPATT diodes, depending on the structural design and material of the semiconductor:

$$R_T = 20 \ldots 150 \text{ deg/W} \qquad (19.13)$$

The greatest values of the thermal resistance are observed for diodes with a planar structural design and mesa structures. For an inverted mesa structure, $R_T \leq 35$ deg/W; for Schottky barrier diodes, $R_T \approx 20 \ldots 30$ deg/W.

Domestic industry is producing silicon three-layer IMPATT diodes of the 2A706 type with a p^+-n-n^+ structure having the following parameters:

Working frequency range, GHz:	
2A706A (red dot)	8.5 - 10
2A706B (blue dot)	10 - 11.5
2A706V (white dot)	8.5 - 10
2A706G (black dot)	10 - 11.5
Power, mW:	
2A706A	100
2A706B	100
2A706V	50
2A706G	50
Capacitance, pFd	0.2 - 0.5
Breakdown voltage, volts	50 - 120
Efficiency, percent	3.5 - 6
Package parameters:	
Inductance, nanohenries	0.4 - 0.5
Capacitance, picofarads	0.4 - 0.5

Operating current, in mA, is indicated on the individual diode package.

The overall dimensions of the diode package are shown in Figure 19.2.

The static differential diode resistance, $R_0 = dU_0/dI_0$, determined on the basis of its volt/ampere characteristics, amounts to approximately 300 ohms. Because of this, to stabilize the operating current and prevent thermal breakdown, the diode power supply should have an internal resistance of $R_i \gg 300$ ohms. In the absence of such a supply, it is necessary to insert a limiting resistor in series with the diode having a resistance of $R_{lim} \gg 300$ ohms.

To calculate the diode impedance from the data sheet values, it is convenient to represent formula (19.11) in the form:

$$I_x = 0{,}5\pi f^2 C U_{\text{пр}}/f_{\text{пр}}, \qquad I_x = 0.5\pi f^2 C U_{tr}/f_{tr} \tag{19.14}$$

setting $\gamma = 1$ and $m = 7$. The characteristic current as a function of frequency, computed from formula (19.14) for 2A706 diodes is shown in Figure 19.5, where the regions of characteristic current values due to scatter in diode parameters as well as its average value are shown.

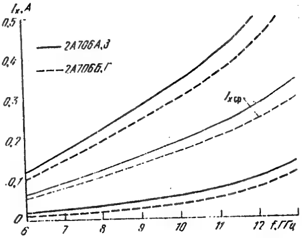

Figure 19.5. The characteristic current of an IMPATT diode as a function of frequency.

The small signal impedance as a function of frequency and direct current, calculated from formulas (19.1) - (19.6) for 2A706A and V diodes is shown in Figure 19.6, where the region of diode impedance values due to scatter in the parameters are indicated for various constant values of β^2. These regions are enclosed between two curves (the solid and dashed lines), corresponding to the extreme permissible values of the diode capacitance (the minimal is the solid curve and the maximum is the dahsed curve) for the same constant value of the parameter $\beta^2 = $ = const. The small circles indicate the values of the impedance at various fixed frequencies which are specified in gigahertz alongside the circles. Constant frequency curves are also shown here. The resistive and reactive components of the impedance of a diode in a package are shown in Figure 19.7 as a function of frequency for the maximum and minimum permissible values of the diode capacitance. As can be seen from the figure, the resistance of the diode is negative in a broad frequency range (about 20 GHz) of $f_1 < f < f_{max}$. The broad band response of the negative resistance of the diode makes it possible to use it for the broad band output stages of active elements of modules. On the other hand, the presence of negative resistance in a very wide band of frequencies can cause the excitation of parasitic self-oscillations at frequencies other than the working frequency, something which creates definite difficulties in assuring circuit stability, all the more since in the region of existence of negative resistance, the diode equivalent circuit (Figure 19.4) has two natural resonances: a series resonance at a frequency of:

$$f_{\text{посл}} = \frac{1}{2\pi}\left(L_{\text{к}} C_{p\text{-}n}\right)^{-1/2}$$

and a parallel resonance at a frequency of:

$$f_{\text{пар}} = \frac{1}{2\pi}\left(L_{\text{к}} \frac{C_{\text{к}} C_{p\text{-}a}}{C_{\text{к}} + C_{p\text{-}n}}\right),$$

where C_{p-n} is the equivalent p-n junction capacitance in the operating mode. Both frequencies depend on the diode direct current I_0, increasing with an increase in this current.

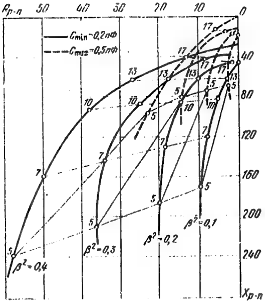

Figure 19.6. The small signal impedance of a 2A706 diode as a function of frequency and the parameter β^2.

When IMPATT diodes are used in output power amplifiers, the dependence of the negative resistance of the p-n junction on the amplitude of the oscillations - the amplitude of the current flowing through the junction I_m, is of considerable importance. In the case of large current amplitudes ($I_m \geq I_x$), the average value over a period of the parameters which determine the impedance of the p-n junction differs from the corresponding small signal values which enter into expressions (19.4) and (19.5), which leads to a reduction in the resistive and reactive components of the p-n junction impedance with a rise in the current amplitude. In this case, the impact of the amplitude of the oscillations on the value of the reactive component of the junction impedance, X_{p-n}, is considerably less than on the value of the resistive component, R_{p-n}, since the slope of X_{p-n} as a function of the current amplitude I_m

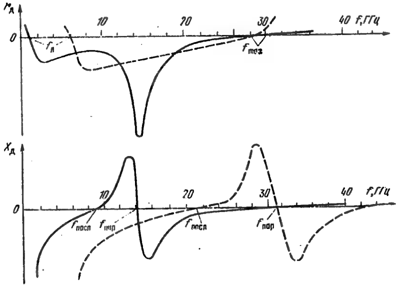

Figure 19.7. The resistive and reactive components of the impedance of an IMPATT diode in a package as a function of frequency for the maximum (———) and minimum (- - -) values of the capacitance.

is approximately an order of magnitude less than the slope of the corresponding function for R_{p-n}. This makes it possible when calculating the quantity X_{p-n} to assume that it is independent of the amplitude of the oscillations.

The negative resistance of the p-n junction of an IMPATT diode as a function of the current amplitude is described by the expression:

$$R_{p\text{-}n} = R_{p\text{-}n}(0)\,\Phi(I_m), \tag{19.15}$$

where $R_{p-n}(0)$ is the small signal value of the negative resistance of the p-n junction (19.1); $\Phi(I_m)$ is a monotonically decaying function. For practical designs of microwave devices using IMPATT diodes, it is convenient to approximate the function $\Phi(I_m)$ with a quadratic parabola:

$$\Phi(I_m) = q - cI_m^2. \tag{19.16}$$

The approximation parameter q and c are chosen on the basis of existing theoretical or experimental curves of the negative resistance as a function of the amplitude of the oscillations.

In generalizing what has been presented here, we shall note some specific features of the application of IMPATT diodes in microwave devices.

The application of IMPATT diodes in the active elements of modules is possible at frequencies from a few gigahertz up to several hundreds of gigahertz, where its negative resistance is manifest. The negative resistance of an IMPATT diode is manifest in a broad frequency range - about 20 GHz, which makes it possible to use it for the realization of broadband output stages of modules. On the other hand, the broadband nature of the negative resistance leads to the necessity of taking special measures to assure the stability of the stages.

The dependence of the maximum permissible diode current on the ambient temperature leads to the necessity of a careful structural design of a good heat sink.

The considerable production process scatter in the parameters of the diode, as well as the poor precision of existing methods of calculating their impedance makes it necessary to employ a large number of control elements in the design of amplifiers and oscillators.

19.3. Microwave Circuits of Oscillators Using IMPATT Diodes

Since the impedance of an IMPATT diode is characterized by a rather large reactive component, the simplest microwave circuit with an IMPATT diode can be represented, as shown in Figure 19.8a, with a resonant circuit L_{equiv} C_{equiv} with the load resistance R_H and the negative resistance r_d inserted in it, where C_{equiv} is the equivalent capacitance of a diode with a reactance $X_d = (\omega C_{equiv})^{-1}$; E_{equiv} is the equivalent inductance of the external circuit with a reactance of $X_{load} = \omega L_{equiv}$.

The model given here for the simplest microwave circuit with an IMPATT diode is justified not only when considering the circuit external to the diode terminals, but also for the circuit internal relative to the "terminals" of the p-n junction. In this case, the components of the impedance at the input terminals of the diode r_d and X_d are replaced in the circuit with the corresponding components of the impedance of the p-n junction R_{p-n} and X_{p-n}, while the reactive components of the package (L_k, C_k) apply to the elements of the external circuit. In this case, the parameters R_H and X_H [R_{load} and X_{load}] designate the resistive and reactive components of the external circuit impedance, referenced to the "terminals" of the p-n junction.

Such a treatment proves to be frequently the most convenient one, since throughout the entire range of frequencies where the resistance of the p-n junction is negative, its reactance is always capacitive. Taking relationships (19.15) and (19.16) into account, we represent the expression for the voltage across the resistance in the form:

$$u = -ai + bi^3, \qquad (19.17)$$

where $a = |R_{p-n}(0)|q$; $b = 4|R_{p-n}(0)|c/3$, and we derive the differential equation for the current:

$$\frac{d^3 i}{dt^3} - M(1 - Bi^2)\,\omega_0 \frac{di}{dt} + \omega_0^2 i = 0. \tag{19.18}$$

Here:

$$M = \frac{a - R_{\text{н}}}{\omega_0 L_{\text{экв}}}; \quad B = \frac{3b}{a - R_{\text{н}}}; \quad \omega_0^2 = \frac{1}{L_{\text{экв}} C_{\text{экв}}}. \tag{19.19}$$

By designating the coefficient in front of the first derivative as:

$$a_{\text{экв}} = 0.5\omega_0 M (1 - Bi^2), \tag{19.20}$$

We shall represent the resulting equation in the form of Van der Pol's equation known from oscillation theory:

$$\frac{d^2 i}{dt^2} + 2a_{\text{экв}} \frac{di}{dt} + \omega_0^2 i = 0,$$

The solution of which is $i = I_m e^{-a_{\text{экв}} t} \sin(\omega_0 t - \varphi)$.

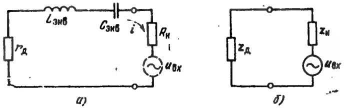

Figure 19.8. Schematic of a microwave device using an IMPATT diode.

It follows from this that the circuit stability (the absence of increasing oscillations in the case of a random perturbation) is assured when the condition aequiv > 0 is met, or as follows from (19.18) - (19.20) for q = 1, when:

$$R_{\text{н}} > |R_{p\text{-}n}(0)|. \tag{19.21}$$

Similarly, the excitation condition can be represented in the form:

$$R_{\text{н}} < |R_{p\text{-}n}(0)|, \tag{19.22}$$

while the condition for steady-state self-excited oscillations (oscillation mode) is: $R_H = [R_{load}] = \overline{R}_{p-n}$ ($\overline{a}_{equiv} = 0$), where $\overline{R}_{p-n}$ is the average value of the negative resistance over an oscillation period.

Since the value of R_{p-n} for each specific diode at a specified frequency is governed by the value of the direct current (19.1), (19.3) and (19.4), then it follows from (19.21) and (19.22) that the choice of the circuit operating mode can be made by means of choosing the load resistance R_{load} or the value of the direct current I_0. The current corresponding to the excitation of self-oscillations for a specified load resistance is called the starting current, I_{start}. In this case, the condition $I_0 > I_{start}$ corresponds to the oscillation condition and the stability condition is $I_0 < I_{start}$.

If an alternating current source is added to the simplest electrical circuit with an IMPATT diode (Figure 19.8a), then when stability condition (19.21) is met, a power gain is established in the circuit for the input oscillations, and when condition (19.22) is met, an external synchronization mode is established for natural oscillations, or a so-called synchronized oscillator mode. Both modes can be used for the operation of the output stages of modules. A free-running oscillator, as a rule, does not find practical application here because of the difficulties of realizing the requisite phase distribution over the elements of an array. However, the parameters of this mode must taken into account in the design work so as to assure the stability of the primary operating mode, i.e., the absence of amplitude and phase jumps in the output signals, which can appear as a consequence of the excitation of parasitic self-oscillation.

The fact is that the realization of the simplest microwave circuit shown in Figure 19.8a in a range of frequencies where the negative resistance of an IMPATT diode is manifest is not possible in practice. To create an external microwave circuit, transmission line sections are usually employed (coaxial, waveguide, stripline, etc.), which are coupled to the load. The oscillating systems which are formed when an IMPATT diode is inserted in such line sections, as a rule, are multiple resonance resonance systems, The appearance of additional (parasitic) resonances is explained by the influence of the parasitic parameters of the diode package, the occurrence of resonant volumes when mounting the diode, the imprecesion in the matching to the load, the presence of spatial resonances in distributed systems, etc. In this case, the equivalent circuit shown in Figure 19.8 is approximate and valid only in a small band of frequencies in the vicinity of each resonant frequency, in the case where adjacent resonant frequencies are separated sufficiently far from each other. The complete equivalent circuit in this case should have the form shown in Figure 19.8b, where the impedance, $Z_H(\omega) = R_H(\omega) + +jX_H(\omega)$ designates the total impedance of the external microwave circuit.

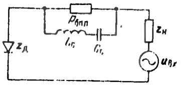

Figure 19.9. Schematic of an IMPATT diode amplifier with a stabilizing microwave network.

One can write the following based on Kirchoff's law for the reduced circuit in the steady-state mode: $Z_H(\omega) + Z_{p-n}(\omega) = 0$, from which the equations for the amplitude and phase balance of the steady-state oscillations follow:

$$R_{\text{н}}(\omega) + R_{p\text{-}n}(\omega) = 0, \tag{19.23a}$$

$$X_{\text{н}}(\omega) + X_{p\text{-}n}(\omega) = 0. \tag{19.23b}$$

Thus, at the natural resonant frequencies of a circuit, which satisfy the phase balance equation, parasitic oscillations can be excited in the case where the negative resistance at these frequencies is not equal to zero. For this reason, when designing the microwave circuit of an IMPATT diode oscillator, it is necessary to take special steps to suppress parasitic self-oscillation. Among them, the use of additional control elements and stabilizing circuits is of the greatest practical significance.

Control elements can be made in the form of short-circuited or open-circuited loop, quarter-wave transformers, inductive or capacitive stops, stubs, etc. The regulatory control of a circuit consists in choosing the point of insertion of the control elements so that the natural resonant frequencies of the circuit prove to be shifted relative to those frequencies where the impedance of the diode exceeds its input resistance. To realize such tuning, one must use several control elements, because of which, the tuning process is extremely complicated. In this case, tuning does not guarantee the stability of a stage with a sharp change in the operating conditions and operating mode (for example, temperature).

The indicated drawbacks are elminiated when stabilizing networks are used. A stabilizing network consists of a stabilizing resonant circuit L_cC_c which is tuned to the working frequency, and a ballast resistor R_{bal}. The diode is connected to the passive external circuit through the stabilizing network (Figure 19.9). The effect of the stabilizing network consists in the fact that at all frequencies, the exception of the working frequency, the negative resistance of the diode is canceled by the positive ballast resistance, and the active resistance, which is connected to the external passive circuit on the diode side, is positive (for this, the ballast resistance should satisfy the stability condition). At the working frequency, the ballast resistance is shunted by the stabilizing tuned circuit and has no influence on the negative resistance connected to the external circuit.

Thus, in the circuit which contains a stabilizing network, the coupling of the negative resistance to the passive external circuit takes place only at the working frequency. In this case, the possibility of the excitation of parasitic self-oscillation is eliminated.

We will note that the schematic of the stabilizing network shown in Figure 19.9 is not the only one possible. At the present time, several variants of such circuits are known. Their structural design can also be diverse.

Considering what has been said above, as well as taking into account the fact that the resistance of an active phased antenna array radiator. i.e.,of the load, changes with a change in the frequency practically arbitrarily outside the range of working frequencies, one can consider the circuit of a microwave network for the output stage of a module using an IMPATT diode with a stabilizing network as the most promising configuration.

19.4. Structural Design Principles

Based on the properties treated above for IMPATT diodes and the specific features of their external microwave networks, one can formulate general requirements placed on the structural design of an IMPATT diode oscillator (GLPD). These are: assuring the specified working frequency, operational mode and operating stability, as well as the transmission of the power developed by the diode to the load with minimal losses in the specified range of frequencies, corresponding to the spectrum of the transmitted signals.

It is correspondingly necessary to provide a resonator or transmission line section in the structure which is coupled to the IMPATT diode and the load, as well as elements for coupling the diode to the resonator, elements for coupling to the input signal source and the load, an impedance transformer and adjusting elements.

The structural design of individual components depends substantially on the type of resonator used.

As a rule, a ferrite circulator (in reflective type amplifiers) or individual coupling elements: capacitive stubs, inductive loops, diffraction holes, etc. (in self-excited oscillators and through transmission type amplifiers) are used for coupling to the load and the input signal source.

The correct fastening of the diode in the resonator is of considerable importance in the structural design. In this case, a good heat sink should be provided as well as minimal contact resistance in the plane where the diode is joined to the resonator. A special clamping terminal is usually employed to secure the diode, where this terminal is fastened in a holder nut, installed in the most massive wall of the resonator. The diode is inserted in the clamp so that the contact to it is made along the lateral surface of the diode package. In this case, the thermal conductivity of the clamp should no worse than the thermal conductivity of copper. Examples of the structural design of diode fasteners are shown in Figure 19.10.

A diode is usually mounted in a resonator so that the number of parasitic resonances is reduced. Resonators with a reduced cross-section are used for this purpose or the dimensions of the resonator are reduced at the diode insertion point.

An IMPATT diode oscillator is realized most simply by using a coaxial resonator [6] as shown in Figure 19.10a. The IMPATT diode (1) is installed in a gap in the center conductor (2) close to the short-circuited wall which forms the heat sink.

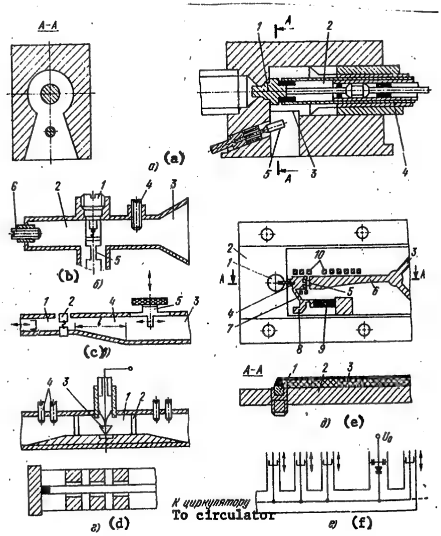

Figure 19.10. Examples of the structural design of microwave devices using IMPATT diodes.

Key:
- a. Coaxial structure;
- b. Toroidal;
- c,d. Waveguide structure;
- e. Stripline;
- f. Structure with several control elements.

The resonator is coupled to the load through a stop (3), and the length of the resonator is changed and tuned to resonance by means of moving the short-circuiting piston (4); the coupling to the load is adjusted by means of changing the position of the coupling stub (5).

The structural design of an IMPATT diode oscillator with a toroidal resonator [1] is shown in Figure 19.10b. The IMPATT diode (1) is mounted in the center of the resonator (2), and coupled to the load through the coupling window (3). The coupling to the load is adjusted by the positioning of the stub (4). Tuning to resonance is accomplished by means of the screw (6). Power is fed to the diode through the microwave filter (5).

Waveguide structures of 3 cm band IMPATT diode amplifiers are shown in Figures 19.10c and d, [5, 7]. The cross-section of a rectangular waveguide for the 3 cm band with a reduced height (1) and an IMPATT diode (2) inserted in it is shown in Figure 19.10c. The waveguide height is 1.27 mm. The transition to a standard 10 x 23 mm waveguide (3) is made through an expanding conical section taper (4). The coupling to the load is adjusted by means of a moving tuning screw (5). In the structure shown in Figure 19.10d, the resonator (1) is formed by a rectangular waveguide section, inclosed between two semi-reflecting inductive stops (2). The IMPATT diode (3) is inserted in the center of the resonator, where the waveguide height is reduced at the point of diode insertion. The coupling to the load and the input signal source is adjusted by changing the width of the inductive stop window. The tuning is accomplished by means of the fine tuning screws (4).

In the stripline structure [6, 8] shown in Figure 19.10e, the IMPATT diode (1) is mounted in the heat sink plate (2) to which the microstrip line circuit (3) is secured. The microwave resonator is formed by a section of 50 ohm line (4), to one side of which the IMPATT diode is connected, while the elements for capacitive coupling to the load (5) and the impedance transformer (6) which matches the input impedance of the 50 ohm load line of the circulator to the diode impedance is connected to the other side. The coupling to the synchronizing signal source and the load is accomplished through the input and output 50 ohm line of the circulator. Bias voltage is fed to the diode through a low pass filter, formed by elements (7 and 8) with stabilizing resistance (9). The circuit is tuned and adjusted by means of the regulating loops (10).

Examples of structural designs of coaxial resonators with several tuning elements in the form of movable quarter-wave transformers and short-circuited loops [9] are shown in Figure 19.10f. The use of additional control elements makes it possible to obtain several resonances in the microwave circuit of the diode, the natural frequencies of which fall in a definite ratio, for example, 1:2 and for this reason, such structures can be used to increase the diode efficiency either in an IMPATT mode or when exciting oscillations in a TRAPATT mode.

The structure of an IMPATT diode oscillator with a stabilizing network [10] is shown in Figure 19.11a, b. Here, the stabilizing resonator (1) which is also simultaneously the load resonator, is formed by a section of rectangular waveguide inclosed between the shorting wall (2) and inductive stop (3), through which coupling to the load is accomplished. The IMPATT diode (4) is inserted in coaxial line (5) which is coupled to the resonator through the coupling hole in the short-circuiting wall. The matched load (6) which is used as a ballast resistor is inserted at the other end of the coaxial line. If the impedance introduced into the coaxial line from the resonator is represented as the impedance of a series LC circuit with a load resistance R_H, then the equivalent circuit of the oscillator can be represented as shown in Figure 19.11c. As can be seen from this figure,

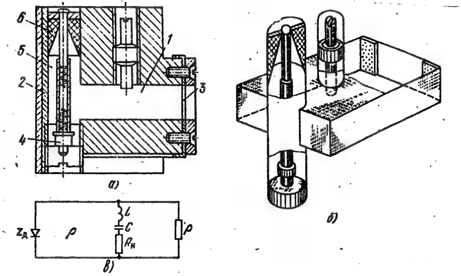

Figure 19.11. Structural design of an IMPATT diode oscillator with a stabilizing network and its equivalent circuit.

the circuit matches that shown in Figure 19.9 if the LC network is treated as a stabilizing and load network simultaneously.

Such a structure can be used as the major component in the structural design of a multiple diode output amplifier module using power addition.

19.5. Principles of Design Calculations of IMPATT Diode Microwave Devices

The goal of the design is to obtain a specified output power P_H at the working frequency f_0. We shall analyze the dependence of the power delivered by the p-n junction of an IMPATT diode on the DC and AC currents flowing through the junction. By employing the theoretical relationship for the negative resistance of the p-n junction as a function of the amplitude of the current flowing through it [1] (19.15) and (19.16), we determine the approximation parameters q and c from the condition for a satisfactory approximation of the function $\Phi(I_m)$ in the range of large amplitudes ($I_m \geq I_x$). We define the parameter q as the value of $\Phi(I_m)$ when $I_m = I_x + I_0$ ($I_m/I_x = 1 + \beta^2$). The parameters q and c depend on the quantity β^2 and are quite well approximated by functions of the form:

$$q \doteq 0{,}8\,(1 - \beta^2); \quad c \doteq 0{,}9 + 3\,(\beta^2)^2. \tag{19.24}$$

We determine the power delivered by the p-n junction, taking (19.15) and (19.16) into account, as:

$$P_{\text{д}} = 0{,}5 I_m^2 \,|R_{p\text{-}n}(0)|\,(q - c I_m^2). \tag{19.25}$$

An optimal value of the current amplitude $I_m = I_{m\ opt}$ corresponds to the maximum value of this power, $P_{d\ max}$, where we determine this optimal current amplitude by differentiating (19.25) with respect to I_m and equating the derivative to zero:

$$I_{m\,\mathrm{opt}} = \sqrt{q/2c}. \tag{19.26}$$

By substituting the value found for $I_{m\ opt}$ in (19.25), we find the maximum power:

$$P_{\text{д}\,\max} = 0{,}125\,|R_{p\text{-}n}(0)|\,q^2/c. \tag{19.27}$$

Expressions (19.25), (19.27) and (19.1) are justified with the assumption that avalanche breakdown occurs simultaneously and uniformly over the entire area of the p-n junction, something which is valid only for ideally uniform p-n junctions. As a rule, actual diodes are not absolutely uniform. Nonuniform breakdown leads to nonuniformity in the current distribution over the area of the p-n junction, because of which, it is as if a portion of the area is cut off, which leads to a reduction in the current flowing in the diode circuit and its output power.

It is rather difficult to take the actual current distribution over the p-n junction area into account, and for this reason, the integral effect of the inhomogeneity of a p-n junction can be taken into account if the concept of the effective or acting area of the p-n junction is introduced, defining it as:

$$S_d = S/n \qquad S_{\text{д}} = S/n, \tag{19.28}$$

where the coefficient n depends on the degree of nonuniformity of the p-n junction and can be determined based on a comparison of the experimental and theoretical values of the negative resistance and the maximum diode output power; n = = 1.8 to 2.7 for 3 cm band silicon mesa structures.

Taking (19.28) into account and substituting the expressions for the p-n junction negative resistance (19.1) and the approximating function (19.24) into (19.27), we derive an expression for the maximum value of the diode output power:

$$P_{\text{д}\,\max} = \frac{A}{n}\,\frac{\beta^2(1-\beta^2)}{0{,}9+3(\beta^2)^2}, \tag{19.29}$$

where

$$A = 0{,}08\,\frac{1}{\omega C}\,\frac{1-\cos\theta}{\theta}.$$

It follows from (19.29) that an optimal value of the parameter $\beta^2_{opt} = 0.325$ or an optimum value of the direct current $I_{0\ opt} = 0.325$ corresponds to the maximum delivered power. For IMPATT diodes which are known at the present time, as a rule, $I_{0\ opt}$ exceeds the maximum permissible current $I_{0\ per}$, and therefore, the power $P_{d\ max}$ is limited in practice by the permissible thermal operating conditions of a diode.

For $I_0 < I_{0\ per}$, the dependence of the output power on the direct current is close to a linear function:

$$P_{d\ max} \approx kI_0 \qquad P_{\text{п}\,\max} \simeq kI_0, \tag{19.30}$$

where the coefficient $k = 4.4$ W/A for a 2A706 type diode.

The range of frequencies where the power does not fall below an indicated level, for example, 100 mW for a 2A706A diode, is usually indicated in the data sheet. In this case, the power delivered by the diode may also be greater in the center of the working band. We will note that the use of a diode is permitted in a wider range of frequencies, however, the data sheet value of the output power is not guaranteed in this case.

For a diode with set parameters (A = const.), by solving equation (19.29) one can determine the parameter β^2, and consequently, the direct current I_0 needed to obtain the specified diode output power:

$$\beta^2 = \frac{1-\sqrt{1-3{,}6a\,(3a+1)}}{2\,(3a+1)}, \tag{19.31}$$

where

$$a = P_{\text{п}\,\max}\, n/A.$$

It follows from (19.31) that the maximum value of the parameter a is limited by the condition $a \leq 0.18$, which is physically explained by the limitation on the maximum output power which can be obtained per unit area of the IMPATT diode p-n junction.

In the presence of losses in the external microwave circuit, the power dissipated in the load is:

$$P_{load} = \qquad P_{\text{н}} = P_{\text{п}\,\max}\,\eta_{\text{к}}, \tag{19.32}$$

where η_k is the resonant circuit efficiency (the efficiency of the external microwave circuit).

An optimal value of the p-n junction resistance corresponds to the maximum power level produced by the p-n junction, where this resistance is defined as follows for $I_m = I_{m\ opt}$ taking (19.28), (19.15) and (19.16) into account:

$$R_{p\text{-}n\,opt} = R_{p\text{-}n}(0)\,nq/2. \tag{19.33}$$

Since the amplitude balance condition (19.23a) must be met in the steady-state self-excited oscillation mode, a definite load resistance corresponds to the maximum value of $P_{d\ max}$, where this resistance is transformed to the "terminals" of the p-n junction:

$$R_{load\ opt} = R_{p\text{-}n\ opt} \qquad R_{н\,opt} = R_{p\text{-}n\,opt}. \tag{19.34}$$

In the case of known diode package parameters L_k, C_k and R_s, this resistance can always be referenced to the diode input terminals (19.5). Thus, in an osicllating mode, the load resistance governs the amplitude of the current flowing through the p-n junction, and is chosen so as to assure a maximum diode output power for a specified supply current I_0.

In this case, since the negative resistance of an IMPATT diode p-n junction is rather low (approximately 10 ohms), while the load resistance also includes the diode loss resistance R_S (a few ohms), the attainable microwave circuit efficiency is usually low:

$$\eta_k \leqq 0.5 \text{ -- } 0.6 \qquad \eta_к \leqslant 0{,}5 \ldots 0{,}6. \tag{19.35}$$

The reactance of the external microwave circuit X_H [X_{load}], transformed to the "terminals" of the p-n junction, is determined from the phase balance condition at the working frequency (19.23b).

The quantity $X_{p\text{-}n}$ (or X_d) in the operating mode is determined by relationships (19.2) - (19.4) and (19.6) for a specified supply current of I_0 = const.

When designing an IMPATT diode oscillator, the working frequency f_0 and the requisite power P_{load} are usually specified. Based on the relationships given here, the following design procedure can be recommended for an oscillator:

1. We select a diode for which the output power at the specified frequency is greater than (or equal to) the requisite value P_H [P_{load}]. We determine the characteristic current I_x (19.14) at the specified frequency.

2. We determine the power delivered by the diode using formula (19.32), specifying the efficiency of the external microwave circuit, η_k, based on relationship (19.35).

3. We determine the value of the parameter β^2 needed to obtain the requisite power $P_{d\ max}$ and the diode direct current I_0 based on expressions (19.31) and (19.10).

If the diode operating current I_0 is specified (for example, it is indicated for the individual diode package), then the value of β^2 can be determined from formula (19.10). Usually, the value of the current corresponding to a definite indicated input power $P_{H\ max}$ is indicated on the data sheet. The current corresponding to any other value of the output power, $P_H \leq P_{H\ max}$, is determined by relationship (19.30), where the coefficient k is found for the indicated values of I_0 and $P_{H\ max}$.

We determine the maximum permissible diode current $I_{0\ per}$ (19.12) for the given temperature T_0, taking (19.13) into account, and we check for the condition that $I_0 < I_{0\ per}$.

We determine the resistive component of the load impedance R_H using formulas (19.34), (19.33), (19.28), (19.24) and (19.1).

5. We determine the reactive component of the load impedance X_H from formulas (19.23) and (19.2).

6. We select the circuit configuration and structural design of the oscillator and calculate the geometric dimensions of the oscillator microwave circuit components for the known values of R_H, X_H and the diode package parameters L_k, C_k and R_S.

The design of an IMPATT diode amplifier coincides in many respects with the design of an oscillator. We shall consider the specific the specific features of the design calculations for a reflective type of IMPATT diode amplifier, in which the resonator containing the IMPATT diode is coupled to the input microwave signal source and the load by means of a ferrite circulator as shown in Figure 19.12. If the diode inserted in the resonator has a negative resistance, then the input resistance of the resonator, which is the load on the line connecting the resonator to the circulator is negative at the section a-a. In this case, the power of the wave reflected from the resonator input exceeds the power of the incident wave, which is equal to the power of the input signal source P_{in}, by an amount P_y, which is equal to the power delivered by the diode (without taking resonator losses into account). In the absence of losses in the line connecting the resonator to the circulator, and in the circulator, the power dissipated in the load, P_H, is equal to the power of the reflected wave, and consequently:

$$P_{load} = P_{in} + P_y = \qquad P_{н} = P_{вх} + P_{у}. \tag{19.36}$$

The power gain is the ratio:

$$K_P = \frac{P_н}{P_{вх}} = \frac{P_{вх} + P_у}{P_{вх}} = 1 + \frac{P_у}{P_{вх}}, \tag{19.37}$$

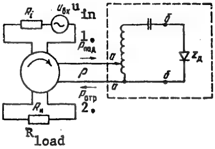

Figure 19.12. A reflective type IMPATT diode amplifier.

Key: 1. $P_{incident}$;
2. $P_{reflected}$.

or, since the input signal source and the load are matched to the circulator:

$$K_P = \frac{P_{отр}}{P_{пад}} = |\Gamma_a|^2 = \left|\frac{z_a - \rho}{z_a + \rho}\right|^2. \tag{19.38}$$

Here P_{OTP} and $P_{пад}$ are the reflected and incident wave power; Γ_a is the coefficient of reflection from the resonator input (at the section a-a); z_a is the resonator input impedance; ρ is the characteristic impedance of the circulator input line.

If we neglect the losses in the resonator, then the power dissipated at the resonator input is equal to the power delivered by the diode:

$$P_у = P_д, \tag{19.39}$$

and the reflection factor from the resonator input is equal to the reflection factor from the diode (at section b-b):

$$\Gamma_a = \Gamma_b = (z_н - z_д)/(z_н + z_д), \tag{19.40}$$

where z_H is the impedance of the external circuit connected to the diode.

Taking (19.40) into account, we represent expression (19.38) in the form:

$$K_P = \left|\frac{(R_н - r_д)^2 + j(X_н + X_д)^2}{(R_н + r_д)^2 + j(X_н + X_д)^2}\right|^2.$$

From this we derive the following for the resonant frequency when the condition $X_{load} + X_d = 0$:

$$K_{P0} = \left|\frac{R_н - r_д}{R_н + r_д}\right|^2 = \left|\frac{1+\alpha}{1-\alpha}\right|^2, \tag{19.41}$$

where $\alpha = -r_d/R_{load}$ is the regeneration coefficient. (19.42)

$$\alpha = -r_д/R_н$$

When operating as an amplifier, the amplitude of the alternating current flowing through the p-n junction, for a specified load resistance, increases with an increase in the input signal power. In this case, since the diode resistance decreases with an increase in the amplitude of the current, then the gain decreases with an increase in the input signal power, as follows from (19.41). The power delivered by the diode expressed as a function of the input signal power has a maximum at a certain value $P_{in} = P_{in\ opt}$ corresponding to the optimum value of the current amplitude $I_m = I_{m\ opt}$ (19.26).

To obtain the maximum output power, the amplifier operating conditions are chosen so that $P_{in} = P_{in\ opt}$. In this case, the power delivered by the diode does not depend on the load resistance, as follows from (19.27), and this resistance is determined from the condition for assuring the necessary gain at the requisite output power.

The gain corresponding to the maximum output power is determined by the following expression based on (19.41), (19.42), (19.33), (19.28), (19.24) and (19.1):

$$K_{P\,\text{opt}} = \left[\frac{(1+0{,}5q)\sqrt{K_{P0}} + (1-0{,}5q)}{(1-0{,}5q)\sqrt{K_{P0}} + (1+0{,}5q)} \right], \qquad (19.43)$$

where

where K_{P0} is the small signal gain, defined by relationship (19.41) for low input signal power levels ($P_{in} \ll P_{d\ max}$).

It follows from (19.43) that the operating gain of an amplifier (the mode corresponding to the maximum output power) is always less than the small signal value and increases with an increase in the latter. When selecting the small signal gain, it is necessary to take into account the fact that to assure amplifier stability under actual operating conditions, the following condition should be met:

$$K_{P0} < 20 \text{ dB} \qquad K_{P0} < 20 \text{ дБ}. \qquad (19.44)$$

We derive the expression for the power of the input signal source and the power dissipated in the load resistance in the maximum output power output mode taking (19.39), (19.34) and (19.37) into account:

$$P_{\text{вх opt}} = P_{\text{д max}}/(K_{P\,\text{opt}} - 1), \qquad (19.45)$$

$$P_{\text{н opt}} = P_{\text{д max}}\, K_{P\,\text{opt}}/(K_{P\,\text{opt}} - 1). \qquad (19.46)$$

When designing an amplifier, just as an oscillator, the values of f_0 and P_{load} are usually specified. The following design procedure can be recommended for an amplifier in a maximum power output mode based on the relationships given above.

1. Assuming $K_{p\ opt} >> 1$ and taking $P_{load\ opt} = P_{d\ max}$ based on (19.46), we select a diode which assures the requisite output power at the specified frequency and determine its characteristic current I_x, employing expression (19.14).

2. We determine the parameters β^2 and q from formulas (19.31) and (19.24) as well as the value of the diode direct current I_0 from formula (19.10).

3. Having specified the value of K_{p0} in accordance with expression (19.44), we determine $K_{p\ opt}$ from formula (19.43) as well as the input signal power P_{opt} and the power dissipated in the load, $P_{load\ opt}$ from formulas (19.45), (19.46), (19.4) and (19.27).

4. We determine the resistive component of the load impedance R_{load} from formulas (19.42), (19.41), (19.33), (19.28), (19.24), (19.5) and (19.1).

5. We determine the reactive component of the load impedance X_{load} from formulas (19.23a), (19.6) and (19.2).

6. We calculate the structural design parameters of the microwave network from the specified values of the load impedance.

Chapter 20. THE STRUCTURAL DESIGN OF MICROWAVE HYBRID INTEGRATED CIRCUIT COMPONENTS

20.1. General Information

Elements with lumped parameters, inductance coils and capacitors as well as with distributed parameters, in the form of sections of unbalanced strip transmission lines are used in the microwave band in hybrid integrated circuits (GIS) at frequencies above 300 MHz.

The use of elements with lumped parameters in hybrid IC's became possible because of the success of modern film technology which makes it possible to assure a high resolution when applying very narrow conducting strips on a dielectric substrate.

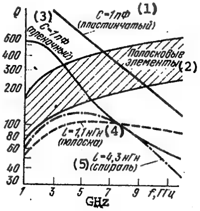

Figure 20.1. The Q of the components of microwave circuits as a function of frequency.

Key:
1. C = 1 pFd (plate capacitor);
2. Stripline elements;
3. C = 1 pFd (film);
4. L = 1.1 nHy (small strips);
5. L = 4.3 nHy (spiral).

Inductance coils and capacitors have the properties of elements with lumped parameters if their geometric dimensions are small as compared to the working wavelength λ: approximately 0.05 to 0.01 λ [1, 3]. If this condition is met, then the well known procedure and formulas for design calculations of coils and capacitors operating at lower frequencies can be used in the calculation of the inductance of coils and the capacitance of capacitors.

Planar printed circuit inductance coils of various shapes and capacitors in the form of plate (three-layer) or comb (single-layer) structures are usually employed in hybrid IC's using microwave components with lumped parameters. Ready-made outboard capacitors, for example, miniature noninductive K10-42 capacitors, are rather widely used in hybrid IC's.

The Q of flat inductance coils at frequencies of from 1 to 8 GHz amounts to 50 to 100, while it is 100 to 600 for film capacitors, which is altogether sufficient for any circuits of practical devices, for example, transistor microwave amplifiers and oscillators. However, the technological difficulties in the fabrication of the elements increase with an increase in frequency and the losses in the elements also increase where these losses are due to the small surface of the conductors.

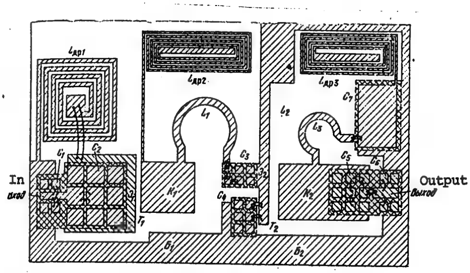
Lдр1
Lдр2
Lдр3
L1
L2
L3
C1
C2
C3
C4
C5
C6
C7
Э1
Э2
K1
K2
T1
T2
Б1
Б2
In
Вход
Output
Выход

Figure 20.2. The hybrid integrated circuit for a decimeter band, two stage transistor power amplifier (Э, Б, K are the connection points for the leads of transistors T_1 and T_2 [the emitter, base and collector leads respectively]).

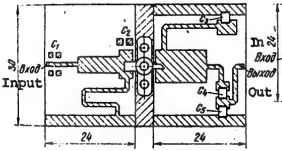
30
Вход
Input
C1
C2
C3
C4
C5
Выход
Out
24
24

Figure 20.3. The circuit board structure of a transistor power amplifier (P_{out} = 4 watts; f = GHz).

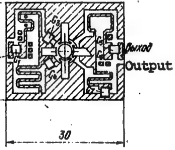
In
Вход
24
C1
C2
C3
C4
Выход
Output
30

Figure 20.4. The hybrid integrated circuit of a transistor, decimeter band power amplifier (P_{out} is 7 to 9 watts).

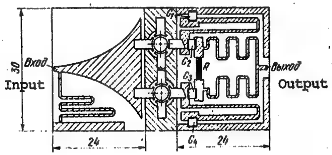
30
Вход
Input
C1
C2
C3
C4
R
Выход
Output
24
24

Figure 20.5. The circuit board structure of a power amplifier using two transistors with power adding in the output circuit.

Sections of an asymmetrical strip transmission line - so-called stripline elements - are the most widespread microwave components of hybrid IC's. Their major advantages are the rather simple structural design and reliability. The substrates of stripline elements usually have a high relative dielectric permittivity ($\varepsilon > 7$). Such elements have been given the name of microstripline elements.

Microwave elements using asymmetrical striplines at frequencies of from 1 to 10 GHz have a Q of 100 to 400. Curves for the Q are shown in Figure 20.1 as a function of frequency for stripline elements and elements with lumped parameters. The graphs show that at frequencies above 3 to 5 GHz, the Q of stripline elements is higher than the Q of elements with lumped parameters.

When designing hybrid IC's, the choice of elements with lumped parameters or stripline elements depends on the requisite electrical and structural design characteristics of the hybrid IC's. Combinations of the various elements are frequently used in practical microwave circuits.

The fine tuning of hybrid IC's entails considerable technological difficulties. For this reason, it is extremely important in the design of hybrid IC's to execute the structural design calculations of the elements with the least error so as to almost completely preclude substantial adjustments to the fabricated circuitry. Examples of hybrid IC's using microwave power transistors are shown in Figures 20.2--20.5.

20.2. The Asymmetrical Transmission Stripline

In the fabrication of printed circuits with asymmetrical strip transmission lines, the conducting strips and the metallized surface are made on opposite sides of the dielectric substrate (Figure 20.6).

A mode close to the T mode propagates in an asymmetrical stripline. Since the dielectric permittivity of the substrate is usually rather high, then the field of the mode propagating along the line is primarily concentrated in the dielectric under the conducting strip. The edge field which occurs during the propagation of the wave in the line where this field is due to the finite width w of the conducting strip, is partially in the air medium above the dielectric. The presence of this field leads to radiation power losses and the creation of parasitic coupling between the conducting striplines forming the circuit of the microwave device. It is recommended [1] that the conducting strips be spaced a distance apart equal to three times the thickness of the dielectric substrate to attenuate this coupling.

To reduce the losses to radiation and eliminate the influence of the line radiation field on the operation of adjacent microwave units, a device using asymmetrical striplines is frequently housed in a closed metal package, which plays the part of a shield. The presence of a shield can exert a marked influence on the operational conditions of a stripline, leading to a change in the wavelength in the line and to the excitation of higher modes in it. In particular, a group of surface waves is excited in a stripline having a substrate made of a

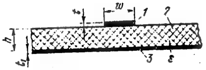

Figure 20.6. Cross-section through an asymmetrical strip transmission line.

Key: 1. Conducting strip;
2. Dielectric substrate;
3. Metalized surface.

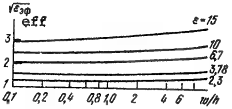

Figure 20.7. The relative effective dielectric permittivity as a function of the ratio w/h for various values of ε.

material with a high relative dielectric permittivity ε. The critical frequency of a low order surface mode [1] is:

f_{cr} [GHz] =

$$f_{кр}\,[ГГц] = c/4h\sqrt{\varepsilon-1} = 75/h\sqrt{\varepsilon-1}, \quad (20.1)$$

where $c = 3 \cdot 10^{11}$ mm/sec is the speed of light in free space; h is the substrate thickness in mm.

The substrate thickness for which a surface wave appears at the working frequency f can be determined from formula (20.1):

$$h_{max} = 75/f\sqrt{\varepsilon-1}. \quad (20.2)$$

In order to prevent operation close to the critical frequency, the substrate thickness of a stripline should be less than h_{max}.

The influence of a shield on the operation of an asymmetrical stripline can be reduced by selecting the distance from the stripline to the walls of the shield. Thus, the shield height H above a stripline should be considerably greater than the substrate thickness. For a line where $\varepsilon > 7$, it is recommended that $H \geq 6...10h$ [014]. The side walls of a shield should be spaced from the edges of the stripline at a distance at least equal to 3h.

When a nondispersive wave close to a T mode propagates in an asymmetrical stripline, the wavelength in the line is [2]:

$$\lambda \simeq \lambda_0/\sqrt{\varepsilon_{eff}}. \qquad \lambda \simeq \lambda_0/\sqrt{\varepsilon_{эф}}, \quad (20.3)$$

where λ_0 is the wavelength in free space; ε_{eff} is the relative effective dielectric permittivity. The quantity ε_{eff} depends on the ratio w/h, the dielectric permittivity of the substrate material ε, the configuration of the boundary between the air ($\varepsilon = 1$) and the dielectric ($\varepsilon > 1$) media and can be calculated from the approximate formula [3]:

$$\varepsilon_{эф} = 0{,}5\,(\varepsilon+1) + 0{,}5\,(\varepsilon-1)\,(1+10h/w)^{-0.5}. \quad (20.4)$$

Based on the estimate given in the literature [2], the error in calculating $\sqrt{\varepsilon_{eff}}$ using formula (20.4) amounts to ± 1%. Curves for $\sqrt{\varepsilon_{eff}}$ are shown in Figure 20.7 as a function of w/h for various values of the relative dielectric permittivity of the substrate material.

When designing hybrid IC's using asymmetrical striplines, the quantity $\sqrt{\varepsilon_{eff}}$ serves as a measure of the decrease in the geometric dimensions of the conducting stripline. Thus, when the electrical length of a line section $\phi = 2\pi l/\lambda_0 = 2\pi l_\varepsilon/\lambda$ is kept constant, the length l_ε of a stripline segment with a substrate made of a dielectric where $\varepsilon > 1$ falls off by a factor $\sqrt{\varepsilon_{eff}}$ times as compared to the length l of the line section with an air dielectric ($\varepsilon = 1$):

$$l_\varepsilon = l/\sqrt{\varepsilon_{eff}} \qquad l_\varepsilon = l/\sqrt{\varepsilon_{эф}}. \tag{20.5}$$

The characteristic impedance of an asymmetrical stripline can be calculated as follows [2]:

$$\rho = \rho_0/\sqrt{\varepsilon_{эф}}. \tag{20.6}$$

Here, ρ_0 is the characteristic impedance of a stripline where $\varepsilon = 1$, in ohms. For $w/h \leq 1$:

$$\rho_0 = 60 \ln (8h/w + w/4h), \tag{20.7}$$

while for $w/h > 1$:

$$\rho_0 = \frac{120\pi}{w/h + 2,42 - 0,44h/w + (1 - h/w)^6}. \tag{20.8}$$

The error in calculating ρ_0 using these formulas amounts to ± 0.25% when w/h = 0...10 and ± 1% when w/h > 10 [2].

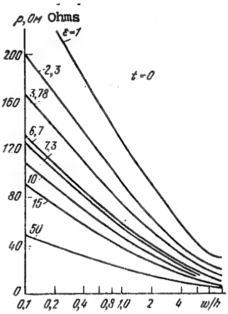

Figure 20.8. The characteristic impedance of an asymmetrical stripline as a function of the ratio w/h for various values of ε.

Curves for the characteristic impedance ρ are shown in Figure 20.8 as a function of w/h for various values of the relative dielectric permittivity of the substrate, where these curves were calculated in accordance with formula (20.6), using formulas (20.4), (20.7) and (20.8). It was assumed in the calculations that the thickness of the conducting strip was t = 0. In reality, t is a finite quantity. It is sufficient in practical cases for the thickness t to be 3 to 5 times greater than the penetration depth Δ (Δ is the distance from the conductor surface at which the amplitude of the current density falls off by a factor of e = 2.718 times). The values of Δ for various metals are given in Table 20.1, where the major characteristics of the conductors are also shown. When w/h > 0.1, this thickness has little influence on the characteristic impedance of a line, and for this reason, one can assume $t \simeq 0$ when computing it.

The characteristic impedance of an asymmetrical stripline (if it is not specified in the design plan) is frequently chosen equal to 50 ohms for convenience in

TABLE 20.1.

(1) Материал проводника	σ, 10^7 См/м	Δ, $10^4/\sqrt{f}$, мкм Micrometers	R_{11}, $10^{-7}\sqrt{f}$ Ом/□	(2) ТКР, 10^{-6} $\frac{1}{°C}$	Адгезия Adhesion
Ag	6,17	6,41	2,5	21	Плохая Poor
Cu	5,8	6,6	2,6	18	Очень плохая Very poor
Au	4,1	7,86	3	15	Та же The same
Al	3,72	8,24	3,3	26	Плохая Poor
W	1,78	11,88	4,7	4,6	Хорошая Good
Mo	1,76	12	4,7	6	» »
Ni	1,14	1,38	55,0	15	»
Cr	0,77	18,07	7,2	9	Очень хорошая Very good
Ta	0,64	19,78	7,2	6,6	Та же The same

Note: f is the frequency in Hz.

Key:
1. Conductor material;
2. Thermal coefficient of expansion, 10^{-6} °C^{-1}

[Conductivity σ, 10^7 mho/m].

connecting the line to radiofrequency connectors and individual microwave units. The use of line sections having a high characteristic impedance, and this means with very narrow conducting strips, is not desirable because of the technological difficulties in their fabrication and the increase in the attenuation in the line.

The attenuation in an asymmetrical stripline, α (in dB per unit of length) is composed of the attenuation due to power losses in the conductor at radiofrequencies α_m, in the dielectric α_d and the losses to radiation α_{rad}. The attenuation in a conductor, assuming that the radiofrequency current flows primarily in a surface layer of thickness Δ, can be approximately determined from formula [014, 3]:

$$\alpha_м \simeq 8{,}68 R_{11}/\rho w, \tag{20.9}$$

while the attenuation in the dielectric is:

$$\alpha_д \simeq 2{,}73 \sqrt{\varepsilon}\, \lambda^{-1}\, \mathrm{tg}\, \delta. \tag{20.10}$$

Here, R_{11} is the specific surface resistance of the current conducting layer in ohms per unit area; tanδ is the dielectric loss angle tangent.

It is difficult to estimate the attenuation in a line due to radiation and it is frequently determined experimentally.

In asymmetrical striplines where $\varepsilon > 7$ and with low losses, the major source of attenuation is the losses α_m. An analysis of formula (20.9) shows that to reduce the losses in a line, one must choose sufficiently thick substrates and wide conducting strips. However, the thickness h in this case should not come close to h_{max}. Moreover, increasing h and w leads to an increase in the line dimensions, something which is undesirable in the structural design of hybrid IC's. To reduce the impact of the thickness of a conducting strip on the value of α_m, it is recommended that t be chosen equal to or greater than 3Δ to 5Δ.

TABLE 20.2.

	Substrate Материал подложки Material	ε	tg δ	(1) Коэффициент теплопроводности, 10^{-3} Вт/(мм · °C)	ТКЛР, 10^{-7} $\frac{1}{°C}$ (2)
		$f = 10$ ГГц, $f = 20$°C GHz			
Polikor	Поликор	9,49...9,8	$1 \cdot 10^{-4}$	25...37,7	75
Sapphire	Сапфир	13,2	$1 \cdot 10^{-4}$	24	66,6
Sapphirite	Сапфирит	9,3...10,1	$1 \cdot 10^{-4}$	21...25	62
22KhS	22ХС	9,2...9,4	$10 \cdot 10^{-4}$	13,4	60
GM	ГМ	9,5...10	$(0,5...1,2) \cdot 10^{-4}$	21...25	64
Brokerit	Брокерит	6,4...6,6	$(2...5) \cdot 10^{-4}$	210	60
ST32-1	СТ32-1	10	$(3...5) \cdot 10^{-4}$	1,045	32
	СТ38-1	7,25...7,5	$(2...10) \cdot 10^{-4}$	1,31...1,4	38
	СТ50-1	8,2	$35 \cdot 10^{-4}$	31,5	50
FLAN-2,8	ФЛАН2,8	2,8	$15 \cdot 10^{-4}$		350
	ФЛАН7,2	7,2	$15 \cdot 10^{-4}$		400
	ФЛАН10	10	$15 \cdot 10^{-4}$		350
	ФЛАН16	16	$15 \cdot 10^{-4}$		250

Key: 1. Coefficient of thermal conductivity, 10^{-3} W/(mm · °C);
2. Thermal coefficient of linear expansion, 10^{-7} °C^{-1}.

When applying a conducting stripline to a dielectric substrate, the adhesion of the metal to the dielectric is taken into account. Because of the fact that copper, aluminum, gold and silver, which have a poor adhesion (see Table 20.1) are most frequently used for the conductors, a thin film of metal having a high specific resistance is initially applied to the dielectric substrate to improve the adhesion. The presence of such a film (sublayer) of thickness t_1, which is comparable to the penetration depth Δ_1 in this film, leads to an increase in the radiofrequency resistance in the conducting strip. If $t_1 \ll \Delta_1$ ($t_1/\Delta_1 < 0.2$), which is typical of many asymmetrical stripline structures, then the sublayer introduces neglectably low losses.

To reduce the losses in microwave elements using asymmetrical striplines, materials are to be used for the conductors which have a sufficiently low specific surface resistance (see Table 20.1) and dielectrics with low losses and good thermal conductivity (see Table 20.2). The Q of such elements at frequencies of 1 to 10 GHz, without taking radiation losses into account, amounts to 100 to 400.

The permissible DC current density, $j_{0\ per}$, in a conducting stripline is determined by the thermal mode of the microwave circuit elements of the amplifier/oscillator. During the design work, the following condition must be met: $j_{0\ per} > j_{0\ op}$, where $j_{0\ op}$ is the DC current density in the conducting stripline in

TABLE 20.3.

Method of Fabricating the Conducting Strip	Permissible Direct Current Density A/mm^2	
	Sitall	Ceramic
Vacuum depostion	30	200
Electrolytic build-up	30	200
Foil application	50	400

[Sitall: ceramic glass similar to pyroceram]

the operating mode. The value of $J_{0\ per}$ depends on the substrate material and the method of fabricating the line. In order to increase $j_{0\ per}$, materials are to be used for the substrates which have sufficiently good thermal conductivity. Some approximate data on the permissible DC current density, $j_{0\ per}$, are given in Table 20.3 and in the literature [6].

20.3. Printed Circuit Inductance Coils

When designing microwave networks around elements with lumped parameters, the requisite inductances of the circuits can be obtained using sections of metal strips with a rectangular cross-section: so-called strip single turn inductance coils (Figure 20.9) or strips bent in the shape of a meander (Figure 20.10) and in the shape of a spiral (Figure 20.11).

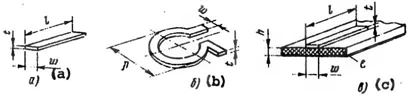

Figure 20.9. Stripline inductance coils.

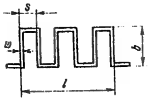

Figure 20.10. A meander type inductance coil.

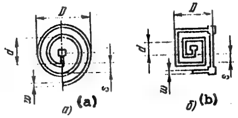

Figure 20.11. Spiral coil.

Stripline single turn inductance coils (Figure 20.9b) have inductances from 0.5 to 4 nanohenries [1]. Flat spiral coils provide for greater inductances (up to 100 nHy), where square spiral coils (Figure 20.11b) make it possible to obtain a greater inductance than in the case of circular coils (Figure 20.11a) for a specified area of the coils on a printed circuit board. The inductance of a coil in the shape of a meander (Figure 20.10) reaches 100 nHy. However, parasitic resonances are observed in these coils at frequencies substantially higher than the working frequency because of the linear sections s and b of a coil, which at high frequencies then behave as line sections with distributed parameters.

The Q of stripline single turn and spiral coils at frequencies above 1 GHz amounts to 50--100 (see Figure 20.1). Spiral inductance coils have a higher Q than single turn coils, but also a greater interturn capacitance. The Q of coils for a fixed inductance value increases in proportion to $\sqrt{f}$ up to frequencies of 5 to 6 GHz, and then falls off with an increase in frequency.

The inductance and Q of a coil depend on its geometric dimensions, as well as on the presence of metallization on the bottom side of the dielectric substrate, even when the metallized side of the dielectric substrate is a considerable distance from the plane of the coil. To preclude the influence of the metallization on coil inductance, the spacing to the metallized surface under the coil for a substrate with $\varepsilon = 10$ should exceed the width of the coil conductor w by a factor of more than 20 times [1]. In those practical cases where this requirement is not met for technological reasons, the calculation of coil inductance must be made taking into account the presence of the metallized surface. Metallization in the same plane that the inductance coil is in has little impact on its inductance, and it is sufficient in practice to make the distance from the coil to the adjacent metallized layer equal to 5 times the width of the coil conductor [1].

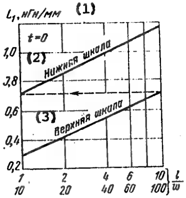

Figure 20.12. The per unit length inductance L_1 as a function of the ratio l/w for a single turn inductance coil without taking the strip thickness into account.

Key:
1. L_1, nHy/mm;
2. Lower scale;
3. Upper scale.

As a result of calculating a coil for a specified inductance, it is necessary to select its geometric dimensions such that they permit obtaining the requisite inductance and which are technologically convenient to realize.

Design Calculations of Coil Inductance. Formulas are given in Table 20.4 for calculating the inductance L or the per unit length inductance L_1 of coils, the shape and designation of the dimensions of which are given in Figures 20.9 - 20.11.

The curves for the per unit length inductance L_1 are shown in Figure 20.12 as a function of the ratio l/w when t = 0 for a single turn coil, calculated using the formula given in Table 20.4. Values of the coefficients C_n used in the calculation of the inductance of meander type coils are given in Table 20.5. The error in the determination of the inductances for these coils on the order of tens of nanohenries amounts to ± 2%, while it runs up to 6% for inductances of about 80 to 100 nHy.

TABLE 20.4

Форма катушки Coil Shape	Расчетная формула Design Formula	Длина проводника катушки Length of Coil Conductor
Single Turn Одновитковая (рис. 20.9, *а*, *б*) Fig. 20.9a, b.	$L_1=0,2\left(\ln\frac{l}{w+t}+1,193+0,2235\frac{w+t}{l}\right)$	$l=\frac{L}{L_1}$
(1) Прямоугольная полоска над металлизированной поверхностью (рис. 20.9, *в*)	$L_1=\begin{cases}0,2\left[\ln\frac{8h}{w}+\frac{1}{32}\left(\frac{w}{h}\right)^2\right], & \frac{w}{h}\leqslant 2,\ t\simeq 0,\\ \frac{0,628}{w/2h+0,9+0,318\ln(w/2h+0,94)}, & \frac{w}{h}>2,\ t\simeq 0\end{cases}$	$l=\frac{L}{L_1}$
Meander Меандр (рис. 20.10) Fig. 20.10	(2) $L=0,1b\,(4n\ln 2a/w-C_n),\ t\simeq 0,$ n — число элементов меандровой линии длиной b C_n — см. табл. 20.5	$l=nb+(n-1)(a-w)$
(3) Плоская круглая спираль (рис. 20.11, *а*)	$L=5(D+d)^2n^2/(15D-7d),\ t\simeq 0,$ $D=d+(2n-1)s+2w,$ n — число витков n is number of turns	$l=\pi n\,[d+0,5s(2n-1)]$
(4) Плоская квадратная спираль (рис. 20.11, *б*)	$L=6(D+1)^2n^2/(15D-7d),\ t\simeq 0,$ $D=d+(2n-1)s+2w,$ n — число витков n is the number of turns	$l=4n\,[d+0,5s(2n-1,5)]$

Примечание. Все линейные размеры катушек выражаются в миллиметрах, индуктивность L — в наногенри, погонная индуктивность L_1 — в наногенри на миллиметр.

Note: All of the linear dimensions of the coils are expressed in millimeters; the inductance L is in nanohenries and the per unit length inductance L_1 is in nanohenries per millimeter.

Key:
1. Rectangular strip above a metalized surface (Figure 20.9c);
2. n is the number of elements of a meander line of length b; C_n - see Table 20.5;
3. A flat circular spiral (Figure 20.11a);
4. A flat square spiral (Figure 20.11b).

TABLE 20.5.

n	2	3	4	5	6	7	8	9	10	11	12
C_n	2,76	3,92	6,22	7,60	9,70	10,92	13,38	14,92	16,86	18,46	20,36

The determination of the geometric dimensions of flat spiral coils for a specified inductance L is made using successive approximations, in which certain geometric dimensions of the coil are specified based on structural design and production process considerations and the missing dimensions are determined using the formulas for L and D. For example, having specified the ratio D/d and using the formula for L, the number of turns n is determined. Then the conductor width w is chosen based on production process considerations and the requisite coil pitch s is found by using the formula for D. If it is convenient to realize this pitch, then the design calculation is terminated at this point.

In order to be able to change the inductance of a coil, part of the coil conductor is subdivided into sections having contact pads for the connection of tap conductors to them (Figure 20.11b).

Design Calculations of the Q of an Inductance Coil. The quality factor of a coil $Q = 2\pi fL/r$ for a specified frequency f and inductance L is determined by its resistance r, which reflects the actual radiofrequency power losses in the inductance coil. This resistance is composed of the coil conductor resistance for the radiofrequency current, r_m, the resistance introduced by power losses in the dielectric substrate r_d, the resistance introduced by radiation power losses, etc. It can be assumed in practice that in a properly designed typical structure, the power losses in a coil are determined primarily by the resistance r_m. In this case, the coil Q is:

$$Q = \frac{2\pi fL}{r_м} = 10^{-9}\,\frac{4\pi fL\,(w+t)}{kR_{11}\,l}\,. \qquad (20.11)$$

Here, k is a coefficient which takes into account the degree of nonuniformity in the current distribution at the edges of the conducting strip. The value of k is determined from the graph shown in Figure 20.13.

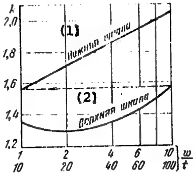

Figure 20.13. The curves for the coefficient k which takes into account the degree of nonuniformity of the current distribution at the edges of the conducting strip.

Expression (20.11) can be used to calculate flat inductance coils of various shapes made from a conductor in the form of a metal strip with a rectangular cross-section (Figure 20.9).

The Q of a single turn coil (Figure 20.9) increases with an increase in the ratio w/l, while the per unit length inductance L_1 decreases. It is frequently desirable when structurally designing such a coil to obtain a sufficiently large value of L_1 at a quality factor of $Q \geq 50...100$. For coils intended for operation at frequencies up to a few gigahertz, this condition can be met when $w/l = 15...20$.

When designing spiral inductance coils, one must consider the fact that the increase in the conductor width w leads to an increase in the coil Q. If it is desirable that the external diameter of the coil D be rather small with a high value of the Q, then it is necessary to reduce the spacing between the turns. This leads to an increase in the interwinding capacitance of the coil. An analysis of the formulas for the Q of flat spiral coils shows that the maximum Q is obtained when $D/d = 5$.

20.4. Capacitors

Primarily film plate capacitors (Figure 20.14), capacitors formed by a short section of an asymmetrical stripline with a low characteristic impedance (Figure 20.15), comb capacitors (Figure 20.16) and outboard miniature ceramic capacitors find applications in hybrid integrated circuit structures.

To tune a circuit by means of varying the capacitance, a block of parallel low capacitance capacitors is made instead of a single capacitor of the requisite nominal value. A structural design of a tunable film capacitor is shown in Figure 20.14b. The upper plate is fabricated in the form of strips of different sizes, the resoldering of which makes it possible to change the capacitance of the capacitor [5].

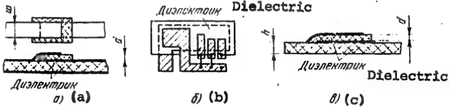

Figure 20.14. Film plate capacitors.

The typical structure of a film capacitor, which is shown in Figure 20.14c, takes the form of two metal plates, separated by a dielectric layer. The film capacitors have a weak external electromagnetic field, and for this reason, can be placed close to other microwave components.

The capacitance of film capacitors used in microwave circuits at frequencies of up to about 2 GHz amounts from a few picofarads to hundreds of picofarads [4]. The Q of such capacitors changes depending on the nominal value and the quality

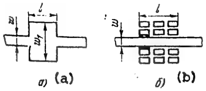

а) (a) б) (b)

Figure 20.15. Capacitors formed by a section of an asymmetrical stripline.

Key: a. With a fixed capacitance;
b. With a variable capacitance (only the conducting strip is shown).

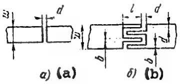

а) (a) б) (b)

Figure 20.16. A comb capacitor to obtain a series capacitance in a microwave circuit.

of the materials of the conductor and dielectric. To reduce losses in a capacitor, metals with a low specific surface resistivity (see Table 20.1) and a low loss dielectric are used for the plates. Aluminum is most frequently used for the plates of capacitors. The dielectrics of film capacitors, besides a small loss angle tangent, should have a high relative dielectric permittivity and electrical strength. Silicon monoxide is most frequently used in the fabrication of film capacitors (see Table 20.6).

A gap in a conducting strip (Figure 20.16a) produces a series capacitance in an asymmetrical stripline. To obtain a considerably capacitance (more than a few picofarads), the gap d should be quite small, something which is difficult to execute in practice. Greater capacitances (up to 10 to 20 pFd) can be obtained if a comb capacitor is used (Figure 20.16b). The capacitor formed by a gap in a strip is a special case of this. Another capacitor structure intended for creating a series capacitance in an asymmetrical stripline is shown in Figure 20.14a. The capacitor takes the form of two short sections of a stripline conductor which overlap lengthwise, where the sections are separated by a dielectric layer. The overlap area of the plates in such capacitor structures does not usually exceed 10 mm^2.

To create a capacitance which is connected in parallel to an asymmetrical stripline, one can use a capacitor in the form of a short section of asymmetrical striplines ($l \ll \lambda$) with a relatively low characteristic impedance (less than 20 ohms) (Figure 20.15). The sectional structure of the capacitor shown in Figure 20.15b makes it possible to change its capacitance.

Outboard miniature capacitors are convenient for applications in hybrid IC's intended for operation at frequencies up to a few gigahertz, since the fabrication of a circuit with such components does not require a complex technology. The Q of miniature outboard capacitors is sufficient for their use in microwave circuits of hybrid IC's in the indicated band.

When designing capacitors, it is necessary to know the relationship of the capacitance of a capacitor to its geometric dimensions and the relative dielectric

TABLE 20.6.

(1) Диэлектрик конденсатора	ε	tg δ при f=1 кГц (2)	$E_{пр}$, 10^5 В/мм (3)
SiO	5...6	0,002...0,01	1...2
SiO_2	3,6...4,2	0,0007...0,005	3...5
GeO	10...12	0,005...0,01	0,5...0,8
Al_2O_3	8 ..19	0,003	8...10

Key:
1. Capacitor dielectric;
2. Tan δ when f = 1 KHz;
3. E_{pr} [electrical strength], 10^5 V/mm.

permittivity of the dielectric used in its construction. A rigorous calculation of the capacitance of plate capacitors taking the edge effect into account is difficult, and for this reason, we shall limit ourselves to an approximate calculation.

Film Plate Capacitor (Figure 20.14c). The capacitance of a capacitor is determined from the well known formula for a plate capacitor:

C [pFd] =

$$C\,[\text{пФ}] = 8{,}85 \cdot 10^{-3}\, \varepsilon S/d. \qquad (20.12)$$

Here, ε is the relative dielectric permittivity; S is the overlap area of the plates in mm^2; d is the dielectric thickness in mm.

Dielectrics with large values of ε are used and d is reduced to increase the capacitance of a capacitor. The minimum thickness d_{min} is determined by the permissible electrical strength of the dielectric.

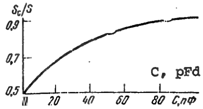

Figure 20.17. On the determination of the area of capacitor plates taking the edge effect into account.

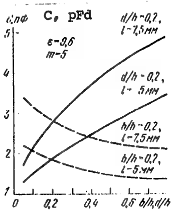

Figure 20.18. The capacitance of a comb capacitor as a function of the geometric dimensions.

For normal operation of a capacitor, the thickness of its dielectric should satisfy the condition:

$$d \geqq d_{min} = u_{work}/NE_{pr} \qquad (20.13)$$

Here, u_{work} is the working voltage between the capacitor plates in volts; E_{pr} is the electrical strength in V/mm; N is a safety factor, taken equal to 0.5--0.7.

When designing a capacitor, the dielectric material is chosen first (see Table 20.6) and then the dielectric thickness d is determined from formula (20.13).

Then, working from the specified value of the capacitance, the requisite overlap area of the plates S is found from formula (20.12). Formula (20.12) yields a somewhat overstated value of S, since it does not take edge effects into account. Because of this, a correction is to introduced into the calculated value in accordance with the approximate graph shown in Figure 20.17, in which S_c is the area taking the correction into account.

It is recommended that the plates be made wide and short so as to reduce losses in the metal plates of a capacitor as well as losses to radiation.

A Capacitor in the Form of a Short Section of Asymmetrical Stripline (Figure 20.15a). The capacitance of such a capacitor can be calculated by working from the easily determined per unit length capacitance of an asymmetrical stripline:

$$C_1\ [\mathrm{pFd/mm}] = 3.33\sqrt{\varepsilon_{eff}}/\rho \qquad C_1\,[\text{пФ/мм}] = 3{,}33\sqrt{\varepsilon_{\text{эф}}}/\rho. \tag{20.14}$$

For a specified capacitance of a capacitor C, the requisite length of a line section is $l = C/C_1$.

Comb Capacitor (Figure 20.16b). The capacitance of a capacitor formed by two "combs", arranged on a dielectric substrate ($\varepsilon > 1$) can be computed from the approximate formula:

$$C\,[\text{пФ}] \simeq 3{,}6\cdot 10^{-8}(\varepsilon+1)\,l\,\times$$
$$\times\left[1+\frac{1{,}9}{(2m-1)(1+d/b)}+3(m-1)\left(\frac{h}{d}\right)^{0{,}25}\left(\frac{b}{h}\right)^{0{,}4388}\right], \tag{20.15}$$

where m is the number of protruding lugs on one side of the capacitor; l is the length of a protruding lug in mm. The error in calculating a capacitance using formula (20.15) does not exceed ± 5%. An example of the capacitance plotted as a function of the geometric dimensions of a comb capacitor is shown in Figure 20.18.

CHAPTER 21. MICROWAVE PHASING DEVICES (PHASE SHIFTERS)

General Remarks

The development of microwave engineering is tied to success in the development of high speed electrically controlled microwave devices. Thus, controlling the phase of microwave signals in antenna equipment is accomplished by means of phase shifters which are controlled by magnetic or electrical fields.

A conditional classification of phase shifters which make it possible to continuously or discretely change the phase of microwave signals can be made using the following criteria: the operational principle and function; the permissible microwave power level (pulse, CW); the working frequency range (wavelength); the structural design (waveguide, coaxial, stripline or microstripline, etc.).

The following requirements are placed on the parameters of phase shifters [1] a working bandwidth of no less than 5 to 15 percent of the carrier frequency; a pulsed transmission power of 5 to 220 KW and an average value of 5 to 50 W; a switching time of 0.1 to 100 μsec; losses of no more than 0.5 to 1.5 dB and good matching (SWR $\leq$ 1.5).

Electrically controlled phase shifters can be designed using diverse controlled elements: semiconductor diodes with various structures (p-n, p-i-n and n-i-p-i-n), ferrites, ferroelectrics, etc. [1-4]. This is due to the function of the phase shifters and the requirements placed on them: providing a high efficiency, high electrical strength, stability of the characteristics, low control power and sufficients operational speed.

There are three methods of phase control: continuous (analog), digital and switched. In the first, the phase shift changes continuously. However, this method is difficult to implement because of the necessity of supplying continuously changing control signals. Moreover, time and temperature instabilities exert a marked influence on the phase characteristics of the phase shifters. This deficiency is also preserved in the case of digital phase control, when a number of operating points are used on the operational characteristics of analog phase shifters, and for this reason, the phase change takes place in a jump by an amount ΔΦ (discrete step). The influence of instabilities is practically eliminated in digitally switched phase shifters [OID], the phase of the electromagnetic oscillations at the output of which can assume fixed values. The stability of such phase shifters is governed by the fact that the controlled elements (ferrite rings or semiconductor diodes) operate in a mode in which only the extreme regions of their operating characteristics are used. This makes it possible to ease the requirements placed on the time and temperature stability of the switchers of digitally switched phase shifters and the controllers, since the requisite phase shift is not governed by the value of the control voltage, but rather by its presence at particular switchers.

Various controlled elements can be used in the construction of phase shifters regardless of the manner of phase control. However, p-i-n diode phase shifters with a continuous phase variation which make use of the change in the conductance component of the diode admittance are of no interest because of the large conductance losses. For this reason, p-i-n diodes are used primarily for switched phase control, for example, by means of turning transmission line sections on or off which change the overall length of the channel. A characteristic feature of phase shifters with a continous phase change is the use of controlled veractors: elements with a controllable capacitance [3]. Ferrites are used both in phase shifters with a continuous phase change and in discretely switched phase shifters [2, 4].

The major parameters of an electrically controlled phase shifter are: the phase control range $\Phi_{min} \ldots \Phi_{max}$; the losses introduced by the shifter L; the traveling wave ratio at the input (or the absolute value of the reflection factor Γ). Moreover, specific requirements can be imposed, for example, on the shape of the phase-frequency response (its linearity).

It is convenient to introduce a "phase shifter quality" parameter for the comparative evaluation of phase shifters:

$$K_\Phi \text{ [deg/dB]} = \Phi/L \qquad K_\Phi \text{ [град/дБ]} = \Phi/L.$$

Digitally switched phase shifters are completely characterized by maximum phase shift values Φ and L as well as the smallest phase jump (discrete step).

In phase shifters using ferrites, controlled by an external magnetic field, electromagnets must be used (in the majority of cases, of considerable size and weight), which have an operating speed of $10^{-6} \ldots 10^{-5}$ sec, something which limits their application. In this respect, microwave phase shifters designed around semiconductor devices are more promising, in which the phase shift is controlled with the action of an electric field. For this reason, we shall consider the operational principle, major types and characteristics of semiconductor phase shifters, as well as the procedure for determining their major parameters.

21.1. Semiconductor Phase Shifters

The change in the input impedance of semiconductor devices with the action of a control voltage is used in semiconductor phase shifters. In this case, the semiconductor device can be inserted in the channel in series or parallel, as shown in Figure 21.1, where Z and Y are the normalized impedance and admittance of the semiconductor device for a series and parallel configuration respectively:

$$z = \frac{R}{\rho_0} + j\frac{X}{\rho_0} = r + jx; \quad y = \frac{G}{Y_0} + j\frac{B}{Y_0} = g + jb, \qquad (21.1)$$

where R = 1/G and X = 1/B are the resistive and reactive components of the impedance of the semiconductor device; $\rho_0 = 1/Y_0$ is the characteristic impedance of the line in which the semiconductor device is inserted.

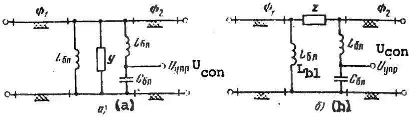

Figure 21.1. Schematic of the insertion of a semiconductor device in a line.

a. Parallel; b. Series.

The impedance of a semiconductor device can change with the action of the control voltage U_{con} of the source (Figure 21.1). Decoupling the control circuits and transmission channel is accomplished by network L_{bl} and C_{bl}. If the lower frequency ω_H in the transmitted signal spectrum is considerably higher than the maximum frequency Ω_{con} in the control voltagespectrum (which is usually the case), then the values of L_{bl} and C_{bl} are chosen from the relationship:

$$\omega_н L_{бл} \gg \rho_0 \gg 1/\omega_н C_{бл}. \tag{21.2}$$

If the frequencies ω_H and Ω_{con} are commensurate, then the control circuit and the transmission channel should be decoupled by a filter network with a cutoff frequency falling above Ω_{con} and having an attenuation (i.e., a decoupling) no worse than the specified value at the frequency ω_H. In this sense, the network L_{bl} and C_{bl} which is shown in Figure 21.1 takes the form of a very simple low pass filter (FNCh) and can be designed not only by working from expression (21.2), but also using microwave filter theory. In this case, one can provide for the guaranteed decoupling during phase shifter operation within the frequency band and in many cases, reduce the dimensions of the circuit L_{bl} and C_{bl}, by appropriately choosing the cutoff frequency of the low pass filter.

Inserting the semiconductor device (a varactor or p-i-n diode) in the line causes both a reflection of a portion of the microwave power by virtue of the mismatch at the insertion point and its partial absorption in the semiconductor device (ohmic losses).

Using wave transmission matrices, we write the resulting transmission matrix [t] for the circuit of Figure 21.1a:

$$[t]=\begin{bmatrix} t_{11} & t_{12} \\ t_{21} & t_{22} \end{bmatrix}=[t_1][t_2][t_3]\simeq$$

$$\simeq\begin{bmatrix} (1+y/2)e^{j(\Phi_1+\Phi_2)} & y/2 \\ -y/2 & (1-y/2)e^{-j(\Phi_1+\Phi)} \end{bmatrix}, \qquad (21.3)$$

where $[t_1]$ and $[t_3]$ are the transmission matrices of line sections having an electrical length of $\Phi_{1,2} = 2\pi l_{1,2}/\lambda_{line}$, where λ_{line} is the working wavelength in the line; l is the geometric length of the line; $[t_2]$ is the transmission matrix of a four-pole network with an admittance y. The approximate sign in (21.3) is due to the fact that we neglected the losses in the line itself as well as the dimensions of the semiconductor device as compared to λ.

We determine the losses L introduced by the semiconductor device into the channel from expression (21.3):

$$L = P_{in}/P_{out} = \quad L=P_{вх}/P_{вых}=10\lg|t_{11}|^2=10\lg[(1+0{,}5g)^2+(0{,}5b)^2]. \qquad (21.4)$$

In this case, the absolute value of the reflection factor is:

$$\Gamma=\sqrt{(g^2+b^2)/(4+g^2+b^2)}. \qquad (21.5)$$

Similar expressions can also be derived for the circuit of Figure 21.1b; in this case, g is replaced with r and b is replaced with x.

21.2. Semiconductor Phase Shifters with a Continuous Phase Change

In phase shifters of this type, both the resistive and reactive components of the impedance of the semiconductor device change with the action of the controlling voltage. For varactors, the change in U_{con} within the range of permissible values (with the p-n junction cut off) leads to a change in primarily the reactive component of the impedance. In this case, the change occurs in a relatively narrow range and rather smoothly. This is responsible for the use of varactors primarily in phase shifters with a continuous phase change. At the same time, the resistive component of the impedance changes in p-i-n diodes with the action of U_{con} in a wide range (changes in almost a jump), which limits their application in phase shifters with a continuous phase change.

Semiconductor phase shifters with continuous phase change can be both transmissive and reflective types.

A transmissive semiconductor phase shifter can be designed in the circuit configurations of Figure 21.1. Its operational principles consists in the fact that with a change in the capacitive susceptance (Figure 21.1a), the electrical length of the line in which this susceptance is inserted also changes. Neglecting the resistive losses of the diode, one can write the following for the phase shift introduced by the phase shifter:

$$\Phi \simeq \Phi_0 + \mathrm{arctg}\,(b/2), \qquad \Phi \approx \Phi_0 + \arctan(b/2) \tag{21.6}$$

where $\Phi_0 = \Phi_1 + \Phi_2$. $\Phi_0 = \Phi_1 + \Phi_2$.

For the circuit of Figure 21.1b, it is necessary to substitute x for b in this expression. A drawback to this circuit is the fact that in the process of controlling the phase, the phase shifter introduces considerable losses, which are caused by reflection from the controlled element [see (21.4)]. When $g < 1$, the reflection losses in a single element phase shifter are substantially greater than the resistive losses. For this reason, the quality of a simple one element phase shifter is poor: $K_\Phi \leq 15$ deg/dB.

An improvement in the parameters of a phase shifter is achieved by introducing additional devices into the circuitry (two and four pole networks), as well as by increasing the number of controlled elements.

A phase shifter circuit configuration with a compensating reactance is also possible, where an equivalent inductance in the form of a short-circuited line section is inserted in parallel with the controlled capacitance C. This line section, $l_{s.c.}$, can cancel, at a particular frequency, either the initial value of the susceptance b, due to the minimum capacitance of the element (primarily the capacitance of the package, C_k), or the value of b corresponding to the average value of the controlled capacitance. In both cases, the result is an expansion of the phase control range without increasing the insertion losses L, something which leads to an increase in K_Φ. The length $l_{s.c.}$ is determined from the condition:

$$\omega C/Y_0 = -\cot(2\pi l_{s.c.}/\lambda_{line}) \quad = \quad \omega C/Y_0 = -\mathrm{ctg}\,(2\pi l_{кз}/\lambda_{л}),$$

where C is the controlled capacitance for the control voltage selected on the volt-farad characteristic. To design a phase shifter with such compensation at a fixed frequency, the resulting susceptance b, $\cot(2\pi l_{s.c.}/\lambda_{line})$ is to be substituted in place of the susceptance b in the formulas for calculating the losses, phase shift and reflection factor.

Multiple element phase shifters based on controlled capacitances represent a cascade configuration of single element phase shifter circuits.

Increasing the number of controlled elements considerably complicates the calculation of the phase shifter parameters: the absolute value of the transmission gain and the phase shift. In this case, it is expedient to use a computer employing the tools of wave transmission and scattering matrices.

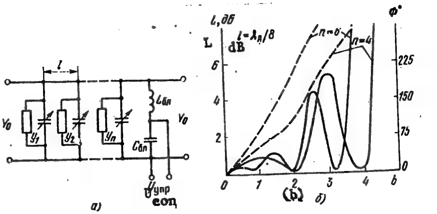

Figure 21.2. Schematic of a multiple element phase shifter with a continuous phase change (a) and its amplitude (solid curves) and phase (dashed curves) characteristics (b).

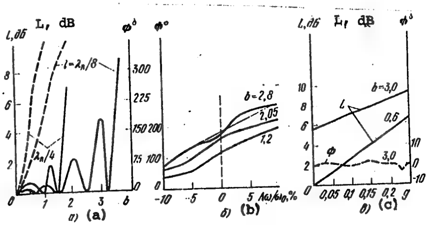

Figure 21.3. The amplitude-phase (a) and phase-frequency (b) characteristics of a nine element phase shifter; the influence of the resistive losses on the insertion attenuation and the phase shift (c).

A general equivalent circuit of a phase shifter with a continuous phase change and an arbitrary number of controlled elements is shown in Figure 21.2a. The task consists in finding the insertion losses as the coefficient of the first line of the first row of the resulting transmission matrix [t] of the entire device: $[t] = [t_1]\,[t_2] \ldots [t_n]$, where $[t_i]$ are the transmission matrices of the sections (the line sections l_1, l_2 and the controlled capacitance C(U) in the case of ideal isolating networks).

The reflection factor from the phase shifter is also determined from the values found for the coefficients of the resulting transmission matrix [t]. Thus, the characteristics of multiple element phase shifters are: a range of phase change of $\Phi_{min} \ldots \Phi_{max}$, the insertion losses L and the absolute value of the reflection factor Γ; these are defined as functions of the normalized admittance of the controlled capacitance C(U).

In a phase shifter with n identical equidistantly spaced varactors, by virtue of the change in their capacitance from C_{min} to C_{max}:

$$\Phi \simeq -n\left(\operatorname{arctg}\frac{\omega C_{max}}{2Y_0}-\operatorname{arctg}\frac{\omega C_{min}}{2Y_0}\right).$$

Here, the influence of multiple reflections between varactors on the phase shift was not taken into account, which is permissible in a first approximation if their reflection factors with respect to the absolute value of Γ 1, ..., n $\leq$ 0.25.

The formula cited here can serve as the basis for selecting the number of elements in the design of a phase shifter. Characteristics of phase shifters with a continuous phase change for various numbers of equidistantly spaced control elements [3] are available at the present time which have been calculated on a computer and plotted.

The case where the resistive losses in the controlled elements can be neglected (g = 0) is of practical interest, and then the losses in a phase shifter are determined only by the reflection losses. The amplitude and phase characteristics of phase shifter with different numbers of elements are shown in Figure 21.2b for this case. It follows from the figures that with an increase in the number of elements, the phase shift is practically proportional to the reactive component; the nonuniformity in the characteristics of the insertion losses increases with an increase in the number of elements.

The influence of the spacing between elements on phase shifter parameters is illustrated in figure 21.3a. Depending on this spacing, the slope of the phase characteristic (the dashed lines) also changes as does the nonuniformity of the insertion losses (the solid lines). Based on the curves of Figure 21.3a, one can determine the attainable minimal insertion losses and their nonuniformity for a specified Φ in a specified range of frequencies. The inverse problem can also be solved: find the range of frequencies within which the permissible insertion losses L are preserved with the attainable value of Φ. (In this case, it is necessary to keep in mind the feasible range of change in b.) One can also estimate the bandwidth of a phase shifter, comparing its characteristics for various spacings between the elements, i.e., for different electrical lengths of the line sections.

It can be seen from Figure 21.3b that in step with an increase in the normalized capacitive admittance, the nonlinearity of the phase characteristic increases within the passband.

Where there are resistive losses in the controlled elements, the phase relationships in a multiple element phase shifter practically do not change. A practically linear relationship exists between the insertion losses of a phase shifter and the conductance component of the admittance of the controlled capacitance (Figure 21.3c).

Some general requirements for the parameters of controlled elements can be formulated based on the characteristics treated here and optimal circuit design approaches can be found. These requirements can be reduced to the following. The maximum capacitances of controlled phase shifter elements with a continuous phase change should not have a normalized susceptance of $b \geq 2.5$ to 3. Otherwise, it is impossible to obtain operationally acceptable values of the amplitude modulation level during the phase control process in the frequency passband. If it is necessary to have low values of the SWR for a specified change in the phase shift Φ, then the number of controlled elements is to be increased and the maximum capacitive susceptance b reduced. However, with a significant increase in the number of elements ($n > 9$ to 10), the resistive losses corresponding, for example, to $g = 0.1$, yield too much attenuation.

With certain requirements placed on the working frequency range, a positioning of the elements where $l = \lambda_{line}/4$ can prove to be optimal. Then the quality of the phase shifter increases because of the increase in the slope of the phase characteristic and the possibility of reducing the number of controlled elements.

Thus, while the quality of a single element phase shifter is primarily determined by its reflection losses, the quality of a multiple element phase shifter depends on the value of the normalized conductance g of the controlled element.

As a rule, the major components of reflective phase shifters with a continuous phase change are short-circuited line sections with varactors; reflecting sections. They can be connected to the common channel either directly or through multipole networks (Figure 21.4). The controlled elements regulate the signal phase on the path to the short-circuiter and back. The characteristics of a reflective multi-element phase shifter are calculated using the same method as for a transmissive one, but the values of the parameters obtained as a result of the calculation are doubled (with the exception of the phase shifter quality, $K_\Phi = 2\Phi/2L$).

A 3 dB directional coupler (slotted and loop bridges) or some other multipole network which posses similar characteristics can be used to segregate the incident and reflected waves. The insertion of the controlled elements by means of the indicated multipole network on the whole forms a transmissive phase shifter configuration (see Figure 21.4). In the circuit of Figure 21.4a., the directional coupler is loaded at the outputs (2 and 3) into reflective phase shifters, which in the general case each contain one or more controlled elements.

In the case of identical reflecting sections with a single controlled element without resistive losses and an ideal directional coupler, the insertion phase shift is equal to twice the phase shift provided by a short-circuited line section and the controlled element [3]:

$$\Phi = \operatorname{arctg} \frac{-2\,[b - \operatorname{ctg}(2\pi l/\lambda_л)]}{1 - [b - \operatorname{ctg}(2\pi l/\lambda_л)]^2},$$

where $b = \omega C/Y_0$ is the normalized capacitive susceptance of the varactor; l is the distance from the element to the short-circuiter of the reflecting section.

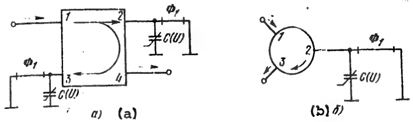

Figure 21.4. Circuits of reflective phase shifters using a 3 dB bridge (a) and a circulator (b).

Circulators can be used to separate the incident and reflected waves in reflective phase shifters (Figure 21.4b). Such a phase shifter can also contain different numbers of controlled elements. The insertion shift for a phase shifter with one controlled element is determined in a manner similar to that for a phase shifter with a bridge circuit. Two controlled elements (varactors) in a reflecting section are sufficient to change the phase shift from 0 to 360°.

It follows from the analysis of semiconductor phase shifter operation that they have a comparatively poor quality K_Φ and considerable nonuniformity of the insertion losses within the range of phase change. The indicated drawbacks limit the range of applications of these phase shifters.

21.3. Discretely Switched Semiconductor Phase Shifters

As is well known [1] p-i-n diodes can sharply change (with a jump) the resistive component of the impedance in a wide range with the action of a control voltage U_{con}; however, the reactive component is small and almost does not change at all. The sharp change in the diode impedance is used in discretely switched phase shifters*. In this case, the ohmic losses in the diode are small, since the following conditions are met (for the parallel insertion of the diode in the line):

---

*In the following, we shall call a discretely switched phase shifter simply a discrete [digital] phase shifter for the sake of simplicity.

$$Y_1 \simeq g_1 = \rho_0/r_{for} >> 1; \qquad Y_2 \simeq g_2 = \rho_0/r_{inv} << 1 \qquad (21.7)$$

$$y_1 \simeq g_1 = \rho_0/r_{\text{пр}} \gg 1, \quad y_2 \simeq g_2 = \rho_0/r_{\text{обр}} \ll 1,$$

where Y_1 and Y_2 are the p-i-n diode admittances for the forward and inverse bias modes respectively; ρ_0 is the characteristic impedance of the line (see Figure 21.1a) in which the p-i-n diode is inserted.

In expressions (21.7), the reactive components of the diode admittance b_1 and b_2 are taken equal to zero. When g_2 from (217) is substituted in (21.4) and (21.5), it is not difficult to convince onself that the losses in the diode and absolute value of the reflection factor are small. This is explained by the fact that the inverse resistance of the diode r_{inv} is high and it practically does not shunt the transmission line.

If the value of g_1 from (21.7) is substituted in the same equations (21.4) and (21.5), then we obtain greater losses and a higher value of Γ: practically all of the power is reflected [this follows from (21.5) when $g_1 >> 1$ and $b_1 \simeq 0$ are substituted].

The nearly total reflection of the power from the diode in the case of forward bias can be employed, for example, to design a reflective phase shifter. If a radio frequency signal is fed to the input of the circuit of Figure 21.1a and the output is short-circuited then such a reflective phase shifter provides for two insertion phase delays: with forward biasing of the diode, the wave is reflected from the diode, and with inverse biasing, it is reflected from the short-circuited end of the line. The difference between the insertion phase delays is a discrete step (jump) in the phase of such a phase shifter.

The series insertion of a diode can be treated in a similar fashion (Figure 21.1b). In this case, the diode opens the line in the case of inverse biasing and allows a wave to pass through low insertion losses in the case of forward biasing. By using two or more diodes and the appropriate circuit designs, one can provide for switching the microwave power from one line to another. This circumstance is also utilized in digital semiconductor phase shifters.

Digital semiconductor phase shifters make it possible to eliminate the majority of deficiencies inherent in continuous semiconductor phase shifters, specifically: improve the quality factor ($K_\phi \simeq 200$ deg/dB), reduce the SWR (K_{st} [SWR] ≤ 1.5), equalize losses for various phase shifts and control large microwave power levels (especially in a reflection mode). The possiblity of obtaining the characteristics enumerated above in a wide frequency band (up to an octave and more) is also important, something which makes it possible to use such phase shifters in phased antenna arrays. The possibility of obtaining the requisite phase-frequency characteristics and assuring stability also promotes this to no small extent.

The design calculations for discrete semiconductor phase shifters are carried out using matrix analysis tools.

The operational principle of digital semiconductor phase shifters is rather simple. The large number of circuit designs which have been realized at the present time is due to the widescale use of phse shifters of this type. For this reason, primarily the specific features of the circuit design solutions for digital phase shifters of various types to obtain a requisite phase characteristic and the specific operatonal features with such a characteristic are treated in the following, and where necessary, the design equations are given. The treatment takes into account the predominant application of digital phase shifters in phased arrays.

We shall initially consider digital phase shifters which make it possible to obtain only one discrete phase step, and then we will show how by using them as component elements in multiple element discrete phase shifters, one can obtain the requisite number of discrete phase steps.

Semiconductor digital phase shifters can be broken down into three main groups according to the operational principle: with switched line sections (Figure 21.5a), reflective with incident and reflected wave isolators (Figure 21.5b, c) and the periodically loaded line type (Figure 21.5d, e) [5].

Phase shifters using switched line sections are the simplest and most obvious in terms of the operational principle. The difference in the electrical length of the line section corresponds to the phase shift of $\Delta\Phi = \Phi_2 - \Phi_1$ (Figure 21.5a).

The following can be numbered among the advantages of phase shifters of this group: the diodes have practically the same insertion losses for both values of the phase delay (slight deviations are possible only by virtue of the change in the length of the switched line sections); the circuit is convenient for microstripline fabrication; it is compact (especially for small phase shifts). The drawbacks are: the relatively large number of diodes (up to four per phase shifter element); the necessity of supplying control signals of different polarities; phase shifter losses do not depend on the phase shift, while in all other groups of phase shifters, the losses fall off with a decrease in the phase shift [5].

Phase shifters of the second group have become widespread (Figure 21.5b, c). Both reciprocal multipole networks (directional couplers, bridges) and nonreciprocal (most often circulators) are used as the device to segregate the incident and reflected waves. In this case, the energy reflected from the diodes falls entirely in the output arm of the multipole network. The phase shift itself (discrete phase step) at the output of the phase shifters of the second group is formed by virtue of the phase change in the reflection factor when the diodes are switched in the appropriate line section, which are connected to the separating device: $\Delta\Phi = \arg(\Gamma_1/\Gamma_2)$.

Merits of phase shifters in this group are the minimum number of diodes which are used (down to one per element) for any phase shift, as well as the possibility of separate optimization of the isolation device (with respect to decoupling and matching) and the manner of inserting the diodes (based on the requisite phase function within the passband, the balance of the insertion losses in the two phase states, etc.).

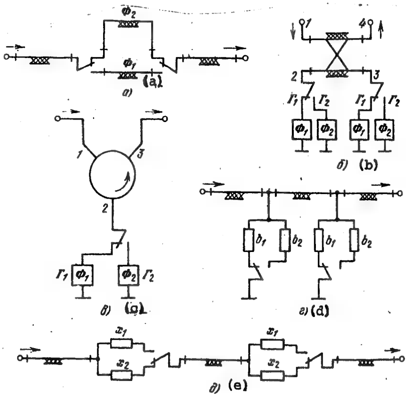

Figure 21.5. Circuits of discretely switched phase shifters.

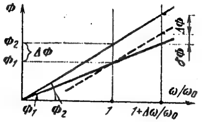

Figure 21.6. The phase characteristics of switched nondispersive line sections.

The operational principle of periodically loaded line type phase shifters consists in the fact that the electrical length of a line increases when a shunting capacitance is inserted and decreases when an inductance is inserted. To reduce reflections from inhomogeneities, represented by the shunting capacitance or inductance, a pair of identical reactive elements is used, spaced at a distance apart approximately equal to a quarter wavelength. For good matching, the shunting reactances should be rather small, but this leads to small phase shifts (usually, no more than 45 degrees), which limits the application of the phase shifter. The phase shift in the phase shifters shown in Figures 21.5d and [illegible] is determined by the following relationships respectively: $\Delta\Phi = \arctan(b_1/2) - \arctan(b_2/2)$ and $\Delta\Phi = \arctan(x_1/2) - \arctan(x_2/2)$.

Phase Shifters with Switched Line Sections. The great diversity of the phase shifters in this group is due primarily to the requirements placed on the form of the phase-frequency characteristic and the minimum phase shifter dimensions for large discrete phase steps. We shall consider the operation of the phase shifter shown in Figure 21.a within the passband. The electrical length of the switched nondispersive line sections are:

$$\Phi_{1,2} = 2\pi l_{1,2}/\lambda_0, \qquad (21.8)$$

where λ_0 is the wavelength corresponding to the center frequency of the specified bandwidth (Figure 21.6).

The phase characteristics of the switched line sections, which take the form of straight lines running through the origin. are depicted in Figure 21.6. In the case of tuning off of the center frequency, as follows from Figure 21.6 there appears an increment in the phase jump, $\delta\Phi$, related to the frequency difference $\Delta\omega/\omega_0$ by the ratio (we consider the diodes to be ideal switches):

$$\delta\Phi = \Delta\Phi\Delta\omega/\omega_0, \qquad (21.9)$$

where $\Delta\Phi = \Phi_2 - \Phi_1$ is the phase shift at the center frequency. It follows from this that a phase shifter of the type shown in Figure 21.5a provides for a phase shift which changes linearly with frequency, and consequently, a time delay which is independent of frequency. For this reason, such a phase shifter is convenient for use in wideband devices with a constant time delay. However, the bandwidth and the maximum phase shift are limited by resonance phenomena which occur when the length of a disconnected line section becomes a multiple $\lambda/2$. In this case, the disconnected line section becomes in essence a high Q resonator, which is weakly coupled to the connected line section by virtue of the capacitance of the diode cutoff switches (Figure 21.7a). Because of this, the insertion losses at the resonant frequency increase, and moreover, phase errors appear.

To increase the decoupling between line sections and the channels, one can use the circuit shown in Figure 21.7b with a permanent structural connection of both channels to the incoming and outgoing lines. The disconnection of one of the channels is accomplished by shorting its input and output to ground. In this case, the length of the line sections from branch point A to the points of diode insertion is $\lambda_p/4$, where λ_p is the wavelength corresponding to resonance in the disconnected channel. When a forward bias is supplied, the upper diodes (in accordance with the schematic of Figure 21.7b) are turned on. In this case, the quarter-wave short-circuited line sections have an infinitely high input impedance at branch point A, which also creates increased isolation. The lower diodes are cut off, and consequently have no influence on the operation of the channel with an electrical length Φ_1 (the channel length is determined by the length of the line section between branch points A - A).

Phase shifters of the type of Figure 21.5a can also be used in systems where it is necessary to have the phase shift independent of frequency. In this case, expression (21.9) is the phase error $\delta\Phi$ introduced by such a phase shifter. A constant phase shift in a wide frequency band (up to an octave and more) can be obtained by using a dispersion line in a channel where this line has a shorter electrical length and takes the form of coupled lines connected to each other at one end as shown in Figure 21.8a. The length of the coupling region is $\lambda_0/4$, where λ_0 is the average wavelength of the working band. The phase-frequency characteristic of such a coupled line is [5]:

$$\Phi = \Phi_1 = \arccos\left[\frac{(1+\alpha)/(1-\alpha)-\mathrm{tg}^2\,\Phi_{0C}}{(1+\alpha)/(1-\alpha)+\mathrm{tg}^2\,\Phi_{0C}}\right], \qquad (21.10)$$

where $\alpha = 10^{-C/20}$; C is the crosstalk attenuation in dB; $\Phi_{OC} = 0.5\pi\lambda_0/\lambda$ is the electrical length of the coupling region.

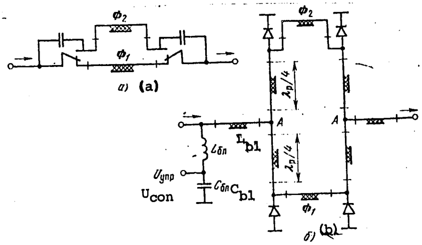

Figure 21.7. Variants of phase shifters with switchable channels and increased isolation between them.

The phase-frequency characteristic corresponding to expression (21.10) is shown in Figure 21.8b by the curve Φ_1. The phase-frequency characteristic Φ_2 of a nondispersive line section is also shown in this same figure. A schematic of a phase shifter using lines having the characteristics Φ_1 and Φ_2 is shown in Figure 21.8c.

If the length of a nondispersive line section is chosen so that its phase-frequency characteristic Φ_2 is parallel to a straight line passing through a point with abscissas of Φ_1 and Φ_2 which are equally spaced from the point $\Phi_{OC} = \pi/2$ (Figure 21.8b), then at frequencies corresponding to the point Φ_1, $\pi/2$ and Φ_2, the phase shift introduced by the phase shifter is equal to a certain quantity $\Delta\Phi$, while at the remaining points which fall outside the range $\Phi_1 < \Phi_{OC} < \Phi_2$, a phase error appears which does not exceed $\delta\Phi$.

The phase-frequency characteristic $\Phi_2 = \gamma\Phi_{OC}$ is a straight line passing through the origin, where γ is an angular coefficient which is found from the condition: when $\Phi_{OC} = \pi/2$, we should have $\Phi_2 = \pi + \Delta\Phi$. From this, $\Phi_2 = 2(1 + \Delta\Phi/\pi)\Phi_{OC}$. The points Φ_1 and Φ_2 are defined as the abscissas for which the discrete phase step of a single stage phase shifter of the type shown in Figure 21.8c is:

$$\Delta\Phi \doteq 2\left(1+\frac{\Delta\Phi}{\pi}\right)\Phi_i - \arccos\frac{(1+\alpha)/(1-\alpha)-\mathrm{tg}^2\,\Phi_i}{(1+\alpha)/(1-\alpha)+\mathrm{tg}^2\,\Phi_i},$$

where i = 1, 2. By solving this equation for α and introducing the band coverage overlap coefficient $K_\omega = \Phi_2/\Phi_1$, we obtain:

$$\frac{1+\alpha}{1-\alpha} = \mathrm{ctg}^2\left[\frac{\pi+\Delta\Phi}{1+K_\omega} - \frac{\Delta\Phi}{2}\right]\mathrm{tg}^2\left(\frac{\pi}{1+K_\omega}\right). \qquad (21.11)$$

The value of α found from (21.11) is used for the design calculations of a network of the type of Figure 21.8a.

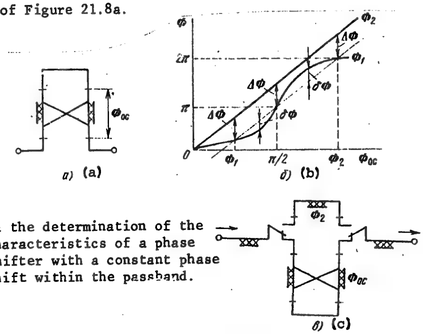

Figure 21.8. On the determination of the characteristics of a phase shifter with a constant phase shift within the passband.

Phase shifters with switched channels, which are intended for operation in the lower portion of the microwave band, have considerable dimensions. One of the ways of reducing the overall dimensions of a phase shifter in this case is replacing the switched line sections with reactive four-pole networks with lumped elements [5]. As is well known, the transmission matrix of a uniform lossless transmission line (Figure 21.9a) has the form:

$$[a]=\begin{bmatrix}\cos\Phi & j\rho_0\sin\Phi\\ \dfrac{j\sin\Phi}{\rho_0} & \cos\Phi\end{bmatrix}. \qquad (21.12)$$

The classical transmission matrices, $[a_\Pi]$ and $[a_T]$ of Π and T symmetrical four-pole networks with lumped reactive elements (Z_1 and Z_2 in Figure 21.9b, c) are defined by the expressions:

$$[a_\Pi]=\begin{bmatrix}1+Z_2Y_1 & Z_2\\ 2Y_1+Z_2Y_1^2 & 1+Z_2Y_1\end{bmatrix}. \qquad (21.13)$$

$$[a_T]=\begin{bmatrix}1+Z_1Y_2 & 2Z_1+Z_1^2Y_2\\ Y_2 & 1+Z_1Y_2\end{bmatrix}, \qquad (21.14)$$

where $Y_1=1/Z_1$; $Y_2=1/Z_2$.

The four-pole networks treated here can be considered equivalent to a transmission line section in the case where the corresponding elements of their transmission matrices are equal (at a fixed frequency). By equating the elements of matrices (21.12) and (21.13), we obtain the values of Z_1 and Z_2 of a Π four-pole network, expressed in terms of the parameters ρ_0 and Φ of a line section:

$$Y_1=j\frac{\operatorname{tg}(\Phi/2)}{\rho_0},\quad Z_2=j\rho_0\sin\Phi,\quad \pi>\Phi>0;$$

$$Z_1=-j\frac{\rho_0}{\operatorname{tg}(\Phi/2)},\quad Y_2=-j\frac{1}{\rho_0\sin\Phi},\quad 2\pi>\Phi>\pi. \qquad (21.15)$$

Similarly, for a T network:

$$Z_1=j\rho_0\operatorname{tg}(\Phi/2),\quad Y_2=j\frac{\sin\Phi}{\rho_0},\quad \pi>\Phi>0;$$

$$Y_1=-j\frac{1}{\rho_0\operatorname{tg}(\Phi/2)},\quad Z_2=-j\frac{\rho_0}{\sin\Phi},\quad 2\pi>\Phi>\pi. \qquad (21.16)$$

Expressions (21.15) and (21.16), taking into account the symbols adopted in Figures 21.9b and c, make it possible to draw the conclusion that Π and T four-pole networks, which are equivalent to a line section of length $\pi > \Phi > 0$ at the working wavelength λ_0, have the structure of a low pass filter (FNCh) section; for

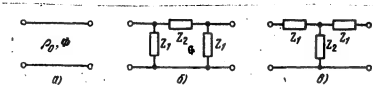

Figure 21.9. The equivalent representation of a section of uniform transmission line.

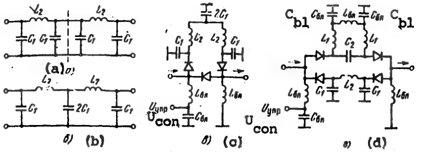

Figure 21.10. Examples of circuits of discrete phase shifters with lumped reactive elements.

$2\pi > \Phi > \pi$, these four-pole networks have the structure of a high pass filter (FVCh) section. Moreover, it follows from expressions (21.15) and (21.16) that one of these four-pole networks cannot successfully realize an equivalent line section of length $\Phi = \pi$. Possible circuits for constructing a network for a line section of electrical length $\Phi = \pi$ are shown in Figure 21.10. The series connection (Figure 21.10a) presupposes the use of two Π four-pole networks, each of which is equivalent to a section of line with a length of $\Phi = \pi/2$. It is obvious that this networks reduces to the form of the network in Figure 21.10b. A phasing section of a phase shifter for a discrete phase step of $\Delta\Phi = \pi$ using a network of the kind shown in Figure 21.10b is shown in Figure 21.10c.

Another structural variant of a phasing section for a discrete phase step of $\Delta\Phi = \pi$ is shown in FIgure 21.10d. Two Π four-pole networks are also used here, one of which, having the structure of a low pass filter section (C_1, L_2) is equivalent to a line section with a length of $\Phi = \pi/2$, while the other, having the structure of a high pass filter section (L_1, C_2) is equivalent to a line section with the length of $\Phi = 3\pi/2$.

One element of a phase shifter for other discrete phase steps can be made in a similar manner. We will note that the circuit configurations treated here for the elements of discrete phase shifters can made using a T section four-pole network (Figure 21.9c).

Reflective phase shifters with isolators are differentiated according to the type of isolating devices used and the methods of obtaining the specified discrete phase step. In contrast to phase shifters with switched channels, in reflective phase shifters it is necessary to equalize the losses in both phase states, which is achieved through different circuit design solutions.

The major requirement which should be satisfied by the mutual isolation device of such phase shifters is that of assuring a 3 dB power division among the two arms with a phase shift of 90 degrees. In line with a T mode, primarily the following isolating devices are employed: a loop bridge (Figure 21.11a), a ring bridge (Figure 21.11b) and a coupler with electromagnetic coupling (Figure 21.11c). In waveguide phase shifters, primarily a 3 dB bridge is used for these purposes, since the sizes of other devices with similar characteristics are considerably greater.

We shall consider the methods of obtaining a discrete phase step in reflective phase shifters. The first method is similar to that used in phase shifters with a continuous phase shift change (see Figure 21.4a) with the only difference that the diode resistance can assume only two values: either close to the resistance which provides for a short circuit at the point of diode installation (in this case, power is reflected from the diode) or close to a resistance which provides for a no-load mode (in this case, the reflection takes place from the short circuited end ofthe line in which the diode is inserted). The discrete phase step is $\Delta\Phi = 2\Phi_1$, where Φ_1 is the electrical length of the line from the point of diode insertion to the short circuited end of the line. With this method, it is difficult to achieve identical insertion losses in both phase states, since the reflection occurs in one case from the diode and in the other from the short-circuiter. To equalize the losses in both phase states and expand the working bandwidth, a loop is inserted in the line coupling the diode and the isolating device [5]. In this case, the requisite values of the reflection factors are determined by the point of insertion of the loop, its length and characteristic impedance.

As has already been noted, elements with multiple discrete steps, which are shown in Figure 21.12, can be realized in reflective phase shifters. In this structural design, two loops Φ_1 and Φ_2 are connected at a common point. The characteristic impedances (ρ_1 and ρ_2) and the length of these loops are chosen so that when switching the bias voltage of the diodes, the susceptance of the first loop at the common point is equal to $\pm jb_1$, and $\pm jb_2$ at the second point. The combination of these susceptances yields four values of the total susceptance at the common point: $j(b_1 + b_2)$, $j(b_1 - b_2)$, $j(b_2 - b_1)$, $-j(b_1 + b_2)$. Four values of the discrete phase step are provided in this case. The dimensions of such a phase shifter are slightly larger than the dimensions of a single digit phase shifter with one discrete step, since only one separating device is used.

A phase shifter with a nonreciprocal isolator - a circulator - operates just as the phase shifter shown in Figure 21.5c does. The use of circulators provides for smaller dimensions and a smaller number of diodes, which is responsible for lower losses.

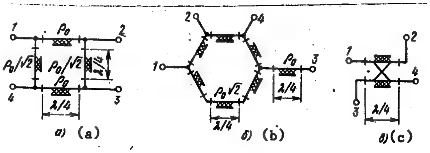
1
2
3
4
ρ_0
$\rho_0/\sqrt{2}$
$\lambda/4$
а) (a)
$\rho_0\sqrt{2}$
б) (b)
в)(c)

Figure 21.11. Isolators for digital phase shifters.

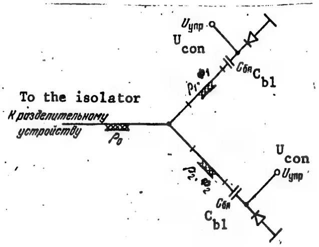
$U_{упр}$
U con
$C_{бл}$ C b1
ρ_1, Φ_1
To the isolator
К разделительному устройству
ρ_0
ρ_2, Φ_2
U con
$U_{упр}$
$C_{бл}$
C b1

Figure 21.12. An example of the realization of a multiply discrete element of a phase shifter.

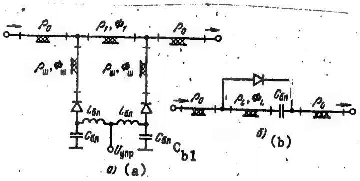
ρ_0
ρ_1, Φ_1
ρ_0
$\rho_ш, \Phi_ш$
$\rho_ш, \Phi_ш$
$L_{бл}$
$L_{бл}$
$C_{бл}$
$U_{упр}$
$C_{бл}$ C b1
а) (a)
ρ_0
ρ_L, Φ_L
$C_{бл}$
ρ_0
б) (b)

Figure 21.13. Circuits for obtaining the necessary susceptances (a) and reactances (b) in a phase shifter of the periodically loaded line type.

Phase shifters of the periodic loaded line type differ in the methods of realizing the reactance inserted in the line to change the line's electrical length. The reactive elements inserted in the transmission line can be made in the form of loops. The length and characteristic impedance of the loops are chosen from the condition for obtaining the requisite input susceptance; usually $b_1 = b_2 = b$, where b is the shunting susceptance (Figure 21.5d). A shcematic of such a phase shifter with parallel loops is shown in Figure 21.13a. Phase shifters of the periodically loaded line type with a series configuration of distributed reactances also find application (see Figures 21.5e and 21.13b).

Multiple Element Discrete Phase Shifter. The major requirement placed on them is the requirement of assuring a phase change with a discrete step $\Delta\Phi$ in a particular range of values from Φ_{min} to Φ_{max} (in the general case from 0 to 2π). The discrete step $\Delta\Phi$ is determined by working from the requirement placed on the characteristics of the device in which the given multiple place phase shifter will operate. Usually, a multiple digit phase shifter contains n_1 digits. Each digit can exist in only one of two phase states (a single discrete step digit): there is no phase delay (or the insertion delay is taken as zero); or the insertion phase delay is $\Delta\Phi_i$, where i is the number of the digits.

The minimum number of digits n_1 in this case is assured through the choice of the following values of $\Delta\Phi_i$:

$$\begin{aligned} \Delta\Phi_1 &= \Delta\Phi, \\ \Delta\Phi_2 &= \Delta\Phi_1 + \Delta\Phi = 2\Delta\Phi, \\ \Delta\Phi_3 &= \Delta\Phi_2 + \Delta\Phi_1 + \Delta\Phi = 4\Delta\Phi, \\ &\cdots\cdots\cdots\cdots \\ \Delta\Phi_n &= \Delta\Phi + \sum_{i=1}^{n-1} \Delta\Phi_i = 2^{n-1}\Delta\Phi. \end{aligned} \tag{21.17}$$

The range of phase change from 0 to 2π will be covered if the overall phase delay introduced by all of the digits is:

$$\Phi = \Delta\Phi_1 + \Delta\Phi_2 + \ldots + \Delta\Phi_n = 2\pi - \Delta\Phi. \tag{21.18}$$

By using equations (21.17) and (21.18), we obtain:

$$n_1 = 1 + \log_2 (\pi/\Delta\Phi). \tag{21.19}$$

It follows from (21.19) that n_1 is an integer with the condition $\Delta\Phi = \pi/2^m$ is met, where m are also integers.

Digital phase shifters which have already been described are used to realize the discrete digits. The selection of the type of digital phase shifter is made based on various criteria. For example, if minimal average insertion losses are required, then one can employ phase shifters of the periodically loaded line type as the lowest order digits (i.e., the digits with the small discrete phase steps), and for digits with larger discrete phase steps, one can use phase shifters with switched channels. In this case, a gain is obtained in the average insertion losses both as compared to the case where all digits are realized using phase shifters with switched lines as well as the periodically loaded line type.

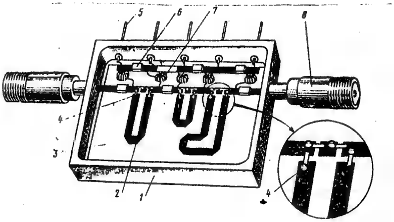

Figure 21.14. The structural design of a three element microstripline phase shifter.

Key: 1. Phase shifter housing;
2. Stripline conductor;
3. Dielectric plate;
4. PIN diodes;
5. Power supply terminals for the PIN diodes;
6. Blocking capacitors;
7. Choke;
8. Coaxial to stripline transition.

This is explained by the fact that phase shifters using switched lines introduce approximately the same losses for any discrete steps, while phase shifters with periodically loaded lines have low losses for small discrete steps. At the same time, the losses in phase shifters of this type increase with large discrete phase steps.

One of the possible structural designs of a phase shifter using switched line section is shown in Figure 21.14.

CHAPTER 22. MICROWAVE FILTERS.

22.1. The Classification of Microwave Filters

Electrical filter is the term for a passive linear network with a sharply pronounced frequency selectivity. Filters are very widely used in radio systems for the frequency selection of the requisite signal against a background of other signals or interference. A filter is frequently used to suppress interfering signals.

In the microwave band, a filter takes the form of a transmission line which includes inhomogeneities, matched in a definite frequency band and sharply mismatched outside of this band. In this sense, filter operation is similar to the operation of a broadband matching device. (A filter is sometimes used for broadband matching). It is apparent that to reduce losses within a passband, a filter should be made of reactive elements.

At the present time, the most widespread procedure for microwave filter design is the procedure in accordance with which the low frequency prototype of the filter is designed initially, in this case determining the inductances and capacitances for the loaded Q's of the resonant circuits of the prototype. Then the question of the realization of the calculated elements with the appropriate inhomogeneities or resonant systems in the selected transmission line is resolved. Thus, it is necessary to have an equivalent circuit of the microwave filter for design calculations based on this procedure.

The equivalent circuit imparts clarity to the design calculations and makes it possible to use techniques which have been well worked out in the theory of low frequency filters for the design of a microwave filter. However, it must be remembered that the equivalent circuit reflects the actual microwave device with only a certain degree of precision. It frequently does not take into account various parasitic scattering fields, equivalent to additional capacitances and inductances. It is also necessary to remember that resonant microwave systems (volumetric resonators, line sections) are multiple resonance systems, something which is not at all taken into account in the equivalent circuit. The transient processes in the equivalent circuit and actual device will also be different.

The main parameter of a filter is its frequency characteristic: the working attenuation $L(f)$ or the reflection factor $\Gamma(f)$ as a function of frequency. We recall that $L = 1/(1-\Gamma^2)$.

Filters are broken down into low pass (FNCh), high pass (FVCh), bandpass (PPF) and bandstop or rejection (PZF) filters.

Bandpass and bandstop filters are most frequently used in the microwave band, although, for example, low pass filters are used to filter the higher harmonics of oscillators and frequency multipliers. Bandpass filters are sometimes used both as low pass and as high pass filters. The right side of the frequency response is used for a low pass filter and the left side for a high pass filter.

The following are usually specified in the design calculations for a bandpass filter: the cutoff frequencies for the passband f_{pr} and f_{-pr}, the mismatch tolerances (Γ_{pr}) or the insertion losses L_{pr} within the passband, the stopband cutoff frequency is f_z and f_{-z} and the minimum permissible losses within the stopband L_z or Γ_z.

It is obvious that the optimal shape of the frequency response would be a rectangular form, in which the frequencies pass through and the blocked frequencies coincide: $f_{pr} = f_z$ and $f_{-pr} = f_{-z}$. However, such a response shape is obtained only with an infinite number of filter sections. In actual devices, the slope of the frequency response curve is determined by the kind of function L(f), which in turn, depends on the number of sections and the Q's of the tuned circuits in the sections.

With respect to the passband, bandpass filters are broken down into narrow band for which the relative passband is less than 5% ($[2\Delta f_{pr}/f_0] \cdot 100 < 5$), average bandwidth filters ($5 < 100 \cdot 2\Delta f_{pr}/f_0 < 20$) and broadband filters ($[2\Delta f_{pr}/f_0] \cdot \cdot 100 > 20$). Here, $f_0 = \sqrt{f_{pr} f_{-pr}}$ is the center frequency of the passband.

In low frequency filters, the filter sections are connected directly to each other and there is strong mutual coupling between the sections. In microwave filters, the sections can be coupled directly to each other by means of coupling elements (such microwave filters are called indirectly coupled filters), or through quarter-wave line sections (quarter-wave coupled filters), where the series resonant circuits are transformed by line sections into parallel resonant circuits.

Microwave filters can also be classified according to the type of line which is used to construct the filter: waveguide, coaxial and stripline filters.

22.2. The Design of the Low Frequency Filter Prototype

The determination of the parameters of a filter prototype is a problem of parametric analysis, i.e., the filter elements must be found based on the known frequency response of the filter. In order to make the design procedure more general, in which the numerical calculations for a specific sample are minimal, all of the quantities are normalized. Normalizing impedances consists in the fact that the load impedances at both ends of the filter are considered equal to unity. For a load resistance of R, all of the prototype resistances are increased by a factor of R times; the frequency response of the filter does not change in this case. If the filter is not matched within the passband at either end, then an ideal transformer which provides for matching should be used.

Then the frequencies are normalized so that the normalized frequency at the edge of the passband is equal to unity. We make the substitution:

$$\nu = k_1 \omega \tag{22.1}$$

If k_1 is chosen from the condition that $k_1 = 1/\omega_{pr}$, then at the boundary of the passband, the equality $\nu = 1$ will be observed. In this case, all of the filter reactances should be multiplied by the actual cutoff frequency ω_{pr}.

When solving a problem of parametric synthesis of filters, all of the types of filters are reduced to a single prototype. Such a prototype is most often a low pass filter.

The transition from one filter to another is made by substitution of a frequency variable. Thus, the transition from a frequency ω to a frequency defined by the equality:

$$\nu = -k_2/\omega, \tag{22.2}$$

will transform a low pass filter into a high pass filter.

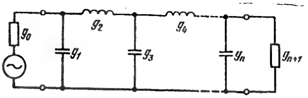

Figure 22.1. Schematic of a prototype filter.

A substitution of variables of the kind:

$$\nu = k_3 \omega_0 (\omega/\omega_0 - \omega_0/\omega), \tag{22.3}$$

transforms a low pass filter into a bandpass filter. The values of the cutoff frequencies for the bandpass filter and its passband can easily be derived from formula (22.3):

$$\omega_{\text{пр}} \omega_{-\text{пр}} = \omega_0^2; \quad 2\Delta\omega = \omega_{\text{пр}} - \omega_{-\text{пр}} = \nu_{\text{пр}}/k_3 = 1/k_3. \tag{22.4}$$

Here ω_0 is the center frequency of the passband.

To derive a stopband filter from a low pass filter, two conversions, (22.2) and (22.3), must be applied sequentially.

Thus, any of the filters can be designed on the basis of a single low pass filter prototype in the form of a ladder circuit (Figure 22.1).

When designing a filter, it is first of all necessary to have the frequency characteristic specified, L(f), such that the filter can be realized, i.e., the design calculations should not lead to quantities which are not physically feasible.

Three types of filters have become the most widespread, categorized according to the type of frequency response:

1. Filters with a Chebyshev characteristic, the function of the working attenuation of which is described by means of Chebyshev polynomials of the first kind:

$$L = 1 + h^2 T_n^2 (\nu/S). \tag{22.5}$$

Here, $\nu = f/f_0 - f_0/f$ is the frequency variable;

$$h = |\Gamma_{\text{пр}}| / \sqrt{1 - |\Gamma_{\text{пр}}|^2},$$
$$h = \sqrt{L_{\text{пр}} - 1}$$

is the amplitude coefficient; S is a scale factor which normalizes the cutoff frequency; n is the degree of the Chebyshev polynomial; $\nu_{pr}/S = 1$.

The frequency response of a three section filter is shown in Figure 22.2. A filter with a Chebyshev frequency response (a Chebyshev filter) is optimal in the sense that in the case of identical starting data, of all of the filters which can be described, it has the smallest number of sections. The slope of the frequency response is the maximum of all of the filters which can be used. A drawback to the filter is the pulsation of the insertion losses within the passband and the nonlinearity of the phase-frequency characteristic.

2. Filters with a maximally flat response (Figure 22.3):

$$L = 1 + h^2 (\nu/S)^{2n}. \tag{22.6}$$

The insertion losses within the passband vary from the maximum values at the edge of the band to zero at the center frequency. A merit of the filter is the linearity of the phase-frequency response.

3. Filters made of identical resonators are the simplest to fabricate and align. The frequency response of the filter is described by a Chebyshev polynomial of the second kind and has greater operations within the passband, especially at its boundaries. To reduce the oscillations, the Q's of the end sections are cut in half. However, a major advantage of the filter is lost in this case: the identical nature of the sections. The phase response of the filter is nonlinear. The filter finds fewer applications as compared to filters of the first two types.

We will note that a filter which has a frequency response described by a function using a Zolotarev fraction has the greatest slope of the frequency characteristic. The response has oscillations within the passband and within the stopband. The filter has not found widescale application since special sections with mutual inductances are required to make it.

In formulas (22.5) and (22.6), the degree of the polynomials n is equal to the number of filter sections, and one can derive the expressions to calculate the number of sections from these formulas.

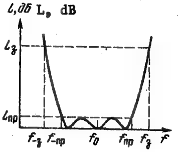

Figure 22.2. Frequency response of a bandpass filter described by a Chebyshev polynomial.

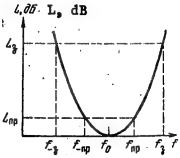

Figure 22.3. Maximally flat response of a bandpass filter.

For a Chebyshev filter, the number of sections is:

$$n \geqslant \frac{\operatorname{Arch}\sqrt{(L_{з}-1)/(L_{пр}-1)}}{\operatorname{Arch}(\nu_{з}/\nu_{пр})}. \qquad (22.7)$$

For a filter with a maximumally flat response:

$$n \geqslant \frac{\lg\sqrt{(L_{з}-1)/(L_{пр}-1)}}{\lg(\nu_{з}/\nu_{пр})}. \qquad (22.8)$$

If in calculations using formulas (22.17) and (22.18) [sic] the number n proves to be fractional, it is rounded off to the nearest whole value (usually the greater one).

After determining the number of filter sections, the components of the ladder circuit are found (Figure 22.1) as well as the loaded Q's of the bandpass filter sections. This is the most labor intensive part of the problem.

There are two known methods of overcoming the computational difficulties. In the first, the general laws governing the distribution of the parameters of the circuit components are ascertained. These governing laws are studied and then generalized. In the second approach, tables and graphs are drawn up for the most frequently encountered cases of filter design.

The simplest distribution of the values of g can be successfully established for a filter with a maximally flat response, for which:

$$g_k = 2\sin[\pi(2k-1)/2n], \qquad (22.9)$$

where k is the number of the branch reckoned from the filter input (Figure 22.1).

It follows from formula (22.9) that when $n = 1$, $g_1 = 2$, when $n = 2$, $g_1 = g_2 = \sqrt{2}$, when $n = 3$, $g_1 = g_3 = 1$, $g_2 = 2$, etc. The filter is symmetrical.

The transition to a bandpass filter is made by substituting variables in accordance with formula (22.3). In this case, the loaded Q's of the resonant circuits are determined from the formula:

$$Q_{к} = Q_{Ф}\, g_k/2 = Q_{Ф} \sin[\pi(2k-1)/2n]. \qquad (22.10)$$

Here:

$$Q_{Ф} = \sqrt[n]{h}/S \qquad (22.11)$$

is the loaded Q of the entire filter at the three decibel level.

For a Chebyshev filter, there is no formula as simple as (22.9). The coefficients g can be calculated from the following formulas:

$$g_1 = 2a_1/\gamma,\ g_k = 4a_{k-1}a_k/b_{k-1}g_{k-1}, \qquad (22.12)$$

where

$$a_k = \sin[\pi(2k-1)/2n];\ b_k = \gamma^2 + \sin^2(\pi k/n),\ \gamma = \operatorname{sh} \beta/2n,$$

$$\beta = \ln[\coth(L\ [\mathrm{dB}]/17.37)]$$

$$\beta = \ln[\operatorname{cth}(L\ (дБ)/17{,}37)].$$

The transition to a bandpass filter is also made by substituting variables in accordance with formula (22.3). The loaded Q's of the filter resonant circuits are determined from the formula:

$$Q_{н} = g_k/2S. \qquad (22.13)$$

In filters with quarter-wave coupling, it is necessary to take into account the influence of the frequency sensitivity and dispersive properties of the quarter-wave line sections. The initial loaded Q of the filter sections is determined from the formulas:

$$Q^0_{к} = Q_{к}(\lambda_0/\lambda_{б0})^2 - \pi/4\ (\text{средние звенья}), \qquad \text{(center sections)} \quad (22.14)$$

$$Q^0_{к} = Q_{к}(\lambda_0/\lambda_{б0})^2 - \pi/8\ (\text{крайние звенья}). \qquad \text{(end sections)} \quad (22.15)$$

We shall briefly deal with the problem of synthesizing a bandstop filter. A bandpass filter is taken as the prototype here. By applying the transformation (22.2) to it, we obtain a bandstop filter. The Chebyshev frequency characteristics of the bandpass and bandstop filters are shown in Figure 22.4. As can be seen from Figure 22.4, the cutoff frequencies for the bandwidth and the insertion losses are the same for both filters:

$$\nu_{\text{пр ппф}} = \nu_{\text{пр пзф}} = S, \quad \nu_{-\text{пр ппф}} = \nu_{-\text{пр пзф}}; \tag{22.16}$$

$$L_{\text{пр ппф}} = L_{\text{пр пзф}}, \quad L_{\text{з ппф}} = L_{\text{з пзф}}. \tag{22.17}$$

[ппф = bandpass filter; пзф = bandstop filter].

The conversion (22.2) transforms the cutoff frequencies of the stopbands and the loaded Q's of the tuned circuits:

$$(\nu_{\text{з ппф}}/S)(\nu_{\text{з пзф}}/S) = 1, \tag{22.18}$$

$$(Q_{\text{к ппф}}\, S)(Q_{\text{к пзф}}\, S) = 1. \tag{22.19}$$

When equalities (22.18) and (22.19) are observed, the number of sections in both filters is the same.

Yet another type of filter is used in the microwave band which does not have any analog at lower frequencies: the stepped filter. It consits of line sections of equal length and different input impedances. In contrast to a stepped matching transformer (taper), the change in the characteristic impedance from step to step takes place nonmonotonically here. The design procedure for a stepped filter is based on the use of a stepped transition as the prototype. The frequency response of a Chebyshev stepped filter is described by the formula:

$$L = 1 + h^2 T_n^2 (\sin \Phi / S), \tag{22.20}$$

where Φ is the electrical length of one step.

A comparison of the frequency responses of a filter and a transition show that the frequency response of a filter is shifted by $\pi/2$, i.e., there where the transition has a stopband the filter has a passband. The length of the step amounts to half the resonant wavelength. The filter bandwidth is twice as narrow as the bandwidth of the transition.

Thus, the solution of the problem of prototype synthesis of a bandpass microwave filter is completed with the determination of the number of filter sections and the calculation of the loaded Q's of the resonant systems of the sections.

At the present time, tables and auxiliary computed graphs are given in the reference literature for the parameters of filters which are encountered most frequently in practice, for example, [1, 4, 5, 014], because of which the design calculations of a filter prototype are speeded up substantially.

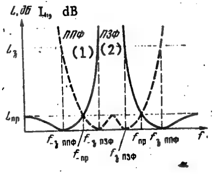

Figure 22.4. The frequency responses of Chebyshev bandpass and bandstop filters.

Key: 1. Bandpass filter;
2. Bandstop filter.

22.3. The Structural Execution of Microwave Filters

The execution of the structural design of the filters in the microwave band can be extremely diverse.

A spatial resonator is used as a microwave resonator. With careful fabrication, it has an extremely high Q: up to 15.000 - 20,000 in the centimeter band and dimensions which are too large. For this reason, it is used in the short wave portion of the centimeter band and the millimeter band as the resonant systems of a filter for very narrow band filters.

The major types of resonators of microwave filters are the resonant sections of transmission lines, which are open circuited, short-circuited or loaded into reactances.

As is well known, short-circuited and open circuited line sections, the length of which is a multiple of a whole number of quarter-wavelengths possess resonant properties. Such systems, just as volumetric resonators, are multiple resonance systems. The inherent Q of a resonant line section with a T-mode is defined by the formula:

$$Q_0=\pi\sqrt{\varepsilon}/\lambda_0\,\alpha, \tag{22.21}$$

where α is the coefficient of attenuation in the line.

The natural Q of coaxial and stripline resonators, filled with a dielectric, amounts to 250 to 400 in the decimeter band. For resonators filled with air, the Q is increased up to 500 to 600. For waveguide resonators, the natural Q can be calculated from the formula:

$$Q_0=\frac{\pi}{\alpha_n\,\lambda_n}\left(\frac{\lambda_n}{\lambda}\right)^2. \tag{22.22}$$

A waveguide resonator has an inherent Q of several thousand at centimeter wavelengths.

The topology of a half-wave resonator using striplines is depicted in Figure 22.5a. The equivalent circuit of the resonator is shown in Figure 22.5b. When the center of the resonator is shifted (Δl), the amount of its coupling to the line changes, i.e., the loaded Q changes. The greater Δl, the higher the loaded Q of the resonator.

The structural design of a three-section stripline bandstop filter with quarter-wave coupling is depicted in Figure 22.6. The degree of coupling is adjusted by means of the gap between the main stripline and the end face of the resonators.

As a rule, microwave filters are transmissive devices. For this reason, through transmission resonators find the greatest application in them. We shall deal in more detail with two types of transmissive resonators: a waveguide bounded on two sides by reactive inhomogeneities, and a resonator made with coupled striplines. These resonators find the greatest applications in microwave filters.

A waveguide resonator is depicted in Figure 22.7. It takes the form of a waveguide bounded at the end faces by reactances, in this case, inductive stops with a normalized susceptance b. The resonant length of the resonator for the case of inductive susceptances of $b < 0$ is determined from the formula:

$$l_0=\frac{\lambda_{\text{в}0}}{2\pi}\left(n\pi-\operatorname{arctg}\frac{2}{|b|}\right),\quad n=1,2,3,\ldots \tag{22.23}$$

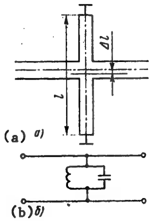

Figure 22.5. A stripline resonator.

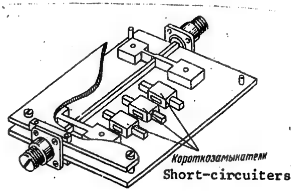

Figure 22.6. A bandstop filter.

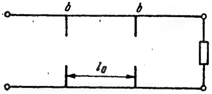

Figure 22.7. A resonator in the form of a line limited by inhomogeneities.

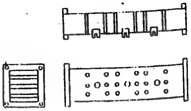

Figure 22.8. A waveguide bandpass filter.

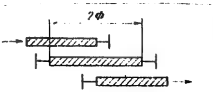

Figure 22.9. A bandpass filter resonator using coupled striplines.

The loaded Q of the resonator is:

$$Q_{\text{н}} = \frac{\sqrt{b^4+4b^2}}{4}\left(\frac{\lambda_{\text{в}0}}{\lambda_0}\right)^2\left(n\pi + \operatorname{arctg}\frac{2}{|b|}\right). \tag{22.24}$$

For large and small values of b, formula (22.24) can be simplified. When $|b| > 50$,

$$Q_{\text{н}} = \frac{n\pi}{4}b^2\left(\frac{\lambda_{\text{п}0}}{\lambda_0}\right)^2. \tag{22.25}$$

and for small values of $|b|$, the quantity $\arctan(2/|b|) \to \pm\pi/2$ and:

$$Q_{\text{н}} = \frac{|b|}{2}\left(\frac{\lambda_{\text{п}0}}{\lambda_0}\right)^2\left(n\pi \pm \frac{\pi}{2}\right). \tag{22.26}$$

For a filter with quarter-wave couplings, the spacing between adjacent sections is determined from the formula:

$$l_{k,\,k+1} = (2m-1)\,\lambda_{\text{в}0}/4 - k\lambda_{\text{в}0}/2 + l_k\, l_{k+1}/2,\ m = 1, 2, \ldots \tag{22.27}$$

An array of inductive stubs and inductive stops is used as the reactive inhomogeneities in waveguide transmissive resonators. The natural Q's of centimeter band resonators with inductive stubs amount to 1,500 to 2,000, and with inductive stops, 3,000 to 4,000.

A three-section bandpass filter with quarter-wave couplings is depicted in Figure 22.8. The susceptance here is formed by the array of three inductive stubs. The capacitive screws, which are placed in the center of each resonator, are intended for the experimental alignment of the filter.

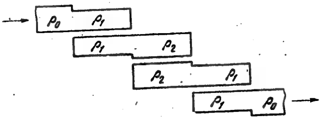

Figure 22.10. A bandpass filter.

Another widely used through transmission resonator is a resonator made with coupled striplines. The resonant sections of line are coupled together with distributed electrical and magnetic coupling. Filters using such resonators are small, structurally simple and their production can be automted. The resonator of a bandpass filter using coupled lines is depicted in Figure 22.9. In it, Φ is the electrical length of the coupling section, at the frequency equal to $\Phi_0 = \pi/4$. The free arms of the line can be short-circuited as depicted in Figure 22.9, or open-circuited. The loaded Q of a resonator circuit using coupled striplines is defined by the approximate formula:

$$Q_{load} = \quad Q_н = \pi/4r^2, \tag{22.28}$$

where r is the coupling resistance, determined by the structural parameters of the line: the width and thickness of the strip, the spacing between the bases and the spacing between the coupled striplines. The gap between the striplines exerts the major influence on r. Formula (22.28) yields better precision, the greater Q_{load} is. The error in the calculation when $Q_{load} > 20$ does not exceed 1%, and when $Q_{load} = 5$, it increases up to 8%.

The working attenuation function of a resonator using coupled striplines is:

$$L = 1 + \left(\frac{1}{r\sin\Phi} - r\sin\Phi\right)\frac{1+r^2}{r^2}\cos^2\Phi. \tag{22.29}$$

It is convenient to calculate the coupling resistance r in terms of the cross-talk attenuation of a directional coupler made with coupled lines:

$$C = (1+r^2)/r^2. \tag{22.30}$$

By means of series connecting the sections, one can obtain a bandpass filter. The direct connection of the filter sections is depicted in Figure 22.10, where only the conducting strip is shown.

A variant of a stripline bandpass filter is a filter using opposing stubs.

22.4. A Design Procedure for Microwave Filters

The technical requirements placed on microwave filters can be extremely diverse. First of all, the frequency characteristics of a filter are important. Additional requirements can be placed on filters which follow from specific operational or production features. It is not always possible to meet all of the technical requirements. The designer should have a clear-cut idea of the entire complex in which the filter will be used.

The frequency properties of a filter are usually specified in terms of the parameters f_{pr}, f_{-pr}, L_{pr}, f_z, f_{-z} and L_z. Filter design begins with the selection of the frequency response. We shall make one note: for a Chebyshev filter with an even number of sections, the normalized output resistance R_{out} is not equal to unity, but rather to $\tanh^2(\beta/4)$, i.e., an ideal transformer is needed to match the filter to the line. For this reason, Chebyshev filters with an even number of sections are rarely used: it is simpler to add one section.

In the following design step, the number of sections is determined by using formulas (22.7) and (22.8).

Then it is necessary to select the type of resonator coupling: direct or quarter-wave. The length of a filter with direct coupling is less, and therefore, if strict limitations are placed on the filter length, then a direct connection of the sections is selected. Stripline filters are also most often direct coupled filters, something which is explained by their structural compactness.

The length of quarter-wave coupled filters increases somewhat because of the connecting line section. A merit of such filters is the smaller amount of coupling between the sections, which makes it possible to independently tune the filter section by section. The ohmic losses in filters with quarter-couplings is less, and the calculated characteristics are in better agreement with the actual ones, which is explained by the lower values of the loaded Q's of the individual resonators. The fabrication tolerances are less stringent here. A drawback to quarter-wave coupled filters is the considerable length and limited bandwidth, which should not exceed 15%.

The subsequent design consists in finding the loaded Q's of the prototype filter sections. The calculations can be made using formulas (22.9) - (22.13), or what is simpler, by making use of the extensive reference literature [1, 5, 014]. Then the problem of the practical realization of the resonators is solved. In this case, first the type of line, resonant frequency and passband are selected. The design calculation procedure is governed by the specific type of resonator and is not given here.

We shall limit ourselves to some recommendations are general guidelines. Very narrow band filters with a bandwidth of 0.5 to 1% can be realized only by using high Q systems: spatial resonators, waveguides and air filled striplines.

Waveguide filters are used at frequencies 5 to 10 GHz. The majority of these filters are through transmissive resonators with quarter-wave coupling (figure 22.8). If the resonator is formed by inductive stubs, then the filter bandwidth is limited to 20%. With a greater bandwidth, stubs are needed which prove to be too thin to replace with inductive stops. The tuning screws of the sections make it possible to change the resonant wavelength of a resonator by 3 to 5%.

Stripline filters are used in very wide range of wavelengths from tens of decimeters up to 3 cm. At longer wavelengths, the dimensions increase greatly and at shorter wavelengths, the requisite fabrication precision increases. Stripline filters using resonators with end coupling are designed for wavelengths of 60 to 4 cm and bandwidths of 0.5 to 5%. With a greater bandwidth, the gaps between the sections prove to very small. Stripline filters using opposing stubs operate well at wavelengths of 70 to 5 cm with bandwidths of 2 to 50%. They are quite compact and well suited for production, and for this reason have found very widescale application.

A common drawback to stripline filters is the difficulty of experimental alignment, which is accomplished by changing the dimensions of the conducting stripline.

Coaxial filters are used at decimeter and meter wavelengths.

The geometric dimensions of resonators and other filter components are calculated based on their equivalent circuits and using reference literature [1, 3, 4, 7].

For transmissive waveguidel resonators and end coupled stripline resonators, the length and loaded Q of a resonator can be determined form formulas (22.23) – (22.27).

Microwave filters are manufactured in accordance with the third precision class with a purity of the current carrying surfaces of no worse than $\nabla 6$ ... $\nabla 7$.

If the ohmic losses α in a filter do not exceed 1 dB, then they have little influence on the frequency response, shifting it along the ordinate.

We will note that literature has appeared in recent years which is devoted to automated (computer) filter design. The use of a computer makes it possible to vary the change in many filter parameters, optimizing its requisite characteristics [6].

CHAPTER 23. DIRECTIONAL COUPLERS AND DIRECTIONAL FILTERS USING COUPLED STRIPLINES

Stringent requirements for cost reduction, increasing reliability as well as reducing size and weight are placed on microwave band radio equipment, including antenna arrays, both with mechanical and electrical scanning.

These requirements can be met to a certain extent by using strip transmission lines in the antenna arrays. They are used as the channelizing feeder system in the decimeter band, and serve as the basis for the realization of individual feeder channel components in the decimeter and centimeter bands (power dividers, directional couplers, filters, etc.); the use of lumped reactive elements make it possible to use striplines in the meter wavelength range also.

The use of striplines in antenna arrays makes it possible to realize structures which are more suited for production and have low size, weight and cost.

To be numbered among the drawbacks of stripline structures are primarily the high losses (especially in the centimeter band) as compared to waveguide and coaxial transmission lines.

When comparing the possibilities for using microstripline and stripline elements in antenna equipment, one must keep in mind the following. The use of microstripline elements is expedient and justified when fabricating individual components and assemblies for both active and passive antenna arrays (phase shifters, mixers, converters, amplifiers, etc.). However, in excitation circuits for antenna arrays (the simplest series and parallel circuits or more complex ones with a large number of directional couplers and filters), the advantages of microstripline construction are lost because of the considerable losses in a long feeder channel.

Questions of design calculations and planning of directional couplers (NO) using coupled lines as well as loop type directional filters (NF) designed around directional couplers are treated in this chapter.

Directional couplers are used in antenna arrays primarily for the following:

--To obtain the requisite amplitude-phase distribution in the radiators of an array;

--To decouple the radiators of an array, something which is especially important for correct operation of a phased array;

--In compensating circuits to reduce the influence of the affect of the change in input impedances of radiators during electrical beam scanning of a phased antenna array;

--As elements of more complex radio frequency assemblies (phase shifters, amplifiers, etc.).

Directional filters find application in transceiving (reradiating) antenna arrays for the segregation of the receive and transmit channels.

23.1. The Classification of Directional Couplers and Filters and Their Operating Characteristics

A directional coupler is an eight-pole system. The directional coupler transmission line through which the greatest power flows is called the primary line, while the line in which a part of the power is split off is called the secondary line. Directional couplers with three types of directivity are shown in Figure 23.1.

The major characteristics of directional couplers are: the crosstalk attenuation, the directivity, the decoupling, the matching of the arms of the coupler to the input feed lines (SWR), the phase relationships for the voltages in the output arms and the working attenuation in the primary line.

The crosstalk attenuation is defined as the ratio of the primary line input power to the output power of the working arm of the secondary line. For example, for the coupler depicted in Figure 23.1a, the crosstalk attenuation is:

$$C_{12} = 10 \lg (P_1/P_2). \tag{23.1}$$

The directivity is the ratio of the powers at the output of the working and nonworking arms of the secondary line. For example, for Figure 23.1a, the directivity is:

$$C_{24} = 10 \lg (P_2/P_4). \tag{23.2}$$

The decoupling [isolation] is defined as the ratio of the primary line input power to the output power of the secondary line nonworking arm. For the eight-pole network of (Figure 23.1a):

$$C_{14} = 10 \lg (P_1/P_4). \tag{23.3}$$

The working attenuation of the primary line is defined as the ratio of the powers at the input and output of the primary line. For Figure 23.1a:

$$C_{13} = 10 \lg (P_1/P_3). \tag{23.4}$$

The matching of the directional coupler arm with the input feed line is characterized by a standing wave ratio which is measured from the input arm of the directional coupler, when matched loads are connected to the remaining arms.

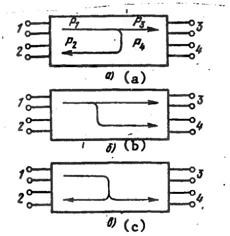

Figure 23.1. Three types of directional coupler directivity.

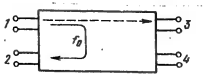

Figure 23.2. A diredtional filter in the form of an eight-pole device.

To determine the band coverage properties of directional couplers, the major characteristics are determined as function of frequency (wavelength).

Depending on the crosstalk attenuation $|C|$, directional couplers are broken down into devices with strong coupling ($|C| = 0...10$ dB) and weak coupling ($|C| > 10$ dB). Directional couplers which have different power levels in the output arms ($|C| = 3.01$ dB), fall in a special class of configurations: hybrid or 3 dB directional couplers.

Of the small directional couplers used in practice, the following have become the most widespread:

1) Coupled line couplers are the most compact broadband devices with respect to the frequency characteristics of the working parameters; they make it possible to realize both strong and weak coupling;

2) Loop couplers are the simplest to fabricate and provide for the simplest topological configuration of the output networks in mixers, phase shifters and switchers for active phased antenna arrays;

3) Cascade coupled line couplers make it possible to increase the bandwidth of the device with a slight increase in structural complexity.

Directional filters are eight-pole devices which are used for the frequency segregation of signals. If a microwave power source is connected to one of the filter arms, for example, to arm 1 (Figure 23.2), then at a certain frequency f_0, almost all of the power will go to arm 2 (the directional coupling arm). With a change in frequency, a redistribution of the microwave power flux takes place: the power in arm 2 is reduced, while the power in arm 3 (the direct coupled arm) increases. If a matched load is connected to the arms of the filter, then with a change in frequency, practically no power is split off to arm 4 (the isolated arm).

Directional filters are made as loop types, with capacitive coupling and with quarter-wave coupling lines. We shall treat questions of the design calculations and structural design of single loop directional filters which use directional couplers with coupled lines.

The main characteristics of directional filters are: the insertion loss factor for the directional coupling circuit; the attenuation factor for the direct coupling circuit, as well as these factors as a function of frequency.

The insertion loss factor (attenuation coefficient) for the directional coupling circuit is defined as the ratio of the primary line input power to the output power of the working arm of the secondary line (Figure 23.2):

$$L_{\text{dir.coup.}} = \quad L_{\text{нс}} = 10\lg(P_1/P_2). \qquad (23.5)$$

The ratio of the powers at the primary line input and output is called the attenuation factor for the direct coupling circuit:

$$L_{\text{dir.coup.}} = \quad L_{\text{пс}} = 10\lg(P_1/P_3). \qquad (23.6)$$

The matching of a directional filter to the input feed line is characterized by the SWR.

The definition of the directivity for directional couplers and directional filters coincides with (23.2).

Directional couplers and filters can be designed around two types of striplines: symmetrical (Figure 23.3a-c) and asymmetrical (Figure 23.3d). A drawback to an asymmetrical stripline is the lack of shielding (the impossiblity of designing "multistory" modules around them), and the elevated losses due to radiation losses in the line where $\varepsilon < 10$. The expediency of using asymmetrical striplines with a high relative dielectric permittivity $\varepsilon \geq 10$ (they are called microstriplines) was discussed at the beginning of the chapter.

Questions of the design of directional couplers and filters using coupled symmetrical striplines will be treated in the following. The major parameters of such lines (characteristic impedance, attenuation, Q and ultimate power) are related to the geometric dimensions (the thickness t and width w of the conducting strip, thickness b and width a of the substrate) as well as its type (configuration, dielectric permittivity, specific conductivity of the material).

A detailed procedure for calculating the geometric dimensions of a stripline for a specified characteristic impedance is given in [014, 015, 1-6]. Also given there are the types of substrates and the limitations on the dimensions of a symmetrical stripline with a transverse electromagnetic wave are treated.

23.2. The Main Design Equations for Single Section T Mode Coupled Line Directional Couplers

Parallel Coupled Lines. Lines of various configurations (Figure 23.4) can be used in T-mode coupled line directional couplers.

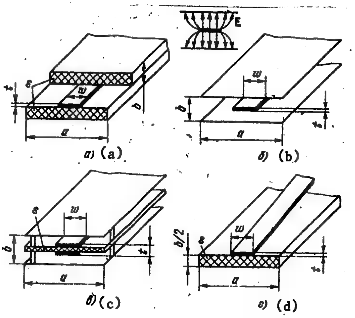
E
ε
t
w
b
a
а) (a)
w
b
a
t
б) (b)
ε
w
b
t
a
в) (c)
b/2
ε
w
a
t
г) (d)

Figure 23.3. Striplines.

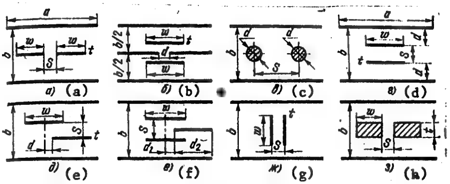
a
b
w
w
t
S
а) (a)
b/2
b/2
w
t
d
w
б) (b)
d
d
b
S
в) (c)
a
w
d
b
t
S
d
г) (d)
w
b
S
t
d
д) (e)
w
b
S
d₁
d₂
е) (f)
b
w
t
S
ж) (g)
w
b
t
S
з) (h)

Figure 23.4. Coupled symmetrical striplines of various configurations.

Primarily the following are used in directional couplers with loose coupling: striplines with thin conductors (Figure 23.4a); striplines with thin conductors coupled through a slot (Figure 23.4b); striplines with circular inner conductors (Figure 23.4c). The following are used in directional couplers with strong coupling: striplines with two thin inner conductors, parallel to the outer plates (Figure 23.4d); similar striplines with displaced conductors (Figure 23.4e); an insert type configuration with thin conductors (Figure 23.4f); striplines with

with two thin inner conductors perpendicular to the outer plates (Figures 23.4g) and those with thick rectangular rods (Figures 23.4h).

The use of a line with a particular configuration depends on many factors. However, configurations shown in Figure 23.4a is most frequently used for loose coupling, directional couplers with sidewall coupling, while the figure of 23.4d for the case of strong coupling is used for directional couplers with end face coupling.

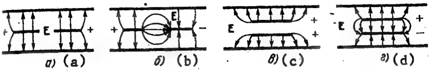

Figure 23.5. The electrical lines of force in coupled striplines with even and odd excitation.

Design Equations. Identical coupled lines represent a symmetrical eight-pole network, the analysis and synthesis of which can be accomplished by means of a classical transmission matrix or using wave transmission and scattering matrices with the symmetry analysis technique. In accordance with this method, the task of studying a directional coupler using identical coupled lines reduces to the description of the processes in the two pairs of four-pole networks for the case of in-phase (even) and out-of-phase (odd) excitation (Figure 23.5).

The scattering matrix of an ideally matched directional coupler using coupled lines with isolated arms (1 and 4 in Figure 23.1a), where this coupler represents a symmetrical eight-pole network, has the form:

$$[S]=\begin{bmatrix} 0 & s_{12} & s_{13} & 0 \\ s_{12} & 0 & 0 & s_{13} \\ s_{13} & 0 & 0 & s_{12} \\ 0 & s_{13} & s_{12} & 0 \end{bmatrix}, \tag{23.7}$$

where
$$s_{12}=\frac{jK\sin\Phi}{\sqrt{1-K^2}\cos\Phi+j\sin\Phi};$$
$$s_{13}=\frac{\sqrt{1-K^2}}{\sqrt{1-K^2}\cos\Phi+j\sin\Phi};$$
$$s_{11}=1;\ s_{14}=0;$$

In this case:

$$K=\frac{\rho_{0ч}-\rho_{0н}}{\rho_{0ч}+\rho_{0н}};\quad \Phi=\frac{2\pi}{\Lambda}l, \tag{23.8}$$

$\rho_{OЧ}$ and ρ_{OH} are the normalized characteristic impedances for even and odd excitation respectively; $\Lambda = \lambda/\sqrt{\varepsilon}$ is the wavelength in the stripline; l is the length of the coupling line; λ is the wavelength in air.

It must be kept in mind that the following relationships hold true:

$$|s_{12}|^2+|s_{13}|^2=1 \tag{23.9}$$

is the unitary condition for the scattering matrix;

$$\rho_{0н}\,\rho_{0ч}=1 \tag{23.10}$$

is the condition for ideal matching and isolation.

It follows from formulas (23.7) and (23.8):

1. The power distribution between inputs 3 and 2 of the directional coupler (Figure 23.1a) depends on the electrical length of the coupling line Φ. As a rule, we choose:

$$l=\Lambda_0/4\ (\Phi=\pi/2), \tag{23.11}$$

where Λ_0 is the center wavelength of the working frequency band, defined in the transmission line (λ_0 is the center working wavelength; ε is the relative dielectric permittivity of the substrate). At this wavelength, the scattering matrix element S_{12} (or the coupling) is maximum, while the absolute value of the coupling coefficients between the lines at the center frequency when $\Phi = \pi/2$ is equal to $K = |S^0_{12}|$ and is defined by expression (23.8).

2. The phase difference in the signals at output 3 and 2 amounts to 90°, which is easily established from (23.7):

$$\arg(s_{13}/s_{12})=\pi/2,$$

where the signal phase leads at output 2, which follows from (23.7), (23.8) and the inequalities $\rho_{0\ \text{even}} > \rho_{0\ \text{odd}}$ and $K > 0$.

It is convenient to represent formulas (23.7) and (23.8) in the form:

$$s_{12}=\frac{K\sin\Phi}{\sqrt{1-K^2\cos^2\Phi}}\,e^{j\psi}, \tag{23.12}$$

$$s_{13}=\frac{\sqrt{1-K^2}}{\sqrt{1-K^2\cos^2\Phi}}\,e^{j(\psi-\pi/2)}, \tag{23.13}$$

where

$$\psi = -\operatorname{arctg}\left(\frac{1}{\sqrt{1-K^2}}\operatorname{tg}\Phi\right), \qquad (23.14)$$

$$\rho_{0ч} = \sqrt{(1+K)/(1-K)},\ \rho_{0н} = \sqrt{(1-K)/(1+K)}. \qquad (23.15)$$

At the center frequency of the passband ($1 = \Lambda_0/4$):

$$|s^0_{12}|^2 = 1 - |s^0_{13}|^2 = K^2. \qquad (23.16)$$

In accordance with expression (23.1)-(23.4), we write the main characteristics of coupled line directional couplers, assuming for the sake of definition that arm 1 is the input arm (Figure 23.1a):

The voltage standing wave ratio at the input:

$$K_{ст} = \frac{1+|s_{11}|}{1-|s_{11}|}, \qquad (23.17)$$

The crosstalk attenuation:

$$C_{12} = 10\lg\frac{1}{|s_{12}|^2}, \qquad (23.18)$$

The working attenuation

$$C_{[illegible]} = 10\lg\frac{1}{|s_{13}|^2}, \qquad (23.19)$$

The isolation

$$C_{14} = 10\lg\frac{1}{|s_{14}|^2}, \qquad (23.20)$$

The directivity:

$$C_{[illegible]} = 10\lg\frac{|s_{12}|^2}{|s_{14}|^2}. \qquad (23.21)$$

Bandwidth Properties. It follows from expressions (23.12) - (23.15) that the quadrature relationships between the voltages in the output arms of directional couplers using identical coupled lines are preserved at all frequencies.

The elements S_{11} and S_{14} of the scattering matrix are equal to zero at all frequencies if condition (23.10) is met, i.e., in this case the directional coupler is ideally matched ($SWR_1 = 0$) and possesses ideal isolation $C_{14} \to \infty$ (the directivity $C_{24} \to \infty$).

By substituting (23.12) and (23.13) in (23.18) and (23.19), we obtain:

$$C_{12} = C^0_{12} + \Delta C_{12}, \qquad (23.22a)$$

$$C^0_{12} = 10\lg(1/K^2), \qquad (23.22b)$$

where

$$\Delta C_{12}=10\lg[1+(1-K^2)\operatorname{ctg}^2\Phi]; \qquad (23.22c)$$

$$C_{13}=C^0_{13}+\Delta C_{13}; \qquad (23.23a)$$

$$C^0_{13}=10\lg\frac{1}{1-K^2}, \qquad (23.23b)$$

$$\Delta C_{13}=10\lg(1-K^2\cos^2\Phi). \qquad (23.23c)$$

In the expressions given here, C^0_{12} and C^0_{13} are the directional coupler parameters at the center frequency of the band; ΔC_{12} and ΔC_{13} are the deviations in the directional coupler parameters from their average value within the working frequency band.

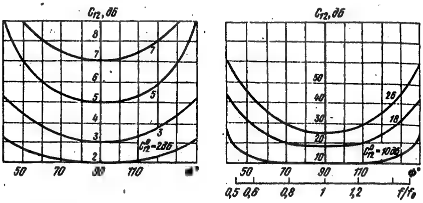

Figure 23.6. The frequency responses of the crosstalk attenuation of a directional coupler using coupled lines.

TABLE 23.1

C^0_{12}, дБ	3	5	10	20	30	40
$\Delta f_{0,5}$, %	64	55	48	45	44	43
$\Delta f_{0,2}$, %	38	33	27	24	23	22

The frequency characteristics of the crosstalk attenuation, calculated in accordance with (23.22a) - (23.22c), are shown in Figure 23.6 and together with Table 23.1 ($\Delta f_{0.5}$ and $\Delta f_{0.2}$ are the bandwidths in percent at the 0.5 and 0.2 dB levels of deviation from C^0_{12} respectively) make it possible to estimate the bandwidth properties of very simple directional couplers using coupled lines. When $C^0_{12} \to \infty$, $\Delta f_{0.5}$ tends to the ultimate value of 42%.

Directional Coupler Operation with Unmatched Loads. A detailed study of the impact of unmatched loads with complex reflection factors Γ_1, Γ_2, Γ_3 and Γ_4, connected to the corresponding arms 1--4 of a coupled line directional coupler on its major characteristics is made in [015]. A conclusion of practical importance follows from [015]: that it is necessary to carefully fabricate the coaxial to stripline (or waveguide to stripline) junctions, the points where the directional coupler joins other radio frequency assemblies, which are the major sources of inhomogeneities, so that $|\Gamma_i| < 0.05$; in this case, all of the major characteristics of the directional coupler will differ to an insignificant extent from the nominal values.

23.3. Extended Bandwidths Directional Couplers Using Coupled Lines

The bandwidth of coupled line directional couplers can be extended by increasing the number of sections of equal electrical length Φ which are cascaded together. Such multiple section directional couplers, although they make it possible to obtain multiple octave bandwidths, are nonetheless larege in size as compared to the extremely simple directional couplers described in the precious sections, something which makes it difficult to use them in antenna arrays. Design relationships are given in this paragraph for a compact tandem directional coupler, in which a cascade configuration of two directional couplers, HO1 and HO2 (Figure 23.7), is used to widen the bandwidth.

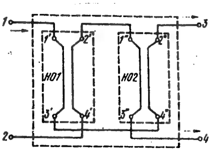

Figure 23.7. The topology of a tandem directional coupler consisting of two directional couplers.

With such a configuration, the production process realization of a directional coupler with strong coupling is also simplified and the requirements placed on the tolerances during coupler fabrication are reduced. Generally speaking, several directional couplers can also be connected in a similar manner. When a signal is fed to arm 1, output signals appear in arms 4 and 3; arm 2 is decoupled. A tandem directional coupler [10] is a symmetrical eight-pole network with the coupling shown in Figure 23.1b; for it, we shall use symbols with a subscript "T": the crosstalk attenuation is C_{14T}, the working attenuation is C_{13T}, the directivity is C_{42T} and the decoupling is C_{12T} (cf. formulas (23.1) - (23.4)).

The parameters $C_{mn\,T}$ are defined on analogy with (23.18) - (23.21), with the substitution of $S_{mn\,T}$ for S_{mn}, where $S_{mn\,T}$ are the elements of the scattering matrix of the tandem directional coupler, which are found by known methods in terms of the scattering matrix s_{mn} for HO1 and HO2 (Both HO's [directional couplers] are assumed to be identical: $K_1 = K_2 = K$, while the connecting sections are equal).

Then:

$$s_{14T} = \frac{2jr\sin\Phi}{(\cos\Phi + j\sqrt{1+r^2}\sin\Phi)^2}; \qquad (23.24)$$

$$s_{13_T} = \frac{1 - r^2 \sin^2 \Phi}{(\cos \Phi + j\sqrt{1 + r^2} \sin \Phi)^2}. \qquad (23.25)$$

$$s_{12_T} = 0, \; s_{11_T} = 0,$$

where $r = K/\sqrt{1 - K^2}$; Φ is the electrical length of the coupling region of H01 and H02; K is the coupling coefficient at the center frequency for H01 (or H02).

At the center frequencies ($\Phi = \pi/2$):

$$|s^0_{14_T}| = K_T = 2K\sqrt{1 - K^2}, \qquad (23.26)$$

$$|s^0_{13_T}|^2 = 1 - |s^0_{14_T}|^2. \qquad (23.26a)$$

Expression (23.26) defines the crosstalk attenuation of a tandem directional coupler (K_T) based on the known coupling coefficient K for H01 (or H02); the inverse relationship to (23.26), which takes into account the feasibility of the directional couplers comprising the tandem configuration is:

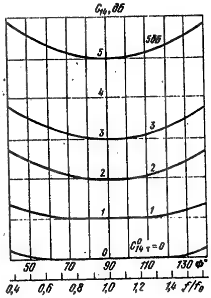

Figure 23.8. The frequency characteristics of the coupling [coefficient] of tandem directional couplers using coupled lines.

$$K = \sqrt{1 - \sqrt{1 - K_T^2}} \Big/ \sqrt{2}. \qquad (23.27)$$

The crosstalk attenuation as a function of frequency is:

$$|s_{14_T}| = \frac{2K\sqrt{1 - K^2} \sin \Phi}{1 - K^2 + K^2 \sin^2 \Phi}. \qquad (23.28)$$

Then:

$$C_{14_T} = 10 \lg \frac{1}{|s_{14_T}|^2} = C^0_{14_T} + \Delta C_{14_T}, \qquad (23.29a)$$

where: $$C^0_{14_T} = 10 \lg \frac{1}{|s^0_{14_T}|^2} = 10 \lg \frac{1}{4K^2(1 - K^2)} \qquad (23.29b)$$

determines the coupling at the center frequency ($\Phi = \pi/2$);

$$\Delta C_{14T} = 10\lg\left(\frac{1-K^2+K^2\sin^2\Phi}{\sin\Phi}\right)^2 \qquad (23.29c)$$

is the deviation of the coupling of the tandem directional coupler from the average value in the working frequency band.

TABLE 23.2

C^0_{14T}	0	1	2	3	5	7	10	18	26	30	40
$\Delta f_{0.5}$	190	150	110	105	100	95	90	95	84	83	82
$\Delta f_{0.2}$	140	110	75	70	65	60	55	50	48	46	44

The frequency characteristics of the coupling coefficient, calculated in accordance with (23.28)--(23.29), are shown in Figure 23.8 and in conjunction with Tables 23.2 ($\Delta f_{0.5}$ and $\Delta f_{0.2}$ are the bandwidths in percent at the 0.5 dB and 0.2 dB levels for the deviation from C^0_{12T} respectively) make it possible to estimate the bandwidth properties of extremely simple tandem directional couplers using coupled lines.

It must be kept in mind that the electrical lengths of the sections 2'-2" and 3'-4", which join the directional couplers (Figure 23.7), are to be made identical.

23.4. The Characteristic Impedances of Coupled Lines in the Case of in-Phase and Out-of-Phase Excitation

It should be noted that the expressions cited in §23.2 are valid for directional couplers using identical lines regardless of the configuration of the latter. The structural (geometric) dimensions and the electircal characteristics of directional couplers are related by means of the characteristic impedances for the case of in-phase (even) $\rho_{0\ \text{even}}$ and out-of-phase (odd) $\rho_{0\ \text{odd}}$ excitation.

The determination of the values $\rho_{0\ \text{even}}$ and $\rho_{0\ \text{odd}}$ represents a rather complex mathematical problem, for the solution of which three main methods are used: the solution of Laplace's equation with boundary conditions, a solution using the technique of conformal mapping and the precise calculation of the stripline capacitance.

Coupled Striplines with Lateral Coupling (Figure 23.4a). For a zero thickness (t/b = 0), the precise value of the characteristic impedance $\rho_{0\ \text{even}}$ is computed from the formula:

$$\rho_{0_{\text{ч}}} = \frac{30\pi}{\sqrt{\varepsilon}}\,\frac{K(k'_{\text{ч}})}{K(k_{\text{ч}})}, \qquad (23.30a)$$

where $K(k'_ч)$ is a complete elliptical integral of the first kind;

$$k_ч = \text{th}\left(\frac{\pi}{2}\frac{w}{b}\right)\text{th}\left(\frac{\pi}{2}\frac{w+S}{b}\right); \quad k'_ч = \sqrt{1-k_ч^2}. \tag{23.30b}$$

The precise value of the characteristic impedance is:

$$\rho_{0\ \text{odd}} = \rho_{0н} = \frac{30\pi}{\sqrt{\varepsilon}}\frac{K(k'_н)}{K(k_н)}, \tag{23.31a}$$

where:

$$k_н = \text{th}\left(\frac{\pi}{2}\frac{w}{b}\right)\text{cth}\left(\frac{w+S}{b}\right); \quad k'_н = \sqrt{1-k_н^2}. \tag{23.31b}$$

One can employ the following formulas with a high degree of precision (an error of less than 1% for $w/b \leq 0.35$), when calculating $\rho_{0\ \text{even}}$ and $\rho_{0\ \text{odd}}$ for conducting strips of zero thickness:

$$\rho_{0ч} = \frac{94,15/\sqrt{\varepsilon}}{\frac{w}{b}+\frac{\ln 2}{\pi}+\frac{1}{\pi}\ln\left[1+\text{th}\left(\frac{\pi S}{2b}\right)\right]}; \tag{23.32a}$$

$$\rho_{0н} = \frac{94,15/\sqrt{\varepsilon}}{\frac{w}{b}+\frac{\ln 2}{\pi}+\frac{1}{\pi}\ln\left[1+\text{cth}\left(\frac{\pi S}{2b}\right)\right]}. \tag{23.32b}$$

The values of $\rho_{0\ \text{even}}$ and $\rho_{0\ \text{odd}}$ as a function of the geometric dimensions of the coupled lines are shown in Figure 23.9 in the forms of nomograms. A straight line joining the specified values of $\rho_{0\ \text{even}}$ and $\rho_{0\ \text{odd}}$, positioned on the outside scales, will yield the value of w/b and S/b at the intersection of the center scale.

Striplines with Lateral Coupling (Figure 23.4b, c and h). For coupled striplines with conductors having a thickness greater than 0 ($t/b \neq 0$) (Figure 23.4h), the formulas for the calculation of $\rho_{0\ \text{even}}$ and $\rho_{0\ \text{odd}}$ and the corresponding tables and graphs are given, for example, in [1, 6]. The values of $\rho_{0\ \text{even}}$ and $\rho_{0\ \text{odd}}$ are calculated for the configuration of Figure 23.4b using the formulas in [1, 5], and for the configuration in Figure 23.4c, using the formulas in [5].

End Face Coupled Striplines (Figure 23.4d). The equations for ρ_0 even and ρ_0 odd of coupled striplines of zero thickness (t/b = 0) with end face coupling have the form:

$$\rho_0 \text{ even} = \quad \rho_{0_{ч}} = \frac{188{,}3/\sqrt{\varepsilon}}{w/(b-S)+(\ln 4)/\pi+C/\pi\varepsilon_a}, \qquad (23.33a)$$

$$\rho_0 \text{ odd} = \quad \rho_{0_{н}} = \frac{188{,}3S/b\sqrt{\varepsilon}}{w/(b-S)+C/\pi\varepsilon_a}, \qquad (23.33b)$$

where:

$$\frac{C}{\varepsilon_a} = \frac{S}{b-S}\ln\frac{b}{S} - \ln\left(1-\frac{S}{b}\right).$$

These equations are valid when

$$w/b \geq 0.35 \quad = \quad w/b \geqslant 0{,}35, \qquad (23.33c)$$

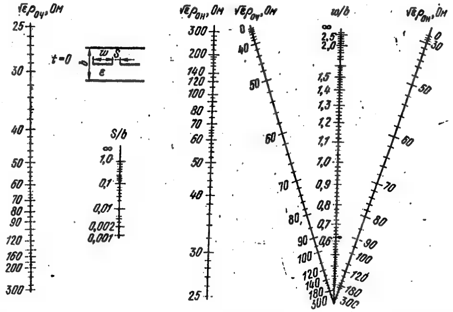

Figure 23.9. Nomograms for the determination of the dimensions S/b (a) and wb (b) in coupled striplines for specified values of $\rho_{0ч}$ [characteristic impedance with in-phase (even) excitation] and $\rho_{0н}$ [characteristic impedance with out-of-phase (odd) excitation]

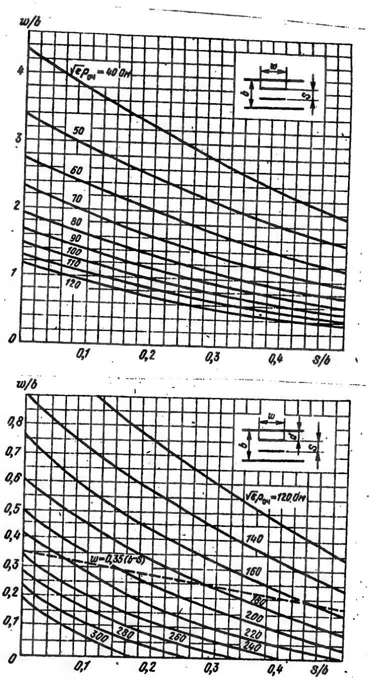

Figure 23.10. The geometric dimensions of coupled striplines with end-face coupling.

If these conditions are not met, the precision of the conformity of the dimensions to the characteristic impedances decreases.

The dimensions of coupled striplines are shown in Figure 23.10 as a function of the characteristic impedance $\rho_{0\ \text{even}}$ for the case of in-phase excitation. To take the finite thickness of a conductor into account ($t/b \neq 0$), one should use Kon's corrections [5, 6].

Striplines with End-Face Coupling (Figure 23.4e-g). To calculate $\rho_{0\ odd}$ and $\rho_{0\ even}$ for the configuration depicted in 23.4e, one must make use of the results of [9]; the characteristic impedance of the lines shown in Figure 23.4f, g were treated in [5].

Coupled microstrip lines with end-face coupling (a configuration similar to Figure 23.4a) are treated in [014, 015].

23.5. The Relationship Between the Structural and Electrical Characteristics

A Stripline Directional Coupler with Lateral Coupling (Figure 23.4a). The relationship between the structural and electrical characteristics is determined from expressions (23.32a) and(23.32b) after substituting $\rho_{0\ even}$ and $\rho_{0\ odd}$ from (23.15) in them and after the appropriate transformations. Then:

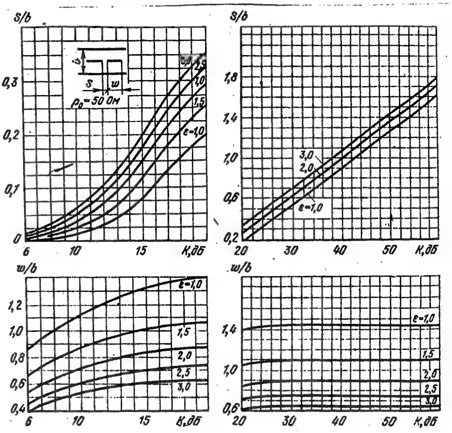

Figure 23.11. On the determination of the geometric dimensions of directional couplers with side coupling.

$$\frac{S}{b}=\frac{1}{\pi}\ln\left[\operatorname{cth}\frac{94,15\pi K}{\rho_0\sqrt{\varepsilon}\sqrt{1-K^2}}\right], \qquad (23.34)$$

$$\frac{w}{b}\,\frac{94,15}{\rho_0\sqrt{\varepsilon}}\sqrt{\frac{1-K}{1+K}}-\frac{1}{\pi}\ln[2(1+\exp\varkappa)], \qquad (23.35)$$

where $\varkappa=-188,3\pi K/\rho_0\sqrt{\varepsilon}\,\sqrt{1-K^2}$.

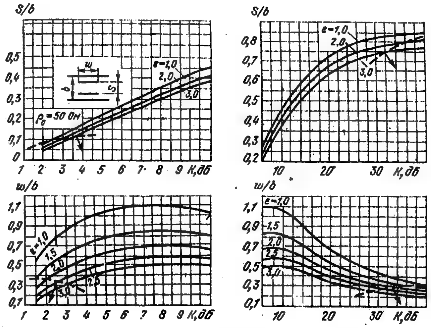

Figure 23.12. On the determination of the geometric dimensions of directional couplers with end-face coupling.

Values of the structural parameters S/b and w/b are shown in Figure 23.11 as a function of the coupling coefficient at the center frequency $C_{12}^0 = K$ for $\rho_0 = 50$ ohms at values of the relative dielectric permittivity of the subsrate ε of from 1 to 3.

It is useful to employ extensive material from graphs and tables (especially when the ratio t/b ≠ 0) in the calculations [6].

For K < 10 dB, the dimension S can become infeasible either structurally or in terms of the production process, and then it is preferable to employ end face coupling (see Figure 23.4d).

Stripline Directional Coupler with End-Face Coupling (Figure 23.4d). The relationship between the structural design and electrical characteristics is determined by expressions (23.33a) and (23.33b):

$$\frac{S}{b}=\sqrt{\frac{1-K}{1+K}}\left[\sqrt{\frac{1-K}{1+K}}-\frac{\sqrt{\varepsilon}\,\rho_0\ln 4}{188{,}3\pi}\right]; \tag{23.36}$$

$$\frac{w}{b}=\left[\frac{188{,}3}{\sqrt{\varepsilon}\,\rho_0}\left(\sqrt{\frac{1-K}{1+K}}\left(\frac{S}{b}\right)\left(1-\frac{S}{b}\right)\right]+\frac{1}{\pi}\left[\left(1-\frac{S}{b}\right)\times\right. \quad (23.37$$

$$\left.\times\ln\left(1-\frac{S}{b}\right)+\left(\frac{S}{b}\right)\ln\left(\frac{S}{b}\right)\right]. \tag{23.37}$$

Curves for the parameters S/b and w/b are shown in Figure 23.12 as a function of the coupling coefficient at the center frequency $C_{12}^{0} = K$ for $\rho_0 = 50$ ohms and for various values of ε. The limitations imposed on (23.36) and (23.37) as well as by inequalities (23.33c) reduce the accuracy of the relationship of the geometric dimensions and the coupling coefficient in the region falling below the dashed lines.

To determine S from the ratio S/b found from (23.36), the following relationship should be used (see Figure 23.4d):

$$S=\frac{2dS/b}{1-S/b}. \tag{23.38}$$

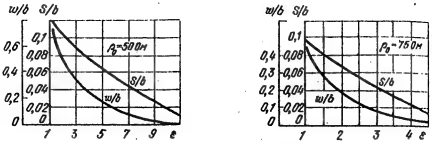

Figure 23.13. On the calculation of the geometric dimensions of a 3 dB directional coupler with in-phase coupling.

Stripline directional couplers with end-face 3 dB coupling occupy a special place in the design of antenna arrays; the curves for w/b and S/b are shown to these couplers in Figure 23.13 as a function of the dielectric permittivity ε for $\rho_0 =$ = 50 and 75 ohms.

23.6. The Major Design Relationships for Single Loop Directional Filters Using Striplines

A single loop directional filter using striplines can be obtained from two directional filters by connecting terminals 2' - 1" and 4' - 3" (Figure 23.14).

The design procedure for such directional filters, which presupposes the design of the microwave structure around a prototype filter with lumped parameters [5], has a number of limitations and in some cases yields a perceptible error, and for this reason, we shall give theoretical relationships, the basis for which is the tool of wave matrices [7]. Such an approach makes it possible to use the basic expressions derived in §23.2.

The scattering matrix of a single loop directional filter with equilateral loops and identical coupling ($K_1 = K_2 = K$), consisting of identical directional couplers with coupling sections (H01 and H02) of equal electrical length Φ (Figure 23.14) has the following form (for the sake of determinancy, we assume that the first arm 1' is the input):

$$[S_\Phi] = \begin{bmatrix} 0 & s_{12\Phi} & s_{13\Phi} & 0 \\ s_{12\Phi} & 0 & 0 & s_{13\Phi} \\ s_{13\Phi} & 0 & 0 & s_{12\Phi} \\ 0 & s_{13\Phi} & s_{12\Phi} & 0 \end{bmatrix}, \tag{23.39}$$

where $$s_{12\Phi} = \tilde{s}_{12}^2/(1 - \tilde{s}_{13}^2) \tag{23.40}$$

is the transmission gain of the directional filter from one line to another through the directional coupling channel;

$$s_{13\Phi} = \tilde{s}_{13} + \tilde{s}_{12}^2\,\tilde{s}_{13}/(1 - \tilde{s}_{13}^2) \tag{23.41}$$

is the transmission gain of the directional filter from one line to another through the direct coupling channel;

$$\tilde{s}_{12} = s_{12}\,e^{-j\Phi}, \quad \bar{s}_{13} = s_{13}\,e^{-j\Phi}; \tag{23.42}$$

S_{12} and S_{13} are determined by (23.12) - (23.14).

The frequency properties of the various filter networks are defined by the expression for the input losses L as a function of frequency. For the directional coupling channel (1'-2" and 3'-4") in accordance with (23.5):

$$L_{\text{dir.coup.}} = L_{\text{нс}} = 10\lg\frac{1}{|s_{12\Phi}|^2}. \tag{23.43}$$

Taking (23.39) - (23.42) and (23.12) - (23.14) into account:

$$L_{\text{нс}}=10\lg\left[1+\left(\frac{2\sqrt{1-K^2}}{1-\sqrt{1-K^2}}\operatorname{ctg}\Phi\right)^2\right]. \tag{23.44}$$

There follows from the unitary nature of the matrix $[S_\phi]$ (23.39):

$$|s_{12\Phi}|^2+|s_{13\Phi}|^2=1. \tag{23.45}$$

Then, taking (23.6) and (23.44) into account, we derive the following expression for the attenuation of the directional filter in the forward circuit (1'-3', 2"-4"):

$$L_{\text{пс}}=10\lg\frac{1}{|s_{13\Phi}|^2}=10\lg\left[1+\left(\frac{1-\sqrt{1-K^2}}{2\sqrt{1-K^2}}\operatorname{tg}\Phi\right)^2\right]. \tag{23.46}$$

Thus, the frequency characteristics of the channels of the filter considered here, without taking losses into account, are governed by functions (23.44) and (23.46). By analyzing them, one can establish the frequency properties of directional filters.

1. The directional coupling channel behaves as a bandpass filter with periodically alternating passbands. The argument of the frequency characteristic is cotΦ, and for this reason, its zeros are located at the points $\Phi_0 = (2n - 1)\pi/2$, while the poles are located at the point $\Phi_\infty = n\pi$, n = 1, 2, 3...

2. The forward channel is similar in terms of its frequency properties to a stopband filter. The stopbands alternate periodically, and in this case, the argument of the frequency characteristic is tanΦ. The poles of the curve $L_{\pi c}$ [forward insertion losses] are located at the points $\Phi_\infty = (2n - 1)\pi/2$, while the zeros are located at the points $\Phi_0 = n\pi$, n = 1, 2, 3, ...

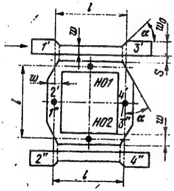

Figure 23.14. Outline drawing of a single loop directional filter.

3. With a decrease in the coupling coefficient K, the passbands and the stopbands are narrowed, and vice-versa, with an increase in K both bands widen, where these functions are nonlinear.

Specifically, the indicated relationships are established from the following considerations. We introduce the approximating function:

$$L_{\text{нс}}=10\lg[1+h^2(\operatorname{ctg}\Phi/\operatorname{ctg}\Phi_m)^2], \tag{23.47}$$

where Φ_m is the electrical length corresponding to the edge of the specified passband of the directional filter; h is a coefficient which defines the nonuniformity of the frequency response within the passband.

By equating the right sides of (23.44) and (23.47), and then solving the resultant equality for K, taking into account the fact that K [0, 1], we obtain:

$$K=\sqrt{1-\left(\frac{h}{h+2\,|\,\mathrm{ctg}\,\Phi_m\,|}\right)^2}. \tag{23.48}$$

At the resonant frequency f_0, all of the energy should be transmitted via the directional coupling channel; in this case, in accordance with (23.44), $F_0 = (2n - 1)\pi/2$. To assure the minimum loop dimensions (of the directional filter), one is to set n = 1, and taking (23.8) into account, we have:

$$\Phi_0=\pi/2;\quad f_m=f_0+\Delta f,\quad \Phi_m=\Phi_0 f_m/f_0=\Phi_0\lambda_m/\lambda_0, \tag{23.49}$$

$$l=\Lambda_0/4=\lambda_0/4\sqrt{\varepsilon}, \tag{23.50}$$

where $f_m(\lambda_m)$ is the frequency (wavelength) corresponding to the edge of the specified passband; Δf is half of the passband.

The design of a directional filter is completed with the plotting of the frequency characteristics for $L_{\mathrm{dir.coup.}}$ (23.44) and $L_{\pi c}$ (23.46), shown in Figure 23.15 for one special case of the values of directional filter parameters.

23.7. The Influence of Tolerances on the Parameters of Directional Couplers

When fabricating printed circuit directional couplers and filters, it is important to esimate the impact of the structural (geometric) tolerances on such parameters as the crosstalk attnuation, isolation and standing wave ratio of the inputs [014, 015, 8].

Curves for the change in the most important parameters of a side coupled directional coupler (Figure 23.4a) are shown in Figure 23.16 as a function of the tolerances for the geometric dimensions: the width of the conducting strip in the coupling region w, the gaph S and the dimension b for various coupling coefficients K. Increasing the width by Δw and the spacing between them by ΔS reduces the coupling in a directional coupler by ΔC, while increasing the dimension b causes the coupling to increase.

It follows from the graphs that with identical tolerances for $\Delta w/w$ and $\Delta S/S$, changing the gap S has a great effect in the case of weak coupling and changing w does the same with strong coupling.

It should also be noted that making the gap S in directional couplers with strong coupling $|C^0| < 10$ dB with a precision of even 10 percent ($\Delta C \leq 0.2$ dB is structurally difficult to do because of the small size of the gap itself.

Curves for the crosstalk attenuation (S_{12}), isolation (C_{14}), working attenuation of the primary line (C_{13}) and the SWR are shown in Figure 23.17 as a function of the relative change in the gap (S/S_0) and the width of the conducting strip in the coupling region (w/w_{nom}) (w_{nom} is the nominal width of the conducting strip in the coupling region) for a directional coupler with end-face coupling (Figure 23.4d); the graphs are plotted taking into account the losses in the dielectric substrate. It follows from the graphs that making the width of the strips in the coupling in the coupling region with a precision of $\pm10\%$, for example, and the width of the gap with a precision of $\pm5\%$ changes the degree of coupling by $\Delta C_{12} \pm 0.2$ dB; in this case, $C_{14} > 30$ dB, while the SWR < 1.1. The influence of the losses for the materials considered here primarily brought about a finite amount of isolation and a change in the crosstalk and working attenuations of less than 0.1 dB.

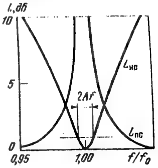

Figure 23.15. Theoretical frequency responses.

$f/f_0 = 1.0048$ ($2\Delta f_0/f_0 = 1\%$);

h = 0.5 dB.

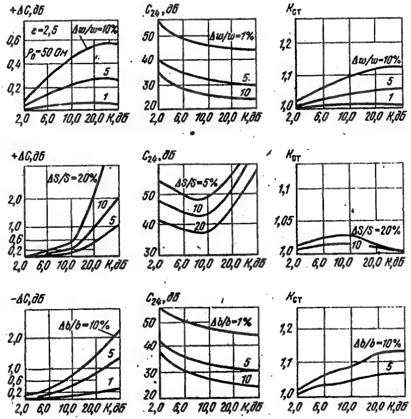

Figure 23.16. On the influence of tolerances on the dimensions of a directional coupler with end-face coupling ($\rho_0 = 50$ ohms, $\varepsilon = 2.5$. [K_{ct} = SWR].

The curves sh own

The curves shown in Figure 23.17 make it possible to draw the conclusion which is of practical importance that it is possible to construct directional couplers with a crosstalk attenuation of 2 to 8 dB only by changing the gap S (Figure 23.4d) with a constant width of the strip in the coupling region (designed for C^0_{12} = 5 dB).

The tolerance for the coupling section length l can be easily estimated, taking (23.8) into account, by means of the curves shown in Figures 23.6.

We will note that in the realization of directional filters, it is necessary to specify such tolerances for the geometric dimensions of the directional couplers (H01 and H02 in Figure 23.14) that they are equal in terms of their absolute value and opposite in sign.

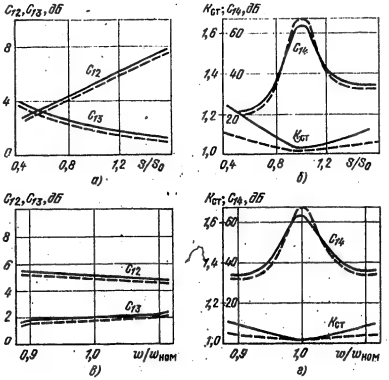

Figure 23.17. On the influence of tolerances on the parameters of a directional coupler with end-face coupling (ρ_0 = 50 ohms):

Solid curves are for CF-2A substrate material;
Dashed curves are for FAF-4 substrate material.

On the Precision of the Realization of Printed Circuit Directional Coupler Dimensions. In the fabrication of microwave printed circuits using striplines made of foil materials, better precision in the reproduction of the circuit dimensions is realized using photochemical technology: down to ±0.025 mm (± 0.1 mm when the drawing is made with Whatman's paper and ±0.05 mm when the drawing is made on glass).

The process of cutting out the conductors with the requisite configuration can be used successfully in the case of nonseries production of striplines; in this case, the precision of the reproduction of the major dimensions of a directional coupler can be kept within ±0.1 mm, and for couplers with end coupling, dielectric inserts are used which make it possible to change the gap size with a precision of ±0.03 mm and less.

23.8. The Structural Design of Directional Couplers and Filters Using Coupled Striplines.

Some Recommendations for the Structural Design of Printed Circuit Directional Couplers and Filters. The correctness of the structural design of printed circuit directional couplers and filters using coupled lines determines their electrical characteristics to a considerable extent. Besides the limitations imposed on the dimensions of striplines with the dominant mode, the following recommendations should be adhered to [0.14, 0.15, 1-6]:

1. The bend angle of a stripline α (see Figure 23.14) (the necessity of a bend arises in the fabrication of a directional filter for the sake of convenience in bringing the conducting stripline into a coaxial-stripline jucntion or to a matched load, etc.), is to be chosen equal to 30...45°.

Fastening screws are to be provided for a tight contact between the upper and lower circuit boards of directional couplers and filters, where these screws are arranged at a distance of no closer than 2b to 3b from the conducting strips. The fastening screws also serve to suppress higher modes at the points of connection of coaxial to stripline transitions and other inhomogeneities.

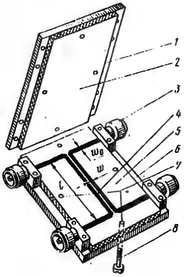

Figure 23.18. A directional coupler with lateral coupling.

Key: 1, 6. Fastening boards;
2. Upper circuit board of the directional coupler;
3. RF plug connector;
4. Conducting strips;
5. Lower circuit board of the directional coupler;
7. Holes for the fastening screws;
8. Fastening screws.

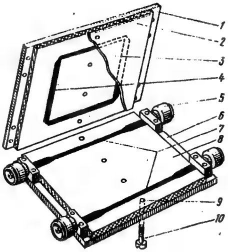

Figure 23.19. A directional coupler with end-face coupling:

Key: 1,6. Fastening boards;
2. Upper board of the directional filter;
3. Dielectric spacer;
4. Conducting strips;
5. RF plug connector;
7. Conducting strips;
8. Lower board of the directional filter;
9. Holes for the fastening screws;
10. Fastening screws.

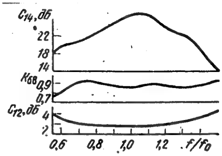

Figure 23.20. Experimental characteristics of a directional coupler with end-face coupling.

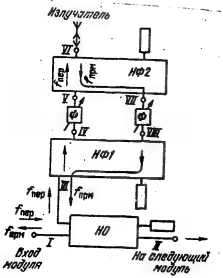

Figure 23.21. Block diagram of a transceiving module of a phased antenna array.

Key: 1. Radiator;
2. NF2 = directional filter filter 2;
3. Directional filter 1;
4. Directional coupler;
5. f_{trans};
6. $f_{receive}$;
7. Module input;
8. To the next module.

3. When manufacturing a large batch of the elements considered here, it is expedient to experimentally work out their corner sections using breadboarded models, since, strictly speaking, corner inhomogeneities slightly change the equivalent length of a line section. Another effective method of aligning a directional filter is the use of four tuning screws, arranged about the perimeter of the loop at intervals of $\Lambda 0/4$, as shown in Figure 23.14 (the small dark circles).

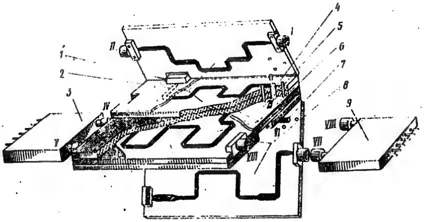

Figure 23.22. A multilevel configuration of a transceiving module of a phased antenna array.

Key:
1. Matched load;
2. Upper and lower boards of the directional coupler;
3. Transmitting channel phase shifter;
4. Multilevel RF transition;
5. Dielectric spacer of directional filter 1;
6. Upper and lower boards of directional filter 1;
7. Module output to the radiator;
8. Upper and lower circuit boards of directional filter 2;
9. Receive channel phase shifter.

Structural designs of coaxial to stripline and waveguide to stripline transitions are treated in [014, 015, 1-6]. An example of the design of a lumped matched load is shown in Figure 23.22, while a distributed load is shown in [014, 015].

Practical Structural Designs for Directional Couplers and Filters. Structural designs of directional couplers and filters are shown in Figures 23.18 and 23.19. The construction of tandem directional couplers, designed in accordance with Figures (23.7), is facilitated when the directional couplers are realized using lines with end-face coupling; in the case of directional couplers with side coupling, it is necessary to use layer to layer transitions (Figure 23.22).

The correctness of the design calculations and structural design solution, arrived at in the planning stage, is evaluated during the process of laboratory tests. Special cases of the appropriate frequency responses are shown in Figure 23.15 for directional filters and in Figure 23.20 for directional couplers.

A block diagram of a transceiving module for a phased array which is used in directional couplers and filters is shown in Figure 23.21, while its realization in a three-level design is shown in Figure 23.22. The conductors of the symmetrical striplines are made in the form of a meander to reduce the longitudinal dimensions; the directional couplers and filters are made with end-face coupling.

The module (Figure 23.21) operates as follows: the signal at the transmit frequency f_{trans} from the input of module (I) is fed through the directional coupler with the corresponding division to the next module (II) and through the level to level transition (4) (Figure 23.22) to the input (III) of the directional filter NF1. Then the signal (f_{trans}) is further fed through the forward coupling channel of NF1 to the input (IV) of the phase shifter of the transmitting channel, and following the appropriate phasing, to the input (V) of NF2 [directional filter 2], through the forward coupling channel of which the signal (f_{trans}) is fed to the input (VI) of the phased array radiator.

In the reception mode, the signal (f_{rec}) is fed from the output (VI) of the radiator via the directional coupling channel of directional filter 2 to the input (VII) of the receive channel phase shifter, and following the appropriate phasing, is fed to the input (VIII) of directional filter 1, and through the directional coupling channel to the input (III) of the directional coupler and through the level to level transition (IV) (Figure 23.22) and the directional coupler to the input of the module (I).

23.9. The Design Procedure

When designing printed circuit directional couplers and filters, besides the requirements placed on the major electrical characteristics, there are limitations on the size and weight, temperature and radiation conditions, power handling capacity, etc., which follow from the requirements placed on an antenna array. Before setting about the calculation of the electrical characteristics in the general case, it is necessary to choose the type of stripline and its characteristic impedance, as well as the type of coupling (side, end-face, mixed) for the directional couplers and filters, working from an entire series of contradictory requirements, where one is governed by the requirements of §23.2 and §23.9 as well as [014, 015- 1-6]. We shall limit ourselves to the treatment of the simplest cases, introducing the following symbols to facilitate the presentation: P is the power (CW or pulsed) transmitted through the directional coupler (or filter) in KW; f_0 (or λ_0) is the center working frequency (or wavelength) of a directional coupler or the resonant frequency (or wavelength) of a directional filter in MHz (or cm); $\pm\Delta f$ (or $\pm\Delta\lambda$) is the working bandwidth, in MHz (or cm); ΔC is the permissible deviation of the crosstalk attenuation of a directional coupler from the average value within the passband, in dB; C^0_{12} is the crosstalk attenuation of a directional coupler at the center frequency* in dB; C^0_{14T} is the crosstalk attenuation of a tandem directional coupler at the center frequency**, in dB; C_{min} is the minimum isolation (or directivity) in the working passband, in dB; $K_{CT\ max}$ [SWR_{max}] is the maximum value of the standing-wave ratio within the working passband at the input to a directional coupler (or directional filter); $2\Delta f$ (or $2\Delta\lambda$) is the passband of a directional filter, in MHz (or cm); $h = L_{HC}$ (f_m) is the attenuation factor at the boundary of the passband in the directional coupling channel, dB; $f_{\pi c}$ (or $\lambda_{\pi c}$) is the frequency (or wavelength) of the signal transmitted through the forward coupling channel of a directional filter, in MHz (or cm); L_{HC} ($f_{\pi c}$) is the attenuation factor at the frequency $f_{\pi c}$ in the directional coupling channel, in dB; $|\Gamma_i|$, $i = 1, 2, 3, 4$ is the absolute value of the reflection factors from inhomogeneities in the inputs of a directional coupler (for example, coaxial to stripline transitions); ρ_0 is the characteristic impedance of the supply feed lines, ohms; $b/2$ is the dielectric substrate thickness, in mm; t is the thickness of a conducting strip, in mm; and ε is the relative dielectric permittivity of the substrate.

---

* For the sake of definition, we assume that arm 1 is the input (Figure 23.1a).

** See Figure 23.1b.

We shall consider the variant of the specifications for the calculation of the structural and electrical parameters of a directional coupler using coupled lines. The following are specified: P, f_0, C^0_{12} (or C^0_{14T}, $\pm\Delta f$ (or ΔC), C_{min}, SWR_{max}, the line is a symmetrical stripline, ρ_0, and the dielectric substrate: ε, $b/2$, t and the type of coupling in the directional coupling is either side or end-face.

The following design calculation procedure is recommended.

1. Determine the width of a conducting strip, w_0 (Figures 23.18 and 23.19), using the procedure given in [1-6, 014, 015], and then determine the a dimension of the stripline (Figure 23.3a), taking into account the limitations in this dimension [1-6].

2. Find the attenuation, Q as well as the ultimate power by using [014, 015, 1-6].

3. Using the graphs of Figures 23.6 and 23.8, and Tables 23.1 and 23.2, establishing the agreement between the passband $\pm\Delta f$ and the permissible coupling nonuniformity, giving preference to the simplest directional couplers because of their structural simplicity.

Using formulas (23.18) and (23.16), determine the coupling coefficients K for the specified C^0_{12}. However, if a tandem directional coupler is selected, then we find the coupling coefficient of a tandem directional coupler, K_T, for the specified C_{14T} using (23.29b) and (23.25), and then we find the coupling coefficients K from (23.27).

4. Determine the coupling line length 1 of the directional coupler using formulas (23.11).

5. Using expressions (23.15), find $\rho_{0\ even}$ and $\rho_{0\ odd}$.

6. Using the known values of $\rho_{0\ even}$ and $\rho_{0\ odd}$, determine the dimension of the conducting strip in the coupling region w, and the gap S, using formulas (23.30)-(23.32) or the graphs of Figure 23.9 for a directional coupler with side coupling and formulas (23.33) or the graphs of Figure 23.10 for a directional coupler with end-face coupling. One can also employ formulas (23.34) - (23.37).

For directional couplers where ρ_0 = 50 ohms and ε = 1, 1.5, 2, 2.5 and 3, the dimensions S and w are most simply determined from the graphs of Figures 23.11 and 23.12, plotted in accordance with (23.34)-(23.37).

It is expedient to use the curves shown in Figure 23.13 to determine the dimensions of a 3 dB directional coupler with in-face coupling where ρ_0 = 50 and 75 ohms.

Equation (23.38) is to be used to determine S in the ratio S/b in a directional coupler with end-face coupling.

7. The frequency resonse $C_{12} = C_{12}(f)$ is plotted for the simplest directional couplers, or $C_{14T} = C_{14T}(f)$ is plotted for tandem directional couplers in accordance with formulas (23.22) and (23.29), or the appropriate curves from Figures 23.6 and 23.8 are used.

8. Where necessary, find the phase relationships at the outputs from formulas (23.12) - (23.14), (23.24) and (23.25) respectively.

9. Estimate the influence of the nonideal nature of the matched loads and the corresponding coaxial stripline transitions (or other inhomogeneities at the outputs of the directional coupler) on K, C_{min} and SWR_{max} from the specified values of $|\Gamma_i|$, using §23.2.

10. Working from the requirements placed on the values of C_{12}^0 (or ΔC_{12}), C_{min} and SWR_{max}, set the appropriate tolerances for the precision in the realization of the geometric dimensions of the directional coupler, as indicated in §23.7.

11. Draw the directional coupler (Figures 23.18, 23.19 and 23.22) taking into account the recommendations for the structural design of printed circuit directional couplers.

Notes: 1. If the type of stripline and coupling in the directional coupler are not stipulated, then it is recommended that they be selected where is one is governed in this case by the considerations indicated in the literature [014, 015, 1-6].

2. If the passband of the directional couplers considered here using coupled lines do not satisfy the technical requirements, it can be widened by using multiple section directional couplers or two or more tandem directional couplers [014, 015].

It must be kept in mind that the use of a tandem directional coupler substantially improves the isolation (or directivity) as compared to the simplest directional couplers, for which because of structural and production process factors, the decoupling does not exceed 20 to 30 dB.

We shall further consider the specification variant for the calculation of the structural design and electrical parameters of single loop directional filters using coupled lines. Required: design a directional filter which segregates the receive channel (arm 2" in Figure 23.14) and transmit channel (arm 3') when working into a common antenna (arm 1'); a matched load is connected to the free arm of the directional filter (4").

The following are specified: P, $f_0 = f_{rec}$, $2\Delta f$, $h = L_{HC}$ (f_m), $f_{\pi c} = f_{trans}$, L_{HC} $(f_{\pi c})$, the line is a symmetrical stripline, the value of ε for the substrate, b/2, t, and the type of coupling in the directional coupler is either in-phase or side coupling.

The following design calculation procedure is recommended:

1. Perform calculations similar to those in paragraphs 1 and 2 for directional couplers.

2. Calculate the geometric length of one side of the loop l (Figure 23.14) using formula (23.50).

3. Using formulas (23.49), find f_m and Φ_m.

4. Determine the coupling coefficient K at the frequency f_0 using formula (23.48).

5. The dimensions of the conducting strip in the coupling region and the gap are determined using the procedure of paragraphs 5 and 6 for directional couplers.

6. Plot the frequency function $L_{HC} = L_{HC}$ (f/f_0) and $L_{\pi c} = L_{\pi c}(f/f_0)$ (see Figure 23.15) in accordance with expressions (23.44) and (23.46).

7. Where necessary, find the phase relationships at the directional filter outputs from expressions (23.40) - (23.42) and (23.12) - (23.14).

8. Make the drawing of the directional filter (Figures 23.14, 23.19 and 23.22), taking into account the recommendations for the structural design of printed circuit directional couplers and filters (§23.8 and [014, 015 and 1-6]).

Notes: 1. The notes of paragraph 11 for directional couplers also remain valid for directional filters.

2. In single loop directional filters using coupled lines, the parameters $h = L_{HC}(f_m)$ and $L_{HC}(f_{\pi c})$ are not completely independent, and for this reason, in satisfying the requirements for the attenuation at the boundary of the passband in the directional coupling channel (h), one may not obtain an altogether satisfactory value of $L_{HC}(f_{\pi c})$. One can partially avoid the indicated correlation by using single loop directional filters with different lengths of the loop sides [7], or by completely using single loop two section directional filters [5]. It is recommended that dual loop directional filers be used to increase the directional properties.

CHAPTER 24. STRIPLINE MICROWAVE POWER DISTRIBUTION SYSTEMS

24.1. The Function and Major Characteristics of Microwave Power Distribution Systems

In a hole series of radio engineering systems for the microwave band, devices are needed which make it possible to divide the power of the source in a definite ratio in several channels or to add the power into a common load. Such functions are performed by multichannel excitation systems for phased arrays which produce the requisite amplitude-phase distribution of the field in the antenna apertures, as well as by power adders for several generators. Two-channel power adders (or dividers) find widescale use in modulators, frequency converters and other radio engineering equipment.

As a rule, passive bidirectional (reciprocal) devices are used for microwave power distribution.

A divider with a common input 0 and N outputs (Figure 24.1) is a multiport network with 2(N+1) poles and can be used as an adder with N outputs and one common input zero by virtue of the reciprocity principle.

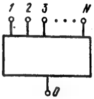

Figure 24.1. A microwave power distribution device in the form of a multiport network.

The following requirements are placed on microwave power distribution devices:

--Providing for a definite distribution of the amplitudes and phases of the signals of the N outputs (or inputs) in a specified frequency range;

--Matching the common input of the divider or N inputs of the adder in the working frequency band;

--Providing for the isolation of the N outputs (inputs) within the passband to reduce the mutual coupling of the channels;

--A high system efficiency;

--A sufficiently simple structural design, small overall dimensions, high reliability and low cost.

Stripline distribution systems based on hybrid integrated circuits (GIS) satisfy the requirements enumerated above to a certain extent. Because of the fact that the possibility for experimental alignment is almost completely lacking in such devices, the theoretical analysis of the circuits and computer methods of analyis and optimization of the working characteristics become of great importance.

The working characteristics of power distribution systems are uniquely defined in terms of the elements of their scattering matrices in the following fashion: the standing wave ratio at the i-th input is:

$$\mathrm{SWR}_i = \quad K_{\text{ст}\,i} = (1+|S_{ii}|)/(1-|S_{ii}|); \tag{24.1}$$

the crosstalk attenuation between the central input (0) and the i-th output is:

$$C_{0i} = 20\lg 1/|S_{0i}|; \tag{24.2}$$

The nonuniformity of the crosstalk attenuation within the frequency band is:

$$\Delta C_{0i} = C_{0i} - C'_{0i} \tag{24.2a}$$

(C'_{0i} is the crosstalk attenuation at the center frequency); the isolation between the i-th and j-th channels is:

$$C_{ij} = 20\lg\frac{1}{|S_{ij}|}. \tag{24.3}$$

The phase relationships of the signals at the outputs are determined by the arguments of the elements of the scattering matrix.

24.2. The Comparative Performance of Various Types of Microwave Power Distribution Systems

The stripline distribution systems used in microwave equipment are distinguished by the number of channels, structural configurations, working frequency band, power handling capability and construction.

Nondirectional distributors formed by branching transmission striplines are the simplest in structural terms. A considerable drawback to such circuits is the impossibility of simultaneously completely matching all of the inputs and decoupling the channels. Because of the finite amount of isolation, a change in the load impedances of the distributor during scanning can lead to considerable deviations of the signal amplitudes and phases at the outputs. This limits the application of nondirectional devices as excitation systems for phased antenna arrays.

Directional distribution devices (Figure 24.2) provide for matching all of the inputs at the center frequency and isolating the channels. Both directional and nondirectional distribution systems are broken down into series (chain) (Figure 24.2a) and parallel (Figure 24.2b, c) types according to the principle for the channelizing of the microwave power.

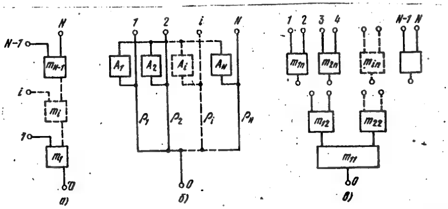
N
N-1
m_{N-1}
i
m_i
1
m_1
0
а)
1
2
i
N
A_1
A_2
A_i
A_N
ρ_1
ρ_2
ρ_i
ρ_N
0
б)
1 2 3 4
N-1 N
m_{1n}
m_{2n}
m_{in}
m_{12}
m_{22}
m_{11}
0
в)

Figure 24.2. Series (a) and parallel (b, c) microwave power directional distributors.

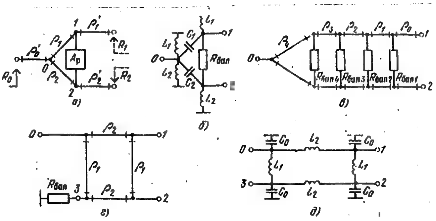
1
ρ_1'
ρ_1
ρ_0'
A_p
R_1
0
ρ_2
ρ_2'
R_2
R_0
2
а)
L_1
C_1
1
0
$R_{бал}$
L_2
C_2
L_2
б)
ρ_3
ρ_2
ρ_1
ρ_0
1
ρ_4
0
$R_{бал4}$
$R_{бал3}$
$R_{бал2}$
$R_{бал1}$
2
в)
0
ρ_2
1
ρ_1
ρ_1
$R_{бал}$
3
ρ_2
2
г)
0
C_0
L_2
C_0
1
L_1
L_1
3
C_0
L_2
C_0
2
д)

Figure 24.3. Circuit configurations of dual channel microwave power dividers.

Series systems are distinguished by their compactness, however, they have a number of substantial drawbacks. First of all, the range of variation in the cross-talk attenuation of the dual channel dividers incorporated in the device increases with an increase in the number of channels, which limits the possibility of using certain types of dual channel dividers, and also generates definite technological difficulties in the realization of the device. The unequal electrical length of the paths from the common input to each radiator leads to a different phase-frequency response of the transmission gains of the channels. Moreover, the distributor units which are closest to the central input pass the maximum power, and for this reason, they should possess an increased electrical strength.

The drawbacks enumerated above are inherent to a lesser extent in parallel distribution systems. Distributors using quarter-wave transmission line sections, depicted in Figure 24.2b, find application in the case of a small number of outputs (less than 10). If resistances are used as the isolating four-port networks $[A_i]$, connected in a star configuration, the device realizes an in-phase uniform power distribution. The frequency properties of such distributors depends substantially on the number of channels, where the SWR of the common input as compared to the SWR of the outputs is a more pronounced function of both the number of channels and the frequency. Thus, within an octave range, the maximum SWR where the number of channels is $N = 3$ and $N = 25$ is 1.75 and 7.5 respectively, while the SWR of the outputs under the same conditions does not exceed 1.1. The efficiency of a distributor likewise falls off with increasing N and in an octave amounts to 0.93 and 0.41 when $N = 3$ and $N = 25$ respectively [1].

A common drawback to such power distributors is the increase in the characteristic impedances of the quarter-wave line sections with an increase in the number of channels, something which makes their technical realization difficult. Moreover, the circuit topology cannot be represented in the form of a flat structure: intersections of the conductors are unavoidable, which likewise represents an inconvenience in the realization of stripline distributors.

A binary power distribution circuit ("christmas tree") has become the most widespread (Figure 24.2c). In this case, the device composed of 3 dB power dividers realizes an in-phase 2^n-channel system with a uniform amplitude distribution of the field at the outputs. When dividers are used which have a division factor other than 1, one can design a system with a specified power distribution for an arbitrary number of channels.

In the low frequency portion of the microwave band, the dimensions of devices using distributed transmission line sections become impermissibly large. One of the ways of reducing the overall dimensions is replacing each line section with its analog using lumped elements [4]. In this case, the working bandwidth of the devices is narrowed, however, within $\leq 10\%$ passband, they can successfully replace systems using distributed elements.

The following can be used as the constituent assemblies of branched distributors: ring configurations, loop quadrature bridges and directional couplers using coupled lines, the isolated outputs of which are loaded into matched impedances (Figure 24.3).

24.3. Calculating the Electrical Parameters and Characteristics of Two Channel Power Distributors

Recommendations are given in this section for the calculation of the electrical parameters of the equivalent circuits of distribution devices (the characteristic impedances of quarter-wave transmission line sections and the parameters of lumped elements), as well as for the elements of their scattering matrices.

Single section ring configurations (Figure 24.3a) assure that the signals at outputs 1 and 2 are in phase when power is fed to the 0 input or provide for summing in-phase signals fed to outputs 1 and 2 in the common 0 channel. They are formed by quarter-wave line sections with characteristic impedances ρ_1 and ρ_2 as well as a decoupling four-port netork (A_p) between terminals 1 and 2. Dual channel power dividers are inserted in the common circuit by means of connecting line sections having characteristic impedances of ρ'_0 and ρ'_1 amd ρ'_2.

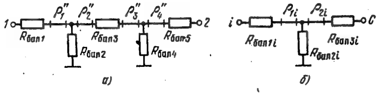

a) б)

Figure 24.4. Dual channel (a) and multichannel (b) power divider circuits with decoupling four-port networks.

In the simplest case, a ballast resistor R_{bal} inserted in series is used as the isolating four-port network. If the length of all of the sections are equal to $\lambda/4$ at the center frequency, then to achieve complete matching and isolation, the parameters of the device are calculated from the following formulas:

$$\rho'_2=\rho'_1\sqrt{\frac{R_2 m}{R_1}};\quad R_{бал}=\frac{\rho_1'^2}{R_1}(m+1);$$
$$\rho_2=\rho_1 m;\quad \rho'_0=\frac{\rho_1}{\rho'_1}\sqrt{\frac{R_1 R_0 m}{m+1}}, \tag{24.4}$$

where $m = P_1/P_2$ is the power division factor. The characteristic impedances ρ_1 and ρ'_1 are chosen arbitrarily in a range of 25 to 150 ohms.

The maximum attainable power division factor of such devices in a stripline design is limited by the feasible values of the characteristic impedances of the lines and does not exceed five.

Dividers with an isolating four-port network (Figure 24.4a), comprised of four quarter-wave line sections with characteristic impedances ρ'' and resistances R_{bal} which differ from the general case have a greater range of change in the coefficient m. One can use modifications of an isolating four-port network whch are obtained by excluding the parallel resistances or shorting the series resistances (with the exception of the last one). For example, a divider with one resistor $R_{bal\ 2}$ (or $R_{bal\ 4}$) takes the form of a ring configuration with a length of $3\lambda/2$ with a matched load at one output. Devices with symmetrically arranged decoupling resistors have a more uniform frequency response of the working characteristics.

It must be noted that the presence of the additional line sections ρ''_1--ρ''_4 narrows the working bandwidth of the devices as compared to a divider having only a resistor as the decoupling four-port network.

The matching of all inputs and the isolation at the center frequency are achieved when the following equations obtain [2].

The characteristic impedances of the quarter wave sections:

$$\rho_1=\sqrt{(m+1)R_0R_1/m}\quad \rho_2=\sqrt{(m+1)R_0R_2}. \tag{24.5}$$

The elements of the normalized transmission matrix of the isolating four-port network:

$$A_{11\text{p}}=\sqrt{m\frac{R_1}{R_2}},\ A_{22\text{p}}=\sqrt{\frac{R_2}{mR_1}},\ A_{12\text{p}}=\frac{m+1}{\rho_0}\sqrt{\frac{R_1R_2}{m}},\ A_{21\text{p}}=0. \tag{24.6}$$

The parameters of the isolating four-port network, R_{bal}, and ρ'' are determined by means of equating the elements of its transmission matrix at the center frequency to the corresponding elements $A_{11\text{p}}$ and $A_{12\text{p}}$ (24.6). In this case, there is the possibility of a free choice of at least one of the parameters R_{bal} or ρ'', which is used in the optimization of the frequency properties of the device. For example, the transmission matrix of the isolating four-port network with one resistor $R_{\text{bal }3}$ when $\rho''_1=\rho''_3$ and $\rho''_4=\rho''_2$ has the form:

$$[A_\text{p}]=\begin{bmatrix}(\rho''_1/\rho''_2)^2 & R_{\text{бал}\,3}\\ 0 & (\rho''_2/\rho''_1)^2\end{bmatrix}, \tag{24.7}$$

Consequently:

$$R_{\text{bal }3}=\quad R_{\text{бал}\,3}=(m+1)\sqrt{R_1R_2/m};\ \rho''_1=\rho''_2\sqrt{mR_1/R_2}. \tag{24.8}$$

The value of ρ''_2 can be chosen arbitrarily in a range of 25 to 150 ohms.

An analysis of the working characteristics of ring dividers without connecting sections can be made using the expresssions given in [2]:

--The reflection factor at the i-th input is:

$$\Gamma_i=\frac{A_{12}-z_i(A_{11}+A_{22}-2)}{A_{12}+z_i(A_{11}+A_{22}-2)}; \tag{24.9}$$

--The working attenuation function is:

$$L_{ij}=20\lg\left|\frac{[A_{12}+z_i(A_{11}+A_{12}-2)}{2(\bar{A}+\tilde{A}_{12})}\sqrt{\frac{z_j}{z_i}}\right|, \qquad (24.10)$$

where Z_i and Z_j are the normalized complex impedances of the load and generator in the general case (i, j = 0, 1, 2); [A], $[\bar{A}]$ and $[\tilde{A}]$ are the transmission matrices of the cascaded four-port networks between the feed points and the load. For example, in the case of the excitation of the 0 input

$$[A]=[A_{\rho 1}][A_{z1}][A_{p}][A_{z2}][A_{\rho 2}].$$

When calculating L_{01}:

$$[\bar{A}]=[A_{\rho 1}];\ [\tilde{A}]=[A_{p}][A_{z2}][A_{\rho 2}].$$

When calculating L_{02}:

$$[\bar{A}]=[A_{\rho 1}][A_{z1}][A_{p}];\ [\tilde{A}]=[A_{\rho 2}],$$

where

$$[A_z]=\begin{bmatrix}1 & 0\\ z^{-1} & 1\end{bmatrix}$$

is the transmission matrix of the impedance inserted in parallel;

$$[A_\rho]=\begin{bmatrix}\operatorname{ch}\gamma l & \rho\operatorname{ch}\gamma l\\ \rho^{-1}\operatorname{sh}\gamma l & \operatorname{ch}\gamma l\end{bmatrix}$$

is the transmission matrix of a line section with a length l having a normalized characteristic impedance of ρ; $\gamma = \alpha + j\beta$ is the propagation constant.

The transmission matrices for the case where inputs 1 and 2 are driven are computed in a similar manner. This algorithm is convenient for machine analysis of six and eight port bridge microwave circuits which are not ideal in the general case (ring configuration, a dual loop bridge), which can be represented in the form of a closed ring of elementary four-port networks with distributed or lumped elements.

A multi-section divider (Figure 24.3c) has a greater working bandwidth than the circuits considered here. The number of sections in dividers which are used in practice does not exceed four.

For a divider with uniform power division, the normalized characteristic impedances of the quarter-wave line sections with respect to ρ_0 can be determined from Table 24.1 as well as the isolating resistors of a n-section device as a function of the requisite frequency coverage factor $k = f_B/f_H$ [f_{upper}/f_{lower}] and the maximum values of the working characteristics at the edge of the band: the SWR of inputs 0, 1 and 2, and the isolation of the channels.

TABLE 24.1

n	$R_{бал\,4}$, Ом	$R_{бал\,3}$, Ом	$R_{бал\,2}$, Ом	$R_{бал\,1}$, Ом	ρ_4, Ом	ρ_3, Ом	ρ_2, Ом	ρ_1, Ом	C_{12}, дБ	$K_{ст\,1,2}$	$K_{ст\,0}$	k
2	—	—	1,86	5,32	—	—	1,67	1,2	36,6	1,007	1,036	1,5
2	—	—	1,96	4,82	—	—	1,64	1,22	27,3	1,021	1,106	2,0
3	—	1,9	3,75	10,0	—	1,8	1,41	1,11	38,7	1,015	1,029	2,0
3	—	2,14	4,23	8,0	—	1,74	1,41	1,15	27,9	1,038	1,105	3,0
4	2,06	3,45	5,83	9,64	1,8	1,54	1,3	1,16	26,8	1,039	1,1	4,0

Key:
1. $R_{bal.4}$, ohms;
2. $R_{bal.3}$, ohms;
3. ρ_4, ohms;
4. C_{12}, dB;
5. $K_{CT\,1,2} = SWR_{1,2}$;
6. SWR_0.

Dual loop directional couplers (Figure 24.3d) are quadrature bridge configurations. When the 0 input is excited, the power is divided between outputs 1 and 2 in a ratio of m, where at the center working frequency, the output 2 signal lags the output 1 signal by $\rho/2$ in phase. When the device is used as a power adder, the signal at input 2 should be fed in with a phase lead of $\rho/2$ with respect to input 1.

The characteristic impedances of the quarter-wave line sections with loads equal to ρ_0 are chosen from the relationship:

$$\rho_1=\rho_0\sqrt{m}\,;\ \rho_2=\rho_0\sqrt{m/(m+1)}\,. \qquad (24.11)$$

In practical circuits, m does not usually exceed 3 - 4 because of the technological difficulties of fabricating lines with a high characteristic impedance.

The analysis of the operating characteristics of a dual loop bridge is made using formulas (24.9) and (24.10). Dual channel dividers based on loop bridges have a smaller bandwidth than ring configurations.

Dividers using lumped elements are anlogs of devices using quarter-wave sections (Figure 24.3b, e). Their electrical parameters, the capacitances and inductances of Π and T section filters are calculated from the formulas [4]:

$$L = \rho/2\pi f_0;\ C = 1/2\pi f_0\rho, \qquad (24.12)$$

where ρ is the characteristic impedance of an equivalent quarter-wave transmission line section; f_0 is the center frequency.

The analysis of the operating characteristics is also made using formulas (24.9) and (24.10).

A directional coupler using coupled lines takes the form of a quadrature bridge, the characteristics of which are determined by the parameters of the coupled lines. The electrical design and analysis of the working characteristics of such devices are given in Chapter 23.

Dual channel dividers, designed around directional couplers using coupled lines, have the greatest working bandwidth of all of the devices considered here. However, there are serious technological difficulties with the realization of dividers with strong side coupling because of the strict tolerances for the dimensions of the striplines.

24.4. The Calculation of the Electrical Parameters and Characteristics of Multi-Channel Power Distribution Systems

N-channel distribution systems using quarter-wave transmission line sections (Figure 24.2b) realize the requisite power distribution at the outputs if the characteristic impedances of the line sections are determined by the expression [2].

$$\rho_i = \sqrt{R_i R_0/P_i}, \qquad (24.13)$$

where R_0 is the internal resistance of the generator; R_i is the load resistance of the i-th output; P_i is the normalized power at the i-th output and $\sum\limits_{i=1}^{N} P_i = 1.$

To achieve ideal matching of all inputs and isolation between the channels at a fixed frequency, the transmission matrix $[A_i]$ of the isolating four-port networks should have the form:

$$[A_i] = \begin{bmatrix} \frac{1}{A_{22\,1}}\sqrt{\frac{P_i R_i}{P_1 R_1}} & \frac{A_{22\,1}}{\rho_0}\sqrt{\frac{P_1}{P_i} R_1 R_i} \\ 0 & A_{22\,1}\sqrt{P_1 P_1/P_i R_i} \end{bmatrix}. \qquad (2.14)$$

These four-port networks can be realized in the form of the circuit depicted in Figure 24.4b, as well as its simpler variants, obtain by eliminating or shorting one or two of the R_{bal} resistances. The impedances of the quarter-wave sections, ρ_{1i} and ρ_{2i}, as well as the resistances $R_{bal\ i}$ are determined by means of equating the transmission matrix of the four-port network and the $[A_i]$ matrix (Figure 24.14). For example, for a circuit with one resistor $R_{bal\ 1i}$:

$$R_{бал\,1i} = R_i; \quad \rho_{1i} = \frac{\rho'_1}{\rho'_2}\,\rho_{2i}\sqrt{\frac{P_i R_i}{P_1 R_1}}.$$

The impedances ρ'_1, ρ'_2 and ρ_{2i} can be chosen arbitrarily in a range of 25 to 150 ohms.

In the special case of uniform power distribution among the channels ($P_1 = P_2 = \ldots = P_N = 1/N$) and identical loads $R_0 = R_1 = R_i = \ldots = R_N = \rho_0$, the characteristics impedances of the line sections and the isolating resistances are equal and are determined by the equations: $\rho_1 = \rho_i = \ldots = \rho_N = \rho_0\sqrt{N}$, $R_{bal\ 11} = R_{bal\ 12} = \ldots = R_{bal\ 1N} = \rho_0$. In this case, the resistances $R_{bal\ 2i}$, $R_{bal\ 3i}$ and the line section impedances ρ_{1i} and ρ_{2i} are absent and the circuit of the distributor is the most wideband circuit of the multichannel dividers of this class.

It is expedient to perform a computer analysis of the operating characterstics of N-channel distribution systems using quarter-wave impedance transformers by means of reducing the multiport network to a six-port network and then make use of expressions (24.9) - (24.10).

The calculation of the parameters of multichannel systems (Figure 24.2a, c) reduces to the determination of the power division factors of each individual two-channel divider and the subsequent calculation of the parameters of its components in accordance with the recommendations of §24.3.

In series type dividers (Figure 24.2a), the power division factor of the individual branches are defined by the expression:

$$m_i = \frac{1}{P_i}\sum_{k=i+1}^{N} P_k. \tag{24.15}$$

In particular, with uniform power distribution among the N outputs, the division factors of two-channel dividers incorporated in a chain circuit configuration are equal to:

$$m_i = N - 1, \quad i = 1, 2, \ldots, N - 1. \tag{24.16}$$

Chain type circuits are conveniently realized using quadrature bridges. In this case, the signals at the outputs are made in-phase by inserting phasing sections with a length of 3λ/4 between the adjacent chain components. Where dual loop bridges with striplines are used, the overall number of circuit outputs is limited: $N \leq 10$. When directional couplers with coupled lines are used, one can construct circuits with a greater number of channels. However, difficulties arise in this case with the realization of the last assemblies of the device having a factor m close to unity.

For 2^n-channel parallel systems (Figure 24.2c), the power division factor of each i-th branch of the j-th stage is determined by the expression:

$$m_{ij} = \sum_{k=a(i-1)+1}^{a(i-1/2)} P_k \Bigg/ \sum_{k=a(i-1/2)+1}^{a_i} P_k, \qquad (24.17)$$

where

$$j = 1, 2, \ldots, n; \; i = 1, 2, \ldots, 2^{j-1}; \; a = 2^{n-j+1}.$$

In the case of uniform power distribution, all dual channel dividers have a division factor of m = 1 among the outputs of a binary system and are quite well realized using ring and dual loop configurations.

The operating characteristics of N-channel binary divider are defined in terms of S-parameters in accordance with (24.1) - (24.3). In this case, the scattering of the device can be obtained by topological or matrix methods [3]. In the case of large values of N, iterative methods of calculating complex microwave networks are more optimal from the viewpoint of the efficient utilization of the immediate access memory of a computer, and sometimes also the machine time as well.

It should be noted that the recommendations given here for the electrical design of microwave power distributors are valid for systems with low dissipative losses. In the short-wave portion of the microwave band, besides taking losses into account, it is also necessary to estimate the impact of inhomogeneities in T or Y configuration lines, the bending of a line, etc. [014, 5].

24.5. An Approximate Design Procedure for Power Distribution Systems

The design calculations for the parameters of a microwave power distribution system can be broken down into the electrical and the structural design calculations.

Initially, by working from the specific requirements placed on the number of channels and the working frequency band, the structural configuration of the device is selected taking the recommendations of §24.4 into account. Thereafter, in the course of the electrical design calculations, the parameters of the equivalent circuits are determined: the characteristic impedances of the line and the lumped elements. For branched series and parallel type systems (Figure 24.2a, c), the power division factors of the constituent assemblies are calculated beforehand, and then the parameters of the dual channel dividers.

After calculating the electrical parameters of the circuit, the scattering matrix is drawn up and the operating characteristics of the device within the frequency band are calculated. To establish the production process tolerances, the working characteristics are studied where scatter is present in the parameters of the circuit components: differences of the load and characteristic impedances from the normal values, as well as in the line lengths and parameters of the lumped elements. In the case of unsatisfactory results, the circuit parameters must be optimized, and possibly also the circuit structure.

The calculated parameters of equivalent circuits serve as the initial data for the structural design. In this design stage, the material and dimensions of the circuit substrate are selected, and the structural dimensions of the transmission lines and lumped film elements are calculated (see [014, 015, 6], as well as Chapter 8 in this book).

The concluding step in the design is that of working out the circuit topology.

BIBLIOGRAPHY

Main Literature

01. Markov G.T., Sazonov D.M., "Antenny" ["Antennas"], Moscow, Energiya Publishers, 1975.

02. Kyun R., "Mikrovolnovyye antenny" ["Microwave Antennas"], Translation from the German edited by M.D. Dolukhanova, Moscow, Sudostroyeniye Publishers, 1967.

03. "Skaniruyushchiye antennyye sistemy SVCh in 3-kh t." ["Microwave Scanning Antenna Systems, in Three Volumes"], Translation from the English edited by R. Khansen, Moscow, Sovetskoye Radio Publishers, 1966-1970.

04. "Antennyye reshetki: Obzor zarubezhnykh rabot" ["Antenna Arrays: A Review of Foreign Literature"], edited by L.S. Benenson, Moscow, Sovetskoye Radio Publishers, 1966.

05. "Antenny i ustroystva SVCh: Raschet i proyektirovaniye antennykh reshetok i ikh izluchayushchikh elementov" ["Microwave Antennas and Devices: The Design Calculations and Planning of Antenna Arrays and Their Radiating Elements"], Edited by D.I. Voskresenskiy, Moscow, Sovetskoye Radio Publishers, 1972.

06. Drabkin A.D., Zuzenko V.L., Kislov A.G.,, "Antenno-fidernyye ustroystva" ["Antennas and Feedlines"], Moscow, Sovetskoye Radio Publishers, 1974.

07. Zhuk M.S., Molochkov Yu.B., "Proyektirovaniye antenno-fidernykh ustroystv v 2-kh t." ["The Design of Antennas and Feedlines, in Two Volumes"], Moscow, Energiya Publishers, 1966, Vol 1; 1973, Vol 2.

08. Amitey N., Galindo V., Vu Ch., "Teoriya i analiz fazirovannykh antennykh reshetok" ["The Theory and Analysis of Phased Antenna Arrays"], Translation from the English edited by G.T. Markov, A.F. Chaplin, Moscow, Mir Publishers, 1974.

09. TIIER [PROCEEDINGS OF THE IEEE], 1968, Vol 56, No 11, "Antennyye reshetki s elektricheskim skanirovaniyem" ["Electrical Scanning Antenna Arrays"].

010. TRUDY MAI [PROCEEDINGS OF MOSCOW AVIATION INSTITUTE], 1964, No 159, "Skaniruyushchiye antenny" ["Scanning Antennas"], Edited by L.N. Deryugin.

011. TRUDY MAI, 1973, No 274, "Mikrovolnovyye skaniruyushchiye antenny" ["Microwave Scanning Antennas"], Edited by D.I. Voskresenskiy.

012. Vendik O.G., "Antenny s nemekhanicheskim dvizheniyem lucha" ["Antennas with Nonmechanical Beam Steering"], Moscow, Sovetskoye Radio Publishers, 1955.

013. "Phased Array Antennas", Edited by A.A. Oliner, G.H. Knittel, Dedham, Artech House, 1972.

014. Maloratskiy L.G., "Mikrominiatyurizatsiya elementov i ustroystv SVCh" ["The Microminiaturization of Microwave Components and Devices"], Moscow, Sovetskoye Radio Publishers, 1976.

015. Maloratskiy L.G., Yavich L.R., "Proyektirovaniye i raschet SVCh elementov na poloskovykh liniyakh" ["The Planning and Design Calculations of Microwave Stripline Components"], Moscow, Sovetskoye Radio Publishers, 1972.

For Chapter 2

1. Voskresenskiy D.I., Ponomarev L.I., Filippov V.S., "Vypuklyye skaniruyushchiye antenny" ["Convex Scanning Antennas"], Moscow, Sovetskoye Radio Publishers, 1978.

2. Vorob'yev V.V., "Ustroystva elektronnogo upravleniya luchom FAR" ["Electronic Beam Steering Devices for Phased Antenna Arrays"], ZARUBEZHNAYA RADIOELEKTRONIKA [FOREIGN RADIOELECTRONICS], 1976, No.1, pp 68-108.

For Chapter 3

1. "Skaniruyushchiye antennyye sistemy SVCh v 2-kh t." ["Microwave Scanning Antenna Systems, in Two Volumes"], Translation from the English edited by G.T. Markov, A.F. Chaplin, Moscow, Sovetskoye Radio Publishers, 1966, Vol 1; 1969, Vol 2.

2. Shnikin H., "Electronically Scanned Antennas", MICROWAVE J., 1960, No 12, pp 67-72, 1961, No 1, pp 57-64.

For Chapter 4

1. Voskresenskiy D.I., Ponomarev L.I., Filippov V.S., "Vypuklyye skaniruyushchiye antenny" ["Convex Scanning Antennas"], Moscow, Sovetskoye Radio Publishers, 1978.

2. Voskresenskiy D.I., "Kommutatsionnaya antenna s shirokugol'nym elektricheskim skanirovaniyem" ["A Switched Antenna with Wide Angle Electrical Scanning"], IZV. VUZOV SSSR. RADIOTEKHNIKA [PROCEEDINGS OF THE HIGHER EDUCATIONAL INSTITUTES OF THE USSR. RADIO ENGINEERING], 1963, Vol 6, No 6, pp 688-694.

3. Voskresenskiy D.I., Gudzenko A.I., "Diapazonnost' ostronapravlennykh dugovykh antennykh reshetok" ["Bandwidth of Pencil Beam Arc Antenna Arrays"], IZV. VUZOV SSSR. RADIOELEKTRONIKA [PROCEEDINGS OF THE HIGHER EDUCATIONAL INSTITUTES OF THE USSR. RADIOELECTRONICS], 1968, Vol 11, No 5, pp 441-451.

4. Stark J.L., Bell C.V., Notest R.A., et al., "Microwave Components for Wideband Phased Arrays", PROC. IEEE, 1968, Vol 56, No 11, pp 1908,-1923.

5. Bogolyubov V.N., Yeskin A.V., Karbovskiy S.B., "Upravlyayemyye ferritovyye ustroystva SVCh" ["Controllable Microwave Ferrite Devices"], Moscow, Sovetskoye Radio Publishers, 1972 (Elementy radioelektronnoy apparatury) [(Radioelectronic Equipment Components)].

6. Goebels F.G., Forman B.J., Nonnemaeker C.H., "Electronic Scanning of Linear Slot Arrays Using Diode Iries [sic]", TRANS. IEEE, 1968, Vol AP-16, No 1, pp 8-14.

7. Khardman, "Razvitiye RLS s fazirovannoy antennoy reshetkoy za posledneye desyatiletiye" ["The Development of Radars with a Phased Antenna Array over the Last Decade"], ZARUBEZHNAYA RADIOELEKTRONIKA [FOREIGN RADIOELECTRONICS], 1971, No 1, pp 39-58.

For Chapter 5

1. Pistol'kors A.A., "Obshchaya teoriya diffraktsionnykh antenn" ["The General Theory of Diffraction Antennas"], ZhTF [JOURNAL OF TECHNICAL PHYSICS], 1944, Vol 14, No 12, pp 693-702; 1946, Vol 16, No 1, pp 3-10.

2. "Posobiye po kursovomy proyektirovaniyu antenn" ["Textbook on Course Required Antenna Design Work"], VZEIS [All-Union Correspondence Electrical Engineering Institute for Communications], Moscow, 1967.

3. Yatsuk L.P., Smirnova N.V., "Vnutrenniye provodimosti nerezonansnykh shcheley v pryamougol'nom volnovode" ["Internal Admittances of Nonresonant Slots in a Rectangular Waveguide"], IZV. VUZOV SSSR. RADIOTEKHNIKA [PROCEEDINGS OF THE HIGHER EDUCATIONAL INSTITUTES OF THE USSR. RADIO ENGINEERING], 1967, Vol 40, No 4, pp 359-369.

4. Veshnikova I.Ye., Yevstropov G.A., "Teoriya soglasovannykh shchelevykh izluchateley" ["Matched Slotted Waveguide Theory"], RADIOTEKHNIKA I ELEKTRONIKA [RADIO ENGINEERING AND ELECTRONICS], 1965, Vol 10, No 7, pp 1181-1189.

5. Yevstropov G.A., Tsarapkin S.A., "Issledovaniye volnovodno-shchelevykh antenn s identichnymi rezonansnymi izluchatelyami" ["A Study of Slotted Waveguide Antennas with Identical Resonant Radiators"], RADIOTEKHNIKA I ELEKTRONIKA, 1965, Vol 10, No 9, pp 1663-1671.

6. Yevstropov G.A., Tsarapkin S.A., "Raschet volnovodno-shchelevykh antenn s uchetom vzaimodeystviya izluchateley po osnovnoy volne" ["The Design of Slotted Waveguide Antennas Taking into Account Dominant Mode Mutual Coupling of the Radiators"], RADIOTEKHNIKA I ELEKTRONIKA, 1966, Vol 11, No 5, pp 822-830.

7. Shubarin Yu.V., "Antenny sverkhvysokikh chastot" ["Microwave Antennas"], Khar'kov, State University, 1960.

8. Shirman Ya.D., "Radiovolnovody i ob"yemnyye rezonatory" ["Radio Waveguides and Spatial Resonators"], Moscow, Svyaz' Publishers, 1959.

9. Reznikov G.B., "Samoletnyye antenny" ["Aircraft Antennas"], Moscow, Sovetskoye Radio Publishers, 1962.

For Chapter 6.

1. Yershov L.I., Kremenetskiy S.D., Los' V.F., "Elektrodinamika vzaimovliyaniya v nerezonansnykh volnovodno-shchelevykh reshetkakh" ["The Electrodynamics of Mutual Coupling in Nonresonant Slotted Waveguide Arrays"], IZV. VUZOV SSSR, RADIOELEKTRONIKA, 1978, No 2, pp 48-54.

2. Los' V.F., Kosmodamianskaya N.S., "Metod rascheta amplitudno-fazovogo raspredeleniya polya v raskryve volnovodno-shchelevykh reshetok s uchetom vnutrennego vzaimodeystviya izluchateley" ["Method of Calculating the Amplitude-PhaseDistribution of the Field in the Aperture of Slotted Waveguide Arrays Taking Internal Mutual Coupling of the Radiators into Account"], "Antenny" ["Antennas"], Edited by A.A. Pistol'kors, Moscow, Svyaz' Publishers, 1969, No 5, pp 24-32.

3. Bakhrakh L.D., Yershov L.I., Kremenetskiy S.D., Los' V.F., "Elektrodinamicheskiye faktory vzaimovliyaniya i raschet volnovodno-shchelevykh reshetok" ["Electrodynamic Factors of Mutual Coupling and the Design of Slotted Waveguide Arrays"], DAN SSSR [REPORTS OF THE USSR ACADEMY OF SCIENCES], 1978, Vol 243, No 2, pp 314-317.

4. Repin V.M., "Difraktsiya elektromagnitnykh poley na sisteme shcheley" ["The Diffraction of Electromagnetic Fields in a System of Slots"], VYCHISLITEL'NYYE METODY I PROGRAMMIROVANIYE [COMPUTER METHODS AND PROGRAMMING], Moscow State University, 1968, No 16, pp 112-121.

5. Yatsuk L.P., Zhironkina A.V., Katrich V.A., "Vozbuzhdeniye pryamougol'nogo volnovoda naklonnoy i krestoobraznoy shchelyami" ["Excitation of a Rectangular Waveguide with Oblique and Cross-Shaped Slots"], "Antenny", Edited by A.A. Pistol'kors, Moscow, Svyaz' Publishers, 1975, No 22, pp 46-60.

6. Fel'd A.N., Benenson L.S., "Antenno-fidernyye ustroystva v 2-kh ch." ["Antennas and Feedlines; in Two Parts"], Moscow, VVIA [Air Force Engineering Academy], 1959, Part II.

7. Markov G.T., "Vozbuzhdeniye pryamougol'nogo volnovoda" ["Excitation of a Rectangular Waveguide"], TRUDY MEI [PROCEEDINGS OF MOSCOW POWER ENGINEERING ISNTITUTE], 1956, No 21, pp 16-34.

8. Fridberg P.Sh., Garb Kh.L., Levinson I.B., "Uchet tolshchiny stenki v shchelevykh zadachakh elektrodinamiki" ["Taking Wall Thickness Into Account in Slot Problems of Electrodynamics"], RADIOTEKHNIKA I ELEKTRONIKA, 1968, Vol 13, No 12, pp 2152-2161.

9. Yevstropov G.A., Tsarapkin S.A., "Raschet volnovodno-shchelevykh antenn s uchetom vzaimodeystviya izluchateley po osnovnoy volne" ["The Design of Slotted Waveguide Antennas Taking Dominant Mode Mutual Coupling of the Radiators into Account"], RADIOTEKHNIKA I ELEKTRONIKA, 1966, Vol 2, No 5, pp 822-830.

10. Breithaupt R.W., Macormick G.T., "Traveling Wave Arrays of Mismatched Elements", TRANS. IEEE, 1971, Vol AP-19, No 1, pp 4-11.

11. Bakhrakh L.D., Kremenetskiy S.D., "Sintez izluchayushchikh sistem" ["The Design of Radiating Systems"], Moscow, Sovetskoye Radio Publishers, 1974.

12. Dayliz S.Yu., Akishin B.A., "Issledovaniye skhemy zameshcheniya naklonno--smeshchennogo volnovodno-shchelevogo izluchatelya" ["Study of the Equivalent Circuit of an Obliquely Displaced Slotted Waveguide Radiator"], in the book, "Antenny i SVCh uzly radiotekhnicheskikh ustroystv" ["Antennas and Microwave Assemblies for Radio Electronic Equipment"], Sverdlovsk, 1976, pp 16-23.

For Chapter 7.

1. Schwartzman L., Stangel, J., "The Dome Antenna", MICROWAVE J., 1975, Vol 18, No 10, pp 31-34.

2. Voskresenskiy D.I., Ponomarev L.I., Filippov V.S., "Vypuklyye skaniruyushchiye antenny" ["Convex Scanning Antennas"], Moscow, Sovetskoye Radio Publsihers, 1978.

3. Voskresenskiy D.I., "Ostronapravlennoye izlucheniye s vypuklykh poverkhnostey" ["Pencil-Beam Radiation from Convex Surfaces"], IZV. VUZOV SSSR. RADIOTEKHNIKA, 1964, Vol 7, No 3, pp 276-282.

4. Yamaykin V.Ye., "Optimizatsiya amplitudnogo raspredeleniya na kruglom sinfaznom raskryve s zatenennoy tsentral'noy oblast'yu" ["Optimization of the Amplitude Distribution in a Circular In-Phase Aperture with a Shaded Central Region"], IZV. VUZOV SSSR, RADIOELEKTRONIKA, 1969, Vol 12, No 6, pp 578-599.

5. Yamaykin V.Ye., "Optimizatsiya perioda FAR" ["Optimization of the Period of a Phased Antenna Array"], "Antenny", Edited by A.A. Pistol'kors, Moscow, Svyaz' Publishers, 1975, Vol 22, pp 20-35.

For Chapter 9.

1. Munson R.E., "Conformal Microstrip Antennas and Microstrip Phased Arrays", TRANS. IEEE, 1974, Vol AP-22, pp 74-78.

2. Anders G., Derneryd, "Linearly Polarized Microstrip Antennas", TRANS. IEEE, 1976, Vol AP-24, No 11, pp 846-851.

3. Tiuri M., Tallqir'st S., Urpo S., "Chain Antenna", Int. IEEE AP-s Symposium Programm and Dig. [sic], Atlanta, Ga., New Youk, 1974, pp 274-277.

4. Walter K., "Antenny begushchey volny" ["Traveling Wave Antennas"], Translation from the English edited by A.F. Chaplin, Moscow, Energiya Publishers, 1970.

5. Tokumaru Shinobu, Shibacaki Taro, "Phased Arrays, Composed of Parallel Fed Two Element Dipoles in a Rectangular Arrangement", TRANS. INST. ELECTR. AND COMM. ENG. JAP., 1976, Vol 156-B, No. 11, pp 521-528.

6. Stark L., "Radiation Impedance of a Dipole in an Infinite Planar Phased Array", RADIO SCIENCE, 1966, Vol 3, pp 361-375.

7. Chang V.W.H., "Infinite Phased Dipole Array", PROC. IEEE, 1968, Vol 56, No 11, pp 1068-1070.

8. Galejt T., "Excitation of Slots in a Conducting Screen Above a Lossy Dielectric Half Space"], TRANS. IRE, 1962, Vol AP-10, pp 443-443 [sic].

For Chapter 10.

1. Indenbom M.V., "Algoritm analiza i optimizatsii direktornykh izluchateley v beskonechnoy ploskoy antennoy reshetke" ["Algorithm for the Analysis and Optimization of Yagi Radiators in an Infinite Planar Antenna Array"], INF. LISTOK/VIMI, [INFORMATION SHEET OF THE VIMI], Series ILT9-13-11, 1980, No 80-0599.

2. Indenbom M.V., Filippov V.S., "Analiz i optimizatsiya direktornykh izluchateley v ploskoy antennoy reshetke" ["Analysis and Optimization of Yagi Radiators in a Planar Antenna Array"], IZV VUZOV SSSR. RADIOELEKTRONIKA, 1979, No 2, pp 34-41.

3. Walter K., "Antenny begushchey volny" ["Traveling Wave Antennas"], Translation from the English edited by A.F. Chaplin, Moscow, Energiya Publishers, 1970.

4. Polak E., "Chislennyye metody optimizatsii" ["Numerical Optimization Methods"], Moscow, Mir Publishers, 1974.

5. Ganston M.A.R., "Spravochnik po volnovym soprotivleniyam fidernykh liniy SVCh" ["Handbook on the Characteristic Impedances of Microwave Feedlines"], Moscow, Svyaz' Publishers, 1976.

6. U.S. Patent 3845490, NKI 343-821.

7. Vay Kaychen', "Teoriya i proyektirovaniye shirokopolosnykh soglasuyushchikh tsepey" ["Theory and Design of Broadband Matching Networks"], Moscow, Svyaz' Publishers, 1979.

For Chapter 11.

1. Titov A.N., Sapsovich B.I., "Fazirovannaya reshetka kak antennaya sistema s iskusstvennym dielektrikom" ["A Phased Array as an Antenna System with an Artificial Dielectric"], "Antenny", Edited by A.A.Pistol'kors, Moscow, Svyaz' Publishers, 1970, No 8, pp 67-80.

2. Nittel' G., Khessel' A., Oliner A., "Nulevyye provaly v diagramme napravlennosti elementa fazirovannoy antennoy antennoy reshetki i ikh svyaz' s napravlennymi volnami" ["Null Dips in the Directional Pattern of an Element of a Phased Antenna Array and Their Relationship to Directed Waves"], TIIER [PROCEEDINGS OF THE IEEE], 1968, Vol 56, No 11, pp 71-88.

3. Elenberger A., Shvartsman L., Topper L., "Nekotoryye trebovaniya k geometrii volnovodnykh reshetok s lineynoy polyarizatsiyey" ["Some Requirements Placed on the Geometry of Waveguide Arrays with Linear Polarization"], TIIER, 1968, Vol 56, No 11, pp 116-128.

4. Borzhiotti G., "Analiz periodicheskoy ploskoy fazirovannoy reshetki metodom sobstvennykh voln" ["Eigenmode Analysis of a Periodic Planar Phased Array"], TIIER [PROCEEDINGS OF THE IEEE], 1968, Vol 56, No 11, pp 132-150.

5. Chaplin A.F., Khzmalyan A.D., Ryakovskaya M.L., "Priblizhennyy spektral'nyy analiz bol'shikh antennykh reshetok" ["Approximate Spectral Analysis of Large Antenna Arrays"], Moscow, Vysshaya Shkola Publishers, 1980, Issue 3, pp 101-121.

For Chapter 12.

1. Lee S.W., Jones W.R., "On the Suppression of the Radiation Nulls and Broadband Impedance Matching of Rectangular Waveguide Phased Arrays", TRANS. IEEE, 1971, Vol AP-19, No 1, pp 41-51.

2. Sushkevich V.I., "Neregulyarnyye lineynyye volnovodnyye sistemy" ["Irregular Linear Waveguide Systems"], Moscow, Sovetskoye Radio Publishers, 1967.

3. Fel'dshteyn A.L., Yavich L.R., Smirnov V.P., "Spravochnik po elementam volnovodnoy tekhniki" ["Handbook on Waveguide Equipment Components"], Moscow, Sovetskoye Radio Publishers, 1967.

For Chapter 13.

1. Fel'd Ya.N., "Shchelevyye antenny" ["Slot Antennas"], Moscow, Sovetskoye Radio Publishers, 1948.

2. "Vychislitel'nyye Metody i Programmirovaniye" ["Computer Methods and Programming"], Moscow State University, Moscow, 1973, Issue 20.

3. Il'inskiy A.S., Grinev A.Yu. Kotov Yu.V., "Issledovaniye elektrodinamicheskikh kharakteristik rezonatorno-shchelevogo izluchatelya s istochnikami vozbuzhdeniya v ploskosti shcheli" ["Study of the Electrodynamic Characteristics of a Slotted Resonator Radiator with the Excitation Sources in the Plane of the Slot"], RADIOTEKHNIKA I ELEKTRONIKA, 1978, Vol 23, No 5, pp 922-930.

4. Grinev A.Yu., Il'inskiy A.S., Kotov Yu.V., "Kharakteristiki skanirovaniya rezonatorno-shchelevoy periodicheskoy antennoy struktury s dielektricheskim pokrytiyem" ["The Scanning Characteristics of a Slot Resonator Periodic Antenna Structure with a Dielectric Coating"], IZV VUZOV SSSR. RADIOTEKHNIKA, 1978, Vol 21, No 12, pp 1822-1833.

5. Grinev A.Yu. Kotov Yu.V., "Mashinnyy metod analiza i chastichnogo parametricheskogo sinteza rezonatorno-shchelevykh antennykh struktur" ["Computer Method for the Analysis and Partial Parametric Synthesis of Slotted Resonator Antenna Structures"], IZV. VUZOV SSSR. RADIOELEKTRONIKA, 1978, Vol 21, No 2, pp 30-35.

6. Kotov Yu.V., "Issledovaniye elektrodinamicheskikh kharakteristik rezonatorno-shchelevykh struktur" ["Study of the Electrodynamic Characteristics of Slotted Resonator Structures"], CHISLENNYYE METODY ELEKTRODINAMIKI [NUMERICAL METHODS OF ELECTRODYNAMICS], Moscow State University, Moscow, 1978, Issue 3, pp 26-40.

For Chapter 14.

1. "SVCh ustroystva na poluprovodnikovykh diodakh: Proyektirovaniye i raschet" ["Microwave Devices Using Semiconductor Diodes: Design Calculations and Planning"], Edited by I.V. Mal'skiy, B.V. Sestroretskiy, Moscow, Sovetskoye Radio Publishers, 1969.

2. Vlasov V.I., Berman Ya.I., "Proyektirovaniye vysokochastotnykh uzlov radiolokatsionnykh stantsiy" ["The Design of the Radio Frequency Assemblies of Radars"], Leningrad, Sudpromgiz Publishers, 1961.

3. USSR Patent No. 358740, Published in Bulletin No. 34, 1972.

4. Voskresenskiy D.I., Mikheyev S.M., Popov V.V.,"Kommutatsionnaya skaniruyushchaya poluprovodnikovaya antennaya reshetka" ["Switched Semiconductor Scanning Antenna Array"], TRUDY MAI [PROCEEDINGS OF MOSCOW AVIATION INSTITUTE], 1973, No 274, pp 5-15.

5. Popov V.V., "Issledovaniye razbrosa parametrov elementov izluchatelya antennoy reshetki" ["Study of the Scatter in the Parameters of the Elements of an Antenna Array Radiator"], TRUDY MAI, 1973, No 274, pp 79-90.

6. Kanareykin D.B., Pavlov N.F., Potekhin V.A., "Polyarizatsiya radiolokatsionnykh signalov" ["Radar Signal Polarization"], Moscow, Sovetskoye Radio Publishers, 1966.

7. Fel'dshteyn A.L., Smirnov V.P., Yavich L.R., "Spravochnik po elementam volnovodnoy tekhniki" ["Handbook on Waveguide Equipment Components"], Moscow, Sovetskoye Radio Publishers, 1967.

For Chapter 16.

1. Aronov V.L., Mazel' Ye.Z., "Sovremennoye sostoyaniye v oblasti razrabotki moshchnykh VCh i SVCh tranzistorov" ["The State of the Art in the Development of High Frequency and Microwave Transistors"], in the book, "Poluprovodnikovyye pribory i ikh primeneniye" ["Semiconductor Devices and Their Applications"], Edited by Ya.V. Fedotova, Moscow, Sovetskoye Radio Publishers, 1971, No 25, pp 7-29.

2. Kaganov V.I., "Tranzistornyye radioperedatchiki" ["Transistorized Radio Transmitters"], Moscow, Energiya Publishers, 1976.

3. "Radioperedayushchiye ustroystva na poluprovodnikovykh priborakh" ["Radio Transmitting Equipment Using Semiconductor Devices"], Edited by R.A. Valitov, and I.A. Popov, Moscow, Sovetskoye Radio Publishers, 1973.

4. Chelnokov O.A., "Tranzistornyye generatory sinusoidal'nykh kolebaniy" ["Transistorized Sine Wave Generators"], Moscow, Sovetskoye Radio Publishers, 1975.

5. "Proyektirovaniye radioperedayusychikh ustroystv SVCh" ["The Design of Microwave Radio Transmitting Equipment"], Edited by G.M. Utkin, Moscow, Sovetskoye Radio Publishers, 1979.

6. Kiyko G.I., Lib Yu.H., et al., "Issledovaniye shirokopolosnogo tranzistornogo usilitelya moshchnosti s raspredelennymi parametrami" ["Study of a Broadband Transistorized Power Amplifier with Distributed Parameters"], "Poluprovodnikovyye pribory v tekhnike elektrosvyazi" ["Semiconductor Devices in Electrical Communications Equipment"], Moscow, Svyaz' Publishers, 1975, No 15, pp 19-26.

For Chapter 17.

1. "Radioperedayushchiye ustroystva na poluprovodnikovykh priborakh" ["Radio Transmitting Equipment Using Semiconductor Devices"], Edited by R.A. Valitov, I.A. Popov, Moscow, Sovetskoye Radio Publishers, 1973.

2. Koptev G.I., Panina T.A., "Raschet uslilitel'nykh i umnozhitel'nykh kaskadov transzistornykh peredatchikov" ["The Design of Amplifier and Multiplier Stages for Transistorized Transmitters"], Moscow, Moscow Power Engineering Institute, 1975.

3. Kaganov V.I., "Tranzistornyye radioperedatchiki" ["Transistorized Radio Transmitters"], Moscow, Energiya Publishers, 1976.

4. Petrov B.Ye., Tereshina G.N., "Transistornyye generatory" ["Transistor Oscillators"], Moscow, MEIT, 1975.

5. Chelnokov O.A., "Tranzistornyye generatory sinusoidal'nykh kolebaniy" ["Transistorized Sine Wave Generators"], Moscow, Sovetskoye Radio Publishers, 1975.

6. Kiyko G.I., Limb Yu.N., et al., "Issledovaniye shirokopolosnogo tranzistornogo usilitelya moshchnosti s raspredelennymi parametrami", "Poluprovodnikovyye pribory v tekhnike elektrosvyazi", Moscow, Svyaz' Publishers, 1975, No 15, pp 19-26.

7. Granovskaya R.A., Petrov S.B., "Proyektirovaniye SVCh tsepey tranzistornykh generatorov s vneshnim vozbuzhdeniyem, vypolnyayemykh v vide gibridnykh integral'nykh skhem" ["The Design of Microwave Networks of Transistorized, Externally Excited Oscillators/Amplifiers Made in the Form of Hybrid Integrated Circuits"], Moscow, Moscow Aviation Institute, 1977.

8. Sobol G., "SVCh primeneniya tekhnologii integral'nykh skhem" ["Microwave Applications of Integrated Circuit Technology"], in the book, "Poluprovodnikovyye Pribory SVCh" ["Semiconductor Microwave Devices"], Edited by F. Brand, Moscow, Mir Publishers, 1972, pp 83-96.

9. Grey P., Grekhem R., "Radioperedatchiki" ["Radio Transmitters"], Moscow, Svyaz' Publishers, 1965.

10. Atabekov G.I., "Osnovy teorii tsepey" ["Principles of Network Theory"], Moscow, Energiya Publishers, 1969.

11. Rayev M.D., Shvarts N.Z., "Soglasovaniye kompleksnykh soprotivleniyy v SVCh mikroelektronike" ["Matching Complex Impedances in Microwave Microelectronics"], IZV. VUZOV SSSR. RADIOELEKTRONIKA, 1972, Vol 11, No 6, pp 728-737.

12. Mattey D.L., Yang L., Dzhons Ye.M., "Fil'try SVCh, soglasuyushchiye tsepi i tsepi svyazi, v 2-kh t." ["Microwave Filters, Matching Networks and Coupling Networks, in Two Volumes"], Moscow, Svyaz' Publishers, 1971, Vol 1.

For Chapter 18.

1. Granovskaya R.A., Shkalikov V.N., "Osobennosti primeneniya v peredayushchikh aktivnykh antennykh reshetkakh moduley s umnozheniyem chastoty" ["Specific Features of the Application of Frequency Multiplier Modules in Active Transmitting Antenna Arrays"], IZV. VUZOV SSSR. RADIOELEKTRONIKA, 1978, No 2, pp 69-73.

2. Vizel' A.A., Pil'don V.N., "Metody rascheta optimal'nykh parametrov umnozhiteley chastoty na nelineynoy yemkosti poluprovodnikovykh diodov" ["Methods of Calculating the Optimal Parameters of Frequency Multipliers Using the Nonlinear Capacitance of Semiconductor Diodes"], ELEKTRONIKA I YEYE PRIMENENIYE [ELECTRONICS AND ITS APPLICATIONS], 1974, Vol 5, No 7, pp 173-213.

3. Kaganov V.I., "Tranzistornyye radioperedatchiki" ["Transistorized Radio Transmitters"], Moscow, Energiya Publishers, 1976.

4. Shkalikov V.N., Lutin E.A., "O fazovykh kharakteristikakh varaktornykh umnozhiteley chastoty" ["On the Phase Characteristics of Varactor Frequency Multipliers"], RADIOTEKHNIKA, 1973, Vol 28, No 10, pp 60-66.

5. Lutin E.A., Telyatnikov L.I., Shkalikov V.N., "Fazovyye kharakteristiki Dvukhkonturnogo umnozhitelya chastoty na diode s nakopleniyem zaryada" ["The Phase Characteristics of a Two Tuned Section Frequency Multiplier Using a Charge Storage Diode"], RADIOTEKHNIKA, 1975, Vol 30, No 10, pp 52-60.

6. "Proyektirovaniye moduley SVCh: Diodnyye generatory, usiliteli i umnozhiteli SVCh" ["The Design of Microwave Modules: Diode Microwave Oscillators, Amplifiers and Multipliers"], Edited by G.P. Zemtsov, Moscow, Moscow Aviation Institute, 1973 (Summary of Lectures).

7. "Radioperedayushchiye ustroystva na poluprovodnikovykh priborakh" ["Radio Transmitting Equipment Using Semiconductor Devices"], Edited by R.A. Valitov and I.A. Popov, Moscow, Sovetskoye Radio Publishers, 1973.

8. Bob Weirather, "Good Microstrip Multipliers Don't Just Happen", ELECTRONIC DESIGN, 1971, No 3, pp 36-39.

For Chapter 19.

1. Tager A.S., Val'd-Perlov V.M., "Lavinno-proletnyye diody i ikh primeneniye v tekhnike SVCh" ["Avalanche and Transit Diodes and Their Applications in Microwave Engineering"], Moscow, Sovetskoye Radio Publishers, 1968.

2. Kolosov M.V., Peregonov S.A., "SVCh generatory i usiliteli na poluprovodnikovykh priborakh" ["Microwave Oscillators and Amplifiers Using Semiconductor Devices"], Moscow, Sovetskoye Radio Publishers, 1974.

3. Khaddad G.G., "Printsipy raboty i osnovnyye svoystva LPD" ["Operational Principles and Major Properties of IMPATT Diodes"], ZARUBEZHNAYA RADIOELEKTRONIKA [FOREIGN RADIOELECTRONICS], 1972, No 1, pp 75-92.

4. "Poluprovodnikovyye pribory SVCh" ["Microwave Semiconductor Devices"], Edited by F. Brand, Translated from the English, Moscow, Mir Publishers, 1972.

5. "SVCh poluprovodnikovyye pribory i ikh primeneniye" ["Microwave Semiconductor Devices and Their Applications"], Edited by G. Watson, Translated from the English, edited by V.S. Etkin, Moscow, Mir Publishers, 1972.

6. "Mikroelektronika i poluprovodnikovyye pribory" ["Microelectronics and Semiconductor Devices"], Edited by A.A. Vasenkov and Ya.A. Fedotov, Moscow, Sovetskoye Radio Publishers, 1976, No. 1.

7. Bouers H., Midford T., Plants S., "Impatt Diode Multistage Transmission Amplifiers", TRANS. IEEE, 1970, V. MTT-18, No 11, p 943-948.

8. Kayl F.N., Midford T.A., "LPD v integral'nom ispolnenii" ["Integrated Circuit IMPATT Diodes"], TIIER [PROCEEDINGS OF THE IEEE], 1967, Vol 55, No 12, pp 130-132.

9. Magalkhayes F.M., K. Kurrokova, "Perestraivayemyy generator dlya izmereniya kharakteristik IMPATT diodov" ["Tunable Generator for the Measurement of IMPATT Diode Characteristics"], TIIER, 1970, Vol 58, No 6, pp 111-113.

For Chapter 20.

1. Sobol G., "SVCh primeneniye tekhnologii integral'nykh skhem" ["Microwave Applications of Integrated Circuit Technology"], in the book, "Poluprovodnikovyye pribory SVCh" ["Microwave Semiconductor Devices"], Edited by F. Brand, Moscow, Mir Publishers, 1972, pp 83-86.

2. Schneider M.U., "Microstrip Lines for Microwave Integrated Circuits", BELL SYSTEM TECHNICAL JOURNAL, 1969, Vol 48, No 5, pp 1421-1444.

3. Sobol G., "Ispol'zovaniye tekhniki integral'nykh skhem dlya sozdayniya SVCh oborudovaniya" ["The Use of Integrated Circuit Hardware for the Design of Microwave Equipment"], ELEKTRONIKA [ELECTRONICS], Vol 40, No 6, 1967, pp 33-46.

4. Colton M., et al., "SVCh integral'nyye skhemy na elementakh s sosredotochenymi postoyannymi i perspektivy ikh primeneniya" ["Microwave Integrated Circuits Using Elements with Lumped Constants and Prospects for Their Application"], ZARUBEZHNAYA RADIOELEKTRONIKA, 1972, No 4, pp 104-123.

5. Demin V.V., Gorelikov N.I., Gotra Z.Yu., "Plenochnyye mikroskhemy i miniatyurizatsiya" ["Film Integrated Circuits and Miniaturization"], L'vov, Kamenyar, 1972.

6. Dolkart V.M., Novik G.Kh., "Konstruktivnyye i elektricheskiye kharakteristiki mnogosloynykh pechatnykh plat" ["Structural and Electrical Characteristics of Multilayer Printed Circuit Boards"], Moscow, Sovetskoye Radio Publishers, (Biblioteka radiokonstruktora) [(Radio Designer's Library)].

For Chapter 21.

1. "SVCh ustroystva na poluprovodnikovykh diodakh" ["Microwave Devices Using Semiconductor Diodes"], Edited by I.V. Mal'kiy and B.V. Sestroretskiy, Moscow, Sovetskoye Radio Publishers, 1969.

2. Mikaelyan A.L., "Teoriya i primeneniye ferritov na SVCh" ["Theory and Application of Ferrites at Microwave Frequencies"], Moscow, Energiya Publishers, 1963.

3. "Upravlyayushchiye ustroystva SVCh" ["Microwave Control Devices"], N.T. Bova, et al., Kiev, Tekhnika Publishers, 1973.

4. Upravlyayemyye ferritovyye ustroystva SVCh" ["Controlled Microwave Ferrite Devices"], V.N. Bogolyubov, et al., Moscow, Sovetskoye Radio Publishers, 1972.

5. Averbukh M.E., Bkhlokhin V.N. [sic], Miroshnichenko A.S., "Diskretnyye mikropoloskovyye fazovrashchateli na p-i-n diodakh" ["Digital Microstrip Line Phase Shifters Using PIN Diodes"], "Elektronika" Central Scientific Research Institute, Moscow, 1976, No. 1.

For Chapter 22.

1. Fel'dshteyn A.L., Yavich L.R., Smirnov V.P., "Spravochnik po elementam volnovodnoy tekhniki" ["Handbook on Microwave Equipment Components"], Moscow, Sovetskoye Radio Publishers, 1967.

2. Fel'dshteyn A.L., Yavich L.R., "Sintez chetyrekhpolyusnikov i vos'mipolyusnikov na SVCh" ["Design of Four and Eight Port Networks for Microwave Frequencies"], Moscow, Svyaz' Publishers, 1971.

3. Al'tman D., "Ustroystva SVCh" ["Microwave Devices"], Translated from the English, Edited by I.V. Lebedev, Moscow, Mir Publishers, 1968.

4. Khanzel L., "Spravochnik po raschety fil'trov" ["Filter Design Handbook"], Translated from the English, edited by L.Ye. Znamenskiy, Moscow, Sovetskoye Radio Publishers, 1974.

5. Mattey Dl., Yang L., Dzhons Ye.M., "Fil'try SVCh, soglasuyushchiye tsepi i tsepi svyazi, v 2-kh t." ["Microwave Filters, Matching Networks and Coupling Networks, in Two Volumes"], Moscow, Svyaz' Publishers, 1974.

6. Maloratskiy L.G., "Mikrominiatyurizatsiya elementov i ustroystv SVCh" ["Microminiaturization of Microwave Components and Devices"], Moscow, Sovetskoye Radio Publishers, 1976.

7. Kozlov V.I., Yufit G.A., "Proyektirovaniye SVCh ustroystv s pomoshch'yu EVM" ["Computer Assisted Design of Microwave Devices"], Moscow, Sovetskoye Radio Publishers, 1976.

For Chapter 23.

1. Ganston M.A., "Spravochnik po volnovym soprotivleniyiyam fidernykh liniy SVCh" ["Handbook on the Characteristic Impedances of Microwave Feedlines"], Translated from the English, Edited by A.Z. Fradin, Moscow, Svyaz' Publishers, 1976.

2. "Konstruirovaniye i raschet poloskovykh ustroystv" ["Structural and Design Calculations for Stripline Devices"], Edited by I.S. Kovalev, Moscow, Sovetskoye Radio Publishers, 1974.

3. "Poloskovyye linii i ustroystva SVCh" ["Microwave Devices and Striplines"], Edited by V.M. Sedov, Khar'kov, Vysshaya Shkola Publishers, 1974.

4. Kovalev I.S., "Osnovy teorii i rascheta ustroystv SVCh" ["Principles of the Theory and Design of Microwave Devices"], Minsk, Nauka i Tekhnika Publishers, 1972.

5. Mattey D.L., Yang L., Dzhons YeM.T., "Fil'try SVCh, soglasuyushchiye tsepi i tsepi svyazi v 2-kh t" ["Microwave Filters, Matching Networks and Coupling Networks; in Two Volumes"], Translation from the English edited by A.V. Alekseyev and F.V. Kushner, Moscow, Svyaz' Publishers, 1971, 1972 [sic].

6. Fel'dshteyn A.L., Yavich L.R., Smirnov V.P., "Spravochnik po elementam volnovodnoy tekhniki", Moscow, Sovetskoye Radio Publishers, 1967.

7. Mashkovets B.M., Tkachenko K.A., "Volnovoy metod sinteza odnopetlevykh napravlennykh fil'trov na poloskovykh" ["The Wave Method of Synthesizing Single Loop Directional Filters Using Striplines"], ELEKTROSVYAZ', 1969, No 6, pp 21-28.

8. Goyzhevskiy V.A., Levin A.F., Golovchenko V.G., "Vliyaniye dopuskov na parametry pechatnykh napravlennykh otvetviteley" ["The Influence of Tolerances on the Parameters of Printed Circuit Directional Couplers"], IZV. VUZOV SSSR. RADIOELEKTRONIKA, 1973, Vol 16, No 3, pp 89-95.

9. Shelton J.P., "Impedances of Offset Parallel Split Transmission Lines", TRANS. IEEE, 1966, Vol MTT-14, No 1, p 7-13.

10. Metcalf W.S., "Cascading Four-Port Networks"], MICROWAVE T. [sic], 1969, Vol 12, No 9, pp 14- 17.

For Chapter 24.

1. Kaganov V.I., "Tranzistornyye radioperedatchiki" ["Transistorized Radio Transmitters"], Moscow, Energiya Publishers, 1976.

2. Myakishev .BYa., Solovtsov P.A., "Mnogokanal'nyy SVCh delitel' moshchnosti s proizvol'nym amplitudnym raspredeleniyem na vykhodakh" ["Multichannel Microwave Power Divider with an Arbitrary Amplitude Distribution at the Outputs"], IZV. VUZOV SSSR. RADIOELEKTRONIKA, 1978, No 2, pp 118-121.

3. Silayev M.A., Bryantsev C.F., "Prilozheniye matrits i grafov k analizu SVCh ustroystv" ["The Application of Matrices and Graphs to the Analysis of Microwave Devices"], Moscow, Sovetskoye Radio Publishers, 1970.

4. Tsarenkov V.S., "Mnogoplechiye deliteli (summatory) moshchnosti SVCh na sosredotochennykh elementakh" ["Multiloop Microwave Power Dividers (and Adders) Using Lumped Elements"], RADIOTEKHNIKA I ELEKTRONIKA, 1975, No. 5, Vol 16, pp 943-948.

5. Nefedov Ye.I., Fialkovskiy A.T., "Poloskovyye linii peredachi: Teoriya i raschet tipichnykh neodnorodnostey" ["Strip Transmission Lines: Theory and Design of Typical Inhomogeneities"], Moscow, Nauka Publishers, 1974.

6. "Osnovy proyektirovaniya mikroelektronnoy apparatury" ["Fundamentals of the Design of Microelectronic Equipment"], Edited by B.F. Vysotskiy, Moscow, Sovetskoye Radio Publishers, 1977.

COPYRIGHT: Izdatel'stvo "Radio i svyaz'", 1981

8225
CSO: 8144/0181

- END -